



Conference Proceedings International Conference on Defence and Space Technologies (ICDST) 2019

On August 23-25, 2019

**Supported by TEQIP III and
Technically Co-Sponsored by**



Organised By

**Department of Electronics & Communication
Engineering**

**Institute of Engineering & Technology,
Lucknow, U.P.-226021**

**An Autonomous and Constituent Institute of
Dr.APJ Abdul Kalam Technical University, U.P.**

www.ietlucknow.ac.in



राजनाथ सिंह
RAJNATH SINGH



रक्षा मंत्री
भारत
DEFENCE MINISTER
INDIA

Date : 19-08-2019

Message

I am happy to know that the **Institute of Engineering and Technology, Lucknow (Uttar Pradesh)** is organizing an **International Conference** on "**Defence and Space Technologies**" **ICDST-2019** from 23rd to 25th August, 2019 at Lucknow and also coming out with a souvenir to mark the occasion.

I congratulate all the management of the Institute on organizing the International Conference and wish for souvenir's successful publication.

With good wishes,

(Rajnath Singh)



**INTERNATIONAL CONFERENCE ON
DEFENCE AND SPACE TECHNOLOGIES**

ICDST-2019

(23-25 AUGUST 2019)

Institute of Engineering and Technology, Lucknow-226021

An Autonomous and Constituent Institute of

Dr. APJ Abdul Kalam, Technical University, Uttar Pradesh

Chief Patron

Prof. Vinay Kumar Pathak

Vice Chancellor Dr. APJ Abdul Kalam
Technical University, Uttar Pradesh

Patron

Prof. H.K.PALIWAL

Director, IET Lucknow

General Chair

Prof. Yatindra Nath Singh

EE, IIT, Kanpur

Conference Chair

Prof. V.K.Singh

ECE, IET Lucknow

Prof. S.R.P. Sinha

ECE, IET Lucknow

Coordinators

Prof. SubodhWairya

Head, ECE, IET Lucknow

Prof. O.P. Singh

Coordinator, TEQIP,

IET, Lucknow,

Convener

Dr. RCS Chauhan

Electronics & Communication Engg.

IET Lucknow

Organizing Secretaries

Dr. Arun Tiwari

Head, Mechanical Engineering

IET Lucknow,

Dr. Y.N. Singh

Head, Computer Science & Engineering

IET Lucknow,

Dr. Satyendra Kumar Singh

Head, Electrical Engineering

IET Lucknow,

Dr. Dhananjay Singh

Head, Chemical Engineering

IET Lucknow,

Dr. Pradeep Bajpayee

Registrar, IET Lucknow,

Mr. Abhishek Nagar

System Manager, IET Lucknow,



Message

For any country, it is important to continuously innovate and develop new technology to strengthen its defence capability. This also needs strong space and nuclear programmes. Strong defence means also maintaining strong democracy independent of influence of other countries. Further, any such efforts also lead to developments which can be used to improve life of common man. There have been many technologies which have been in use in other domains but were left out of space and defence research.

All these efforts need collaboration and interaction between different agencies and academicians. A conference like ICDST-2019 provides such opportunities. We expect all participants to pick up ideas and build further more intellectual capital on them. I hope this will lead to more interaction and innovative developments in time to come.

At the end, I would like to thank all the volunteers and faculty in IET (AKTU) and many others who have made sustained efforts to make this conference feasible at such a short notice. I also hope all the participants will have some intellectual stimulus to take with them and pursue it. Let us hope to get more opportunities where research outcome as a result of these stimuli will be shared.

(Dr. Yatindra Nath Singh)

General Chair, ICDST-2019

Professor, EE

Dean of Infrastructure and Planning

IIT Kanpur-208016

डॉ० दिनेश शर्मा



उप मुख्यमंत्री
उत्तर प्रदेश

99-100, विधान भवन,
लखनऊ

दिनांक: 14-08-2019

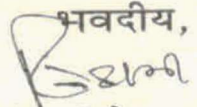


संदेश

मुझे यह जानकर अतीव प्रसन्नता हो रही है कि इन्स्टीट्यूट आफ इंजीनियरिंग एण्ड टेक्नालाजी लखनऊ द्वारा "Defence and Space Technologies" ICDST-2019 विषय पर अन्तराष्ट्रीय सम्मेलन आयोजित किया जा रहा है, जिसमें देश विदेश के प्रतिष्ठित वैज्ञानिक, शिक्षाविद्, शोधकर्ता छात्र एवं विशेषज्ञ भाग लेंगे। स्वाभाविक है कि वे सभी इस अवसर पर अन्तरिक्ष विज्ञान से संबंधित विषयों पर विचार विमर्श करेंगे। इस अवसर पर एक स्मारिका का प्रकाशन भी प्रस्तावित है।

विगत वर्षों कुछ वर्षों से हमारा देश अन्तरिक्ष के क्षेत्र में सफलता के नये आयाम स्थापित किये हैं। हम रक्षा और अंतरिक्ष अनुप्रयोगों के लिए अनेकों परीक्षण कर रहे हैं और सफल हो रहे हैं। हमारा देश अति तीव्रगति से विश्वभर में अन्तरिक्ष के माध्यम से सैन्य शक्ति में अपना बर्चस्व बना चुका है। हमें विश्वास है कि सम्मेलन में आये रक्षा एवं अन्तरिक्ष विशेषज्ञ सारगर्भित चर्चा करेंगे। इस अवसर पर प्रकाशित होने वाली स्मारिका में उपयोगी लेख तथा साहित्य प्रकाशित किये जाएंगे जिससे जनमानस लाभान्वित होगा।

सम्मेलन की सफलता एवं स्मारिका के सफल प्रकाशन के लिए कृपया मेरी शुभकामनायें स्वीकार करें।

भवदीय,

(डॉ० दिनेश शर्मा)

प्रो० एच०के० पालीवाल,
निदेशक,
आई.ई.टी. लखनऊ।

आशुतोष टण्डन "गोपाल जी"

मंत्री

प्राविधिक शिक्षा एवं
चिकित्सा शिक्षा विभाग



कार्यालय : 2238896

सी.एच. : 2213251

कक्ष संख्या 59-59ए, मुख्य भवन
विधान भवन, लखनऊ



दिनांक 19/08/19

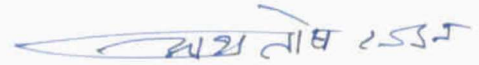
संदेश

मुझे यह जानकर प्रसन्नता हो रही है कि आई0ई0टी0 लखनऊ द्वारा 23 अगस्त, 2019 से 'डिफेन्स एण्ड स्पेस टेक्नोलॉजीज' ICDSI-2019 विषय पर 03 दिवसीय एक अन्तर्राष्ट्रीय कान्फ्रेंस का आयोजन किया जा रहा है। इस अवसर पर एक स्मारिका का प्रकाशन भी किया जायेगा।

वर्तमान समय में हमारा देश रक्षा व अंतरिक्ष अनुसंधान के क्षेत्र में तेजी से प्रगति के पथ पर अग्रसर है। हाल ही में चन्द्रयान-2 का प्रक्षेपण इसका उदाहरण है।

मुझे आशा है कि इस 03 दिवसीय अन्तर्राष्ट्रीय कान्फ्रेंस में रक्षा व अंतरिक्ष विज्ञान से जुड़े विशेषज्ञ गहन विचार विमर्श करेंगे, जिसका लाभ विद्यार्थियों, अध्यापकों व तकनीकी संस्थानों को मिल सकेगा।

कान्फ्रेंस के सफल आयोजन व स्मारिका के प्रकाशन हेतु मेरी हार्दिक शुभकामनाएं।



(आशुतोष टण्डन)

डॉ जी. सतीश रेड्डी
Dr G. Satheesh Reddy

FNAE, HFCSI, FRIN (London), FMACANUD (Russia), FAeSI, FRAeS (UK),
HFPMAI, FSSWR, FIET (UK), FIE, FAPAS, FIETE, AFAIAA (USA)



सत्यमेव जयते

भारत सरकार
Government of India



सचिव, रक्षा अनुसंधान तथा विकास विभाग
एवं
अध्यक्ष, डीआरडीओ

Secretary, Department of Defence R&D
&
Chairman, DRDO



MESSAGE

Space has emerged as the new dimension to be explored and conquered by the budding scientists of the future. It gives me immense pleasure to know that Institute of Engineering and Technology, Lucknow, a constituent institute of Dr APJ Abdul Kalam Technical University, Uttar Pradesh, is organizing the "International Conference on Defence and Space Technologies" (ICDST-2019) from 23-25 August 2019.

I am sanguine that the conference with prominent personalities from DRDO, ISRO and reputed institutes of National Importance, will unwind new horizons, prove to be a milestone and motivate the young engineers to focus on the defence of the country by actively participating in research and development. IET Lucknow has proved that the technical acumen and hidden knowledge in the vast area of this country can be tapped for meaningful scientific valuation, making India a global leader in Defence and Space Technologies.

I wish the conference ICDST-2019 a grand success and sincerely hope that the path breaking step will be the guiding beacon for other institutes to follow.

Jai Hind!

New Delhi
21 August 2019

(Dr G Satheesh Reddy)

रक्षा मंत्रालय, रक्षा अनुसंधान तथा विकास विभाग, डीआरडीओ भवन, राजाजी मार्ग, नई दिल्ली-110011

Ministry of Defence, Department of Defence R&D, DRDO Bhawan, Rajaji Marg, New Delhi-110011

दूरभाष / Phone : 011-23011519, 23014350, फैक्स / Fax : 011-23018216, ई-मेल / E-mail : secvdrdo@brd.drdo.in



प्रो. श्री निवास सिंह
कुलपति
Prof. S. N. Singh
FIEEE, FNAE, FIET, FIE(I), FIETE
Vice-Chancellor

मदन मोहन मालवीय प्रौद्योगिकी विश्वविद्यालय

Madan Mohan Malaviya University of Technology

गोरखपुर-273 010 (उ.प्र.) भारत

Gorakhpur-273 010 (U.P.) India

(Formerly : Madan Mohan Malaviya Engineering College, Gorakhpur)

(Estd. 1962)



Dated : 14th August, 2019

Message

I am delighted to know that the Institute of Engineering and Technology, Lucknow is organizing three days International Conference on “**Defence and Space Technologies**” **ICDST – 2019** during 23-25 August, 2019 and publishing a proceedings/souvenir of the conference. The objective and theme of the International conference is very useful and I hope that this International Conference will provide a platform to the academicians, researchers and participating engineers and faculty members to share their views and expertise with other participants. Being Chairman of IEEE (India), R-10, and Vice-Chancellor of M.M.M. University of Technology, Gorakhpur I hope that the conference will focus on the areas relevant to the society and will come up with some solutions to the problems faced by academicians.

I sincerely believe that the Conference shall provide opportunity to the seasoned researchers and young minds working in this domain to interact, discuss and deliberate to motivate engineering students, research scholars and faculty members to contribute the nation by producing technologies for defence of country and space technologies with their applications for human kind. This conference will increase the involvement of UG, PG, PhD. Students and faculty members of Engineering Institutions in research and project development in the field of defence and space research to make India a global leader in Defence and Space Technologies.

I wish this Conference to be fruitful, meaningful and also a grand success!

(Prof. Sri Niwas Singh)
Chairman, IEEE (India), R-10/
Vice-Chancellor



Prof (Dr) K T V Reddy
B.Tech, M.Tech & P.hD (IIT Bombay)
President

The Institution of Electronics and Telecommunication Engineers (India)

2, Institutional Area, Lodi Road, New Delhi - 110 003

Tel. : 011-43538811(O)

Fax : 011-24649429

Mobile : +91 9820701995

E-mail : president@iete.org

drktvreddy@gmail.com

Website : www.iete.org



MESSAGE

I am glad to know that Institute of Engineering and Technology, Lucknow, UP is organizing an International Conference on Defence and Space Technologies (ICDST-2019) from 23rd -25th Aug 2019.

Space is increasingly being militarized with three quarters of all satellites launched by space agencies to act as the eyes, ears and voice of the modern military commander. Today, almost every phase of military planning and execution depends on space-based systems and every aspect of warfare – from strategic targeting of nuclear missiles to covert operations by special forces – has an essential space link. Realizing that future wars will be controlled by the electromagnetic spectrum, nations are eager to gain an edge in space: the definitive ‘high ground’ where tomorrow’s wars may be won or lost.

India has also added several milestones in its scientific and technological progress in the last four decades, from explorations in space, nuclear and defence technology to inventions that have improved everyday life. Systems such as the anti-satellite (ASAT) weapon that India tested last March can attack low orbiting satellites used for reconnaissance and ocean surveillance. The ASAT test enabled India to join an elite group of nations – the US, Russia and China – with ASAT capability. The US and Russia are far ahead in the ASAT game having launched ‘space mines’ capable of crippling even spacecraft in higher geostationary orbits.

However, in the current scenario there is a need to build international legal regimes to limit the weaponisation of space. There is an urgent requirement to restrain the use of this technology with sensible controls, at least for averting the space-based arms race.

I congratulate the management of IET, Lucknow for organizing the International Conference on such a significant theme and convey my wishes for its splendid success.

Prof (Dr) KTV Reddy

प्रो० विनय कुमार पाठक
कुलपति

Prof. Vinay Kumar Pathak
Vice-Chancellor



डॉ० ए०पी०जे० अब्दुल कलाम प्राविधिक विश्वविद्यालय
उत्तर प्रदेश, लखनऊ

Dr. A.P.J. ABDUL KALAM TECHNICAL UNIVERSITY
Uttar Pradesh, Lucknow

Dated: 14.08.2019

MESSAGE

I am delighted to know that Institute of Engineering and Technology (IET), Lucknow is organizing an International Conference on **"Defence and Space Technologies"** ICDST-2019 on 23-25 August, 2019.

It is a matter of great honour and pleasure for me to write a message to be published in the proceedings/souvenir being brought out by IET.

The theme of the Conference was quite appropriate to the changing scenario of technological advancements happening all around in different fields. It is an established fact that without the availability of new and improved materials one cannot envisage the development of new devices and without new devices one cannot imagine the developments progressing forward. This will create a lot of opportunities for collaborative research and this way, the main purpose of organizing this conference would be served and we are sure of it happening in times to come.

We must felicitate the organizers for publishing the proceedings/souvenir of the conference. This will be a useful reference guide for future. This will serve also as the link for appraisal of the recommended path forward and the action plans drawn at the end of the conference.


(Prof. Vinay Kumar Pathak)
Vice-Chancellor



**INTERNATIONAL CONFERENCE ON
DEFENCE AND SPACE TECHNOLOGIES
ICDST-2019**

(23-25 AUGUST 2019)

Institute of Engineering and Technology, Lucknow-226021

An Autonomous and Constituent Institute of

Dr. APJ Abdul Kalam, Technical University, Uttar Pradesh

Chief Patron

Prof. Vinay Kumar Pathak

Vice Chancellor Dr. APJ Abdul Kalam
Technical University, Uttar Pradesh

Patron

Prof. H.K.PALIWAL

Director, IET Lucknow

General Chair

Prof. Yatindra Nath Singh

EE, IIT, Kanpur

Conference Chair

Prof. V.K.Singh

ECE, IET Lucknow

Prof. S.R.P. Sinha

ECE, IET Lucknow

Coordinators

Prof. SubodhWairya

Head, ECE, IET Lucknow

Prof.O.P.Singh

Coordinator, TEQIP,
IET, Lucknow,

Convener

Dr. RCS Chauhan

Electronics & Communication Engg.
IET Lucknow

Organizing Secretaries

Dr.ArunTiwari

Head, Mechanical Engineering
IET Lucknow,

Dr. Y.N. Singh

Head, Computer Science & Engineering
IET Lucknow,

Dr. Satyendra Kumar Singh

Head, Electrical Engineering
IET Lucknow,

Dr. DhananjaySingh

Head, Chemical Engineering
IET Lucknow,

Dr. Pradeep Bajpayee

Registrar, IET Lucknow,

Mr. Abhishek Nagar

Syatem Manager, IET Lucknow,



It give me immense pleasure to announce that the Institute of Engineering and Technology, Lucknow is going to organize an International Conference on Defence and Space Technologies (ICDST-2019) on 23-25, Aug 2019 with the aim to provide a platform for researchers in academia and industries to share and present their ideas, research experiences and outcomes and future vision in the area. I am confident that the conference presentations and discussions will give opportunities among the academicians, corporate delegates and research scholars to enrich their knowledge and pave the way for more innovative research in the field of defence and space technologies.

On behalf of Institute of Engineering Technology (a constituent Institute of Dr. APJ Abdul Kalam, Technical University, Uttar Pradesh), I take this opportunity to welcome all the distinguished Guest, Speakers, Scholars and Researchers presenting papers and the participants to this esteemed event.

I wish the conference a great success.

(Prof. H.K. Paliwal)

Director, IET Lucknow



**INTERNATIONAL CONFERENCE ON
DEFENCE AND SPACE TECHNOLOGIES**

ICDST-2019

(23-25 AUGUST 2019)

Institute of Engineering and Technology, Lucknow-226021

An Autonomous and Constituent Institute of

Dr. APJ Abdul Kalam, Technical University, Uttar Pradesh

Chief Patron

Prof. Vinay Kumar Pathak

Vice Chancellor Dr. APJ Abdul Kalam
Technical University, Uttar Pradesh

Patron

Prof. H.K.PALIWAL

Director, IET Lucknow

General Chair

Prof. Yatindra Nath Singh

EE, IIT, Kanpur

Conference Chair

Prof. V.K.Singh

ECE, IET Lucknow

Prof. S.R.P. Sinha

ECE, IET Lucknow

Coordinators

Prof. SubodhWairya

Head, ECE, IET Lucknow

Prof.O.P.Singh

Coordinator, TEQIP,
IET, Lucknow,

Convener

Dr. RCS Chauhan

Electronics & Communication Engg.
IET Lucknow

Organizing Secretaries

Dr.ArunTiwari

Head, Mechanical Engineering
IET Lucknow,

Dr. Y.N. Singh

Head, Computer Science & Engineering
IET Lucknow,

Dr. Satyendra Kumar Singh

Head, Electrical Engineering
IET Lucknow,

Dr. DhananjaySingh

Head, Chemical Engineering
IET Lucknow,

Dr. Pradeep Bajpayee

Registrar, IET Lucknow,

Mr. Abhishek Nagar

System Manager, IET Lucknow,



I am delighted to share that the Department of Electronics Engineering at Institute of Engineering and Technology Lucknow is organizing the "**International Conference on Defense and Space Technologies**" during 23rd August, 2019 to 25th August, 2019. The main aim of this conference is to provide a platform to researchers from academia and practitioners from industry to share their innovative ideas and cutting edge research in the fields of defense and space technologies. I am pleased to note that the conference has received immense response from the research community.

I am sure that the scholars participating in this conference would be greatly benefitted from it. I would like to congratulate the organizing committee members of the conference for their relentless efforts to organize this event.

I heartily welcome all the distinguished speakers, authors and the participants to the conference. I wish the conference a great success.

Professor V. K. Singh
Conference Chair, ICDST 2019



**INTERNATIONAL CONFERENCE ON
DEFENCE AND SPACE TECHNOLOGIES**

ICDST-2019

(23-25 AUGUST, 2019)

Institute of Engineering and Technology, Lucknow - 226021
An Autonomous and Constituent Institute of
Dr. APJ Abdul Kalam, Technical University, Uttar Pradesh



Chief Patron

Prof. Vinay Kumar Pathak
Vice Chancellor Dr. APJ Abdul Kalam
Technical University, Uttar Pradesh

Patron

Prof. H.K.PALIWAL
Director, IET Lucknow

General Chair

Prof. Yatindra Nath Singh
EE, IIT, Kanpur

Conference Chair

Prof. V.K.Singh
ECE, IET Lucknow
Prof. S.R.P. Sinha
ECE, IET Lucknow

Coordinators

Prof. Subodh Wairya
Head, ECE, IET Lucknow
Prof. O.P. Singh
Coordinator, TEQIP,
IET, Lucknow,

Convener

Dr. RCS Chauhan
Electronics & Communication Engg.
IET Lucknow

Organizing Secretaries

Dr. Arun Tiwari
Head, Mechanical Engineering
IET Lucknow,
Dr. Y.N. Singh
Head, Computer Science & Engineering
IET Lucknow,
Dr. Satyendra Kumar Singh
Head, Electrical Engineering
IET Lucknow,
Dr. Dhananjay Singh
Head, Chemical Engineering
IET Lucknow,
Dr. Pradeep Bajpayee
Registrar, IET Lucknow,
Mr. Abhishek Nagar
System Manager, IET Lucknow,



Welcome to ICDST 2019!

It is my great pleasure to welcome you to the International Conference on Defence and Space Technologies (ICDST-2019) which takes place in beautiful city Lucknow, Uttar Pradesh on August 23 – August 25, 2019. It has been a real honor and privilege to serve as the Coordinator of the conference. A reasonable motivation through the topical events of the conference may certainly enrich the skills of researchers. Hence it is my ardent wish and even suggestion to grab the opportunities of these sort and participation and certainly will carve a niche to shape a brighter future.

We are grateful to all authors who trusted us with their work; without them there would be no conference. The final result would not have been possible without the dedication and hard work of many colleagues.

We sincerely thank all the speakers and delegates for their participation and various organization. Special thanks are due to the General chair, Conference chairs and to all external referees for the quality and depth of the reviews, and their sense of responsibility and responsiveness under very tight deadlines. We also gratefully acknowledge the efforts that have been put in by our Institute, Organizing Secretaries, members of the various organizing committee, supporting faculty and staff of Electronics and communication Engineering departments, student volunteers and Media.

I Congratulate and appreciate sincerely for all the efforts of Dr. RCS Chauhan (Convener) of the conference and all those who may cooperate in making this occasion a grand success.

Prof. Subodh Wairya
Coordinator, ICDST 2019



**INTERNATIONAL CONFERENCE ON
DEFENCE AND SPACE TECHNOLOGIES**

ICDST-2019

(23-25 AUGUST, 2019)

Institute of Engineering and Technology, Lucknow - 226021

An Autonomous and Constituent Institute of

Dr. APJ Abdul Kalam, Technical University, Uttar Pradesh

Chief Patron

Prof. Vinay Kumar Pathak

Vice Chancellor Dr. APJ Abdul Kalam
Technical University, Uttar Pradesh

Patron

Prof. H.K.PALIWAL

Director, IET Lucknow

General Chair

Prof. Yatindra Nath Singh

EE, IIT, Kanpur

Conference Chair

Prof. V.K.Singh

ECE, IET Lucknow

Prof. S.R.P. Sinha

ECE, IET Lucknow

Coordinators

Prof. SubodhWairya

Head, ECE, IET Lucknow

Prof.O.P.Singh

Coordinator, TEQIP,
IET, Lucknow,

Convener

Dr. RCS Chauhan

Electronics & Communication Engg.
IET Lucknow

Organizing Secretaries

Dr.ArunTiwari

Head, Mechanical Engineering
IET Lucknow,

Dr. Y.N. Singh

Head, Computer Science & Engineering
IET Lucknow,

Dr. Satyendra Kumar Singh

Head, Electrical Engineering
IET Lucknow,

Dr. Dhananjay Singh

Head, Chemical Engineering
IET Lucknow,

Dr. Pradeep Bajpayee

Registrar, IET Lucknow,

Mr. Abhishek Nagar

Syatem Manager, IET Lucknow,



Welcome to ICDST 2019!

It gives me immense pleasure that Department of Electronics and Communication Engineering is organizing ICDST 2019 from 23-25 August, 2019. Being a leading technical institute in north India, IET is expected to have guidance and leadership in latest technological development occurring in our society. I am feeling proud that this conference will serve the same purpose. It will motivate our faculty members along with our students. It is my firm belief that this conference will definitely inculcate some technical curiosity in our students.

I congratulate to the organizing team for their great efforts.

I wish all the success for the ICDST 2019.

Prof. O.P. Singh
Coordinator, ICDST 2019
Coordinator, TEQIP-III



**INTERNATIONAL CONFERENCE ON
DEFENCE AND SPACE TECHNOLOGIES
ICDST-2019**

(23-25 AUGUST 2019)

Institute of Engineering and Technology, Lucknow-226021
An Autonomous and Constituent Institute of
Dr. APJ Abdul Kalam, Technical University, Uttar Pradesh

Chief Patron

Prof. Vinay Kumar Pathak

Vice Chancellor Dr. APJ Abdul Kalam
Technical University, Uttar Pradesh

Patron

Prof. H.K.PALIWAL

Director, IET Lucknow

General Chair

Prof. Yatindra Nath Singh

EE, IIT, Kanpur

Conference Chair

Prof. V.K.Singh

ECE, IET Lucknow

Prof. S.R.P. Sinha

ECE, IET Lucknow

Coordinators

Prof. SubodhWairya

Head, ECE, IET Lucknow

Prof. O.P. Singh

Coordinator, TEQIP,

IET, Lucknow,

Convener

Dr. RCS Chauhan

Electronics & Communication Engg.

IET Lucknow

Organizing Secretaries

Dr. Arun Tiwari

Head, Mechanical Engineering

IET Lucknow,

Dr. Y.N. Singh

Head, Computer Science & Engineering

IET Lucknow,

Dr. Satyendra Kumar Singh

Head, Electrical Engineering

IET Lucknow,

Dr. Dhananjay Singh

Head, Chemical Engineering

IET Lucknow,

Dr. Pradeep Bajpayee

Registrar, IET Lucknow,

Mr. Abhishek Nagar

System Manager, IET Lucknow,



Welcome to ICDST 2019!

ICDST 2019 was fortunate to attract a high interest among the community, and the main conference received 53 submissions from 10 states in India. The submissions span 4 tracks. The high number of submissions provided an excellent opportunity for a high-quality program, but also called for a demanding and laborious paper evaluation process. The 37 members of the Technical Program Committee worked efficiently and responsibly under tight time constraints to produce at least two reviews for each paper that provided the basis for the final paper selection. The reviewing and selection process led to 25 regular papers and 1 invited papers for the main conference, resulting in an acceptance rate of 47%. Given the large number of submitted manuscripts and the tight time and space constraints, many strong submissions could not be accepted. To allow the conference participants to benefit from further worthwhile and stimulating research results, 25 papers were accepted for presentation at main conference. The main program of ICDST 2019 covers three days and includes streams of up to three parallel sessions. The program is further enriched by three keynote presentations offered by renowned researchers in the field, We are grateful to all authors who trusted us with their work; without them there would be no conference. The final result would not have been possible without the dedication and hard work of many colleagues. Special thanks are due to the session chairs, conference chairs, the members of the Technical Program Committees, the General Chair, and to all external referees for the quality and depth of the reviews, and their sense of responsibility and responsiveness under very tight deadlines.

Dr. RCS Chauhan

Convener, ICDST 201

Technical Committee

1. Dr. Upendra Kumar, Assistant Professor, Computer Science and Engineering, IET Lucknow
2. Dr. Anita Yadav, Professor, Computer Science and Engineering, HBTU Kanpur
3. Dr. Rachna Asthana, Professor, Electronics Engineering, HBTU Kanpur
4. Dr. Ashok Kumar Sankhwar, Associate Professor, Electronics Engineering, HBTU Kanpur
5. Dr. Ashutosh Singh, Associate Professor, Electronics Engineering, HBTU Kanpur
6. Dr. Piyush Jaiswal, Assistant Professor, Center for Advanced Studies, AKTU, Lucknow
7. Dr. Arun Kumar Singh, Associate Professor, Electronics and Communication Engineering, REC, Kannauj
8. Dr. T. Srinivas, Professor, Electronics and Communication Engineering, IISc. Bangalore
9. Dr. Yatindra Nath Singh, Professor, Electrical Engineering, IIT Kanpur
10. Dr. K.S. Venkatesh, Professor, Electrical Engineering, IIT Kanpur
11. Dr. Ashish Dutta, Professor, Mechanical Engineering, IIT Kanpur
12. Dr. Kumar Vaibhav Srivastava, Professor Electrical Engineering, IIT Kanpur
13. Dr. Nischal Verma, Electrical Engineering, IIT Kanpur
14. Dr. Ruchir Gupta, Computer Science and Engineering, IIT BHU
15. Dr. Ashish Kumar Singh, Professor, Electrical Engineering, MNNIT Allahabad
16. Dr. Anil Kumar Singh, Professor & Head, Computer Science and Engineering, MNNIT Allahabad
17. Dr. Yogendra Prajapati, Associate Professor, Electronics Engineering, MNNIT Allahabad
18. Dr. Rajat Kumar Singh, Associate Professor & Head, Electronics Engineering, IIIT Allahabad
19. Dr. Karam Veer Arya, Professor, Computer Science and Engineering, ABV IITM, Gwalior, MP
20. Dr. Bhartendu Nath Mishra, Professor and Head, Bio-Technology, IET Lucknow
21. Mr. Ashish Kumar Srivasata, HAL Lucknow
22. Dr. Vinod Kumar Singh, Professor, Electronics and Communication Engineering, IET Lucknow
23. Dr. Sita Ram Prasad Sinha, Professor, Electronics and Communication Engineering, IET Lucknow
24. Dr. Neelam Srivastava, Professor, Electronics and Communication Engineering, IET Lucknow
25. Dr. Subodh Wairya, Professor, Electronics and Communication Engineering, IET Lucknow
26. Dr. RCS Chauhan, Associate Professor, Electronics and Communication Engineering, IET Lucknow
27. Dr. R.K. Singh, Assistant Professor, Electronics and Communication Engineering, IET Lucknow
28. Mr. Amit Kumar, Assistant Professor, Electronics and Communication Engineering, IET Lucknow
29. Dr. Dhananjay Singh, Associate Professor & Head, Chemical Engineering, IET Lucknow
30. Dr. Vijay Shankar Tripathi, Professor, Electronics and Communication Engineering, MNNIT Allahabad
31. Dr. Manoj Kumar Shukla, Professor, Electronics and Communication Engineering, HBTU Kanpur
32. Dr. Kuldeep Sahay, Professor, Electrical Engineering, IET Lucknow
33. Dr. Satyendra Kumar Singh, Associate Professor & Head, Electrical Engineering, IET Lucknow
34. Dr. Dinesh Kumar Srivastava, Professor & Head, Electronics Engineering, BIET Jhansi
35. Dr. Surendra Kumar Sriwas, Assistant Professor, Electronics Engineering, BIET Jhansi
36. Ms. Punam Pradeep Kumar, Scientist G, SAC, ISRO, Ahmadabad
37. Dr. Deepesh Singh, Associate Professor, Civil Engineering, HBTU Kanpur
38. Dr. Sanjiv Kumar Saxena, Assiatant Professor, Electrical Engineering, HBTU Kanpur
39. Dr. Archana Singh, Assiatant Professor, Electrical Engineering, HBTU Kanpur
40. Dr. Parul Yadav, Assiatant Professor, MCA, IET Lucknow
41. Dr. Ashwani Kumar Rathore, Associate Professor, Chemical Engineering, HBTU Kanpur
42. Dr. Rajani Bisht, Associate Professor, Electronics and Communication Engineering, HBTU Kanpur
43. Dr. Neelendra Badal, Professor & Head, Computer Science and Engineering, KNIT Sultanpur
44. Dr. Pawan Tiwari, Assistant Professor, Computer Science and Engineering, IET Lucknow
45. Dr. Arun Kumar Tiwari, Associate Professor & Head, Mechanical Engineering, IET Lucknow
46. Dr. Y.N. Singh, Professor & Head, Computer Science and Engineering, IET Lucknow

Research Paper Submitted to ICDST 2019

Paper Id	Authors	Title	Decision	Remark
01.	Aditya Kumar, Manmohan Singh Yadav and Shafeeq Ahmad	Performance Evaluation of Autonomus Data Density Clustering	REJECT	
02.	Ashi Jain and Shilpi Sharma	Quantum Cryptography	ACCEPT	
03.	Varri Venkateswara Rao	Implementation of Low density Parity Check system using Probabilistic Gradient descent bit flipping Decoder	REJECT	
04.	Vignesh S Ballisitc	Impact Analysis of Kevlar-29 with the reinforcement of Graphene Nanoparticles	REJECT	Incomplete
05.	Ashish Kumar and Prof. Imraan Khan	Modelling Of Solar System With Boost Converter and MPPT	REJECT	
06.	Ashish Kumar and Prof. Imraan Khan	Modeling and Simulation of Grid Connected Solar System With Boost Converter And MPPT	REJECT	
07.	Priyanka Shakya, Ashish Dwivedi and Ram Chandra Singh Chauhan	Designing of an Encrypted Cordic Core Processor For Defence Application Using Aes Algorithm	REJECT	Incomplete
08.	Pritam Sinha, Sangam Bhalke and Vijesh Arora	Ku band monolithic GaAs pHEMT Driver Amplifier	accept?	
09.	Akhilendra Krishna and Vijesh Arora	An L-Band 6-bit Digital Phase Shifter MMIC for Phased Array Applications	accept?	
10.	Shubham Verma, Amit Gupta, Vipin Kumar Tripathi and Vivek Srivastava	Systematic Study of Channel Model in Internet of Underwater Things, Efficient Resource Allocation Scheme and Challenges Arising	REJECT	Incomplete
11.	Vineet Kumar Verma	Performance Analysis of Single Precision Floating Point Multiplier with a Carry Save Adder and with a Carry Look Ahead Adder	REJECT	Incomplete
12.	Alok Kumar Shukla and Ashutosh Nandi	Analyzing the effect of Source/Drain Gaussian Profile on Underlap DG-MOSFET with Air Spacer	ACCEPT	
13.	Najva N and Abdul Saleem	Robotic Arm Movement and Trajectory Control Using Neural Networks	ACCEPT	
14.	Vivek Chamoli and Anamika Bhatia	Implementation of robust target tracking algorithm for Infrared- Image sequence (IR-video)	reject?	
15.	Shashank Yadav, Upendra Kumar and Esha Tripathi	Automated Plant Leaf Recognition using Combined Texture Features and Deep Learning based Classifier	accept?	
16.	Esha Tripathi, Upendra Kumar, Surya Prakash Tripathi and Shashank Yadav	Automated Image Splicing Detection using Texture based Feature Criterion and Fuzzy Support Vector Machine based Classifier	reject?	
17.	Jitender Kumar, Vinod Kumar, Vinay Kumar Singh, Fahim Fahim, Upendra Mittal, Devendra S Barlewar and A T Nimal	GC-SAW and GC-FID Performance comparison for Fast analysis of volatile organic compounds	ACCEPT	
18.	Fahim, Mainuddin, Upendra Mittal, Jitender Kumar, Devendra Barlewar and A. Theodore Nimal	Passive SAW Temperature sensor for Remote application	ACCEPT	

Paper Id	Authors	Title	Decision	Remark
19.	Manoj Bhatt and Sanjay Mathur	A Committee Machine Neural Network for mitigating nonlinear distortion in the High Power amplifier	ACCEPT	
20.		Incomplete submission		
21.	Nivedita Singh and Manoj Shukla	Channel Estimation of DWT based MIMO-OFDM System in Wireless Communication	accept?	
22.	Richa Pathak and Amit Kumar	Design and Analysis of a low power accuracy configurable adder at transistor level	REJECT	Incomplete
23.	Divya Srivastava and Krishna Raj	Comparative Analysis of Redundant signed digit and Hybrid Signed Digit Number Representation	ACCEPT	
24.	Anamika Tiwari and Krishna Raj	Hybridized Concept of Histogram Equalization and Image Fusion for Underwater Image Enhancement	REJECT	Incomplete
25.	Divya Srivastava and Krishna Raj	Cordic implementation and comparative analysis on serial and parallel CORDIC	REJECT	Incomplete
26.	Ram Chandra Chauhan, Yatindra Nath Singh and Rachna Asthana	Design of Minimum Correlated and Maximal Clique Sets of One Dimensional Unipolar Orthogonal Codes	ACCEPT	
27.	Anupam Tiwari	Blockchain Based Space Assets	REJECT	Incomplete
28.	Reetam Negi and Chhagan Charan	Analysis of Covariance based detection technique under Rayleigh fading over cooperative sensing for Cognitive Radio Networks	ACCEPT	
29.	Raveen Katakamu, Bv Subba Rao, Rvs Satyanarayana	Design and Implementation of Antenna Array beam formation for Multi Function Radar by considering thinning effect	ACCEPT	
30.	Pradeep Kumar, Gaurav Kumar, Shivam Rajput, Kishore Jadhav, Daniel Kj and Suwarna	Datar Study and Optimisation of High Current Pulsed Power Components for Pulse Forming Network Powering Electro Magnetic Launcher	ACCEPT	
31.	Smitha Krishnan	Influence of Geometric Design Parameters on Performance of Electromagnetic Bearings for Spacecraft Actuators	REJECT	Incomplete
32.	Smitha Krishnan	Torque Ripple Minimization in BLDC Motors by Back-EMF Shaping	REJECT	Incomplete
33.	Smitha Krishnan	Design of Low Ripple Magnetic Gear for Spacecraft Applications	REJECT	Incomplete
34.	Ruchi Ruchi and Umesh Ghanekar	Improved Digital Image steganography Using Five- Directional PVD	ACCEPT	
35.	Himanshu Bhushan, Dr. Sachin Singh, Amit Kumar	Modeling and Control of Power Flow in Direct-Drive Permanent- Magnet Wind Energy Systems Connected to Grid	REJECT	
36.	Sandeshwari Yadav, Ajay Kumar Yadav and Som Pal Gangwar	Comparative analysis of FFT, DCT and DWT based OFDM system using different modulation technique	REJECT	
37.	Aditya Kumar, Manmohan Singh Yadav and Shafeeq Ahmad	Performance Analysis of Autonomus Data Density Clustering	accept?	
38.	Krishna Kumar, Imran Khan and Anwar Ahmad	Power Quality Control of DFIG Using Smart Neural Learning	REJECT	

Paper Id	Authors	Title	Decision	Remark
39.	Huma Anwar, Imran Khan and Anwar Ahmad	A Review on optimal parameter setting for directional relay in multi machine system	REJECT	
40.	Krishna Kumar, Imran Khan and Anwar Ahmad	Power Quality Control of DFIG Using Smart Neural Learning”	reject?	
41.	Huma Anwar, Imran Khan and Anwar Ahmad	Optimal Parameter Setting for Directional Relay in Multi Machine System	reject?	
42.	Manoj R	Realization and Performance Evaluation of High Frequency Miniaturized 6 Windigenous HMCDC-DC Converter for Space Application	ACCEPT	
43	Raveen Kumar K, Bv Subba Rao and Dr Rvs Satyanarayana	Design and Implementation of Antenna Array beam formation for Multi Function Radar by considering thinning effect	REJECT	
44.	Jamal Arif and Som Pal Gangwar	An Efficient Water marking Process Based on 3 level DWT and FFT Technique	REJECT	
45	Snigdha Singh, Abhinay Choudhary and Manoj Kumar Jain	A Novel Universal Reversible Logic on QCA	accept?	
46.	Lakshman Konathala and Rajasekhar Karumuri	Design and Implementation of 4:3 counter Using bit stacking	REJECT	
47.	Ruchin Agrawal, Dr. Amitabh Kumar Srivastava and Dr. Anjani Kumar Nigam	AHP and GIS-based site suitability analysis for desirable innocuous facilities in an Urban Area	ACCEPT	
48.	Rohit Samkaria and Varnita Verma	Real Time Bridge Structural Health Monitoring using Internet of Things(IoT)	accept?	
49.	Gayatri Tiwari and Ram Chandra Singh Chauhan	A Review on Inter-Satellite links Free Space Optical Communication	ACCEPT	
50.	Parvesh Mamgain and Jasraj Meena	Droid Analyzer: Efficient Framerwork for Android Malware Detection	accept?	
51.	Sapna Tomar and Om Prakesh Singh	Chemical and Physical Analysis;Effect of the Ground Water at the Town of Achhnera, Agra	ACCEPT	
52.	Upendra Kumar Mishra, Vishal Singh Chandel and Om Prakash Singh	Cerium Oxide Based Gas Sensors: A Short Review	REJECT	
53.	Narendra Yadava and Rajeev Kumar Chauhan	Performance Optimization of Nano-scale FDSOI MOS transistors for RFIC Application	ACCEPT	

Accepted =25

Rejected = 28

Total = 53

International Conference on Defence and Space Technologies,
ICDST 2019 on Aug 23-25, 2019
Institute of Engineering and Technology, Lucknow
Program Schedule

23/08/2019 (Friday)

Activity	Time	Venue	Responsibility	Contact No.
Registration	8-10 am	Auditorium Gate	Richa Parihar, Vinay Kumar	09451951176 08699095986
Inauguration	10:0 – 11:30am	Auditorium	Pragati Shukla/ Gaytri Tiwari	07800939548
High Tea	11:30–12:00 noon	Auditorium Hall	Jitendra Shukla	08750502402
Key Note Lecture	12:00–1:00 pm	Auditorium	Abhishek Srivastav	06307506516
Lunch Break	1:00 -2:00 pm	Auditorium Hall	Jitendra Shukla	08750502402
Invited Lecture 1	2:00 – 3:00 pm	Auditorium	Pradeep Verma	09453478332
Invited Lecture 2	3:00 – 4:00 pm	Auditorium	Alok Jain	08756625384
Evening Tea	4:00 – 4:30 pm	Auditorium Hall	Jitendra Shukla	08750502402
Invited Lecture 3	4:30 – 5:00 pm	Auditorium	Pooja Gupta	08896175367
Invited Lecture 4	5:00 – 5:30 pm	Auditorium	Alok Jain	08756625384
Invited Lecture 5	5:30 – 6:30 pm	Auditorium	Usha Sharma	09873939570
Dinner	7:30 – 8:30 pm	Ramanujam Hostel	Jitendra Shukla	08750502402

Inauguration:

Welcome & Lamp Lightening	10:00 am – 10:05 am
Welcome of Chief Guest, Guests of Honour and Others	10:05 am – 10:10 am
Welcome Address by Honourable VC, AKTU	10:10 am – 10:20 am
Address by General Chair, Prof. Y.N.Singh, IIT Kanpur	10:20 am – 10:30 am
Address by Guest of Honour, Prof. S.N.Singh, IIT Kanpur	10:30 am – 10:40 am
Address by Guest of Honour, Prof. KTV Reddy, IETE, New Delhi	10:40 am – 10:50 am
Address by Chief Guest,	10:50 am – 11:25 am
Vote of thanks by Prof. H.K. Paliwal, Director, IET Lko.	11:25 am – 11:30 am
Key Note Lecture: Prof. T. Srinivas, ECE, IISc Bangalore	12:00 pm – 01:00 pm
Invited Lecture 1: Dr. Nilesh M. Desai, Ad. Director SAC, ISRO Ahmadabad	02:00 pm – 03:00 pm
Invited Lecture2: Prof. C.S. Upadhyay, Aerospace Engg, IIT Kanpur	03:00 pm – 04:00 pm
Invited Lecture3: Dr. S.B.Yadaw, Scientist H (retd.) DMSRDE, Kanpur	04:30 pm – 05:00pm
Invited Lecture4: Dr. Santosh Kumar Pandey	05:00 pm – 05:30pm
Invited Lecture5: Prof. K.V.Arya, CSE, IIITM, Gwalior	05:30 pm – 06:30pm

24/08/2019 (Saturday)

Activity	Time	Venue	Responsibility	Contact No.
Registration	08.00 –10:00 am	Auditorium Gate	Richa Parihar, Vinay Kumar	09451951176 08699095986
Invited lecture 6	10:00 –11:00 am	Auditorium	Gaytri Tiwari	07800939548
High Tea	11:00 – 11:30 am	Auditorium Hall	Jitendra Shukla	8750502402
Invited Lecture 7	11:30 – 12:30 pm	Auditorium	Abhishek Srivastav	06307506516
Invited Lecture 8	12:30 – 01:30 pm	Auditorium	Anum Khan	07800318000
Lunch Break	01:30 - 02:30 pm	Auditorium Hall	Jitendra Shukla	08750502402
Paper	02:30 – 04:30 pm	LT 11/Committee	Richa Parihar	09451951176
Presentation I/II		Hall	/Abhishek Srivastava	06307506516
Invited Lecture 9	02:30 – 03:30 pm	Auditorium	Pradeep Verma	09453478332
Invited Lecture 10	03:30 – 04:30 pm	Auditorium	Alok Jain	08756625384
Evening Tea	04:30 – 05:00 pm	Auditorium Hall	Jitendra Shukla	08750502402
Invited lecture 11	05:30 – 06:30 pm	Auditorium	Pooja Gupta	08896175367
Dinner	07:30 – 8:30 pm	Ramanujam Hostel	Jitendra Shukla	08750502402

Invited Lecture 6: Prof. R. Gunasundari, ECE, Ponducherry Engineering College, Puducherry

Invited Lecture 7: Dr. K. Jayathilakan, DFR Lab, DRDO Mysore

Invited Lecture 8: Prof. Ashish Dutta, Mechanical Engineering, IIT, Kanpur

Invited Lecture 9: Prof. K.S. Venkatesh, Electrical Engineering, IIT, Kanpur

Invited Lecture 10: Dr. Jaideep Srivastava, Professor, Computer Science and Engineering, University of Minnesota, Minneapolis, USA

Invited Lecture 11: Prof. K. Raj, Electronics and Communication Engineering, HBTU Kanpur

Paper Presentation I (Defence and Space Technologies), 24 Aug 2019, 2:30 – 4:30pm , Venue: LT11,
Session Chair:

1. Prof. D.K. Srivastava BIET Jhansi,
2. Dr. Virendra Kumar Goswami, Ex Wing Commander (IAF),
3. Dr. Sanjiv Saxena, EE, HBTU Kanpur

Responsibility: Mr. Indra Singh (07503014757), Ms. Snigadha (08004663145)

Paper id	Author	Time	Venue	Responsibility	Contact
8, 13, 17, 18, 30, 42, 47, 50					

Paper Presentation II (Electronics and Information Communication Technology),
24 Aug 2019, 2:30 – 4:30pm , Venue: Committee Hall (below director office),

Session Chair:

1. Prof. Manoj Kumar Shukla HBTU Kanpur,
2. Dr. Ashutosh Kumar Singh, ECE, HBTU Kanpur
3. Dr. Ajay Pratap Singh, CSE, Amity, Lucknow

Responsibility: Mr. Abhinay Choudhary (06395565226), Mr. Rashid Jamal (08840163495)

Paper id	Author	Time	Venue	Responsibility	Contact
2, 21, 26, 34, 37, 48					

25/08/2019 (Sunday)

Activity	Time	Venue	Responsibility	Contact No.
Registration	08:00 – 10:00 am	Auditorium Gate	Richa Parihar, Vinay Kumar	09451951176 08699095986
Invited lecture 12	10:00 – 11:00 am	Auditorium	Gaytri Tiwari	07800939548
High Tea	11:00 – 11:30 am	Auditorium Hall	Jitendra Shukla	08750502402
Invited Lecture 13	11:30 – 12:30 pm	Auditorium	Abhishek Srivastav	06307506516
Invited Lecture 14	12:30 – 01:30 pm	Auditorium	Anum Khan	07800318000
Lunch Break	01:30 – 02:30 pm	Auditorium Hall	Jitendra Shukla	08750502402
Paper	02:30 – 04:30 pm	LT11/ Committee	Richa Parihar	09451951176
Presentation III/IV		Hall	/ Abhishek Srivastava	06307506516
Invited Lecture 15	02:30 – 03:30 pm	Auditorium	Pradeep Verma	09453478332
Invited Lecture 16	03:30 – 04:30 pm	Auditorium	Alok Jain	08756625384
Evening Tea	04:30 – 05:00 pm	Auditorium Hall	Jitendra Shukla	08750502402
Valedictory	05:30 – 06:30 pm	Auditorium	Pooja Gupta	08896175367
Dinner	7:30 – 8:30 pm	Ramanujam Hostel	Jitendra Shukla	08750502402

Invited Lecture 12: Dr. Virendra Kumar Goswami, Ex Wing Commander (IAF)

Invited Lecture 13: Prof. Ashutosh Kumar Singh, NIT Kurukshetra, Hariyana

Invited Lecture 14: Ms. Punam Tyagi, SG, Space Application Center, ISRO, Ahmadabad

Invited Lecture 15: Ms. Leena Kohli Kapoor, SG, Space Application Center, ISRO, Ahmedabad,

Invited Lecture 16: Mr. Asif Siddiqui, Head Ground Station, ISRO Lucknow

Paper Presentation III (Defence and Space Technologies), 25 Aug 2019, 2:30 – 4:30pm , Venue: LT11,
Session Chair:

1. Prof. A.K. Singh, CSE, MNNIT, Allahabad,
2. Dr. Ashish Srivastav, HAL Lucknow
3. Dr. Archana Singh, EE, HBTU Kanpur

Responsibility: Mr. Ashish Dwivedi (09807443304), Ms. Richa Pathak (08090105634)

Paper id	Author	Time	Venue	Responsibility	Contact
9, 19, 28,29,49,51					

Paper Presentation IV (Electronics and Information Communication Technology), 25 Aug 2019,
2:30 – 4:30pm , Venue: Committee Hall (below director office),

Session Chair:

1. Prof. Vinay Kumar Srivastava, ECE, MNNIT Allahabad,
2. Prof. Shirshu Verma, ECE, IIIT Allahabad,
3. Dr. Ashok Kumar Sankhwar, ECE, HBTU Kanpur

Responsibility: Mr. Vivek Mishra (09648173491), Ms. Priyanka Bharti (07388064692)

Paper id	Author	Time	Venue	Responsibility	Contact
12, 15, 23,45, 53					

Abstract of Key Note/Invited Lectures

Photonics for Defence and Space applications.

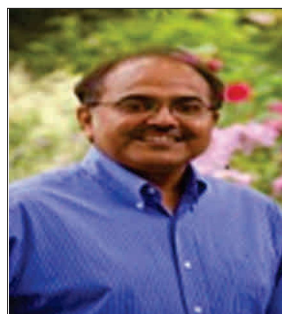


Prof. Srinivas Talabattula
Applied photonics Lab, ECE Department
Indian Institute of Science, Bangalore

Abstract

Photonics is the science and technology involving light wave-particles. Recently photonics is playing an important role all over the world in all applications ranging from communications to sensors. In this lecture we focus on photonics applications to defence and space. After a brief introduction, the following topics will be addressed: photonic integrated circuits, microwave photonics, micro-optoelectro-mechanical systems and quantum communications. Specific examples from our recent work will be included, such as sub-micro-Newton force sensor based on photonic bandgap structures, integrated optic micro-ring resonator based pressure and acceleration sensors, high speed electro-optic modulators, optical delay-line based antenna beam steering networks, and implementation of the emerging quantum photonic systems for secure communications.

Adaptive Machine Learning on Data From Body Wearables, and Its Application for War-fighter Sleep Health



Prof. JAIDEEP SRIVASTAVA
Computer Science and Engineering
University of Minnesota Minneapolis, USA

Abstract:

How can adaptive machine learning technology be applied to disparate domains like body sensors, network sensors/anomaly detection and chemical/biological sensors. This talk first presents a translational science approach to human health through sleep analysis creating novel state-of-the-art deep learning algorithms to empower both clinicians and patients. It then discusses a machine learning based approach to detecting anomalous and suspicious behaviors from cyber-security logs, based on which we can develop system that improves the detection accuracy significantly, as well as shortening the time-to-detection. The talk concludes with how the approach of adaptive machine learning can be used to analyze data in real time from chemical/biological sensors for the senior leadership for effective decision-making.

“Indian Space Programme: Achievements and Future Plans”



Niles M. Desai

Additional Director, Space Application Center, ISRO, Ahmadabad

Research Driven by Demands of the Defence Sector, Some Accidental Experiences



Prof C.S. Upadhyay

Mechanical Engineering, IIT Kanpur

Personnel Protective Systems against Bullets



DR. S.B. YADAV

Scientist H(Retd.) DMSRDE, Kanpur (DRDO)

How to define/solve a problem in your area of interest and write a research paper?



Dr. Santosh K Pandey
Scientist 'D'/Joint Director
Government of India, Ministry of Electronics and IT

Abstract

Any research study has three major pillars- problem definition; innovation/idea to solve the problem & methods to get results; and presentation: paper/patent. Out of these, defining a research problem is the foremost step in any research study. It is essential that problem should be defined with focused objective/s and scope after doing a critical review of existing literature and feasibility study. Proposed solution to the identified problem should have innovation/novelty in the light of existing contributions supported by analytical study, simulation, implementation/try out for performance results and comparison with results of existing methods in order to establish quality of the proposed contribution. Finally, the outcome/s of the research study is presented to the society/related stakeholders in form of a paper/patent. All three pillars are very crucial for conducting a quality research. However, it has been observed that mostly, these are not taken care appropriately, which results in compromising the quality of research/paper. The invited talk attempts to deliberate on these facts in a comprehensive way with special attention to write a good research paper. The talk also touches upon some thrust areas of research in accessibility, e Learning and software security along with key points for writing good R&D project proposal.

Cost and Availability Analysis for Corrective Maintenance in Aircrafts



Prof. K. V. Arya

ABV-Indian Institute of Information Technology & Management, Gwalior

Abstract of Lecture

Maintenance is undertaken to ensure the system continues to deliver the intended performance in a reliable and safe manner. Since it is a supportive or auxiliary process therefore, maintenance has no direct profitable output yet it constitutes an indispensable part of any production or operation process. Maintenance plays an integral role in military aircrafts operations in defense as the critical nature of operations implies that any failure is not tolerable at any point during missions. In aircraft, maintenance or MRO (Maintenance, Repair and Overhaul) is the performance of tasks required to ensure the continuing airworthiness of an aircraft or aircraft part, including overhaul, inspection, replacement, defect rectification and the embodiment of modifications, compliance with airworthiness directives and repair. Due to secrecy of data in military aircrafts, limited understanding of root cause failure characteristics of a highly complex system, inappropriate means of diagnosing the condition of the system and inability to duplicate the field conditions in the laboratory the much research had not been published in military domain. This talk is focused on development of a maintenance pattern in military aircraft items at components level (MRO stage) throughout their life cycle. The will help in deducting the item design and tests at different operational modes and maintenance echelons for better alignment to reduce the number of maintenance events cost as well as better planning of the spare parts during full life cycle of a military aircraft

WEARABLE TECHNOLOGIES



Dr. R. GUNASUNDARI
Professor, Department of ECE,
Pondicherry Engineering College,

Abstract

The global demand for connected devices is growing, with trends such as the Internet of Things (IoT) and home automation setting certain expectations from users. This is driven by developments in communications protocols and sensor technology, which has made it easier to integrate network connectivity and remote-control systems into an increasingly wide variety of devices. As such, these technologies are becoming increasingly common in a wide range of sectors, from military and defence to retail and security. For the military, interconnected and portable devices are most desirable for soldiers on covert operations, but there has been a growing trend of wearable technologies for wider military use. It is predicted that 350 million wearable devices will be in use worldwide by 2018, so it's no surprise that these technologies would also be put to use in military applications. Wearable technologies will enable soldiers to be tracked with greater accuracy, making it easier in high alert operations to monitor the safety of soldiers and reduce the risk of errors. Developments in technology fields like nano-info and biotechnology are directly or indirectly assisting growth in the wearable technologies domain. A wide range of ideas from smart fibres to new materials to augmented/ambient reality is resulting in evolution of a new domain of wearable technologies. military aircraft

Defence and Space Food Technologies



Dr.K.Jayathilakan

DRDO- Defence Food Research Laboratory, Mysore - 570011

Abstract of Lecture

Food technologies are a broad-based field encompassing the traditional technologies like dehydration, salting, sugaring, baking, frying etc. Over the decades, the technological advancements have resulted in several innovative technologies for various applications. Among the dehydration techniques freeze-drying maintains the quality of products which is quite close to that of fresh product. During freeze drying the thermal evaporation of moisture is through elimination at low temperatures under vacuum. Hurdle technology helps to preserve the foods for a period of 2-4 months and is applicable to fruits, vegetables and their products, meat and fish products and sparingly used for cereal products preservation. Hurdle technology is an intelligent combination of hurdles such as pH, temperature, water activity, redox potential, preservative etc. to ensure the microbial safety as well as sensory and nutritional acceptance. Membrane technology is used in the manufacture of clarified juices, for initial concentration through ultra filtration, nano-filtration and reverse osmosis processes. These processes save a lot of energy as well as gives better quality product.

Thermal treatment is the most widely used technology for preservation of foods. Thus retort processing of foods is the most promising technology for both vegetarian and non-vegetarian foods in the ready-to-eat form. Sterilization temperatures in the range of 110 – 125°C are used for low acid foods with the main objective of inactivating the undesirable micro-organisms. High pressure technology is a novel non-thermal processing method of food preservation where the food is subjected to high hydrostatic pressure in the range of 100-600 Mpa at room temperature. Though high pressure processing equipment is very costly, it is a promising technology for stabilization of food against spoilage and helps to improve rheological and functional properties of foods. Aseptic processing is the method of choice for getting sterile quality product where the multilayer laminate packs are used and the sterile product is filled under sterile conditions.

At the advent of consumers demand for nutritious foods, health consciousness, the recent strategy in the field is the development of functional foods with specific health benefits, to counter/replace the medicines or modulate some of the physiological actions. The functional foods are a three-way concept wherein the agricultural or animal origin serves as raw material, specific ingredient components exert functionality and functional component imparts physiological action. The scientific basis of claims for functional foods is a part of the research and the functionalities cover the aspects of reduction in cholesterol and hypertension as well as being anti carcinogenic, antidiabetic, tumor suppressors, from the diseases prevention angle, while, from nutritional supply or value addition point of view, they cover the supply of dietary fibre, vitamins, minerals, functional fibre, essential fatty acids etc., in turn good health to the consumers. Nanotechnology is the emerging technique with a great potential for delivering bioactive compounds. Food design through innovative ingredient technology is the present trend which encompasses the use of statistical approach for development of processed products, by which multidimensional comparison of ingredients as well as responses for optimization of ingredients composition can be achieved. The advancement in food science, requirement of processed convenience foods, and improved buying status of consumers, have led to the development of technologies in the field and strategic applications of these will provide the consumer a better quality food.

Food, a basic need, plays an important role in keeping the Armed Forces personnel in fighting fit condition. The foods satisfying the Indian palate and the dietary habits are generally preferred. The processed food products are ideally suited to withstand the various climatic conditions from the scorching heat of Rajasthan desert to sub-zero temperatures of Himalayas and to hot-humid conditions of Assam. The various factors like the nutritional status of the product, long shelf-life, reducing cooking time, suitable packaging for the required shelf-life, as well as withstanding the transportation hazards, light weight packs vis-a-vis quality of the product pertaining to the sensory attributes fall under the umbrella of Defence quality requirements. Beside to these, depending on the operational tasks to be carried out, the ration scale in terms of the calorie requirements has to be stipulated to achieve the successful performance of the personnel during field operations. Diverse food patterns for land, sea and air operations demand a specific requirement based on logistics. Thus, the Defence requirements of food are specific. Logistics demand that these foods should provide convenience, light in weight, have longer shelf-life and acceptable quality as well as they should be easily available commercially.

A human flight space mission requires a high quality, shelf stable food supply. Developing foods for Indian space mission is a challenging task, where the crew members are to be provided with traditional nutritious, palatable, food in a convenient form. Food is an important component of life support system and plays a key role in space mission. The packaging material used for space foods must also confer to the availability of space in the storage area, protection, ease of identification, ability to withstand high 'g', zero g and high vibration as well as providing ease during reconstitution and dispensing. DFRL has competency in developing packaging systems against aviation stresses and thus it can be extrapolated to development of packaging system for space foods. Space foods are food products especially created and processed for consumption by the astronauts in outer space. For an astronaut food is a most important physiological factor. It is vital for optimum work capacity adaptive powers and health.

The food has specific function of providing balanced nutrition for the health of individuals working in space, while being easy and safe to store, prepare and consume under the low gravity environment of contemporary manual space craft.

There are limitations to weight and volume when travelling and the microgravity conditions experienced in space also affect the food packaging. Currently there is limited storage space and no refrigeration. The essential quality criteria required for the space foods are light weight, low volume, quick preparation time, easy consumability, low fragmentation, high acceptability, wholesomeness, nutrient adequacy, stability, variety, gastrointestinal compatibility and above all the most challenging criteria to be identical to what is consumed back home. Diets were designed to supply each crew member with all the recommended dietary allowances of vitamins and minerals necessary to perform in the environment of space. There were mainly eight categories of space food - Rehydratable, thermo stabilized, intermediate moisture, natural form, irradiated, frozen, fresh and refrigerated foods. Food and how it is eaten and packaged have been greatly affected by the unique microgravity environment of space. The presence of microgravity has had an enormous impact on the development of space food packaging, food selection and related food system requirements.

Design and intelligent control of mobile manipulator systems for space applications



Prof. Ashish Dutta

Dept. of Mechanical Engineering, IIT Kanpur, Kanpur 208016

Abstract of Lecture

A Mobile Manipulator consists of a mobile base with an arm mounted on it, and is used to perform tasks like drilling, welding, pick and place etc. As it has to move safely on very rough terrain the design of the mobile base consists of a rocker-bogie mechanism. A new potential field based path planning algorithm has been developed to find a path from an initial point to a final goal point that ensures stability, minimum energy consumption and time. The standard pseudo inverse methods of redundancy resolution cannot be used in real time and hence a learning based method using a two stage KSOM network has been used to learn the forward kinematics solution and also track the end effector during motion. In the first stage the KSOM performs the redundancy resolution of the system and in the second stage it corrects the error during the actual motion. Once the network is trained for a particular terrain, the corresponding joint angles and wheel velocities for tracking a desired end effector trajectory can be found in real time. Simulation and experimental results for tracking different end effector trajectories on an uneven terrain proves the efficiency of the proposed method.

Natural Daylight Color Visualization for Multispectral Imaging in NIR (700-100nm)



Prof. K. S. Venkatesh
Electrical Engineering, IIT Kanpur

Abstract:

From the time of Alexander, darkness has been a matter of interest to military tactical planning, a great asset or a great problem, depending on which side is asked. For offensive operations, with proper information, darkness is an asset, for the defenders, it is a big problem. In this talk, we present two powerful developments that impact our operations in darkness. The first development is an innovation that provides approximate colour vision in the dark, using illuminating wavelengths outside the visible range, hence unlikely to be detected by the enemy. No existing night vision system provides even approximate colour, and the presence of colour greatly enhances the responses of a person compared to monochrome imagery. The second development uses thermal imaging in the 3-5 micron band, which is already quite prevalent. But due the inherent levels of noise present in thermal imagery, distant objects such as tanks which might have a distinct thermal profile, but occupy a very size in the image can easily go undetected due to the very low signal to noise ratio. We present a solution that applies a 'track before detect' policy to detect virtually undetectable that exhibit consistent motion in the scene and localize them in the video. Both these inventions are the work of former students of the lab who are scientists at IRDE Dehradun

Concepts of Designing and Implementation of Efficient DSP Systems



Prof. Krishna Raj
Electronics and Communication Engineering, HBTU Kanpur

Abstract of Lecture:

The lecture is focused on design, simulation and implementation of efficient DSP algorithms that will be beneficial to the teachers/researchers of this field. This lecture has two parts. A good choice of arithmetic system and internal number representation that affects both efficient implementation of the machine operations and the accuracy of approximated real arithmetic. The first part of the lecture covers design of efficient adder and multiplier using hybrid signed digit number system. The second section covers several high-level architectural transformations that can be used to design families of architectures for a given DSP algorithm. These transformations include pipelining, retiming, unfolding, and systolic array design methodology. In this lecture we will also discuss the concept of designing FIR filter using Hybrid signed digit adders for addition and fast multipliers. We designed different traditional adders and signed digit adders. Comparison of the computational speed and complexity of different traditional adders and HSD adders will also be discussed in this lecture. This HS Dadder is a tradeoff between speed and complexity. This significantly enhances the performance of the filters/systems.

Application OF Remote Sensing To Study the Impact of Atmospheric Phenomena on Defense Operations During War & Peace".



DR. VIRENDRA KUMAR GOSWAMI
Ex Wing Commander (IAF) and Former Vice Chancellor

ABSTRACT

This is an humble appeal to all the Research Scholars and the young minds in particular ,to come out with innovative solutions of the problems faced by the Armed Forces (Air Force ,Army & Navy) during war and peace operations due to adverse Atmospheric phenomena resulting adverse unprecedented weather conditions by making use of remote sensing technologies e.g. High Resolution Satellite imageries, data access, assimilation, HPC & cloud computing for real-time analysis.

The Armed Forces believe in “More you sweat in Peace, less you bleed in War”. Surprise ,3Is (Improvement, Innovation, Invention) & forecasting (Predicting/Planning) are the important principles of war. This appeal is a synthesis of the few glimpses of the practical experience of the Speaker /Author of Atmospheric Phenomena(impact of Adverse weather conditions) on conducted Defense Operations During War & Peace at home & abroad, amalgamated with the few innovative solutions cum forecasting techniques to meet the challenges of adverse Atmospheric Phenomena during the Air Operations by making use of Remote Sensing (Satellites) as these are comparatively less vulnerable , more secure & accurate during War as well as for Mock practices/war exercises during Peace.

Lastly, still unsolved mysteries of adverse atmospheric phenomena affecting the Armed Forces War & Peace Operations with probable solutions have been put in your court of brilliant innovative mind to explore in the defense of your Country, Climate change and humanity in totality

Design and Testing of Testing of Reversible Circuits



Prof. Ashutosh Kumar Singh
NIT Kurukshetra, Hariyana

Abstract of Lecture

Reversible logic circuits are theoretically proven for providing nearly energy-free computation. It has wide applications in the field of quantum computing, optical computing, and nanotechnology. The true functioning of these circuits is another issue where testing plays an important role to meet the destiny of future electronics, since reversible circuits perform bijective functions in which a unique output state is obtained from every input state. Therefore, the operations are fully controllable and observable. This property is utilized by the researchers to incorporate testability in these circuits. Several testing methodologies have been proposed in the literature for the recognition of various types of fault models by means of single-/multiple-bit faults detection, as any fault occurrence results in the change of single/multiple values of bits to the output wires of the circuit. These methodologies are well-categorized in three main classifications, explicitly, designing using proposed gates designing using modification of standard circuits or gates, and designing with inbuilt testability features. It is noticed that the parity preservation and generation principle is preferred in most of the methods due to bijective property of reversible logic circuits. The researchers either proposed novel gates or modified the original circuit in order to produce the necessary information for testing by means of parity bits. The combination of $R1$ and $R2$ online testable gates to form testable logic block TB and the combination of OTG with Feynman gate to form are the major innovations seen in the case of designing using proposed gates methodology. The conversion of a standard gate to form testable reversible cell (TRC) extended Toffoli gate-based conversion and gates cascading approach is found prominent in the case of designing using modification methodology. The process of designing leads to a large increment in operating costs in terms of number of inputs, gate count, quantum cost (QC), and garbage output (GO). In the above context, we present a method of converting an arbitrary circuit into corresponding testable design. In the proposed work, parity preserving gates are first converted into their respective modified testable cells (MTCs), which are used to design an arbitrary circuit. The resulting circuit is cascaded with a derived identity gate to incorporate test and locate functionality which provides full coverage of several types of fault models under single-bit fault detection. Multiple controlled Fredkin (MCF)-gates-based circuits are taken for design and implementation process.

nd humanity in totality

Overview of Space Borne Microwave Sensors & Technology Trends

MS. PUNAM TYAGI

SG, Space Application Center Ahmedabad ,(Unit of ISRO)

Abstract of Lecture:

Remote Sensing is the science of making inferences about material objects from measurements, made at a distance, without coming into physical contact with the objects under study. Remote sensing system consists of a sensor to collect the radiation and a suitable platform - an aircraft, balloon, rocket, satellite - on which a sensor can be mounted. The information received by the sensor is suitably processed & interpreted to survey/ study various natural resources like agriculture, forestry, minerals, water, marine, Ocean, atmosphere etc. In this lecture we present a short retrospective overview of Space Borne Microwave Sensors– current status and future trends. Some representative space borne Radar sensors and their applications focus areas will be discussed. Key Radar technology elements & Indigenous development will be presented.

Satellite Communication in Service of Nation

MS. LEENA KOHLI KAPOOR

SG, Space Application Center Ahmedabad ,(Unit of ISRO)

Abstract of Lecture

SATCOM applications are the most significant dimensions of societal applications of space technology in India. In SATCOM the thrust areas are satellite based tele-education, tele-medicine, satellite based broadband services, VSAT network for Disaster Management, Mobile Satellite Service and Satellite based Navigation. Various applications like Distress Alert Transmitter, Automatic Weather Station, Tsunami Early Warning System, etc have been operational since long and have already proved their utility. In India, the Mobile Satellite Services (MSS) has been of great importance for national disaster management and for strategic & special application needs. Advanced MSS Satellites have allowed the development of miniaturized terminals for popular MSS applications. In near future, development and implementation of Broadband Internet and other VSAT applications based on Multi Spot beam high power, high throughput satellites on Ku/Ka frequency bands will further extend the boundaries of societal applications of space technology.

INDIAN SPACE EXPLORATION MISSIONS: AN OVERVIEW

ASIF SIDDIQUI
ISTRAC/ ISRO, LUCKNOW

Abstract of Lecture

The hallmark of Indian Space Programme is the application-oriented focus and the benefits that have accrued to the country through these programmes. Indian Space programme encompasses research in areas like Astronomy, Astrophysics, Planetary and Earth Sciences, Atmospheric Sciences. Balloons, Sounding Rockets, Space Platforms and Ground based facilities supporting these research efforts. Not only does it help in the enhancement of science & technology levels in country, but also promotes industrial growth, international cooperation & societal benefits, besides inspiring young minds & harvest national pride.

Significant accomplishments in Science and Space Exploration Missions include Chandrayaan-1, Mangalyaan, and Astro Sat& Chandrayaan-2. Aditya-L1 is another future mission which focuses on the study of sun. The long cherished dream to send a human in space received a big push with the announcement of the Gaganyaan Programme last year. With the success milestones achieved in the various space exploration missions, using indigenous technology, the Indian space programme occupies its own pride of place in the global space exploration scenario.

Table of Contents

S.No.	Paper Id	Authors	Title	Page Numbers
1	2	Ashi Jain, Shilpi Sharma	Quantum Cryptography	1-7
2	8	Pritam Kumar Sinha, Sangam Bhalke, Vijesh Arora	Ku-band Monolithic GaAs pHEMT Driver Amplifier	8-11
3	9	Akhilendra Krishna, Seema Tomar, Rakhi Kumari, Sangam Bhalke, Vijesh Arora	An L-Band 6-bit Digital Phase Shifter MMIC for Phased Array Applications	12-17
4	12	Alok Kumar Shukla, Ashutosh Nandi	Analyzing the effect of Source/Drain Gaussian Profile on Underlap DG-MOSFET with Air Spacer	18-25
5	13	Najva N, Abdul Saleem	Model reference controller approach for robot arm tracking using neural networks	26-37
6	15	Shashank Yadav, Upendra Kumar, Esha Tripathi	Automated Plant Leaf Recognition using Combined Texture Features and Deep Learning based Classifiers	38-45
7	17	Jitender Kumar ¹ , Vinod Kumar, Vinay Kumar Singh, U. Mittal, Fahim, Devendra S Barlewar, A. T. Nimal	GC-SAW and GC-FID Performance Comparison for Fast Analysis of Volatile Organic Compounds	46-51
8	18	Fahim, Mainuddin, Upendra Mittal, Devendra Barlewar, Jitender Kumar, A.T.Nimal	Passive SAW Temperature Sensor for Remote Applications	52-56
9	19	Manoj Bhatt, Sanjay Mathur	A Committee Machine Neural Network for mitigating nonlinear distortion in the Nonlinear High Power amplifier	57-62
10	21	Nivedita Singh, M.Shukla	Channel Estimation of DWT based MIMO-OFDM System in Wireless Communication	63-69

11	23	Divya Srivastava, K.Raj	A relative analysis of Hybrid Signed Digit adder to Redundant Signed Digit Adder	70-82
12	26	R. C. S. Chauhan, MIEEE, Y. N. Singh, SMIEEE, R. Asthana, SMIEEE	Design of Minimum Correlated, Maximal Clique Sets of One-Dimensional Uni-polar (Optical) Orthogonal Codes	83-109
13	28	Reetam Negi, Chhagan Charan	Analysis of Covariance based detection technique under Rayleigh fading over cooperative sensing for Cognitive Radio Networks	110-117
14	29	BV Subba Rao, Raveen Kumar K, Dr RVS Satyanarayana	Design and Implementation of Antenna Array beam formation for Multi Function Radar by considering thinning effect	118-130
15	30	Pradeep Kumar V, Gaurav Kumar, Shivam Rajput, Kishore Jadhav, KJ Daniel, Suwarna Datar	Study and Optimisation of High Current Pulsed Power Components for Pulse Forming Network Powering Electro Magnetic Launcher	131-137
16	34	Ruchi, Umesh Ghanekar	Improved Digital Image Steganography Using Five-Directional PVD	138-145
17	37	Aditya Kumar, Manmohan Singh Yadav, Dr. Shafeeq Ahmad	Performance Evaluation of Autonomous Data Density Clustering	146-151
18	42	Manoj R, Sureshkumar A, Rekha A R, Krishnakumar J	Realization and Performance Evaluation of High Frequency Miniaturized 6W Indigenous HMC DC-DC Converter for Space Applications	152-159
19	45	Snigdha Singh, Abhinay Choudhary, Manoj Kumar Jain	A Novel Universal Reversible Logic on QCA	160-168
20	47	Ruchin Agarwal, Amitabh Kumar Srivastava, Anjani Kumar Nigam	AHP and GIS-based site suitability analysis for desirable innocuous facilities in an Urban Area	169-181
21	48	Rohit Samkaria, Varnita Verma	Real-Time Bridge Structural Health Monitoring using Internet of Things (IoT)	182-189

22	49	Gayatri Tiwari, Ram Chandra Singh Chauhan	A Review on Inter-Satellite links Free Space Optical Communication	190-196
23	50	PARVESH MAMGAIN JASRAJ MEENA	Droid Analyzer: Efficient Framerwork for Android Malware Detection	197-206
24	51	Sapna Tomar, O.P.Singh	Chemical and Physical Analysis; Effect of the Ground Water at the Town of Achhnera, Agra	207-211
25	53	Narendra Yadava, R. K. Chauhan	RF Performance Evaluation of Nanoscale FDSOI MOS Transistors	212-228

Quantum Cryptography

Ashi Jain¹, Shilpi Sharma²

¹student, Department of CSE, ASET, Amity University Uttar Pradesh, 201303, India ²professor, Department of CSE, ASET, Amity University Uttar Pradesh, 201303, India

ashij07@gmail.com¹, ssharma22@amity.edu²

Abstract

Quantum Cryptography is an important technology that is beneficial in securing information in long term cryptosystems. Every day, in almost every region of the world the researchers are trying their level best to secure such enormous and sensitive information which are considered at risk of attack at any time. But now researchers have found the way of securing information at a quantum level that is by Quantum Cryptography. Quantum Computers are giving significant advantages to the society today in several areas. Some of the advantages can be: they are able to break much of the current cryptography; they are faster and makes the work more prominent while giving efficient results. While quantum computers have some disadvantages also but its positive impacts outweigh its negative impacts so easily. Security for cyberspace and personal information in the Future Internet should be considered as an important element for the human survival. Here quantum cryptography plays a significant role and becomes the first consideration. Quantum Cryptography relies on the principle of Quantum – Mechanics. This paper discusses briefly what quantum cryptography is and then explains its advantages and disadvantages. After this, analyze the status of Quantum Cryptography in Future Generation. It also explains how, Quantum Cryptography plays its major role in providing security for various applications especially cyberspace security for the future Internet that is securing information so that no one else can read the message and it is kept safe.

Keyword: QuantumCryptography, Heisenberg uncertainty principle, principle of polarization, photon, secret key cryptography, encryption, quantum mechanics.

1. Introduction

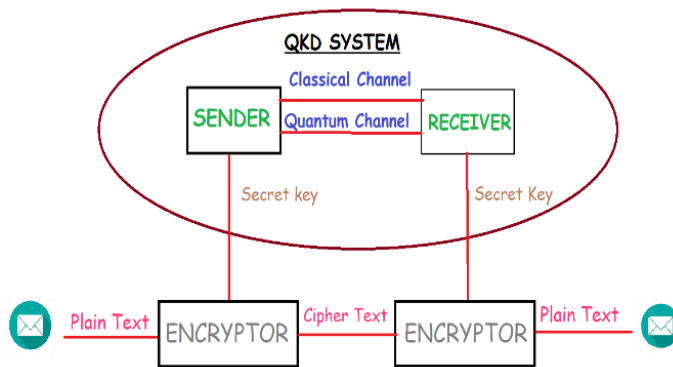
Quantum Cryptography was introduced by the works of Stephen Wiesner and Gilles Brassard. In the early 1970s Wiesner conceived the concept of quantum conjugate coding. Both the researchers came to know about the idea of how to use quantum physics for transmitting significant messages between sender and receiver. The transmission of messages was achieved by using individual photons from a sender to a receiver through an optic fiber. [1] The objective of Quantum Cryptography is to keep the information secure and safe from eavesdropper. The two important pillars for Quantum Cryptography are: Heisenberg Uncertainty Principle and Polarization of a Photon. Now let us understand how Heisenberg Uncertainty Principle is related with Quantum Cryptography i.e. one cannot know absolutely everything about the state of a quantum. With the help of polarization of photon the information can only be known when it is measured i.e. an eavesdropper cannot copy unknown quantum states. [2] In 1984, Bennet and Brassard introduced the first quantum cryptographic communication protocol which was known as BB84, proposing quantum key distribution. QKD is an important approach that is beneficial for generating and distributing random keys based on principle of quantum physics. In QKD, information is sent through polarization of a photon. [3] A common type of encryption is based on secret key cryptography. It says that information can be converted into readable format if and only if proper secret key is entered.[4] Classical Cryptography is the most useful in securing information as it is dependent on public and private keys. It majorly helps in forming many technological solutions to the problems that arise in the computer and also helps in securing information. [5] The key technologies which can be used to ensure security of information are

cryptography and network security. Quantum Cryptography is the most significant branch under Cryptography which relates quantum mechanics with classical cryptography. [6]

1.1. QKD SYSTEM

The first quantum cryptographic communication protocol mainly known as BB84, introducing a new and innovative concept known as quantum key distribution. QKD is an approach that is dependent on the quantum laws of physics and is mainly used for generating and distributing random keys in order to secure information. QKD basically allows two people to generate a random shared secret key which is available to them only that is no one else can see it. This key can be further used and applied to encrypt and decrypt messages in order to provide security to the information. In QKD, information is sent through polarization of a photon. The photons are sent via an optical fiber. The QKD system mainly contains quantum channel and a classical channel. The quantum channel consists of a transparent optical path which is used to pass single photons. The classical channel is closely tied to quantum channel for timing requirements and it is not necessary to be optical.

Figure 1. A pictorial representation of working of QKD System.



QKD SYSTEM BLOCK DIAGRAM

1.2. ADVANTAGES OF QUANTUM CRYPTOGRAPHY

Now let's discuss the advantages of Quantum Cryptography.

- a) Encryption is the process of converting information or data into a code so that it can only be read by certain people. Hence encryption techniques protect the information and personal details like bank accounts, dob etc. from unauthorized access.
- b) It is simply not possible for someone to steal information that belongs to two people. Here quantum cryptography plays the major important role.
- c) Now it is not possible to copy the data if it is in the quantum state. If someone intentionally tries to read that encoded data then quantum state may change its existing state.
- d) Quantum Cryptography is simple to use and also requires less resources to ensure its proper functioning.
- e) The basic function of quantum cryptography is to secure information when passed from one person to another, based on fundamental laws of physics rather than mathematical algorithms and computing technologies.

1.3. DISADVANTAGES OF QUANTUM CRYPTOGRAPHY

Where there are advantages of quantum cryptography, thereby it has disadvantages also.

- a) While information travelling through an optic fiber, it may be possible that polarization of photon may change its state due to some specific changes. Because of that it will be very hard and difficult to discover, track and stop an eavesdropper. Then there are little chances to secure information in serious situations. As a result the information can get into wrong hands.

- b) Another negative impact of quantum cryptography is: COST. The cost is considered in terms of time and money. The cost is in terms of time because of addition of more cryptographic techniques while processing information can cause delay.
- c) Quantum Cryptography cannot protect information from those threats that emerge from poor design of systems.
- d) Selective Access Control is another fundamental need of keeping the information secure which is not provided in quantum cryptography.
- e) Quantum cryptography does not allow to send keys to two or more different locations because quantum principles do not allow this. Therefore, it needs a separate channel between the initial source and final destination which can perform the assigned function.

But it is observed that positive impacts of quantum cryptography have outweighed the negative impacts of it.

1.4. FUTURE STATUS OF QUANTUM CRYPTOGRAPHY

Cyberspace security in the future should be examined as an important element because secure information is important for human survival. MOOC is a new online course which is introduced by Cal Tech and Deft University which thereby helps engineers, scientists and cybersecurity researchers to prepare for quantum computing in future and its associated needs with a course on quantum cryptography. In near future, Quantum Cryptography will focus on the principles of quantum mechanics which can be helpful to create secured lines of communication. It will also take the advantage of quantum effects for example entanglement which can be further used to apply cryptographic tasks that will give security beyond the reach of classical cryptography. Quantum cryptography will offer a great help in the field of finance, energy, healthcare, space etc. It will help us to improve global markets, traffic, climate, cure diseases and so on.

Hence in future, quantum cryptography will be such a powerful technology that it will make the life of human beings better and there will be no cases of threats or frauds regarding cyberspace.

1.5. EMERGING TRENDS IN QUANTUM CRYPTOGRAPHY

Today many hackers still can crack the toughest internet security codes or important information. To solve this major problem, researchers are trying their level best and finding the unique properties that drive quantum computers to create a secure platform where no one can see the secret message without permission.

The new and powerful technique that the researchers have found is that quantum cryptography is capable of generating and allocating the encryption security codes at megabit per second rates. It is five to ten times faster than the existing methods and it can run at several systems at single time.

The researchers ensure that this particular technique is safe from all the cybersecurity attacks.

2. Literature Review

This paper explains the basic meaning of quantum cryptography and how it is related to quantum key distribution. The research paper explains the characteristics of quantum cryptography, weaknesses of modern digital cryptosystems and the application of this technology and its limitations.[7]

Quantum key distribution (QKD) or also called as quantum key exchange (QKE) secures the information that relies on the laws of quantum mechanics. In this paper QKE is being compared with traditional key establishment protocols in order to secure information. [8]

In this paper, quantum cryptography in wireless network has been described briefly, and it initiates a scheme that is integrating quantum cryptography which is helpful for the distribution of the encryption keys and securing information. [9]

In this paper, we study how the protection of QKD is finite and significant described under the law of quantum physics. We are also able to know those summarization steps, that are required and followed in order to ensure

that the particular information is read by the correct person. Also, this paper demonstrates how two-way QKD protocols can be considered in the security analysis.[10]

It is understood that quantum cryptography creates interconnection between mathematics and quantum physics. Thus, the objective of this research paper was to discuss the traditional application of quantum cryptography and quantum key distribution. This paper also figures out some relevant developments in the context of quantum cryptography. [11]

It is familiar that cryptography protects the information and personal details from the sender to the receiver. Now the combination of 3AQKDP which is called as implicit and 3AQKDPMA which is called as explicit quantum cryptography helps to provide more authenticated secure information between two people. This paper discusses the same thing. This research paper also explains the application of cryptography in various fields.[12]

It is familiar that cryptography is an art of science that secure information between sender and receiver with the help of common key. Today in cryptography, security is based on mathematical complexity of the algorithm. This paper explains the radical use of quantum mechanics for cryptography. [13]

Quantum Cryptography is a very popular technology that helps to communicate people in a secure environment. This research paper has its objective to mark the rise of quantum cryptography and explain quantum key distribution and quantum network and analyze its advantages. [14]

Because of development of science and technology, cyberspace security has become a serious issue for the Internet in near future. Hence in this paper, the focus is to analyze characteristics of quantum cryptography and also explain its benefits in the future Internet [15]

3. Methodology

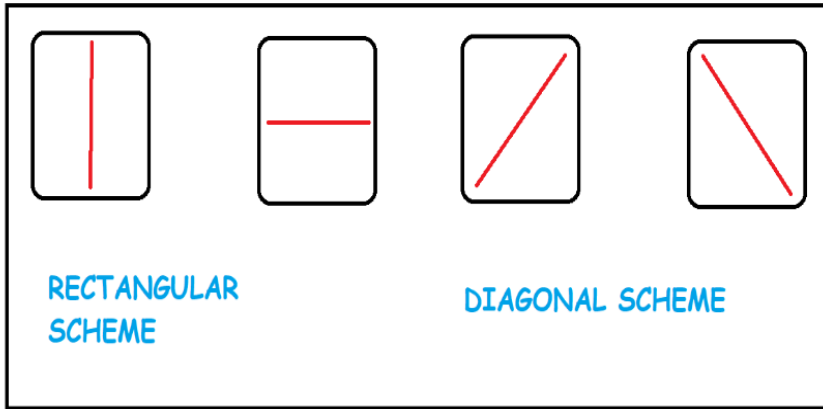
Cryptography simply means to keep a message secret during transmission through untrusted channel. The encoding and decoding of messages are performed by Secret Key. Secret Key Cryptography is where the message is only known to sender and receiver and anyone can see the message but they can't read it without the key. The key is used to keep your conversation safe.

Modern computer will soon be replaced by Quantum Computer. One type of Cryptography is Quantum Cryptography. Quantum Cryptography is the process of securing information by converting it into unreadable format called as cipher text. The information can be converted to readable format if and only if proper key is entered. What makes it powerful is that it is not dependent on maths but it relies on laws of physics.

Suppose Alice wants to send a private message to Bob, for that Alice encrypt the message using a key made up of ones and zeros. Then Alice send the key to Bob by a secure line but remember that no one else sees the key. But a random person says an eavesdropper enters into the secure line and has read all the messages and then their secret will be publicly known. But it would never happen if they use quantum cryptography.

Here the key is a stream of photons or light particles. Photons have a property called spin which can be changed when it passes through a filter: vertical, horizontal and two diagonals. There are two schemes: diagonal scheme and rectilinear scheme.

Figure 2. A diagram representing difference between the two schemes used in quantum cryptography.



Two schemes: Rectangle scheme and Diagonal Scheme.

Now Alice start sending Bob photons switching between filters at random. Now here's where Heisenberg Uncertainty Principle plays an important role. The only way Bob can measure a photon's spin is by passing it through a filter. If Bob measures a photon with rectilinear filter she will guess it correctly and it will be noted out as 1. But if it uses diagonal filter the photo spin will be altered as it passes through and it will be noted out as 0. And hence she will get the information wrong! The laws of physics prevent her from knowing the key. Now for ensuring whether Alice has sent the message to Bob only Alice has to do certain things. Alice has to call Bob and tell him which scheme she has used for what photon. Alice doesn't need to tell whether it was 1 or 0, just tell Bob whether it was rectilinear or diagonal. If she used right filter then Alice's information has been sent to the right person and it is secured.

Figure 3. Represents the photo spins. If it is 1 then the message is sent to correct person and if it is 0 then Message is sent to wrong person.



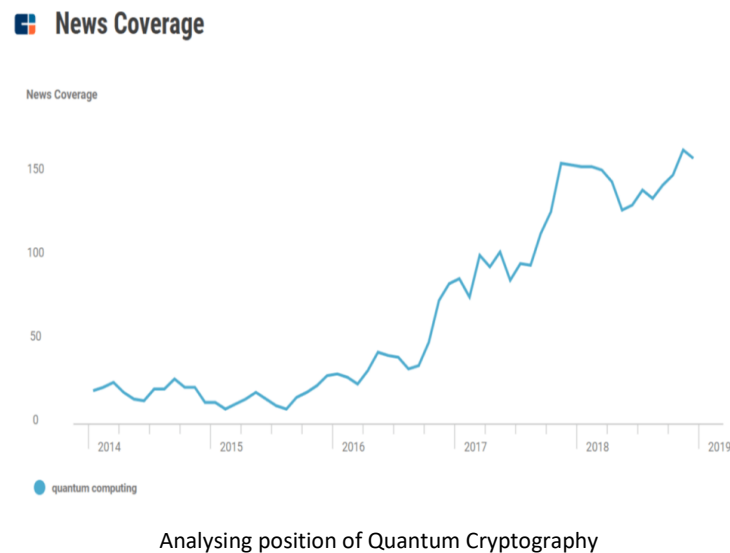
Photo spin in Quantum Cryptography

4. Result

We are now familiar that quantum cryptography is a process of how to keep the information secure by converting it into unreadable format commonly known as cipher text. The information can be converted into unreadable format if and only if proper secret key is inserted.

Quantum computers are rejuvenating characteristics of cybersecurity and network. Some of the biggest technologies like Google, Microsoft, Intel etc. are taking this field quantum cryptography on a high level and has given it a speedy rise. Let's see how.

Figure 4. A graph showing the status of Quantum Cryptography in the recent years.



Quantum computers provide advantage for solving different types of computer problems. These problems need various methods related to technology in order to make the complete analysis of the problem and then find its solution.

Today, the most powerful quantum computers offer a mix of powerful classical systems boosted by impressive quantum capabilities. And it is expected that by 2030, we could see quantum computers outpace classical counterparts.

5. Conclusion

In this research paper, several advantages and disadvantages of quantum cryptography were discussed in order to make the people aware of its impacts in network security now and in the future.

Despite of numerous advantages in the field of quantum cryptography, there still are a lot of challenges that it had to face in near future. But hopefully the positive impacts of quantum cryptography will outweigh its negative impacts soon.

Quantum cryptography is one of the most popular topics in the computer industry. In order to withstand quantum computers, new cryptosystems should be explored more and taken into consideration especially those which are not based on discrete logarithm problems. In this way quantum cryptography will give more positive results.

As discussed, quantum cryptography depends upon two important pillars, one is Heisenberg Uncertainty Principle and the other is Principle of Photon Polarization. Without these two principles, quantum cryptography stands nowhere. Both the principle is supporting the functioning of quantum cryptography in one way or the other. Hence the characteristics of quantum cryptography can solve the problem of cyber security for the future internet. Also, it provides various security applications which is useful for securing information.

6. Future Work

It is true that quantum cryptography is the most popular topic in the field of science and technology. Quantum cryptography can change our life completely. Immediate applications of quantum cryptography can consist of

more energy efficient materials, weather forecasting and other applications of artificial intelligence. The future work of Quantum Cryptography should be of identifying the core element which supports the functioning of quantum cryptography by the same time enhancing the quality of that element to get more of its advantages. We can also find the solution to the problems that are faced by Quantum Cryptography.

Then we can understand how quantum cryptography can be improved in order to satisfy the needs of the people in future. In near future we can also justify how quantum cryptography plays a significant role in Internet of Things and Cyberspace.

With further new approach and modification in theory and practical, quantum cryptography could be the first application of quantum mechanics at the single quantum level.

7. References

- [1] Singh, A., & Sharma, N. Quantum Key Distribution: A Secure Key Exchange Method in Quantum Cryptography.
- [2] Lal, A. K., Rani, A., & Sharma, S. (2008). The New Approach of Quantum Cryptography in Network Security. *International Journal Of Emerging Technology and Advance Engineering*, ISSN, 2250-2459.
- [3] Padamvathi, V., Vardhan, B. V., & Krishna, A. V. N. (2016, February). Quantum Cryptography and Quantum Key Distribution Protocols: A Survey. In 2016 IEEE 6th International Conference on Advanced Computing (IACC) (pp. 556-562). IEEE.
- [4] Rao, A., Rathan, M., Srinivas, Y., Vijayasekhar, J., Krishna, N., Jaliparthi, R., ... & Rani, S. (2012). A Note on Quantum Cryptography '. *International Journal on Computer Science & Engineering*, 4(9), 1540-1544.
- [5] Jeyaseelan, M. A. S., & Priya, M. S. M. Practical quantum cryptography for secure free-space communications.
- [6] Zhou, T., Shen, J., Li, X., Wang, C., & Shen, J. (2018). Quantum cryptography for the future internet and the security analysis. *Security and Communication Networks*, 2018.
- [7] Nguyen, T. M. T., Sfaxi, M. A., & Ghernaoui-Hélie, S. (2006). 802.11 i encryption key distribution using quantum cryptography. *JNW*, 1(5), 9-20.
- [8] Sharbaf, M. S. (2009, April). Quantum cryptography: a new generation of information technology security system. In 2009 Sixth International Conference on Information Technology: New Generations (pp. 1644-1648). IEEE.
- [9] Abushgra, A., & Elleithy, K. M. (2015, April). Security of quantum key distribution. *ASEE*.
- [10] Aleksic, S., Winkler, D., Franzl, G., Poppe, A., Schrenk, B., & Hipp, F. (2013, July). Quantum key distribution over optical access networks. In *Proceedings of the 2013 18th European Conference on Network and Optical Communications & 2013 8th Conference on Optical Cabling and Infrastructure (NOC-OC&I)* (pp. 11-18). IEEE.
- [11] Lopes, M., & Sarwade, N. (2014). Cryptography from quantum mechanical viewpoint. *arXiv preprint arXiv:1407.2357*.
- [12] Scarani, V., & Renner, R. (2008, January). Security bounds for quantum cryptography with finite resources. In *Workshop on Quantum Computation, Communication, and Cryptography* (pp. 83-95). Springer, Berlin, Heidelberg.
- [13] Marhoefer, M., Wimberger, I., & Poppe, A. (2007). Applicability of quantum cryptography for securing mobile communication networks. *Long-Term and Dynamical Aspects of Information Security: Emerging Trends in Information and Communication Security*, 97-111.
- [15] De Wolf, R. (2017). The potential impact of quantum computers on society. *Ethics and Information Technology*, 19(4), 271-276.
- [16] Paterson, K. G., Piper, F., & Schack, R. (2007). Quantum cryptography: A practical information security perspective. *Nato Security Through Science Series D-Information and Communication Security*, 11, 175.
- [17] Navez, P., & Van Assche, G. (2002). A method for secure transmission: Quantum Cryptography. Center for quantum information and communication, Ecole Polytechnique, Université Libre de Bruxelles.
- [18] Sharma, R. D. (2011). Quantum cryptography: a new approach to information security. *International Journal of Power System Operation and Energy Management (IJPSOEM)*, 1(1), 11-13.
- [19] Fehr, S. (2010). Quantum cryptography. *Foundations of Physics*, 40(5), 494-531.
- [20] Marhoefer, M., Wimberger, I., & Poppe, A. (2007). Applicability of quantum cryptography for securing mobile communication networks. *Long-Term and Dynamical Aspects of Information Security: Emerging Trends in Information and Communication Security*, 97-111.

Ku-band Monolithic GaAs pHEMT Driver Amplifier

Pritam Kumar Sinha^{*1}, Sangam Bhalke², Vijesh Arora¹

¹ Scientist, Solid State Physics Laboratory Delhi, Timarpur Lucknow Road, Delhi-110054, India,

² DGM, GAETEC, Hyderabad-500069, India

pritam.et@gmail.com¹, vijesharora@gmail.com¹

Abstract

Objectives: This paper presents the design and measurement of a Ku-band (16GHz - 18GHz) MMIC driver amplifier. This MMIC amplifier was fabricated with a 100 μ m thick substrate using 0.13 μ m InGaAs/AlGaAs/GaAs pHEMT technology. This two stage MMIC driver amplifier demonstrated a measured linear gain of 16dB with gain flatness of less than ± 0.5 dB, Noise figure less than 5dB and the measured output power at 1dB gain compression is better than 25dBm. This amplifier therefore provides reasonable output power and noise figure.

Keywords: Ku-band, driver amplifier, satcom, GaAs MMIC, SSPA

1. Introduction

Today's wireless application gives the requirements of high linearity, low noise and high bandwidth. High performance and high linearity MMIC driver amplifiers for Ku-band applications have been increasingly receiving demands in both commercial wireless communications, such as point-to-point digital radio and satellite applications for its reduction in cost, size & system complexity. Recently, GaAs monolithic-microwave integrated-circuit (MMIC) technology has been expected with more reasons to extend its area to the commercial communications. Because many products need the operation range located in the sub-gigahertz to a few gigahertz, the GaAs MMIC is then continuously growing. It is especially suitable for the high linearity and low noise applications.

When the PA operates at its nonlinear region, it will cause serious signal distortion. Therefore, it is desirable for power amplifier to linearly amplify RF signal efficiently. However higher efficiency can only be possible when the power amplifier operates at its maximum output power which is normally a non-linear region. In communication systems, class-A amplifiers are generally known for better linearity, however it will suffer from lower efficiency so class-AB mode is preferred to have moderate efficiency. Noise figure is another important parameter for a driver amplifier other than linearity. But all the parameters could not be achieved simultaneously. So there exists a trade-off between these parameters.

In this work we report a 16GHz to 18GHz GaAs pHEMT driver amplifier MMIC which is the building block of solid state power amplifiers (SSPA) for applications such as satellite communications systems. The 0.13 μ m PHEMT device used in common-source amplifier which has the advantage of lower noise figure as well as higher gain. RLC Feedback technique has been incorporated to get better gain flatness. The specialty about this circuit is that this MMIC demonstrates minimum noise figure as well as sufficient output power with flatter gain response simultaneously.

2. Circuit design

The basic working of the driver amplifier is to drive the succeeding power amplifier with minimum distortion at the input of PA. Driver amplifiers are generally operated in linear class-A mode to enable high linearity and high gain, thereby keeping spurious signals generated by the PA low, by reducing inter-modulation products. In the present design, driver amplifier MMIC consists of 2-stages with the power drive ratio of 1:2 to achieve required gain and output power. The peripheries of the PHEMTs are 0.6mm, 1.2mm for the first and power stage respectively. The driver requires a bias voltage of 4.0V & draws total quiescent current of 420mA (approx). The simplified block

diagram is shown in fig (1) below, where M1 & M3 is the input & output matching network respectively. M2 is the inter-stage matching network. The total chip dimension is 2.5mm x 3.3mm.

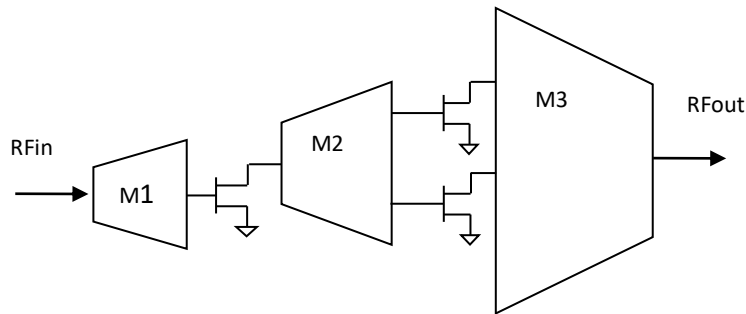


Fig. 1. Block diagram of the driver amplifier

The process selected for the Ku-band driver amplifier is 0.13um GaAs PHEMT foundry process. The device has maximum f_T of 108 GHz. The MMIC process used for this design has two level of interconnect metals with air-bridge, metal-insulator-metal capacitor and thin film resistors. Since the f_T is higher, stability of the amplifier over the entire frequency range is a major concern. Stability analysis was done on both stages to make sure there was sufficient margin over process variation. The process is designed to operate with a peak voltage upto 4.5V. Normally power amplifiers are preceded by driver amplifier since PA operates at saturation for maximizing output power & efficiency. Driver amplifier enhances the overall gain requirement and the gain flatness as well. Thus a driver amplifier should have good linearity so that minimum nonlinearity comes at the input of the PA. In this design RLC feedback topology have been incorporated at the first stage for attaining reverse gain slope & therefore ensure gain flatness. The fabricated chip microphotograph is shown in fig (2).

To design the driver amplifier the output matching network, which transforms the maximum output power to the 50Ω system is designed first. The required large signal load impedance $Z_{opt,Q2}$ is composed of $R_{opt,Q2}$ and $C_{ds,Q2}$. In this design the optimum large signal load impedance was $15.8+j*6.3\Omega$. Due to the fact that GaAs PHEMT is potentially unstable, a resistor (in parallel with a capacitor) is added in series with each device. The value of this stabilizing resistor must be small enough that it would not dissipate much power and reduce the overall gain and efficiency.

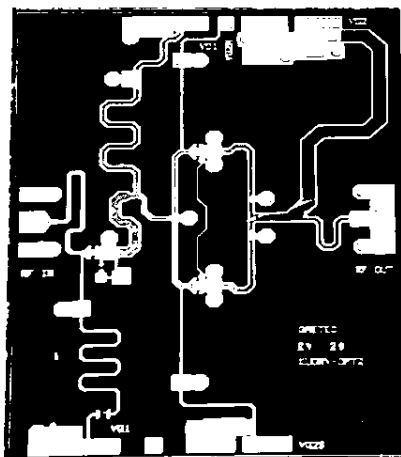


Fig. 2. Fabricated chip photograph of driver amplifier (2.5mm x 3.3mm)

On the other hand, too small value series resistor before device can't guarantee the stability of the device. After the output matching network is added, the inter-stage matching network is then designed to match the output of the driver stage to the input of the power stage in order to reduce the mismatch loss. At the same time we also consider power matching for the R_{opt} & C_{ds} of the first stage device. The inter-stage matching consists of blocking capacitor & tree structure of the power stage. RLC Feedback topology has been incorporated at the first stage & then both the 1st stage and inter-stage is optimized to get better output power flatness. All the microstrip lines, capacitors, inductors, etc used in the circuit are finally EM simulated to validate the passive models used to design the circuit.

3. Measured Performance

The MMIC has been designed in such a way that all the drain biases are situated at North side and the gate biases are at the South side of the MMIC as per the requirement. The amplifier was tested under CW mode of operation. Gain flatness is one of the critical parameter of this circuit; small signal gain of 16dB with flatness of better than ± 0.5 dB is achieved over the band as shown in fig (3). Fig (3) also shows gain plot of the circuit at small signal level as well as at 1dB compression point. Next important parameter is the driver amplifier linearity as discussed in this paper; fig (4) shows the measured output power versus input power performance of the circuit where it is observed that the saturated power of this driver amplifier at three different frequency point viz. 16GHz, 17GHz and 18GHz is 27dBm.

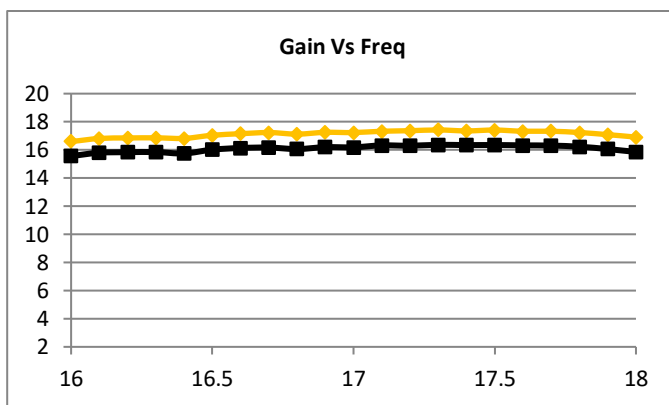


Fig. 3. Measured Gain at 1dB compression of the driver amplifier

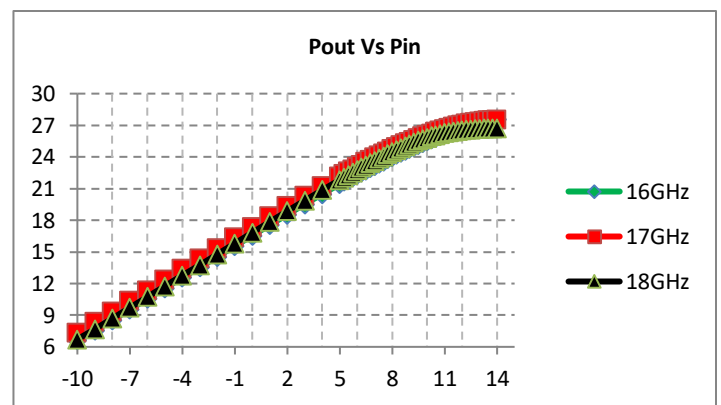


Fig.4. Measured P1dB of the driver amplifier

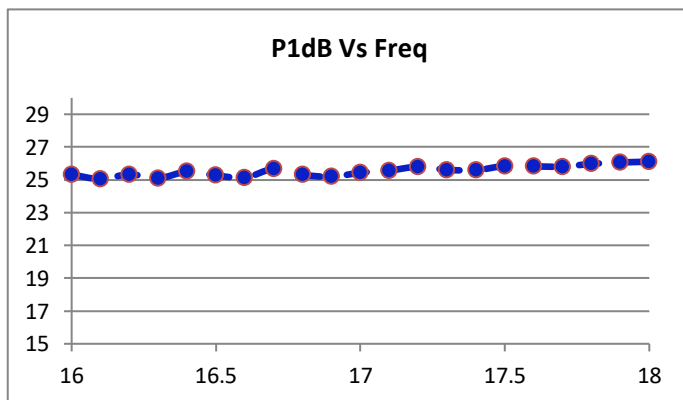


Fig.5. Measured Output power at 1dB compression over the band of the DA

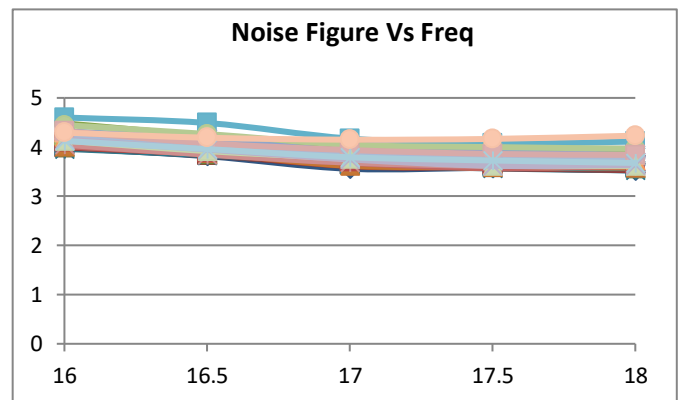


Fig.6. Measured Overall Noise figure of the driver amplifier

The P1dB variation over the frequency band is shown in fig (5) where it is well beyond 25dBm. The measured PAE performance varies from 22.4% to 24% from 16GHz to 17.5GHz frequency band. Normally driver amplifiers are operated at linear region which is well below the 1dB compression point, in this case the maximum output power required from this driver is 21dBm for the system which is in the linear region as depicted in fig (4). Finally the measured noise figure performance of the driver amplifier is shown in fig (6). On-wafer noise figure were measured at various locations yield noise figure < 5dB which is very appropriate for SSPA application.

3. Tables

Table 1: PERFORMANCE COMPARISON OF VARIOUS GaAs BASED MMIC AMPLIFIER.

Parameters	Ref [4]	Ref [5]	Ref [6]	Ref [7]	Ref [8]	This Work
Frequency (GHz)	13-15	12-13	14-17	12-17	-	16-18
P1dB (dBm)	30.2@14GHz	>29	>30	27	>22@15GHz	>25
Noise figure(dB)	-	-	-	-	-	<5
Gain (dB)	13.1-15.2	>20	29-32	18-20	>22	>16
Gain flatness (dB)	1.9	-	3	2	-	1
No. of stages	2	2	4	2	2	2
PAE(%)	22.5	49-52	27.5	-	37(max)	22.4-24
Technology	0.35µm GaAs pHEMT	0.25µm GaAs pHEMT	0.35µm GaAs pHEMT	0.15µm GaAs power pHEMT	0.15µm GaAs pHEMT	0.13µm GaAs pHEMT

3. Conclusion

We proposed two-stage, low-power Ku band amplifier for Ku band Satcom applications. Both good linearity and low noise figure have been achieved. However higher output power utilizes bigger device size, which ultimately reduce the circuit noise figure so there exists a trade-off between these two. In this circuit the devices & the topology have been chosen in such a way so that optimum P1dB, Lower Noise figure and flatter gain response is ensured.

Table1 shows comparison of various MMIC amplifiers of almost similar band where we found that the present work provides better response in terms of gain flatness & noise figure. This work has demonstrated decent noise figure with reasonable P1dB among other references. Moreover due to class-A mode of operation, PAE ranges moderately between 22.4% to 24%, which thus ensure better linearity as compared to other classes of operation.

References

- [1] Nuri Saydam, Korkut Yegin, "Ku Band Amplifier Design for Satcom Systems," 24th Telecommunications forum TELFOR 2016, IEEE
- [2] H.Z.Liu, C.C.Wang and Y.H. Wang, "A Four-Stage Ku-Band 1 Watt PHEMT MMIC Power", 2002 IEEE GaAs digest.
- [3] S. C. Cripps, RF Power Amplifiers for Wireless Communications, 2nd ed. Norwood, MA: Artech House, 2006.
- [4] H.Z. Liu, C.H. Lin, C.K.Chu, M.P. Hong, Y.H. Wang, C.H. Chang, C.L. Wu and C.S. chang, " A Self-bias Ku-band 1 Watt PHEMT Power amplifier MMIC with A compact source capacitor".2005 IEEE proc
- [5] Maulik L. Bhavsar, Puja Srivastava, Apurba Bhattacharya, SAC, Ahmedabad, "A Ku- band 1 Watt 2-stage Power amplifier MMIC for Space with 52% Power Added Efficiency".2016 APMC
- [6] C.W. Huang, S.J Chang, W.Wu, C.L. Wu, C.S. Chang, "A Ku-Band Four stage PHEMT 1W MMIC Power amplifier",2006 Microelectronics journal 37 Elsevier.
- [7] A. Bessemoulin, Y.H. Suh, D.Richardson, S.J. Mahon, J.T. Harvey, "A compact 500mW Ku-band Power Amplifier MMIC in 3 x 3mm² quad flat packages", 2006 European microwave integrated circuits conference.
- [8] Rasidah S., Amiza Rasm, Siti Maisurah M.H., A.I.A Rahim, M.R.Yahya, "15GHz Medium Power Amplifier Design for Ku-band Applications", RSM2011 Proc, Kota Kinabalu, Malaysia.

An L-Band 6-bit Digital Phase Shifter MMIC for Phased Array Applications

Akhilendra Krishna*¹, Seema Tomar¹, Rakhi Kumari¹, Sangam Bhalke², Vijesh Arora¹

¹ Scientist, Solid State Physics Laboratory, Lucknow road Timarpur, Delhi- 110054, India,

²DGM, GAETEC, Vignayankancha Post, Hyderabad-500069, India

akhilendra@sspl.drdo.in¹, vijesh.arora@sspl.drdo.in

Corresponding author*: Phone: +91-11-2390-3612

Abstract

This paper presents the design and performance an L-band 6-bit digital phase shifter. Simple filter topologies were utilized for minimizing the switching device count. Each bit of the switched filter phase shifter was optimized for achieving phase shifting accuracy; the MMIC covers the 1.0 - 1.5 GHz band with rms phase error less than 6.3° and peak phase error less than 10.5°. The Insertion loss is 6.0±0.8 dB, and rms amplitude error is within 0.58 dB.

Keywords: MMIC Phase Shifter, Reconfigurable filters, L-Band and GaAs FET.

1. Introduction

Phase shifters are extensively used for electronic beam scanning in radar and satellite applications. This is because they are compact and consume negligible power. Topologies based on switched filters have good phase response, relatively smaller size and provide wider bandwidth.

In this work we present an optimum switched filter six bit digital phase shifter design using only fifteen GaAs switching devices and eight control lines. The proposed implementation was optimized for insertion loss variations along with good phase accuracy. The novelty of this design is that the lower four bits 5.625°, 11.25°, 22.5° and 45° require a single control signal for each of phase bit, i.e. complimentary control logic requirement is circumvented. 45° bit has been designed using single control line for the first time as per author's knowledge. Thus the phase shifter needs only 15 FETS with 8 control lines for attaining 0-360° phase control, and is therefore appropriate for integration in multi-function core chip. The phase shifter was fabricated using the space qualified G7S GaAs process and exhibits an rms phase error <6.3°, maximum phase error < 10.5° and an insertion loss of 6.0 ±0.8 dB with rms insertion loss variation <0.58 dB . Lower device count, simplified switching control and low rms amplitude and phase errors are realized.

2. Circuit Design

The 5.625° phase shift is obtained by switching a single GaAs FET across a capacitor. Schematic of 5.625° bit is shown in Figure 1. The design equation [3] for the capacitor C1 in terms of phase shift ϕ , centre frequency ω_0 and impedance Z_0 is:

$$C_1 = \frac{1}{2 Z_0 \omega_0 \tan \phi} \quad (1)$$

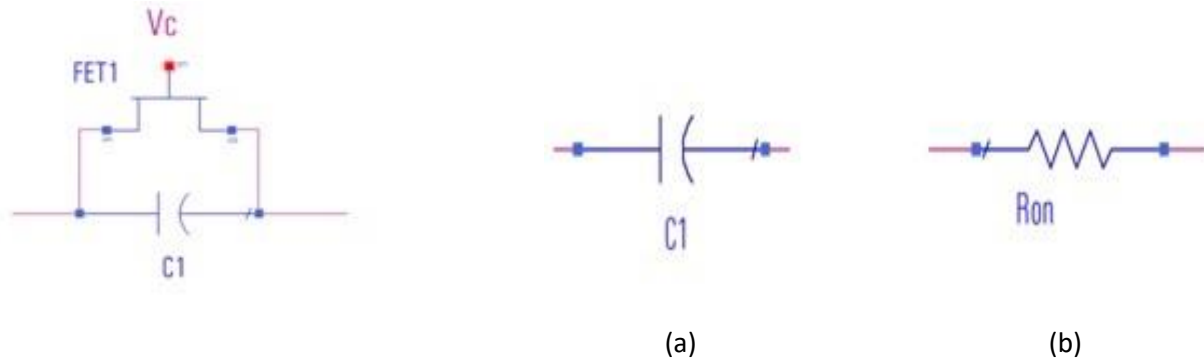


Fig. 1. Topology of 5.6250 bit: (a) Reference state and (b) Phase shifting state

The circuit in Fig. 2, comprising of a reconfigurable filter, is employed for 11.25°, 22.5° and 45° degree bits [3]. This topology uses only two switching devices and a single control line for providing the requisite phase shift. In the reference state both FETs are OFF and the phase shift is provided when both FETs are turned ON, the simplified topologies is shown in Fig.3 (a) & (b) . The design equations [2], [6], [12] for L, C1 and C2 in terms of phase shift ϕ , centre frequency ω_0 and impedance Z_0 are:

$$L = \frac{Z_0 \tan \frac{\phi}{2}}{\omega_0} \quad (2)$$

$$C_1 = \frac{1}{2 \omega_0^2 L} = \frac{\cot \frac{\phi}{2}}{2 \omega_0 Z_0} \quad (3)$$

$$C_2 = \frac{\sin |\phi|}{\omega_0 Z_0} \quad (4)$$

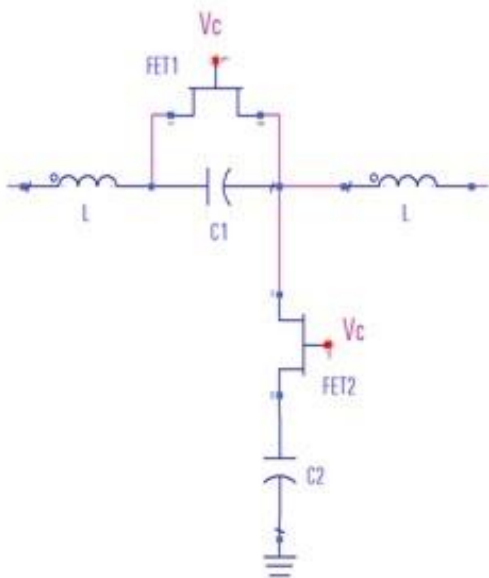


Fig. 2. Topology of 11.25°, 22.5° and 45° bits

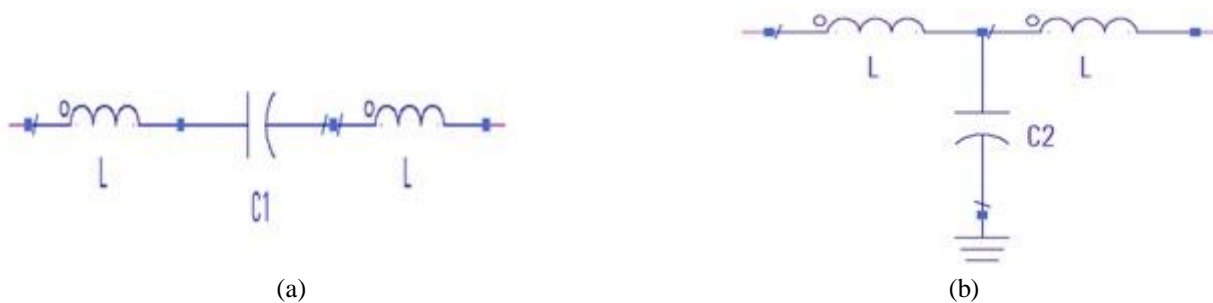


Fig. 3. Equivalent circuits (a) Reference state (b) Phase shifting state

The higher phase shift bits i.e. (90° and 180°) have been designed using switched High pass-Low pass sections and SPDT switches. A pair of low insertion loss SPDT switches is used to switch between a low pass/high pass filter. The FET size was optimized to achieve low insertion loss and reasonable isolation using only two devices per switch. Circuit diagrams of 90° and 180° bit are shown in Figure 4 and 5. The 90° bit is a third order filter sections while 180° bit uses fifth order filter sections.

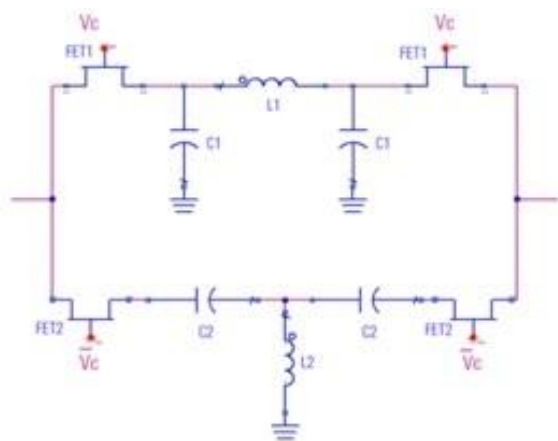


Fig. 4. Circuit diagram of the 90° bit

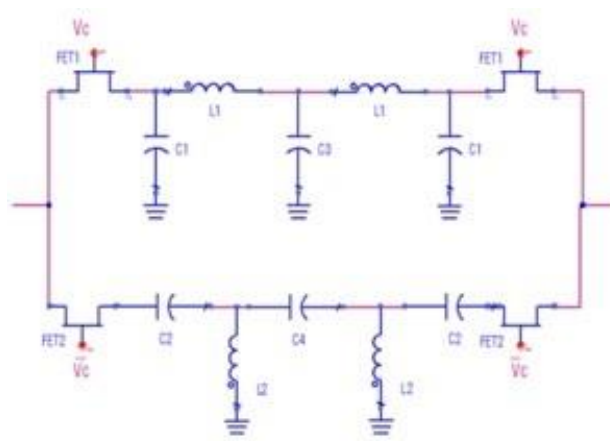


Fig. 5. Circuit diagram of the 180° bit

Devices used in the individual bits are shown in table 1. After finalizing the bit design, they were ordered appropriately to minimize loading. The bit sequencing is depicted in figure 6.

Table1: DEVICES FOR EACH BIT

SIZE (μm)	5.625°	11.25°	22.5°	45°	90°	180°
FET 1	900	900	900	900	1200	1200
FET 2	-	600	600	600	1200	1200

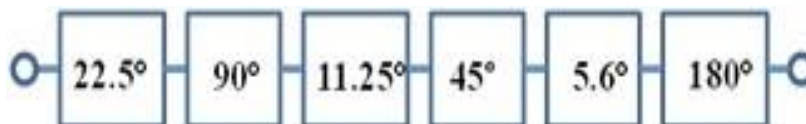


Fig. 6. Bit sequencing

3. Measurement Results

The integrated six bit MMIC is measured and the results of six major phase shifting bits are shown in Fig.7. The phase shifter Insertion loss is less than 6.8 dB in all four. Insertion Loss is shown in Fig.8.

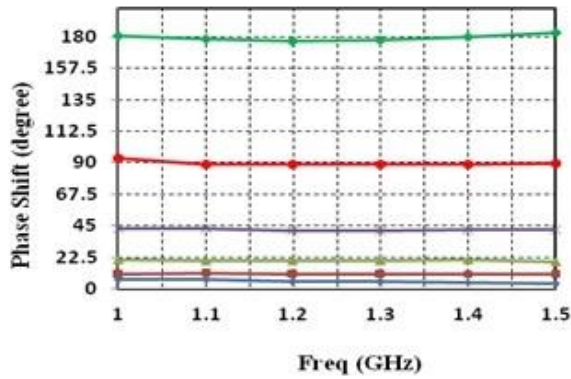


Fig. 7. Phase shifting performance of the cardinal bits

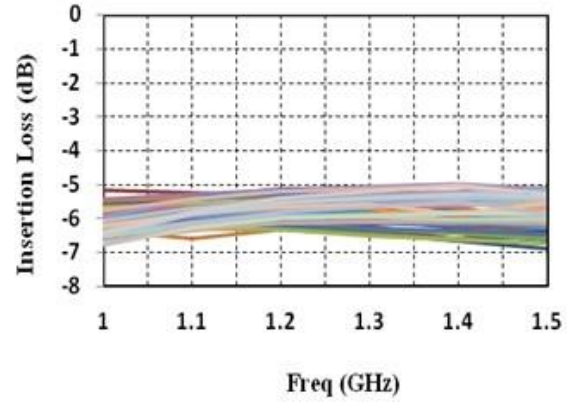


Fig. 8. Insertion loss variation

The phase shifter has good return losses and depicted in Figs. 9 & 10.

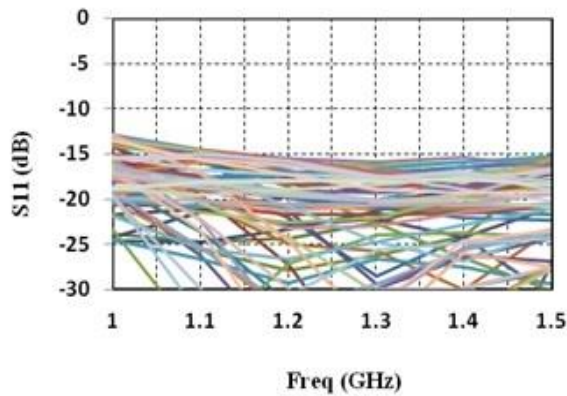


Fig. 9. Input return loss

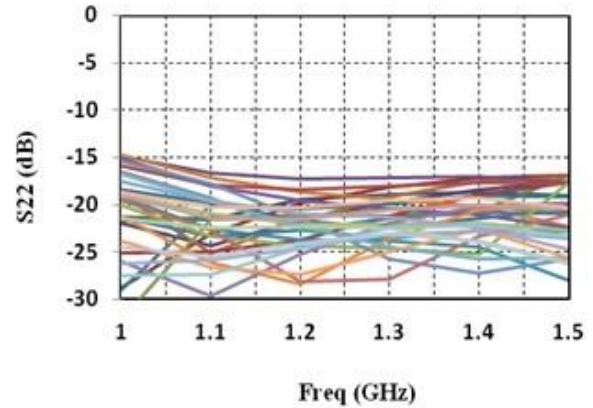


Fig. 10. Output return loss

The RMS error [1] is better than 6.3° and maximum phase error less than 10.5° and shown in Fig.11. The RMS amplitude error is plotted in Fig.12.

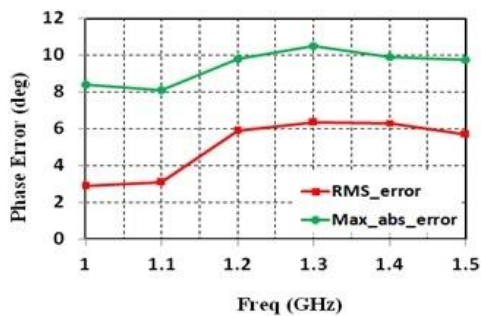


Fig. 11. Phase error

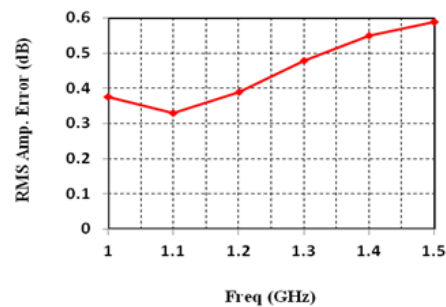


Fig. 12. Amplitude error

The fabricated MMIC phase shifter is shown in Fig.13.

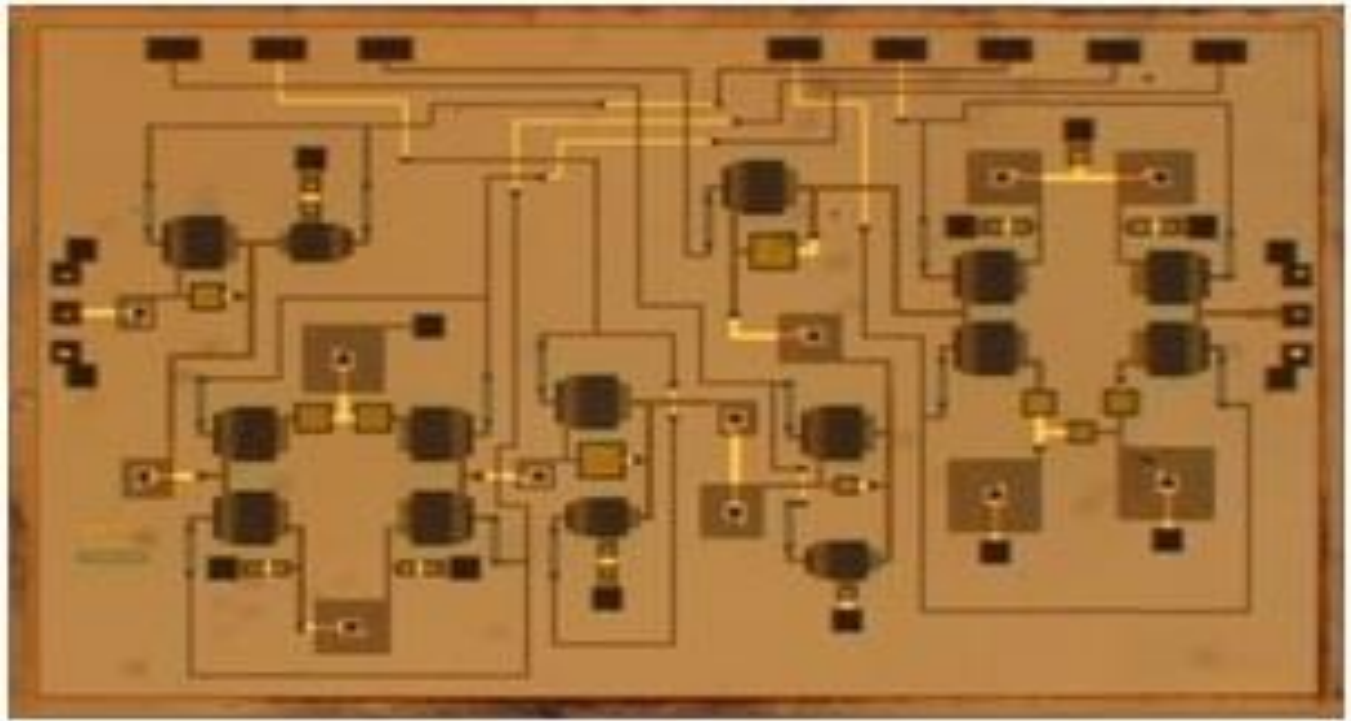


Fig. 13. Photograph of MMIC phase shifter: 5.2mm x 3.5mm

The comparison of performance of GaAs MMIC based phase shifter is shown in table 2.

4. Conclusion

An L-band MMIC phase shifter has been implemented using only 15 FETs and 8 control lines. This MMIC has RMS phase error $<6.3^\circ$ and insertion loss of 6.0 ± 0.8 dB with RMS amplitude error <0.58 dB, with good impedance matching. The input power handling P1dB is 23 dBm.

5. Acknowledgement

The authors thank Director SSPL and Dr S.L Badnekar for their support and encouragement. The contributions of Fabrication and Measurement teams at GAETEC, Hyderabad are also acknowledged.

Table2: PERFORMANCE of GaAs MMIC BASED PHASE SHIFTERS

Freq. Range (GHz) & (Fractional Bandwidth)	No. of Bits	No. of FETs	Switch control lines	Insertion Loss (dB)	RMS Phase Error	References
1.4 -2.4 (52%)	4	16	7	3.5 \pm 0.6	< 4°	[3]
L-band (20%)	5	40	10	8.2	<2.4	[4]
2.2-2.3 (4.4%)	5	24	10	4.9 \pm 0.5	<7°	[5]
1.4- 2.4 (52%)	6	20	10	3.8 \pm 0.8	<4°	[6]
1.0- 1.4 (33%)	6	27	12	9.0 \pm 0.5	NA	[7]
12 – 13 (8%)	6	18	11	6.1 \pm 0.6	< 1.3°	[8]
S and C band (10%BW)	5	15	10	6.1 \pm 0.6	<2.8°	[9]
8 – 12 (40%)	6	18	11	7.6	< 3.3°	[10]
1.0 -1.5 (40%)	6	15	8	6.0 \pm 0.8	< 6.3°	This work

6. References

- [1] Inder J. Bhal and David Conway, “ L- and S- Band Octave Compact Bandwidth 4-bit MMIC Phase Shifters” *IEEE Trans. Microwave Theory Tech.*, vol. no. 56, no.2, pp. 293-299, Feb 2008.
- [2] Inder J. Bhal, and Prakash Bhartiya, “Microwave Solid State Circuit Design”, *John Willey and Sons*, Second Edition, 2003.
- [3] Qun Xiao, “A Compact L-band Broadband 4-bit MMIC Phase Shifter with low phase error,” *Proceedings of the Asia-Pacific Microwave Conference*, 2011, pp. 291-294.
- [4] Kensuke Nakajima, Noriharu Suematsu, Eiji Taniguchi, Hideji Takeda, Toshinbo, Yoshinobu Sasaki and Tadarshi Takaji, “L- band Glass-Epoxy 5-bit Phase Shifter Module Using SW-Bank Chips and Low Cost L,C Chips” *IEEE MTT-S International Microwave Symposium Digest*, vol. 3, pp. 1593-1596, June 2000.
- [5] M. Rhodes, A.A Lane, “Monolithic Five-Bit Phase Shifter for Artemis Space Application,” *IEE Colloquium of Active and Passive components for Phased Array Systems*, pp. 10/1- 10/4, 1992.
- [6] Qun Xiao, “A Compact L-band Broadband 6-bit MMIC Phase Shifter with low phase error,” *Proceedings of 6th European Microwave Integrated Circuits Conference*, 2011, pp. 410-413
- [7] N. D. Doddamani, Harishchandra, and Anil V. Nandi, “Design of SPDT Switch, 6- bit Digital Attenuator, 6- bit Digital Phase Shifter for L-band T/R Module using 0.7 μ m GaAs MMIC Technology,” *IEEE-ICSCN2007*, Feb. 22-24,2007.pp.302-307.
- [8] A. Sharma, A. Kumar and A.N. Bhattacharya, “A Ku- band 6-bit Digital Phase Shifter MMIC for Phased Array Antenna System,” *IEEE International Microwave and RF Conference (IMaRC)*, 2015.
- [9] M. Hangai, M. Hieda, N. Yunoue, Y. Sasaki and M. Miyazaki, “S and C- band Ultra-Compact Phase shifters Based on all- Pass Network,” *IEEE Transactions on Microwave Theory and Techniques*, vol.58, no. 1, January 2010.
- [10] Qi Wang, Pengpeng Sun, Xiaojuan Chen, Tingting Yuan, Lei Pang, Xinyu Liu and Weijun Luo, “Design of an X-Band 6-bit Phase Shifter,” 8th International Symposium on Computational Intelligence and Design, 2015, pp. 539-542.
- [11] Robert V. Garver, “Broad-Band Diode Phase Shifters” *IEEE Trans. Microwave Theory Tech.*, MTT-20, vol. no. 5, pp. 314-323, Nov 1982.
- [12] Liam Devlin, “The Design of Integrated Switches and Phase shifters” *IEE Tutorial Colloquium Design of RFIC and MMICs*, pp. 2/1- 2/14, 1999.
- [13] Koul S. K., Bhat B., “Microwave and Millimeter Wave Phase Shifters” *Artech House*, 1991.

Analyzing the effect of Source/Drain Gaussian Profile on Underlap DG-MOSFET with Air Spacer

Alok Kumar Shukla¹, Ashutosh Nandi²

¹School of VLSI Design and Embedded System National Institute of Technology, Kurukshetra, India ²Department of Electronics and Communication Engineering National Institute of Technology, Kurukshetra

mr.alokkumarshukla@gmail.com¹Kurukshetra, India
ashutosh.chl@gmail.com²

Abstract—The present work has analyzed the effect of lateral Source/Drain (S/D) Gaussian profile on the underlap DG-MOSFET with air spacer. The impact of lateral straggle (σ) on I_{on}/I_{off} ratio, threshold voltage (V_t), subthreshold slope (SS), and DIBL have been studied at a different value of channel thickness. This paper shows that when lateral straggle of the S/D Gaussian profile (σ) is varied from 1nm to 4nm, I_{on}/I_{off} ratio, V_t , SS and DIBL deteriorates by ~2decade, ~47.7%, 35%, and ~145% respectively for 15 nm channel thickness based underlap DG-MOSFET. These deteriorations are restricted to ~1 decade, 2.5%, 12%, and ~95% when t_{si} is scaled down to 7nm. It is further observed that for 7 nm t_{si} based device the deterioration in all the above parameters are negligible when σ is restricted to an achievable value of 3 nm (junction depth ~12 nm). All the results were carried out using Sentaurus TCAD simulation tool.

Keywords— Lateral straggle, drain induced barrier lowering(DIBL), underlap length, air spacer

1. INTRODUCTION

In a MOSFET (metal oxide semiconductor field effect transistor) family, the channel length is one of the most important parameter. The short channel effects (SCEs) are an important issue when the size of the device is reduced to nanometer technology. Several MOSFET modeling techniques are used to eliminate these effects [1],[2]. Double gate (DG) MOSFET is a successful option for further scaling of MOSFET [1]. In DG-MOSFET, the electrostatic integrity (EI) of the device increases, which further enhance the device performance. To control the lateral spread of source/drain (S/D) electric field in the channel region, International Technology Roadmap for Semiconductor guides the creation of an ultra-shallow junction [3]. Recently Chuang et al. [4] reports an ultra-shallow junction of ~12nm ($\sigma=3$ nm) by monolayer doping process when the S/D region is doped with 10^{20} cm⁻³. Scaling down the DG-MOSFET, the channel thickness could contribute to an undesirable rise in resistance and junction capacitance in source(S)/drain(D) region, which could reduce the drive current [5].

There are many research groups [6], [7], who have used the symmetric underlap DG MOS for reducing SCEs [8]. The parasitic capacitance of the device can also be reduced by introducing S/D underlap region [9]. In 2017, Mandal et al. [10] reported the analog performance of symmetric as well as asymmetric underlap DG-MOSFET with optimized underlap length. However, Koley et al. [11] found that asymmetric underlap DG-MOSFET is successful only for reducing the effect of DIBL.

Spacer dielectrics have a dominant position for reducing the fringe capacitance. Due to the least dielectric, the air is the most attractive substance for the spacer region. This may decrease the fringe capacitance which further decreases the total device capacitance [12]. In 2010, Park et al. [13] reported that the gate fringing field loses its control over channel edge

due to use of air spacer, this reduces the drain current. However, the device with an air spacer is able to aim better inverter delays, switching energy and switching charge than oxide spacer based device [13]. The effective approach to improve CMOS efficiency and to decrease active power consumption has been proved with low-K spacer. Currently the value of relative dielectric constant is ~ 4 for low-K spacer materials, while the C_{eff} is smallest for air spacer. Also air spacers in NAND flash memories and in DRAM have been published. In 2016, Cheng et al. [14] report 10 nm FinFET CMOS with air spacer. Recently Gupta et al. [15] used air spacer for underlap TG-FinFET and concluded the reduction in fringe capacitance. It is noted that S/D lateral Gaussian doped MOSFETs provide greater flexibility in regulating the device's off-state drive current [16]. For the first time, Nandi et al. [16] used Gaussian doping into DG-MOSFET in the S/D region. Afterward, Singh et al. [5], [17] proposed the model for Gaussian doped underlap DG-MOSFET.

As air spacer plays an important role in reducing the fringe capacitance of the device, therefore the study concerning the effect of lateral S/D Gaussian profile on air spacer based underlap DG-MOSFET is carried out in the present work.

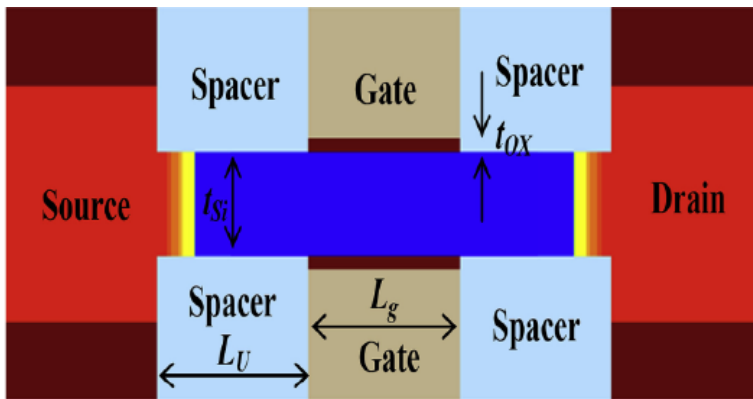


Fig. 1. Schematic view of symmetric underlap DG-MOSFET with air spacer.

2. STRUCTURE AND SIMULATION SETUP OF THE DEVICE

The schematic view of the air spacer based underlap DG-MOSFET with S/D lateral Gaussian doping profile can be seen from figure 1. Air gap spacer is formed by carbon decomposition on the sidewall of the gate stack, followed by SiN deposition and reactive ion etching, resulting in SiN carbon encapsulation. Finally, to extract the deposited carbon, Oxygen plasma is used [15]. In order to decrease sheet resistance and improving gate efficiency, a metal gate is used. The doping of the channel is 10^{16} cm^{-3} with Boron concentration to reduce the impact of mobility degradation while the S/D concentration is kept high to 10^{20} cm^{-3} with arsenic concentration [18]. The S/D doping profile ($N_{SD}^{\pm}(x)$) is expressed as [16]:

$$N_{SD}^{\pm}(x) = \frac{\left(N_{SD(p)} e^{-\frac{x^2}{2\sigma^2}} + N_{SD(p)} e^{-\frac{(L_g-x)^2}{2\sigma^2}} \right)}{\left(1 + s_D e^{((E_F-E_D)/kT)} \right)}$$

Where N_{sdp} stands for peak of the Gaussian profile and σ represents the straggle parameter of

the S/D Gaussian doping. Donor energy level E_D and Fermi energy level E_F is set as per [16]. The S/D underlap DG-MOSFET is simulated using Sentaurus TCAD tool. In the simulation setup, the drift-diffusion model is used that considers the effect of MLDA quantization with empirical parameter β [19], [20]. The simulation setup also includes the Shockley-Read-Hall (S-R-H) generation/recombination model, band to band Auger recombination model, old Slotboom bandgap narrowing model and Lombardi mobility model [21]-[24]. Nandi et al. [20] has calibrated the simulation model with experimental data. We have used the same model in our simulation set up.

3. PERFORMANCE VARIATION WITH LATERAL STRAGGLE AND CHANNEL THICKNESS

In the present section, the channel thickness of DG-MOSFET is varied with different lateral straggle in order to study SCEs. Values and unit of different parameters have been listed in Table I.

TABLE I. VALUES AND UNIT OF DIFFERENT PARAMETERS

<i>Parameters</i>	<i>Notations</i>	
	<i>Values</i>	<i>Unit</i>
Gate voltage (V_{gs})	1.1	V
Gate length (L_g)	18	nm
Channel doping (N_a)	10 16	cm -3
Gate work function (Φ_M)	4.6	eV
Source/Drain doping (N_{sdp})	10 20	cm -3
Degenerated doping (N_{de})	2.7×10^{19}	cm -3
Gate oxide thickness (t_{ox})		nm
Drain voltage (V_{ds})	1.1	V
Gate underlap length (LU)	10	nm

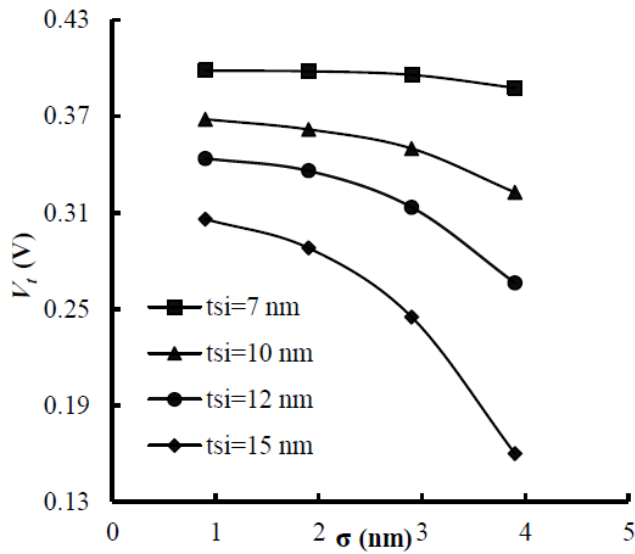


Fig. 2. The threshold voltage V_t versus lateral straggle σ for different values of t_{si} .

The threshold voltage variation can be studied in Fig. 2. It is observed that for the variation of straggle parameter σ from 1 nm to 4 nm, the threshold voltage deteriorates by ~47.7 % (0.306 V to 0.16 V) at $t_{si}=15$ nm. This deterioration is restricted to ~2.5 % (0.398 V to 0.388 V) when t_{si} is reduced to 7 nm. It is also evident from the figure that V_t is almost constant when straggle parameter σ is changed from 1 nm to 3 nm at $t_{si}=7$ nm. The voltage roll-off can also be studied from Fig. 2. It is observed from the figure that the V_t roll-off is minimum at lower t_{si} ($t_{si}=7$ nm) when σ is varying from 1 nm to 4 nm. This is because at $t_{si}=7$ nm the gate electrostatic integrity is much better which actually restrict the spread of lateral S/D electric field at higher σ .

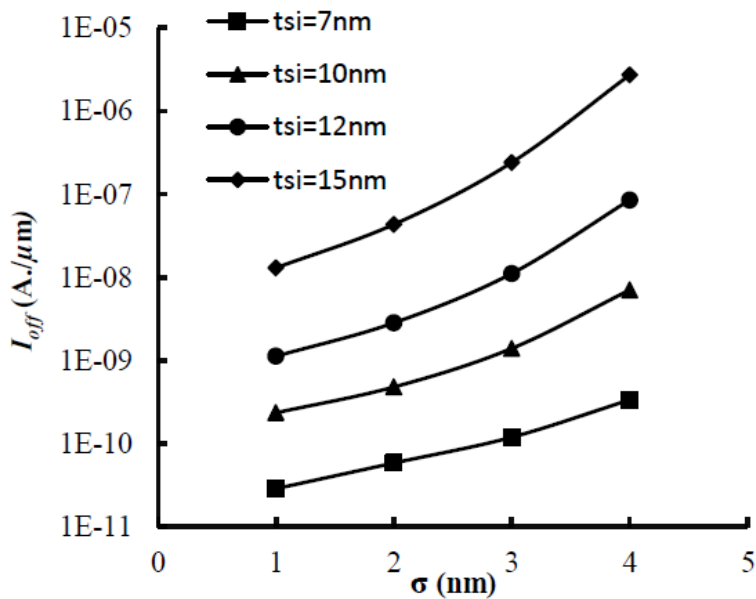


Fig. 3. Variation of I_{off} with lateral straggle σ for different values of t_{si} .

The variation of off current (I_{off}) with straggle parameter (σ) at different

t_{si} can be seen from figure 3. As seen from the figure, off current increases with σ while it decreases with the scaling of t_{si} . If σ is varying from 1 nm to 4 nm, it is noted that off current increases almost ~ 2 decade (1.30×10^{-8} A./ μm . to 2.71×10^{-6} A./ μm .) for $t_{si} = 15$ nm based device, while the off current increase is restricted to ~ 1 decade (2.88×10^{-11} A./ μm . to 3.37×10^{-10} A./ μm .) when t_{si} scaled down to 7 nm. It is also concluded that for a constant σ of 1 nm the off current decreases by almost ~ 3 decades when t_{si} is reduced from 15 nm to 7 nm. On the contrary, when σ is increased to a constant value of 4 nm, the decrease in off current by ~ 4 decade is observed for $t_{si} = 7$ nm based device as compared to $t_{si} = 15$ nm based device.

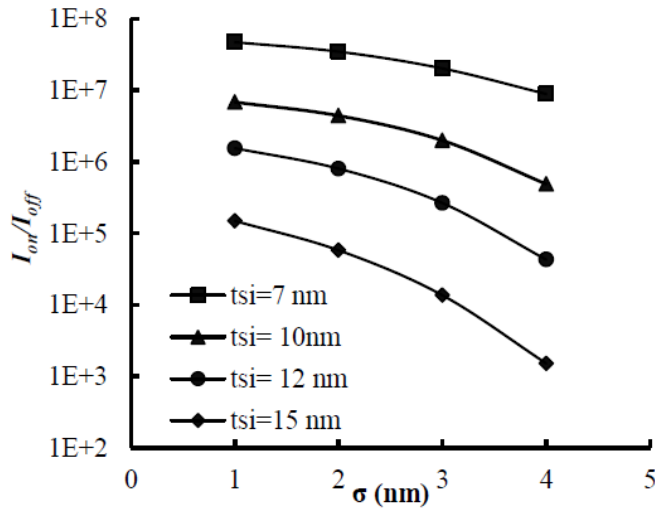


Fig. 4. Variation of I_{on}/I_{off} ratio with lateral straggle σ for different values of t_{si} .

Similarly Fig. 4 demonstrates that as lateral straggle increases the I_{on}/I_{off} ratio of the device decreases when others parameters are constant. Further the I_{on}/I_{off} ratio improves when t_{si} scaled from 15 nm to 7 nm, for a constant value of σ .

From figure 4, it can be seen that the I_{on}/I_{off} ratio decreases by ~ 2 decade for the variation of σ from 1 nm to 4 nm at $t_{si} = 15$ nm while it is ~ 1 decade at $t_{si} = 7$ nm. Importantly it is observed that the deterioration in I_{on}/I_{off} ratio is restricted to $\sim 47.3\%$ when lateral straggle σ is changed from 1 nm to an achievable value of 3 nm for $t_{si} = 7$ nm based device.

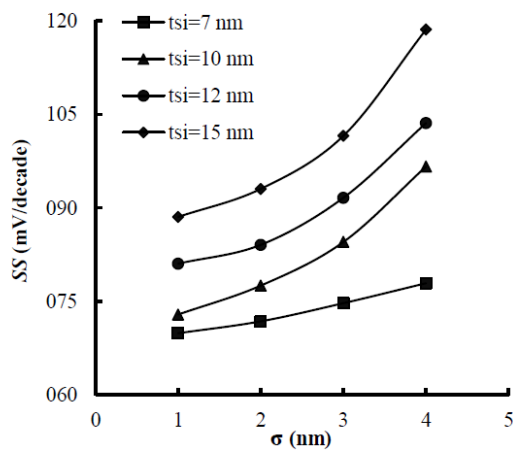


Fig. 5. Subthreshold slope variation with lateral straggle σ for different values of t_{si} .

The variation of the subthreshold slope with varying σ and for different t_{si} is indicated in Fig. 5. It is concluded from the figure that the subthreshold slope is enhanced by $\sim 34.5\%$ (119 mV/decade to 77.9 mV/decade) for $\sigma = 4$ nm and $\sim 21\%$ (88.5 mV/decade to 69.9 mV/decade) for $\sigma = 1$ nm when t_{si} is scaled from 15 nm to 7 nm. And for a constant value of t_{si} , the subthreshold slope is deteriorated by $\sim 35\%$ (88.5 mV/decade to 119 mV/decade) for $t_{si} = 15$ nm while the deterioration is $\sim 12\%$ (69.9 mV/decade to 77.9 mV/decade) for $t_{si} = 7$ nm when σ varies from 1 nm to 4 nm. This further verifies the S/D electric field is rapidly increasing when σ is increased as discussed earlier. However, the deterioration is negligible ($\sim 7\%$) for the variation in σ from 1 nm to an achievable value of 3 nm at $t_{si} = 7$ nm.

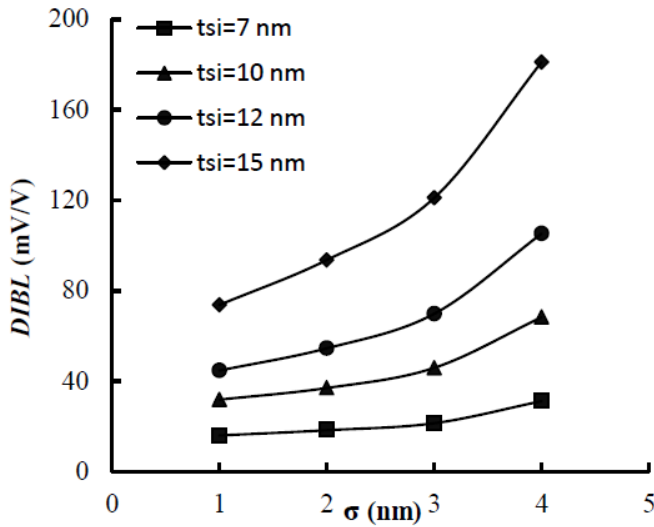


Fig. 6. DIBL versus lateral straggle σ for different values of t_{si} .

Now, from Fig. 6, it is noted that the DIBL is increased with lateral straggle σ . As t_{si} is scaled from 15 nm to 7 nm, DIBL is improved by $\sim 82\%$ (181.016 mV/V to 31.121 mV/V) and $\sim 78\%$ (73.647 mV/V to 15.952 mV/V) for $\sigma = 4$ nm and $\sigma = 1$ nm respectively. It is also concluded that there is a minimal change ($\sim 33\%$) in DIBL when σ varies from 1 nm to 3 nm. Hence it is concluded that the SCEs can be enhanced by scaling the t_{si} at achievable σ of 3 nm.

4. CONCLUSION

In this paper, we have analyzed the effect of S/D lateral straggle on the air spacer based underlap DG-MOSFET in conjunction with the channel thickness. The subthreshold behavior of the device in terms of V_t , SS, DIBL, I_{off} , I_{on}/I_{off} deteriorates for the variation of lateral straggle σ from 1 nm to 4 nm. However, scaling the t_{si} from 15 nm to 7 nm restricts this deterioration of the subthreshold behaviour. Although, SCEs increases with σ , however, at $t_{si} = 7$ nm, there is a marginal change in V_t , SS, DIBL and I_{on}/I_{off} by 0.5%, 7%, 33% and $\sim 47\%$ respectively when σ varies from 1 nm to an achievable value of 3 nm.

5. REFERENCES

- [1] A. Nandi, N. Pandey, S. Dasgupta, "Analytical modeling of DG- MOSFET in subthreshold regime by green's function approach," *IEEE Trans. Electron Devices*, vol. 64, no. 8, pp. 3056-3062, Aug. 2017.
- [2] A. Nandi, N. Pandey, and S. Dasgupta, "Analytical Modeling of Gate- Stack DG-MOSFET in Subthreshold Regime by Green'sFunction Approach," *IEEE Trans. on Electron Devices*, vol. 65, no. 99, pp. 1-5, Oct. 2018.
- [3] International Technology Roadmap for Semiconductors (ITRS) 2007 for Metrology. Available:www.itrs.net.
- [4] S. S. Chuang, T. C. Cho, P. J. Sung, K. H. Kao, H. J. H. Chen, Y. J. Lee, M. I. Current, and T. Y. Tseng, "Ultra-shallow junction formation by monolayer doping process in single crystalline Si and Ge for future CMOS devices," *ECS J. Solid State Sci. Technol.*, vol. 6, no. 5, pp. P350–P355, Apr.2017.
- [5] K. Singh, M. Kumar, E. Goel, B. Singh, S. Dubey, S. Kumar, and S. Jit, "Analytical modeling of potential distribution and threshold voltage of gate underlap DG MOSFETs with a source/drain lateral Gaussian doping profile," *Journal of Electronic Materials*, vol. 45, no. 4, pp. 2184-2192,2016.
- [6] B.C. Paul, A. Bansal, and K. Roy, "Underlap DGMOS for digital subthreshold operation," *IEEE Trans. Electron Devices*, vol. 53, no. 4, pp. 910-913, Apr.2006.
- [7] T. Schulz, W. Rosner, L. Risch, A. Korbel, and U. Langmann, "Short channel vertical sidewall MOSFETs," *IEEE Trans. Electron Devices*, vol. 48, no. 8, pp. 1783-1788,2001.
- [8] A. Bansal, B.C. Paul, and K. Roy, "Modeling and optimization of fringe capacitance of nanoscale DGMOS devices," *IEEE Trans. Electron Devices*, vol. 52, no. 2, pp. 256-262,2005.
- [9] V. Trivedi, J. G. Fossum, and M. M. Chowdhury, " NanoscaleFinFET with gate-source/drain Underlap," *IEEE Trans. On Electron Devices*, vol. 52, no. 1, pp. 56-62, Dec.2004.
- [10] A. Mandal, D. Saha, D. Ghosal, S. Bhattacharya, A. Kundu, and M. Kar, "Symmetric/asymmetric underlap DG-MOSFET: A study of analog/RF performance using non-quasi static approach," *Devices for Integrated Circuit*, pp. 837-840, Mar.2017.
- [11] K. Koley, B. Syamal, A. Kundu, N. Mohankumar, and C. Sarkar, "Subthreshold analog/rf performance of underlap DG-FETs with asymmetric source/drain extensions," *Microelectronics Reliability*, vol. 52, no. 11, pp. 2572-2578, Nov.2012.
- [12] E. Huang, E. Joseph, H. Bu, X. Wang, N.Fuller, C. Ouyang, E. Simon yi, H. Shobha, T. Cheng, A. Mallikarjunan, I. Lauer, S.Fang, W. Haensch, C.-Y. Sung, S.Purushothaman, and G. Shahidi, "Low-k spacers for advanced low power CMOS devices with reduced parasitic capacitances," *Proc. SOI Conf. IEEE*, pp. 19-20, Oct.2008.

- [13] J. Park, C. Hu, "The effects of vacuum spacer transistors between high performance and low stand-by power devices beyond 16nm," *Proc. Solid-state and Integrated Circuit Technology*, pp. 1823-1825, Nov. 2010.
- [14] K. Cheng, C. Park, C. Yeung, S. Nguyen, J. Zhang, X. Miao, M. Wang, S. Mehta, J. Li, C. Surisetty, and R. Muthinti, "Air spacer for 10nm FinFET CMOS and beyond," *International Electron Devices Meeting (IEDM)*, pp. 17-1, Dec. 2016.
- [15] S. Gupta, and A. Nandi, "Effect of air spacer on analog performance of underlap tri-gate FinFET," *Superlattices and Microstructures*, vol. 109, pp. 693-701, 2017.
- [16] A. Nandi, A. K. Saxena, and S. Dasgupta, "Analytical modeling of a double gate MOSFET considering source/drain lateral Gaussian doping profile," *IEEE Trans. on Electron Devices*, vol. 60, no. 11, pp. 3705-3709, 2013.
- [17] K. Singh, S. Kumar, E. Goel, B. Singh, M. Kumar, S. Dubey, and S. Jit, "Subthreshold Current and Swing Modeling of Gate Underlap DG MOSFETs with a Source/Drain Lateral Gaussian Doping Profile," *Journal of Electronic Materials*, vol. 46, no. 1, pp. 579-584, 2017.
- [18] S. Gupta and A. Nandi, "Temperature analysis of underlap GAA- SNWTs for analog/RF applications," *Microelectronics J.*, vol. 90, pp. 58-62, Aug. 2019.
- [19] S. Tayal and A. Nandi, "Study of temperature effect on junctionless Si nanotube FET concerning analog/RF performance," *Cryogenics (Guildf.)*, vol. 92, pp. 71-75, Jun. 2018.
- [20] A. Nandi, A.K. Saxena, S. Dasgupta, "Design and analysis of analog performance of dual-k spacer underlap N/P-FinFET at 12 nm gate length," *IEEE Trans. Electron Devices*, vol. 60, no. 5, pp. 1529-1535, May 2013.
- [21] S. Gupta and A. Nandi, "RF performance enhancement in underlap Tri-Gate FinFET," in *2018 2nd International Conference on Inventive Systems and Control (ICISC)*, 2018, pp. 760-762.
- [22] S. Tayal, S. Gupta, A. Nandi, A. Gupta, and S. Jadav, "Study of Inner- Gate Engineering Effect on Analog/Radio Frequency Performance of Conventional Si-Nanotube Field Effect Transistor," *J. Nanoelectron. Optoelectron.*, vol. 14, no. 7, pp. 953-957, Jul. 2019.
- [23] S. Gupta and A. Nandi, "Enhancing Frequency Performance of Underlap Tunnel Field-Effect Transistor for Analog/RF Applications," *J. Nanoelectron. Optoelectron.*, vol. 14, no. 5, pp. 716-722, May 2019.
- [24] Sentaurus device User Guide, 2016.

Model reference controller approach for robot arm tracking using neural networks

Najva N^{*1}, Abdul Saleem ²

¹Research scholar, Dept. of Electrical and Electronics Engineering, Government Engineering College, Thrissur, Kerala, 680009, India

²Assistant Professor, Dept. of Electrical and Electronics Engineering, Government Engineering College, Thrissur, Kerala, 680009, India

najvahassan@gmail.com¹, abdulsaleempk@gmail.com²,

Corresponding author*: Phone: +91-9961727772

Abstract

An accurate mathematical model is much useful for the development of a precise controller. The dynamics of robot arm motion is highly nonlinear and can have uncertainties. Artificial neural networks are universal approximators and so it can be considered as a best choice to approximate the dynamics of robot arm motion. This paper proposes a neural network based model reference controller (MRC) for robot arm trajectory tracking. A neural network based reference model is initially trained such that it follows any desired reference trajectory. The neural network controller is trained to drive the error between actual plant and reference model to a value which is approximately zero. Simulations are done to validate the proposed method and found that the neural network based MRC is capable of following desired trajectories with approximately zero tracking error. The performance of the proposed method is compared with PID controller and is found that the instantaneous control input and total control effort of the proposed controller is very small.

Keywords: neural networks, model reference controller, kinematics, dynamics, tracking error

1. Introduction

Robot manipulators are electro-mechanical devices which are capable of performing a variety of functions in a more flexible working environment, and at a lower production cost. The various applications include industrial, educational and medical field apart from their applications in farm, home, hospital and military. The robots can work in unpredictable and hazardous situations where a human faces very difficult to reach. One of the objectives of the robot is its arm movement from an initial position to a target position. Planning a robot arm trajectory satisfying obstacle avoidance and developing an appropriate method to control trajectory tracking are important research problems in robotics. An effective trajectory tracking controller should be able to track the desired trajectory with minimum tracking error, lesser control input, and minimum total control effort.

The objective of robot arm tracking is to develop a controller such that the robot arm can move along the desired trajectory. This can be achieved by controlling the joint angles of the arm. The joint angle for a particular end effector orientation and position is calculated by inverse kinematics. Since robot arm dynamics are highly nonlinear, a closed-form solution of joint angles is not feasible. Neural networks are capable of handling uncertainties and unexpected parameter variations in nonlinear plants and so neural network based controllers can be considered as a better solution to robot arm trajectory control problems.

In literature, numerous methods are suggested for effective trajectory tracking of robot arm. Bingol and Akpolatin [1] proposed a pattern search algorithm based PID controller for the trajectory control of the robot arm. The pattern search algorithm uses a set of vectors called patterns, to determine which points to search at each iteration and for each iteration, this algorithm searches a point, from the pattern around the current point, such that the value of the objective function is improved. The optimization algorithm presented in this paper requires more

time to complete trajectory tracking. In [2], Younus et.al. proposed a PID controller, whose control parameters are tuned using a genetic algorithm. This method controls the robot arm with less tracking error as compared with the conventional PID controller. An adaptive computed torque control algorithm is presented by Guo and Zhang [3] for trajectory tracking. The adaptive control is capable of compensating the parametric uncertainties but is limited to robots with 2-DOF. Linear estimation techniques together with a computed torque control law are used in [3]. The tracking performance was improved by Lin and Chen [4] who developed a model reference adaptive control which considered the variations at the end effector load. The dynamics uncertainties are considered in the work proposed by Wang and Feng [5]. Fractional order Fuzzy based PID controller where parameter tuning is done by using Fuzzy logic is developed by Reham and Mohammad [6]. Sinha and Mishra [7] developed a controller based on sliding mode, which provides robustness against uncertainties to control the robot arm. The controller guarantees stability in Lyapunov sense but the chattering effect could not be eliminated completely. The chattering effect is reduced by using a twisting sliding mode controller by Boudoua and Hamerlain [8] for the control of pneumatic artificial muscles robot arm. However, this method does not guarantee the stability of the overall system. In [9], Paraklev and Jafarov proposed a robust PD-sliding-mode controller for avoiding the instability problem. Even though this method avoid the instability problem it produced tracking error. For under actuated robots, a model-based adaptive variable structure control scheme is proposed by Su [10]. A simple sliding mode control scheme for robot arm control is presented used by Bailey [11]. The design complexity is reduced greatly here. A trajectorycontroller which uses the variable structure theory is proposed in [12] by Yeung and Chen. This method considered parameter variations and the controller can be used for a higher number of links.

Due to the uncertainties in the dynamic model and possible variations in system parameters, an adaptive controller is highly appreciated. The effects of modeling uncertainties decreases the performance of the controller in terms of tracking accuracy and control input. Conventional methods fails to model the nonlinearities and uncertainties in the robot arm dynamics. An effective trajectory tracking controller should possess the least tracking error and low control input. Also, its maximum control input requirement and total control effort should be minimized.

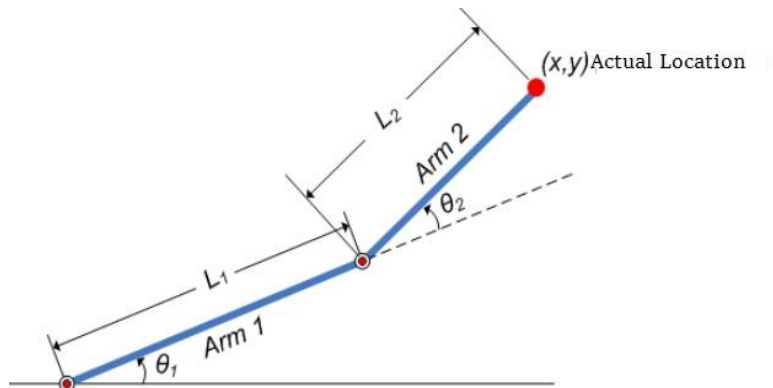
This paper proposes a model reference neural network based trajectory controller which gives the best performance in terms of tracking error, control input, total control effort and maximum torque as compared to conventional PID controllers. Herein, two neural network architectures are used: one as the controller and the other as the reference model. The reference model is trained such that it can follow any reference trajectory. The controller is trained using large number of randomly generated reference trajectories and the weights are updated to minimize the error between reference trajectory and the output of the NN based plant model. After training, the neural network structure is connected to the robot arm.

The rest of this paper is organized as follows. Section 2 formulates the tracking problem. A brief introduction of neural networks is presented in section 3. The proposed methodology is described in section 4. Simulation results are presented and analyzed in section 5. Finally, the concluding remarks are presented in section 6.

2. Problem Formulation

A robot arm with two degrees of freedom consists of two links as shown in Figure 1. L_1 and L_2 are the link lengths of Arm 1 and Arm 2 and their joint angles are θ_1 and θ_2 respectively. The two links are connected together to a revolute joint known as elbow and the first link is fixed to a revolute joint called shoulder.

Figure 1. Robot arm



The relation between position and orientation of a robot arm is obtained from its forward kinematics which can be derived using Denavit-Hartenberg (DH) convention as

$$x = L_1 \cos \theta_1 + L_2 \cos(\theta_1 + \theta_2) \quad (1)$$

$$y = L_1 \sin \theta_1 + L_2 \sin(\theta_1 + \theta_2) \quad (2)$$

where θ_1 and θ_2 are joint angles.

Equations (1) and (2) gives the position of the robot arm at any instant. These two equations imply that the position of the arm can be controlled by changing the angle θ_1 or θ_2 which can be achieved by applying torque. Thus the torque acts as the control input of the robot arm tracking. The robot dynamics is represented by the equation

$$\frac{d^2\phi}{dt^2} + g \sin\phi + a \frac{d\phi}{dt} = u \quad (3)$$

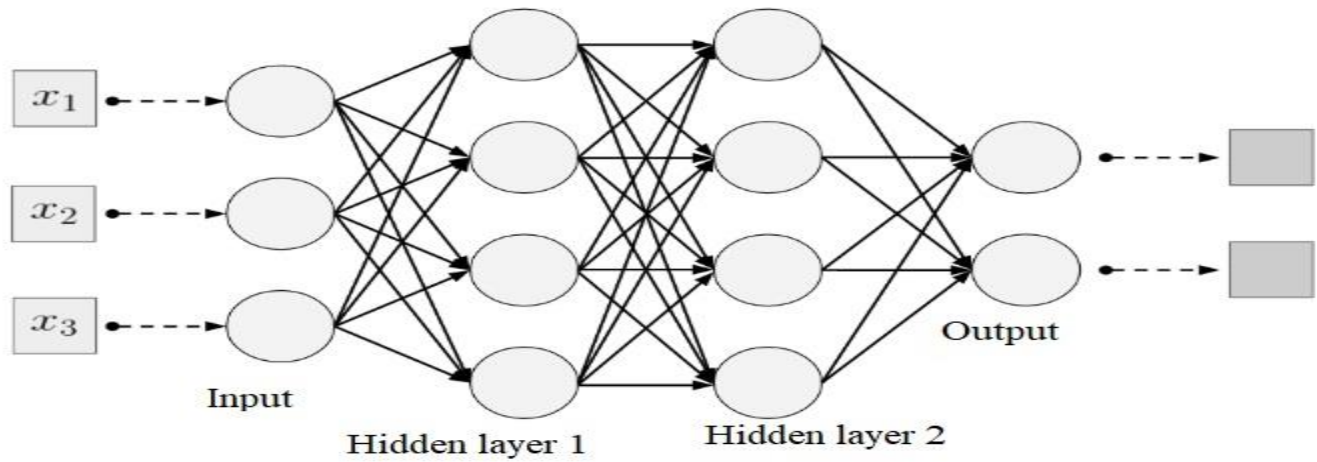
where u is the control signal, ϕ is the angle to be controlled and a, g are constants.

The dynamic equation considers frictional and gravitational forces. The objective of robot arm trajectory tracking is to design a control input u such that robot arm moves along the desired trajectory as close as possible such that total control effort is minimized. In this work, artificial neural network is used as the controller to solve the trajectory tracking problem.

3. Neural Networks

Artificial neural network (ANN) is a mathematical model that mimics the structure and function of biological neural networks. The basic building block of an ANN is neurons. A neuron receives the weighted sum of the outputs of all neurons connected to it as its input, which is passed to an activation function to compute the neuron output. A multi-layer NN consists of an input layer, one or more hidden layers and an output layer. The commonly used activation functions are sigmoid function, ReLU function hyperbolic tangent, leaky RELU, softmax, swish. ANNs have the ability to learn and model nonlinear and complex relationship, and capable of generalization. A neural network learns by updating its weights. Back propagation algorithm is one method used for NN training. In back propagation, the weights are adjusted such that a cost function is minimized. The sum of squares of errors is a proper choice of cost function. Here, the error is the difference between the desired output and actual output. A neural network structure is shown in Figure2.

Figure 2. Neural network structure



The net input by a neuron is given by

$$net_j = \sum_{i=1}^n w_{ij} x_j + b_j \quad (4)$$

where x is the output of the incoming neuron of the previous layer, w is the weight, b is the bias and n is the number of neurons in the previous layer. If the sigmoid function is used as the activation function, then the output of each neuron can be computed by using

$$out_j = \frac{1}{1+e^{-net_j}} \quad (5)$$

A typical cost function can be the sum of squares of errors defined as

$$E = \sum \frac{1}{2} (target - output)^2 \quad (6)$$

The weights are adjusted such that the cost function is minimized. A common method used for updating the weights is to find how much changes occurs to the cost function for a given change in the weight, which is computed as

$$\frac{\partial E_{total}}{\partial w_i} = \frac{\partial E_{total}}{\partial out_{01}} * \frac{\partial E_{out_{01}}}{\partial net_{01}} * \frac{\partial net_{01}}{\partial w_i} \quad (7)$$

and the weight is updated using the formula

$$w_{n+1} = w_n + \alpha \frac{\partial E_{total}}{\partial w_i} \quad (8)$$

where α is learning factor. The training is continued until the cost function is reduced to an acceptable value. The proposed method uses a neural network based controller trajectory to control a robot arm trajectory.

4. Proposed Methodology

The proposed methodology uses the concept of model reference controller presented in [13]. Herein, two neural networks (i) the reference plant, and (ii) the controller are used

Figure 3. Plant reference model

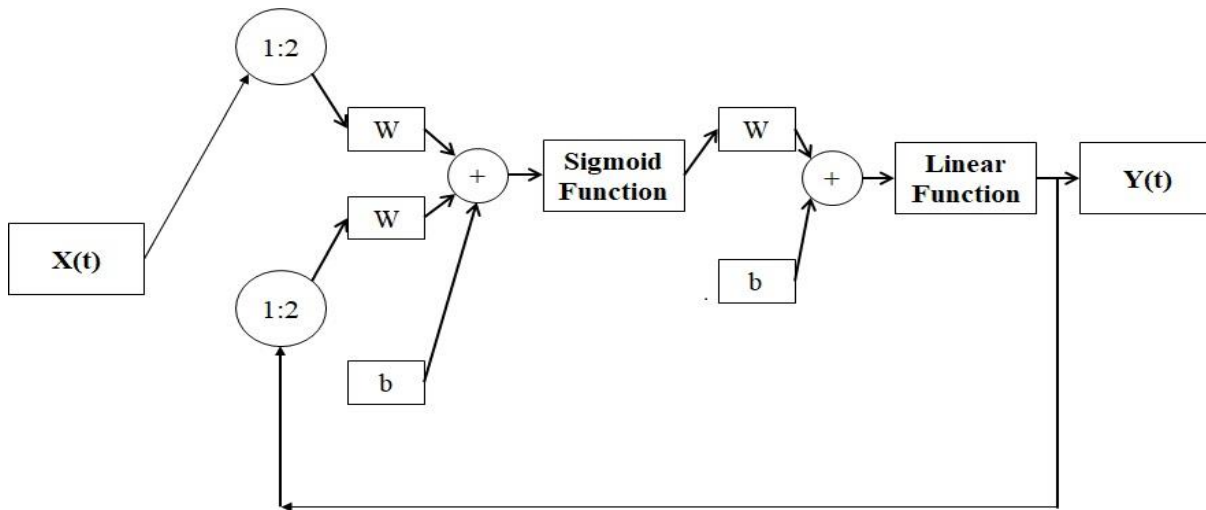
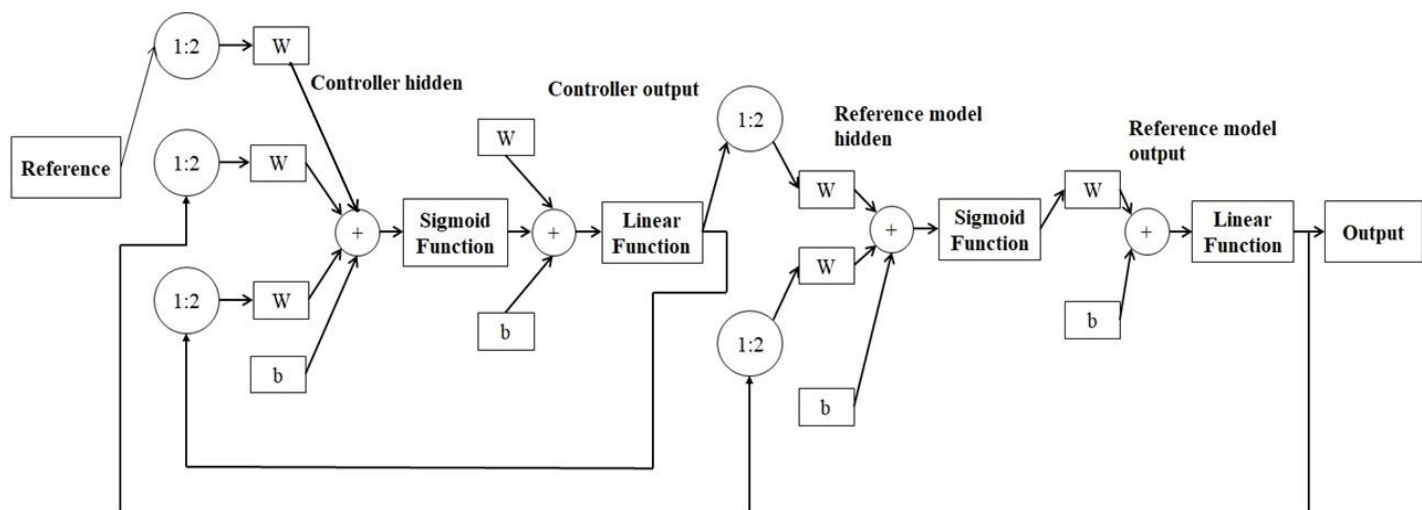


Figure3 represents the NN structure of the plant reference model. The inputs to the network are desired trajectory and the output of the model. Initially, the reference model is trained until the error between output of the model and its input attains zero or a very small value. A trained plant reference model is capable of following any desired trajectory. Hence, the output of this model can be used to train the controller.

The next step is to train the controller. Figure4 shows the schematic structure during the controller training. It consists of two sub networks, (i) controller and (ii) the referenceplant. Inputs to the controller are the desired trajectory, controller output, and the output of the plant reference model. Inputs to the reference model are the controller output, and the model output.

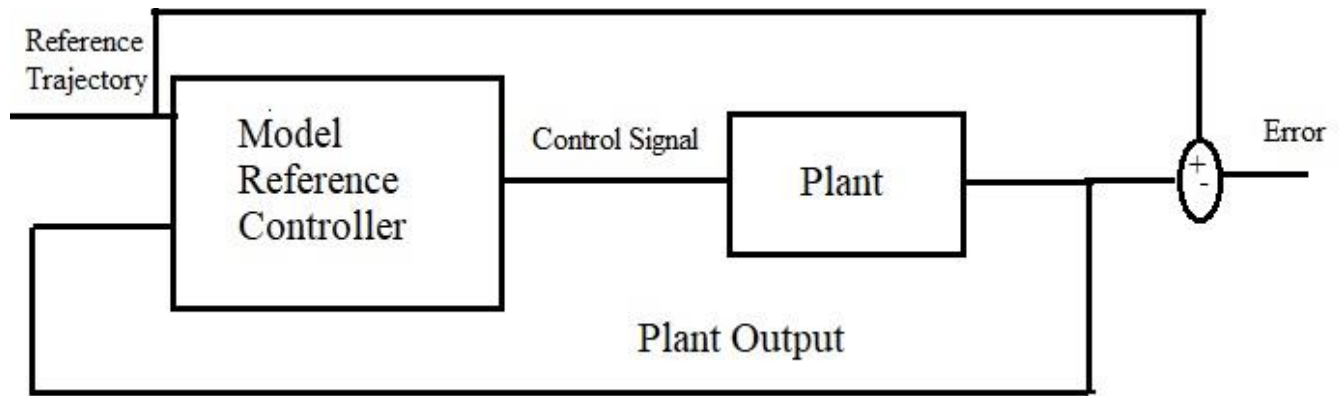
A number of randomly generated desired trajectories are given for training, to the controller input and the weights of the NN are adjusted until the difference between desired trajectory and the reference plant is zero or very small. The advantage of this technique is that there is no need of an actual plant for training the network. Back propagation algorithm is used for training.

Figure 4. Plant reference model + Neural network controller



Once the neural networks are trained, then the controller can be connected to the robot arm, as shown in Figure5. The desired trajectory and the output of the robot arm are the inputs to the model reference controller which consists of the two sub-networks of the Figure4. The controller output is connected to the plant.

Figure 5. Simulation set up



5. Results and Discussion

The performance of the proposed methodology is tested by simulation experiments. SIMULINK set up is used for simulation. The robot arm is modeled using the SIMULINK. The numerical values $a = 2$ and $g = 10$ are considered for the coefficients of the dynamic model given by equation (3). Three different trajectories are considered. First, the reference model is trained and then the controller is trained by giving a set of randomly selected desired trajectories as input. After training, the error between the desired trajectory and the output of reference plant is zero. The three cases discussed subsequently uses this trained model reference controller. To illustrate the effectiveness of the proposed method, the results are compared with that obtained for a PID controller based robot arm trajectory tracking.

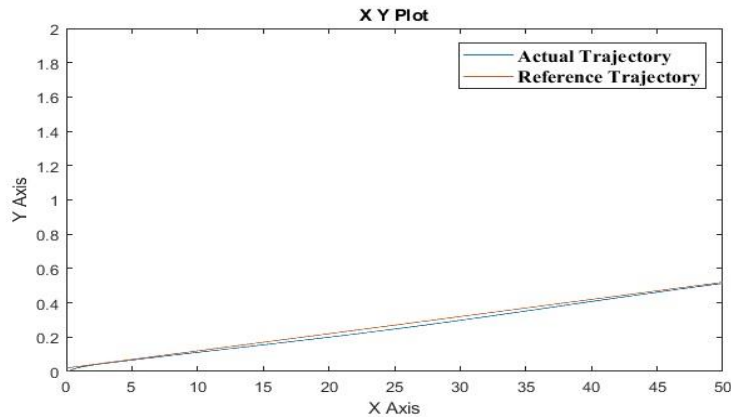
5.1. Case. 1

A straight line given by equation.

$$y = 0.02 + 0.02 * t \quad (9)$$

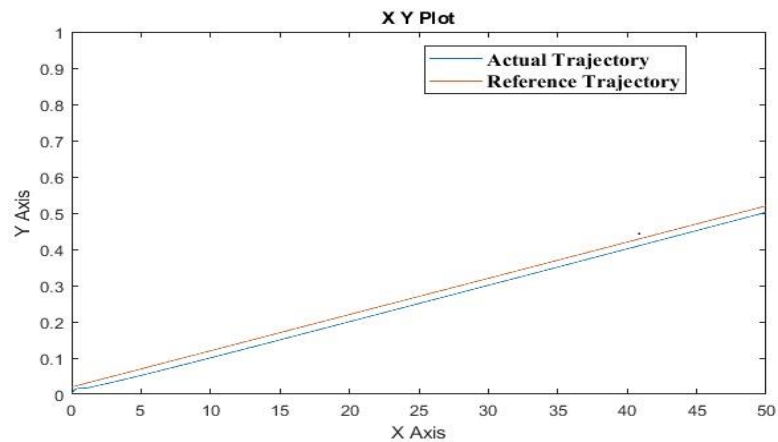
is considered as the reference trajectory. The objective is that the robot arm should track this trajectory with a minimum tracking error by applying minimum control. The neural network controller is trained using the reference trajectory. Figure 6 shows the tracking of straight-line trajectory by the NN model reference controller.

Figure 6. Trajectory tracking using NN Controller (Case 1)



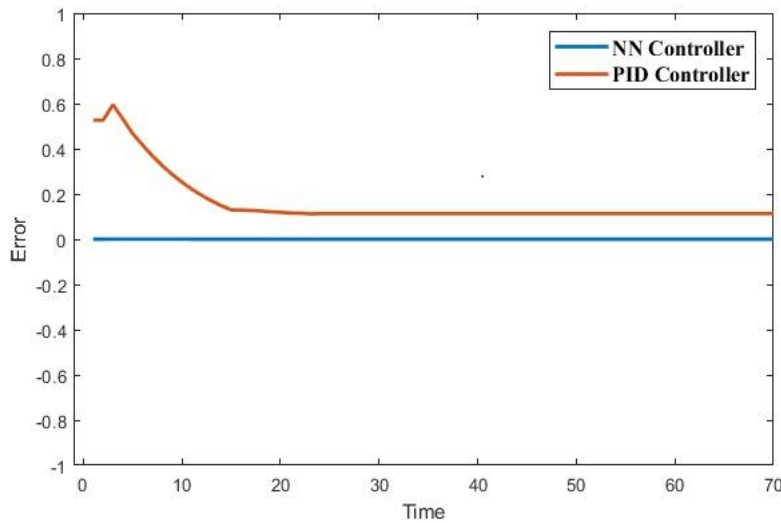
It shows that the robot arm is capable of following very close to the desired trajectory. However, the trajectory tracked by PID controller is not so close to the desired trajectory which can be observed from Figure 7. For this case, the PID parameters are chosen as $K_p = 12$, $K_d = 8$, $K_i = 5$.

Figure 7. Trajectory tracking using PID Controller (Case 1)



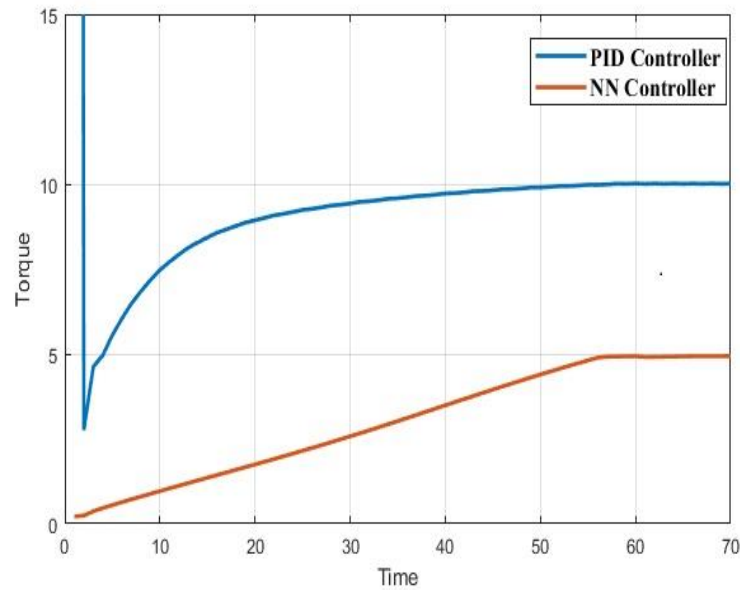
The error vs time plot shown in Figure 8 illustrates that the tracking error of the neural network controller is less than the error of the PID controller. The tracking error of the NN controller is very near to zero. The control signal u is plotted against time t , for both PID and neural network controller, which are shown in Figure9. It is obvious from the figure that the PID controller requires more torque. Also, at all instants of time, the torque requirement of the NN controller is less than that required for PID controller.

Figure 8. Time history of tracking error: comparison of controllers (Case 1)



Another achievement is that maximum torque requirement is also small for the NN controller. The total control effort in a PID controller is very large than the NN controller.

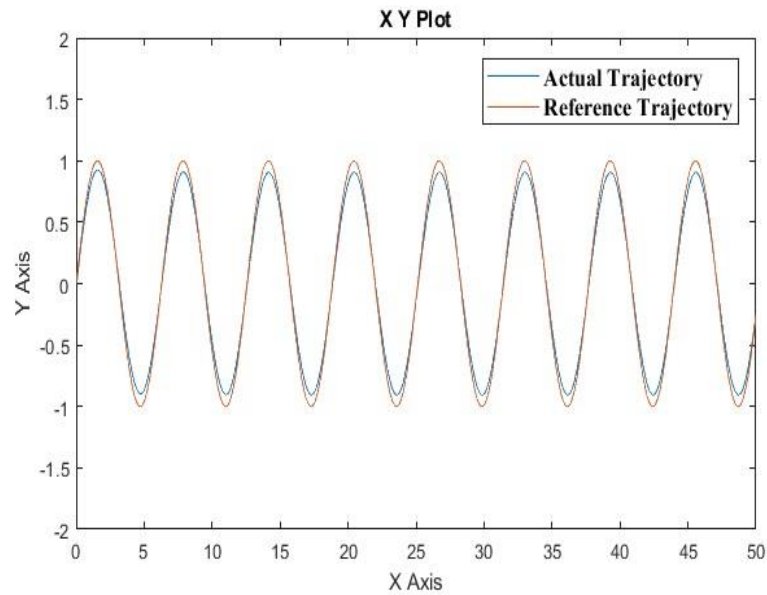
Figure 9. Time history of control input: comparison of controllers (Case 1)



5.2 Case. 2

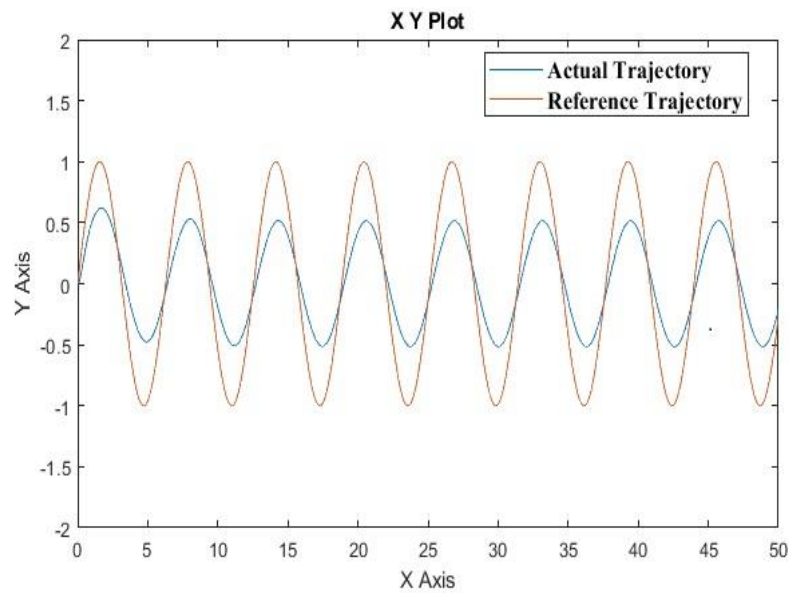
In practical applications, the robot arm hardly required to move in a sinusoidal path. For a theoretical interest and to illustrate the effectiveness of the NN controller, we considered a sinusoidal trajectory. The trajectory tracking plots with the NN controller and the PID controller are shown in Figure 10 and Figure 11.

Figure 10. Trajectory tracking using NN controller (Case 2)



The plots clearly illustrates that the NN controller gives a much smaller tracking error as compared to the PID controller. The K_p, K_d, K_i parameters of the PID are having the values 25, 8 and 15 respectively.

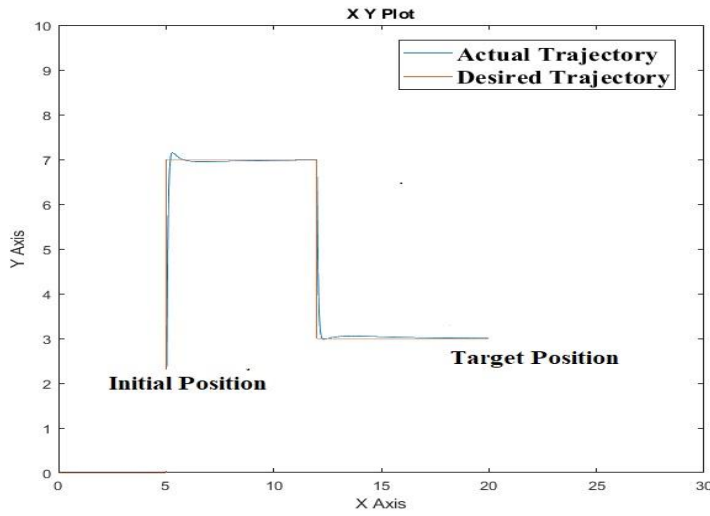
Figure 11. Trajectory tracking using PID controller (Case 2)



5.3. Case. 3

Consider a case where the objective of the robot arm is to pick an object from an initial position to a target position along a reference trajectory as shown in Figure 12.

Figure12. Trajectory tracking using NN controller (Case 3)



Simulations were done for both NN and PID controllers and the tracking trajectories are depicted in Figure12 and Figure13. The PID parameters were taken as $K_p = 53$, $K_d = 10$, $K_i = 25$.

Figure 13. Trajectory tracking using PID controller (Case 3)

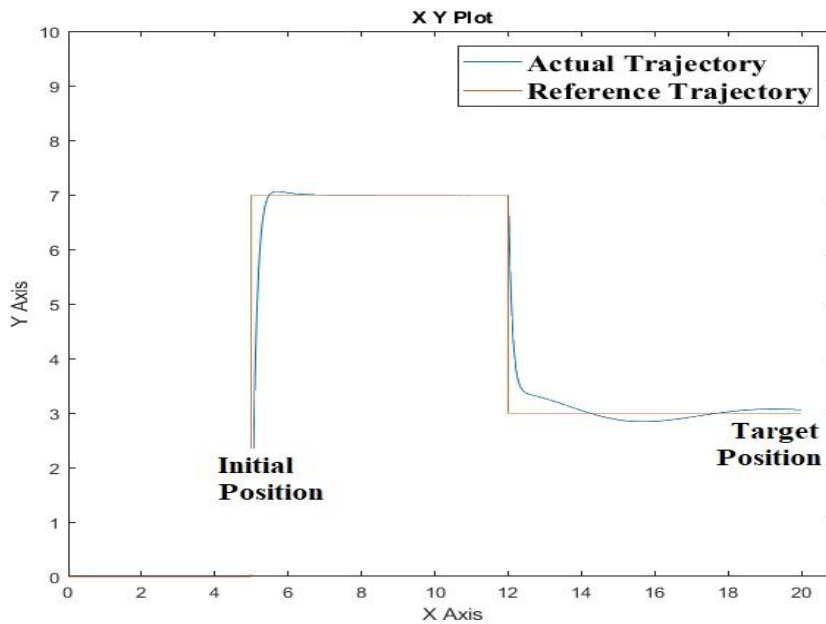


Table 1 shows the total control effort required by the two controllers for the three different cases. The table clearly illustrates that the NN based controller requires lesser control effort as compared to PID tracking controller

Table 1: Total control effort: Comparison of two controllers

	Case 1	Case 2	Case 3
NN controller	584.76	4.19×10^4	3.09×10^4
PID controller	3575.67	5.88×10^4	5.13×10^4

The simulation results illustrates that the neural network based model reference controller has more accuracy, requires less torque and minimum control effort. The robot dynamics is nonlinear and behaves in an unpredictable way. The adaptive property of neural networks make it very suitable for approximating any nonlinear dynamics and thus nullifying the effect of model uncertainties. Also, the controller is trained to adapt to all possible reference trajectories. Hence, the model reference NN controller is capable of tracking any desired trajectory with least tracking error. In addition, the NN controller minimizes the control input to the plant. The total control effort is also less with the NN controller.

6. Conclusion

This paper presented a neural network based model reference controller for trajectory control of robot arm. The proposed NN based controller consists of two neural networks, the plant model and the controller. First, the reference model is trained such that it can follow any reference trajectory and then the controller and reference model is trained for a number of different random reference trajectories such that the tracking error is very near to zero. The trained neural networks are connected to the plant. Simulations are done for three different cases for both proposed NN controller and conventional PID controller. The simulation results illustrated that, as compared to PID controller, the proposed method exhibited superior performances with respect to tracking error, total control effort, and maximum torque requirement.

References

- [1] Bingol, Mustafa Can, Zuhtu Hakan Akpolat, and Gonca Ozmen Koca. "Robust control of a robot arm using an optimized PID controller." *International Conference Mechatronics*. Springer, Cham, 2017.
- [2] Youns, Majed D., Salih M. Attya, and Abdulla I. Abdulla. "Position Control Of Robot Arm Using Genetic Algorithm Based PID Controller." *AL Rafdain Engineering Journal* 21.6 (2013): 19-30.
- [3] Guo, L. S., and Q. Zhang. "Adaptive trajectory control of a two DOF closed-chain robot." *Proceedings of the 2001 American Control Conference*. (Cat. No. 01CH37148). Vol. 1. IEEE, 2001.
- [4] Lin, Ming-Chang, and Jian-Shiang Chen. "Experiments toward MRAC design for linkage system." *Mechatronics* 6.8 (1996): 933-953.
- [5] Fan, Liu, and Er Meng Joo. "Linear and nonlinear PD-type control of robotic manipulators for trajectory tracking." *IEEE Conference on Industrial Electronics and Applications*, 2009.
- [6] Mohammed, Reham H., Fahmy Bendary, and Kamel Elserafi. "Trajectory tracking control for robot manipulator using fractional order-fuzzy- PID controller." *International Journal of Computer Applications* 134.15 (2016): 8887.

[7] Sinha, Abhinav, and Rajiv Kumar Mishra. "Smooth sliding mode controller design for robotic arm." *International Conference on Control, Automation, Robotics and Embedded Systems (CARE)*. IEEE, 2013.

[8] Boudoua, S., M. Hamerlain, and F. Hamerlain. "Intelligent twisting sliding mode controller using neural network for pneumatic artificial muscles robot arm." *2015 International Workshop on Recent Advances in Sliding Modes (RASM)*. IEEE.

[9] Parlak, i, M. N. A., E. M. Jafarov, and Y. 'Istefanopulos. "Design of robust PD-sliding mode controller for robot position systems with parameter perturbations." *IFAC Proceedings Volumes 36.7 (2003): 105- 110*.

[10] Su, Chun-Yi, and Yury Stepanenko. "Adaptive variable structure set point control of under actuated robots." *IEEE Transactions on Automatic Control 44.11 (1999): 2090-2093*.

[11] Bailey, Eric, and Aristotle Arapostathis. "Simple sliding mode control scheme applied to robot manipulators." *International journal of Control 45.4 (1987): 1197-1209*.

[12] Yeung, Kai S., and Yon P. Chen. "A new controller design for manipulators using the theory of variable structure systems." *IEEE Transactions on Automatic Control 33.2 (1988): 200-206*.

[13] Youcef-Toumi, Kamal, and Osamu Ito. "A time delay controller for systems with unknown dynamics." *Journal of dynamic systems, measurement, and control 112.1 (1990): 133-142*

Automated Plant Leaf Recognition using Combined Texture Features and Deep Learning based Classifiers

Shashank Yadav¹, Upendra Kumar^{*2}, Esha Tripathi³

¹ Research Scholar, Department of Computer Science & Engineering, Institute of Engineering and Technology Lucknow, 226021, India

² Assistant Professor, Department of Computer Science & Engineering, Institute of Engineering and Technology Lucknow, 226021, India

³ Research Scholar, Department of Computer Science & Engineering, Institute of Engineering and Technology Lucknow, 226021, India

shashankyadav48@gmail.com¹, upendra.ietlko@gmail.com², tripathi.asha@gmail.com³

Corresponding author*: Phone: +919415452072

Abstract

Plant recognition plays an important role in various applications used by environmental experts, chemists and botany experts. Human can recognize plants manually but it is a prolonged and low-efficiency process. This paper presents an automated system for identifying plant species based on leaf images. Automatic recognition of plants is useful for medicine, foodstuff, and reduction of chemical wastage during crop spraying. It is also useful for identification and preservation of species. A hybrid texture and colour based feature extraction method is applied on digital leaf images to produce robust feature after pre-processing the image. Thereafter a combination of machine learning methods, such as KNN (k-Nearest Neighbours), SVM (Support Vector Machine), and ANN (Artificial Neural Network) is applied on dataset for plant classification. This dataset contains 32 types of leaves. The outcomes of this work proved that success rate of plant recognition can be enhanced up to 94% with ANN classifier when both shape and colour features are utilized.

Keywords— *Plant Recognition, Support Vector Machines, k-Nearest Neighbour, Artificial Neural Network*

1. Introduction

Plants perform a significant role for maintaining the ecology system of the Earth. Recently, several plant species are at risk of extinction. However, automatic plant recognition is helpful for a multitude of sectors such as medicine, food, reducing chemical waste during crop spraying, as well as identifying and preserving species. It is therefore very important to design a plant safety database¹. For this the first step is to teach a computer how to classify plants. There are many types of species of plants approximately ranging from 220,000 to 420,00 and many ways for recognizing a plant by using flower, fruit, root, leaf etc., but due to mass availability of leaves almost in all seasons and also having higher number of distinct features such as colour, distinct appearance, and internal structures, can be better utilized to differentiate various plant species^{2,3}. Many researchers have worked on classification of plant species using leaf based features and machine learning methods.

Studies on various databases belonging to plant species are available in the literature. Among those, it has been identified that the Flavia leaf database was the most frequently used dataset, although other set of leaf databases were also used by some researchers. Therefore Flavia leaf database is used in this work for the recognition of plant leaves. Generally three features are used to estimate the class of plant species, which can be used separately such as shape based descriptor, intrinsic texture feature based histogram, and a fine-scale margin histogram. Thereafter, these features can be combined to identify the class of plant species.

Satti et al. (2013)² proposed a technique for the plant identification by using leaves digital images. They preferred the features of leaves in place of flowers, fruits, root, stem etc. There are many openly available leaf image datasets such as Flavia dataset, Leafsnap dataset, Intelengine dataset, Image CLEF dataset and many others but in this work Flavia dataset was used. The proposed methodology contains three steps: preprocessing step, extraction of features and classifying the objects. The preprocessing technique is to enhance data images before feature extraction. The features were utilized as the classifier inputs for proper classifying the objects. Thereafter, the

outputs were confirmed and compared by using ANN and Euclidean KNN classifier. The neural network was accomplished with 1907 sample leaves which are related to 33 different plant species extracted from Flavia database. The performance of the proposed technique showed 93.3% accuracy by using ANN classifier.

The research suggested by ArunPriya et al. (2012)⁴, contained three stages. First was preprocessing in which gray scale transforming and enhancement of boundary was performed. Second one was feature extraction in which the standard DMF was derived from five basic features and then for recognizing the leaf Support Vector Machine (SVM) classification technique was used. In the research, twelve leaf features were used, that were identified after then orthogonalized into five principal variables. For SVM, these variables were used as input data.

According to Kadir et al. (2011)⁵, generally the authors did not include colour feature, because colour was not recognized as a key feature to the recognition of leaves. They used features like shape, vein, colour, and texture to classify a leaf. In this research, a neural network called Probabilistic Neural network (PNN) was implemented for classification. Their result gave average accuracy of 93.75% on Flavia dataset that contains 32 kinds of plant leaves.

This current research applied different classification techniques (KNN, SVM, ANN) on Flavia leaf database, and found that the accuracy percentage of ANN is very high i.e. 93.95 %.

2. Materials and Methods

2.1. Preprocessing steps

2.1.1. RGB image to gray image conversion

Scanners or digital cameras are used to acquire the leaf images. The image format is JPG and images of all leaves are in 640 x 480 resolutions. The orientation of leaves can be in any direction while acquiring images. First of all an RGB image is converted into a grayscale image. The equation (1) describes a formula that is used to transform a pixel's RGB value into grayscale value¹.

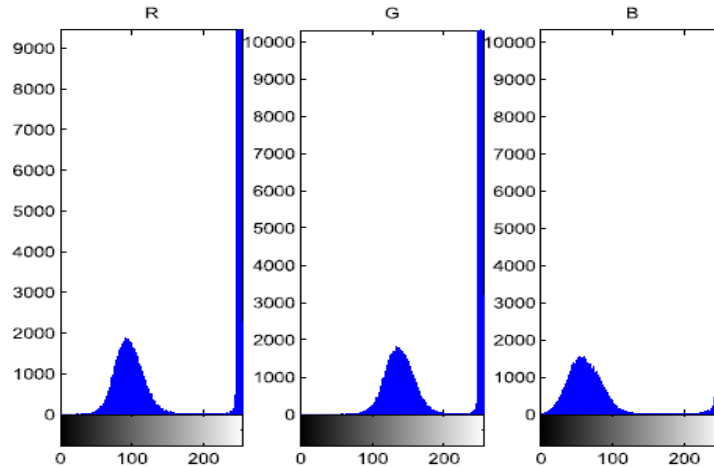
$$\text{gray} = 0.2989 * R + 0.5870 * G + 0.1140 * B \quad (1)$$

where R, G, B related to the colour components of the pixel.

2.1.2. Gray scale image to binary image conversion

For converting grayscale image into binary image, the level is identified according to the RGB histogram¹. The pixel values corresponding to R, G, B components of leaf images were accumulated for 1600 different leaves to construct the histogram. Each colour histogram contains two peaks shown in figure 1. The left peak shows those pixels which contain leaf part (object), and the right peak shows those pixels which contain white background part. The lowest point between two peaks is 240 approximately as an average. Therefore the level 0.94 (240/255=0.941) is selected.

Figure 1: RGB histogram of leaf

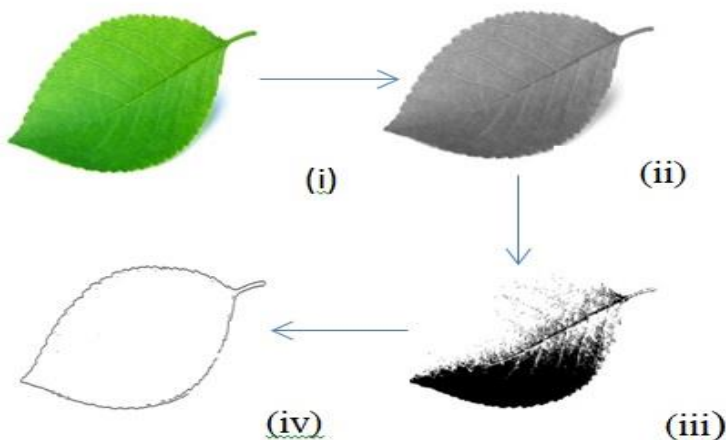


All pixels presented in the input image (with luminance higher than the level by the value one) are replaced by output image and restored all other pixels with value zero. To filter noises, a rectangular averaging filter of size 3×3 is used. Therefore pixel values are 0 or 1 as a rounded value.

2.1.3 Improvement of boundary

The first thing that appears in the mind when mentioning the shape of the leaf might be the margin of a leaf¹. So the next step is convolving the image with the Canny Edge Detection. Canny edge detection is a method for extracting structural information from various visual objects and it helps in reducing the quantity of data in order to process it easily. Generally, this method has been used in various computer vision based applications^{6,8}. Similar kind of method can also be applied in our dataset to improve the boundary of image. Figure 2 shows the steps of pre-processing of leaf images used in this work.

Figure 2: Pre-processing steps
 (i) Input image, (ii) Gray scale image,
 (iii) Binary image (iv) Contour extraction.



2.2.Extraction of features

2.2.1.Fundamental features of Geometry

- **Diameter:** The longest distance between any two points is defined as diameter on the boundary of the leaf. Letter D is used to denote the diameter.
- **Area of Leaf:** The area of leaf is calculating by numbering of pixels whose binary value is 1 on flatter leaf image. Letter A is used to denote the area of leaf.
- **Perimeter of Leaf:** By counting the number of pixels available on leaf margin, the perimeter of leaf can be calculated. Letter P is used to denote the perimeter of leaf.
- **Physiological Length of leaf:** For calculating the physiological length of leaf, human requires to indicate the two ends of the leaf main vein by mouse clicking. The length is described as the distance between the two ends. LP is used to denote the physiological length.
- **Physiological Width of leaf:** This width can be calculated by drawing a line which passes through the two ends of the main vein such that infinite lines can be plotted perpendicular to that line¹. The largest distance between points of intersection pairs is considered as the physiological width. Wp is used to denote the physiological width. Due to being discrete the coordinates of pixels the research considers two lines that are perpendicular if their degree is $90^\circ \pm 0.5^\circ$

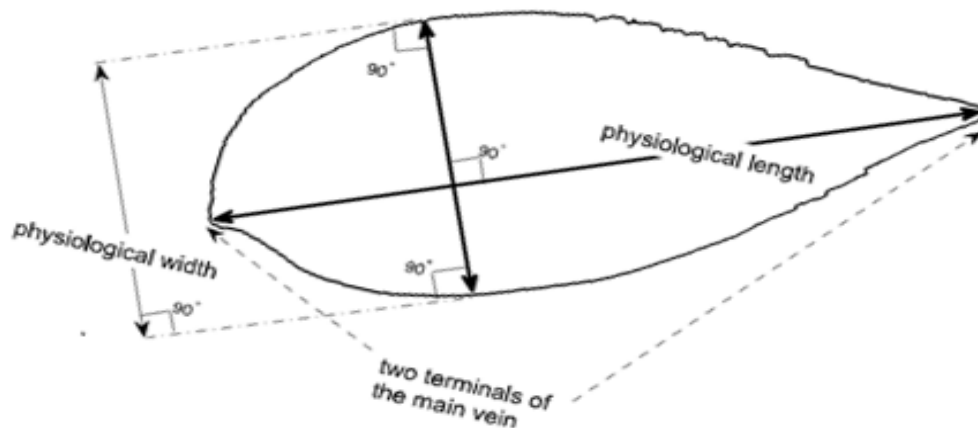


Figure 3: *Physiological length and physiological width relationship*

2.2.2.Digital morphological feature

- **Aspect ratio of length and width:**The ratio of Lp (physiological length) to Wp (physiological width) i.e. Lp/Wp is considered as aspect ratio.
- **Perimeter ratio of diameter:**The ratio of perimeter to diameter is denoted by the ratio of leaf perimeter P and leaf diameter D i.e. P/D .
- **Perimeter ratio of physiological length & physiological width:**The ratio of P (leaf perimeter) and the addition of Lp (physiological length) and Wp (physiological width) i.e. $P/(Lp + Wp)$ is considered as perimeter ratio of physiological length and physiological width.
- **Form factor:** The form factor is utilized to define the variance between a circle and a leaf. It is declared as $4\pi A/P^2$, where A belongs to the leaf area and P belongs to the perimeter of the leaf margin.
- **Rectangularity:** The resemblance between a leaf and a rectangle is declared as rectangularity. It is calculated by the formula $LpWp/A$, where Lp belongs to the physiological length, Wp belongs to the physiological width and A belongs to the leaf area.

- **Narrow factor:** The ratio of the D (diameter) and Lp (physiological length) i.e. D/Lp is declared as narrow factor.
- **Irregularity:** A characteristics i.e. irregularity (dispersion)⁵ to handle with an irregular shaped object e.g. the leaf. This feature is defined as:

$$Dispersion = \frac{\max\left(\sqrt{(x_i - \bar{x})^2 + (y_i - \bar{y})^2}\right)}{\min\left(\sqrt{(x_i - \bar{x})^2 + (y_i - \bar{y})^2}\right)} \quad (2)$$

Where (\bar{x}, \bar{y}) belongs to leaf centroid, and (x_i, y_i) is the pixel coordinate in the leaf outline. The above Eq.2 is used for calculation the ratio between radius of the maximum circle that covers the region and minimum circle that can be contained inside the region. Therefore, value of dispersion will increase as the size of region expands. But the dispersion has a few limitations that is unaffected with small discontinuity occurs in shape, for example a leaf with crack.

2.2.3 Colour features

Colour moments signify colour features to describe a colour image. The characteristics which can be considered are standard deviation, mean, kurtosis, and skewness. Three characteristics are extracted from each plane R, G, and B for RGB colour space^{5,7}. The following formulas are used to define these characteristics.

$$Mean \mu = \frac{1}{PQ} \sum_{x=1}^P \sum_{y=1}^Q M_{xy} \quad (3)$$

$$Standard \ Deviation \ \sigma = \sqrt{\frac{\sum_{x=1}^P \sum_{y=1}^Q (M_{xy} - \mu)^2}{PQ}} \quad (4)$$

$$Skewness \ \theta = \frac{\sum_{x=1}^P \sum_{y=1}^Q (M_{xy} - \mu)^3}{PQ\sigma^3} \quad (5)$$

$$Kurtosis \ \gamma = \frac{\sum_{x=1}^P \sum_{y=1}^Q (M_{xy} - \mu)^4}{PQ\sigma^4} \quad (6)$$

Where P, Q are the dimension of image. Mxy is colour values on columns xth and row yth.

2.3.Support Vector Machine

Supporting vector machines (SVMs) in machine learning are supervised learning models that investigate information which is utilized for classification. Given a collection of training examples, each example marked as closeness to one or the other categories, an SVM training method creates a model that allocates new instances to one category or the other. This SVM model¹² is used for representing the examples of space points, and plotted to divide the separate category examples by a clear gap. That gap should be as wide as possible. New instances are then mapped into the same space, predicting that they belong to a class based on which side of the gap they fall.

In a high or infinite-dimensional space, a support vector machine creates a hyperplane or set of hyperplanes. SVM can be utilized for regression, classification, or other tasks for example outliers detection. Instinctively, a good separation can be achieved by the hyperplane which has the longest distance to the nearby training data point of any class. For the less generalization error of the classifier, margin should be larger.

2.4. k-Nearest Neighbour Algorithm

The k-nearest neighbour algorithm (KNN)¹¹ is used for classification as well as regression. It is a non-parametric process in pattern recognition. The inputs which are used for KNN consists of k training examples in the feature space. The output relies on whether the classification uses KNN.

In the KNN classification the outcome is the membership of the class. An object is categorized by its neighbour’s majority vote with the most prevalent class among its k nearest neighbours. k is a positive integer which is typically small. If k= 1, the object is simply allocated to the single nearest neighbour’s class. It is a learning algorithm of instance-based or lazy learning, where the purpose is only locally approximated and all other working is suspended until classification. The simplest machine learning algorithm is the KNN algorithm.

2.5. Artificial Neural Network

Artificial neural networks (ANNs) are the systems for computing, which are nearly motivated by the biological neural networks which compose brains of animal⁹. These types of systems learn to execute processes by taking examples, normally without programming with any process-specific instructions. An ANN is considered as a group of linked units or nodes which are called artificial neurons. These artificial neurons are assumed as the neurons in a biological brain. Every connection can convey a signal from one neuron to another neuron. An artificial neuron which is receiving a signal, that neuron can execute it and then send signal to additional neurons which are connected to it. The main aim of the ANN process is to resolve difficulties in the same manner that a human brain would.

Normally, in the implementation of ANN, signal present in a connection among artificial neurons (edges) is real number, and outcome of every neuron is evaluated with the help of non-linear function which is the sum of input neurons. The model used for classification has four layers i.e. first input layer, first hidden layer, second hidden layer and fourth layer (output layer). Numbers of neurons are contained by input layer equal to size of feature vector. First hidden layer contains 768 neurons (number of classes ×size of feature vector), second hidden layer contains 32 neurons. Output layer contains 32 neurons, the output produced in the form of vector with binary values of size equal to total number of classes. Total 32 types of plant leaves were used in this work, so the number of classes is 32.

3. Results and Discussion

To examine our proposed model, Flavia dataset¹⁰ was used. This dataset comprises 32 types of leaf species and each has minimum 50 digital images. In first set of results, 40 images were used for training the network model and remaining 10 were used for testing. Similarly in second set of results, 30 images were used for training the network and remaining 20 were used for testing.

In this work, a variety of test dataset was experimented from the Flaviadatabase using KNN, SVM and ANN. The results from the data sets via different classifier are with respect to its ratio of training vs. testing sets per species.

Result Set-I

Table 1: Accuracy results for various classifiers with digital morphological features.

Classifier model	Accuracy	Accuracy
	Trainingvstesting ratio(40/10)	Trainingvstesting ratio(30/20)
KNN(k=3)	71.87%	70.47%
KNN(k=5)	65%	68.75%
SVM	81.25%	72.66%
ANN	93.94%	93.94%

Result Set-II

Table 2:Accuracy results for various classifiers with hybrid of digital morphological and colour features.

Classifier Model	Accuracy	Accuracy
	Trainingvs testing ratio(40/10)	Trainingvs testing ratio(30/20)
KNN(k=3)	72.66%	70.47%
KNN(k=5)	65%	68.75%
SVM	83.75%	72.66%
ANN	93.95%	93.94%

As shown in the table, combination of physical Feature, colour (with kurtosis), mean and standard deviation provides the best outcome with effectiveness of 94%. According to the results all types of characteristics have significant role. The ANN classifier is the most efficient of them all. In case of hybrid feature set, corresponding accuracy of different classifiers produced better results than the model using only morphological features.

4. Conclusion

By using the proposed methodology in this work, the automated system can categorize automatically 32 types of plants by using leaf images from the flavia dataset. A variety of machine learning classifiers i.e ANN, kNN and SVM were used for training the model. Before classification a hybrid texture features (a combination of 13 different features) were extracted from input data. The experimental outcome points out that around 94% accuracy can be achieved by using this method. The outcome is more effective than the work done in various existing literatures. Observing the classification accuracy, the proposed methodology is comparatively better than other methods, which in turn is fast during execution, effective in identifying and simple while implementing.

References

[1] Wu SG, Bao FS, Xu EY, Wang YX, Chang YF, Xiang QL. A Leaf Recognition Algorithm for Plant Classification Using Probabilistic Neural Network. *arXiv:0707.4289v1 [cs.AI]*, 2007 July; 1-6.

[2] Satti V, Satya A, Sharma S. An automatic leaf recognition system for plant identification using machine vision technology. *International Journal of Engineering Science and Technology (IJEST)*. 2013 April; 5(4), 874-879.

[3] Chaki J, Parekh R. Plant Leaf Recognition using Shape based Features and Neural Network classifiers. (*IJACSA*) *International Journal of Advanced Computer Science and Applications*. 2011; 2(10), 41-47.

[4] ArunPriya C, Balasaravanan T, Antony ST. An Efficient Leaf Recognition Algorithm for Plant Classification Using Support Vector Machine. *Proceedings of the International Conference on Pattern Recognition, Informatics and Medical Engineering*. 2012 March; 428-432.

[5] Kadir A, Nugroho LE, Susanto A, Insap P, Santosa PI. Leaf Classification Using Shape, Color, and Texture Features. *International Journal of Computer Trends & Technology*. 2011 July to August; 225-230.

[6] Vijayashree T, Gopal A. Authentication of Leaf Image Using Image Processing Technique. *ARNP Journal of Engineering and Applied Sciences*. 2015 May; 10(9), 4287-4291.

[7] Turkoglu M, Hanbay D. Recognition of plant leaves: An approach with hybrid features produced by dividing leaf images into two and four parts. *Applied Mathematics and Computation*. 2019; 1-14.

[8] Jeon WS, Rhee SY. Plant Leaf Recognition Using a Convolution Neural Network. ***International Journal of Fuzzy Logic and Intelligent Systems***. 2017 March; 17(1) 26-34

[9] Zhu X, Zhu M, Ren H. Method of plant leaf recognition based on improved deep convolutional neural network. ***Elsevier (Cognitive Systems Research)***. 2018; 223–233.

[10] Flavia. <http://flavia.sourceforge.net>. Date accessed: 15/04/2019

[11] Nearest Neighbour. <http://scikit-learn.org/stable/modules/neighbors.html#nearest-neighbor-algorithms>. Date accessed: 15/04/2019

[12] Support Vector Machine. <http://scikit-learn.org/stable/modules/svm.html#svr>. Date accessed: 15/04/2019

GC-SAW and GC-FID Performance Comparison for Fast Analysis of Volatile Organic Compounds

Jitender Kumar¹, Vinod Kumar², Vinay Kumar Singh*³, U. Mittal¹, Fahim¹, Devendra S Barlewar¹,
A. T. Nimal¹

¹ Solid State Physics Laboratory, Delhi-110054, India

² Department of Chemistry, Kirori Mal College, University of Delhi, Delhi-110007, India

³ Department of Chemistry, Sri Aurobindo College, University of Delhi, Delhi-110017, India

jitender.tilwalia@gmail.com¹, vinod7674@gmail.com²,

vinayksdu@gmail.com³, upendra_mittal@yahoo.co.in¹, fahimdurani1@gmail.com¹, devendra@sspl.drdo.in¹, atnimal@yahoo.com¹

Corresponding author*: vinayksdu@gmail.com

Abstract

Background/Objectives: This work was initiated for the development of gas chromatograph (GC) based chemical agent detector and compares the response of Surface Acoustic wave (SAW) detector with Flame Ionization Detector (FID) for the development of a reliable and fast vapour analyzer.

Methods/Statistical analysis: An uncoated 433.92 MHz SAW device was used as Gas Chromatography (GC) detector and its response was compared with conventional FID detector. The response of the detectors was analyzed by using standard mixture of seven Volatile Organic Compounds or Toxic Industrial Chemicals (VOCs/TICs). Besides this comparison various key parameter of GC i.e. Flow, temperature and length of GC column were optimized for fast GC. **Findings:** After analyzing the data of both the detectors, it was observed that the resolution of chromatograms with SAW detector showed more resolved peaks as compare to the FID detector for the same GC parameters.

Improvements/Applications: It is concluded that the SAW detector is more suitable technology for fast and reliable analysis of chemical vapors.

Keywords: Capillary column, Detector, GC, SAW, TICs, VOCs.

1. Introduction

Surface Acoustic Wave (SAW) device used in 1979 first time as gas sensing and in 1964 as detector^{1,2}. Gas chromatograph is a technique which is used for the analysis of organic volatile compounds by using various detectors. In literature researcher optimized the various parameters for development fast gas chromatography^{3,4,5,6,7}. The sensitivity and resolution are the key parameter of any gas chromatography-based system. Mostly in the analysis and identification in field scenario, the combinations of these techniques with selective or non-selective detectors are used for the detection of chemicals. The Flame ionization (FID), Thermal conductivity (TCD), photo-ionization (PID) etc., are non-selective detectors whereas nitrogen phosphorous (NPD), electron capture (ECD), or mass (MS) are selective detectors (Table 1)^{3,4,8,9}.

Table: 1 Major detector for gas chromatography

Parameter	FID	NPD	FPD	MS	ECD	SAW
Sensitivity(g/s)	2×10^{-12}	2×10^{-13}	1×10^{-12}	1×10^{-9}	5×10^{-14}	1×10^{-15}
Dynamic Range	1×10^7	1×10^5	1×10^5	1×10^6	1×10^2	1×10^7
Selectivity	No	Yes	Yes	Yes	Yes	No

SAW detector used as Non-selective GC detector, which shows the linear response towards the mass change over the surface of the detector^{10,11}. To the best of our knowledge and literature the resolution study has not been done earlier. In this paper we are presenting, how the resolution of detector is affected with variation of gas chromatograph parameters. Different detector needs different types of gases for the operation as per the detector requirement. The FID needs Hydrogen and Zero Air in the ratio of 1:10. However the SAW detector does not require specific gases for the operation.

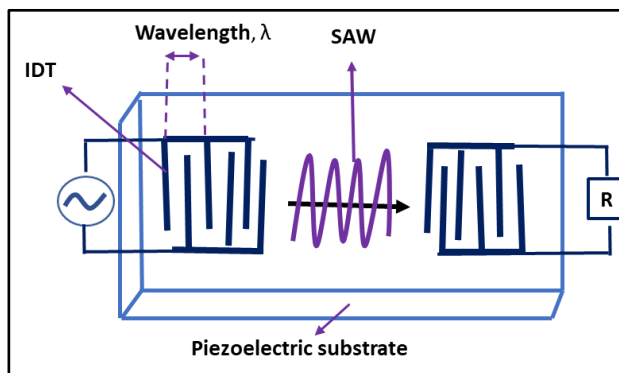
2. SAW detector operation

A SAW device consists of a piezoelectric substrate with two transducers called inter digital transducers (IDT) input and output IDTs. On applying the RF signal on input IDTs, it generates the surface acoustic wave on the surface of device and vice versa happened on the output IDT. (Figure1)^{9,12,13,14}. It works on the principle of mass loading, when the vapour molecules are eluted from the capillary column and adsorbed on the surface of detector hence SAW velocity changes and it reflected as the change in resonance frequency of SAW detector. This relationship had been represented by Sauerbrey equation (1)^{15,16}.

$$\Delta f = - \frac{2f_0^2}{A\sqrt{\rho_q\mu_q}} \Delta m \tag{1}$$

Where Δf -frequency change, f_0 - resonant frequency, Δm - mass change (g), A - active crystal area, ρ_q - density of substrate material and μ_q - Shear modulus of substrate.

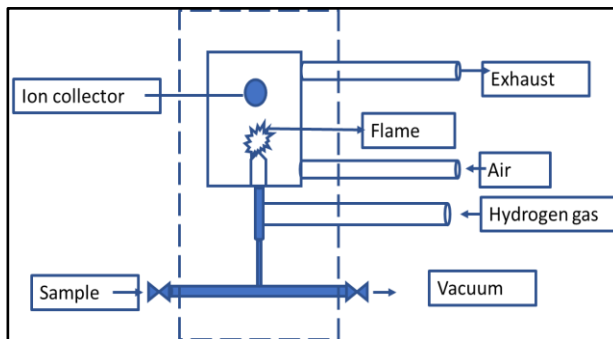
Figure 1. Schematic of SAW device



3. FID detector operation

The FID operation is based upon the ions which were formed during the combustion of organic compounds in the flame of hydrogen. The response of the detector is based on the concentration of ions in the gas sample^{17,18}. Schematic is shown in Figure 2.

Figure 2. Schematic of FID



For FID detector operation, a high temperature and fuel gases (mixture of hydrogen and zero air gas) are required.

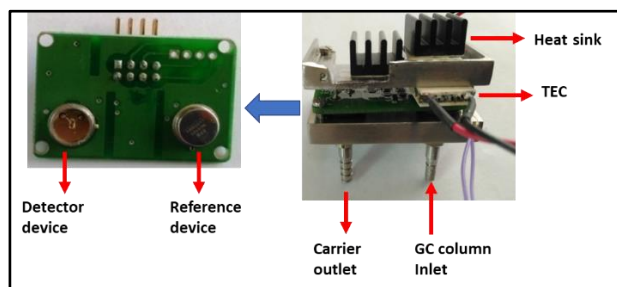
In Gas Chromatograph technique separates the mixture of different compounds between mobile and stationary phase of capillary column over a period called retention time and time-resolved chemical spectra known as chromatogram. Different chemical constituents of the sample travel through the column at different rates depending upon their physical and chemical properties, the interaction of sample will be different with the phases (mobile and stationary). In order to achieve, the non-overlapping peaks of compounds the GC parameters i.e. length of column, flow of carrier gas, temperature etc. has to be optimized. The eluted vapors of samples from the column are detected by Detector^{8,9}.

4. Experimental

For performing the experimental work, a conventional GC with FID detector (Make chemito-1000) system was used. A 433.92 MHz one-port SAW oscillator used as a detector (Figure 3) which have two identical SAW device, one act as detector and another as a reference. A small Thermoelectric cooler (TEC)(Size - 12.3×12.3 mm, (make Laird Technologies, part No. 177-1753) used to maintain the SAW detector temperature at room temperature. The temperature of assembled SAW detector is measured by PT1000 RTD. The SAW detector enclosure assembly is shown in Figure3. The detector cell has the provision for connecting the capillary column to the SAW detector (Figure 3). It has been designed specifically for exposing only one SAW device. Thedetector response of SAW detector is considered in terms of frequency shift.

For entire experiment Rtx-200 narrow bore capillary column was used with 0.2µl sample. The injector port was kept at 130°C. A standard mixture was prepared by mixing the entire 7 analytical grade VOCs in equal ratio.

Figure3. SAW detector

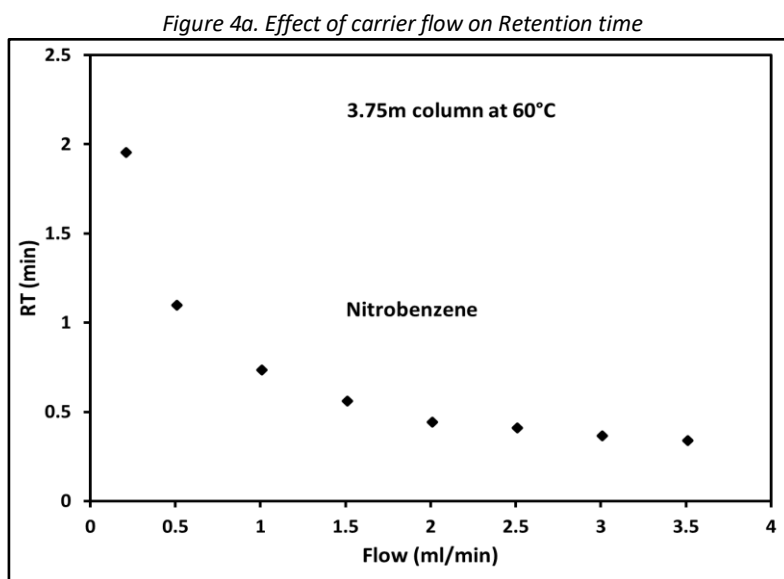


The responses of both detectors were recorded at various parameters of GC. Initially 30m, 15m, 7m, and 3.75m meters capillary column were used at various oven temperature and carrier flow rate using FID detector. Since the

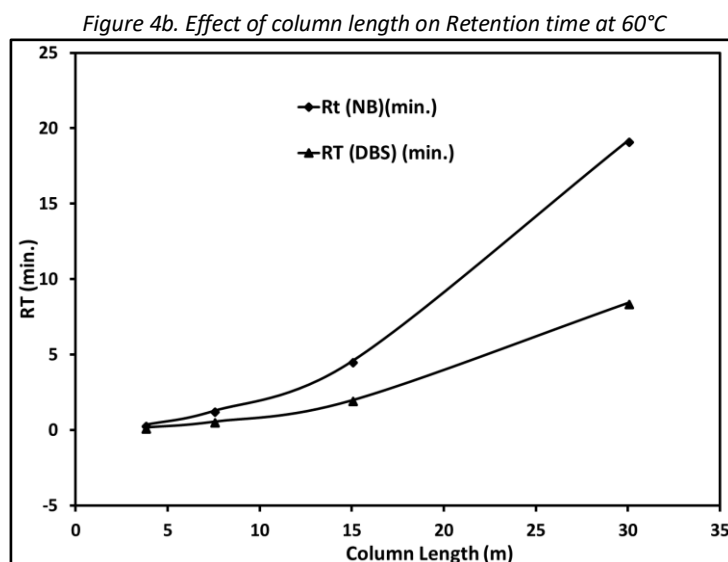
chromatogram with 7m column was well resolved whereas the chromatogram became unresolved at 3.75m. Therefore the 3.75m column was selected for comparing the chromatogram of mixture of compounds with SAW and FID detector.

5.Result and Discussion

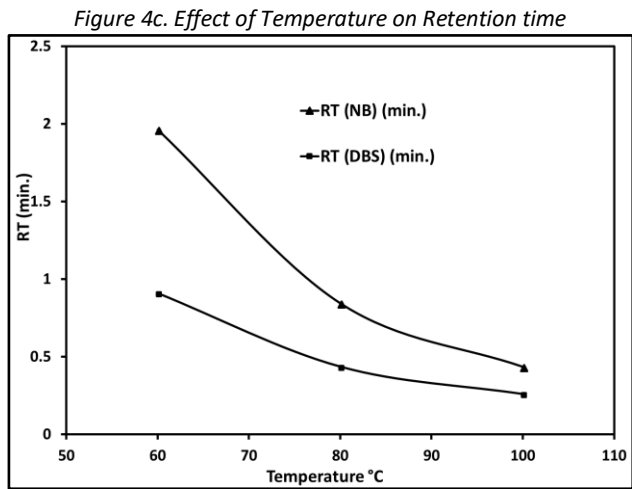
A mixture of seven compounds (Methanol, Toluene, Xylene, Dimethylformamide, 1,5-Dichloropentane, Dibutyl sulfide and Nitrobenzene) were used for the injection in conventional GC system with FID detector as well as SAW detector. The responses of both the detectors were measured with different parameters of GC system. The retention time of nitrobenzene was recorded with different flow rate of the carrier gas (nitrogen gas) and found that at higher flow rate of carrier gas the resolution of chromatogram decreases (Figure 4a).



Similarly, at 60°C the Nitrobenzene (NB) and Dibutyl sulfide (DBS) response was recorded at various length of the capillary column and found that the retention time drastically reduced with decreasing the length of capillary column (Figure 4b).



The same mixture of seven compounds were also injected to the injector port and recorded the at different temperature. The resolution/retention time of the chromatogram reduced with higher the temperature of the oven (Figure 4c).

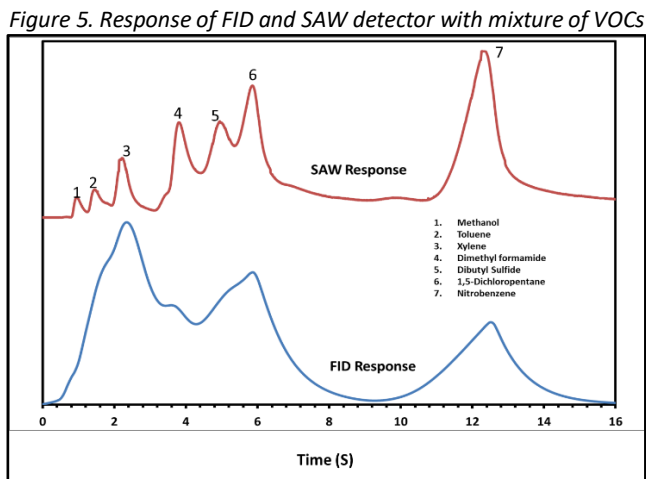


As per the analysis of the data it was observed that the resolution is critically dependent on three key parameter of GC i.e flow rate of carrier, Temperature of oven and length of capillary column. It was also observed that the resolution of chromatogram of mixture of seven VOCs with FID at 60°C and with reduced length of column (3.75m) were less resolved as compared to the SAW detector.

As per the result it has been observed that the chromatogram with SAW detector is more resolved, less tailing and sharp peaks. However, the FID operates at higher temperature and it gives the less resolution and less sharp peaks (for same GC parameters) due to slow response time as compare to the SAW detector. Therefore, the following could be the possible reason for higher resolution of SAW detector as compared to the FID (figure 5):

1. Low active area on the surface of the uncoated SAW detector
2. Fast adsorption and desorption of eluted compounds
3. Low operating temperature

Therefore, the SAW technology can be used for the fast analysis of VOCs.



6. Conclusion

This paper describes the comparative study for Fast GC using FID and SAW detector. Both the detectors are capable of detecting of organic compounds in vapour phase. Due to the rugged and smaller size of the SAW detector, it can be used for the development of portable chemical detection system and does not require specific gases for its operation. As compared to the FID, SAW detector can resolve more no. of compounds within specified time.

7. Acknowledgment

Authors are thankful to Dr. Seema Vinayak, Director SSPL- DRDO, for her continuous support. Authors are also thankful to Pooja Rajput, Pallav Tripathi, Milap Singh, Sanjay and Chandani Kumari of SAW Group at SSPL for their support and patronage.

References

- [1] W. H. King, Jr, Piezoelectric sorption detector, *Analytical Chemistry* 36 (9) (1964) 1735–1739.
- [2] Wohltjen H, Dessy R. Surface acoustic wave probe for chemical analysis II Gas Chromatography detector. *Analytical Chemistry*. 1979 August;51 (9) ,1465–1477.
- [3] Bartelt-Hunt S L, Knappe R U, Morton A B. A Review of chemical warfare agent simulants for the study of environmental behavior. *Critical Reviews in Environmental Science and Technology*. 2008 January;38,112–136.
- [4] Faricha A, Suwito, Rivai M, Nanda M A, Purwanto D, Rizki Anhar R P. Design of electronic nose system using gas chromatography principle and surface acoustic wave sensor. *Telkomnika* .2018 August;16 (4), 1458-1467.
- [5] Watson G W, Staples E J. SAW resonators as vapor sensors. *IEEE Symposium on Ultrasonics*. 1990, 311–314.
- [6] Watson G W, Horton W, Staples E J. Gas chromatography utilizing SAW sensors. *Proceeding Ultrasonics Symposium*. 1991,305–309.
- [7] Staples E J, Matsuda T, Viswanathan S. Real time environmental screening of air, water and soil matrices using a novel field portable GC/SAW system. *Proceeding Environmental Strategies for the 21st Century Asia Pacific Conference Singapore* .1998, 8–10.
- [8] Popiel S. Chemical warfare agents: GC analysis, *Encyclopedia of Chromatography*.(Third edition 1): 2009, 1, 396-402.
- [9] Berezkin V G, Drugov V G. Detectors for the gas chromatographic determination of Impurities. *Journal of Chromatography Library* .1991 ;49,25-34.
- [10] Faricha A, Suwito, Rivai M, Nanda M A, Purwanto D, Rizki Anhar R P. Design of electronic nose system using gas chromatography principle and surface acoustic wave sensor. *Telkomnika* .2018 August; 16 (4), 1458-1467.
- [11] Watson G W, Staples E J. SAW resonators as vapor sensors. *IEEE Symposium on Ultrasonics*. 1990, 311–314.
- [12] Slobodnik A J. Surface acoustic waves and SAW materials. *Proceeding IEEE*. 1976, 581-595.
- [13] Mittal U, Islam T, Nimal A T, Sharma M U. Fabrication of high frequency surface acoustic wave (saw) devices for real time detection of highly toxic chemical vapors. *International Journal on Smart Sensing and Intelligent Systems*. 2015 September; 8 (3) ,1601-1623.
- [14] Fahim, Mainuddin, Mittal U, Kumar J, Nimal A T, Sharma M U. Single chip readout electronics for SAW based gas sensor systems. *IEEE Conferences*,2017, 1-3.
- [15] Sauerbrey G. The use of quartz crystal oscillators for weighing thin layers and for micro weighing applications. *Z Physics*.1959;155,206-222.
- [16] Liu J, Lu Y. Response mechanism for surface acoustic wave gas sensors based on surface-adsorption. *Sensors*. 2014 April;14(4),6844-6853.
- [17] Dewulf J, Langenhove H V. Analysis of volatile organic compounds using gas chromatography. *Trends in Analytical Chemistry*.2002; 21, 637-646.
- [18] Zhu X, Sun J, Ning Z, Zhang Y, Liu J. High performance mini-gas chromatography-flame ionization detector system based on micro gas chromatography column. *Review Of Scientific Instruments* .2016;87, 1-4.

Passive SAW Temperature Sensor for Remote Applications

Fahim*¹, Mainuddin², Upendra Mittal¹, Devendra Barlewar¹, Jitender Kumar¹, A.T.nimal¹

¹*Solid State Physics Laboratory, Delhi-54, India*

²*Department of Electronics and Communication Engineering, Jamia Millia Islamia University, Delhi-25, India*
fahimdurani@yahoo.com, mainuddin@jmi.ac.in

Abstract

Background/Objectives: This paper presents the realization of a wireless Surface Acoustic Wave (SAW) temperature sensor for moving or rotating parts like fast rotating engine of fighter jets, hazardous environments like chemically contaminated chambers of high voltage areas, embedded areas like tyres and concrete.

Methods/Statistical analysis: SAW temperature sensors are fabricated on a piezoelectric crystal substrate using IC planar technology. The velocity of SAW is influenced by the temperature of substrate and is exploited for sensing applications. The substrate material and crystal cut determine the sensitivity and temperature range. SAW temperature sensors are known to be very sensitive, linear, fast and reliable.

Passive SAW sensors operate without on-board power supply using a dedicated readout unit. The readout unit transmits interrogation signal to the sensor tag which receives and re-transmits it with temperature modified value.

Findings: In this paper, 434 MHz quartz one port resonator SAW device was developed. A meander line dipole antenna was designed and connected with SAW device. SAW sensor along with antenna forms a sensor tag which can be fixed on any platform for which temperature is to be measured. An interrogator unit was designed and implemented using a transceiver IC and FPGA. The sensor system was tested on test bed and it performed stable temperature readout.

Keywords: SAW, temperaturesensor, passive operation, antenna, wirelesssensing, interrogator.

1. Introduction

Measurement of temperature of rotating or moving parts of machinery is a challenging task particularly when real-time data is required. Traditionally, temperature measurement has been done by measuring the change in resistance (RTDs and thermistors), radiation from objects (IR meters), voltage produced at the junction of two dissimilar electrical conductors (Thermocouples) or voltage drop across a silicon PN junction diode. For applications considered here, thermocouples and RTDs, though passive, require wired connections, slip rings or external transmitters to communicate. Likewise, the challenges at high voltage transmission station and switchboxes is even more stringent. The presence of metallic cables or contacts can cause catastrophic faults.

One of the methods employed for remote temperature measurement is infrared thermometry. This however requires the object to be in direct line of site and the measurements can be done on periodic basis rather than in continuous mode. The other approach involves the use of battery powered transmitters connected to the sensors. These, however, are plagued by issues like size, periodic battery replacement, mounting on fast moving and vibrating platforms, lack of suitability for high temperatures.

In SAW based temperature sensors, acoustic waves are induced electrically into a piezoelectric substrate. These waves are influenced by substrate temperature before re-converting back to electrical form. SAW temperature sensors are small sized (a few millimeter size and few hundred micron thickness) and therefore can respond rapidly to temperature changes. Some substrate materials are very sensitive to temperature change and offer a high resolution. SAW sensors are reliable, easy to fabricate (IC planar technology), compatible with standard CMOS process and provide stable performance¹. One significant and distinct advantage of SAW technology is its ability for passive operation. This feature makes it amenable to wireless operation in remote and harsh environment. SAW wireless temperature sensing was first demonstrated by Bao et al. in 1987². It offers many advantages over traditional methods. These include

- Passive operation: No external batteries are required for operation. This eliminates the need for battery monitoring and replacement³.

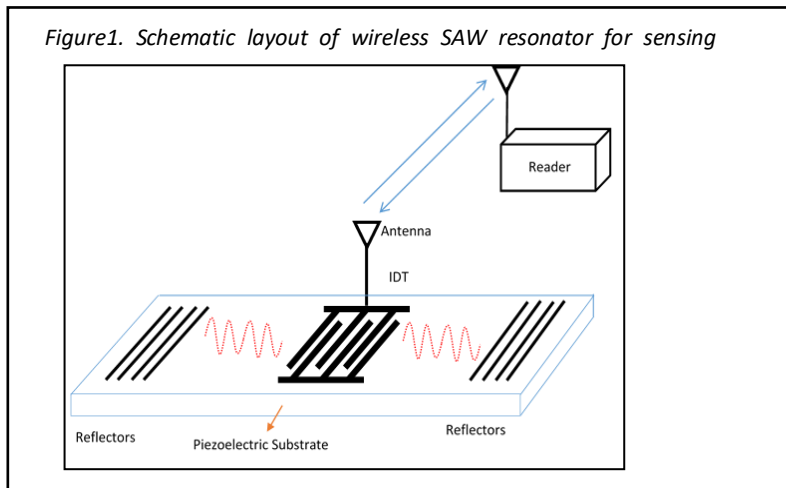
- Non-Invasive: As no power or signal wires are required, the sensor can be used in vacuum sealed chambers, power equipment and contaminated environments.
- Wireless readout: Temperature can be measured remotely using interrogators. This makes them apt for rotating applications and unreachable places.

The above advantages offered by SAW wireless technology makes them highly suitable for many critical applications considered in this paper⁴. The next section describes the technological aspects and system considerations leading to the development of passive SAW temperature sensor for remote applications.

2. Passive SAW Sensor Technology

SAW devices have been extensively researched and used for many decades. Due to its numerous features, research in SAW technology continues to be in a positive trend. Commercially, SAW has excelled in two main application areas – communication systems and sensing⁵. In sensing, SAW has been used for realizing physical, chemical and biological sensors. Chemical and biological are realized using selective coatings on the SAW device which binds the target molecules/antigens leading to mass loading on the device^{6,7}. SAW physical sensors work on the principle that change in physical parameters, like temperature, pressure, strain etc., cause change in wave properties like velocity and phase.

Passive SAW sensor consists of sensor tag and a reader/interrogator. Figure 1 shows diagram of a typical passive SAW physical sensor. The sensor tag comprises of SAW device and antenna while the interrogator consists of a



transceiver, antenna and processor. SAW devices used in most passive sensor applications are resonators instead of delay lines as they have lower losses and hence a longer range (distance) of operation⁸. Resonators have one (or two) interdigital transducer (IDT) in the middle and reflectors on both sides. IDT is connected to the Antenna and receives the interrogator signal. The interrogator transmits a signal burst having frequency close to the frequency of SAW resonator-device. The resonator antenna which is designed for device frequency range picks up the interrogator signal and through IDT induces SAW along the surface of the piezoelectric substrate. The waves are reflected by the reflectors to the IDT and transmitted back to the interrogator. The frequency of back-reflected signal is, however, affected by the physical environment of the device. The change in frequency thus contains the information about the physical quantity to be measured. The frequency changes in SAW device due to variation in temperature is described in Eq. 1 as temperature coefficient of frequency (TCF)⁹.

$$TCF = \frac{1}{f_0} \frac{df_0}{dT} = \frac{1}{v} \frac{dv}{dT} - \frac{1}{\lambda} \frac{d\lambda}{dT} \quad (1)$$

Where T is temperature of SAW device, λ is the wavelength and v is the SAW velocity in substrate.

In the present work, the SAW device has been designed and fabricated and used for temperature sensing application. The following sections describe the design of SAW temperature sensor, antenna and interrogator.

3. SAW Temperature Sensor

The interdigitated electrodes were fabricated on a circular 3" substrate of crystalline quartz substrate. The crystal was first carefully cleaned and then after a thin film of aluminum metal of thickness of 0.2 μm was deposited on the substrate using thermal evaporation technique. The thickness of the aluminum is an important

parameter and is predetermined for interdigitated electrode fabrication; the thickness uniformity across the profile of the wafer is also very important to ensure consistent behavior from one electrode to another. The wafer was then coated with a photoresist solution of photosensitive polymer. Positive photo resists like AZ 1350 are used for device because of their high resolution. After coating with photoresist it was spun at high speed so as to form a thin uniform layer. Then it was baked at 90°C for about half an hour to harden the layer. Thereafter the wafer was exposed to ultraviolet light through photomask which defines the geometry of the pattern to be produced on the wafer. Substrate was subsequently put in a developing solution. The exposed regions undergo a chemical reaction and are removed. The metal below the cleared photoresist was etched using appropriate etchant, leaving a metal pattern on the device corresponding to the pattern on the mask.

For the present work we have used the device fabricated on a ST-X Quartz piezoelectric substrate. The ST-X Quartz substrate is known to have zero TCD (temperature coefficient of delay) at room temperature. Fabricated SAW device have the 1.81 μm multiple thin electrodes and 1.81 μm gap and the chip size is 2x3 mm². The fabricated substrate was inspected for short or opens in the interdigitated electrode pattern. As shown in Figure 2 the electrode on the substrate was first inspected using optical microscope (Metzer) at 100x.

The device was also characterized by using Scanning Electron Microscope (SEM) for the confirmation that the fabricated electrode has the same dimension as per the design as shown in Figure 3.

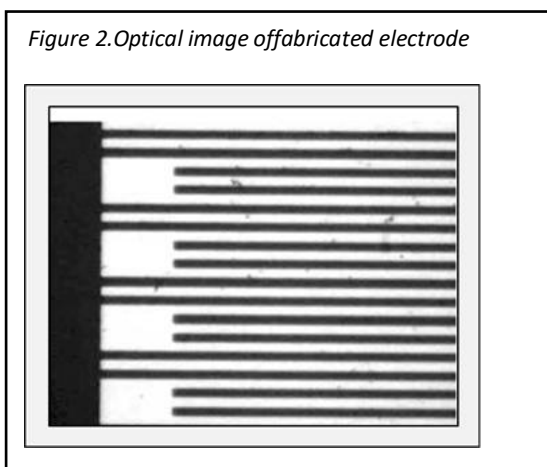


Figure 2. Optical image of fabricated electrode

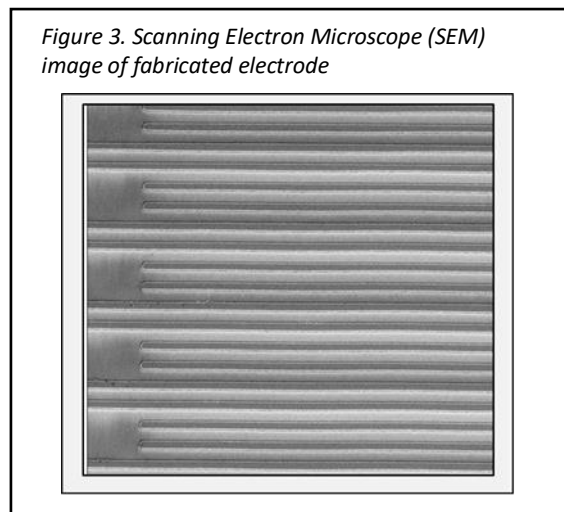


Figure 3. Scanning Electron Microscope (SEM) image of fabricated electrode

4. Antenna for SAW resonator

The communication link between reader and sensor tag is achieved using a radio link. A meander line antenna was designed, fabricated and attached to SAW device to carry out the wireless temperature sensing. This configuration has been chosen in order to make overall antenna shorter by folding the connector back and forth. Although the efficiency and bandwidth decreases in meander configuration yet it suits short range sensor applications. The antenna has been fabricated on a single sided FR4 PCB ($\epsilon_r=4.4$) with $L_c = 38\text{mm}$, $L_a = 3\text{mm}$ and $L_b = 7\text{mm}$. The design has a bandwidth of 30MHz and efficiency of 39%, however, the variation in bandwidth and efficiency due to temperature change will alter the values during operation. The layout of meander line antenna is shown in Figure 4.

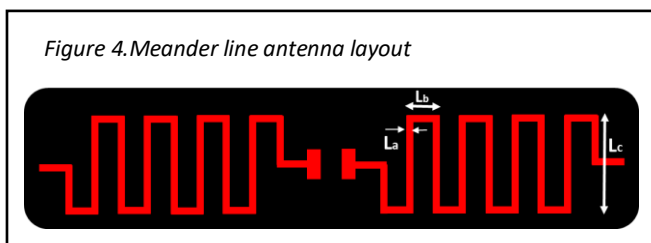


Figure 4. Meander line antenna layout

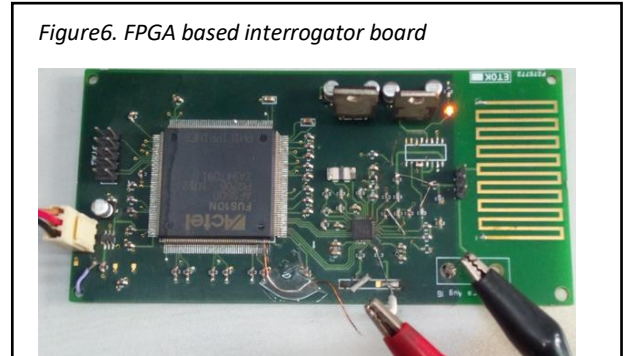
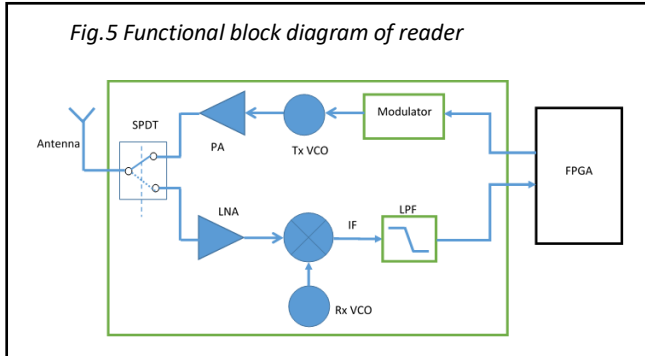
5. Interrogator/reader

The interrogator/reader unit comprises of transmit and receive part both sharing an antenna through a switch. The unit is required to generate and transmit a short RF-Burst and immediately switch to receiver mode to capture the reflection from SAW sensor tag. It has to further process the received signal and determine the

temperature as a function of frequency shift between the transmitted and received signal. A functional block diagram of interrogator unit shown in Figure 5.

The reader used in this work was developed using MAX 7030 transceiver IC (Make –Maxim semiconductor, USA). The device generates a typical power output of +10dBm for a 50Ω and has a typical sensitivity of -114dBm. It has an internal RF switch through which Tx and Rx can be connected to a common external antenna.

ActelSmartFusion FPGA (AFS200) was used for control and processing. The Tx/Rx timings and automatic gain control signal are generated in FPGA. The receiver signal is amplified using a Low Noise Amplifier (LNA) and the

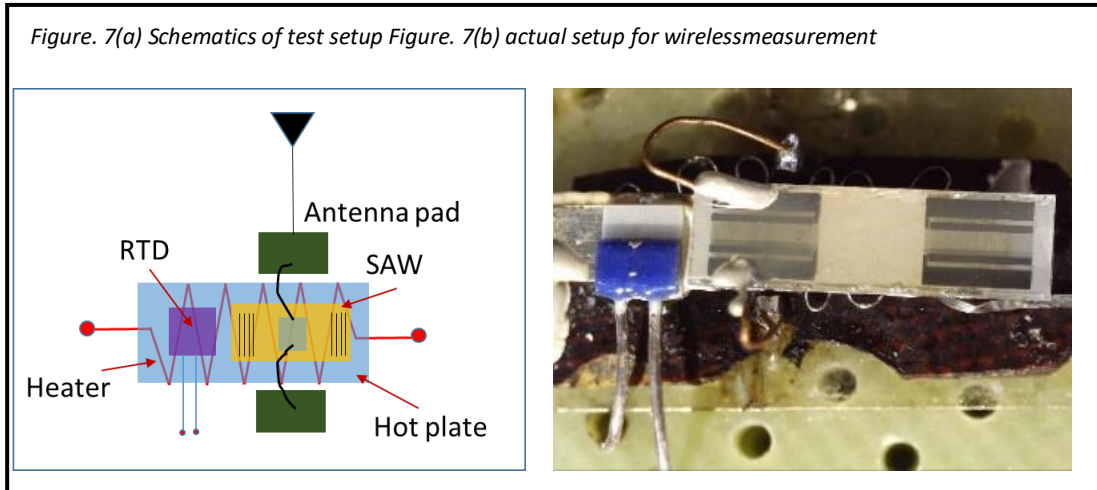


amplified output is mixed with Local Oscillator output (LO). The LNA has a maximum achievable gain of 30dB. The LO is generated using a fixed integer Phase-locked loop (PLL). Actual fabricated board with reader and FPGA based controller circuit is shown in Figure 6.

The mixer down-converts the input RF to 10.7MHz intermediate frequency (IF). MAX7030 has an integrated image rejection of the mixer, a unique feature. The IF output is fed to FPGA input pin for frequency counting.

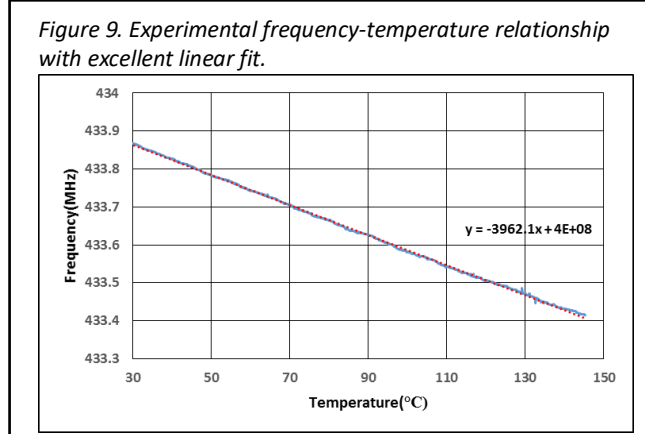
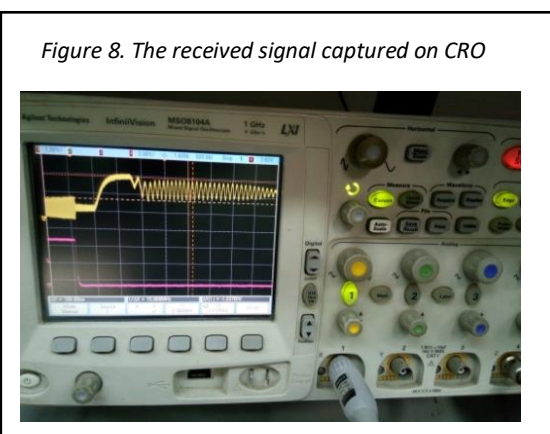
6. Measurement results and discussion

Figure7(a) and 7(b) show the schematic and actual test setup for wireless temperature measurement. The SAW sensor was bonded with the antenna to form SAW tag. A micro-heater based hot plate arrangement was



made just under the SAW sensor. A thermal conductive layer was used for a good thermal contact. The heater was powered by a dc-power source and a PT100 RTD was placed on the hot plate for temperature calibration. The reader unit was connected to a PC through RS232 interface for thorough data analysis.

The measurements were carried out by increasing the temperature of hot plate from ambient to 150°C



gradually. The received signal from the interrogator is captured with CRO as shown in Figure 8 and showed a linear variation in SAW frequency over the temperature range shown in Figure 9. The experiment was repeated for several cycles and similar results were obtained indicating stable and repeatable response. The measurements were reasonably stable up to 50 cm and deteriorated rapidly after that even though a spectrum analyzer detected reasonably good reflected signal even up to 2 m range.

7. Conclusion

A passive wireless temperature sensor based on SAW resonator has been developed for remote applications. The sensor has shown a linear response to temperature change (30 °C to 150 °C) and a range of 0.5 m was achieved even though there is a scope of increasing the range. Passive SAW sensors offer a wide range of applications where conventional methods are difficult to implement. With advancement in fabrication of SAW devices and piezoelectric material, high frequency devices in GHz are being realized. Such devices are even smaller in size and require smaller antennas. Material like Langasite has a higher temperature range compared to Quartz and LiNO₃.

8. Acknowledgment

Authors are extremely thankful to Dr. Seema Vinayak, Director SSPL, for allowing and supporting this work. They are also thankful to Mr J S Rawat Sc G, Pallav Kumar Tripathi Sc E and Puja Rajput JRF for their support and patronage. Authors would also like to thank Dept. of Electronics and Information Technology (DEITY) for their support under Visvesvaraya Scheme.

9. References

- [1] Tian, X.-G.; Liu, H.; Tao, L.-Q.; Yang, Y.; Jiang, H.; Ren, T.-L. High-resolution, high-linearity temperature sensor using surface acoustic wave device based on LiNbO₃/SiO₂/Si substrate. *AIP Adv.* 2016, 6, 095317
- [2] Bao X.Q., Burkhard W., Varadan V.V., Varadan V.K. SAW Temperature sensor and remote reading system, *Proc. of the IEEE Ultrasonic Symposium*, pp 583-585, 1987.
- [3] L. Reindl, I. Shrena, S. Kenshil, R. Peter, "Wireless measurement of temperature using surface acoustic waves sensors", *Proc. Frequency Control Symp. PDA Exhibit/Proc. IEEE Int. 17th Eur. Frequency Time Forum*, pp. 935-941, 2003.
- [4] L. M. Reindl, I. M. Shrena, "Wireless measurement of temperature using surface acoustic waves sensors", *IEEE Trans. Ultrason. Ferroelectr. Freq. Control*, vol. 51, pp. 1457-1463, Nov. 2004.
- [5] L. Reindl, G. Scholl, T. Ostertag, H. Scherr, U. Wolff, F. Schmidt, "Theory and application of passive SAW radio transponder as sensors", *IEEE Trans. Ultrason. Ferroelectr. Freq. Control*, vol. 45, no. 5, pp. 1281-1292, Sep. 1998.
- [6] Afzal A., Iqbal N., Mujahid A., Schirhagl R. Advanced vapor recognition materials for selective and fast responsive surface acoustic wave sensors: A review. *Anal. Chim. Acta.* 2013;787:36–49
- [7] O. Tigli and M. E. Zaghoul, "Surface acoustic wave (SAW) biosensors," 2010 53rd IEEE Int. Midwest Symp. Circuits Syst., pp. 77-80, Aug. 2010.
- [8] W. Buff, "SAW sensors for direct and remote measurements", 2002 IEEE Ultrason. Symp., pp. 420-428, 2002.
- [9] Lim C, Wang W, Yang S, et al. Development of SAW-based multi-gas sensor for simultaneous detection of CO₂ and NO₂. *Sensors and Actuators B: Chemical*, 2011, 154(1): 9

A Committee Machine Neural Network for mitigating nonlinear distortion in the Nonlinear High Power amplifier

Manoj Bhatt¹, Sanjay Mathur²

¹Department of Electronics and Communication Engineering GBPUA&TPantnagar-263153, INDIA, ²Department of Electronics and Communication Engineering GBPUA&TPantnagar-263153, INDIA
mb914491@gmail.com¹, mathur_sanjay@rediffmail.com²

Abstract—The tradeoff between bandwidth efficiency and power efficiency with nonlinear distortion in a modern communication system, i.e., High speed (High bit rate) communication has become a more prominent problem due to the nonlinear characteristic of High Power Amplifier (HPA). To obtain the peak gain from the HPA, it has to operate in its saturation region, which is highly nonlinear. In the absence of any preceding signal processing, the HPA is forced to back-off at the input side, which in turn results in a sufficient back-off on the output side too. Hence, for long-distance or digital satellite communication channels it is inevitable to use HPA to obtain sufficient transmission power, but at the same time, the high bit rate modulation schemes having a high peak to average power ratio are very susceptible to the nonlinearity of HPA causing nonlinear distortions in the modulated signal. Therefore it is necessary to compensate nonlinearity introduced by HPA. For that, we need a very effective predistorter. This article proposes a new predistortion technique based on neural network committee machine using a Mixture of Experts (MOE), and it is achieved in two steps. In the first step, we modeled the memoryless Saleh model's AM-to-AM and AM-to-PM conversions. In the second step, an approximation of the Saleh inverse transfer function is modeled, and we have used it to implement the predistorter. The approach is applied to 16-QAM transmissions, and the results obtained in the first step show that the Mixture of Experts based HPA has an excellent level of similarities of AM-to-AM and AM-to-PM characteristics as obtained by Saleh model. The results obtained from the second step demonstrate the linearization performance of the predistorter, as achieved through the MOE model.

Keywords—16-QAM, HPA nonlinearity, Saleh Model, Predistorter, Linearization, MOE

1. INTRODUCTION

In all long-distance communication systems, such as satellite communication or mobile communication we compulsorily require High power amplifier (HPA) to boost low power information signal such as speech signal for transmitting it over long distances. HPA has a non-linear characteristic, and for a power-efficient communication system, it must be operated near saturation, which falls the nonlinear region or region this severely distorts the information signal. These nonlinear distortions become more vulnerable when the communication system demands bandwidth-efficient modulation techniques such as Quadrature Amplitude Modulation (QAM) [1] with large envelope fluctuation or high peak-to-average power ratios (PAPR), which are more sensitive to the power amplifier nonlinearities. This distortion occurs in the form of spectral re-growth, which leads to adjacent channel interference and violations of the out-of-band emission requirements mandated by regulatory bodies. It also causes in-band distortion, which degrades the bit error rate (BER) performance [1], which we observe in the form of squeezing and twisting in the constellation of the transmitted signal.

To reduce the HPA nonlinearity, there exist two schemes, namely “Back-off” approach and linearization. “Back-off” approach is mostly a trivial solution for handling the nonlinearity of HPA although with this approach the output signal of PA clears the criteria related to the mandatory spectrum mask and error vector magnitude (EVM) or mean square error (NMSE). But at the same time, it leads to an assembly of the costly and power-incompetent transmitter, because of the low HPA efficiency in the low input power regions [2]. Due to this incompetence of “Back-off” approach, the need for power-efficient linearization techniques is growing immensely, and various linearization techniques are proposed. Sperlich [3] demonstrated a performance comparison of these major linearization techniques and concluded that amongst all the linearization techniques, Digital Predistortion (DPD) is the most cost-effective and mostly used linearization technique, which provides higher efficiency and greater flexibility. Further, modeling of the nonlinear characteristics of the PAs can be done by using either a transistor level approach or a system-level approach; one such example is behavioral technique. The behavioral model is the most efficient and low complexity approach for characterizing the nonlinearity and predistorter of the PAs. Nonlinear PAs literature explains various behavioral models for the modeling of nonlinear Amplitude-to-Amplitude (AM-to-AM) and Amplitude-to-Phase (AM-to-PM) characteristic of power amplifiers such as Rapp model, Ghorbani model, Taylor model, and Saleh model, etc. Development of a good DPD predistorter depends on the ability to develop an accurate and simple PA behavioral model. Therefore we used Saleh model for modeling memoryless nonlinear power amplifier because it matches well with the practical AM-to-AM and AM-to-PM characteristics of TWTA and has lower complexity as compared to the other state-of-the-art behavioral models since it requires only two parameters to compute the nonlinearity of the power amplifier [4, 5].

Many researchers have suggested that neural network has an excellent capability to represent complex nonlinear system or function and efficiently used as DPD to linearize nonlinear PAs [6–11] and a comparative study is also done by Rawat and Ghannouchi [12] for different DPD linearizers over performance with mildly nonlinear to highly nonlinear PAs, and the study suggests that machine learning (ML) based linearizers are better suited for the application. Although the design parameters are

relatively higher, ML linearizers are gaining more popularity recently [12]. The working principle of a DPD linearizer is explained in the methodology section. Hence considering these facts, this article proposes a new digital predistortion technique based on neural network committee machine, also known as Mixture of Experts (MOE). It is achieved in two steps; in the first step, we modeled the memoryless Saleh model's AM-to-AM and AM-to-PM conversions with the help of the MOE model. In the second step, an approximation of the Saleh inverse transfer function is modeled through the MOE model. The paper presents simulation results for 16-QAM modulation.

2. METHODOLOGY

This section explains various schemes as utilized in the current article to achieve the predistortion. It explains the basic concepts of predistorter, Saleh model, MOE, and how we have utilized various modules to build an efficient predistorter.

2.1 Predistorter Concept

In predistortion, a predistorter is placed before the power amplifier, and this predistorter should have a response just inverse to that of the amplifier's nonlinear response so that cascading of these two forms a linear system having a linear response and the output signal of the system is amplified by a constant gain. The working principle of a predistortion concept is shown in "Fig. 1"

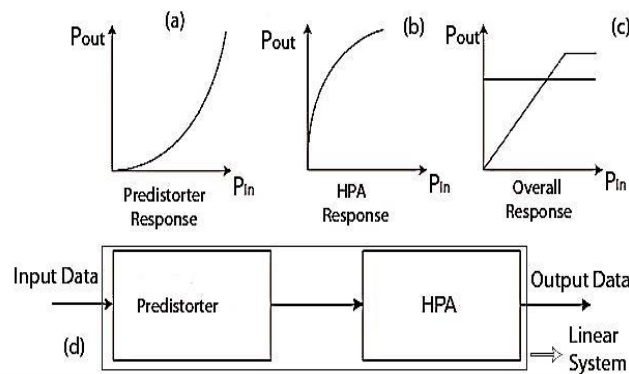


Fig.1. Working principle of a PD linearizer; (a) Predistorter response, (b) Power amplifier response, (c) Linearized output, (d) Block diagram of Predistortion concept.

During the predistortion operation, the nonlinear predistorter generates intermodulation distortion (IMD) products that are in anti-phase with the IMD products produced by the power amplifier, reducing the out-of-band emissions and finally, at the predistortion output, these IMDs products cancel each other and constant gain amplified power is achieved

2.2 Saleh Model

The Saleh model is empirical, and a frequently used model for memory-less power amplifier due to its low parameter complexity and is specially designed for modeling a TWT amplifier. The Saleh model is recommended as the standard PA model by the IEEE broadband wireless access group and is suitable as a base for designing linearization techniques such as predistorters. The two-parameters in Saleh model are gain $\Upsilon(|x|)$ and phase conversion $\phi(|x|)$ functions, which are given by (1) [4].

$$\Upsilon(|x|) = \frac{a_\alpha |x|}{1 + \beta_\alpha |x|^2}; \quad \phi(|x|) = \frac{a_\rho |x|^2}{1 + \beta_\rho |x|^2} \quad (1)$$

Where a_α , β_α , a_ρ , and β_ρ are the distortion parameters that are fitted to the measured data.

2.3 MOE

MOE was proposed by Jacobs et al. [13] in 1994, and it is a type of neural network committee machine with a modular structure network that follows supervised learning [14]. It is used for regression, classification problem [15], and fusion applications in healthcare, finance, surveillance, and recognition [16] fields. In the MOE architecture, a group of experts and a single gate cooperate to resolve a nonlinear supervised learning problem following the Divide-and-Conquer principle [14]. In Divide-and-Conquer algorithms, a complex non-linear problem is divided into simpler problems or a set of linear problems, and the solution of each simpler problems can be combined to solve the complex non-linear problem. The architecture of MOE is shown in "Fig. 2" [14], and it can be viewed as a tree-structured architecture having three main components; K number of experts that are either regression functions or classifiers, a gate that makes soft partitions of the input space and tells each expert about in which regions the individual expert would work best and a probabilistic model to combine the experts and the gate [17]. The parameters of both experts and gate for these regions can be learned or estimated by using Expectation and Minimization (EM) based learning algorithms such as iteratively-reweighted least squares (IRLS) [13] or single-loop EM [17] etc. "Fig 2 (b)" shows the signal flow graph of a single neuron single layer expert network and the output generated by expert k is presented as the inner product of the input vector \mathbf{x} and the synaptic weight vector \mathbf{w}_k of this neuron and b is the bias term, as given by (2).

$$y_k = \mathbf{w}_k^T \mathbf{x} + b \quad (2)$$

"Fig. 2 (c)" shows the single layer signal flow graph of the gating network, which consists of K neurons and each neuron assigned to a specific expert. Unlike the experts, the neurons of the gating network are non-linear, with their activation functions defined by (3).

$$g_k = \frac{\exp(\mu_k)}{\sum_{j=1}^K \exp(\mu_j)} \quad (3)$$

This is also called the Softmax activation function, where μ_k is the inner product of the input vector \mathbf{x} and the synaptic weight vector \mathbf{a}_k , i.e. $\mu_k = \mathbf{a}_k^T \mathbf{x} + b$ [14].

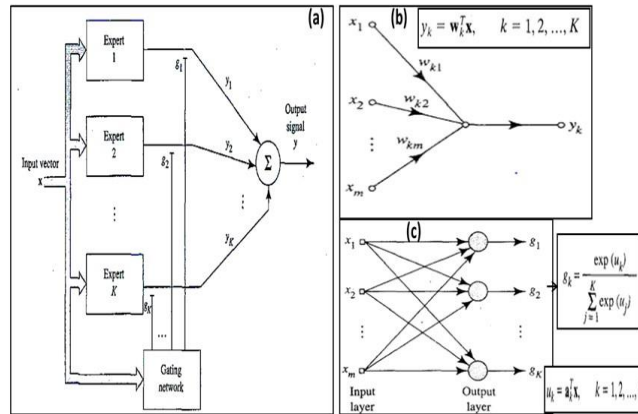


Fig.2. (a) Block diagram of Original MOE, (b) Signal flow graph of a single linear neuron of Expert, (c) Signal flow graph of a single neuron for the gating network [14].

Several researchers have used the EM algorithm for learning or training the parameters of the expert networks and gating network. The EM algorithm is a two steps algorithm. In the first step, the expectation of log-likelihood function is calculated in terms of the parameters of the expert networks and the gating network and in the second step, the values of the parameters of the expert networks and the gating network are calculated, that maximize the expectation of log-likelihood function. One disadvantage of EM algorithm is whenever any component of the MOE has nonlinear nature, then maximization concerning that component's parameters are analytically unsolvable even for the simplest generalized linear case. In the original MOE, proposed by Jacobs et al. [13], it was difficult to apply EM to some parts of the MOE architecture because of the nonlinearity of the softmax gating network. This made the maximization concerning the parameters in gating network nonlinear and analytically unsolvable even for the simplest generalized linear case [17]. For removing it, Xu et al. [17] proposed an alternative model for MOE by introducing an alternative gating function. This form is chosen so that the maximization concerning the parameters of the gating network can be handled analytically. Since we have used the EM algorithm as a learning algorithm, therefore, we used the alternative model of MOE [17] in this article.

2.4 MOE based Predistortion

For devising MOE based predistortion, various components are considered in the explained manner. X and Y are considered to be the input and target data of the form $X = \{\mathbf{x}^n\}_{n=1}^N$ and $Y = \{\mathbf{y}^n\}_{n=1}^N$ respectively with N number of training points. The set of MOE component parameters is represented by Ω . The parameters of the gate and experts are represented by ϕ_g and ϕ_e respectively, therefore $\Omega = (\phi_g, \phi_e)$. For simplification, vector \mathbf{x}^n and \mathbf{y}^n are denoted as \mathbf{x} and \mathbf{y} further in our article. The total probability of observing target vector \mathbf{y} for a given input vector \mathbf{x} in terms of the experts can be stated as equation (4), (5). In the following equations, vector $f_l(\mathbf{x}, w_l)$ represents the output of the l^{th} expert, w_l represents the synaptic weight of the l^{th} expert and Σ_l represents the covariance matrix.

$$\begin{aligned} P(\mathbf{y}|\mathbf{x}, \phi_g, \phi_e) &= \sum_{l=1}^L P(\mathbf{y}, l|\mathbf{x}, \phi_g, \phi_e) \\ &= \sum_{l=1}^L g_l(\mathbf{x}, \phi_g) P(\mathbf{y}|\mathbf{x}, l, \phi_e) \end{aligned} \quad (4)$$

$$P(\mathbf{y}|\mathbf{x}, l, \phi_e) = \frac{1}{(2\pi)^{\frac{n}{2}} * |\Sigma_l|^{\frac{1}{2}}} \exp\left\{-\frac{1}{2}(\mathbf{x} - f_l(\mathbf{x}, w_l))^T \Sigma_l^{-1} f_l(\mathbf{x}, w_l)\right\} \quad (5)$$

Where L is the number of experts, $g_l(\mathbf{x}, \phi_g)$ is the probability of selecting the l^{th} expert, and $P(\mathbf{y}|\mathbf{x}, l, \phi_e)$ is the probability of generating \mathbf{y} for a given \mathbf{x} through l^{th} expert. In the original MOE model, the gating function $g_l(\mathbf{x}, \phi_g)$ is represented by the following softmax function (6).

$$g_l(\mathbf{x}, \phi_g) = \exp(\gamma_l(\mathbf{x}, \phi_g)) / \sum_{k=1}^L \gamma_k(\mathbf{x}, \phi_g) \quad (6)$$

Where $\gamma_k(\mathbf{x}, \phi_g), k=1, \dots, L$ are the outputs of the gating function, but this form of softmax function has nonlinearity in nature and maximization part of the EM algorithm is not analytical solvable. Therefore to overcome this problem, we have used an alternative form of gating function as given in Xu et al. [17], presented in (7).

$$g_l(\mathbf{x}, \phi_g) = (\alpha_l * P(\mathbf{x}|\phi_{g,l}) / \sum_{k=1}^L (\alpha_k * P(\mathbf{x}|\phi_{g,k}))$$

$$\sum_l \alpha_l = 1 \text{ and } \alpha_l \geq 0$$

$= (\alpha_l * P(\mathbf{x}|\phi_{g,l}) / P(\mathbf{x}, \phi_g)$ (7) Where α_l and $\phi_{g,l}$ are the components of ϕ_g i.e. $\phi_g = \{\phi_{g,l}, \alpha_l\}$ and $P(\mathbf{x}, \phi_g) = \sum_{k=1}^L (\alpha_k * P(\mathbf{x}|\phi_{g,k}))$. $P(\mathbf{x}|\phi_{g,l})$ is further given by (8).

$$P(\mathbf{x}|\phi_{g,l}) = \frac{1}{(2*\pi)^{n/2} * |\Sigma_l|^{1/2}} \exp\left\{-\frac{1}{2}(\mathbf{x} - \mu_l)^T \Sigma_l^{-1}(\mathbf{x} - \mu_l)\right\} \quad (8)$$

Where μ_l and Σ_l are mean and covariance respectively.

Now, the total probability of observing target vector \mathbf{y} for a given input vector \mathbf{x} in terms of the experts can be written as (9) or (10).

$$P(\mathbf{y}|\mathbf{x}, \phi_g, \phi_e) = \sum_l \frac{\alpha_l * P(\mathbf{x}|\phi_{g,l})}{P(\mathbf{x}, \phi_g)} P(\mathbf{y}|\mathbf{x}, \phi_e) \quad (9)$$

$$P(\mathbf{y}, \mathbf{x}) = \sum_l \alpha_l * P(\mathbf{x}|\phi_g) * P(\mathbf{y}|\mathbf{x}, \phi_e) \quad (10)$$

Finally, the EM training algorithm's steps and equations as stated in Xu et al. [17] are used for updating the parameters of the MOE network that maximize the log-likelihood of the probability equation (10), i.e., $\ln(P(\mathbf{y}, \mathbf{x}))$. "Fig. 3" shows the proposed DPD predistortion block diagram.

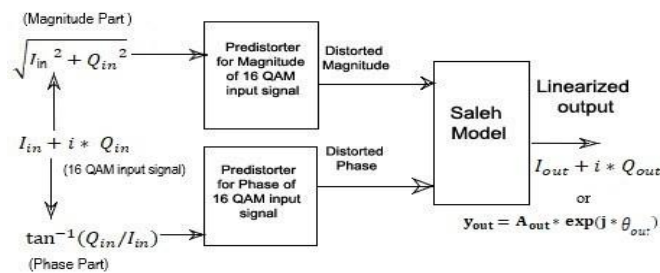


Fig. 3. Block Diagram of DPD predistortion.

Here two MOE networks are used for performing the function of predistorter, in which one network deals with the magnitude part of the 16-QAM input signal, and the other one deals with the phase part of the 16-QAM input signal. The output obtained from these two blocks has the same form as the input signal of the predistorter and is further applied to the Saleh model for obtaining linearized output at the HPA output. Finally, the magnitude and phase part of the output signal are combined according to the following (11) to obtain the total output.

$$y_{out} = A_{out} * \exp(j * \theta_{out}) \quad (11)$$

Where A_{out} and θ_{out} are the magnitude and phase of the output signal, respectively.

3. RESULTS AND DISCUSSION

To evaluate the performance of the proposed method, the simulations are done in MATLAB. The following sections explain Saleh model modeling and digital predistortion modeling.

3.1 Saleh Model Modeling

For obtaining the characteristic of Saleh model, we have used equation (1), and the considered distortion parameters for Saleh model are $\alpha_\alpha = 2.0587$, $\beta_\alpha = 1.0517$, $\alpha_\rho = 4$ and $\beta_\rho = 2.1$. The same characteristic is obtained through our MOE method also, which uses three experts and one gating network. "Fig. 4 (a)" and "Fig. 5 (a)" show that these two characteristics superimpose with mean square error (MSE) of the order of 2.2483×10^{-5} (or -46.4815 dB) and 5.560×10^{-5} (or -42.5493 dB) respectively. "Fig. 4 (b)" and "Fig. 5 (b)" show that below 45 iterations, log-likelihood function attains constant value which explains that no further updation is required for the parameters of experts and gating networks. This reflects the speed of the method.

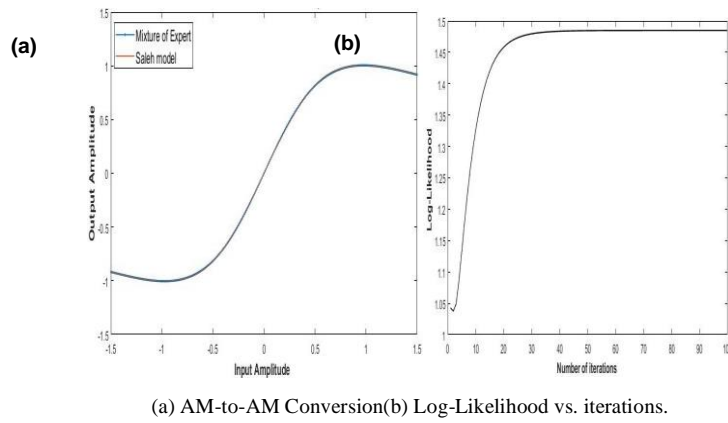


Fig. 4. AM-to-AM conversion modeling.

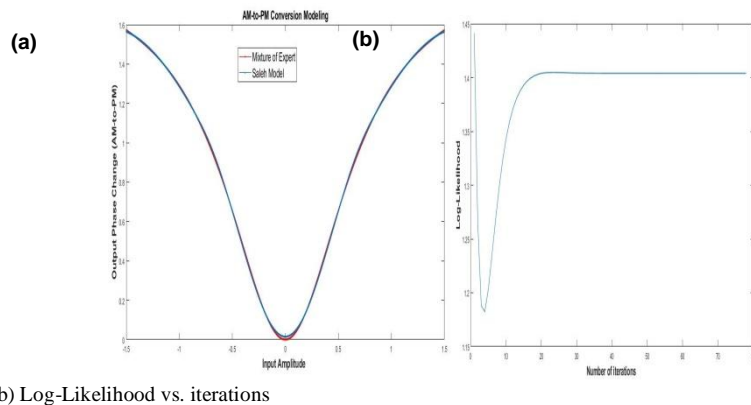


Fig. 5. AM-to-PM Conversion Modeling.

3.2 Digital Predistortion Modeling

In the subsequent step, MOE is used to design a digital predistorter. The performance of the proposed method for predistortion is evaluated in two steps. In the first step, we approximated the inverse of the Saleh characteristic through MOE method. For that, we applied the reverse order of the input and output signals of the Saleh model, i.e., input as output and output as an input signal to the MOE for the same parameters as considered in the above case. The obtained results denoted by $g(x)$ in "Fig. 6" are compared with the inverse Saleh AM-to-AM characteristic denoted by $A^{-1}(x)$. "Fig. 6" shows that $g(x)$ is very close to the exact inverse of $A^{-1}(x)$ with the MSE of the order of 1.1157×10^{-5} (or -49.5245 dB).

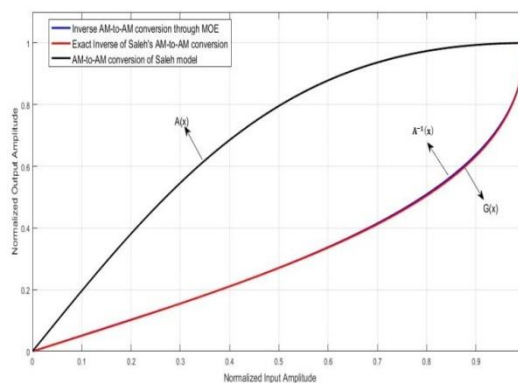
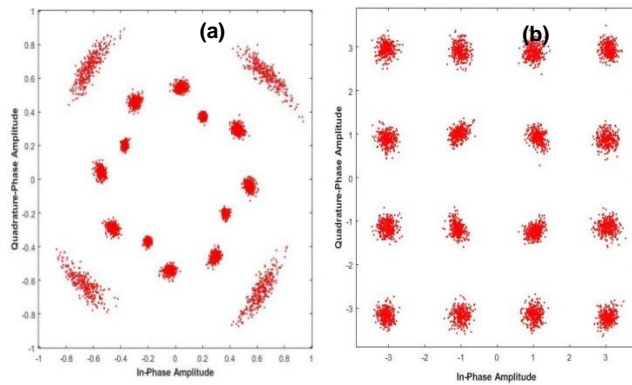


Fig. 6. Comparison of inverse AM-to-AM characteristics as obtained through Saleh model and our proposed method.

After that, $g(x)$ is used as predistorter, which is placed just before the HPA for achieving digital predistortion. The DPD evaluation in the time domain is presented using the 16-QAM signal in "Fig. 7". The signal constellation diagram in "Fig. 7 (a)" shows the effect of the PA nonlinearity without predistorter and "Fig. 7 (b)" shows the effect of PA nonlinearity with predistorter. As can be seen from the constellation diagram, the use of a predistorter for the compensation of nonlinear distortion caused by HPA is justified.



(a)HPAoutputwithoutpredistorter(b)HPAoutput withpredistorter.

Fig. 7. Constellation of 16-QAM System.

4. CONCLUSION

This article presents a MOE based neural network method for modeling the memoryless Saleh behavioral model and also a predistorter for linearizing the non-linearity introduced by the Saleh model. The modeling results of our method has an excellent level of similarities with a high level of MSE and a small number of neurons, i.e., six neurons each for AM-to-AM and AM-to-PM conversion characteristic of Saleh model and inverse AM-to-AM characteristic of Saleh model. Log-Likelihood vs. Iterations results show that it requires lesser number of iterations which indicates the reported method has a high speed for convergence. The predistorter based result is clearly showing the linear improvement in the 16-QAM constellation diagram using the DPD approach presented in the article.

5. REFERENCES

- [1] R. Singla and S. Sharma, "Digital predistortion of power amplifiers using look-up table method with memory effects for LTE wireless systems," *EURASIP Journal on Wireless Communications and Networking*, vol. 330, pp. 1-8, 2012.
- [2] Evolved Universal Terrestrial Radio Access (E-UTRA); Base Station (BS) radio transmission and reception (Release 11), 3GPP TS 36.104 V11.3.0 Std., Dec. 2012.
- [3] R. Sperlich, "Adaptive power amplifier linearization by digital pre-distortion with narrowband feedback using genetic algorithms," Ph. D. dissertation, Georgia Institute of Technology, Georgia, 2005.
- [4] A. A. A. Saleh, "Frequency-independent and frequency-dependent nonlinear models of TWT amplifiers," *IEEE Transactions on communications*, vol. 29, pp. 1715-1720, 1981.
- [5] H. Al-kanan, X. Yang, and F. Li, "Saleh Model and Digital Predistortion for Power Amplifiers in Wireless Communications Using the Third-Order Intercept Point," *Journal of Electronic Testing*, pp. 1-7, 2019.
- [6] M. Ibnkahla, et al. "Neural networks for modeling nonlinear memoryless communication channels," *IEEE Transactions on communications*, vol. 45, pp. 768-771, 1997.
- [7] M. Ibnkahla, "Neural network predistortion technique for digital satellite communications," *IEEE International Conference on Acoustics, Speech, and Signal Processing. Proceedings (Cat. No. 00CH37100)*, vol. 6, 2000.
- [8] N. Naskas and Y. Papananos, "Neural-network-based adaptive baseband predistortion method for RF power amplifier," *IEEE Transactions on circuits and systems II: express briefs*, vol. 51, pp. 619-623, 2004.
- [9] T. Liu, S. Boumaiza, and F. M. Ghannouchi, "Dynamic behavioral modeling of 3G power amplifiers using real-valued time-delay neural networks," *IEEE Transactions on Microwave Theory and Techniques*, vol. 52, pp. 1025-1033, 2004.
- [10] M. Isaksson, D. Wisell, and D. Ronnow, "Wide-band dynamic modeling of power amplifiers using radial-basis function neural networks," *IEEE Transactions on Microwave Theory and Techniques*, vol. 53, pp. 3422-3428, 2005.
- [11] M. Rawat, K. Rawat, and F. M. Ghannouchi, "Adaptive digital predistortion of wireless power amplifiers/transmitters using dynamic real-valued focused time-delay line neural networks," *IEEE Transactions on Microwave Theory and Techniques*, vol. 58, pp. 95-104, 2009.
- [12] M. Rawat and F. M. Ghannouchi, "Distributed spatiotemporal neural network for nonlinear dynamic transmitter modeling and adaptive digital predistortion," *IEEE transactions on instrumentation and measurement*, vol. 61, pp. 595-608, 2011.
- [13] M. I. Jordan and R. A. Jacobs, "Hierarchical mixtures of experts and the EM algorithm," *Neural computation*, vol. 6, pp. 181-214, 1994.
- [14] S. Haykin, *Neural networks: A comprehensive foundation*, Prentice Hall PTR, 1994.
- [15] K. Chen, L. Xu, and H. Chi, "Improved learning algorithms for mixture of experts in multiclass classification," *Neural networks*, vol. 12, pp. 1229-1252, 1999.
- [16] S. E. Yuksel, J. N. Wilson, and P. D. Gader, "Twenty years of mixture of experts," *IEEE Transactions on neural networks and learning systems*, vol. 23, pp. 1177-1193, 2012.
- [17] L. Xu, M. I. Jordan, and G. E. Hinton, "An alternative model for mixtures of experts," In *Advances in neural information processing systems*, pp. 633-640, 1995.

Channel Estimation of DWT based MIMO-OFDM System in Wireless Communication

Nivedita Singh¹, M.Shukla²

Electronics Engineering Department¹, Electronics Engineering Department²

Harcourt Butler Technical University¹, Kanpur, Uttar Pradesh, India¹

Harcourt Butler Technical University², Kanpur, Uttar Pradesh, India²

nivedita.sakshi@gmail.com¹, mkshukla@hbtu.ac.in²

Abstract-The channel estimation is quite mathematically complex process as observed by the researchers throughout the world, in wireless communication platform. It is being done for getting the accurate estimate of the channel behavior and impulse response. The combined MIMO-OFDM system has brought a drastic change in wireless network for avoiding ISI and increasing capacity link of a channel. In general the Fast Fourier Transform (FFT) Tool in place of Discrete Fourier Transform (DFT) has been adopted with the OFDM system for fast and easy computation. However, the problem of higher bit error rate was still the matter of concern. To further avoid this problem researcher's has adopted a better method by utilizing the combined MIMO-OFDM system with Wavelet Transform Tool for improving BER performance of the system. This paper basically analyzes 5×5 wavelet based MIMO-OFDM system which has been taken in order to analyze the system performance for higher count of transmitter/receiver compared to conventional systems (i.e. 2×2). The results have been discussed by using BER versus SNR graph. The simulation results, have the DWT based MIMO-OFDM system with channel coding which has demonstrated improved BER performance than the DWT based MIMO-OFDM system without channel coding against interference and noise. Also, the throughput comparison performance of system with different code rates has been demonstrated in the paper which helps to understand the relation between the SNR range, throughput and different modulation scheme for the system. The channel capacity for different transceiver systems by utilizing the water filling algorithm has been demonstrated, that shows, larger the count of transmitter and receiver, greater will be the capacity of channel to carry the information bits.

Keywords: Multiple-Input Multiple-Output (MIMO), Orthogonal Frequency Division Multiplexing (OFDM), Bit Error Rate (BER), Inter Symbol Interference (ISI), Cyclic Prefix (CP), Continuous Wavelet Transform (CWT), Discrete wavelet Transform (DWT).

I-INTRODUCTION

Wireless communication is a term that allows all the procedures and form of connecting and communicating between the several networks wirelessly. The main objective of this technology is to provide larger area coverage, high quality data rates services and better spectral efficiency, but the wireless network is adversely affected by the multipath interference. To attain the high performance and robustness in our communication system, the channel estimation scheme is required². The impulse response of the channel will help in knowing the important information for designing and planning of wireless systems¹. This paper considers Least Square channel estimation method which is a training sequence based channel estimation technique.

In order to eliminate the ISI effect, OFDM is being used. It is a combination of multiplexing and modulation both. It divides the available spectrum into multiple sub channels and converts the frequency selective channel to multiple flat fading channels for higher data transmission rate. Because of this, the symbol duration get larger than the delay spread of the channel, which helps to handle ISI. OFDM digital implementation is possible by using mathematical tool called as FFT and IFFT. Cyclic prefix is like a guard interval which is inserted in OFDM symbol in order to avoid further the ISI problem, but has drawback of decrease in the spectral efficiency and high power consumption⁵. To create multi-dimensional wireless communication system, MIMO has been considered, a multiple antenna system with an efficient spatial diversity technique which enhances the multipath propagation in order to increase range, capacity and reliability of wireless communication system⁷.

In the proposed work, 5×5 DWT based MIMO-OFDM system in AWGN channel has been considered for observing the performance of system with higher count of transmitter and receiver against the noise and interference. In the literature, the 2×2 system was considered to be the conventional by the researchers. In this paper, the least square channel estimation has been adopted to estimate the channel parameters as it is supposed to be better in computing channel coefficients for higher number of transmitter/receiver. In this paper, MIMO-OFDM systems is considered in which the FFT and IFFT tool in OFDM system get replaced with DWT and IDWT respectively, in order to attain much higher spectral efficiency than the conventional one. The introduction section of this paper includes the literature Survey also, which demonstrates existing FFT-OFDM system. Further in section II the proposed model DWT-OFDM system with MIMO is shown. The DWT- OFDM system is more robust against multipath fading effects and interference as compared to FFT based OFDM systems [5]. In section III and IV the effect of CP on spectral efficiency of system and the LS channel estimation technique has been discussed respectively. At last in section V and VI the results based on MATLAB simulation have shown and the conclusion is drawn based on the computed results.

The MIMO-OFDM system proves to be more efficient than the other proposed systems. The MIMO block focuses on sending signals of multiple users at a time by using same channel bandwidth. The problem of ISI (Inter Symbol Interference) is resolved with the help of OFDM part and available spectrum is being utilized efficiently by multiple users with the help of MIMO system³. During transmission, the multipath propagation is perceived as interference, degrading a receiver's ability to recover the transmitted signal, however the MIMO system utilizes this disability to increase throughput and reliability of system⁴. It allows multiple users in a single channel to work parallelly. The MIMO system spreads the same total power over different antennas to achieve higher array gain which helps to improve the spectral efficiency⁴.

To achieve the required bit rate, OFDM multicarrier transmission systems has been adopted, as it follows the basic principle of orthogonality to avoid ISI and ICI, in which the subcarriers are spaced closely in frequency domain without interfering to each other. Previously, multiple sinusoidal generators were used to generate these orthogonal sub-carriers, because of which the OFDM system has large and complex structure. To avoid this complexity, researchers started using DFT instead of sinusoidal generators for getting the sub-carrier. Further, researcher adopted new mathematical tool FFT instead of DFT, as FFT based OFDM structure has less computational complexity. The basic idea behind this is to transmit the each single information stream onto the separate carrier parallelly. It allows transmission of multiple information streams at a time without interference of each other in a lesser bandwidth.

To generate the OFDM signal, first consider the spectrum required by the input data and the modulation scheme which is used for symbol mapping. The bit stream of input signal is encoded, where the redundant bits are added for security and reliability reason. These encoded bits are passed through serial to parallel buffer stage so that it divides the single stream information into multiple sub-streams. Further this parallel binary generated data is mapped and converted into waveform pattern by the help of modulation scheme (BPSK, QPSK, QAM). This is done to easily load that data onto analog carrier and to easily identify the error pattern by the help of constellation diagram. The phase and amplitude of carrier is being decided with the help of modulation scheme. Each sub stream is being modulated onto a subcarrier by IFFT operation.

The problem of ISI occurs when the transmitted symbol interferes with itself and receivers do not decode the transmitted signal correctly. To resolve this issue, symbols are padded with guard interval named as cyclic prefix, which acts a buffer region to save the transmitted OFDM symbol from ISI⁵. This cyclic prefix transforms the linearly Convolutional channel to cyclic Convolutional channel. The OFDM transmitter and receiver can be seen in fig.1. The signal is passed through AWGN/Rayleigh channel and received at receiver end. In order to reconstruct signal back, there is removal of cyclic extension, which converts the received symbol parallelly again by serial to parallel buffer and demodulate it by using FFT tool .Equation for IFFT

$$x(n) = \frac{1}{N} \sum_{l=0}^{N-1} X(l) e^{i*2*\pi*l*n/N} \quad (1)$$

Equation of FFT is

$$X(l) = \sum_{k=0}^{N-1} x(n) e^{-i*2*\pi*l*n/N} \quad (2)$$

Here, N denotes the total number of sub-carrier, and l denotes the lth sub-carrier on which the data is being loaded.

II-DWT BASED MIMO-OFDM SYSTEM

In the proposed system the basic principle of DWT-MIMO-OFDM system has taken into consideration, in which the IDWT tool is used for modulation and DWT tool is used for demodulation. It is an additional approach to study signal in both time and frequency domain⁴. The wavelet transform is more preferred tool over Fourier transform as it has better frequency and time localization. It has been considered better for the study of non-stationary signals. They both satisfy the rule of orthogonality and used as a carrier in OFDM system. Wavelet basically means a small (finite length) oscillatory wave with amplitude that starts at zero, increases, and again settles down to zero. The wavelet transform is a mathematical tool used to give time-frequency representation of signal⁶. It helps to analyze at what interval of time, the signal has that frequency component. Generally, it has categorized into two formats one is continuous wavelet transform (CWT) and other one is discrete wavelet transform (DWT). DWT does not mean evaluation of signal is being done in discrete domain, whereas it symbolizes the evaluation of signal is being taken in continuous domain with the discretization of scaling and translational parameters. The CWT tool is being avoided in OFDM as it evaluates the coefficients on each scale causing numerous unwanted coefficients to represent the signal, which increases the redundancy and complexity at receiver side.

The wavelet basis function is given by⁶

$$W(s,\tau) = (1/\sqrt{s}) \psi((t-\tau)/s) \quad (3)$$

It dilates, translates and scaled the mother wavelet $\psi(t)$ ⁶. Here, s is a scaling parameter decides the width of the wavelet and τ is the translating parameter decides the duration of the wavelet. The above equation is representation of continuous wavelet transform (CWT) basis function. For discrete wavelet transform (DWT) the researchers has derived the basis function by the help of CWT, by putting some specified value, which evaluates the coefficient for representing the signal at some specific scale. It follows the Heisenberg uncertainty principle which states that one cannot know what spectral component can exists at what instances of time, we can only have the information about the time interval in which certain band of frequency exists.

DWT mainly decompose the signal into a set of mutually orthogonal wavelet basis functions and has filters of different cutoff frequencies which is used to analyze the signals at different scales⁹. The signal is decomposed into successive bands from which one is passed through low pass filter and other one is passed through high pass filter repeatedly⁵. The low passed one produces approximation that is eliminating the high frequency component, leaving out the details and considering only approximate part of signal so they are called as approximate coefficients. The signal which is passed through a high pass filter is used to analyze the high frequencies generating the detail coefficient leaving out the approximate part of signal by considering the detailed one only. Each level gives the detailed and approximated coefficients, till the further decomposition of signal is not possible. Fig.2 represents the basic DWT/IDWT structure and fig.3.shows the three level decomposition of signal having a series of low pass and high pass filter.

Equation for IDWT of X(K) is given by¹²

$$(x(n)) = \sum_{m=-\infty}^{\infty} \sum_{k=-\infty}^{\infty} X(m, k) 2^{m/2} \psi(2^m n - k) \quad (4)$$

Equation for DWT of x(n) is given by¹¹

$$X(m, k) = \sum_n x(n) 2^{m/2} \psi(2^m n - k) \quad (5)$$

The scale is changed by up-sampling and down-sampling (sub-sampling) operations. It reduces some sample of the signal. $\psi(m, k)$ is mother wavelet function, m represents the translation scale. Fig.4 shows the transmitter/receiver structure for DWT-MIMO-OFDM system. The input bits are first taken by encoder to encode bit stream with a particular code rate. Then the encoded stream is sent to modulator for converting the input binary stream to waveform pattern. Again the symbol is passed through the Serial to parallel buffer for further transmission. The symbol gets loaded to M-band wavelet carrier by the help of IDWT tool. These symbols are transmitted through the channel and get demodulated by using DWT tool at receiver end.

III-CYCLIC PREFIX

Due to signal propagation phenomena, such as reflection, diffraction or say multipath, a receiver can receive several delayed versions of same signal. At the receiver all these multipath components are summed and multiple symbols being received simultaneously overlap with each other called as ISI. If the bandwidth of the transmitted signal is very large compared to the bandwidth of channel, then there will be effect of interference in the symbol. But if the symbol length gets increase (or can say bandwidth of transmitted symbol get decreases) then the effect of ISI can be mitigated. In order to increase the symbol length, the copy of last part of symbol is being inserted at initial point of symbol as shown in fig.5 below. The receiver can identify the end points of each symbol and correctly correlates the information and helps to eliminate the ISI.

N_{cp} denotes the length of the cyclic prefix, N_{fft} is the IFFT window length and N show the number of sub carriers. It compensates for ICI and ISI but it consumes a considerable amount of spectrum and power⁸. Assuming the channel having maximum delay of m , insert cyclic prefix of duration n greater than channel impulse response m . It consumes large transmission energy and cause a loss in data rate of

$$\frac{\text{Cyclic prefix}(n) \times 100\%}{\text{Cyclic prefix}(n) + \text{Number of subcarrier}(N)} \quad (6)$$

It reduces spectral efficiency and data rates because it does not contain any information⁸. As, increase in length of symbol further to overcome ISI, it reduces the overall power efficiency and disperses the transmitter energy results in loss of SNR which is given by

$$-10 \log_{10} \frac{(\text{Total OFDM Symbol length} - \text{Cyclic Prefix length})}{\text{Total OFDM symbol length}} \quad (7)$$

The waveform being used in wavelet transform are longer than the normal transform duration, because of which DWT-OFDM symbols overlap in time domain and gives better frequency localization⁹. In result it does not require cyclic prefix to extend the symbol duration in order to mitigate ISI. Also, FFT-OFDM symbols are passed through rectangular shape of window generating larger side lobes, this is avoided in case of DWT-OFDM. Moreover, it reduces the complexity of system from FFTs $O(N \log_2 N)$ to $O(N)$ ¹⁰. The DWT-OFDM not only saves the bandwidth by not adding CP to OFDM symbol but also saves the transmission power and enhances the capacity of system.

IV-CHANNEL ESTIMATION

Channel estimation is a mathematical estimation of what is exactly happening in environment. It allows receiver to approximate and measure the effect of channel on signal, so that ISI and noise can be removed from it¹³. In proposed model pilot sequence based channel estimation called as Least Square Channel estimation technique has been considered. In this a reference carrier named as pilot symbol is known at receiver end in terms of position or pattern and used for channel estimation. The transmitted and received signal is represented in vector and matrix form for the ease of evaluation. For any l^{th} subcarrier, the received vector can be represented as

$$Y(l) = X(l)H(l) + W(l) \quad (8)$$

$H(l)$ represents the channel coefficient across l^{th} subcarrier and $X(l)$ represents the symbol loaded onto l^{th} subcarrier. For N subcarrier after rearrangement, the received signal in matrix form can be represented as

$$\begin{bmatrix} Y(0) \\ \vdots \\ Y(N) \end{bmatrix} = \begin{bmatrix} X(0) & 0 & 0 & \dots & 0 \\ 0 & X(1) & \ddots & \vdots & \\ 0 & 0 & \dots & X(N) & \end{bmatrix} \times \begin{bmatrix} H(0) \\ \vdots \\ H(N) \end{bmatrix} + \begin{bmatrix} W(0) \\ \vdots \\ W(N) \end{bmatrix} \quad (9)$$

Y is $N \times 1$ receiver pilot output matrix in subcarrier domain, X is $N \times N$ diagonal invertible matrix whereas W is a $N \times 1$ noise matrix in sub carrier domain. Estimate of coefficient on l^{th} subcarrier is given by

$$\hat{H} = X^{-1}Y \quad (10)$$

Where X^{-1} is the pseudo-inverse of X and is given by

$$\begin{bmatrix} \frac{1}{X(0)} & 0 & 0 & \dots & 0 \\ 0 & 0 & \vdots & \ddots & 0 \\ 0 & 0 & \dots & \dots & \frac{1}{X(N)} \end{bmatrix} \quad (11)$$

So, by above discussion FFT of channel coefficients has been found. In order to find the channel taps estimate take IFFT of the estimate of subcarrier coefficient.

$$\hat{H} = Y(l)/X(l) \quad (12)$$

V-SIMULATION RESULTS

In this paper, DWT based MIMO-OFDM system performance has been measured in SNR versus BER graph. The required simulation parameters are shown in table-1 and their performance is being compared in fig.6 and fig.7. As fig.6 and fig.7 shows inverse relation in SNR and BER, on increase of SNR the noise content in signal decreases and the probability of occurring error also decreases. In fig.6 the five transmitter and five receiver antennas perform this communication process without channel coding resulting in increase in BER as increase of order of modulation scheme. QPSK has lowest BER compared to 16-QAM and 64-QAM, which also matches to the theoretical reason of sending lesser bits at a time results in lower tendency of occurring error.

Fig.7 shows performance and comparison of system with Convolutional coding with two different rate and modulation scheme. It is said to be Convolutional encoder as it performs a Convolution of input streams with encoder impulse response. As, channel codes adds redundancy to the codes provide protection to the information bits which enhanced the BER performance of signal. The BER performance of QPSK, 16-QAM, 64-QAM with code rate of 1/2 and 3/4 follows the same order for occurrence of error as shown in fig.7. As, for lower code rate means higher the number of bits for data error detection and correction process, so performance of the system enhances but have less bandwidth efficiency. For higher code rate and order of modulation of system greater will be the rate of occurrence of error, so 64-QAM with code rate 3/4 has the higher probability of error.

Table-2 refers for the comparison among considered conventional system (2x2) and the proposed system (5x5). The results show that as the number of transmitter and receiver increases then the performance of system gets degraded. For proposed system, BER has increased compared to the conventional one. Major effect on system can be seen for lower SNR values, as the noise content in signal is higher, chances of occurring error is high for any system. As, on increase in transmitting antennas, it results in transmission of more bits for multiple user (by using MIMO scheme) independently causes more possibility of occurring errors, which can be seen in simulation results.

Throughput is an important indicator of performance and quality of network connection. It is the rate of successful message transmission over a communication channel. Fig.9 shows the throughput performance of system with different code rate and modulation schemes. It indicates that higher the code rate and order of modulation scheme better will be the throughput performance of system. Theoretically it is being measured with the Shannon formula. At the lesser value of SNR system did not performed well but as SNR got improved the rate of successful transmission of data enhances resulting in good throughput performance of system. After a certain range of SNR, the performance of the system gets constant.

Fig.8 represents the average capacity of a MIMO system for different number of transmitter/receiver antenna. Further, the capacity versus SNR graph has been shown for the analysis. As, the number of transmitter/receiver increases, capacity to carry more information (bits) also increases. Hence, there is proper channel utilization. This paper includes the water filling algorithm for allocating the optimal transmitting power for independent multiple parallel channels, computing the capacity of the MIMO channel for a given noise power of 10⁻⁴ watt and SNR range of -10 dB to 20 dB. As, the SNR range of -10 dB to 50 dB is considered suitable for voice and wireless network, that's why this paper includes the above stated SNR range. The 3x2 and 2x3 diversity scheme has almost same capacity for carrying information however, 4x4 has the maximum one. The total capacity for a MIMO channel is given by Shannon channel capacity theorem

$$\sum_{i=1}^t \text{Log}_2(1 + P_i \sigma_i^2 / \sigma_n^2) \text{ bits/s/Hz} \quad (13)$$

Here t is the number of transmitting antenna σ_i^2 is gain of ith stream of channel obtained by the singular value decomposition of channel matrix, σ_n^2 is power of noise present in the channel and P_i denotes the transmitted power of the ith signal. Here, P_i is calculated by water filling algorithm, where

$$P_1 + P_2 + P_3 \dots \dots \dots P_t < P_{\text{total}} \quad (14)$$

and P_i is $(1/\lambda - \sigma_n^2 / \sigma_i^2)$, here λ is Lagrange's multiplier.

VI-CONCLUSION

The transmission rate of DWT-MIMO-OFDM system gets improved by the dynamic adjustment of radio transmitter modulation schemes, which ensures the higher data throughput and spectral efficiency with higher order of modulation. The primarily defined DWT tool in place of FFT tool helps to avoid insertion of cyclic prefix, that leads to bandwidth and power saving of a wireless communication system. The simulation results of the proposed system with and without channel coding has been demonstrated showing channel coding helps to detect and correct the errors, causing decrease in BER performance of the system. The simulation results for throughput performance of the system with different modulation order/schemes, and code rate shows that there is a trade-off

between the BER performance and code rate of system. As, on increase in code rate and the count of transmitter and receiver there is increase in carrying more number of bits through available channel and also in probability of occurring error. So, by using higher count of transmitter/receiver helps in transmitting more information at a time but with a drawback of higher BER.

REFERENCES

- [1] Pu Liang, Fang Yuan, Li Wei, Wang Zhisen, "Channel estimation in mobile wireless communication", *International conference on communication and mobile computing*, 2010, PP 77-80.
- [2] Bhagwatkar Sonali A., Patil B.P. and Satpute Bhalchandra S., "Performance of MMSE Channel Equalization for MIMO-OFDM system", *International conference of computing communication control and automation*, 2016.
- [3] Venkatasubramanian Akhilesh, Krithika.V and Partibane.B, "Channel estimation for a Multi-User MIMO-OFDM-IDMA system", *International Conference on Communication and Signal Processing*, April 2017, PP 1823-1826.
- [4] Sharma Vishal, Kaur Harleen and Singh Gurpreet, "BER Assessment of MIMO incorporated W-OFDM Wireless Communication System", *International Conference on Advanced Computing and Communication Technologies*, 2015, PP 463-466.
- [5] Meenakshi D., Prabha S. and Raajan N.R., "Compare the performance analysis for FFT based MIMO-OFDM with DWT based MIMO-OFDM", *IEEE international conference on emerging trends in computing, communication and Nanotechnology*, , 2013, PP 441-445.
- [6] Agboje Oboyerulu E., Idowu-Bismark Olabode B., Ibhaze Augustus E. "Comparative analysis of Fast Fourier Transform and Discrete wavelet based MIMO-OFDM", *International Journal on communication antenna and propogation*, vol.7 april 2017.
- [7] Shubhangi, Chaudhary R., Patil Anil J. and Yadav Ashwini V., "WLAN-IEEE 802.11 ac:Simulation and performance evaluation with MIMO-OFDM", *Conference on advances in Signal Processing* , 2016, PP 440-445,.
- [8] Al-Jzari Amar, Kostanicliva, "Cyclic Prefix length Determination for orthogonal frequency division Multiplexing system over different wireless channel models based on maximum excess delay spread", *American Journal of Engineering and applied sciences*.
- [9] Gupta Abhishek, Nigam Prateek, Chaurasia Vijayshri, "A review on wavelet transform as a substitute to cyclic prefix removal in FFT In OFDM", *International Journal of engineering sciences and research technology*, February 2014, PP 827-830,.
- [10] Gupta Mahesh Kumar, Shrivastava Sarika, Raghuvanshi A.S., Tiwari S., "Channel Estimation for Wavelet Based OFDM System". *International conference on devices and communications*, February 2011.
- [11] Broughton S.A, Bryan K., "Discrete Fourier analysis and Wavelets," John Wiley, New Jersey, 2009
- [12] OLtean Marius, Nafornita Miranda, "Errors per scale statistics for a wavelet OFDM transmission in flat fading channels", *6th IEEE International Symposium on intelligent Signal Processing,* Aug 2009, PP.119-124.
- [13] Yantaoqiao, Yu Songyu, Su Pengcheng, Zhang Lijun , "Iterative algorithm of least square channel estimation in MIMO-OFDM", *IEEE trans. On broadcasting*, vol 51, PP 631-640 march 2005.

Figures and Tables

Figure.1 FFT based OFDM transceiver system

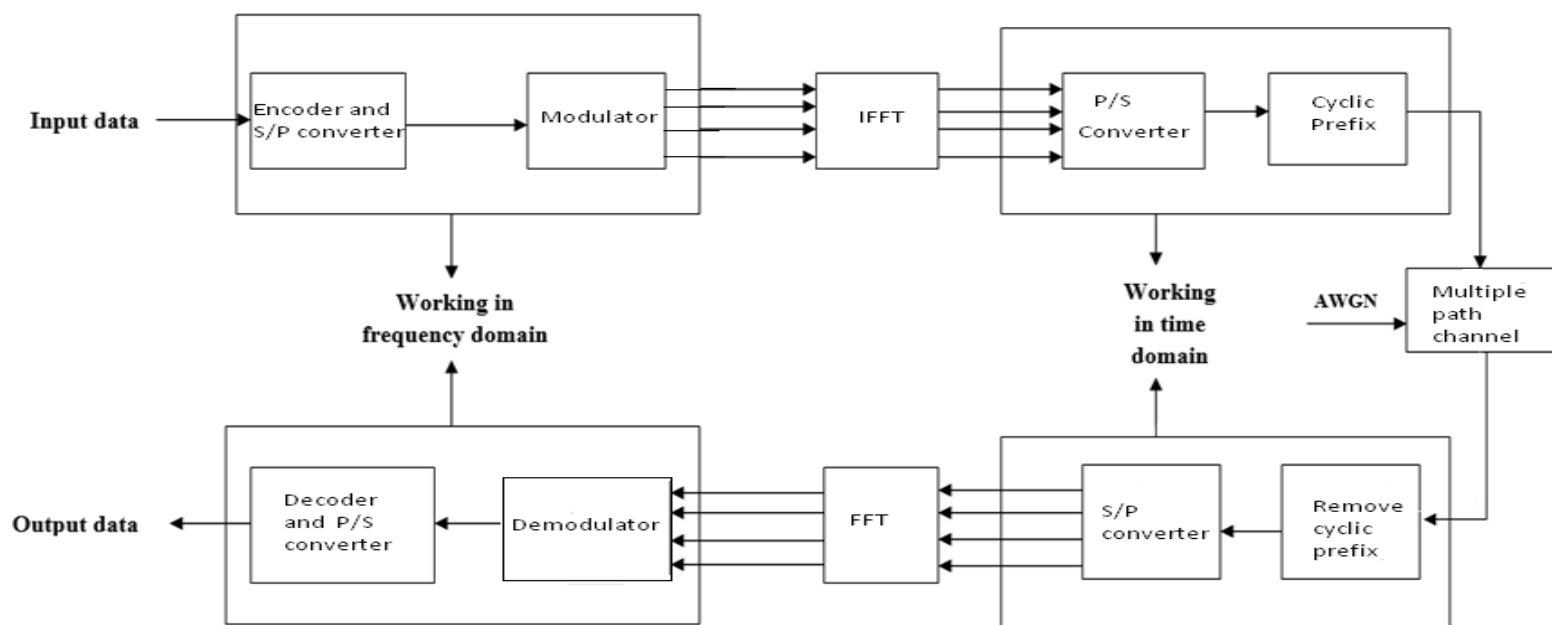


Figure.2. Decomposition and Reconstruction of signal using DWT and IDWT

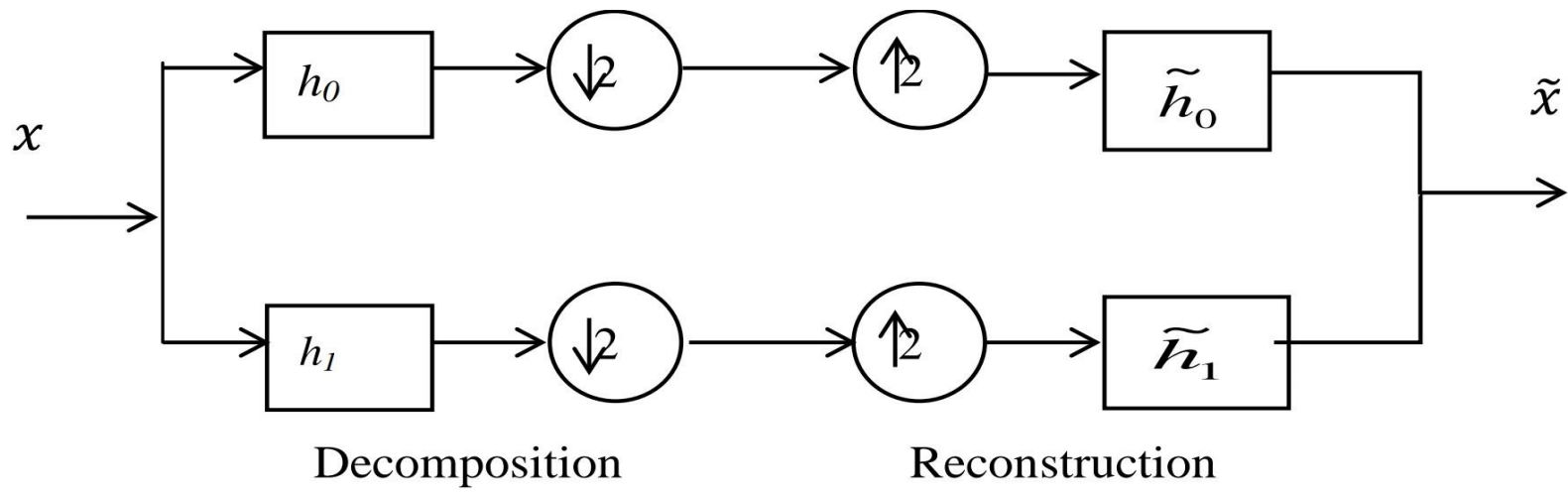


Figure.3. DWT structure

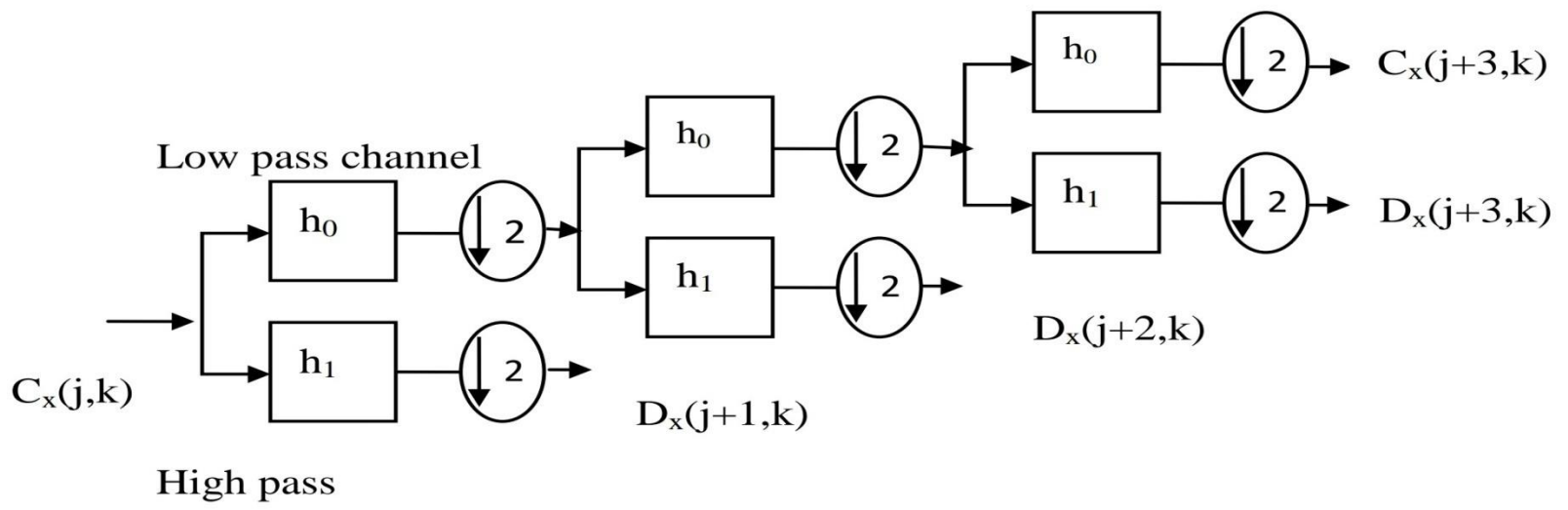


Figure.4. DWT based OFDM transceiver system

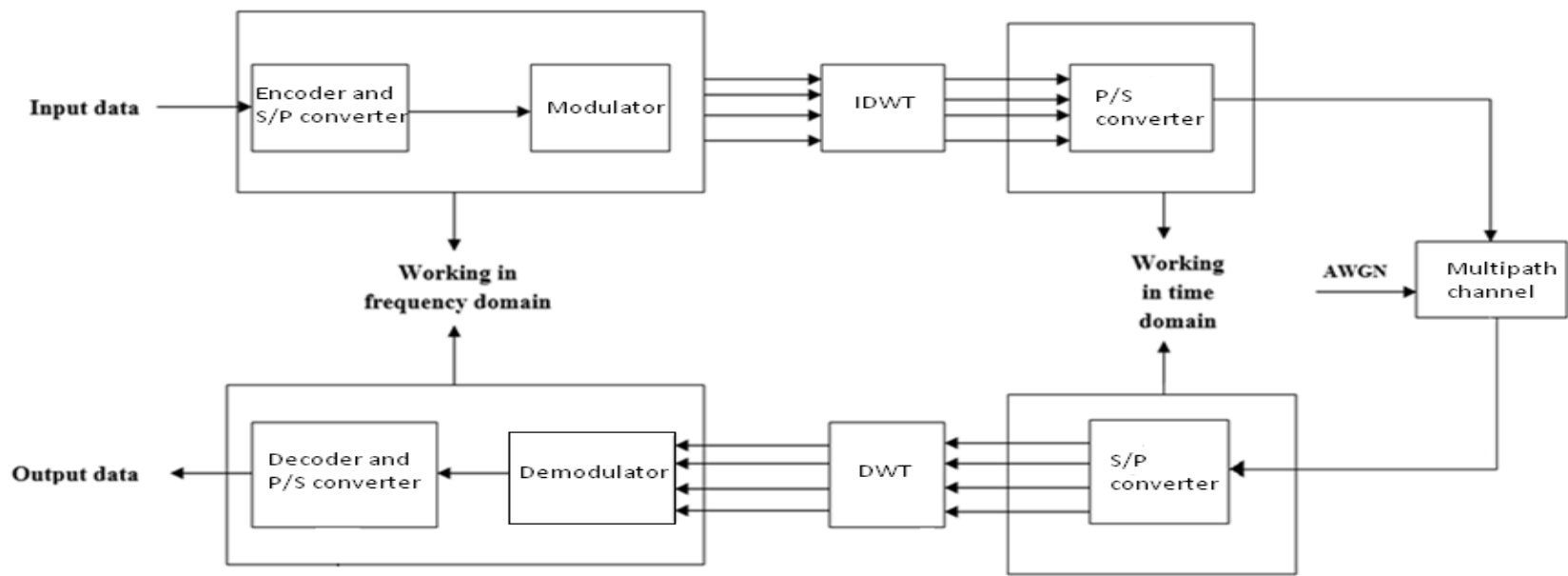


Figure.5. OFDM symbol for FFT

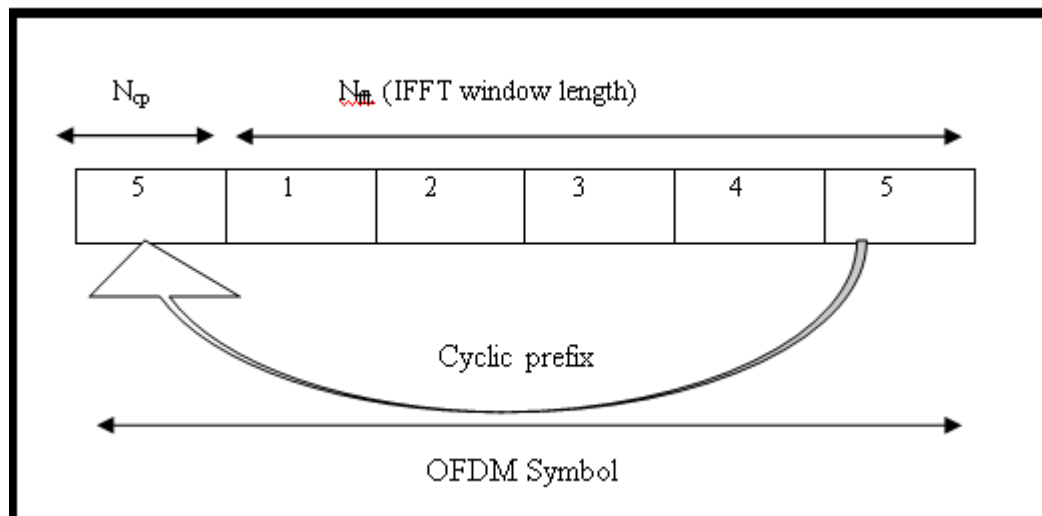


Figure.6. BER performance of system without channel coding

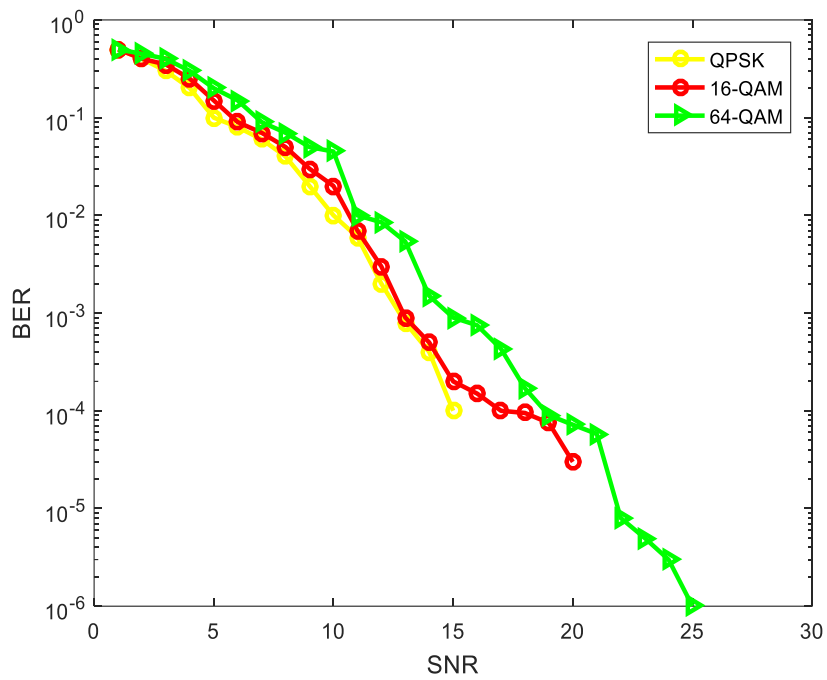


Figure.7. BER performance of system with Convolutional Channel coding

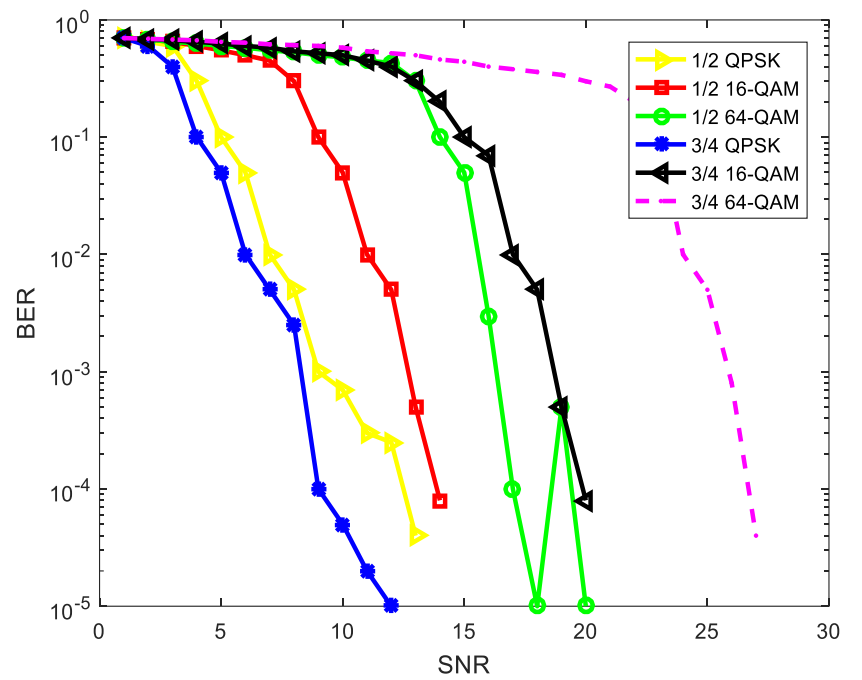


Figure.8. Average Capacity of a MIMO system for different number of Tx-Rx antennas.

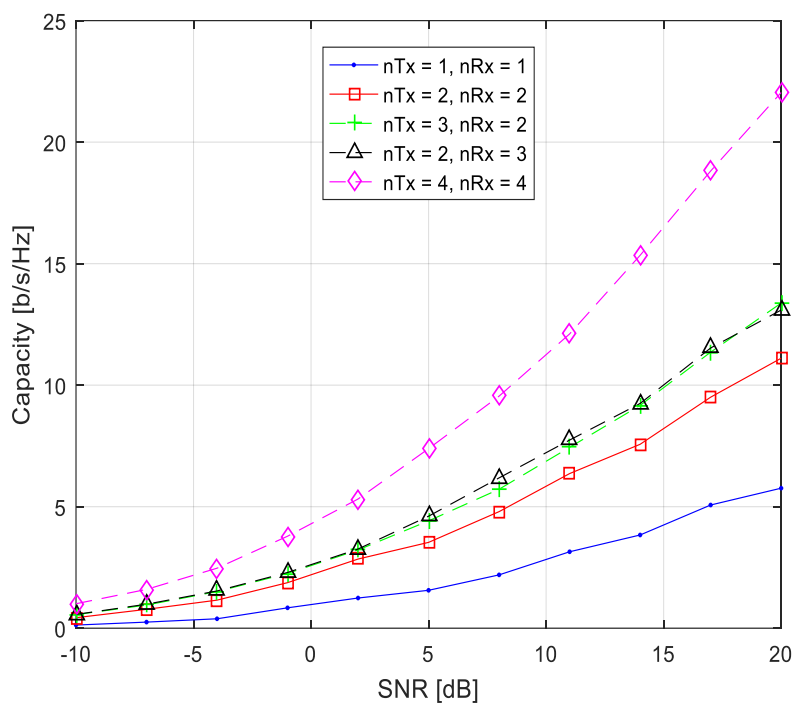


Figure.9. Throughput performance of system with channel

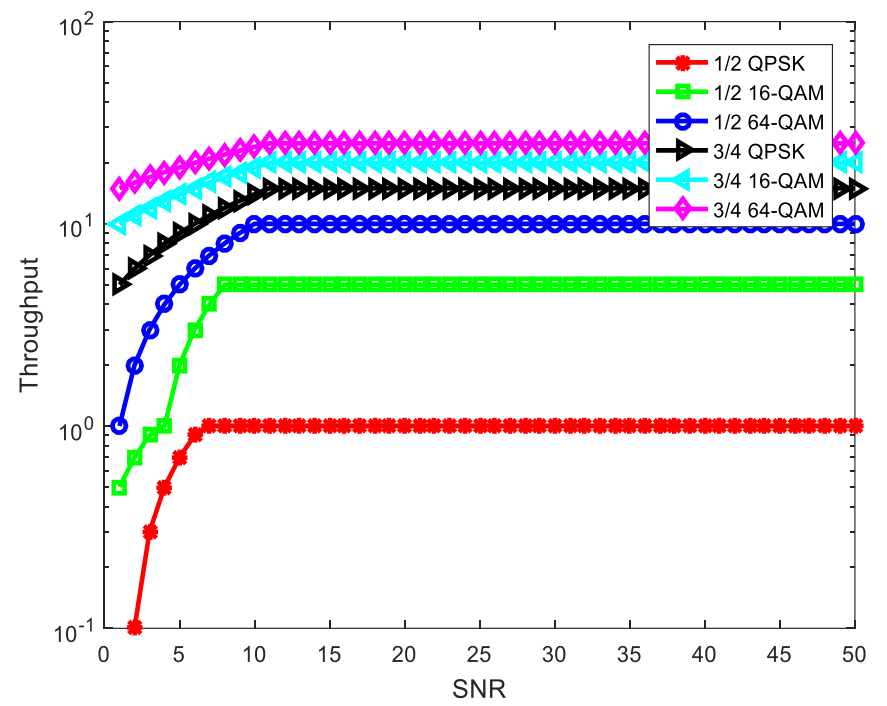


Table 1: System specification table

Parameter	Specification DWT-MIMO-OFDM system
Channel Model	AWGN channel
Modulation	QPSK,16-QAM,64-QAM
Diversity Scheme	5x5
Channel estimation	Least square
Number of subcarriers	1024
Code Rate	1/2 and 3/4

Table-2: DWT-MIMO-OFDM system comparison table

	Specification DWT-MIMO-OFDM system	Specification(proposed model) DWT-MIMO-OFDM system
Channel Model	AWGN channel	AWGN channel
Modulation	QPSK	QPSK,16-QAM,64-QAM
Diversity Scheme	2x2	5x5
Channel estimation	Least square	Least square
Code Rate	1/2	1/2, 3/4

A relative analysis of Hybrid Signed Digit adder to Redundant Signed DigitAdder

Divya Srivastava¹, K.Raj²

Electronics Engineering Department¹, Electronics Engineering Department²

Harcourt Butler Technical University¹, Kanpur, Uttar Pradesh, India¹

Harcourt Butler Technical University², Kanpur, Uttar Pradesh, India²

divya.sri7v@gmail.com¹, kraj_biet@yahoo.com²

Abstract— The number representation is one of the important aspects of arithmetic operations such as adders and multipliers can have a lower delay by using an adequate number system. Adders are the important circuit for many of the digital signal processing application, not only it is used for addition but also function as a filtering component, for multiplexing and also for the division. Thus a circuit performance can be evaluated on its base adder and eventually on the number system implemented. Increasingly high demands are rising for faster computational performance by lowering the delay and using a compact space. This demands a trade-off between computational speed and lesser silicon area. Hybrid signed digit adder is a better alternative compared to the traditionally signed digit and redundant signed digit number system. In this paper, a comparative analysis is done considering the various adders based on the gate delays generated on increasing the bit length. Individual performances are then compared with the proposed Hybrid signed digit adder. Carry Save Adder and Carry Skip Adder are also been subsumed in this paper. The paper discusses designing an optimum adder which has a proper trade-off in-between area, speed, and power.

Keywords— *Ripple carry adder, Carry save adder (CSA), Carry Skip Adder, Carry look ahead adder, Redundant Signed Digit Adder, Propagation Delay, Hybrid signed Adder.*

I. INTRODUCTION

The implementation of the arithmetic algorithms has gone through continuous development for achieving the greater computational speed along with a reduction in silicon area and power dissipation¹⁹. To accomplish this aim choosing a correct number representation scheme plays a trivial role in designing¹⁸. Eventually, a proper trade-off is required to balance all the requirement in a single design space. Binary digit representation is one of the popular number representation systems, shows an interesting result in terms of the trade-off¹. Redundant number representation^{3,4}, is an extension to signed digit representation. It provides a faster arithmetic operation in a fixed time constraint. Redundant number system finds its application in a various digital signaling application such as FFT¹⁷, Floating-point addition⁸ and can be used as a conversion and reconversion of number during designing. The basic signed digit number system which is also know as the binary signed digit number representation show the positive number with a 0 and the negative number with 1. But the general signed digit number represent the signed magnitude as well as the unsigned magnitude with the help of the number set of {-1,0,1}. By using this representation, the redundancy of the system is increases which is the basic principle for the “carry-free” addition adder system. The carry-less propagation meaning is that the carry generated in one stage will not transfer to other stage or it can limit to a particular length of the word length. This process is very much useful in multi-operand system as it gives the designer a faster result compared to the earlier design. The Signed digit number system is basic this type carry-free propagation of the adder. The Signed digit number system will limit the carry of the addition to single unit place.

The design of the adder based on the signed digit number system representation is faster but have higher complexity compared to normal design. This make us to propose a dsign which can be comparatively lower in complexity front of the design. The typical RBSD adder performs the carry limited addition in two stages 1). Design computation stage, here the intermediate carry along with sum are generated. Both of the positive carries as well as negative carries are entertained to through next weighted stage 2). Addition of the intermediate stage the output of the prior stage is done in RBSD form without the requirement of carry bit as input from the prior stage¹⁶.

The hybrid-redundant number which is a subclass of redundant number systems can be used for optimum design of the digit-parallel addition algorithms.

The (HSD) number systems described in ⁵, which is formed by signed as well as unsigned numbers digits positioned alternatively to each other. This number system provides a strong alternative to the redundant number system for designing point of view. The hybrid signed digit representation had some limitation^{6,12} which are mentioned as below:

- There is a considerable amount of difference in the range which is used for positive and negative numbers, which may lead to improper implementation of subtraction algorithm.
- There is no circuitry used to accelerate the carry propogation in HSD. This absence of the circuitry is due to the fact that HSD doesn't use a standard adder cell in its circuitry.
- HSD doesn't have the symmetric approach to the designing due to which it's designing is complex to implement.

A comparative analysis is obtained for the various adder having the different number representation. The analysis is basically done on terms of delay during the computational time of the adders and also on the complexity on designing they show during the designing process. The initial section i.e. the second section describes about the redundant number system a prime focus is given to the RBSD representation and the conversion and reconversion of the RBSD to and from the binary representation in also evaluated in tabular format. The third section of the paper gives the basic ideas about the different adders used in the paper and advantages along with the disadvantages the bring to the table. Finally in the fourth section discussion is made about the proposed HSD adder. A basic algorithm of HSD adder is described in detail. The later section of the paper shows the detailed results and comparative analysis obtained about these adders circuits. The conclusion section conclude this paper with the future scope of the paper that is the implementation of the carry-save adder in HSD to further enhance the scope of the HSD adder.

The RBSD adder shows a better result when compared to the SD adder as the latter shows ineffective in dealing with the redundancy produced by the adder during the carry less addition. Thus the RBSD comes handy and over comes this short coming of the SD adder but this luxury is achieved on the cost of area and complexity. A HSD adder which shows a slightly lower result compared to the RBSD adder have the simplicity of the SD adder and the redundancy handling capacity of the RBSD adder, thus showing a optimum results as having the best of the both world.

II. FUNDAMENTAL OF REDUNDANT SIGNED DIGIT NUMBER

Redundant binary signed number system (RBSD) which uses radix-2 representation, by using (-1, 0, 1) to represent any number. The radix-2 representation can express any number in more than one form, this property of radix-2 is exploited by RBSD representation⁶. The RBSD representation has found its application in the various field especially in digital signal processing and also while performing the normal arithmetic operation in computer-oriented programming. The basic model of RBSD was suggested by Robertson in 1959 and again by Avizienis in 1961³. The arithmetic operation performed using RBSD have a faster computational time as there is a concept of "carry-free".

The Signed digit(SD) system is a symmetric number system and assumed to have the values from $[i=-\alpha, \dots, -1, 0, 1, \dots, \beta]$ having the algebraic values[13].

$$X_v = \sum_{i=-\alpha}^{\beta} x_i r^{-i} \quad (1)$$

The value of r and x' can be chosen so that the preceding conditions should be contented. That is:

- The ' r ' radix should be a positive integer.
- The algebraic value of X_v when equal to 0 must have a distinctive representation.
- A complete parallel addition, as well as the subtraction, should be obtained for all the digit in the two's complement representation form.

The α must have the maximum values that are in the range of $[r - 1]/2 \leq \alpha \leq r - 1$ [10]. For getting the least redundancy, the highest value of α should be $\alpha = [r/2]$. If the value of $r = 2$, this representation of the number is called an RBSD number system¹⁵. Considering that the RBSD is better in comparison to the Binary Signed Digit there is a requirement to understand the conversion of these two number system to explore the dependency they have on each other

A. Conversation of Binary digit to RBS digit:

The procedure to convert Binary to RBSD is done: Firstly decimal number 12 is converted into binary. The obtained value is 1100. Now, this binary digit representation is converted to RBSD as follow¹⁵.

- The first digit namely x_i can be written in the digit position as (0,1,2,3).
- The borrow function will generate the digit B_i which was denoted in the one's digit position. B_i is the left shifted resultant of the x_i .
- Generation of D_i is done just by changing the 1's in x_i to $\bar{1}$. Here $\bar{1}$ is -1.

The RBSD z_i is obtained by adding the B_i & D_i .

B. Conversion from RBS digit to binary digit:

Assuming ' z_i ' is represented in RBSD form and ' x_i ' is represented in binary digit then[16] From table

$$z_i^+ = z_i^+ - z_i^- \quad (2)$$

Where,

z_i^+ =only for the positive digits are changed to 1

z_i^- =only for the negative digits are changed to

III. ADDER BASIC BACKGROUND

The wide range of the multi-bit adders is compared with the typical RBSD and proposed HSD adders. A comparative analysis is obtained for the same in this paper. The timing reports gives the delay of the computation time produced by each of these adders. Eventually leading us to an optimum adder design that is the HSD adder.

A. Ripple Carry Adder

A single FA(full adder) can perform the arithmetic addition of the two one-bit inputs while performing addition for multi-bit inputs there is a need of carries to flow from one full adder to others. This flow of carries resembles a ripple kind form thus coined the term Ripple carry adder. RCA is a group of multiple FA which are in cascaded form and are connected in series with each other¹⁶. The output carry of the single-stage is made to propagated to the preceding stage's as a input carry to them and then the addition is performed accordingly.

The disadvantage of RCA:

- For performing the N bits of addition, there is a requirement for N full adder blocks. Thus on increasing the input bits, the power consumption will also increase, bits and power dissipation have a linear dependency in RCA.
- As output carries from one stage need to propagate to the next block, so the delays increases. Thus the delay has a linear dependency on the number of bits.

Maximum delay that could occur for an N-gate RCA can be calculated as

$$t = 2N + 1 \quad (3)$$

then total maximum delay of RCA is :

$$T_d = (N - 1)t_c + t_s \quad (4)$$

T_d = Is the total delay of the RCA.

t_c = Is the delay time due to carry.

t_s = Is the delay time due to sum.

It is observed that delay is mostly due to the time involvement in carry propagation. The delay for RCA is **O(n)**. Here n denotes the number of bits .

B. Carry Look Ahead Adder

The carry look ahead adder circuit generate carries parallely in time. Thus due to this parallel generation of carry bits, there is a requirement for an extra circuitry¹⁶. A CLA needs more area and power due to the parallel carry generation. In the carry look ahead adder the circuit when the two bits are provided the circuit will preprocess whether the result that will be obtained after the addition will be a carry or not. This preprocessing done by the adder limits the time required by the circuit for computation.

From the figure 2 it is clear that due to the simultaneous generation of the carry, the carry of the system is minimized and this delay is almost equal to no delay in receiving the carry from the previous stage. This property of the CLA enables the system to faster computation and also the inherent quality of reversible logic based circuits make the CLA a favorable choice for the designer.

Let's assume that the G_i be generating the function(i.e. generation of the carries) and P_i be the propagating function(i.e. propagation of the carries).

Both of these function can be described as below equations:

$$G_i = A . B \quad (5)$$

$$P_i = (A \oplus B) . C_i \quad (6)$$

The equation (5) describe about the Carry equation of the Carry look ahead adder

$$C_{i+1} = A . B + (A \oplus B) . C_{in} \quad (7)$$

The adder sum is described in the below equation:

$$S_i = A \oplus B \oplus C \quad (8)$$

From the equations (5),(6) we can observe that the sum is independent of the carry. Thus we can make the circuit a carry-free propagation circuit by generating all the carry at the same time. The carry generation can be summed for the n bits of the carry is:

$$C_n = A_{n-1} \cdot B_{n-1} + (A_{n-1} \oplus B_{n-1}) \cdot C_{n-1} \quad (9)$$

C. Carry Select Adder

Carry Select Adder(CSA) is similar to RLA the difference lies on designing, the carry of the system is selected prior thus the delay generated due to the propagation from one stage to other is nullified. In CSA the carry gets repeatedly and simultaneously set and reset (i.e. selected as 0 and 1). The result of the selected carries and the result of the output carries are feed as inputs to a multiplexer circuitry and eventually, the designer gets a single weighted output at the output terminal. So, no delay in waiting for the previous stage output carry to perform the addition in the present stage².

The MUX generate the output equations for sum and carry. The resultant sum function is:

If carry equal to 1 then

$$S_0 = A_0 \oplus B_0 \oplus C_0 \quad (10)$$

If carry equal to 0 then

$$S_0 = A_0 \oplus B_0 \quad (11)$$

D. Carry Save Adder

The multiplication operation requires to add multiple summands, the technique of adding these summands is referred to as CSA. A CSA is redundant signed digit adder and it is similar to RCA the only difference is that Carry save adder doesn't propagate the carry through stage rather store the carries and later calculate it.

The addition operation of the three N-bit numbers :

- The addition of A and B will produce an intermediate sum U. This intermediate sum will add with C and generate the output Z(output of the First stage). A vector function generates the intermediate sum bit. This vector function also saves the carry of the present stage.
- At the later step of the computation, the sum and carry are added to produce the output Z which is the desired output from the system.

Advantage of Carry Save Adder:

- The sum and carry vector function are generated in a fixed time constraint. Also, the sum and carry are available parallelly which means that the delay time can be minimized using CSA.
- Carry Save Adder use N numbers of full adder blocks that will generate sum and carry individually. The entire sum of the circuit can be calculated after getting the prior output(intermediate outputs) shifted to the left by one bit.

E. Carry SKip Adder

The carry skip adder that is also called as the carry-bypass adder, is an improvement to RCA. The CSKA uses a RCA with carry bypass path(this bypass path provide the skip logic). The whole architectural bits are divided into K even numbers of the stages. Every K_i stage has a carry bypassing path which will forward

the input carry to the next stage(K_{i+1}) stage. When the binary input bits are in favorable form they can be rippled down to K_{i+1} th stage by using the bypass path. The skipping algorithm of CSA is done by bailing out a group of consecutive adder stages one at a time to reduce the carry propagation time⁹.

IV. PROPOSED HYBRID SIGNED DIGIT ADDER

Hybrid signed digit system representation is similar to the partial RS systems representation weighting radix-2 number systems. The HSD representation holds some redundant radix-2 positions, but maximumly nonredundant positions. The HSD representation has advantage compare to other representation as it limits the carry flow(propagation) chain to fixed-length(i.e. it can limit the carry propagation up to $(d+1)$ th position here d will be the longest distance separating two adjacent digits)¹¹.

The HSD adder can select carry for the propagation and can consider any value among $\{-1,1,0\}$ this is similar to the signed digit number system. This pre-selection of the carry bits helps HSD adder to reduce the carry propagation chain to $(d+1)$ th position¹⁵. HSD adder which is also used to implement the multiplier block of HSD multiplier, the basic idea behind is to multiple two HSD digits is done by shifting the digits left and then add them using the HSD adder.

Algorithm for HSD adder:

The HSD addition can be considered as $a_i = m_i + m'_i$ for the radix-2b(for HSD and SD representation). Considering m_i and m'_i as the signed digits numbers and m_{i-1} and m'_{i-1} as the unsigned position digits. The signed position digit will generate the intermediate sum when m_i and m'_i are provided as inputs. Below is the consideration to be taken for the intermediate sum and carry generation in HSD addition¹⁵

- When $m_i = m'_i = 1$, then intermediate sum equal to 0 and intermediate carry equal to 1.
- When m_i and m'_i are non-negative number and only one input of m_{i-1} and m'_{i-1} is non zero, then intermediate sum equal to $\bar{1}$ and intermediate carry equal to 1.
- When $m_i = m'_i = 0$,
then intermediate sum equal to 0 and intermediate carry equal to 0.
- When at least one inputs m_i and m'_i is non-negative and m_{i-1} and m'_{i-1} are also nn-negative, then intermediate sum equal to $\bar{1}$ and intermediate carry equal to 1.
- When both input m_i and m'_i is non-negative,
then intermediate sum equal to $\bar{1}$ and intermediate carry equal to 0.

V. EVALUATION AND SIMULATED RESULTS

The analysis is done based on gate delay of each adder. Through the analysis we observed that on varying number of bits, the delay of RCA is increases but, this behavior is limited on terms of area used and output power received. The delay of the RCA is 20ns for a 4 bit addition. In the figure 7 we sees that the output at 500 nanosecond is 4A which means the one's digit give $A(9+1=10 \sim A)$ and ten's place give the output 4 which on whole is 4A.

The Carry look ahead adder have an extra circuitry for parallel addition of the numbers due to which area requirement is higher compare to any adder discussed in this paper. A CLA have a 13.5 nanoseconds of delay compare to Carry save adder which have a delay of 16.74 nanoseconds but, as the bit increases the complexity of the design increases and thus the delay to the adder increases for a 32 bit CLA adder have a delay of 35.02 nanoseconds. From the figure 8 we observed that the carry input firstly initiated at 200ns, then at 600ns and again at 800ns and the output carry generated at 700ns.

From figure 9 the carry save adder which resembles the RSD adder have a gate delay of 18ns the gate delay is keep on increasing as the carry storing and separate evaluation of the carry take area that is greater than the RCA adder but less than that of the CLA. From the waveform we can observe that the carry ship adder which shows a improved result than the RCA by providing a bypassing path to the carry. The CSA

due to this skipping carry algorithm lowers its area requirement to 30% compared to the CSA circuit. Also the skipping algorithm provides a faster computational timing to the circuit. A 4-bit CSK adder has a 16 ns gate delay which makes this adder faster among every other adder used in this paper. The high computational speed comes at the cost of complexity. As CSK adders acquire 57% more area than RCA adders. From figure 10, an observation can be made that the carry gets high only on 200 ns and 600 ns and the output 1 (for inputs C and 5) shows that the resultant is 17 (i.e. 10001).

A HSD adder shows a result which better suits the designer. HSD adders have a higher delay compared to CSK adders but much less than RBSD adders which are traditionally used for addition. Table 4 shows a comparative analysis of the adders and from there an observation can be made that a 4-bit HSD adder required only 15.02 ns of delay which is less than most of the adders used in the paper.

The above observations can be understood more prominently by the tabulation method. Figure 10 describes the delay behavior of the CLA in comparison with the RBSD adder; it is quite obvious that the RBSD adder provides a faster computation than the CLA adder.

From figure 12, an observation can be made that HSD adders provide a better result in terms of gate delay when the number of bits is increasing.

VI. CONCLUSION

HSD adders are an integration of signed and unsigned bits which are placed in an alternative behavior, due to this hybrid nature, the HSD representation enjoys the benefits of both simplicity in addition and carry-free propagation. HSD adders show a proper trade-off between cost, area, and computational timing, which is the requirement of modern technologies in the VLSI industry. The HSD adder can introduce a CSA to its benefits to get the optimum adder design in terms of computational timing, area, and power. The HSD adder algorithm can be further explored to get the optimum HSD multiplier design, which is a key component in digital image and signal processing.

VII. REFERENCE

- [1]. Parhami, *Computer Architecture: Algorithms and Hardware Designs*, Oxford University Press, 2000.
- [2]. Deepti Obul Reddy, P. Ramesh Yadav, Carry Select Adder with Low Power and Area Efficiency, *International Journal of Engineering Research and Development*, Volume 3, Issue 3 (August 2011), pp. 29-35.
- [3]. Avizienis, A., Signed-Digit Number Representations for Fast Parallel Arithmetic, *IRE Trans. Electronic Computers*, Vol. 10, pp. 389-400, September 1961.
- [4]. Gonzalez, A. F., and P. Mazumder, Redundant Arithmetic, Algorithms and Implementations, *Integration: the VLSI Journal*, Vol. 30, pp. 13-53, November 2000.
- [5]. Phatak, D. S., and Koren, I. Hybrid Signed-Digit Number Systems: A Unified Framework for Redundant Number Representations with Bounded Carry Propagation Chains. *IEEE Trans. on Computers*, Special issue on Computer Arithmetic, vol. TC-43, no. 8, Aug. 1994, pp. 880-891.
- [6]. Phatak, D. S. Redundant Binary Representations, *IEEE Trans. Computers*, Vol. 50, No. 11, pp. 1267-1278, November.
- [7]. K. D. Tocher, Technique for multiplication and division for automatic binary computers, *Quarterly J. Mech. Appl. Math.*, vol. 11, part 3, pp. 364-384, 1958.
- [8]. Amir Kaivani and Seokbum Ko, Floating-Point Butterfly Architecture Based on Binary Signed-Digit Representation, *IEEE Transactions on Very Large Scale Integration (vlsi) systems*, 1063-8210, 2015.
- [9]. Sujan Sarkar, Jishan Mehedi. Design of hybrid (CSA-CSkA) adder for improvement of propagation delay, 2017 Third International Conference on Research in Computational Intelligence and Communication Networks (ICRCICN), 2017.

International Conference on Defence and Space Technologies, ICDST 2019, Aug 23-25, 2019, IET Lucknow, India

- [10]. H. Makino, Y. Nakase, H. Suzuki, H. Morinaka, H. Shinohara and K. Makino, An 8.8-ns 54×54-bit multiplier with highspeed redundant binary architecture, IEEE J. SolidState Circuits, vol. 31, pp. 773-783, 1996.
- [11]. Krishna Raj and Suman Lata, Fast Processing Using Signed Digit Number System, India International Journal of Electronics Engineering, 2(1), 2010, pp. 173-175.
- [12]. Behrooz pamami, Senior Member, Generalized Signed-Digit Number Systems : A Unifying Framework for Redundant Number Representations , IEEE Transactions On Computers, Vol. 39, No. 1. January 1990
- [13]. T. C. Chen, Maximal redundancy signed-digit systems, Proc. Symp. Comput. Arithmetic, Urbana, IL, June 1985, IEEE Computer Society Press, pp. 296-300.
- [14]. Vishal Awasthi, Krishna Raj, Development of Optimum Addition Algorithm using Modified Parallel Hybrid Signed digit (MPHSD) Technique, 2013 3rd IEEE International Advance Computing Conferenc.
- [15]. Smita Sharma, Akanksha Singh, KrashnKant Gupta, Addition of Redundant Binary Signed Digits Using RBSD Adder, 2015 International Conference on Futuristic trend in Computational Analysis and Knowledge Management (ABLAZE) 2015.
- [16]. N. Ravindran, R. Mary Lourde. An optimum VLSI design of a 15-BIT ALU, 2015 International Conference on Information and Communication Technology Research (ICTRC), 2015.
- [17]. K Raj, B Kumar and P Mittal, FPGA Implementation and Mask Level CMOS Layout Design of Redundant Binary Signed Digit Comparator, IJCSNS International Journal of Computer Science and 2009.
- [18]. Rajkumar Tomar, Praveen Kumar Singh and Krishna Raj, A Review of CORDIC Algorithm and Architecture with Application for Efficient Designing, International Journal of Scientific & Engineering Research Volume 4, Issue 8, AUGUST 2013 ISSN 2229-5518.

Table 1: Conversion table from Binary digit to RBS digit.

Digital Position	4	3	2	1	0
$X=(12)_{16}=(1100)_2$		1	1	0	0
$(D_i)_2$		$\bar{1}$	$\bar{1}$	0	0
$(B_i)_2$	1	1	0	0	
RBSD $Z_i=(D_i)_2+(B_i)_2$	1	0	$\bar{1}$	0	0

Table 2: Conversion table from RBS digit to Binary digit

$z_i^-(143)_{RSD}$	1	$\bar{1}$	0	0	1	0	0	0	$\bar{1}$
z_i^+	1	0	0	0	1	0	0	0	0
z_i^-	0	1	0	0	0	0	0	0	1
$x=(143)_2$	0	1	0	0	0	1	1	1	1

Figure 1. Ripple carry adder for 4 bit input and sum S and carry C_{in} and C_{out} .

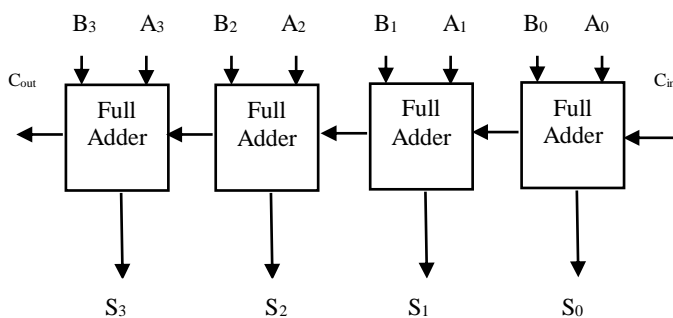


Figure 2. Carry Look Ahead Adder with multi-bit input taking C_0 as input carry and generating sum and carry

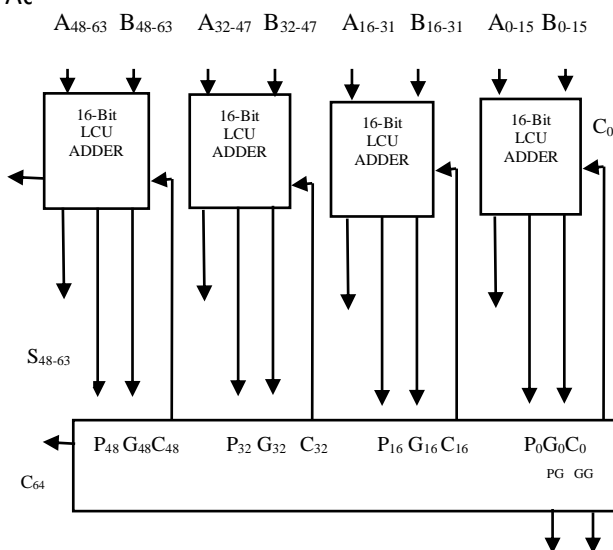


Figure 3. Carry Select Adder with 4 bit input with 0/1 C_{in} as input carry and C_{out} as output carry.

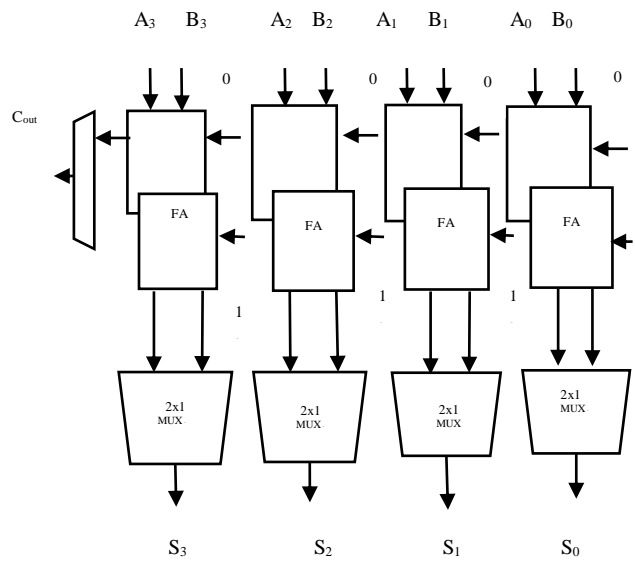


Figure 4. Carry save adder v eration stage.

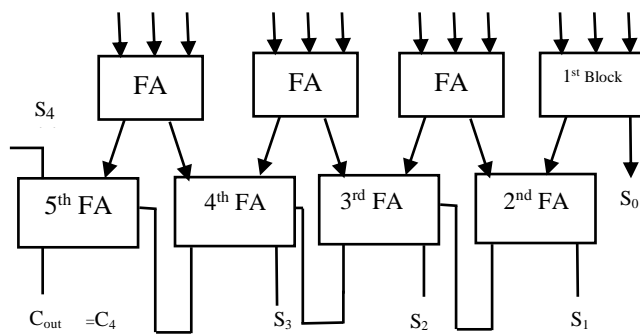


Figure 5. Carry skip adder for 8 bit input

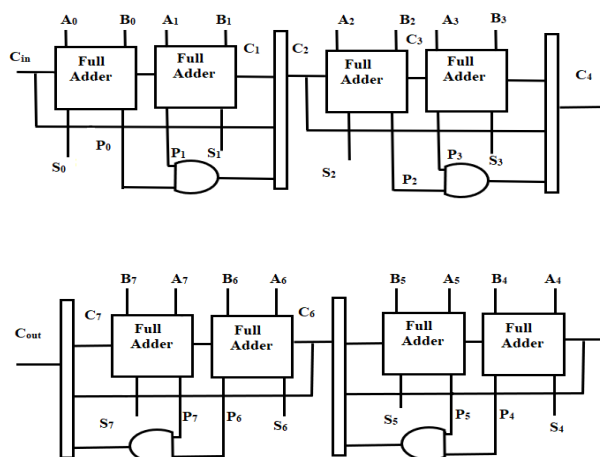


Figure 6. HSD adder for m_i and n_i addition.

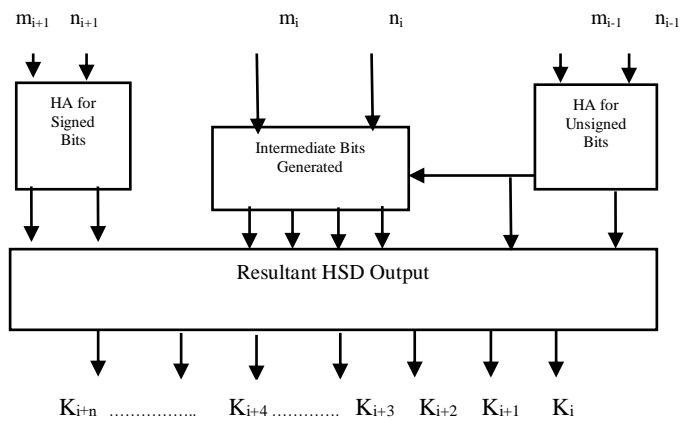


Figure 7. Waveform of Ripple carry adder which shows how the addition is performed in respect to the addition of the two number.



Figure 8. Waveform of Carry look ahead adder the output shows a less delay of the gates.



Figure 9. Waveform of Carry Save adder which shows how the addition is performed in respect to the addition



Figure 10. Waveform for Carry skip adder the output was simulated for 700ns and carry is observed.

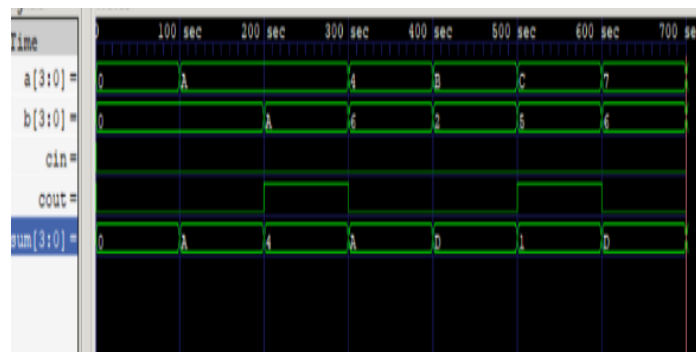


Table 3. Observation table to analyze the delay performance of the CLA and RBSD adder for different number of the bits

No. of Bits	Delay evaluated based on the gate count	
	CLA	RBSD
4 bits	13.5	16.74
8 bits	19.80	16.74
16 bits	25.02	16.80
32 bits	35.02	16.80

Figure 11. Graphical representation of the CLA adder in comparison with the RBSD adder is made for 4 bits to 32 bits.

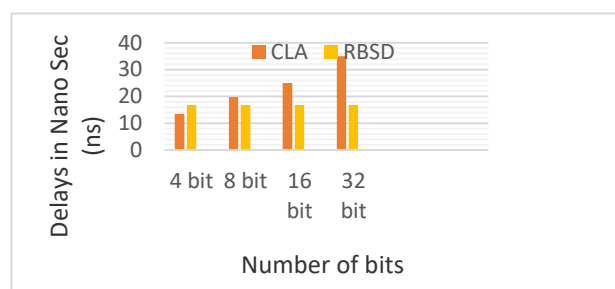
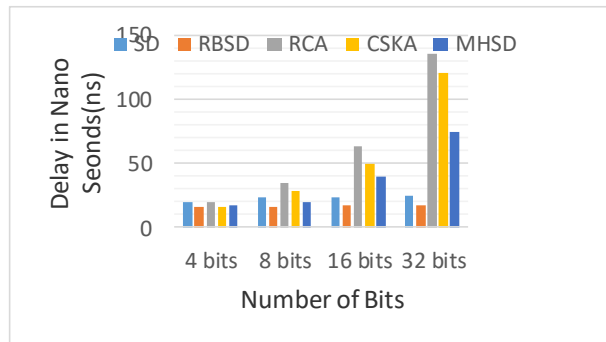


Table 4. Observation table for the delay performance analysis of the various adders for different number of the bits.

No. of bits	Delay evaluated based on the gate count					
	SD	RBSD	RCA	CSKA	CSA	HSD
4 bits	20	16.74	20	16	18	15.02
8 bits	24	16.74	35	29	20	15.02
16bit	24.21	16.80	64	50	40	15.02
32 bit	24.25	16.80	136	120	75	15.02

Figure 12. Graphical representation of adders in comparison with the gate delay produced for 4 bits to 32 bits



Design of Minimum Correlated, Maximal Clique Sets of One-Dimensional Uni-polar (Optical) Orthogonal Codes

R. C. S. Chauhan¹, MIEEE, Y. N. Singh², SMIEEE, R. Asthana³, SMIEEE

Abstract: — This paper proposes an algorithm to search a family of multiple sets of minimum correlated one dimensional uni-polar (optical) orthogonal codes (1-DUOC) or optical orthogonal codes (OOC) with fixed as well as variable code parameters. The cardinality of each set is equal to upper bound. The codes within a set can be searched for general values of code length 'n', code weight 'w', auto-correlation constraint less than or equal to λ_a , and cross-correlation constraint less than or equal to λ_c , such that $n \gg w > (\lambda_a, \lambda_c)$. Each set forms a maximal clique of the codes within given range of correlation properties (λ_a, λ_c) . These one-dimensional uni-polar orthogonal codes can find their application as signature sequences for spectral spreading purpose in incoherent optical code division multiple access (CDMA) systems.

Index Terms: — Auto-correlation constraint, Cross-correlation constraint, One dimensional uni-polar orthogonal codes (1-DUOC), Difference of positions representation (DoPR). Extended DoP matrix, Maximal clique sets.

1. INTRODUCTION

TO implement a CDMA system, one need a set of CDMA codes having a desired properties. Usually, there exist more than one set of such sets for given parameters. We desire to find the algorithm to identify all the sets of minimum correlated orthogonal codes [1]-[4]. Similarly, in Optical CDMA multiple sets of minimum correlated one-dimensional uni-polar (optical) orthogonal codes with fixed or variable code parameters are required to increase the channel capacity [5]-[6] and inherent security. The code parameters for one dimensional uni-polar orthogonal codes are code length 'n', code weight 'w', auto-correlation constraint λ_a and cross-correlation constraint λ_c such that $n \gg w > (\lambda_a, \lambda_c)$.

Various one-dimensional optical orthogonal code design schemes for constant weight have been proposed in literature [7]-[13]. These schemes can design single set of optical orthogonal codes corresponding to specific values of code parameters $(n, w, \lambda_a, \lambda_c)$. The sets of 1-DUOC with variable or multi-weight parameter have larger cardinality than that of the set with constant code weight parameter [14]. The set of codes with low code weights provide poor BER performance, then the set of codes with large code-weights are desirable. The set of codes having subsets with different code weight parameters can provide multiple QoS (quality of service) as per the need [14]-[20]. The sets of 1-DUOC or OOC with variable or multi code-length parameter can be used for multi-rate systems employing OOC [5], [21]-[25]. The 1-DUOC with multi-length and multi-weight provide the multi-class set of 1-DUOC with larger cardinality and inherent security [5], [26]-[27] for use in multi-rate systems. The general values or unspecified parameters of the codes increase the inherent security of the system by decreasing the probability of generating same set of signature sequences (pattern) or orthogonal codes [27], unless code parameters are known. It can be said that the sets of 1-DUOC or OOC with general and variable code parameters are needed for systems incorporating OOC for better performance [5],[6].

We have designed the single family of minimum correlated multiple sets for fixed code parameters through proposed maximal clique search method. Secondly two or more such families can be found for various length and weight parameters. Finally one set from each family is searched such that it has minimum correlation with all others. These finally searched minimum correlated maximal clique sets of orthogonal codes with multi-length and multi-weight parameters even with equal or unequal values of auto-correlation constraint and cross-correlation constraint can be put in other family. The auto-correlation constraint for the set of codes designed here is never greater than two. The cross-correlation constraint for set of codes is always equal to one but this may exceeds to two for multiple sets of codes with fixed or variable code parameters representing tradeoff between larger cardinality and better BER performances. Each set has maximum number of codes which is given by upper bound of the set [28]-[33] such that the codes within every set form a maximal clique. In graph theory, a clique is a sub-graph such that each pair of nodes in the sub-graph is connected or adjacent. We can represent all codes as nodes and a link exist between two nodes if cross-correlation is less than or equal to λ_c . A sub-set of codes where each possible pair of codes has a link between them is the clique set [47].

In the next section, the basic properties and characteristics of one dimensional uni-polar (optical) orthogonal codes and their multiple maximal clique sets are discussed in brief which have been proposed already in [5],[6],[28]-[38]. In section III, the difference of position (DoP) representation and extended DoP (EDoP) matrices of the 1-DUOC are explored with the help of references [6],[39]-[40]. The section IV describes the method of finding maximum non-zero shift auto-correlation and cross-correlation values of 1-DUOC through conventional method as well as using EDoP matrices of uni-polar codes. In section V, an algorithm to design minimum correlated, maximal clique sets of 1-DUOC with constant as well as variable code parameters, have been proposed with the tabulated results and calculation of computational complexity of the algorithm. The last section compares the results with already proposed schemes and algorithms for constructing the sets of 1-DUOC or optical orthogonal codes (OOC). In the end, future scope and applications of the designed codes have been discussed.

2. ONEDIMENSIONALUNI-POLARORTHOGONALCODESAND THEIR MULTIPLESETS

Let two uni-polar code words X and Y belong to a code set with code parameters $(n, w, \lambda_a, \lambda_c)$.

$$X=(x_0, x_1, \dots, x_{n-1}), Y=(y_0, y_1, \dots, y_{n-1}); \forall x_t, \forall y_t \in (0, 1) \forall t.$$

Definition 2.1: [28]

The maximum of non-zero shift auto-correlation of uni-polar or binary code X is given as λ_{ax} [28].

$$\lambda_{ax} \geq \sum_{t=0}^{n-1} x_t x_{t \oplus m} \text{ for } 0 < m \leq n-1. \\ t \oplus m \text{ implies } (t + m) \bmod(n).$$

Example 2.1(a):

Let the code X with length ' n '=13 and code weight ' w '=4, be [0 1 0 1 0 0 1 0 0 0 1 0 0]. For $0 < m \leq 12$, the left circular

shifted binary sequences $(X_1, X_2, \dots, X_{12})$ of the code X, are as follows.

$$X = [0\ 1\ 0\ 1\ 0\ 0\ 1\ 0\ 0\ 0\ 1\ 0\ 0],$$

$$X_1 = [1\ 0\ 1\ 0\ 0\ 1\ 0\ 0\ 0\ 1\ 0\ 0],$$

$$X_2 = [0\ 1\ 0\ 0\ 1\ 0\ 0\ 0\ 1\ 0\ 0\ 0\ 1], \dots,$$

$$X_{12} = [0\ 0\ 1\ 0\ 1\ 0\ 0\ 1\ 0\ 0\ 0\ 1\ 0].$$

The overlapping of weighted bits or non zero shift auto-correlation of code X with its circular shifted binary sequences $(X_1, X_2, \dots, X_{12})$ are $(0, 1, 1, 2, 1, 1, 1, 1, 1, 1, 1, 0)$. The maximum of

all such values is termed as maximum non-zero shift auto-correlation λ_{ax} of the code. It will be 2 in this case.

Definition 2.2: [28]

If X_P is weighted positions representation (WPR) [36] of uni-polar orthogonal code X of length 'n' and weight 'w', the maximum non-zero shift auto-correlation λ_{ax} of the code is given as follows.

$\lambda_{ax} \geq (a + X_P) \cap (b + X_P), (a \neq b), 0 \leq (a, b) \leq n - 1$. X_P contains 'w' integer values showing weighted positions or positions of bit 1's of the code X. Here

$$a + X_P = \{(a + x_P) \bmod n : x_P \in X_P\}.$$

Example 2.2(a):

Let the uni-polar code $X = [1\ 0\ 1\ 0\ 0\ 1\ 0\ 0\ 0\ 1\ 0\ 0\ 0]$ with code-length 'n'=13, and the code-weight 'w'=4, has its weighted positions representation $X_P = (0, 2, 5, 9)$. The circular shifted sequences of the code X, or $(a + X_P)$ or $(b + X_P)$ for $0 \leq (a, b) \leq 12$, are given as following. $[(0, 2, 5, 9), (1, 3, 6, 10), (2, 4, 7, 11), (3, 5, 8, 12), [(0, 4, 6, 9), (1, 5, 7, 10), (2, 6, 8, 11), (3, 7, 9, 12), (0, 4, 8, 10), (1, 5, 9, 11), (2, 6, 10, 12), (0, 3, 7, 11), (1, 4, 8, 12)]$.

The intersection of these circular shifted weighted position sequences $(a + X_P)$ with $(b + X_P)$ is not greater than 2. Hence the maximum non-zero shift auto-correlation of the code X is equal to 2.

Definition 2.3:[6]

If X_P is weighted positions representation [36] of uni-polar orthogonal code X of length 'n' and weight 'w', the maximum non-zero shift auto-correlation λ_{ax} of the code is also given as follows.

$$\lambda_{ax} \geq (X_P) \cap (a + X_P), (0 < a \leq n - 1)$$

Example 2.3(a):

Let us take same code X as in examples 2.1(a) and 2.2(a). The intersection of WPR of code X, $X_P = (0, 2, 5, 9)$ with circular shifted sequences of X or $(a + X_P)$ is not greater than 2. Hence the maximum non-zero shift auto-correlation X is equal to 2.

Definition 2.4: [28],[38]

Auto-correlation constraint λ_a for the set of 1-DUOC is always greater than or equal to maximum non-zero shift auto-correlation λ_{ax} of every code within the set. $\lambda_a \geq \lambda_{ax}$.

Example 2.4(a):

Let the set of one dimensional uni-polar orthogonal codes is (X, Y, Z, A, B) . The maximum non-zero shift auto-correlation λ_{ax} of the codes X, Y, Z, A, B are 1, 2, 1, 2, 2 respectively. The auto-correlation constraint λ_a for the set is maximum of $(1, 2, 1, 2, 2)$ i.e., λ_a

= 2.

Lemma 2.5: [28],[38]

For code X, the maximum non-zero shift auto-correlation λ_{ax} satisfy the following relation, $1 \leq \lambda_{ax} \leq w - 1$, for 1- DUOC with code parameters $(n, w \geq 2)$.

Proof: In the uni-polar code with $w \geq 2$, at least one weighted bit will always overlap with one of the $(n - 1)$ non-zero circular shifted versions. No uni-polar code with its every non-zero circular shifted version results in 'w' overlapped weighted bits. Because 'w' overlapping weighted bits occurs only with the codes un-shifted or zero (mod (n)) circular shifted versions. Then the maximum overlapping of code with its non-zero circular shifted versions is less than w i.e. less than equal to $(w - 1)$. Hence for the code parameters $(n, w \geq 2)$ the values of maximum non-zero shift auto-correlation of the codes lies in the range 1 to $(w - 1)$.

Definition 2.6: [28],[38]

The maximum cross-correlation of a uni-polar code X with another code Y and all the $(n - 1)$ circular shifted versions of code Y is defined as cross-correlation λ_{cxy} for the pair of codes X and Y [28],[38], and satisfies

$$\lambda_{cxy} \geq \sum_{t=0}^{n-1} x_t y_{t \oplus m} \text{ or } \sum_{t=0}^{n-1} y_t x_{t \oplus m} \text{ for } 0 \leq m \leq n - 1$$

Example 2.6(a):

Let the code length 'n'=13, code weight 'w'=4, the uni-polar code X=[0101001000100] and code Y=[1101000 001000]. The maximum non-zero shift auto-correlation of both X and Y is 2. The overlapping of weighted bits of code Y with X and all 12 circular shifted versions of code X i.e. $(X_1, X_2, \dots, X_{12})$ (as given in example 2.1(a)) are (2,0,1,2,1,0,2,1,2,0,2,1,2). The maximum of these cross correlation values is 2 which is the cross-correlation for the pair of codes X and Y, i.e. $\lambda_{cxy} = 2$.

Definition 2.7: [28]

If X_P and Y_P are weighted positions representation (WPR) [36] of uni-polar orthogonal code X and Y respectively with code-length 'n' and weight 'w', the cross-correlation of the pair of code X and Y is given as follows λ_{cxy}

$$\lambda_{cxy} \geq (a + X_P) \cap (b + Y_P), 0 \leq (a, b) \leq n - 1.$$

Example 2.7(a):

Let the code length 'n'=13, code weight 'w'=4, the uni-polar code X= [1 0 1 0 0 1 0 0 0 1 0 0 0] and code Y= [1 1 0 1 0 0 0 0 0 1 0 0 0] with its weighted positions representation $X_P = (0,2,5,9)$ and $Y_P = (0,1,3,9)$ respectively. The circular shifted sequences of the code X, or $(a + X_P)$ with its weighted positions are given as following.

[(0,2,5,9), (1,3,6,10), (2,4,7,11), (3,5,8,12)], (0,4,6,9), (1,5,7,10), (2,6,8,11), (3,7,9,12), (0,4,8,10), (1,5,9,11), (2,6,10,12), (0,3,7,11), (1,4,8,12)]

The circular shifted sequences of the code Y, or $(b + Y_P)$ with its weighted positions are given as following.

[(0,1,3,9), (1,2,4,10), (2,3,5,11), (3,4,6,12), (0,4,5,7), (1,5,6,8), (2,6,7,9), (3,7,8,10), (4,8,9,11), (5,9,10,12), (0,6,10,11), (1,7,11,12), (0,2,8,12)]

The intersection of these circular shifted sequences $(a + X_P)$ and $(b + Y_P)$ with its weighted positions is not greater than 2. Hence the cross-correlation λ_{cxy}

Definition 2.8: [6]

If uni-polar code X and Y of length 'n' and weight 'w' are represented with its 'w' weighted positions, the cross-correlation λ_{cxy} of the code is also given as follows

$$\lambda_{cxy} \geq (XP) \cap (a + YP), (0 \leq a \leq n-1)$$

Alternatively

$$\lambda_{cxy} \geq (YP) \cap (a + XP), (0 \leq a \leq n-1)$$

Example 2.8(a):

Let the code length be 'n'=13, code weight 'w'=4, the uni-polar code X = [1 0 1 0 0 1 0 0 0 1 0 0 0] and code Y = [1 1 0 1 0 0 0 0 0 1 0 0 0] with their weighted positions representation $X_P = (0, 2, 5, 9)$ and $Y_P = (0, 1, 3, 9)$ respectively. The circular shifted sequences of the code Y, or $(a + Y_P)$ are given as in example 2.7(a), (b). The intersection of code X_P and the circular shifted sequences $(a + Y_P)$ with its weighted positions is not greater than 2. Hence the cross-correlation λ_{cxy} of the code X and code Y is equal to 2.

Definition 2.9: [28],[38]

The cross-correlation constraint λ_c for the set of 1-DUOCs is always greater than or equal to cross-correlation λ_{cxy} of any pair of codes within the set. $\lambda_c \geq \lambda_{cxy}; \forall x, y$.

Example 2.9(a):

Let the set of 1-DUOCs be (X, Y, Z, A, B). The pairs of codes within set are (XY, XZ, XA, XB, YZ, YA, YB, ZA, ZB, AB). Let the cross-correlation values for these pairs of codes are (2, 1, 2, 2, 1, 1, 2, 1, 1, 2) respectively. The cross-correlation constraint λ_c for the set is maximum of (2, 1, 2, 2, 1, 1, 2, 1, 1, 2), i.e. $\lambda_c = 2$ for the set of codes (X, Y, Z, A, B).

Lemma 2.10: [28],[38]

For the pair of 1-DUOC with code-parameters $(n, w \geq 2)$, X and Y, the cross-correlation λ_{cxy} satisfies the following relation, $1 \leq \lambda_{cxy} \leq w-1$. Proof: In a pair of uni-polar codes with code parameters $(n, w \geq 2)$, at least one weighted bit of one uni-polar code will always overlapped with other code or one of the $(n-1)$ non-zero circular shifted versions of other code.

Further no uni-polar code will results in 'w' overlapping of weighted bits with other code or non-zero circular shifted versions of other code. Because 'w' overlapping of weighted bits occurs only with its own un-shifted or zero (mod (n)) circular shifted version. Thus the maximum overlapping of code with other code or non-zero circular shifted versions of other code may result in less than w or less than equal to $(w-1)$ overlapping. Hence, for the code parameters $(n, w \geq 2)$, the cross-correlation of the pair of codes lies between 1 to $(w-1)$. The one-dimensional uni-polar

orthogonal codes with $\lambda_{cxy} = 1$ are perfect uni-polar orthogonal codes, while the codes with $1 < \lambda_{cxy}$

are quasi orthogonal.

Theorem 2.11:

The orthogonality and cardinality of the maximal set of one-dimensional uni-polar orthogonal codes are inversely proportional to each other.

Proof:

The pair of uni-polar codes with $\lambda_c = 1$, is termed as maximum orthogonal 1-DUOC pair. While the pair of uni-polar codes with $\lambda_c = w - 1$, is termed as minimum orthogonal pair of 1-DUOC.

For $\lambda_a = \lambda_c = \lambda$ where $1 \leq \lambda \leq w - 1$, the maximum number of one dimensional uni-polar orthogonal codes Z , within a set, is given by following Johnson bound[28]-[31],

$$Z(n, w, \lambda) \leq \left\lfloor \frac{1}{w} \left[\frac{n-1}{w-1} \cdots \cdots \cdots \left[\frac{n-\lambda}{w-\lambda} \right] \right] \right\rfloor = J_A(n, w, \lambda)$$

Here $\lfloor a \rfloor$ represents largest integer less than or equal to a . For $\lambda = w - 1$

$$Z(n, w, w - 1) \leq \left\lfloor \frac{1}{n} {}^n C_w \right\rfloor = \left\lfloor \frac{1}{w} \left[\frac{n-1}{w-1} \cdots \cdots \cdots \left[\frac{n-(w-1)}{1} \right] \right] \right\rfloor$$

which represent maximum number of 1-DUOCs within one set with minimum orthogonality.

$$\text{For } \lambda = 1, Z(n, w, 1) \leq \left\lfloor \frac{1}{w} \left[\frac{n-1}{w-1} \right] \right\rfloor$$

which represents to minimum number of uni-polar orthogonal codes in one set with maximum orthogonality.

For $(\lambda = p)$, $(1 < p < w - 1)$, the cardinality of maximal set is

$$Z(n, w, p) \leq \left\lfloor \frac{1}{w} \left[\frac{n-1}{w-1} \cdots \cdots \cdots \left[\frac{n-p}{w-p} \right] \right] \right\rfloor$$

which is less than the cardinality of maximal set for $\lambda = (p + 1)$

$$Z(n, w, p + 1) \leq \left\lfloor \frac{1}{w} \left[\frac{n-1}{w-1} \cdots \cdots \cdots \frac{n-p}{w-p} \left[\frac{n-(p+1)}{w-(p+1)} \right] \right] \right\rfloor$$

While the orthogonality for the set with $(\lambda = p)$ is greater than for the set with $(\lambda = p + 1)$. It proves that orthogonality and cardinality of maximal set are inversely related to each other.

Lemma 2.12:

The maximal set of 1-DUOCs with parameters $(n, w, \lambda_a, \lambda_c)$ forms a maximal clique of codes.

Proof:

All the codes in a set are such that every pair of codes is having correlation properties within given range. If the codes are assumed to be nodes, then each node is connected with all others with the given properties. This shows that all the codes within set form a clique. If the cardinality of the set is maximum or equal to upper bound; it means that the formed clique of codes is maximal. A code is chosen and we can keep on adding another code to extend the set so that extended set is a clique. Once it is no more possible to extend the set further, we have achieved a maximal clique.

Theorem 2.13:

For the code parameters $(n, w, \lambda_a, \lambda_c)$, the cardinality of maximal clique set and number of maximal clique sets are inversely proportional to each other.

Proof:

As per Theorem 2.1, a single set of the 1-DUOC is possible with minimum orthogonality or $(\lambda=w-1)$ and maximum cardinality. Moreover, for $(\lambda=p)$, $(1 \leq p < w-1)$, the cardinality of the maximal set is less than for $(\lambda=p+1)$. Then more codes are available for forming more sets for $(\lambda=p)$ than for $(\lambda=p+1)$. It proves that cardinality of maximal set and numbers of maximal sets are inversely proportional to each other.

Lemma 2.14:

The minimum cross-correlation among the multiple maximal clique sets for the code parameters $(n, w, \lambda_a, \lambda_c)$

) is equal to $(\lambda_c + 1)$.

Proof:

For the code parameters $(n, w, \lambda_a, \lambda_c)$, the maximal clique set contains the codes with auto-correlation constraint less than or equal to λ_a and cross-correlation constraint less than or equal to λ_c . The cross correlation between two independent maximal clique sets is equal to maximum cross-correlation for the pair of codes. One code is taken from one set and other one from the second. This maximum cross-correlation cannot be less than or equal to λ because both the sets are maximal. It will always be greater than λ_c . Hence the minimum value of the cross-correlation among the multiple independent maximal clique sets is equal to $(\lambda_c + 1)$. This also implies that no code shall be common between two maximal clique sets. If such a code exist, cross correlation between codes taken from two sets will be less than equal to λ_c and thus sets are not maximal clique sets.

To design multiple maximal sets of codes with general values of code parameters $(n, w, \lambda_a, \lambda_c)$, a new method is proposed with difference of position representation (DoPR) and calculation of correlation values. Before discussing the method, the characteristics of difference of positions representation for the one dimensional uni-polar orthogonal codes is discussed in the next section.

3. DIFFERENCE OF POSITIONS REPRESENTATION (DOPR)

Conventionally optical orthogonal codes are represented with their weighted positions [6],[7]-[14], which is not a unique representation of the code because weighted positions always change with circular shift of the code. One-dimensional uni-polar orthogonal codes are assumed to be the same with every circular shift of the code [14] for asynchronous use of the code in the multiple access systems. The difference of positions representation (DoPR) of the code remains same even with circular shift of the code. The DoPR is taken from difference families of optical orthogonal codes discussed in [6],[39]-[40].

Lemma 3.1:

The 'w' differences of consecutive weighted positions of one-dimensional uni-polar orthogonal code remain unchanged for every circular shift of the uni-polar code [14].

Proof:

The uni-polar code X with code length ' n ' and weight ' w '

has ' w ' weighted positions. The binary code X can be put on the periphery of the circle in serial order so that last and first bits of the code are adjacent. Now on every circular shift of the binary code around the circle, the difference of second and first weighted position remains same. Similarly for every circular shift of the code, the difference between $(j+1)^{th}$ and j^{th} weighted positions also remains same. Finally, it can be observed that all the ' w ' differences of consecutive weighted positions of the code remains unchanged on every circular shift of the code. Here $(j) \leq w$ and difference is calculated under modulo n arithmetic.

The lemma 3.1 gives the idea for unique representation of the code having ' w ' differences of consecutive weighted positions of the code. These ' w ' difference of consecutive weighted positions of the code is termed as difference of position representation (DoPR) of the code. There are ' w ' or less than ' w ' circular shifted DoPR of the code. One of these circular shifted DoPR can be standardized to represent the code uniquely.

Example 3.1(a):

Let us take the code $X = [0\ 1\ 0\ 1\ 0\ 0\ 1\ 0\ 0\ 0\ 1\ 0\ 0]$ with its WPR, $X_P = (1,3,6,10)$. The differences of consecutive weighted positions of the code are $(2,3,4,4)$ under modulo $n = 13$ arithmetic. For every circular shifted version of code X , $(X_1, X_2, \dots, X_{12})$, the differences of consecutive weighted positions of these shifted version remain un-changed and these will be $(2,3,4,4)$ or $(3,4,4,2)$ or $(4,4,2,3)$ or $(4,2,3,4)$. The DoPR of the code X is $(2,3,4,4)$ and the circular shifted DoPR of the code are $(3,4,4,2)$, $(4,4,2,3)$, $(4,2,3,4)$.

Lemma 3.2:

The difference of any two weighted positions of the uni-polar code always lies from one to $(n-1)$. □ *Theorem 3.3:[6]*

The sum of all the ' w ' differences of consecutive weighted positions or the elements of DoPR of the uni-polar code is always equal to code length ' n '.

Proof:

For the WPR of uni-polar code X , $X_P = (x_{p1}, x_{pi}, x_{pj}, \dots, x_{pw})$.

First difference d_{x1} of positions $(x_{p1}, x_{pi}) = (x_{pi} - x_{p1})$

Second difference of positions

(x_{pi}, x_{pj}) , $d_{x2} = (x_{pj} - x_{pi})^{(w-1)^{th}}$ difference of positions $(x_{p(w-1)}, x_{pw})$, $d_{x(w-1)} = (x_{pw} - x_{p(w-1)})^{(w)^{th}}$ difference of positions (x_{pw}, x_{p1}) , $d_{xw} = (n + x_{p1} - x_{pw})$ the $(w)^{th}$ difference d_{xw} is calculated under modulo ' n ' arithmetic because $(x_{p1} < x_{pw})$

The sum of all ' w ' differences $= (d_{x1} + d_{x2} + \dots + d_{xw}) = ((x_{pi} - x_{p1}) + (x_{pj} - x_{pi}) + \dots + (x_{pw} - x_{p(w-1)}) + (n + x_{p1} - x_{pw})) = n$

3.4 Formation of Standard DoPR of the Code

The one-dimensional uni-polar orthogonal code has a proper representation as DoPR containing ' w ' differences of consecutive positions (DoPs). The uni-polar code can be represented by any one of the ' w ' circular shifted DoPR. One of these ' w ' circular shifted DoPR can be fixed as standard DoPR following the procedure given below.

Step 1. Out of the ' w ' circular shifted DoPR, the DoPR with last element greater than other

(w-1) DoPs, is selected as standard DoPR of the code.

Example 3.4(a):

Let the uni-polar code with code length n=31, weight w=5, be (2,5,13,4,7) in DoPR. The circular shifted DoPRs are (5,13,4,7,2), (13,4,7,2,5), (4,7,2,5,13), and (7,2,5,13,4). The standard DoPR of the code is (4,7,2,5,13) which has highest element as last one.

Step 2. If after the step '1', the code has more than one DoPR with highest last element but equal to some DoPs of that DoPR, the DoPR with smallest value of first DoP element, is selected as standard DoPR of the code.

Example 3.4(b):

Let the uni-polar code with code length n=31, weight w=5, be (6,6,7,5,7) in DoPR. The other circular shifted DoPRs of the code are (6,7,5,7,6), (7,5,7,6,6), (5,7,6,6,7), (7,6,6,7,5). The

DoPRs selected after step 1 for standard DoPR are (6,6,7,6,7) and (5,7,6,6,7). The standard DoPR of the code is (5,7,6,6,7) with smaller first element.

Step 3. If in the step '2' we get more than one DoPR with highest last and smallest first DoPs, the DoPR with smaller value of second DoP, is selected as standard DoPR.

Example 3.4(c):

Let the uni-polar code with code length n=31, weight w=5, is (6,5,7,6,7) in DoPR. The other circular shifted DoPRs of the code are given as follows (5,7,6,7,6), (7,6,7,6,5), (6,7,6,5,7), (7,6,5,7,6). The DoPRs selected from step 1 for standard DoPR are (6,5,7,6,7) and (6,7,6,5,7). The step 2 could not standardize the code from two DoPR (6,5,7,6,7) and (6,7,6,5,7) of the code because first element of both DoPR is same and equal to 6. The step third results in the standard DoPR of the code as (6,5,7,6,7) with smaller second DoP element out of both circular shifted DoPRs.

Step 4. The process may continue till unique and standard DoPR of the code is found, by comparing third, fourth and so on elements in same fashion.

Lemma 3.5:

In the standard DoPR of the unipolar code of length 'n' and weight 'w', the range of first $\lfloor \frac{w-1}{2} \rfloor$ DoP elements lies from 1 to $\lfloor \frac{n-w+1}{2} \rfloor$ while the range of next $\lfloor \frac{w-1}{2} \rfloor$ DoP elements lies from 1 to $\lfloor \frac{n-w+2}{2} \rfloor$

Proof: Let the standard DoPR of the uni-polar code is $(d_{x1}, d_{x2}, \dots, d_{xw})$. The minimum values of $(d_{x1}, d_{x2}, \dots, d_{x(w-1)})$ are equal to 1 as per lemma 3.2. The first DoP element (d_{x1}) takes its maximum value when $(d_{x2}=d_{x3}=\dots=d_{x(w-1)})=1$ and $(d_{xw} > d_{x1})$ or $d_{xw}=d_{x1}+1$ for standard DoPR. As per Theorem 3.3,

$$(d_{x1} + d_{x2} + \dots + d_{x(w-1)} + d_{xw}) = n \quad \square$$

$$(d_{x1} + 1 + \dots + 1 + (d_{x1} + 1)) = n$$

$$(d_{x1} + d_{x1}) = n - (w - 1)$$

$$d_{x1} = \lfloor (n - w + 1) / 2 \rfloor.$$

Similarly (d_{x2}) or one of first $\lfloor (w-1)/2 \rfloor$ DoP elements $(d_{xi}), (1 \leq i \leq \lfloor (w-1)/2 \rfloor)$, takes its maximum value when other DoP elements except (d_{xw}) equal to one and $(d_{xw} > d_{xi})$ or $(d_{xw} = d_{xi} + 1)$ so that

$$d_{xi} = \lfloor (n - w + 1) / 2 \rfloor \text{ for standard DoPR. One of the next remaining } \lceil (w-1)/2 \rceil \text{ DoP elements except}$$

last DoP element $(d_{xj}), (\lfloor (w-1)/2 \rfloor < j \leq (w-1))$, takes maximum value when other DoP elements except (d_{xw}) equal to one and $(d_{xw} \geq d_{xj})$ or $(d_{xw} = d_{xj})$ for standard DoPR.

As per Theorem 3.3,

$$(d_{x1} + d_{x2} + \dots + d_{x(w-1)} + d_{xw}) = n$$

$$(d_{xj} + (w-2) + d_{xj}) = n$$

$$2d_{xj} = n - (w-2)$$

$$d_{xj} = \lfloor (n - w + 2) / 2 \rfloor.$$

If one of the first $\lfloor (w-1)/2 \rfloor$ DoP elements equal to last DoP element and no element of second half $\lfloor (w-1)/2 \rfloor$ DoP elements equal to last DoP element, the code can be standardized by taking one of its circular shifted versions such that first $\lfloor (w-1)/2 \rfloor$ DoP elements have no DoP element

equal to last DoP element.

Lemma 3.6:

In the standard DoPR of the uni-polar code of length 'n' and weight 'w', last DoP element is in range from $\lfloor n/w \rfloor$ to $(n - w + 1)$.

Proof: Suppose the standard DoPR of the uni-polar code is $(d_{x1}, d_{x2}, \dots, d_{xw})$. The last DoP element (d_{xw}) takes its maximum value when all other DoP elements are minimum or equal to one. Then maximum of (d_{xw}) is equal to $(n - w + 1)$ as per theorem 3.3. This (d_{xw}) takes its minimum value when all other DoP elements are such that their DoP values are just less than or equal to last DoP element. Mathematically some of other DoP elements are equal to $\lfloor n/w \rfloor$, some are $\lceil n/w \rceil$. The minimum value of last DoP element (d_{xw}) will be $\lceil n/w \rceil$.

The maximum non-zero shift auto-correlation and cross-correlation values of the codes can be calculated using the DoPR or standard DoPR. This calculation is easier than the conventional calculation of auto and cross-correlation values of the codes as given in definitions 2.1, 2.2, 2.3, 2.6, 2.7 & 2.8. For the calculation of correlation values, the DoPR is converted into extended DoP matrix of the code. The extended DoP matrix $(w \times (w - 1))$ of the code contains not only differences of consecutive weighted positions but also the differences of any two weighted positions of the code.

Extended DoP (EDoP) Matrix of the Uni-polar Code.

1. There are 'w' rows and $(w-1)$ columns in extended DoP matrix of the code.
2. The first row of extended DoP matrix contains differences of first with all other weighted positions of the code.
3. The w^{th} row of extended DoP matrix contains the differences of w^{th} with all other weighted positions of the code in cyclic order.

In j^{th} row, the difference of i^{th} element with $(i+1)^{\text{st}}$ element can be placed in any column and remaining elements are placed in cyclic order. This means for same code, we can have $(w-1)^w$ EDoP matrices. One of which may be given as follows.

Let us take the code X with DoPR $(d_{x1}, d_{x2}, \dots, d_{xw})$ with weight 'w' and code length $n = d_{x1} + d_{x2} + \dots + d_{xw}$, the EDoP matrix is formed as following

$$\begin{bmatrix} e_{x01} & e_{x02} & \dots & e_{x0(w-2)} & e_{x0(w-1)} \\ e_{x11} & e_{x12} & \dots & e_{x1(w-2)} & e_{x1(w-1)} \\ \dots & \dots & \dots & \dots & \dots \\ e_{x(w-2)1} & e_{x(w-2)2} & \dots & e_{x(w-2)(w-2)} & e_{x(w-2)(w-1)} \\ e_{x(w-1)1} & e_{x(w-1)2} & \dots & e_{x(w-1)(w-2)} & e_{x(w-1)(w-1)} \end{bmatrix}$$

with

$$\begin{aligned} e_{x01} &= d_{x1}; e_{x11} = d_{x2}; \dots; e_{x(w-2)1} = d_{x(w-1)}; e_{x(w-1)1} = d_{xw}; \\ e_{x02} &= d_{x1} + d_{x2}; e_{x12} = d_{x2} + d_{x3}; \\ &\dots; \\ e_{x(w-2)2} &= d_{x(w-1)} + d_{xw}; e_{x(w-1)2} = d_{xw} + d_{x1}; \\ &\dots; \\ e_{x0(w-2)} &= d_{x1} + d_{x2} + \dots + d_{x(w-2)}; e_{x1(w-2)} = d_{x2} + d_{x3} + \dots + d_{x(w-1)}; \\ &\dots; \\ e_{x(w-2)(w-2)} &= d_{x(w-1)} + d_{xw} + d_{x1} + d_{x2} + \dots + d_{x(w-4)}; \\ e_{x(w-1)(w-2)} &= d_{xw} + d_{x1} + d_{x2} + \dots + d_{x(w-3)}; \\ e_{x0(w-1)} &= d_{x1} + d_{x2} + \dots + d_{x(w-1)}; e_{x1(w-1)} = d_{x2} + d_{x3} + \dots + d_{xw}; \\ &\dots; \\ e_{x(w-2)(w-1)} &= d_{x(w-1)} + d_{xw} + d_{x1} + d_{x2} + \dots + d_{x(w-3)}; \\ e_{x(w-1)(w-1)} &= d_{xw} + d_{x1} + d_{x2} + \dots + d_{x(w-2)}. \end{aligned}$$

Example 3.7(a):

Let the DoPR of the code with weight ‘w’ equal to 5 is (a,b,c,d,e) and code length ‘n’=a+b+c+d+e. The extended DoP matrix (5x4) is given as

$$\begin{bmatrix} a & a+b & a+b+c & a+b+c+d \\ b & b+c & b+c+d & b+c+d+e \\ c & c+d & c+d+e & c+d+e+a \\ d & d+e & d+e+a & d+e+a+b \\ e & e+a & e+a+b & e+a+b+c \end{bmatrix}$$

Lemma 3.8:

If ‘a’ is a DoP element of extended DoP matrix of the code, then the DoP element ‘n-a’ also exist in the same extended DoP matrix of the code.

Proof: if ‘a’ is a difference of any

two weighted positions (x_{pi}, x_{pj}) of the codes such that $(i, j) \in (0:n-1)$

i.e. $a = (x_{pj} - x_{pi})$ while the difference between (x_{pj}, x_{pi}) in circular order is $(x_{pi} - x_{pj}) = (n - a)$ in modulo ‘n’ arithmetic. It means that two DoP elements ‘a’ and ‘n-a’ represents the difference of two same weighted positions.

Lemma 3.9:

If first (w-1) consecutive differences of weighted positions EDoP

$$\text{EDoP} \begin{bmatrix} e_{x01} & e_{x02} & \cdots & e_{x0(w-2)} & e_{x0(w-1)} \\ e_{x11} & e_{x12} & \cdots & e_{x1(w-2)} & e_{x1(w-1)} \\ \cdots & \cdots & \cdots & \cdots & \cdots \\ e_{x(w-2)1} & e_{x(w-2)2} & \cdots & e_{x(w-2)(w-2)} & e_{x(w-2)(w-1)} \\ e_{x(w-1)1} & e_{x(w-1)2} & \cdots & e_{x(w-1)(w-2)} & e_{x(w-1)(w-1)} \end{bmatrix}$$

With

$$\begin{aligned} e_{x01} &= d_{x1}; e_{x11} = d_{x2}; \dots; e_{x(w-2)1} = d_{x(w-1)}; \\ e_{x(w-1)1} &= d_{xw} = (n - (d_{x1} + d_{x2} + \dots + d_{x(w-1)})); \\ e_{x02} &= d_{x1} + d_{x2}; e_{x12} = d_{x2} + d_{x3}; \dots; \\ e_{x(w-2)2} &= d_{x(w-1)} + d_{xw} = (n - (d_{x1} + d_{x2} + \dots + d_{x(w-2)})); \\ e_{x(w-1)2} &= d_{xw} + d_{x1} = (n - (d_{x2} + d_{x3} + \dots + d_{x(w-1)})); \dots; \\ e_{x0(w-2)} &= d_{x1} + d_{x2} + \dots + d_{x(w-2)}; \\ e_{x1(w-2)} &= d_{x2} + d_{x3} + \dots + d_{x(w-1)}; \\ e_{x(w-2)(w-2)} &= d_{x(w-1)} + d_{xw} + d_{x1} + d_{x2} + \dots + d_{x(w-4)} = (n - (d_{x(w-3)} + d_{x(w-2)})); \\ e_{x(w-1)(w-2)} &= d_{xw} + d_{x1} + d_{x2} + \dots + d_{x(w-3)} = (n - (d_{x(w-2)} + d_{x(w-1)})); \\ e_{x0(w-1)} &= d_{x1} + d_{x2} + \dots + d_{x(w-1)}; e_{x1(w-1)} = d_{x2} + d_{x3} + \dots + d_{xw} = (n - d_{x1}); \dots; \\ e_{x(w-2)(w-1)} &= d_{x(w-1)} + d_{xw} + d_{x1} + d_{x2} + \dots + d_{x(w-3)} = (n - d_{x(w-2)}); \\ e_{x(w-1)(w-1)} &= d_{xw} + d_{x1} + d_{x2} + \dots + d_{x(w-2)} = (n - d_{x(w-1)}). \end{aligned}$$

Example 3.9(a):

Let the DoPR of the code with weight ‘w’ equal to 5 is (a,b,c,d,e) and code length ‘n’=a+b+c+d+e. The extendedDoPmatrix (5x4) is given as

$$\begin{bmatrix} a & a+b & a+b+c & a+b+c+d \\ b & b+c & b+c+d & n-a \\ c & c+d & n-(a+b) & n-b \\ d & n-(a+b+c) & n-(b+c) & n-c \\ n-(a+b+c+d) & n-(b+c+d) & n-(c+d) & n-d \end{bmatrix}$$

Lemma 3.10:

If first $u < w$ consecutive differences of weighted positions or DoP element $(d_{x1}, d_{x2}, \dots, d_{xu})$ of DoPR $(d_{x1}, d_{x2}, \dots, d_{x(w-1)}, d_{xw})$ of the code are known, the extended DoP matrix for the incomplete code with u DoP or DoP element $(d_{x1}, d_{x2}, \dots, d_{x(w-1)})$ of DoPR $(d_{x1}, d_{x2}, \dots, d_{x(w-1)}, d_{xw})$ of the code are known, the extended DoP matrix is given as follows.

$$\text{EDoP} \begin{bmatrix} e_{x01} & e_{x02} & \cdots & e_{x0(u-1)} & e_{x0u} \\ e_{x11} & e_{x12} & \cdots & e_{x1(u-1)} & e_{x1u} \\ \cdots & \cdots & \cdots & \cdots & \cdots \\ e_{x(u-1)1} & e_{x(u-1)2} & \cdots & e_{x(u-1)(u-1)} & e_{x(u-1)u} \\ e_{x(u)1} & e_{x(u)2} & \cdots & e_{x(u)(u-1)} & e_{x(u)(u)} \end{bmatrix}$$

With

$$\begin{bmatrix} e_{x01} = d_{x1}; \\ e_{x11} = n - d_{x1} \end{bmatrix}$$

$$\begin{bmatrix} e_{x02} = d_{x1} + d_{x2}; e_{x12} = d_{x2} \\ e_{x21} = n - (d_{x1} + d_{x2}); e_{x22} = n - d_{x2} \end{bmatrix}$$

$$\begin{bmatrix} e_{x03} = (d_{x1} + d_{x2} + d_{x3}); e_{x13} = (d_{x2} + d_{x3}); e_{x23} = d_{x3}; \\ e_{x31} = n - (d_{x1} + d_{x2} + d_{x3}); e_{x32} = n - (d_{x2} + d_{x3}); e_{x33} = n - d_{x3} \end{bmatrix}$$

; ...;

$$\begin{bmatrix} e_{x0(u)} = (d_{x1} + d_{x2} + \cdots + d_{xu}); e_{x1(u)} = (d_{x2} + d_{x3} + \cdots + d_{xu}); \\ e_{x2(u)} = (d_{x3} + d_{x4} + \cdots + d_{xu}); \cdots; e_{x(u-1)(u)} = (d_{xu}); \\ e_{xu1} = n - (d_{x1} + d_{x2} + \cdots + d_{xu}); e_{xu2} = n - (d_{x2} + d_{x3} + \cdots + d_{xu}) \\ ; \cdots; e_{x(u)(u-1)} = n - (d_{x(u-1)} + d_{xu}); e_{x(u)(u)} = n - (d_{xu}); \end{bmatrix}$$

Proof: It is obvious that there is no change in EDoP matrix if EDoP element in same row move to another position. The EDoP matrix of Lemma 3.9 is same as EDoP matrix of lemma

3.10 with cyclic shift within rows. It can be verified by examples 3.9(a) and 3.10(a) with i^{th} row being cyclically shifted left $(i-1)$ times.

The advantage of this kind of EDoP representation is that if last k entries of DoPR are deleted, EDoP can be determined by deleting lower k rows and rightmost k column in EDoP representation of complete code.

Example 3.10(a):

Let the DoPR of the code with weight 'w' equal to 5 is

(a, b, c, d, e) and code length $n = (a + b + c + d + e)$. The extended DoP matrix for 1, 2, 3, and 4 consecutive DoP elements of incomplete and complete code is given as following matrices respectively.

$$\begin{bmatrix} a \\ n-a \end{bmatrix},$$

$$\begin{bmatrix} a & a+b \\ n-a & b \\ n-(a+b) & n-b \end{bmatrix},$$

$$\begin{bmatrix} a & a+b & a+b+c \\ n-a & b & b+c \\ n-(a+b) & n-b & c \\ n-(a+b+c) & n-(b+c) & n-c \end{bmatrix},$$

$$\begin{bmatrix} a & a+b & a+b+c & a+b+c+d \\ n-a & b & b+c & b+c+d \\ n-(a+b) & n-b & c & c+d \\ n-(a+b+c) & n-(b+c) & n-c & d \\ n-(a+b+c+d) & n-(b+c+d) & n-(c+d) & n-d \end{bmatrix}$$

4. THE CALCULATION OF CORRELATIONCONSTRAINTS

4.1 Auto-Correlation Constraint:

In the conventional method for calculation of maximum non-zero shift auto-correlation as given in definition 2.1, the weighted bits' positions of code X are compared with circular shifted versions of code X. There are $n(n-1)$ comparisons of binary digits in the calculation of maximum non-zero shift auto-correlation of uni-polar code as given in definition 2.1. The 'n' bits of code X are compared with 'n' bits of each of $(n-1)$ circular shifted versions of code X. These comparisons of weighted bits positions can be further reduced as described below.

Lemma 4.2:

In calculation of the maximum non-zero shift auto-correlation using weighted positions representation (WPR) of the code, there are $(n-1)w$ comparisons of weighted positions (definition 2.3).

Proof: In conventional method for the calculation of the maximum non-zero shift auto-correlation of the uni-polar code, each of 'w' weighted positions of X_P are compared with each of 'w' weighted positions of every $(n-1)$ circular shifted versions (X_{P+a}) , (Definition 2.3). Thus there are $(n-1)w^2$ comparisons of weighted positions in the calculation of the maximum non-zero shift auto-correlation of the code X.

Lemma 4.3:

For the uni-polar code of length 'n' and weight 'w', the total cases of overlapping pairs of weighted bits of uni-polar code with its circular shifted versions in the calculation of maximum non-zero shift auto-correlation (definition 2.1) are

$$\frac{w(w-1)}{2}$$

2

Proof: In the calculation of maximum non-zero shift auto-correlation, first weighted bit of the uni-polar code overlap with next $(w-1)$ other weighted bits by circular shifting. The second weighted bit overlap with next $(w-2)$ weighted bits by circular shifting. Similarly the third and so on up to $(w-1)$ th weighted bit overlap with next $(w-3)$ and so on up to last weighted bit by circular shifting. There are total $(w-1)$ plus $(w-2)$ plus $(w-3)$ plus and so on up to plus one overlapping which may occur in the pairs of codes with its maximum $(n-1)$ circular shifted versions. Total overlapping of weighted bits are $w(w-1)/2$.

Lemma 4.4:

The uni-polar code with code length 'n' and code weight 'w' has 'w' circular shifted versions with first bit as weighted bit of the code.

Example 4.1.4: Let us take the code $X = [0\ 1\ 0\ 1\ 0\ 0\ 1\ 0\ 0\ 0\ 1\ 0\ 0]$ with weighted positions representation $X_P = (1,3,6,10)$. The $w=4$ circular shifted versions of the code with first bit as weighted bit are given as follows

$$X_1 = [1\ 0\ 1\ 0\ 0\ 1\ 0\ 0\ 0\ 1\ 0\ 0\ 0], (X_{P+12}) = (0,2,5,9),$$

$$X_3 = [1\ 0\ 0\ 1\ 0\ 0\ 0\ 1\ 0\ 0\ 0\ 1\ 0], (X_{P+10}) = (0,3,7,11),$$

$$X_6 = [1\ 0\ 0\ 0\ 1\ 0\ 0\ 0\ 1\ 0\ 1\ 0\ 0], (X_{P+7}) = (0,4,8,10),$$

$$X_{10} = [1\ 0\ 0\ 0\ 1\ 0\ 0\ 1\ 0\ 0\ 0\ 0], (X_{P+3}) = (0,4,6,9).$$

In the calculation of maximum non-zero-shift auto-correlation, total cases of overlapping of weighted bits = first weighted bit overlaps with second, third and fourth weighted bits, i.e. three overlapping + second weighted bit overlaps with third, and fourth, i.e. two overlapping + third weighted bit overlaps with fourth weighted bit, i.e. one overlapping = 6 overlapping.

Lemma 4.5:

There are ${}^w C_2 = \frac{w(w-1)}{2}$ pairs of codes formed out of the 'w' circular shifted versions of the code with first bit as weighted bit.

Lemma 4.6:

Total unrepeated overlapping of weighted bits in the all pairs of codes having first bit as weighted bit are $\frac{w(w-1)}{2}$.

Proof: As per lemma 4.5, there are $\frac{w(w-1)}{2}$ pairs of codes having first bit as weighted bit. Each pair has one unrepeated overlapping at first position. Then, there are total $\frac{w(w-1)}{2}$ overlapping of weighted bits.

Theorem 4.7:

The overlapping of weighted bits of uni-polar code with its every circular shifted version equal to overlapping of weighted bits in all the pairs of the 'w' circular shifted versions with first bit as weighted bit of the code.

Proof: As per lemma 4.3, total overlapping of weighted bits of uni-polar code with its every circular shifted versions are $\frac{w(w-1)}{2}$. As per lemma 4.6, the same number of definite overlapping are found in all the pairs of the 'w' circular shifted versions with first bit as weighted bit of the code. Hence all weighted overlapping are covered in both cases.

Theorem 4.8:

The weighted positions of the 'w' circular shifted versions of the code with first bit as weighted bit are given by the rows of EdoP matrix along-with extra first column having zero elements.

Proof: Let us take the code X with DoPR(a,b, c, d, e) with weight $w=5$, and code length $n=(a+b+c+d+e)$. The weighted positions of the code with first bit as weighted bit are $(0, a, a+b, a+b+c, a+b+c+d)$. The circular shifted versions of this code with first bit as weighted bit are

$$(0, b, b+c, b+c+d, b+c+d+e)$$

$$(0, c, c+d, c+d+e, c+d+e+a),$$

$(0, d, d+a, d+a+b, d+a+b+c)$ and
 $(0, e, e+a, e+a+b, e+a+b+c)$.

These circular shifted versions of the code with first bit as weighted bit are same as row element of the following EDoP matrix (example 3.7(a)) along-with extra first column having zero elements.

$$\begin{bmatrix} 0 & a & a+b & a+b+c & a+b+c+d \\ 0 & b & b+c & b+c+d & b+c+d+e \\ 0 & c & c+d & c+d+e & c+d+e+a \\ 0 & d & d+e & d+e+a & d+e+a+b \\ 0 & e & e+a & e+a+b & e+a+b+c \end{bmatrix}$$

Similarly for any weight $w \geq 2$ the theorem can be verified easily.

Theorem 4.9:

The maximum non-zero shift auto-correlation of the uni-polar code is equal to maximum number of overlapping bits among the pairs of ‘w’ circular shifted versions with first bit as weighted bit of the code. OR The maximum non-zero shift auto-correlation of the uni-polar code is equal to the maximum number of common DoP elements between two rows of EDoPmatrix having zero elements in first column.

$$\lambda_{ax} \geq \sum_{j=0}^{w-1} \sum_{l=0}^{w-1} e_{xij}e_{xkl} \text{ for } i = (0:w-1), k = (i+1:w-1)$$

OR

The maximum non-zero shift auto-correlation of the uni-polar code is equal to one plus maximum number of common DoP elements between two rows of EDoP matrix of the code.

$$\lambda_{ax} \geq 1 + \sum_{j=0}^{w-1} \sum_{l=1}^{w-1} e_{xij}e_{ykl} \text{ for } i = (0:w-1), l = (i+1:w-1)$$

$$\text{where } e_{xij}e_{ykl} = \begin{cases} 1 & \text{if } e_{xij}=e_{ykl} \\ 0 & \text{if } e_{xij} \neq e_{ykl} \end{cases}$$

e_{xij} & e_{ykl} are DoP elements of two rows of EDoP matrix along-with first column having zero elements.

Proof: Let us take the code X with DoPR($d_{x1}, d_{x2}, \dots, d_{xw}$) with weight ‘w’ and code length $n = d_{x1} + d_{x2} + \dots + d_{xw}$, the EDoP matrix with zero elements in the first column is formed as follows.

$$\text{EDoP} \begin{bmatrix} e_{x00} & e_{x01} & e_{x02} & \cdots & e_{x0(w-1)} \\ e_{x10} & e_{x11} & e_{x12} & \cdots & e_{x1(w-1)} \\ e_{x20} & e_{x21} & e_{x22} & \cdots & e_{x2(w-1)} \\ \cdots & \cdots & \cdots & \cdots & \cdots \\ e_{x(w-1)0} & e_{x(w-1)1} & e_{x(w-1)2} & \cdots & e_{x(w-1)(w-1)} \end{bmatrix}$$

with

$$e_{x00} = e_{x10} = e_{x20} = \cdots = e_{x(w-1)0} = 0.$$

$$e_{x01} = d_{x1}; e_{x11} = d_{x2}; \cdots; e_{x(w-1)1} = d_{xw}.$$

$$e_{x02} = d_{x1} + d_{x2}; e_{x12} = d_{x2} + d_{x3}; \cdots; e_{x(w-1)2} = d_{xw} + d_{x1}$$

...

$$e_{x0(w-1)} = d_{x1} + d_{x2} + \cdots + d_{xw-1}; e_{x1(w-1)} = d_{x2} + d_{x3} + \cdots + d_{xw}; \cdots;$$

$$e_{x(w-1)(w-1)} = d_{xw} + d_{x1} + d_{x2} + \cdots + d_{x(w-2)}.$$

As per definition 2.1 and theorem 4.7, the maximum non-zero shift auto-correlation λ_{ax} of the uni-polar code is equal to maximum number of overlapping of weighted bits among the pairs of circular shifted versions with first bit as weighted bit of the code. However As per theorem 4.8 and definition 2.3, the maximum non-zero shift auto-correlation of the code is equal to the maximum number of common DoP elements between two rows of EdoP matrix along-with firstcolumn with zero elements

if $e_{xij}e_{xkl} = \begin{cases} 1 & \text{if } e_{xij} = e_{xkl} \\ 0 & \text{if } e_{xij} \neq e_{xkl} \end{cases}$ which represents common elements between two rows of EdoP matrix with first column having zero elements.

$$\lambda_{ax} \geq \sum_{j=0}^{w-1} \sum_{l=0}^{w-1} e_{xij}e_{xkl} \text{ for } i = (0:w-1), l = (i+1:w-1)$$

Or the maximum non-zero shift auto-correlation of the uni-polar code is equal to one plus maximum common DoP elements between two rows of EdoP matrix of the code. As any two rows of EdoP matrix with first column having zero elements always has at least one common element which is zero.

$$\lambda_{ax} \geq 1 + \sum_{j=0}^{w-1} \sum_{l=1}^{w-1} e_{xij}e_{ykl} \text{ for } i = (0:w-1), l = (i+1:w-1)$$

Lemma4.10:

There will be $\frac{(w-1)w^3}{2}$ comparisons of DoP elements in the calculation of maximum non-zero shift auto-correlation using extended DoP matrix with first column having zero elements.

Proof: There are $\frac{(w-1)w}{2}$ pair of rows of extended DoP matrix which are compared in the calculation of maximum non-zero shift auto-correlation of the code. In each pair of rows, there are w^2 comparisons of DoP elements. Thus there are total $\frac{(w-1)w^3}{2}$ comparisons of DoP elements of EdoP matrix take place in the calculation of maximum non-zero shift auto-correlation of the code.

Lemma 4.11:

There are $\frac{w(w-1)^3}{2}$ comparisons of DoP elements in the calculation of maximum non-zero shift auto-correlation using extended DoP matrix of the code.

Proof: There are $\frac{(w-1)w}{2}$ pair of rows of extended DoP matrix which are compared in the calculation of maximum non-zero shift auto-correlation of the code. In each pair of rows, there are $(w-1)^2$ comparisons of DoP elements. Hence there are $\frac{w(w-1)^3}{2}$ total comparisons of DoP elements of EDoP matrix in the calculation of maximum non-zero shift auto-correlation of the code.

Lemma 4.12:

If there is no common DoP elements in the pair of rows of EDoP matrix of code, the maximum non-zero shift auto-correlation of the code is always equals to one [38].

4.13 Cross-Correlation Constraint:

In the conventional method for calculation of cross-correlation for the pair of uni-polar codes as given in definition 2.6, the weighted bits' positions of code X are compared with code Y and circular shifted versions of code Y. Or the weighted bits' positions of code Y are compared with code X and circular shifted versions of code X. There are n^2 comparisons of binary digits in the calculation of cross-correlation of uni-polar code in conventional method (definition 2.6).

These comparisons of weighted bits positions can be further reduced as described below.

Lemma 4.14:

In the calculation of cross-correlation using weighted positions representation (WPR) of the pair of codes, there are (nw^2) comparisons of weighted positions (definition 2.8).

Proof: In the calculation of cross-correlation of the pair of uni-polar codes (definition 2.8), the 'w' weighted positions (WP) of X_P are compared with 'w' weighted positions of Y_P and each of the $(n-1)$ circular shifted versions (Y_{P+a}). There are (nw^2) total comparisons of weighted position in the calculation of cross-correlation of the pair of codes.

Lemma 4.15:

For the uni-polar codes of length 'n' and weight 'w', the definite cases of overlapping of weighted bits of uni-polar code X with code Y and the $(n-1)$ circular shifted versions of code Y are w^2 .

Proof: In the calculation of cross-correlation (definition 2.6), first weighted bit of code X overlap with w weighted bits of code Y in 'w' shifts. The second weighted bit of code X overlap with 'w' weighted bit of code Y in 'w' shifts. Similarly the third and so on upto w^{th} weighted bit of code X overlap with 'w' weighted positions of code Y in 'w' shifts. Thus there are (w^2) total overlapping of weighted bits occurred in the pairs of code X with code Y and the maximum $(n-1)$ circular shifted versions of code Y in the calculation of cross-correlation.

Lemma 4.16:

There are total w^2 pairs of code X and code Y formed out of the 'w' circular shifted versions of both the codes with first bit as weighted bit.

Lemma 4.17:

The definite overlapping of weighted bits in all the pairs of circular shifted versions of codes X and Y having first bit as weighted bit are w^2 .

Proof: As per lemma 4.16, there are w^2 pairs of codes having first bit as weighted bit. Each pair has one definite overlapping at first position. Subsequently there are w^2 definite overlapping of weighted bits.

Theorem 4.18: The overlapping of weighted bits of uni-polar code X with uni-polar code Y and every circular shifted version of code Y equals to the overlapping of weighted bits in all the pairs of code X and code Y formed out of the 'w' circular shifted versions of both the codes having first bit as weighted bit.

Proof: As per lemma 4.15, the definite overlapping of weighted bits of uni-polar code X and code Y along-with every circular shifted version of code Y are w^2 . As well as per lemma 4.17, the same number of definite overlapping are covered in all the pairs of circular shifted versions of code X and code Y having first bit as weighted bit. Hence all definite weighted overlapping are covered in both cases.

Theorem 4.19:

The cross-correlation of the uni-polar codes X and Y is equal to maximum overlapping among the pairs of code X and code Y out of the 'w' circular shifted versions with first bit as weighted bit of both the codes.

OR

The cross-correlation of the uni-polar codes X and Y is equal to maximum common DoP elements between any two rows of EdoP matrices along-with first column with zero elements of code X and code Y respectively.

$$\lambda_{cxy} \geq \sum_{j=0}^{w-1} \sum_{l=0}^{w-1} e_{xij} e_{ykl} \text{ for } i = (0:w-1), k = (0:w-1)$$

OR

The cross-correlation of the uni-polar codes X and Y is equal to one plus maximum common DoP elements between any two rows of EDoP matrices of code X and code Y respectively.

$$\lambda_{cxy} \geq 1 + \sum_{j=1}^{w-1} \sum_{l=1}^{w-1} e_{xij} e_{ykl} \text{ for } i = (0:w-1), k = (0:w-1)$$

$$\text{if } e_{xij} e_{ykl} = \begin{cases} 1 & \text{if } e_{xij} = e_{ykl} \\ 0 & \text{if } e_{xij} \neq e_{ykl} \end{cases}$$

e_{ij} & e_{kl} are DoP elements of the rows of EDoP matrices along-with extra column with zero elements of code X and code Y respectively.

Proof: Suppose the code X with DoPR($d_{x1}, d_{x2} \dots \dots, d_{xw}$) and code Y with DoPR($d_{y1}, d_{y2} \dots \dots, d_{yw}$) with weight 'w' and code length $n = d_{x1} + d_{x2} + \dots \dots + d_{xw} = d_{y1} + d_{y2} + \dots \dots + d_{yw}$ the EDoP matrix along-with first column with zero elements of code X and code Y are formed as follows

$$\text{EDoP(X)} \begin{bmatrix} e_{x00} & e_{x01} & e_{x02} & \cdots & e_{x0(w-1)} \\ e_{x10} & e_{x11} & e_{x12} & \cdots & e_{x1(w-1)} \\ e_{x20} & e_{x21} & e_{x22} & \cdots & e_{x2(w-1)} \\ \cdots & \cdots & \cdots & \cdots & \cdots \\ e_{x(w-1)0} & e_{x(w-1)1} & e_{x(w-1)2} & \cdots & e_{x(w-1)(w-1)} \end{bmatrix}$$

with

$$e_{x00} = e_{x10} = e_{x20} = \dots = e_{x(w-1)0} = 0.$$

$$e_{x01} = d_{x1}; e_{x11} = d_{x2}; \dots; e_{x(w-1)1} = d_{xw}.$$

$$e_{x02} = d_{x1} + d_{x2}; e_{x12} = d_{x2} + d_{x3}; \dots; e_{x(w-1)2} = d_{xw} + d_{x1}$$

...

$$e_{x0(w-1)} = d_{x1} + d_{x2} + \dots + d_{x(w-1)}; e_{x1(w-1)} = d_{x2} + d_{x3} + \dots + d_{xw}; \dots;$$

$$e_{x(w-1)(w-1)} = d_{xw} + d_{x1} + d_{x2} + \dots + d_{x(w-2)}.$$

and

$$\text{EDoP(Y)} \begin{bmatrix} e_{y00} & e_{y01} & e_{y02} & \cdots & e_{y0(w-1)} \\ e_{y10} & e_{y11} & e_{y12} & \cdots & e_{y1(w-1)} \\ e_{y20} & e_{y21} & e_{y22} & \cdots & e_{y2(w-1)} \\ \cdots & \cdots & \cdots & \cdots & \cdots \\ e_{y(w-1)0} & e_{y(w-1)1} & e_{y(w-1)2} & \cdots & e_{y(w-1)(w-1)} \end{bmatrix}$$

OR

$$e_{y00} = e_{y10} = e_{y20} = \dots = e_{y(w-1)0} = 0.$$

$$e_{y01} = d_{y1}; e_{y11} = d_{y2}; \dots; e_{y(w-1)1} = d_{yw}.$$

$$e_{y02} = d_{y1} + d_{y2}; e_{y12} = d_{y2} + d_{y3}; \dots; e_{y(w-1)2} = d_{yw} + d_{y1}$$

...

$$e_{y0(w-1)} = d_{y1} + d_{y2} + \dots + d_{y(w-1)}; e_{y1(w-1)} = d_{y2} + d_{y3} + \dots + d_{yw}; \dots;$$

$$e_{y(w-1)(w-1)} = d_{yw} + d_{y1} + d_{y2} + \dots + d_{y(w-2)}.$$

As per definition 2.6 and theorem 4.18, the cross-correlation λ_{cxy} of the uni-polar codes X and Y is equal to the maximum number of overlapping among the pairs of code X and code Y of the circular shifted versions with first bit as weighted bit of both the codes. However As per definition 2.6 and theorem 4.8, the cross-correlation of the codes X and Y is the maximum number of common DoP elements between the rows of EDoP matrices along-with first column having zero elements for both the codes X and Y.

$$\text{if } e_{xij}e_{ykl} = \begin{cases} 1 & \text{if } e_{xij} = e_{ykl} \\ 0 & \text{if } e_{xij} \neq e_{ykl} \end{cases}$$

$$\lambda_{cxy} \geq \sum_{j=0}^{w-1} \sum_{l=0}^{w-1} e_{xij}e_{ykl} \text{ for } i = (0: w-1), k = (0: w-1)$$

e_{ij} & e_{kl} are DoP elements are the DoP elements of the rows of EDoP matrices along-with

first extra column having zero elements of code X and code Y respectively..

Or the cross-correlation of the uni-polar codes X and Y is equal to one plus maximum common DoP elements between the rows of EDoP matrices of the code X and Y. Because any two rows of EdoP matrices along-with first column having zero elements for code X and Y always has at least one common element as zero.

$$\lambda_{cxy} \geq 1 + \sum_{j=1}^{w-1} \sum_{l=1}^{w-1} e_{xij}e_{ykl} \text{ for } i = (0:w-1), k = (0:w-1)$$

Lemma 4.20:

There are w^4 comparisons of DoP elements in the calculation of cross-correlation using extended DoP matrices along-with first column having zero elements for both the codes,.

Proof: As per lemma 4.16, there are w^2 pair of rows from extended DoP matrices along-with first column having zero elements for code X and Y. In each pair of rows, there are w^2 comparisons of DoP elements. Hence there are w^4 comparisons of DoP elements of both EDoP matrices in the calculation of cross-correlation for the pair of codes X and Y.

Lemma 4.21:

In calculation of cross-correlation using extended DoP matrices of the codes X and Y, there are $w^2(w-1)^2$ comparisons of DoP elements.

Proof: As per lemma 4.16, there are w^2 pair of rows from extended DoP matrices of code X and Y. In each pair of rows, there are $(w-1)^2$ comparisons of DoP elements.

Hence there are $w^2(w-1)^2$ total comparisons of DoP elements of EDoP matrices in the calculation of cross-correlation of the codes X with Y.

Lemma 4.22:

If there is no common DoP elements in the pair of rows of EDoP matrices of the two codes, the cross-correlation of the pair of codes is always equals to one [38].

Theorem 4.23:

The cross-correlation of the uni-polar code X with code parameters (n_1, w_1, λ_{a1}) and code Y with parameters (n_2, w_2, λ_{a2}) is equal to maximum common DoP elements between the any two rows of EdoP matrices along-with first column having zero elements of code X and code Y respectively.

$$\lambda_{cxy} \geq 1 + \sum_{j=1}^{w_1-1} \sum_{l=1}^{w_2-1} e_{xij}e_{ykl} \text{ for } i = (0:w_1-1), k = (0:w_2-1)$$

$$\text{if } e_{xij}e_{ykl} = \begin{cases} 1 & \text{if } e_{xij} = e_{ykl} \\ 0 & \text{if } e_{xij} \neq e_{ykl} \end{cases}$$

e_{ij} & e_{kl} are DoP elements of the rows of EDoP matrices along-with first column having zero elements of code X and code Y respectively.

Proof: it is straight forward through theorem 4.19.

I. DESIGN OF THE MAXIMAL SETS OF 1-DUOC

The maximal sets of 1-DUOC for fixed code parameters $(n, w, \lambda_a=1, \lambda_c=1)$ are designed through maximal clique search method in the proposed algorithm.

5.1. Maximal Clique Search Method:

Suppose the uni-polar code in standard DoPRis(d_1, d_2, \dots, d_w). Let for $u < w$, (d_1, d_2, \dots, d_u) DoPelements of the code are known at one step of following algorithm. The extended DoP matrix of the code withincomplete DoP elements (d_1, d_2, \dots, d_u) is given by lemma

3.10. The maximum non-zero shift auto-correlation and cross- correlation of the pair of codes with incomplete DoP elements can be calculated by theorem 4.9 and theorem 4.19 respectively as well as using lemma 3.10 for EDoP matrices of codes with incomplete DoP elements. In the defined graph of codes with incomplete or complete DoP elements, some maximal clique sets of codes are searched by maximal clique finding algorithms [41-46] or the algorithm proposed here as follows.

Step.1:

Define the connected graph of codes or correlation matrix having binary elements (0,1). In the correlation matrix of codes, the binary digit '1' represent to cross-correlation less than equal to λ_c between two codes while binary digit '0' represent to cross-correlation greater than λ_c between two codes in the matrix. In the defined graph of codes, the binary digit '1' of correlation matrix is equivalent to a straight line between two codes while no line if corresponding binary digit '0' for two codes in correlation matrix. $i=0$. If the size of correlation matrix is large enough, the correlation matrix can be broken into smaller parts which is discussed in the next section. All the codes of graph can be divided into S sub-graphs. Each sub-graph is containing the codes with similar DoP elements of some positions which is clearly mentioned in next sub-section 5.2.

Step.2:

In the defined graph or smaller part of correlation matrix with binary elements, find the codes with highest degree. The smaller part of correlation matrix contains the codes of $(i+1)^{th}$ sub-graph along the rows of matrix while the codes of $(i+2)^{th}$ and other subsequent sub-graphs found along the columns, select one of the codes with highest degree. Put this code inset

A. $i=i+1$. d =highest degree.

Step.3:

If $d > 1$, form another graph or smaller part of correlation matrix containing only the codes connected with highest degree code selected in step-2 at last time and excluding the codes of set A. Jump to step-2

Step.4:

If $d=1$, find the code adjacent with last selected highest degree code as in step-2. Put this code also in set A. The codes of set A form a maximal clique defined by Lemma 2.3. There are total 'i' codes are found in final set A.

Step.5:

More than one maximal clique sets can be searched out of first smaller part of correlation matrix having more than one codes with highest degree by following the step 1 to step 4. The first smaller part of correlation matrix contains the codes of 1st sub- graph along the rows while the codes of 2nd and subsequent sub-graphs found along the columns.

Step.6:

Out of the all the M maximal clique sets found at step 5, a clique sets correlation matrix $M \times M$ can be defined. This matrix contains the elements equivalent to cross-correlation of pair of maximal clique sets. The cross-correlation of a pair of maximal clique

sets is defined as maximum cross-correlation between a pair of codes taken from each maximal clique set of pair. The clique sets correlation matrix can be normalized with elements equal to 'zero' if cross-correlation value is greater than $(\lambda_c + 1)$ and normalized elements equal to 'one' if cross-correlation value is less than equal to $(\lambda_c + 1)$.

Step.7:

By applying step 2 to step 4 over normalized clique set correlation matrix, not for smaller part of correlation matrix as given for the codes, one set of maximal clique sets is searched out having minimum correlated maximal clique sets.

5.2. Algorithm to design minimum correlated maximal cliques set of 1-DUOC:

Step.1:

Input code parameters $(n=n_1, w=w_1, \lambda_a=1, \lambda_c=1)$ Such that $n \gg w > (\lambda_a, \lambda_c)$.

Step.2:

For the code in standard DoPR $(d_1, d_2, \dots, d_{(w-1)}, d_w)$, all possible pairs of unequal values of (d_1, d_2) from the range of (d_1, d_2) given in lemma 3.5 are arranged with serial number of codes with first only two DoP elements.

The maximum

non-zero shift auto-correlation of the code within complete

DoP elements should not greater than one. Any two such codes are defined as related if at least one common DoP elements found otherwise unrelated. A connected graph G can be defined having vertices equal to number of codes formed. One pair of (d_1, d_2) is equivalent to one node or code as well as unrelated codes are equivalent to line drawn between the nodes or code numbers. The codes are related if mutual cross-correlation is greater than one and unrelated if cross-correlation is equal to one.

The counter $s=0$.

Step.3:

From the defined graph G, a set of minimum correlated maximal clique sets is searched by maximal clique search method given at section 5.1. The counter $s=s+1$. If $(s+2)=(w-1)$ go to step-6.

Step.4:

All the codes found with each maximal clique set found at step 3, are rearranged along-with $(s+2)^{\text{th}}$ DoP element which is not equal to last $(s+1)^{\text{th}}$ DoP elements of the code. Each graph of codes corresponding to maximal clique set is redefined as in step-2 such that only those codes are included in the graph having maximum non-zero shift auto-correlation equal to one. The maximum non-zero shift auto-correlation of the code, equal to one means no DoP elements in the rows of EDoP matrix of the code, are repeated in the same EDoP matrix of the code.

Step.5:

If $(s+2) < (w-1)$, go to step-3 and continue.

Step.6:

Each code of last searched each maximal clique set is rearranged with its last DoP element as per theorem-3.3. i.e. $d_w = n - (d_1 + d_2 + \dots + d_{(w-1)})$.

This searched maximal set is group of minimum correlated $(\lambda_c = 2)$ maximal clique

sets of 1-DUOC with $(n=n_1, w=w_1, \lambda_a=1, \lambda_c=1)$.

Step.7:

Similarly for $(n=(n_1, n_2, n_3, \dots), w=(w_1, w_2, w_3, \dots), \lambda_a=1, \lambda_c=1)$ minimum correlated multiple maximal sets of codes are formed for each set of code parameters $(n, w, \lambda_a, \lambda_c)$ as in step-1 to step-6.

Step.8:

Now another graph F is defined for sets of 1-DUOC with different code parameters. The vertices of graph are equivalent to sets of 1-DUOC with different set of code parameters. The line drawn between two vertices is equivalent to the cross-correlation between two sets which is less than or equal to two. No line drawn between two vertices if the two equivalent sets have cross-correlation greater than two. In this defined graph F of sets of 1-DUOC with different set of code parameters, a maximal clique is searched out by algorithm given in sub-section 5.1. This searched clique contains the sets of 1-DUOC with multi-length and multi-weight having auto-correlation constraint equal to one and cross-correlation constraint equal to two. The algorithm proposed in sub-section 5.2 can design sets of codes with specified auto (cross) correlation constraint after some little change in the algorithm.

5. CONCLUSION

In this paper the proposed clique search algorithm design the family of sets of codes with multi-length, multi-weight, auto-correlation constraint equal to one and cross-correlation constraint equal to one for within set while cross-correlation constraint equal to two among the sets with upper bound. These codes are designed for unspecific code parameters which increase inherent security. These codes can be utilized for the purpose of increasing the channel capacity and even for multi-rate system incorporating OOC. The computational complexity of the proposed algorithm designing the multiple sets of codes with variable and general code parameters, is polynomial type if clique search is polynomial. In future a mathematical alternative of clique search method for 1-DUOC or OOC may be explored for reducing the computational complexity of the algorithm proposed here.

6. REFERENCES

- [1] B. Natarajan, Z. Wu, C. R. Nassar, and S. Shattil, "Large set of CI spreading codes for high-capacity MC-CDMA," *IEEE Transactions on Communications*, vol. 52, no. 11, pp. 1862-1866, November-2004.
- [2] F. Vanhaverbeke, and M. Moeneclaey, "Binary signature sets for increased user capacity on the downlink of CDMA systems," *IEEE Transactions on Wireless Communications*, vol. 5, no. 7, pp. 1795- 1804, July-2006.
- [3] F. Vanhaverbeke, M. Moeneclaey, and H. Sari, "DS/CDMA with two sets of orthogonal spreading sequences and iterative detection," *IEEE Communications Letters*, vol. 4, no. 9, pp. 289- 291, September-2000.
- [4] F. Vanhaverbeke, M. Moeneclaey, and H. Sari, "Increasing CDMA capacity using multiple orthogonal spreading sequence sets and successive interference cancellation," *IEEE Conference Proceedings*, pp. 1516-1520, 2002.
- [5] N. G. Tarhuni, T. O. Korhonen, E. Mutafungwa, and M. S. Elmusrati, "Multiclass optical orthogonal codes for multiservice optical CDMA networks," *Journal of Lightwave Technology*, vol. 24, no. 2, pp. 694-704, February-2006.
- [6] M. Buratti, Y. Wei, D. Wu, P. Fan, and M. Cheng, "Relative difference families with

- variable block sizes and their related OOCs,” *IEEE Transactions on Information Theory*, vol. 57, no. 11, pp. 7489-7497, November 2011.
- [7] S. Bitan and T. Etzion, “Constructions for optimal constant weight cyclically permutable codes and difference families,” *IEEE Transactions on Information Theory*, vol. 41, no. 1, pp. 77–87, Jan. 1995.
- [8] Y. Chang, R. Fuji-Hara, and Y. Miao, “Combinatorial constructions of optimal optical orthogonal codes with weight 4,” *IEEE Transactions on Information Theory*, vol. 49, no. 5, pp. 1283–1292, May 2003.
- [9] W. Chu and S. W. Golomb, “A new recursive construction for optical orthogonal codes,” *IEEE Transactions on Information Theory*, vol. 49, no. 11, pp. 3072–3076, Nov. 2003.
- [10] G. Ge and J. Yin, “Constructions for optimal $(v,4,1)$ optical orthogonal codes,” *IEEE Trans. Inf. Theory*, vol. 47, no. 11, pp. 2998–3004, Nov. 2001.
- [11] S. Ma and Y. Chang, “A new class of optimal optical orthogonal codes with weight five,” *IEEE Transactions on Information Theory*, vol. 50, no. 8, pp. 1848–1850, Aug. 2004.
- [12] G. C. Yang and T. E. Fuja, “Optical orthogonal codes with unequal auto- and cross-correlation constraints,” *IEEE Transactions on Information Theory*, vol. 41, no. 1, pp. 96–106, Jan. 1995.
- [13] F. R. Gu and J. Wu, “Construction and performance analysis of variable-weight optical orthogonal codes for asynchronous optical CDMA systems,” *Journal of Lightwave Technology*, vol. 23, pp. 740–748, February 2005.
- [14] D. Wu, P. Fan, H. Li, and U. Parampalli, “Optimal variable-weight optical orthogonal codes via cyclic difference families,” in *Proc. 2009 IEEE International Symposium on Information Theory (ISIT’09)*, pp. 448–452, June 28–July 3, 2009.
- [15] D. Wu, P. Fan, X. Wang, and M. Cheng, “A new class of optimal variable-weight OOCs based on cyclic difference families,” in *Proc. 4th Int. Workshop on Signal Design and its Application in Communications (IWSDA’2009)*, pp. 16–19, Oct. 19–23, 2009.
- [16] D. Wu, H. Zhao, P. Fan, and S. Shinohara, “Optimal variable-weight optical orthogonal codes via difference packings,” *IEEE Transactions on Information Theory*, vol. 56, no. 8, pp. 4053–4060, August 2010.
- [17] G. C. Yang, “Variable weight optical orthogonal codes for CDMA networks with multiple performance requirements,” *Proceedings IEEE GLOBECOM’93*, vol. 1, pp. 488–492, December 1993.
- [18] G. C. Yang, “Variable-weight optical orthogonal codes for CDMA networks with multiple performance requirements,” *IEEE Transactions on Communications*, vol. 44, no. 1, pp. 47–55, January 1996.
- [19] H. Zhao, D. Wu, and P. Fan, “Construction of optimal variable weight optical orthogonal codes,” *Journal of Combinatorial Design*, vol. 18, 2010, pp. 274–291.
- [20] S. V. Maric, O. Moreno, and C. J. Corrada, “Multimedia transmission in fiber-optic LANs using optical CDMA,” *Journal of Lightwave Technology*, vol. 14, no. 10, pp. 2149–2153, October 1996.
- [21] S. V. Maric and V. K. Lau, “Multirate fiber-optic CDMA: System design and performance analysis,” *Journal of Lightwave Technology*, vol. 16, no. 1, pp. 9–17, January 1998.
- [22] E. Intay, H. M. H. Shalaby, P. Fortier, and L. A. Rusch, “Multirate optical fast frequency-hopping CDMA system using power control,” *Journal of Lightwave Technology*, vol. 20, no. 2, pp. 166–177, February 2002.
- [23] W. C. Kowng and G.-C. Yang, “Design of multilength optical orthogonal codes for optical CDMA multimedia networks,” *IEEE Transactions on Communications*, vol. 50, no. 8, pp. 1258–1265, August 2002.
- [24] J.-G. Zhang, “Variable-bit-rate video transmission systems using optical fiber code-

- division multiplexing scheme,” *IEEE Transactions on Consumer Electronics*, vol. 42, no. 4, pp. 874–884, November-1996.
- [26] N. G. Tarhuni and T. O. Korhonen, “Multi-weight multi-length strict optical orthogonal codes,” in *Proc. 6th Nordic Signal Processing Symposium(NORSIG)*, Espoo, Finland, pp. 161–164, June 9–11, 2004.
- [27] Thomas H. Shake, “Security performance of optical CDMA against eavesdropping,” *Journal of Lightwave Technology*, vol. 23, no. 2, February 2005, pp.655-670.
- [28] F. R. K. Chung, J. A. Salehi, and V. K. Wei, “Optical orthogonal codes: Design, analysis, and applications,” *IEEE Transactions on Information Theory*, vol. 35, no. 5, pp. 595–604, May-1989.
- [29] R. Fuji-Hara and Y. Miao, “Optical orthogonal codes: Their bounds and new optimal constructions,” *IEEE Transactions on Information Theory*, vol. 46, no. 11, pp. 2396–2406, November- 2000.
- [30] H. Chung and P. V. Kumar, “Optical orthogonal codes-new bounds and an optimal construction,” *IEEE Transactions on Information Theory*, vol. 36, no. 7, pp. 866–873, July-1990.
- [31] R. Omrani, P. V. Kumar, “Codes for optical CDMA,” *SETA 2006, LNCS 4086*, pp. 34–46, 2006.
- [32] K. Momihara and M. Buratti, “Bounds and Constructions of optimal $(n, 4, 2, 1)$ optical orthogonal codes,” *IEEE Transactions on Information Theory*, vol. 55, no. 2, pp. 514–523, February-2009.
- [33] K. W. Shum, W. S. Wong, and C. S. Chen, “A general upper bound on the size of constant-weight conflict avoiding codes,” *IEEE Transactions on Information Theory*, vol. 56, no. 7, pp. 3265–3276, July-2010.
- [34] R. C. S. Chauhan, R. Asthana, and Y. N. Singh, “A general algorithm to design sets of all possible one dimensional uni-polar orthogonal codes of same code length and weight,” *IEEE conference proceedings (ICCIC-2010)*, pp. 7-13, 28-29 December 2010.
- [35] R. C. S. Chauhan, R. Asthana, and Y. N. Singh, “Uni-polar orthogonal codes: design, analysis and applications,” International Conference on High Performance Computing (HiPC-2010), Student Research Symposium, 19-22 December 2010, Goa, India.
- [36] R. C. S. Chauhan, R. Asthana, and M. Shukla, “Representation and calculation of correlation constraints of one dimensional uni-polar orthogonal codes,” *IEEE conference proceedings (CSNT- 2011)*, pp 483-489, 3-5 June 2011.
- [37] R. C. S. Chauhan, R. Asthana, and M. Shukla, A. Singh, and G. P. Bagaria, “Proposal for one dimensional optical orthogonal codes: Design, analysis and algorithm” *IEEE conference proceedings (CSNT-2011)*, pp 514-519, 3-5 June 2011.
- [38] Jawad A. Salehi, “Code Division Multiple Access Technique in Optical Fiber Network. Part I: Fundamental Principles” *IEEE Transactions on Communication*. Vol. 37, No.8, pp. 824-833, August 1989.
- [39] O. Moreno, R. Omrani, P. V. Kumar, and H. (Francis) Lu, “A generalized Bose Chowla family of optical orthogonal codes and distinct difference sets,” *IEEE Transactions on Information Theory*, vol. 53, no.5, pp. 1907-1910, May-2007.
- [40] C. fan, J. Lee, and Y. Chang, “Constructions of difference systems of sets and disjoint difference families,” *IEEE Transactions on Information Theory*, vol. 54, no.7, pp. 3195-3201, July 2008.
- [41] A. Jagota, M. Pelillo, and A. Rangarajan, “A new deterministic annealing algorithm for maximum clique,” *IEEE Proceedings 2000*, pp.505-508.
- [42] Q. Zhang, J. Sun, and E. Tsang, “An evolutionary algorithm with guided mutation for maximum clique problem” *IEEE Transactions on Evolutionary Computation*, vol. 9, no.2, pp. 192-200, April 2005.

- [43] P. Liu, "Research on greedy clique partition GCP-algorithm," *IEEE conference proceedings (MLC-2011)*, pp 4306-4309, 3-5 August 13-16,2006.
- [44] Y. Zhang, Q. Dang, Z. Jiang, and Y.X. Hunag, "A bit level blocked estimation of distribution algorithm with local search for maximum clique problem" *IEEE conference proceedings (CEC- 2008)*, pp 4112-4117,2006.
- [45] B. Wu, S. Yang, H. Zhao, and B. Wang, "A distributed algorithm to enumerate all maximal clique in Map-reduce," *IEEE conference proceedings (FCST-2009)*, pp 45-51,2009.
- [46] L. Lu, Y. Gu, and R. Grossman, "D-maximal clique: A distribute algorithm for enumerating all maximal clique and Maximal clique distribution" ," *IEEE conference proceedings (ICDMW-2010)*, pp 1320-1327,2010.
- [47] "clique",<http://en.wikipedia.org/wiki/clique>.

Analysis of Covariance based detection technique under Rayleigh fading over cooperative sensing for Cognitive Radio Networks

ReetamNegi¹, ChhaganCharan²

¹Department of Electronics and communication Engineering, National Institute of Engineering and Technology, Kurukshetra, Haryana ²Department of Electronics and communication Engineering, National Institute of Engineering and Technology, Kurukshetra, Haryana

¹negireetam@gmail.com, ²chhagan.charan@nitkkr.ac.in

Abstract— The sensing performance in CRN degrades under fading channel to address its cooperation among multiple secondary users within a certain range is preferred. Moreover, the accurate detection of white spaces under multiple primary users is challenging. A recent study on Eigen value and covariance-based detectors don't require prior knowledge of the primary user by using random matrix theories are proved to be more accurate. In this paper, the outcome of Rayleigh multipath fading channels on spectrum sensing in a multiple primary user environment for covariance-based matrix methods such as CVD, CFN, MME, and EME is analyzed. Simulation results will show the outcomes.

Keywords— Spectrum sensing, Covariance based matrix, Rayleigh Fading, Cognitive Radio.

1. INTRODUCTION

In the past decade, the amount of wireless devices has increased with a huge amount. For these wireless communication systems, we need RADIO spectrum which is limited in the environment. To regulate wireless networks over the large geographical region, the Federal Communications Commission (FCC) has allocated certain policies in a certain time frame over a certain frequency band [1]. Though radio spectrum ranges from 6 KHz to 300 GHz, the long-established spectrum policies lead to a situation in which some bands are fully occupied while others are not used well and wasted. For the underutilized spectrum, Cognitive Radio (CR) is defined which allows secondary users (SU) to opportunistically access unused spectrum bands. In FCC definition, a “CR does spectrum sensing at secondary user (SU) and monitors spectrum usage by locating the underutilized portion of the spectrum” [1].

The CR user in CR networks needs to design very carefully such that they act as outsiders in the spectrum they visit. This makes it necessary to do spectrum management in a well-organized manner and visit the idle channels without causing disturbance to primary users. Whenever there is activity from a primary user, a secondary user must leave the channel. There are spectrum sensing solutions for CR to perform well and check its surroundings with a time. The main aim of spectrum sensing is that a SU must continuously carry out the spectrum sensing in such a way that it does not hamper the PU while the spectrum is still occupied by the primary user. For this, CR hardware should look for spectrum with reduced primary user occupation and utilize them for data transfer [2]. These primary users occupy the primary band called as licensed

channel should immediately leave the channel if any legitimate PU is detected. That is why accurate sensing of wireless channels is important for cognitive radio engineering.

Different sensing algorithms including energy detection [6], the matched filtering [7] and cyclostationary detection have been studied so far. Each of them has different operational requirements, advantages and disadvantages. The main basic method of energy detection (ED) doesn't require the advance knowledge about the information and vigorous to unknown multipath fading. Moreover ED method relies on noise power which makes it more exposed to the noise uncertainty [6], [7]. Practically it is very difficult to obtain precise noise power. To solve this, a recent method of detection is proposed which uses the concept of statistical covariance and auto-correlation of the coming signal. At the receiving filter it is found that on the basis of structure of covariance matrix a received signal is turned in to another matrix for which at the receiver a statistical covariance matrix is obtain. This received matrix has off diagonal elements which are zero when signal is not present. However, for the presence of signal the element of covariance matrix is not equal to zero. Finally on the basis of off diagonal elements, the diagonal elements of covariance matrix are computed to find the presence of signal. Different methods have been employed on the basis of Eigen value of the covariance matrix such as energy with minimum eigen value (EME) [13], maximum-minimum eigen value (MME), covariance absolute value (CAV), Mean to square extreme eigenvalue(MSEE).

Multipath fading and shadowing in the radio spectrum may lead CR to sense wrong information. As well different Cognitive Radios cannot work at the same time. That is why cooperation among different CR is preferred [15]. This increases the performance and accuracy. Previously in literature, hypothesis testing using ED for fading from different sources using single primary user has been investigated and different algorithms are developed. Also, cooperation among spectrum sensing for single input single output (SIMO) and multiple input multiple output (MIMO) systems are redefined and different detection techniques for different multipath fading channels has been studied. However, multiple primary user having multiple fading channels under cooperative spectrum sensing haven't described yet. That is why Eigen value based cooperative spectrum sensing detector is the focus of this paper. The fading consider is Rayleigh fading for multipath channel.

The rest paper is organized as follow. In section II system model and background is discussed. Section III presents the threshold detection for the algorithms. Section IV shows the cooperative spectrum sensing in Rayleigh multipath fading channel. Result and conclusion is drawn in section V and section VI respectively.

2. SYSTEM MODEL AND BACKGROUND

Let M secondary users working together to sense the availability of K primary users and Z samples. Two hypotheses H_0 tells primary user is absent (null) and H_1 tells primary user is present (alternative) , shown as below:

$$H_0: x(n) = \eta(n)$$

$$H_1: x(n) = s(n) + \eta(n)$$

where $s(n)$ is the transmitted signal samples passed through a wireless channel and $\eta(n)$ is the white Gaussian noise samples Robust nature of Energy identification towards fading makes it

one of main detection method. Any information within a source signal is not required for energy detection. In energy detection noise power is required for optimal detection of independent and identically distributed (i.i.d.) signals [12]. The average power (n) of received signal is calculated as

$$P_y(n) = \frac{1}{Z} \sum_{n=0}^{N-1} |c(n)|^2$$

where Z tells about total number of sample present. For Energy detection method we calculate the threshold λ and take a decision if $P(n) > \lambda$ signal exist otherwise does not exist. P_f is determined to know the chance of false alarm.

In Eigen value based detection L consecutive samples are taken and given by following equation.

In Eigen value based detection L consecutive samples are taken and given by following equation [10].

$$x(n) = [x(n) x(n-1) \dots x(n-L+1)]^T$$

$$c(n) = [c(n) c(n-1) \dots s(n-L+1)]^T$$

$$w(n) = [w(n) w(n-1) \dots w(n-L+1)]^T$$

where L is smoothing factor. Consider the statistical covariance matrices define as

$$R_x = E[x(n)x^T(n)]$$

$$R_y = E[c(n)c^T(n)]$$

We can verify that

$$R_y = R_x + \sigma_w^2 I_L$$

Let λ_{max} is maximum and λ_{min} is minimum Eigen values of R_y and ρ_{max} is the maximum and ρ_{min} be minimum Eigen values of R_x . The maximum and minimum Eigen values are define for $\lambda_{max} = \rho_{max} + \sigma_w^2$ and $\lambda_{min} = \rho_{min} + \sigma_w^2$. For $\rho_{max} = \rho_{min}$ it is seen that $R_x = \delta I_L$, where δ is a positive number. Here we calculate if signal is present or not by calculating $\lambda_{max} / \lambda_{min} = 1$ for no signal otherwise $\lambda_{max} / \lambda_{min} > 1$. By using the confine amount of signal samples we can calculate the statistical covariance matrix. Define autocorrelations of the received signal as [8]

$$\lambda = \frac{1}{Z} \sum_{m=0}^{N-1} y(m)y(m-l) \quad l = 0, 1, \dots, L-1$$

The sample covariance matrix approximates the statistical covariance matrix R_y as define below

$$R_y(Z) = \begin{pmatrix} \lambda(0) & \lambda(1) \dots & \lambda(L-1) \\ \lambda(1) & \vdots & \lambda(L-2) \\ \vdots & \vdots & \vdots \\ \lambda(L-1) & \lambda(L-2) \dots & \lambda(0) \end{pmatrix}$$

Different detection methods are proposed by using this covariance matrix.

3. DETECTION PARAMETER AND THRESHOLD

Let P_d be the probable chance to find the signal, which is on hypothesis H_1 , and P_f shows the probable chance of false alarm, which is on hypothesis H_0

A. The Algorithms

We are using limited number of samples and sample covariance matrix $R(N)$ for the detection process in the following described algorithms

Algorithm 1: The Covariance Absolute Value (CAV) Detection

Step 1. Compute the autocorrelation of presented signal and form sample covariance matrix as given in (11).

Step 2. Choose smoothing value L and threshold γ_1 . Threshold should be chosen in this way so it could join the demand for probability of false alarm.

Step 3. Transform the sample covariance matrix.

Step 4. Compute [9]

$$T_1(Z) = \frac{1}{L} \sum_{n=1}^L \sum_{m=1}^L |r_{nm}(Z)|$$

$$T_2(Z) = \frac{1}{L} \sum_{n=1}^L |r_{nn}(Z)|$$

Here $r_n(Z)$ are elements of transformed sample covariance matrix

Step 5. If $T_1(Z) > \gamma_1 T_2(Z)$ Signal is present otherwise signal absent

Since it is not known if signal is present or not present it is difficult to set threshold on the basis of P_d . So we calculate threshold on the basis of P_{fa}

$$P_{fa} = (T_1(Z) > \gamma_1 T_2(Z))$$

$$\approx 1 - Q \left(\frac{\frac{1}{\gamma_1} \left(1 + (L+1) \sqrt{\frac{2}{Z \cdot \pi}} \right) - 1}{\sqrt{\frac{2}{Z}}} \right)$$

where

$$Q(t) = \frac{1}{\sqrt{2\pi}} \int_t^{\infty} e^{-\frac{u^2}{2}} du$$

For CAV detection $P_{fa} \leq P_0$, P_0 is probability of detection then threshold γ_1 is calculated as [9]

$$\gamma_1 \geq \frac{1 + (L + 1) \sqrt{\frac{2}{Z * \pi}}}{1 + Q^{-1}(1 - P_0) \sqrt{\frac{2}{Z}}}$$

Algorithm 2: Maximum to minimum eigenvalue (MME) and Energy with minimum Eigen value (EME) detection

Step1. Compute the samplecovariance matrix $R(N)$ from equation (11).

Step2. Compute the maximum (λ_{max}) and minimum (λ_{min}) eigenvalues of matrix $Rx(N)$

Step3. If $\lambda_{max} / \lambda_{min} > \gamma_2$, signal is present otherwise signal absent for MME detection.

Step 4. If $T1(Z) / \lambda_{min} > \gamma_3$, signal exist otherwise signal not exists for EME detection.

Based on the random theory it is shown that for a given P_f the threshold should be chosen as

$$\gamma_2 = \frac{(\sqrt{Z} + \sqrt{ML})^2}{(\sqrt{Z} - \sqrt{ML})^2} \left(1 + \frac{(\sqrt{Z} - \sqrt{ML})^{-2}}{(Z_{ML})^{\frac{1}{6}}} \right) F_1^{-1}(1 - P_{fa})$$

$$\gamma_3 = \frac{Q^{-1}(P_{fa}) \sqrt{2Z} - \sqrt{MZ}}{\sqrt{M}(\sqrt{Z} - \sqrt{ML})^2}$$

Algorithm 3 Mean to square extreme eigenvalue (MSEE) detection

Step 1: determine test statistic [7]

$$T_3 = \frac{\lambda_{max} + \lambda_{min}}{\sqrt{\lambda_{max} \lambda_{min}}}$$

If $T_3 > \gamma_4$, signal exist otherwise not exists

For the threshold detection it is calculated from the probability of false alarm

$$P_{fa} = P(T_{MSEE} > \gamma_{MSEE} | H_0)$$

The test statistics of MSEE and MME methods are based on the largest and smallest Eigen values; so the value of threshold is determined from the value of MME threshold (γ_2). That

is why (γ_2) is calculated as the function of threshold of MMSE (γ_4). Let $\alpha = \lambda_{max} / \lambda_{min}$ then, $T_{MME} = \alpha$ and $T_{MMSE} = \frac{\alpha + 1}{2\sqrt{\alpha}}$ where, $\alpha > 1$

Since we know the expression for γ_3 we can calculate theoretical expression for P_f .

$$P_{fa} = 1 - F^{-1} \left(\frac{\gamma_2 (\sqrt{Z} - \sqrt{ML})^2 - \mu}{v} \right)$$

$$P_{fa}(\gamma_4) = 1 - F^{-1} \left(\frac{G(\gamma_4) (\sqrt{Z} - \sqrt{ML})^2 - \mu}{v} \right)$$

where

$$G(x) = 2x^2 - 1 + 2x\sqrt{x^2 - 1}$$

Finally, we obtain $\gamma = G^{-1}(\gamma)$

The proposed MMSE method is the transformation of MME method.

Due to lack of connection between the primary user and the CR user, transmission detection technique depends on weak signals only. Because of shadowing primary user signals cannot be determined by the CR user though they have good line of sight to CR receiver [16]. Therefore for more accurate primary transmitter detection, cooperation among different users is preferred. In this cooperation the uncertainty in single user detection is minimized through participation of multiple users. This reduces the multipath fading and shadowing effects and makes better detection probability.

In the previous study channel matrix H may not be specified and the probability parameters are derived for AWGN channel. As a result there is no multipath fading and channel is ideal. Here channel attributes are not specified and channel coefficients are taken in picture. That is why, various factors such as the time taken by a symbol of the detected signal and the sensing time were smaller than the coherence time of channel. Moreover there were no parallel motions between the PUs and SUs. Assuming these factors makes fading unavoidable in spectrum sensing process. In order to achieve higher sensing performance cooperation among multiple secondary users within a certain range is necessary. Rayleigh multipath fading is very prevalent in wireless channel and has SNR with probability distribution function (pdf) [14]

$$f_{\gamma}(\gamma) = \frac{1}{\bar{\gamma}} e^{-\frac{\gamma}{\bar{\gamma}}}$$

Here, γ and $\bar{\gamma}$ represent instantaneous and average SNR, respectively. The optimal decision rule for determining whether primary user is alive or the inactiveness of the user in the frequency band of interest is done by majority decision rule. For majority rule the decision of presence of PU is determined by the presence of half or more PU.

5. RESULTS

The calculations are done for all the covariance based statistical methods under Rayleigh fading. Here value of N_S is very large 10000 and simulations are done for 1000 Monte Carlo simulations. The P_{fa} is taken as 0.1 and $M=1$ for smoothing factor $L=5$. The comparison is shown in below graphs. The aim is to maximize P_d and minimize P_{fa} . Figure 1 and figure 2 shows the probability of detection for different SNR and number of samples (Z) respectively. It is depicted from the graph that the analysis at low SNR gives best performance.

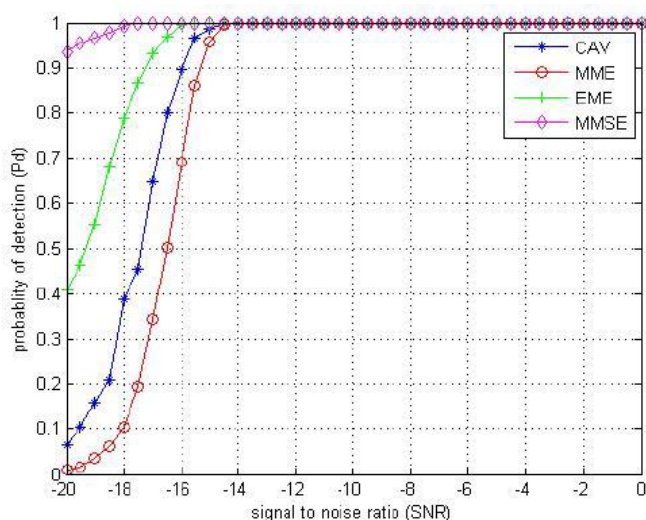


Fig. 1. Probability of detection versus SNR when $Z=5000$, $M=1$ and $L=5$

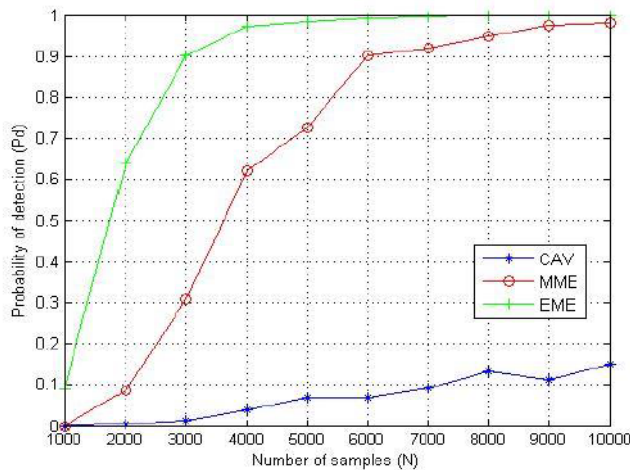


Fig.2. Probability of detection versus number of samples (Z) when SNR=-25dB , M=1 and

6. CONCLUSION

For Rayleigh multipath fading channel different test detectors are analysed under multiple secondary user. All the methods based on sample covariance matrix of the received signal. Statistical theories have been used to set the threshold and obtain the probability of false alarm. Without knowing the prior information of primary user signal various signal has been detected. Moreover these methods are robust to noise uncertainty and also perform well at lowSNR.

7. REFERENCES

- [1] J. Mitola, G. Q. Maguire (1999) Cognitive radio: making software radios more personal, *IEEE Personal Communications*, vol. 6, no. 4, pp.13-18.
- [2] S. Haykin (2005) Cognitive radio: brain-empowered wireless communications, *IEEE Journal*, vol. 23, no. 2, pp.201-220.
- [3] M. T. Masonta, M. Mzyece, and N. Ntlatlapa, "Spectrum decision in cognitive radio networks: A survey," *IEEE Commun. Surveys Tuts.*, vol. 15, no. 3, pp. 1088–1107, 3rd Quart.,2013.
- [4] IEEE 802.22 Wireless RAN (2005) Functional requirements for the 802.22 WRAN standards, IEEE 802.22-05/0007R46
- [5] S. A. Jain , M. M. Deshmukh (2015) , Performance analysis of energy and eigenvalue based detection for spectrum sensing in Cognitive Radio network, *International Conference on Pervasive Computing (ICPC)*, pp.1-5
- [6] R. Zhang, T. J. Lim, Y. Liang, Y. Zeng (2010) , Multi- antenna based spectrum sensing for cognitive radios: A GLRT approach, *IEEE Transactions on Communications*, vol. 58, no. 1, pp.84-88.
- [7] K.Hassan, RGautier, I.Dayoub, E.Radoi, M.Berbineau (2012), Nonparametric multiple-antenna blind spectrum sensing by predicted eigen value threshold, *IEEE*

InternationalConf. Communication (ICC), pp. 1629–1634.

- [8] C. Charan, R.Pandey (2017) , Double threshold based spectrum sensing technique using sample covariance matrix for cognitive radio networks, *2nd International Conference on Communication Systems, Computing and IT Applications (CSCITA)*, pp.150-153.
- [9] Y. Zeng, Y.Liang (2009) , Eigenvalue-based spectrum sensing algorithms for cognitive radio, *IEEE Transactions on Communications*, vol. 57, no. 6, pp.1784-1793.
- [10] P. K. Verma, P. Jain, S. K. Soni (2017),]Performance analysis of blind eigen value with multiple antenna based spectrum sensing in cognitive radio, *Recent Developments in Control, Automation & Power Engineering (RDCAPE)*, pp. 372-377
- [11] K. Bouallegue, I. Dayoub, M. Gharbi ,K. Hassan (2018), Blind Spectrum Sensing Using Extreme Eigenvalues for Cognitive Radio Networks, *IEEE Communications Letters*, vol. 22, no. 7, pp.1386-1389.
- [12] Y. Zeng, Y.-C. Liang, A. T. Hoang, and R. Zhang, “A review on spectrum sensing for cognitive radio: challenges and solutions,” *EURASIP Journal on Advances in Signal Processing*, vol. 2010, Article ID 381465, 15 pages,2010.
- [13] Y. Zeng, C. L. Koh, and Y.-C. Liang, “Maximum eigenvalue detection: theory and application,” in *Proceedings of the IEEE International Conference on Communications (ICC '08)*, pp. 4160–4164, Beijing, China, May2008.
- [14] Salam Al-Juboori*, Sattar J. Hussain and Xavier Fernando “Cognitive Spectrum Sensing with Multiple Primary Users in Rayleigh Fading Channels” www.mdpi.com/journal/electronics , Electronics2014.
- [15] Penna, F.; Garelo, R.; Spirito, M. Cooperative spectrum sensing based on the limiting eigenvalue ratio distribution in wishart matrices. *Commun. Lett. IEEE* 2009, 13,507–509
- [16] Herath, S.; Rajatheva, N.; Tellambura, C. Energy detection of unknown signals in fading and diversity reception. *IEEE Trans. Commun.* 2011, 59,2443–2453.

Design and Implementation of Antenna Array beam formation for Multi Function Radar by considering thinning effect

BV Subba Rao*¹, Raveen Kumar K², Dr RVS Satyanarayana³

¹ Scientist/Engineer-G, Satish Dhawan Space Centre, ISRO, Sriharikota, 524124, INDIA

² Scientist/Engineer-SE, Satish Dhawan Space Centre, ISRO, Sriharikota, 524124, INDIA

³ Professor, Dept of ECE, SV University, Tirupati 517502, INDIA

bvsr@shar.gov.in¹, raven.katakamu@shar.gov.in², v.s.ravinutala@gmail.com³,

Corresponding author*: Phone: +91-9440414514

Abstract

Different kinds of Radars are deployed in ISRO for tracking, surveillance, weather applications. Multi Function Radar with Phased array antenna is planned and designed for combining all three applications in single Radar. Phased array antennas are used for the inherent flexibility to steer the beam electronically and also the need for specialized multi-function radar systems. In the antenna arrays the side lobe level and thinning effect are major problems which cause the wastage of energy and reduction of energy in main beam. In this paper different windowing techniques are used to suppress the side-lobes in planar array antenna, by varying the various parameters like number of antenna elements, scan angle, element spacing and window coefficients.

This paper analyzes the capability of standard DSP based window techniques in order to minimize such side-lobes of a rectangular antenna array beam. Since array design problem is essentially equivalent to the problem of designing FIR digital filters in DSP. The result of antenna gain pattern has been simulated by applying Uniform, Berlet, Barthan, Blackman, Blackman Harris, Bohmanwin, Chebysiv, Gaussian, Hamming, Hanning, Kaiser, Parzen, Taylors and Tukey current windowing distribution techniques . It is revealed that the DSP based windowing for current distribution of antenna array can be used reduction of side lobe in analyzing rectangular and quasi circular array antennas.

Thinning involves reducing total number of active elements in an antenna array without causing major degradation in system performance. Dynamic thinning is the process of achieving this under real-time conditions by using optimization of antenna array element currents. It is required to find a strategic subset of antenna elements for thinning so as to have its optimum performance. From a mathematical perspective this is a nonlinear, multidimensional problem with multiple objectives and many constraints. The present paper discusses an approach for antenna beam forming by considering array thinning. After discussing the basic concept involving antenna array, array thinning, dynamic thinning, and application methodology, simulation results of applying the technique to Quasi planar array are presented. MATLAB software environment is used as the main analysis tool.

Keywords: Multi Function Radar, Tracking Radar, Dual Polari metric Doppler weather Radar, Antenna Array synthesis, Adoptive window synthesis.

1. Introduction

Multi Function Radar consisting of micro strip patch antenna elements operating at S band that are spatially arranged and electrically interconnected to produce a directional radiation pattern in two-dimensional space. The electrical characteristics, orientations, and polarizations of the elements forming part of the array as well as the geometrical arrangement of the array and their interconnections determine the overall performance of the array. Antenna arrays containing large number of elements are frequently used in radar for tracking, communication, astronomy, and other systems. In order to reduce the element count, cost, weight, power consumption, and heat dissipation in these systems, thinning is sometimes performed by removing a percentage of array elements according to a suitable strategy. For a fixed antenna size, the thinning produces antenna arrays much optimized than completely filled arrays, in terms of both hardware and control complexity. Moreover, although by thinning the main lobe width may remain approximately unaltered, there will generally be a reduction in antenna gain and also loss of

control over the radiation pattern outside the main beam. Thinning can be considered as a tool for reducing total number of active antenna elements in an antenna array when the main beam is narrow and the demand on the control of radiations outside the main beam is modest..

The total field of the array is determined by the vector addition of the fields radiated by the individual elements. This assumes that the current in each element is the same as that of the isolated element (neglecting coupling). In practical situation, antenna current distribution follows uniform density function and phase distribution follows Gaussian density function. To provide very directive patterns, it is necessary that the fields from the elements of the array interfere constructively (add) in the desired directions and interfere destructively (cancel each other) in the remaining space. Ideally this can be accomplished, but practically it is only approached. In an array of identical elements, there are at least five controls that can be used to shape the overall pattern of the antenna. These are: 1.The geometrical configuration of the overall array. 2. The relative displacement between the elements 3.The excitation amplitude of the individual elements. 4. The excitation phase of the individual elements 5. The relative pattern of the individual elements.

A. Rectangular Planar array Design

Planar arrays provide additional variables which can be used to control and shape the pattern of the array [1]. Planar arrays are more versatile and can provide more symmetrical patterns with lower side lobes. In addition, they can be used to scan the main beam of the antenna towards any point in space. Applications include tracking radar, search radar, weather radar, remote sensing, communications, and many others [1]. To derive the array factor for the planar array, if M elements are initially placed along x-axis and N elements are initially placed along y-axis as shown in Fig. 1. The array factor of the entire planar array can be written as

$$AF = S_{xm}S_{yn} \quad [1]$$

Where

$$S_{xm} = \sum_{m=1}^M I_{m1}W_{1m}e^{j(m-1)(kd_x \sin \theta \cos \varphi + \beta_x)} \quad [2]$$

$$S_{yn} = \sum_{n=1}^N I_{1n}W_{1n}e^{j(n-1)(kd_y \sin \theta \sin \varphi + \beta_y)} \quad [3]$$

The above equations indicate that the pattern of a rectangular array is the product of the array factors of the arrays in the x and y directions. Where I_{m1} is excitation coefficient of each element. W_{1m} and W_{1n} DSP based window coefficients in x and y direction.. The spacing and progressive phase shift between the elements along x-axis is represented, respectively, by d_x and β_x . If N such arrays are placed next to each other in y-direction, a distance d_y apart and with a progressive phase β_y , a rectangular array will be formed as shown in Fig.1. If amplitude excitation coefficients of the elements of the array in the y direction are proportional to those along the x, the amplitude of (m, n) th element can be written as

$$I_{mn} = I_{m1}W_{1m}I_{n1}W_{1n} \quad [4]$$

The normalized form of antenna array factor

$$AF_n(\theta, \varphi) = \left\{ \frac{1}{M} \frac{\sin(\frac{M}{2}\psi_x)}{\sin(\frac{\psi_x}{2})} \right\} \left\{ \frac{1}{N} \frac{\sin(\frac{N}{2}\psi_y)}{\sin(\frac{\psi_y}{2})} \right\} \quad [5]$$

Where

$$\psi_x = kd_x \sin \theta \cos \varphi + \beta_x$$

$$\psi_y = kd_y \sin \theta \sin \varphi + \beta_y$$

When the spacing between the elements is equal or greater than $\lambda/2$ multiple maximum of equal magnitude can be formed. The principal maximum is referred to as the major lobe and the remaining as the grating lobes. A grating lobe is defined as a lobe other than the main lobe produced by an array antenna when the inter element spacing is sufficiently large to permit the in phase addition of radiated fields in more than one direction. To form or avoid grating lobes in a rectangular array, the same principles must be satisfied as for a linear array. To avoid grating lobes in the xz and yz planes the spacing between elements in x and y direction respectively must be less than $\lambda/2$. For a rectangular array, the major lobe and grating lobes of S_{xm} and S_{yn} are located at

$$kd_x \sin \theta \cos \varphi + \beta_x = \pm 2m\pi \quad m = 0,1,2, \dots$$

$$kd_y \sin \theta \sin \varphi + \beta_y = \pm 2n\pi \quad n = 0,1,2, \dots$$

The phases β_x and β_y are independent of each other and they can be adjusted so that the main beam of S_{xm} is not the same as that of S_{yn} . However, in most practical applications it required that the conical main beams S_{xm} and S_{yn} intersect and their maxima be directed towards same direction. If it is desired to have only one main beam that is directed along $\theta = \theta_0$ and $\varphi = \varphi_0$. The progressive phase shift between the elements in the x and y direction must be equal

$$\beta_x = -kd_x \sin \theta_0 \cos \varphi_0$$

$$\beta_y = -kd_y \sin \theta_0 \sin \varphi_0$$

The directivity of the antenna array $AF_n(\theta, \varphi)$, whose major beam is pointing in the $\theta = \theta_0$ and $\varphi = \varphi_0$ direction.

$$D = \frac{4\pi [AF_n(\theta, \varphi)]_{max} [AF_n(\theta, \varphi)]_{max}^*}{\int_{\varphi=0}^{2\pi} \int_{\theta=0}^{\pi} [AF_n(\theta, \varphi)]_{max} [AF_n(\theta, \varphi)]_{max}^* \sin \theta \, d\theta d\varphi}$$

2. DESIGN FOR MULTI FUNCTION RADAR

Antenna array is designed to control their radiation characteristics by properly selecting the phase and/or amplitude distribution between the elements [6]. It has already been shown that a control of the phase can significantly alter the radiation pattern of an array. In fact, the principle of scanning arrays, where the maximum of the array pattern can pointed in different directions, is based primarily on control of the phase excitation of the elements. In addition, it has been shown that in Fig.19 to Fig.28 a proper amplitude excitation taper between the elements can be used to control the beam width and side lobe level. Typically the level of the minor lobes can be controlled by tapering the distribution across the array. The smoother the taper from the center of the array towards the edges, the lower the side lobe level and the larger the HPBW, and conversely. Therefore a very smooth taper, such as that represented by a binomial distribution or others, would result in very low side lobes but larger HPBW. In contrast, an abrupt distribution such as that of uniform illumination, exhibits the smaller HPBW but highest SLL(-13.5 dB). Therefore if it is desired to achieve simultaneously both very low side lobe level, as well as small half power Beam width a compromised design has to be selected The Antenna array radiation/reception patterns feature undesired minor radiation/reception directions called side lobes.[2]. These can be minimized through application of standard digital filter window functions. . A various DSP based window functions have been proposed in literature and they are used to achieve required to meet design goals. The Spatial DSP based window techniques are Uniform, Barlet, Barthan, Blackman, Blackman Harris, Bohmanwin, Chebysiv, Gaussian, Hamming, Hanning, Kaiser, Parzen, Taylors and Tukey. When Multi function Radar is operating in Target tracking mode uniform window will be used. For Doppler Weather Radar operating mode above mentioned DSP window based Antenna Array is used.

2.1. DSP BASED WINDOW FUNCTIONS REPRESENTATION IN TIME DOMAIN AND FREQUENCY DOMAIN

Doppler radars are now considered to be an indispensable tool in the measurement and forecasting of atmospheric phenomena [2] in space applications. Measurement of the reflectivity and velocity of precipitation particles basically exploits the information contained in the amplitude and phase of the scattered electromagnetic wave. Dual-polarized radar systems [7] can be configured in different ways depending on the measurement goals and the choice of orthogonal polarization states. Doppler radars were upgraded for limited dual-polarization measurements in the linear h/v-basis (for measurement of differential reflectivity and differential propagation phase). Because only copolar signals were involved, the system requirements were much less stringent and significant practical results (e.g. rain rate estimation, hail detection) were obtained fairly quickly. Since antenna performance is critical for achieving high accuracy in the measurement of the weak cross-polar signal, both antenna performance characteristics and formulation of radar observables in the presence of system polarization errors are treated. Calibration issues relevant to polarization diversity systems results in poor estimation of the elements of the covariance matrix from signal samples under three different pulsing schemes. To estimate specific differential phase (Kdp) from range profiles of the differential propagation phase ϕ_{dp} requires SLL of -20dB for Dual polarimetric Radar [7]. To meet this design purpose it is proposed various window techniques.

Rectangular

$$w(n) = 1$$

$$W(e^{j\omega}) = \frac{\sin \frac{\omega N}{2}}{\sin \frac{\omega}{2}}$$

Triangular

$$w(n) = 1 - \frac{2|n|}{N-1}$$

$$W(e^{j\omega}) = \left[\frac{\sin \left[\omega \frac{(N-1)}{4} \right]}{\sin \frac{\omega}{2}} \right]^2$$

Raised Cosine

$$w(n) = \alpha + (1 - \alpha) \cos \frac{2\pi n}{N-1}$$

$\alpha = 0.5$ for Hanning Window
 $\alpha = 0.54$ for Hamming Window

$$W(e^{j\omega}) = \alpha \frac{\sin \frac{\omega N}{2}}{\sin \frac{\omega}{2}} + \left[\frac{1 - \alpha}{2} \right] \frac{\sin \left[\frac{\omega N}{2} - \frac{N\pi}{N-1} \right]}{\sin \left[\frac{\omega}{2} - \frac{\pi}{N-1} \right]} + \left[\frac{1 - \alpha}{2} \right] \frac{\sin \left[\frac{\omega N}{2} + \frac{N\pi}{N-1} \right]}{\sin \left[\frac{\omega}{2} + \frac{\pi}{N-1} \right]}$$

Blackman

$$w(n) = 0.42 + 0.5 \cos \frac{2\pi n}{N-1} + 0.08 \cos \frac{4\pi n}{N-1}$$

$$W(e^{j\omega}) = 0.42 \frac{\sin \frac{\omega N}{2}}{\sin \frac{\omega}{2}} + 0.25 \frac{\sin \left[\frac{\omega N}{2} - \frac{N\pi}{N-1} \right]}{\sin \left[\frac{\omega}{2} - \frac{\pi}{N-1} \right]} + 0.25 \frac{\sin \left[\frac{\omega N}{2} + \frac{N\pi}{N-1} \right]}{\sin \left[\frac{\omega}{2} + \frac{\pi}{N-1} \right]} + 0.04 \frac{\sin \left[\frac{\omega N}{2} - \frac{2\pi n}{N-1} \right]}{\sin \left[\frac{\omega}{2} - \frac{2\pi}{N-1} \right]}$$

$$+ 0.04 \frac{\sin \left[\frac{\omega N}{2} + \frac{2\pi n}{N-1} \right]}{\sin \left[\frac{\omega}{2} + \frac{2\pi}{N-1} \right]}$$

Kaiser

$$w_k(n) = \frac{I_0 \left[\alpha \sqrt{1 - \left[\frac{2n}{N-1} \right]^2} \right]}{I_0(\alpha)}$$

$$W(e^{j\omega}) = \frac{2}{I_0(\alpha)} \frac{\sin \left\{ \frac{N-1}{2} \left[\omega^2 - \left[\frac{2\alpha}{N-1} \right]^2 \right]^{1/2} \right\}}{\left[\omega^2 - \left[\frac{2\alpha}{N-1} \right]^2 \right]^{1/2}}$$

3. RESULTS AND ANALYSYS

The performance comparison in terms of side lobe levels reduction and HPBW changing upon application of various DSP based windows on Antenna array are tabulated in table. The results are indicative of lower side lobe levels and with broader main lobe width which compromise on angular resolution. The Fig.1 shows initially antenna designed for Rectangular Planar array of 48x48 with uniform current distribution. The antenna radiation pattern [3] shown in Fig.2. The achieved side lobe level is only -13 dB and Gain 42.7 dB.. Hence it is modified as Quasi circular planar array shown in Fig.5. The Radiation pattern is shown in Figure.6. The achieved side lobe level -17 dB with Gain of 42.05 dB. For this again to achieve better Side lobe levels Radar array can be operated using Kaiser and Tukey Windowing [10], [11] as shown in Fig.3 and Fig.7.

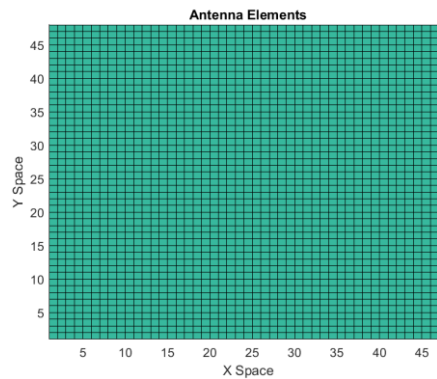


Fig.1. Original rectangular Planer array (48x48) elements

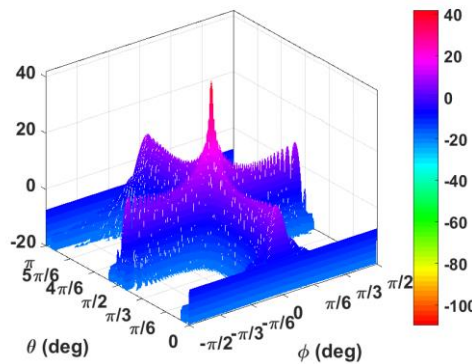


Fig.2. Directivity of antenna Unifrom Current Dtribtion

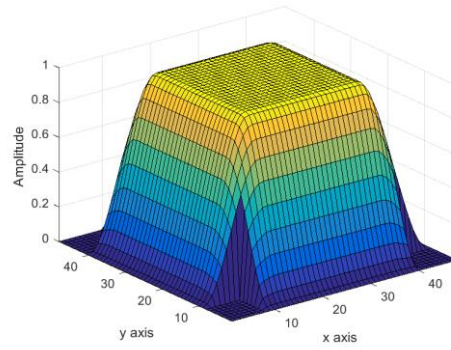


Fig.3. Antenna Current Distribution with Tukey Window

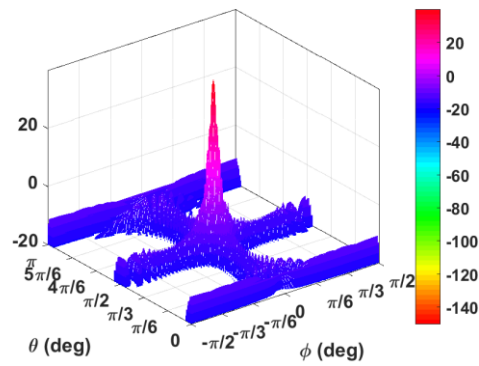


Fig.4. Directivity of antenna Tukey Current Distribution

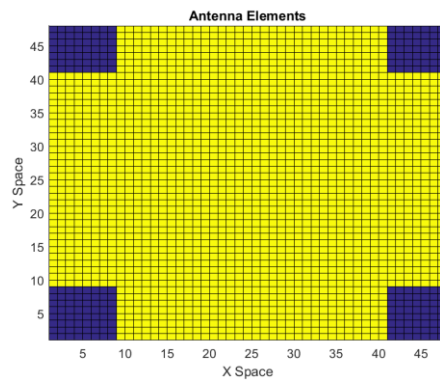


Fig.5. Quasi Circular Planer array (48x48) elements

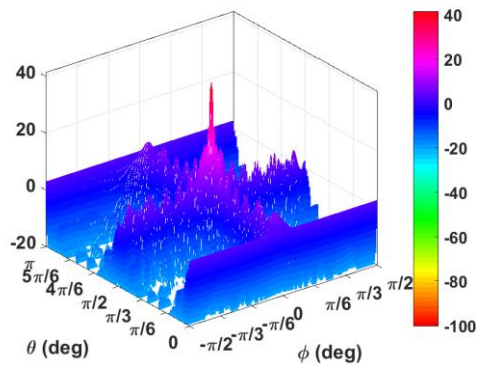


Fig.6. Directivity of antenna Unifrom Current Dtribtion

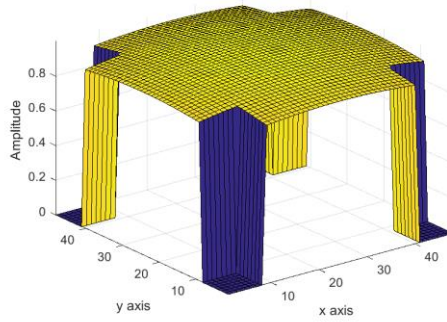


Fig.7. Antenna Current Distribution with Kaiser Window

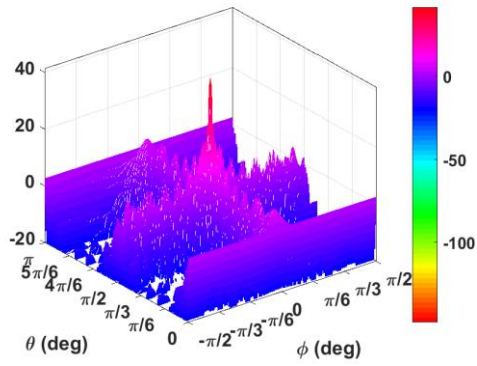


Fig.8. Directivity of antenna Kaiser Current Dtribtion

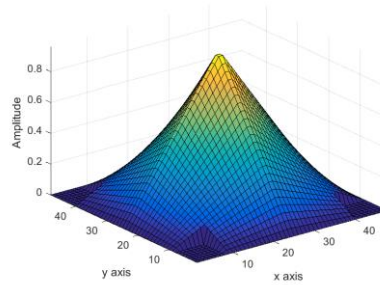


Fig.9 Barlett Window

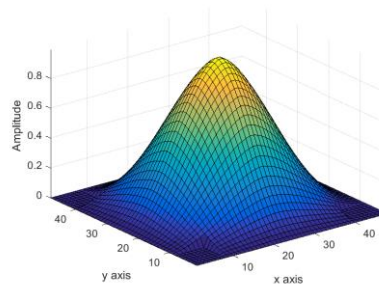


Fig.10. Barthan window

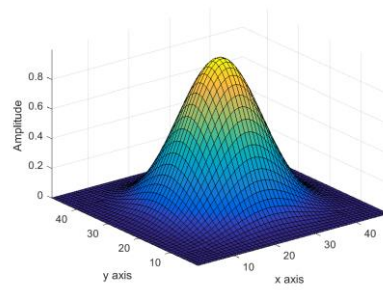


Fig.11. Blackman window

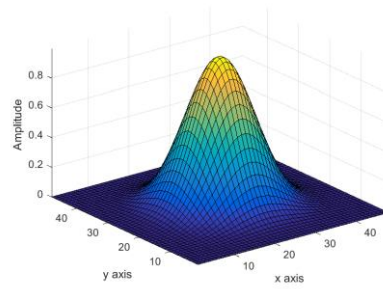


Fig.12. Blackmann Harris Window

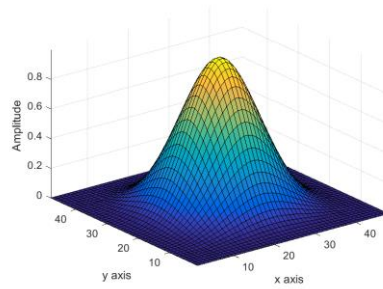


Fig.13. Bohmann Window

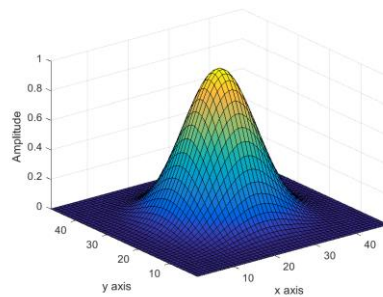


Fig.14. Chebysiv Window

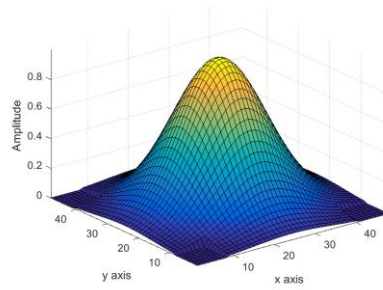


Fig.15. Gaussian window

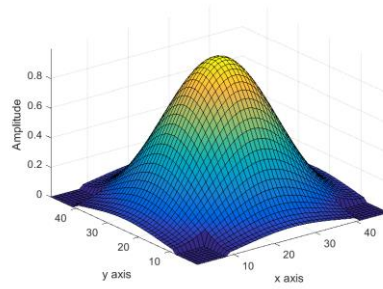


Fig.16. Hamming Window

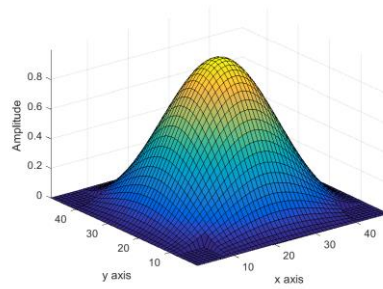


Fig.17. Hanning Window

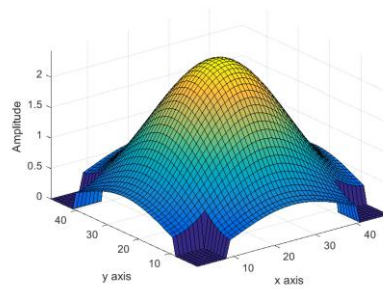


Fig.18. Taylors Window

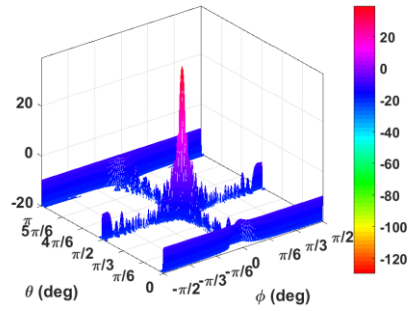


Fig.19. Directivity of antenna Barlett Current Distribution

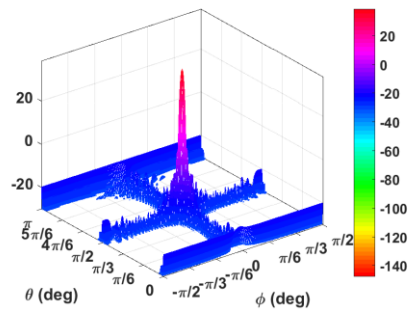


Fig.20. Directivity of antenna Barthaan Current Distribution

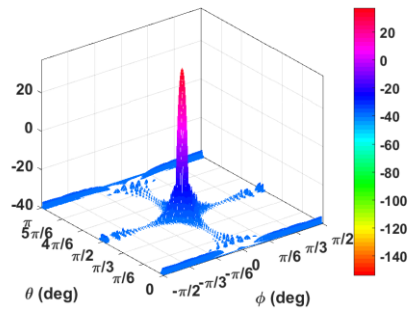


Fig.21. Directivity of antenna Blackman Current Distribution

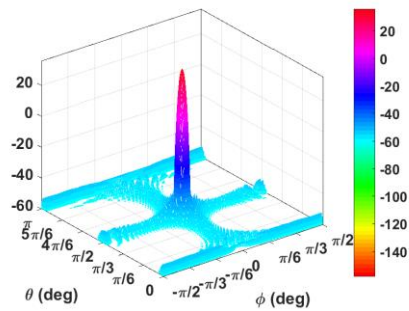


Fig.22. Directivity of antenna BalckmanHarris Current

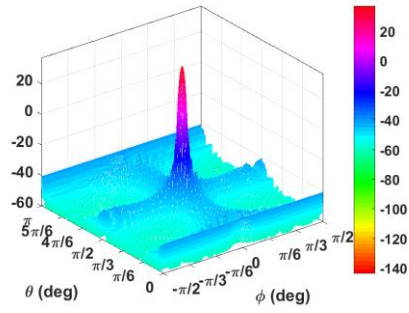


Fig. 23. Directivity of antenna Bohman Current Distribution

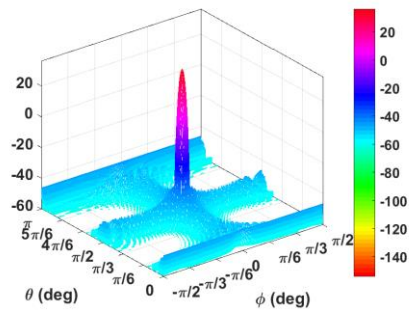


Fig.24. Directivity of antenna Chebysiv Current Distribution

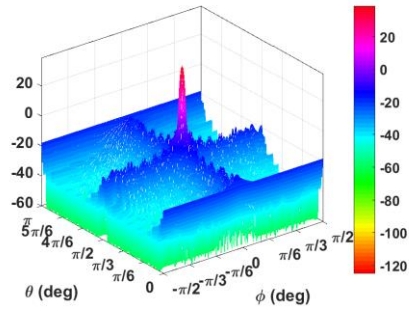


Fig.25. Directivity of antenna Gaussian Current Distribution

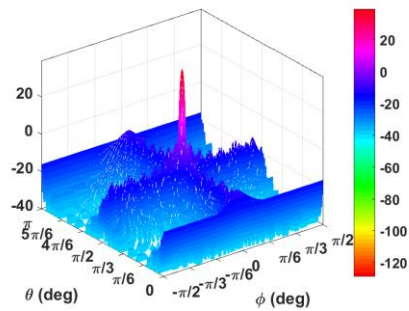


Fig.26. Directivity of antenna Hamming Current Distribution

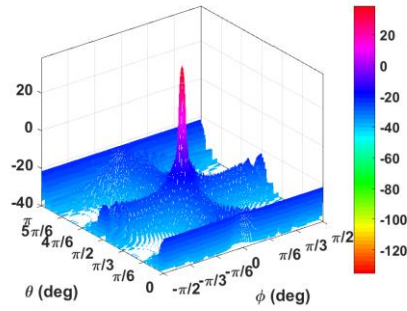


Fig.27 Directivity of antenna Hanning Current Distribution

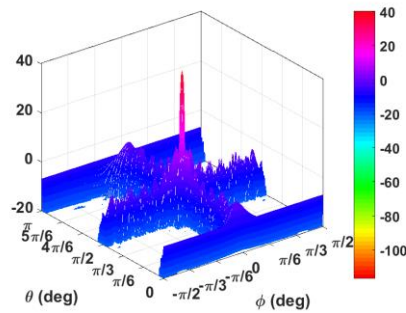


Fig.28. Directivity of antenna Taylor Current Distribution

Analysis of the results obtained shown in the table.1 is indicative of the significance of windowing operations [10],[11] in beam forming in rectangular antenna array based antenna for multi function radar to achieve required Side lobe level and HPBW with optimum Gain. When the Multi function Radar is operated in weather mode the following spatial DSP window based current distributions are tabulated. The antenna current distribution after using various spatial windows are shown in Fig. 9 to Fig.18 and obtained radiation patterns are shown in Fig. 19 to Fig.28.

Window	HPBW (Deg)	FNBW (Deg)	GAIN (dB)	SLL (dB)
Barlett	3.00	3.55	38.51	26.89
Barthan	2.00	2.15	37.89	36.88
Blackman	5.00	7.27	36.97	56.03
BlackHarris	4.00	5.55	35.68	83.13
Bohmann	2.90	4.12	36.68	45.72
Chebysiv	3.00	4.12	36.59	78.05
Gaussian	2.00	3.15	38.50	45.89
Hamming	1.99	3.15	39.01	41.16
Hanning	3.00	4.12	38.53	31.23
Kaiser	1.00	4.12	41.20	16.18
Parzen	3.00	4.12	36.25	54.66
Taylor	2.00	3.87	40.25	30.66
Tukey	2.00	3.72	39.87	15.39
Uniform	1.77	2.00	41.20	13.86

Table.1. Analysis of all window techniques on antenna array

4. Conclusion

Multi function Array Radar is designed in S band frequency for Tracking and Weather applications to meet range safety requirements for launch base station. The Array geometry initially configured with 48x 48 micro strip patch antenna elements with inter element spacing 0.73λ to avoid grating lobes which occur when element spacing is less than the 0.5λ . For Rocket tracking mode operation applications Side Lobe level of -15 dB was proposed and for Dual polarimetry weather radar mode the side lobe level required is more than -20 dB to obtain weather radar meteorology data products. Rectangular planar array consisting of 48 x 48 gives Side lobe level of -13 dB only with gain of 42.7 dB. For Rocket tracking mode Antenna array is tapered as quasi circular with achieved side lobe level of -17 dB and for weather operations antenna array are adopted different window techniques with reduced side lobe level of -22dB. Hence antenna array can be configured/ synthesized for both Tracking and Weather applications. In this paper investigations are made on analysis of rectangular planar array converted to quasi circular array with various DSP based window techniques are used to configure the array for both tracking and Doppler weather radar dual purpose.

5. Acknowledgement

This research was sponsored and supported by Satish Dhawan Space Centre SHAR, Indian Space Research Organization, Dept of Space, and Government of INDIA.

We express our sincere gratitude to department Range Operations, SDSC SHAR. Special thanks to Grahadurai G, Deputy Director, Range Operations, A. Rajarajan, Director, Satish Dhawan Space Centre, Indian Space Research Organization, who have provided immense support for publishing this paper.

References

- [1] C. A. Balanis, Antenna Theory, Analysis and Design. John-Wiley and sons, 2016.
- [2] P. Podder, T.Z. Khan and MH Khan, Comparative performance analysis of hamming, hanning and blackman window, International Journal of Computer Applications, vol 96, June 2014.
- [3] Skolnik. M, Radar Handbook, McGraw-Hill, New York, 3rd Ed., 2008..
- [4] Barton. D.K., Modern Radar System Analysis, Norwood, Mass., Artech House, 1988.
- [5] Richards.M., Fundamentals of Radar Signal Processing, McGraw Hill, New York, 2005.
- [6] Tom Jeffery, Phased Array Radar Design: Application of Radar Fundamentals, SciTech Publishing, Raleigh, NC, 2009.
- [7] V. N. Bringi, V. Chandrasekar, Polarimetric Doppler weather radar: principles and applications, Cambridge University Press, 2009.
- [8] R. S. Elliott, Antenna Theory and Design, Revised Edition, Wiley Interscience, 2018.
- [9] L. Josefsson, P. Persson, Conformal Array Antenna Theory and Design, IEEE Press, John Wiley & Sons, 2006.
- [10] G. Proakis, G. Monolakis, Digital Signal Processing, Principles, Algorithms and applications, Pearson, 2016
- [11] Vijay K Madiset, Digital Signal Processing Handbook, CRC Press, 2018.

Study and Optimisation of High Current Pulsed Power Components for Pulse Forming Network Powering Electro Magnetic Launcher

Pradeep Kumar V¹, Gaurav Kumar², Shivam Rajput³, Kishore Jadhav⁴, KJ Daniel⁵, Suwarna Datar⁶

¹Armament R&D Establishment(Defence Research & Development Organisation) Pune, India²Armament R&D Establishment(Defence Research & Development Organisation) Pune, India³Armament R&D Establishment(Defence Research & Development Organisation) Pune, India⁴Armament R&D Establishment(Defence Research & Development Organisation) Pune, India⁵Armament R&D Establishment(Defence Research & Development Organisation) Pune, India⁶Dept of Applied Physics Defence Institute of Advanced Technology Pune, India
pradeepkumar@arde.drdo.in¹, gauravkumar@arde.drdo.in², srajput@arde.drdo.in³, kbjadhav@arde.drdo.in⁴, kjdaniel@arde.drdo.in⁵, suwarnadatar@diat.drdo.in⁶

Abstract - The Electro Magnetic Gun, commonly known as railgun offer the unique advantage of hyper velocity projectiles, beyond the limit of maximum muzzle velocity offered by the chemical propellant guns. In order to achieve the desired acceleration, the gun needs to be powered by a high magnitude current pulse with peak current of few mega amperes. A pulse forming network (PFN) was developed to generate a current pulse above 1 MA for this purpose. A modular configuration is conceived consisting of 10 capacitor bank modules; each of them is designed to deliver peak current up to 150 kA. The components and subsystem of the PFN were critical and unique to handle pulse currents of the above order and subsequent forces. Capacitors are switched by high current Ignitron switches. A pulse inductor based on bitter magnet configuration was designed and developed to limit the current and shape the pulse as per the requirement. A busbar based system was developed to transfer power between the PFN elements. Specially designed co-axial cables were developed to couple the current from each module to the railgun. The modules were assembled, integrated with the Railgun launcher and test fired to generate a current pulse of 1.1 MA peak with a duration of 3.2 ms, which successfully accelerated a 120 g projectile with a velocity of 2020 m/s.

Keywords: Railgun, Electro Magnetic Launcher, Pulsed Power System, Capacitor Bank

1. INTRODUCTION

Conventional artillery guns using propellants for accelerating projectile have maximum muzzle velocity limited to 1600-1800 m/s and the limitation is attributed to the velocity limitation of the accelerating gases – which in turn accelerate the projectile – as per kinetic theory of gases. Adding more charge is not of significant benefit. Worldwide various other configurations like liquid propellant gun and light gas gun were experimented for higher muzzle velocity, however the Electromagnetic gun or Railgun only turned out to be a near practical solution towards a battle field deployable gun [1].

Railgun works on electro –magnetic propulsion and does not use gas pressure for projectile acceleration. Railgun consists of two parallel long conducting rails along the longitudinal axis separated by long insulator blocks. Another conducting block placed between the rails in sliding contact acts as the armature (Fig.1). When a high pulsed current is introduced into the rails, a huge magnetic field is generated between the rails. The armature behaves as the current carrying conductor in a magnetic field and tends to move according to Lorentz force Law ($J \times B$). The rails experience large amount of repulsive force as well.

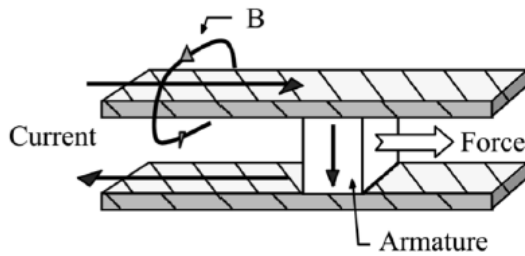


Fig. 1 Principle of Railgun – Schematic

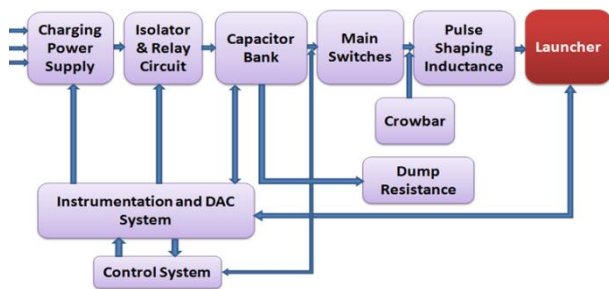


Fig. 2 Components of EM Launch System Powered by a Capacitor Bank

Essential requirement of the system is to generate a high current high voltage electrical pulse, peaking at 100's of kilo Amperes (kA) to few Mega Amperes (MA) [2]. Accordingly a Pulse Forming Network (PFN) was designed and developed to generate a current pulse peaking above 1 MA with a duration of few milliseconds. The components of the EM launch system are shown in Fig 2. The energy from the intermediate storage is delivered through high rating switches to the load (railgun launcher) through a power conditioning circuit. The PFN system consists of the capacitor bank, switches, pulse shaping inductor, interconnecting power transfer lines, and the EM launcher. Each of these components were modelled, simulated, analysed and optimised for the selection of appropriate parameters. Accordingly the systems are designed, fabricated assembled and tested.

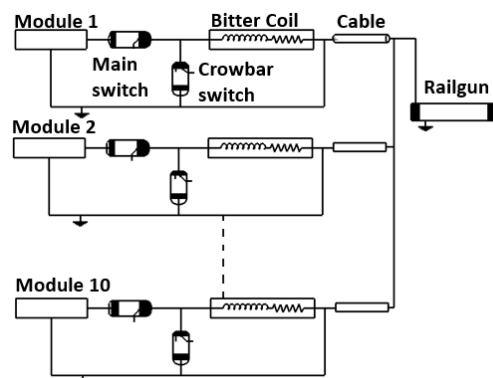


Fig 3: Modular configuration of Capacitor Bank

2. ENERGY STORAGE

For railguns to be used as accelerators for military purposes, it is necessary to deliver tens of MJ's of energy in a matter of milliseconds with currents of the order of MAs. This requires an energy source of very high power rating (of the order of GWs). Such requirements make the power source a complex system. This problem makes it imperative for the power supply to be a two staged system. First, the electrical energy from an electrical generator fed from a prime mover is stored into an intermediate electrical energy storage device (such as capacitor, compulsator, homopolar generator, inductor etc) which can store energy albeit for short duration but can deliver the energy quite rapidly. In the second stage the intermediate storage device transfers high power to the railgun through a pulse forming network

The three primary types of pulsed power systems for electromagnetic launch are capacitive, inductive, and rotating electrical machine [4]. For field deployable systems the energy density (J/cc or J/g) of the systems must be high. Of the three sources rotating electrical machines (eg, Compulsator, Homopolar generator) have the highest energy density but the technology is complex and not readily available as these contain heavy masses rotating at very high speeds. Inductive energy

storage systems contain low loss current carrying inductors which deliver a large current into the gun by means of an opening switch. In inductive energy storage systems, designing an efficient opening switch is the main challenge and often such switches are either destructive or limited to a smaller current. The summary of various pulsed power source with energy density is provided in Table I below:

TABLE I
COMPARISON OF PULSED POWER SOURCES FOR RAILGUN

Device	Method	Energy density (MJ/m ³)
Capacitor	Electrostatic	7
Inductor	Magnetic	140
Rotor	Inertial	640
Battery	Electrochemical	4000
Flux compressor	Chemical	5000-10000

Capacitor bank based pulsed power systems are relatively less complex and have been used worldwide for gun applications [5] - [8]. The operation is simple but the energy density of the capacitors is low when compared to the other two sources and currently, the size of capacitor banks can be very large to match the energy content of a currently available gun propellant round.

Armament Research & Development Establishment (ARDE) developed capacitors as energy storage for its Railgun. The capacitors are rated for 12 kV [9]. Capacitor Bank is arranged in modular configuration with ten modules of 400 kJ form 4 MJ bank, as shown in Fig 3

3. SWITCHING SYSTEM

The modules are to be switched at currents above 150 kA at charging voltage of 11 kV. Simulation results indicate peak current rate, di/dt of 6kA/μs and action integral of 9MJ/Ω. Normal high current switches are not appropriate for these specifications and hence Ignitrons are used as switches which are mercury based switches [10].

A 16 channel trigger system capable of generating pulses of 1.8kV with 4 J energy at each channel was used to trigger the main switch. Effective triggering of crowbar was a real challenge. Various automatic triggering schemes were experimented. Finally an auto-trigger scheme was established by connecting the ignitor of the crowbar to the anode point through a resistor and diode. When the voltage reversal takes place, positive voltage comes at the anode and the crowbar ignitron gets triggered.

4. POWER CONDITIONING

The electrical current pulse from the energy storage has to be properly tailored as per the EM gun requirements [11]. In order to shape the pulse and limit the output current of the capacitor bank module each module is connected to the railgun via an inductor. The function of inductor is to limit the current and continue feeding the railgun even after the capacitors have been cut off from the main circuit. It may be noted that in case of pulsed power systems where large currents are involved each current carrying component experiences enormous force depending on the fields surrounding it. In case of pulse shaping inductor as well as the railgun, the fields are large and as such robust structures have to be designed.

For the pulse shaping inductor bitter coil configuration (Fig 4) was chosen which consists of plates arranged in a coil like fashion rather than coil of wires [12]. The current flows in a helical path through the plates and the forces generated due to current flow is radially outwards and axial compressive. Bitter coil construction is simple and no external reinforcement is required to make it withstand the forces. The inductance can be increased or decreased by changing the number of plates stacked.

The bitter coil has been designed and developed with inductance of 28 μH. It has been tested for currents upto 145 kA for an arc free operation [13].

5. POWER TRANSFER LINES

Two types of power transfer lines are used in the PFN -bus bar/sandwich lines and coaxial cable. It was decided to use busbarlines for connecting capacitors, capacitors to the switches and pulse forming inductor. Coaxial Lines are used as transmission line between module and railgun. These components are designed for minimum inductance, resistance and electro magnetic forces with out causing proximity effects and dielectric breakdown.

5.1 Busbar Lines :

3 mm thick wide copper plates are used as Capacitor Interconnects. Positive and negative terminals are separately interconnected and 3mm thick Glass Reinforced Plastic (GRP) G10 sheets are used as insulator between the plates. In order to ensure minimum forces between the power transfer components, sandwich lines were used for connecting the capacitors to switches and Inductor. In sandwich lines the positive bus bar is sandwiched between the two parallel negative

bus bars. However due to the complexities associated with inter connection with ignitrons and proximity issues, sandwich lines were replaced by two line bus bars.

5.2 Coaxial cable :

This was used in connecting the Pulse forming Inductor to the Railgun. The cable need to be rated for 180 kA with working voltage of 15 kV RMS, as evaluated by simulation studies. It should have sufficient mechanical strength and heat dissipation capability.

As off the shelf cables failed to meet the requirement, a cable was designed and fabricated as per design given by KA Jamison et al [14]. The cable consists of a 12 mm center conductor made of silver coated copper strands . The core position of the strands were counter wound from the outer strand for improved flexibility. The inner dielectric is PTFE tape wrapped and sintered Teflon with a wall thickness of 5.6mm. The outer conductor comprised of double braid of silver plated copper. Each layer was formed from 48 stranded wires which is made from nineteen 30 gauge strands.

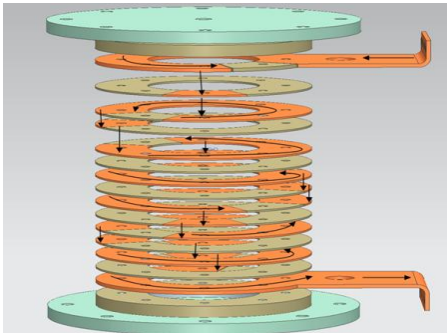


Fig 4. Bitter coil configuration with the current flow directions in the components

The outer dielectric was made of PTFE tape wrapped and sintered Teflon, with wall thickness of 1.6mm. A reinforcing mesh of Kevlar fiber woven over the outer dielectric provided additional strength. Above this is an outer jacket made from flame retardant polyether based polyurethane.

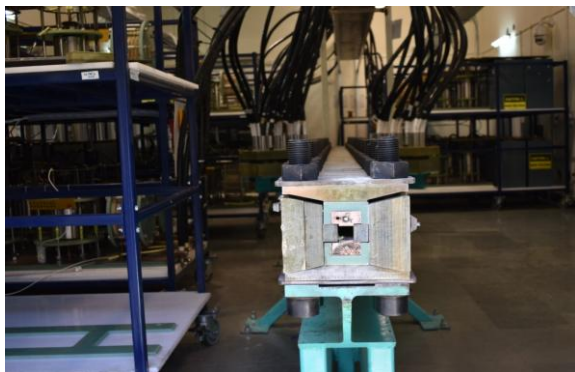


Fig. 5: 30 mm square bore, 4 m long Railgun (ARDE)

6. EM LAUNCHER

The rails carry current and are responsible for the generation of working magnetic field which propels the projectile using well known Faraday's law. In order to keep the rails intact and to avoid bulging of rails, containment structure is required. Unlike a conventional gun, the EM load is not as axi-symmetric as a chemical gun but concentrates more on the rails and part of the containment or support structure. The load is complex such that electromagnetic force varies in time and space along the railgun during launch. The load is also highly transient in nature due to the hypervelocity launch. ARDE railgun launcher is a bolted structure providing very high stiffness to the bore by means of GRP insulation housing with eighty pre-stressed M48 bolts, as shown in Fig 5.

The rail-armature interaction is a unique multi-physics problem and one of the major limitation in the realization of multiple shot railgun. A lot of studies are being carried out to limit ablation and gouging on the rail surface. Besides, thermal management of the rails is also important for multiple shot operation. ARDE has developed simple Railguns of three different configuration, viz

- a. 12 mm square bore, 2 m long
- b. 30 mm square bore, 2 m long and
- c. 30 mm square bore 4m long.

The Railguns a, and b were test fired with 1.6 MJ capacitor bank and the 4 m railgun is test fired with 4 MJ capacitor bank. The ARDE railgun being used currently is shown in Fig 5. This gun enabled to realize the muzzle velocity beyond 2000 m/s for 120 g projectile.

Also ARDE is on the verge of developing an Augmented Railgun, where an improved efficiency, lower operational currents and reduced rail degradation are expected.

7. 4 MJ PULSED POWER SYSTEM

The pulsed power system at ARDE comprises of several units of individual capacitors grouped together called modules [15]. The 4 MJ Capacitor Bank consists of ten 400 kJ modules. Each module comprises of capacitors connected in parallel, a main switching element, a crow barring switch and a pulse shaping element. The modules are designed such that each has a separate triggering unit and are independent of one another (Fig. 6). This helps in providing flexibility in shaping the current pulse. The switching of the modules can be either simultaneous or sequential depending on the requirement of the output load pulse.

The performance was theoretically analysed and optimized with numerous circuit simulations using Microcap and Simulink software. The peak current obtained from the above simulations was well with in the design limit of 1.5 MA. The current reaches its peak value at about 1.6 ms. The time taken for projectile to exit a 4 m railgun is around 3.6 ms. Simulation studies have been validated with experimental results. The simulation results for 1.6 MJ capacitor bank and 4 MJ capacitor bank show excellent agreement with experimental data [16].

8. INSTRUMENTATION AND CONTROL SYSTEM

To understand the performance of the Electromagnetic rail launcher and pulse power subsystems, a data acquisition system has been designed and developed. This include the development of the instrumentation (Sensors) to measure the signals involved in the subsystems of the Railgun and development of easy to use software to acquire and analyze the data from sensors. The system developed is performing reliably to acquire and analyze more than 150 channels.

To trigger and control the subsystems involved in the railgun in, a control system has to be developed which should incorporate high voltage isolation, and free from EMI/EMC interference to provide reliable and robust control system. The development of the control system consists of two parts viz. the triggering and firing system for the Railgun and easy to use software to remotely control and monitor the subsystems involved in the Railgun.

All these systems have been designed and developed such that there is an optical and galvanic isolation between the subsystems and control systems so that even in the event of any failure, safety has been taken care of. Care has taken to leave sufficient scope for addition of higher number of control channels to cater for future requirements.

9. CHALLENGES IN REALISING THE SYSTEM

The need of the sub systems and the components to with stand huge peak currents and mechanical forces created design, manufacturing and integration issues, which were mitigated with careful analysis, step-by-step testing and optimization. Initial module size was considered to be 200 kJ and was latter enhanced to 400 kJ as the former one require more number of components which made the system bulky.



Fig 6: 400 kJ Capacitor modules at ARDE

Each module need to handle currents beyond 150 kA peak at voltage of 11 kV. It was really challenging to operate the switches to handle these currents. Frequent conditioning of Ignitron switches and functional testing was essential to ensure proper operation. Also keeping the integrity of the pulse shaping inductor was difficult. The bitter coil used was of conducting bitter plates connected together by interleaving segmented plates. They are press-fitted using external clamping by using eight bolt-nut arrangements. Due to the heavy compressive force, the plates undergo oscillation during every pulse and the bolting tends to loosen up after multiple firing. This leads to the loss of contact and internal arcing. Added to that huge eddy current was developed on the external metallic clamping plate. This also tends to damage the bolting. Hence frequent bolt tightening or re-assembly of bitter coil was necessary.

The bus-bar structure spread over a vast area and were separated by insulator. Huge separation between positive and negative bus bar induce considerable circuit inductance. Hence it was preferred to keep them closer. Keeping the insulation over the vast surface area, especially at high voltages was very difficult, as micro holes in some insulators and hygroscopic nature of some insulators adversely affected the electrical insulation requirement.

Mega-Ampere current and the forces of tens of Mega Newton on the rail structure made the design and development of Launcher extremely challenging. Proper materials like Oxygen free Copper and Cr.Cu conductors are selected as the rail material and GRP G10 as the insulators. Parametric structural analysis was carried out to evaluate the size of the structural elements to confine the huge electro-mechanical forces.

Development of a proper armature was another challenge in the absence of well defined analytical or computational methodology. Present gun used C-shaped armature developed based on various mechanical, electrical and structural consideration by stringent parametric analysis.

10. EXPERIMENTAL RESULTS

More than 500 static firings and more than 30 railgun firings were carried out with all the three configuration of Railguns. Capacitor banks of 1.6 MJ and 4 MJ had been setup at ARDE which acted as the power sources for the firing.

Static testing is carried out at different voltage to validate the system assembly & simulation results. The rails are shorted with coppers bars at breech end of the railgun to carry out static testing. The current profile is in good agreement with the theoretically modeled pulse.

Projectile firing was also carried out with projectile masses varying from few gram up to 120 g at different charging voltages. The current and velocity profiles were compared with the simulated values after each firing.

Test firing of 120 g projectile with 1.6 MJ capacitor bank at 8kV generated current pulse peaking above 570 kA, which imparted a muzzle velocity of 750m/s. The most significant firing was of 120 g projectile with 4 MJ Capacitor Bank at 7.8 kV under simultaneous triggering. The firing resulted in muzzle velocity of 2024 m/s, very

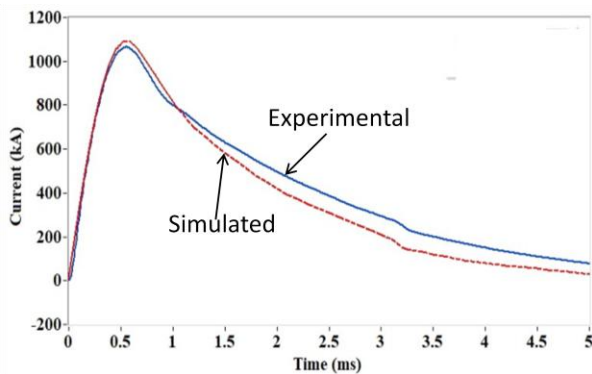


Fig 7: Current Profile at hyper velocity firing

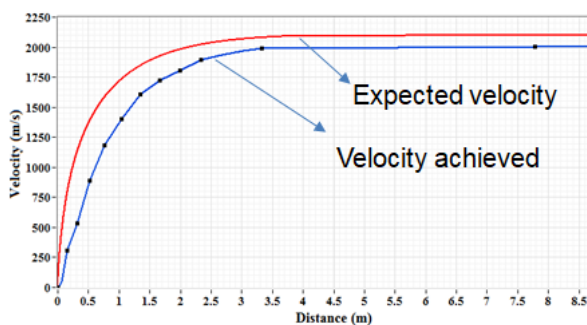


Fig 8: Velocity Profile of Hyper velocity firing

close to the velocity estimated theoretically. Peak current achieved in the test firing was 1095kA, as against simulated value of 1110kA (Fig 7). The velocity profile is presented in the Fig 8.

11. CONCLUSION

As the chemical propellant based conventional armament technology has reached a saturation value as far as velocity is concerned, newer technologies like EM gun is being pursued with great vigour. The railgun, though an electromagnetic accelerator, is much complex than an intricate electrical system. Even if the size of the energy storage equipment and the pulse power system is not an issue, mechanical, thermal and material constraints will continue posing challenges for a practical military grade railgun realization. Development of ablation and gouging resistant rails is necessary. The tribology of the rail-armature interaction needs to be studied to engineer effective rail armature interface.

In line with worldwide trends, ARDE has also started its railgun program with a goal to fire projectile masses above 0.5kg to 2000 m/s. Extensive simulation study has been carried out for the design of the pulsed power and railgun. The experimental results are found in agreement with the simulation results. A peak velocity of 2024 m/s was achieved for 120 g projectile.

12. REFERENCES

- [1] Marshall RA, "Railgunnery: Where have we been? Where are we going?" *IEEE Trans. Magnetics*, vol 37, no 1, pp 440-444, Jan 2001.
- [2] Zizhou Su et al., "Design and simulation of a large muzzle kinetic energy railgun," *IEEE Trans. Plasma Science*, vol. 41, no.5, pp 1416-1420, May 2013.
- [3] John M. Juston and David P. Bauer, "A high performance railgun launcher design," *IEEE Trans. Magnetics*, vol.33, no.1, pp566-570, Jan1997.
- [4] Ian R. McNab, "Pulsed Power Options for Large EM Launchers" *IEEE Transactions On Plasma Science*, Vol. 43, No. 5, May 2015
- [5] Hilmar Peter, Francis Jamet, and Volker Wegner, "Technical Aspects of Railguns," *IEEE Transactions on Magnetics*, vol. 31, no. 1, January 1995
- [6] Harry D. Fair, "Progress in Electromagnetic Launch Science and Technology", *IEEE Trans. Magn.* vol. 43, p. 93 January 2007.
- [7] Gully J.H., "Power supply technology for electric guns," *IEEE Trans. Magnetics*, vol.27, no.1, pp 329-333, Jan1991.
- [8] McNab I.R., "Pulsed power for electric guns," *IEEE Trans. Magnetics*, vol. 33, no. 1, pp 453-460, Jan. 1997.
- [9] G. F. Grater, F. W. MacDougall, M. Hudis, and X. H. Yang, "Characterization of high energy density capacitors under projected U. S. Navy ETC gun operating conditions," in *Proc. IEEE Pulsed Power Conf.*, Albuquerque, NM, June 1995, pp. 509-5
- [10] H.deB.Knight, L.Herbertand and R.C.Maddison, "The ignitron as a switch in high-voltage heavy-current pulsing circuits," *The Institution of Electrical Engineers*, PaperNo.2947, Apr.1959
- [11] M. Del Guercio, "A 4.5-MJ pulsed power supply for railgun experiments," in *IEEE Transactions on Magnetics*, vol. 39, no. 1, pp. 280-284, Jan. 2003.
- [12] Oleg Zaitov and Vladimir A. Kolchuzhin, "Bitter coil design methodology for electromagnetic pulse metal processing techniques"; *Journal of Manufacturing Processes*, 16 (4), 551-562, 2014
- [13] Pradeep Kumar et al – Design and Development of High Current Pulse Shaping Inductor based on Bitter Magnet Configuration for Electro Magnetic Launcher; Unpublished
- [14] KA Jamison, RE Stearns, RB Klug and RD Ford, "High energy cable development for pulsed power application", *IEEE Trans. Magnetics*, vol. 27, no.1, 1991, pp 374-379
- [15] D. Bhasavanich, D. F. Strachan and R. Ford, "4.5 MJ Modular Pulse Power Supply For ET Gun Applications," *Pulsed Power Conference*, 1993. *Digest of Technical Papers*, Ninth IEEE International, Albuquerque, NM, USA, 1993, pp. 772-777
- [16] Pradeep Kumar et al, "Design and development of 4mj capacitor bank based pulsed power system for electromagnetic launcher", *IEEE Trans, Plasma Science*, 47(3), pp1681-1688, Mar 2019.
- [17] F. Deadrick, R. Hawke and J. Scudder, "MAGRAC--A railgun simulation program," in *IEEE Transactions on Magnetics*, vol. 18, no. 1, pp. 94-104, Jan 1982.
- [18] J. S. Bernardes, M. F. Stumborg and T. E. Jean, "Analysis of a capacitor-based pulsed-power system for driving long-range electromagnetic guns," in *IEEE Transactions on Magnetics*, vol. 39, no. 1, pp. 486-490, Jan. 2003

Improved Digital Image steganography Using Five- Directional PVD

Ruchi¹, Umesh Ghanekar²

¹Department of Electronics and Communication Engineering National Institute of Technology, Kurukshetra, Haryana²Department of Electronics and Communication Engineering National Institute of Technology, Kurukshetra, Haryana

Abstract—The combination of Pixel value difference (PVD) and Least Substitution Bit (LSB) is one of the efficient technique for digital image steganography. This paper improvises the existing eight directional PVD and LSB method by using an appropriate neighbourhood. Normally, in combination of PVD and LSB technique, 3x3 block size is considered for embedding of data. Through experimental simulation it is shown that performance of the existing techniques can be improved by considering 3x2 block size in terms of PSNR, Capacity and Quality index.

Index Terms—Steganography, PVD, LSB technique, PSNR, Hiding Capacity

1. INTRODUCTION

Least significant bit (LSB) is an old method for doing steganography in which the last significant bit of the pixel of cover image are replaced by bits of secret image bits. The replacement upto 3 bits in the cover image is undetectable by the human eye. LSB provides the high embedding capacity than any other method. Wu and Tsai [1] researched that edge region of any image tolerates larger changes of pixel values than those in smooth areas. Thus the more amount of data can be concealed in edge region than the smooth region. On this principle another technique ‘pixel value differencing’(PVD) has introduced for doing steganography. In this technique a pair of pixel is taken and the difference between these two pixel are calculated, using the difference value between these pixel a new pixel values are assigned for both these pixel values. The LSB substitution offers a high embedding capacity and PVD offers a higher imperceptibility and combining both these method of steganography[9] we can get both a higher hiding capacity and better imperceptibility. Firstly Khodaei used this hybrid approach of combining LSB substitution and PVD in 1×3 pixel block and then 2×2 size pixel block to exploit the edges in more than one direction to get better performance [2]. In 2×2 pixel block[8] the three directions of edges are considered. Chang and Tseng proposed the 2, 3, and four neighbouring pixels to perform PVD steganography [3]. The technique which was traditionally used for PVD suffers from some problem of step effects in pixel difference histograms of stego images. This problem can be avoided by using two things, (i) exploiting the edges in multiple directions[7] and (ii) using adaptive range table. There are papers which have been proposed based on considering these two things to avoid step effects. Luo et al. given the paper[4] on adaptive PVD steganography with three pixel block which does not suffer from step effects. The problem of using adaptive steganography is that it poses lower hiding capacity. Swain has proposed the hybrid scheme of PVD and LSB substitution for steganography on 3×3 pixel block[5]. The scheme on 3×3 pixel block exploited the eight-directional PVD by finding difference in eight direction. In this technique LSB substitution is done on single pixel value so RS analysis cannot detect it and using edges in multiple direction the PDH analysis cannot detect it. This paper proposes the same algorithm proposed by the Swain on the pixel block of size 3×2 which exploit the edges in five-direction and gives a better performance in terms of PSNR, Quality index and capacity[6].

2. Proposed Technique

The first part of proposed technique algorithm is embedding and the second part is extraction. The embedding is done using range table.1 on a pixel block of size 3×2 which exploit the edges in five direction. The blocks are formed in non overlapping manner. Let us denote the 3×2 block as shown in fig.1. The centre pixel is denoted as O and the surrounding pixel as $b_1 b_2 b_3 b_4 b_5$. Next ‘t’ bit LSB substitution is done on reference pixel O and the changed stego value of reference pixel is O’. The final value of reference pixel value O’ is decided by some calculation.

The last t bit of O is taken whose decimal (integer) value is $B1$ and the last t bit of stego reference pixel O' whose decimal (integer) value is $B2$. Now find the deviation, $dev=B1-B2$. Finally value of O' is given by this as given:

$$O' = \begin{cases} O' + 2^t, & \text{if } dev > 2^{t-1} \text{ and } 0 \leq O' + 2^t \leq 255 \\ O' - 2^t, & \text{if } dev < 2^{t-1} \text{ and } 0 \leq O' - 2^t \leq 255 \\ O', & \text{otherwise} \end{cases} \quad (1)$$

Thus the final modified O' is taken and 5 difference value is calculated for $i=1$ to 5 as given in equation (2).

$$d(i) = |O' - b_i| \quad (2)$$

the difference value $d(i)$ belongs to one of the six ranges. Every range has its own lower bound as l_1 and hiding capacity as t_1 for the range d_1 . Thus l_2, l_3, l_4 and l_5 are the lower bounds and t_2, t_3, t_4 and t_5 are its hiding capacities of the difference values d_2, d_3, d_4 and d_5 respectively.

Now take t_1, t_2, t_3, t_4 and t_5 bits of secret image and convert it into their decimal values as s_1, s_2, s_3, s_4 and s_5 respectively.

Now for $i=1$ to 5 calculate new values using the lower bound of every difference value d_i and add it with the respective decimal value of t bits given as:

$$d'(i) = l_i + s_i \quad (3)$$

Now for $i=1$ to 5 new values of P' and P'' is calculated as given :

$$p' = O' - d'_i \quad (4)$$

$$p'' = O' + d'_i \quad (5)$$

After calculation of p' and p'' , the value of b'_i is taken by the given formula

$$b'_i = \begin{cases} p'_i & \text{if } |b_i - p'_i| < |b_i - p''_i| \text{ and } 0 \leq p'_i \leq 255 \\ p''_i & \text{otherwise} \end{cases} \quad (6)$$

Finally all the stego pixel $O', b'_1, b'_2, b'_3, b'_4, b'_5$ after hiding t, t_1, t_2, t_3, t_4 and t_5 bits of data in $O, b_1, b_2, b_3, b_4, b_5$ respectively is obtained. The example of embedding algorithm can be seen in fig.1.

2.1 Example of embedding and extraction algorithm

The algorithm for extraction are applied similarly on 3×2 pixel block in an non overlapping manner. The block of required size is taken from the stego image and then at starting directly t bit is extracted from the stego block

reference pixel(O'). Then the five surrounding pixel value is taken and each pixel value is subtracted from reference pixel as given in below equation (7) :

<table border="1" style="margin: 0 auto; border-collapse: collapse;"> <tr><td style="padding: 2px 10px;">137</td><td style="padding: 2px 10px;">57</td></tr> <tr><td style="padding: 2px 10px;">130</td><td style="padding: 2px 10px;">88</td></tr> <tr><td style="padding: 2px 10px;">88</td><td style="padding: 2px 10px;">112</td></tr> </table> <p style="text-align: center;">Original block</p> <p style="text-align: center;">Reference pixel=88</p>	137	57	130	88	88	112	<p>Secret bits array: 010111110001111100010</p> <p style="text-align: center;">$88 = (1011000)_2 = 0$</p> <p>After embedding t bit '010' from secret bits array $(1011010)_2 = 90 =$ $O' = 90$</p>	<table border="1" style="margin: 0 auto; border-collapse: collapse;"> <tr><td style="padding: 2px 10px;">137</td><td style="padding: 2px 10px;">57</td></tr> <tr><td style="padding: 2px 10px;">130</td><td style="padding: 2px 10px;">90</td></tr> <tr><td style="padding: 2px 10px;">88</td><td style="padding: 2px 10px;">112</td></tr> </table> <p style="text-align: center;">Original block with changed reference pixel</p>	137	57	130	90	88	112									
137	57																						
130	88																						
88	112																						
137	57																						
130	90																						
88	112																						
<div style="display: flex; justify-content: space-between;"> <div style="width: 30%;"> <p>$d_1 = 90 - 137 = 47$</p> <p>$d_2 = 90 - 57 = 33$</p> <p>$d_3 = 90 - 130 = 40$</p> <p>$d_4 = 90 - 88 = 2$</p> <p>$d_5 = 90 - 112 = 22$</p> </div> <table border="1" style="width: 30%; border-collapse: collapse; text-align: center;"> <tr><td style="padding: 2px 10px;">$l_1 = 32$</td><td style="padding: 2px 10px;">$s_1 = 7$</td></tr> <tr><td style="padding: 2px 10px;">$l_1 = 32$</td><td style="padding: 2px 10px;">$s_2 = 6$</td></tr> <tr><td style="padding: 2px 10px;">$l_1 = 32$</td><td style="padding: 2px 10px;">$s_3 = 1$</td></tr> <tr><td style="padding: 2px 10px;">$l_1 = 0$</td><td style="padding: 2px 10px;">$s_4 = 7$</td></tr> <tr><td style="padding: 2px 10px;">$l_1 = 16$</td><td style="padding: 2px 10px;">$s_5 = 4$</td></tr> </table> <table border="1" style="width: 30%; border-collapse: collapse; text-align: center;"> <tr><td style="padding: 2px 10px;">$d'_1 = 32 + 7 = 39$</td></tr> <tr><td style="padding: 2px 10px;">$d'_2 = 32 + 6 = 38$</td></tr> <tr><td style="padding: 2px 10px;">$d'_3 = 32 + 1 = 33$</td></tr> <tr><td style="padding: 2px 10px;">$d'_4 = 0 + 7 = 7$</td></tr> <tr><td style="padding: 2px 10px;">$d'_5 = 16 + 4 = 20$</td></tr> </table> </div>			$l_1 = 32$	$s_1 = 7$	$l_1 = 32$	$s_2 = 6$	$l_1 = 32$	$s_3 = 1$	$l_1 = 0$	$s_4 = 7$	$l_1 = 16$	$s_5 = 4$	$d'_1 = 32 + 7 = 39$	$d'_2 = 32 + 6 = 38$	$d'_3 = 32 + 1 = 33$	$d'_4 = 0 + 7 = 7$	$d'_5 = 16 + 4 = 20$						
$l_1 = 32$	$s_1 = 7$																						
$l_1 = 32$	$s_2 = 6$																						
$l_1 = 32$	$s_3 = 1$																						
$l_1 = 0$	$s_4 = 7$																						
$l_1 = 16$	$s_5 = 4$																						
$d'_1 = 32 + 7 = 39$																							
$d'_2 = 32 + 6 = 38$																							
$d'_3 = 32 + 1 = 33$																							
$d'_4 = 0 + 7 = 7$																							
$d'_5 = 16 + 4 = 20$																							
<table style="width: 100%; border-collapse: collapse;"> <tr> <td style="width: 33%; padding: 2px 10px;">$p'_1 = 90 - 39 = 51$</td> <td style="width: 33%; padding: 2px 10px;">$p''_1 = 90 + 39 = 129$</td> <td style="width: 33%; padding: 2px 10px;">$b'_1 = 129$</td> </tr> <tr> <td style="padding: 2px 10px;">$p'_2 = 90 - 38 = 52$</td> <td style="padding: 2px 10px;">$p''_2 = 90 + 38 = 128$</td> <td style="padding: 2px 10px;">$b'_2 = 52$</td> </tr> <tr> <td style="padding: 2px 10px;">$p'_3 = 90 - 33 = 57$</td> <td style="padding: 2px 10px;">$p''_3 = 90 + 33 = 123$</td> <td style="padding: 2px 10px;">$b'_3 = 123$</td> </tr> <tr> <td style="padding: 2px 10px;">$p'_4 = 90 - 7 = 83$</td> <td style="padding: 2px 10px;">$p''_4 = 90 + 7 = 97$</td> <td style="padding: 2px 10px;">$b'_4 = 83$</td> </tr> <tr> <td style="padding: 2px 10px;">$p'_5 = 90 - 20 = 70$</td> <td style="padding: 2px 10px;">$p''_5 = 90 + 20 = 110$</td> <td style="padding: 2px 10px;">$b'_5 = 110$</td> </tr> </table> <table border="1" style="margin: 10px auto; border-collapse: collapse; text-align: center;"> <tr><td style="padding: 2px 10px;">129</td><td style="padding: 2px 10px;">52</td></tr> <tr><td style="padding: 2px 10px;">123</td><td style="padding: 2px 10px;">90</td></tr> <tr><td style="padding: 2px 10px;">83</td><td style="padding: 2px 10px;">110</td></tr> </table> <p style="text-align: center;">Stegoblock</p>			$p'_1 = 90 - 39 = 51$	$p''_1 = 90 + 39 = 129$	$b'_1 = 129$	$p'_2 = 90 - 38 = 52$	$p''_2 = 90 + 38 = 128$	$b'_2 = 52$	$p'_3 = 90 - 33 = 57$	$p''_3 = 90 + 33 = 123$	$b'_3 = 123$	$p'_4 = 90 - 7 = 83$	$p''_4 = 90 + 7 = 97$	$b'_4 = 83$	$p'_5 = 90 - 20 = 70$	$p''_5 = 90 + 20 = 110$	$b'_5 = 110$	129	52	123	90	83	110
$p'_1 = 90 - 39 = 51$	$p''_1 = 90 + 39 = 129$	$b'_1 = 129$																					
$p'_2 = 90 - 38 = 52$	$p''_2 = 90 + 38 = 128$	$b'_2 = 52$																					
$p'_3 = 90 - 33 = 57$	$p''_3 = 90 + 33 = 123$	$b'_3 = 123$																					
$p'_4 = 90 - 7 = 83$	$p''_4 = 90 + 7 = 97$	$b'_4 = 83$																					
$p'_5 = 90 - 20 = 70$	$p''_5 = 90 + 20 = 110$	$b'_5 = 110$																					
129	52																						
123	90																						
83	110																						

Figure:1: Embedding algorithm example

$$d'_i = |O' - b'_i| \quad (7)$$

Then check the range of each d'_i from the range table.1. After deciding the range, select its lower bound value. The range decides the number of 't' bits to be extracted. After this the five difference value is calculated as given in eq(8)

$$s_i = |d'_i - l_i| \quad (8)$$

All the obtained s_i value is taken and converted to binary number of t bits as decided by each range. At last all the s_1, s_2, s_3, s_4 and s_5 are converted into their binary bits respectively.

3. 8 directional PVD and LSB substitution of pixel block 3 × 3 block

The cover image is divided into non overlapping block of size 3 × 3. Let us denote the 3 × 3 block as shown in fig.3. where the total elements in the block is the reference pixel ‘O’ and the 8 surrounding pixel as b₁, b₂, b₃, b₄, b₅, b₆, b₇ and b₈. The algorithm of embedding is done on using range table.1. This block exploit the edges in eight directions.

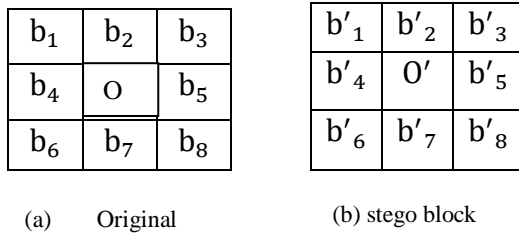


Fig.3 Original and stego block of size 3 × 3

Next ‘t’ bit LSB substitution is done on reference pixel O and the the changed stego value of reference pixel is O’. The final value of reference pixel value O’ is decided by some calculation. The last t bit of O is taken whose decimal (integer) value is B1 and the last t bit of stego reference pixel O’ whose decimal (integer) value is B2. Now find the deviation, dev=B1-B2. Finally value of O’ is given by this as given in eq.(9).

$$O' = \begin{cases} O' + 2^t, & \text{if } dev > 2^{t-1} \text{ and } 0 \leq O' + 2^t \leq 255 \\ O' - 2^t, & \text{if } dev < 2^{t-1} \text{ and } 0 \leq O' - 2^t \leq 255 \\ O', & \text{otherwise} \end{cases} \quad (9)$$

Thus the final modified O’ is taken and 8 difference value is calculated for i=1 to 8 as

$$d(i) = |O' - b_i| \quad (10)$$

the difference value d(i) belongs to one of the six ranges. Every range has its own lower bound as l₁ and hiding capacity as t₁ for the range d₁. Thus l₂, l₃, l₄, l₅, l₆, l₇ and l₈ are the lower bounds for the difference values d₂, d₃, d₄, d₅, d₆, d₇ and d₈. Take t bits of secret image bits and convert it into their decimal values as s₁, s₂, s₃, s₄, s₅, s₆, s₇ and s₈ respectively.

Now for i=1 to 8 calculate new values using the lower bound of every difference value d_i and add it with the respective decimal value of t bits given as:

$$d'(i) = l_i + s_i \quad (11)$$

Now for i=1 to 8 new values of P’ and P’’ is calculated as given :

$$p' = O' - d'_i \quad (12)$$

$$p'' = O' + d'_i \quad (13)$$

After calculation of p’ and p’’, one value of b’_i is taken by this formula

$$b'_i = \begin{cases} p_i' & \text{if } |b_i - p_i'| < |b_i - p_i''| \text{ and } 0 \leq p_i'' \leq 255 \\ p_i'', & \text{otherwise} \end{cases} \quad (14)$$

In extraction part a 3×3 block size is taken from the stego image and 8 difference values of $d_i' = |O' - b_i'|$ are calculated and then 8 values of $s_i = |d_i' - l_i|$. At last all the $s_1, s_2, s_3, s_4, s_6, s_7$ and s_8 are converted into their binary bits respectively which are the desired secret bits of secret image.

4. Experimental Results

All the standard RGB color images are taken from SIPI database which are used in image processing for testing. The embedding and extraction algorithm are performed on MATLAB. All the images are of size 512×512 and the resultant stego images for 3×2 and 3×3 block size are shown in fig.4. Table.3 and table.4 are used to show the performance of PVD and LSB substitution method by using 3×3 and 3×2 block size, respectively.

The evaluation parameters are PSNR, capacity and Quality Index which are shown by eq.no (16), (17) and (18) respectively.

$$MSE = \frac{1}{m \times n} \sum_{i=1}^m \sum_{j=1}^n (p_{ij} - q_{ij})^2 \quad (15)$$

$$PSNR = 10 \times \log_{10} \frac{255 \times 255}{\text{image size in bytes}} \quad (16)$$

Hiding capacity is the total number of bits that an image can conceal. The bits per byte (BPB) shows the average capacity that an image can conceal. It can be defined as given in equation (17).

$$BPB = \frac{\text{Hiding Capacity}}{\text{Image size in Bytes}} \quad (17)$$

Quality index parameter is the measure of structural similarity between the original and stego image. It is denoted by 'Q' and its maximum value can be 1. The formula for calculating 'Q' can be given as in eq.(18)

$$Q = \frac{4\sigma_{us}\bar{u}\bar{s}}{[(\sigma_u^2 + \sigma_s^2)(\bar{u}^2 + \bar{s}^2)]} \quad (18)$$

Where \bar{u} stands for the mean pixel value of original image and \bar{s} is the mean pixel value of stego image. σ_u^2 is the standard deviation of pixel values of original image and the σ_s^2 is the standard deviation of stego image and σ_{us} is the covariance between original and stego image. The following (19), (20), (21), (22) and (23) equations respectively shows the above defined parameters:

$$\bar{u} = \frac{1}{m \times n} \sum_{i=1}^m \sum_{j=1}^n u_{ij} \quad (19)$$

$$\bar{s} = \frac{1}{m \times n} \sum_{i=1}^m \sum_{j=1}^n s_{ij} \quad (20)$$

$$\sigma_u^2 = \frac{1}{m \times n - 1} \sum_{i=1}^m \sum_{j=1}^n (u_{ij} - \bar{u})^2 \quad (21)$$

$$\sigma_s^2 = \frac{1}{m \times n - 1} \sum_{i=1}^m \sum_{j=1}^n (s_{ij} - \bar{s})^2 \quad (22)$$

$$\sigma_{us} = \frac{1}{m \times n - 1} \sum_{i=1}^m \sum_{j=1}^n (u_{ij} - \bar{u})(s_{ij} - \bar{s}) \quad (23)$$

TABLE.4 Results of Swain’s algorithm on 3 × 2 pixel block

Image size 512× 512 × 3	PSNR	Q	Capacity	BPB
Airplane	27.3200	0.9690	2356243	2.9961
Pepper	28.2325	0.9888	2355705	2.9954
Fruits	28.4975	0.9879	2355615	2.9953
Lena	29.7560	0.9903	2352834	2.9944
Average	26.9515	0.9850	2354941	2.9953

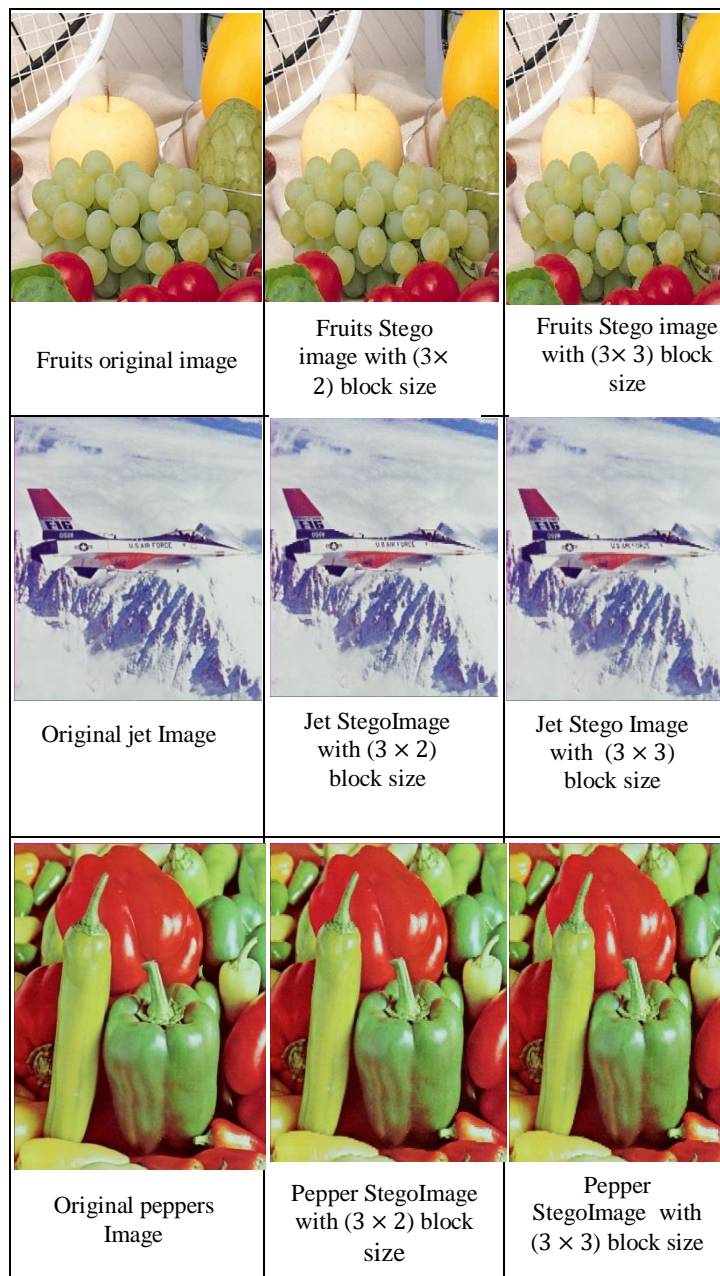
TABLE.3. Results of Swain’s algorithm on 3 × 3 pixelblock

Image size 512× 512 × 3	PSNR	Q	Capacity	BPB
Jet	25.2361	0.950	2347672	2.9852
Pepper	26.1480	0.982	2317085	2.9463
fruits	26.1651	0.979	2347045	2.9844
Lenna	26.4722	0.979	2344311	2.9809
Average	26.00535	0.979	2339028	2.9742

As shown in Table.3 and 4, it is inferred that the results for 3×2 block size are better than 3×3 block size in terms of psnr, quality index and hiding capacity.

Fig.1. Original and stego images of (3 × 2) and (3 × 3) block size.





5. CONCLUSION

In this paper, a technique based on combination of LSB substitution and PVD has been presented. Instead of 3×3 , 3×2 , block size is used to utilize the five directional edges, which helps in improving the performance of the technique in terms of psnr, hiding capacity and quality index. The LSB substitution in steganography provides a high embedding capacity and PVD technique provides a higher imperceptibility. Thus the hybrid technique of LSB and PVD provides steganography of higher embedding with higher imperceptibility. Efficacy of the proposed algorithm is shown on different standard cover and stego images.

6. REFERENCES

- 1.D.-C.Wu andW.-H. Tsai, "A steganographicmethod for images by pixel-value differencing," Pattern Recognition Letters, vol. 24, no. 9-10, pp. 1613–1626, 2003.G. Swain, "A steganographic method combining LSB substitution and PVD in a block," ProcediaComputer Science, vol. 85, pp. 39–44, 2016.

2. C.-C. Chang and H.-W. Tseng, "A steganographic method for digital images using side match," *Pattern Recognition Letters*, vol. 25, no. 12, pp. 1431–1437, 2004.
3. W. Luo, F. Huang, and J. Huang, "A more secure steganography based on adaptive pixel-value differencing scheme," *Multimedia Tools and Applications*, vol. 52, no. 2-3, pp. 407–430, 2011.
4. Gandharba Swain, "Digital Image Steganography Using Eight-Directional PVD against RS Analysis and PDH Analysis", *Hindawi Advances in Multimedia Volume 2018*, Article ID 4847098, 13 pages <https://doi.org/10.1155/2018/4847098>.
5. Mohammed A. Fadhil Al-Husainy, "Image Steganography Method Preserves the Histogram Shape of Image", *European Journal of Scientific Research ISSN*, Vol. 130, no.1, pp.101 – 106, March, 2015.
6. C.-H. Yang, C.-Y. Weng, H.-K. Tso, and S.-J. Wang, "A data hiding scheme using the varieties of pixel-value differencing in multimedia images," *The Journal of Systems and Software*, vol. 84, no. 4, pp. 669–678, 2011.
7. K.C. Chang, C. P. Chang, P. S. Huang, and T. M Tu, "A novel image steganographic method using tri-way pixel-value differencing," *Journal of Multimedia*, vol. 3, no. 2, pp. 37–44, 2008.
8. C.-H. Yang, C.-Y. Weng, S.-J. Wang, and H.-M. Sun, "Varied PVD + LSB evading detection programs to spatial domain in data embedding systems," *The Journal of Systems and Software*, vol. 83, no. 10, pp. 1635–1643, 2010. T. D. Nguyen, S. Arch-Int, and N. Arch-Int, "An adaptive multi bit-plane image steganography using block data hiding," *Multimedia Tools and Applications*, vol. 75, no. 14, pp. 8319–8345, 2016.

Performance Evaluation of Autonomous Data Density Clustering

Aditya Kumar¹, Manmohan Singh Yadav², Dr. Shafeeq Ahmad³
¹M.Tech CSE AIET Lucknow, India, ²Assistant Professor AIET Lucknow, India, ³Director AIET Lucknow, India
akr99akr@gmail.com¹ man1_mohan_100@refiffmail.com² ahmad_shafeeq@rediffmail.com³

Abstract—Clustering can be a type of un-supervised machine learning technique that groups objects inside a dataset based on their resemblance. Clustering techniques which are based on density focuses on collecting objects through the use of objects density data in the clustering method. Different types of clustering techniques based on density were researched in this paper. A fresh method based on clustering data density based on an independent algorithm of data density has been discussed that can be applied to techniques such as pattern recognition, matching and classification. A comparison has been provided between data density and k-means clustering. The results of the experiment show that this method can be used to fix problems data sets with nested objects of varying densities.

Keywords—Autonomous clustering, Data density, unsupervised machine learning, Data Mining.

1. INTRODUCTION

In information analysis and machine learning environments, including data mining and image segmentation, clustering is helpful. Clustering has a number of computer science applications as well as many distinct areas outside computing. Clustering can be used in market studies to form groups of clients with comparable requirements. In bioinformatics, to study hereditary diseases, it is used to define gene groups with comparable patterns of expression. It can be used in chemistry to classify chemical compounds. In the areas of astronomy, psychiatry, archeology and climate science, there are numerous other applications. There are also several ways or categories of these clustering algorithms.

Clustering algorithms can be approximately categorized into seven groups, especially “hierarchical algorithms”, “density-based algorithms”, “partitional algorithms”, “graph-based algorithms”, “combinational algorithms”, “grid-based algorithms”, and “model-based algorithms”. Clustering methods based on density job on the premise that clusters exist in fields with greater data space density. Thus, a local mode or peak density function can characterize each cluster. Two primary benefits of this algorithm are the capacity to find clusters of distinct shapes and sizes even in outer information set and the number of clusters does not need to be specified by customers. The proposed method, algorithms based on density, distinguish dense regions which are measurements separated by regions of low density. One of the most popular clustering methods based on density is the density-based spatial clustering of noise-based applications (DBSCAN), which works on grouping data samples that are very close together in the data space, and marking data samples that are alone in low density as outliers.

DBSCAN delivers high-quality output, but it depends on two parameters indicated and MinPts. It is time consuming to look for each object's nearest neighbors within the development of the cluster and to select distinct starting points result in quite distinct implications. The article focuses on attaining an independent clustering scheme based on information density that will decrease end-user dependence to define clustering parameters.[3]

The rest paper is organized as follows. Section 2 gives a summary of the related works. In Section 3, the algorithm of proposed scheme is presented. Finally, Section 4 concludes the paper and gives some future research.

2. RELATED WORK

For several centuries, numerous clustering algorithms have been suggested. These clustering algorithms are loosely split into five classifications by distinct methodologies: algorithms based on partitioning, hierarchy-based, density-based, graph-based, and model-based. Partitioning-based clustering algorithms partition a data set by the distance from the point to the cluster middle into various clusters, but the amount of output clusters requires specialist or user to be specified. [5]

The benefit of this form of clustering algorithms is their simplicity and effectiveness. However, the clustering findings are prone to non-convex noise and information distribution. K-means and their variants are typical algorithms of this category[6, 7].

Fuzzy c-means is one of the fuzzy clustering algorithms that can allocate a data point to all clusters with a certain degree of affiliation. Hierarchical-based cluster algorithms sometimes obtain a dataset cluster structure referred to as a dendrogram that can be a stratified tree structure that shows objects internal connections. The dendrogram can be developed by agglomerating where considered each object as a cluster or splitting where considering as a cluster the complete dataset.[8]

There are square measure single-link and full-link stratified cluster algorithms on the concept of the linkage criterion [9].

The drawback of this sort of algorithms is that after building a dendrogram for an oversized dataset, it is computationally preventive. Xu, et al. scheduled a mainly based stratified clump density peak methodology, which produces clusters directly on

each achievable clump layer and presents a grid granulation structure to change DenPEHC to cluster large-scale and high-dimensional datasets(LSHD)[10].

A perform model is sometimes used by DBSCAN and stateless person algorithms to predict the indigenous density for each item in a very dataset. This method classifies objects into three types viz. key objects, boundary objects and outliers, by the number of neighbors in the neighborhood of Eps. In addition, the algorithmic program of the NBC uses the magnitude relationship between reverse k-nearest neighbors and k-nearest neighbors to live the native density of objects[11]. However, the numerous overlaps between clusters can not be noticed by “DBSCAN or NBC” and causes a slip-up in clump.

Recently, a rapid density-based clustering algorithmic program referred to as a stateless individual is scheduled in [4], which utilizes dc-neighborhood to estimate indigenous density for points and requires π to search the cluster center as a performance. Zhu, et al. scheduled an algorithmic density-ratio clump program that could determine and evaluate the situation under which the density-based clump algorithms fail, but the “ReCon-DBSCAN” algorithm program needs one additional parameter in DBSCAN and “ReScale-DBSCAN” wants two additional parameters in “DBSCAN”. [12]

A graph like the “kNN graph”, “MST” chart was backed by graph-based clustering algorithms to partition data into clusters. Vertexes and therefore edge weights within the graph depict objects and similarities between objects in a severe manner. For example the “Local time-based algorithms”, recognize the biggest k-1 weights in the MST chart and take them back to create k clusters.[13]

The “CHAMELEON algorithmic” program is predicated on the kNN graph, which first divides the kNN graph into sub-graphs, then fuses sub-graphs to create a hierarchical data structure in accordance with a dynamic model[14]. “Gan et al.” scheduled a graph-based algorithmic clump program called “likelihood propagation,” which could determine clusters with spherical shapes and non-spherical shapes[15].

Model-based algorithms of clustering take into consideration that sample observations emerge from a distribution that is a set of two or a lot of components and that each portion of the blend can be a cluster. These models incorporate Gaussian model[16], Latent Dirichlet Allocation[17], etc.

The primary algorithmic program of expectation-maximization is to infer the parameters in a very combination of “Gaussian models”. “EM algorithmic program”, however, suffers from the slow pace of convergence and hence the risk of optimum neighborhood. Key disadvantages of model-based clustering algorithm square measure that they are originally susceptible to model parameter selection and therefore cluster range.[18]

3. AUTONOMOUS DATA DENSITY BASED ALGORITHM

The Autonomous Data Density based algorithm was provided based completely on the empirical observations of the discrete information samples and data density corresponding to this dataset. The technique requires no user or problem-specific threshold to be predefined and can extract the cumulative closeness of the information sample, its eccentricity and density. As with several other current clustering algorithms, it does not involve users to suggest parameters.

Stage 1: Preparation

In this primary stage, for every unique data sample $ui \in \{u\}N$, $\{u\}N \subseteq \{x\}K$, its local unimodal density DL is calculated, based on below equation:

$$(ui) = \sum(x) d(x, ui) \leq \bar{d} 2Ni qL(ui), \quad (1)$$

where $qL(x)$ is the cumulative proximity measure locally for all the data samples located in the hypersphere with “ ui ” as its centre and “ \bar{d} ” as its radius, “ Ni ” is the number of data samples located within this “hypersphere”; “ \bar{d} ” is the half of the average standardized “Euclidean distance” between the data samples within $\{x\}K$ and is calculated as:

$$\bar{d} 2 = \sum(xj) K j = 1 2 K 2 = \sum \sum d 2(xj, xk) K k = 1 K j = 1 2 K 2 \quad (2)$$

Stage 2: Building the prototypes:

The cluster formation begins with the data sample with the maximum “ DL ”:

$$u_m = \arg \max_{i=1,2,\dots,N} (DL(ui)) \quad (3)$$

Then, all the data samples within the hypersphere with “ u_m ” as the centre and “ $r = \bar{d} 4$ ” as the radius are found out as the initial member of the first cluster $\mathbb{C}1$, and they are ranked based on their standardized Euclidean distances to u_m in an ascending order, which means:

$(z1,) = 0 \leq (z2, u_m) \leq \dots \leq d(zS1, u_m)$ ($zi \in \mathbb{C}1$), and the number of members within $\mathbb{C}1$ is denoted by $S1$. The descending speed of DL at $\mathbb{C}1$ is calculated as:

$$DL'(zi) = DL(z1) - DL(zi); \quad (4)$$

$i = 2, 3, \dots, S1$.

The following condition is checked in regards to DL' :

Condition1:

IF $(DL'(zi) \leq E(DL'(z)) + std(DL'(z)))$,
 $\forall i = 2, 3, \dots, S1$

THEN $(DL(z)$ decreases smoothly)
 ELSE

THEN (D(z) decreases sharply at a certain point) (5)

If Condition 1 is met, it means that $\mathbb{C}1$ is not fully satisfied and the radius of the hypersphere around “ um ” is extended allowing more data samples ($r \leftarrow r \times 1.1$) to be included in $\mathbb{C}1$. In that case, the process is repeated until Condition 1 is unsatisfied.

Once Condition 1 is unsatisfied, it means that (z_i) decreases sharply at the knee point, denoted by “ uk ” where there may be more than one knee points. In that situation, the hypersphere around “ um ” includes data samples from two or more clusters, and (uk) is the maximum radius of the hypersphere around “ um ” which includes data samples from the same cluster. By finding out all the data samples in $\{x\}K$ within the range of $d(uk, um)$ around um , $\mathbb{C}1$ is fully formed: $\mathbb{C}1 \leftarrow \{x | d(x, um) \leq d(uk, um), x \in \{x\}K\}$. After the formation of $\mathbb{C}1$, all its members are excluded from $\{u\}$, $\{x\}K$ and the cluster formation starts again by finding out the next um . The cluster formation process will not stop until $\{u\} = \emptyset$.

During the cluster formation process, there may be some data samples spatially isolated from the majority, which means that $(u,) > d^4 (u \in \{u\} \text{ and } u \neq um)$, for this kind of um , it forms a cluster by itself.

Stage 3: Cluster Fusion

Since the preceding phase can generate too many subtle clusters, the fundamental overlapping clusters are combined together at this point. The fusion operation starts with the smallest support from the cluster and ends when there is no interruption with the one with the largest support.

$\mathbb{C}1$, Condition 2 is checked from the lowest cluster, which also includes the inequality of Chebyshev in the form of standardized eccentricity:

Condition 2:

IF $(\epsilon_{L,i}(\mu_j) < \epsilon_0)$ OR $(\epsilon_{L,j}(\mu_i) < \epsilon_0)$

THEN (\mathbb{C}_i and \mathbb{C}_j are merged together), (6)

where $i=1,2,\dots,C-1$ and $j=i+1,i+2,\dots,C$; $\epsilon_0=5$, which corresponds to the 2σ rule; $\epsilon_{L,i}(\mu_j)$ and $\epsilon_{L,j}(\mu_i)$ are the standardized eccentricities calculated locally within the i th and j th clusters, respectively, and are expressed as ($i \neq j$):

$$\epsilon_{L,i}(\mu_j) = \frac{\sum_{x \in \mathbb{C}_i} d(x, \mu_j)}{\sum_{x \in \mathbb{C}_i} d(x, \mu_i)} \quad (7)$$

$x \in \mathbb{C}_i$.

Once For example, once two clusters, \mathbb{C}_i and \mathbb{C}_j , are merged together ($\mathbb{C}_i \leftarrow \mathbb{C}_i \cup \mathbb{C}_j$), the new cluster center and support are calculated. If \mathbb{C}_i needs numerous clusters to be merged, it will be combined with the closest one. Then, in terms of their supports, all current $C-1$ clusters are re-ranked in the descending order and condition 2 is again verified for another round.

After all the potentially overlapping clusters have been merged, the remaining clusters are considered the data pattern's main modes and the offline algorithm uses the clusters as the final output.

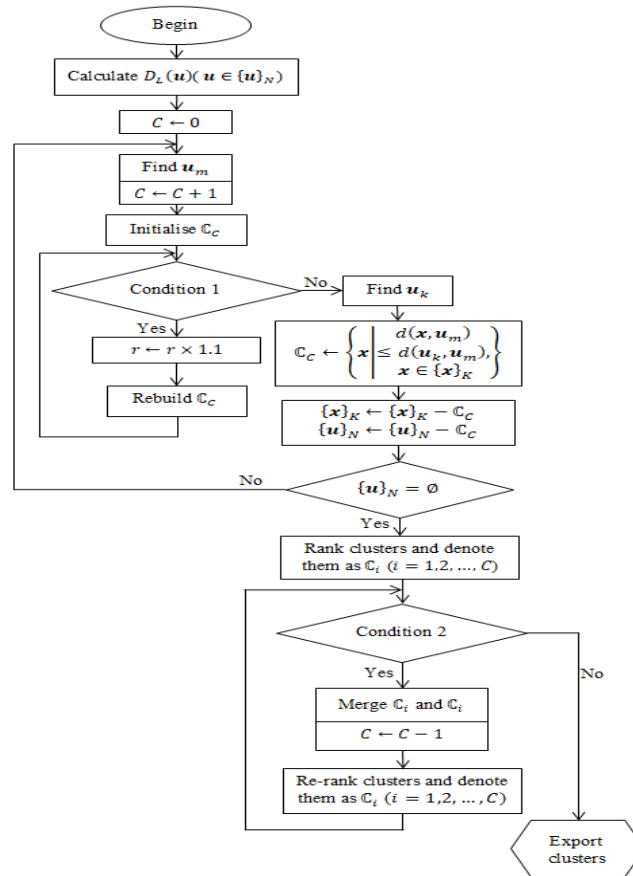


Figure 1:Flowchart of Autonomous Data Clustering

4. SIMULATION RESULTS

In order to test the performance of the newly proposed clustering method, several artificial and benchmark datasets were used in numerical experiments. The artificial datasets were used to test the accuracy of the method, and the benchmark datasets were used to ensure that the method is applicable to real cases.

Two artificial and two benchmark datasets were used in experiments with Euclidean type of distance:

- 1) The first dataset contained 7 clusters of Gaussian.
- 2) The second dataset had 7 clusters Gaussian.
- 3) Iris Dataset with 3 clusters.

Table 1: Gaussian100b dataset

Number of Samples	Number of Distinct Clusters
700	7

Table 2: Cluster Centres

X	Y
0.0247359137171717	0.0692837050505051
0.899709494949495	0.466215454545455
0.120144909090909	0.946071616161616
0.669202600000000	0.830200300000000
0.491926300000000	0.297908400000000
0.449118811881188	0.865216831683168
0.0917844299019607	0.238155392156863

Table 1 and 2 show the cluster centres of the clustered dataset obtained from the proposed method and the k-means method. For the gaussian100b the obtained cluster centre are the same.

Figure 2 shows the clustering plot for the proposed method. As can be seen, 7 distinct cluster groups are obtained shown in various different colors.

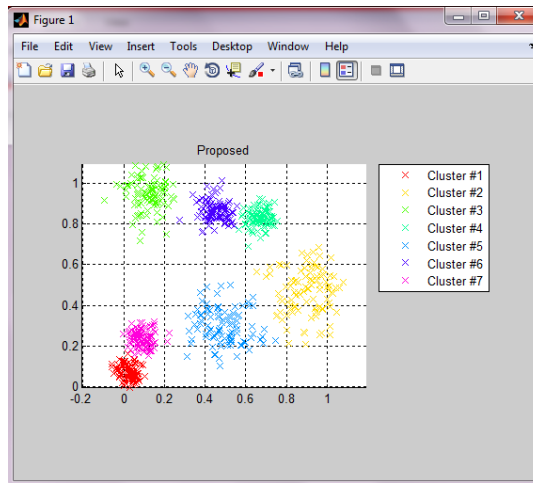


Figure 2: Clustering Plot

Figure 2 shows the cluster plot for k-means algorithm. As can be seen the k-means method is able to identify only 6 distinct clusters of data. Thus, it shows the effectiveness of the proposed method over k-means clustering method

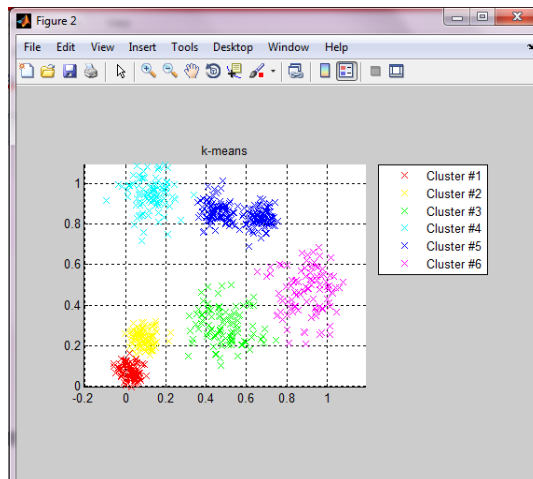


Figure 3: K-means clustering plot

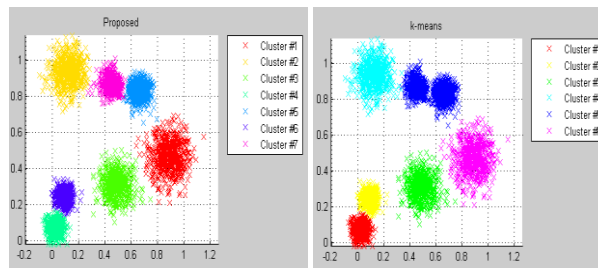


Figure 3: Clustering Plot for proposed and k-means for Dataset 2

Figure 3 shows the clustering plot for dataset 2. The proposed method is able to divide the data into 7 distinct clusters whereas the k-means divides it into 6 clusters only.

5. COCCLUSION

This research work presented a comprehensive research on clustering techniques. Some of the common data clustering methods have been studied especially related to data density based clustering. A method was proposed based on “Autonomus Data density clustering” and the algorithm has been implemented using MATLAB software tool. For comparison of the proposed algorithm k-means clustering method which is one of the most commonly used method in the field of data clustering and data mining is used. The algorithm was applied on various datasets containing different number of samples. Numerical experiments demonstrate that this technique can display outstanding clustering efficiency compared to other techniques that use different types of previous information or assumptions without any user input. Because of the benefits of no user input requirements and the self-generation of collection information properties estimators of clustered datasets, this new technique is a very appealing and efficient data analytics instrument.

6. REFERENCES

- [1] XiaoweiGu, Plamen P. Angelov, "Autonomous data-driven clustering for live data stream", Systems Man and Cybernetics (SMC) 2016 IEEE International Conference on, pp. 001128-001135, 2016.
- [2] D.M.M. Tapas Kanungo, Nathan S. Netanyahu, R.S. Christine D. Piatko, Angela Y. Wu, "An Efficient k-Means Clustering Algorithm: Analysis and Implementation.", *IEEE Trans. on Pattern Analysis and Machine Intelligence*, vol. 24, no. 7, pp. 881-892, Jul. 2002.
- [3] H.-P.K. Martin Ester, Jorg Sander, XiaoweiXu, "A Density-Based Algorithm for Discovering Clusters in Large Spatial Databases with Noise", in *Proc. KDD-96*, 1996, pp. 226-231.
- [4] R. Alex, L. Alessandro, "Clustering by fast search and find of density peaks", *Science*, vol. 344, pp. 1492-1496, 2014.
- [5] D.W.I. RuiXu, "Survey of Clustering Algorithms", *IEEE Trans. on NEURAL NETWORKS*, vol. 16, no. 3, pp. 645-678, Mar. 2005.
- [6] K.S. Rudolf Scitovski, "Analysis of the k-means algorithm in the case of data points occurring on the border of two or more clusters", *Knowledge-Based Systems*, vol. 57, pp. 1-7, 2014.
- [7] A.L. GrigoriosTzortzis, "The MinMax k-Means clustering algorithm", *Pattern Recognition*, vol. 47, pp. 2505-2516, Jul. 2014.
- [8] S. Eschrich, J. Ke, L.O. Hall, D.B. Goldgof, "Fast accurate fuzzy clustering through data reduction", *IEEE Trans. on Fuzzy Systems*, vol. 11, pp. 262-270, Feb. 2003.
- [9] L. Hubert, "Approximate Evaluation Techniques for the Single-Link and Complete-Link Hierarchical Clustering Procedures", *Journal of the American Statistical Association*, vol. 69, pp. 698-704, 2012.
- [10] JiXu, Guoyin Wang, Weihui Deng, "DenPEHC: Density peak based efficient hierarchical clustering", *Information Sciences*, vol. 373, pp. 200-218, 2016.
- [11] Y.Z. Shuigeng Zhou, Jihong Guan, Joshua Huang, "A Neighborhood-Based Clustering Algorithm", *Advances in Knowledge Discovery and Data Mining*, vol. 3518, pp. 361-371, Nov. 2005.
- [12] Ye Zhu, Kai Ming Ting, Mark J.Carman, "Density-ratio based clustering for discovering clusters with varying densities", *Pattern Recognition*, vol. 60, pp. 983-997, 2016.
- [13] Y.Z. OleksandrGrygorash, Zach Jorgensen, "Minimum Spanning Tree Based Clustering Algorithms", in *Proc. ICTAI*, 2006.
- [14] E.-H.H. George Karypis, Vipin Kumar, "CHAMELEON: A Hierarchical Clustering Algorithm Using Dynamic Modelling", *IEEE Computer*, vol. 32, no. 8, pp. 68-75, 1999.
- [15] GuojunGan, Yuping Zhang, Dipak K. Dey, "Clustering by propagating probabilities between data points", *Applied Soft Computing*, vol. 41, pp. 390-399, 2016.
- [16] G. Celeux, G. Govaert, "Gaussian parsimonious clustering models", *Pattern Recognition*, vol. 28, no. 5, pp. 781-793, 1995.
- [17] D.M. Blei, A.Y. Ng, M.I. Jordan, "Latent Dirichlet allocation", *Journal of Machine Learning Research*, vol. 3, pp. 993-1022, 2003.
- [18] A.P. Dempster, N.M. Laird, D.B. Rubin, et al., "Maximum Likelihood from Incomplete Data via the EM Algorithm", *Journal of the Royal Statistical Society*, vol. 39, no. 1, pp. 1-38, 1977.

Realization and Performance Evaluation of High Frequency Miniaturized 6W Indigenous HMC DC-DC Converter for Space Applications

Manoj R¹, Sureshkumar A², Rekha A R³, Krishnakumar J⁴

¹Launch vehicle Inertial Systems Area ISRO Inertial Systems Unit Trivandrum, India ²Launch vehicle Inertial Systems Area ISRO Inertial Systems Unit Trivandrum, India ³Launch vehicle Inertial Systems Area ISRO Inertial Systems Unit Trivandrum, India ⁴
manoj@vssc.gov.in¹, sureshkumar@vssc.gov.in², ar_rekha@vssc.gov.in³, j_krishnakumar@vssc.gov.in⁴

Abstract—The Space craft wheel drive electronics and Launch vehicle inertial sensor electronics typically require low power, low noise power supplies. Commercially available options for Space & MIL grade dc-dc converters operating in input range of 24 - 45V have limited features and performance in terms of EMI, output voltage lines, ripple and efficiency. To improve power supply performance in inertial systems, an indigenous 6W isolated Space and MIL qualified DC-DC Converter has been realized as a Hybrid Micro Circuit (HMC). Weight of the converter realized is 50grams and efficiency up to 70% has been achieved. Design of converter incorporates critical safety features like short circuit and over voltage protection, which are required for high-reliability space applications. HMC dc-dc has also passed EMI tests as per MIL-STD-461C standard. This paper discusses the converter's technical aspects and challenges in realization along with achieved performance and comparison with existing converters.

Keywords—Hybrid Micro Circuit, Flyback, Current mode control, EMI, Space Grade, MIL, House Keeping Bias

1. INTRODUCTION

The Earth imaging satellite reaction wheel drive electronics and launch vehicle inertial sensors electronics require low power, low voltage ripple and better transient response dc-dc converters. The raw bus voltage range in launch vehicle and space craft is 26 – 36V and 28 – 42V respectively. To address both voltage ranges, converters are designed to operate in input range of 24 – 45V. Table 1 gives the typical dc-dc converter requirements of wheel drive and inertial sensor electronics. The technical specifications and qualification levels of converters to operate in space are more comprehensive compared to industrial or commercial standards. Critical design parameters include selection of components, MIL-STD-461C compliance, MIL temperature range, radiation tolerance, output noise, efficiency, regulation and size constraints. Presently available Hi-Rel dc-dc converters offer output voltages in the range $\pm 5V$, $\pm 7V$, $\pm 12V$, $\pm 15V$ etc., lower efficiency at typical and light loading conditions, output cross regulation (up to 5%) and output voltage ripple (up to 50mV_{pp}). Flyback converter is used for dc-dc conversion and electrical isolation since they are simple to operate, have minimum component count and are small in size. The topology along with forward converter is the recommended one for space applications. The current mode control is selected due to features like inherent pulse by pulse current limiting & simpler control loop compensation. Post regulators ensure very tight cross regulation at a slightly lower efficiency. The regulation is ensured using a House Keeping Bias (HKB) and feedback of primary current. Flyback transformer is realized with low leakage inductance, which reduces the MOSFET off state peak voltage, and improves line, load & cross regulations. To minimize the height of the converter, planar cores are used for power transformer. Experimental study is carried out on effect of common mode noise on PWM controller performance. The secondary side post regulators studies are carried for low noise outputs to meet sensitive spacecraft electronics requirements. Another challenge has been in meeting the load transient performance during 1553B transaction, wherein, the load requires additional 550mA current with minimal drop in +5V Output and almost no cross regulation effect. In order to meet this stringent transient, transformer inductance and winding sequence optimization is carried out. To suppress the Electro-Magnetic Interference (Conducted emission, Conducted Susceptibility and Radiated emission) at input side of the flyback converter an optimized in-built single stage series damping EMI filter is realized to meet stringent military standard MIL-STD-461C levels.

Table 1: Design Specifications of DC-DC Converters

Parameters	Specifications
Input Voltage	24 - 45V
Output Capability	5V/500mA, $\pm 15V/150mA$
Output Power	6 W
Output Voltage Ripple	< 20mV _{pp}
Output Regulation	< 0.1% (24-45V) and < 0.5% (No load to 100% load)
Efficiency	~70% (at 100% load)
Frequency	470kHz – 550 kHz
Soft Start	20-40ms (24-45V, Full load)
Radiation Tolerance/	SEE Hardened to LET threshold

Space Grade	upto80 MeV/mg/cm ²
EMI Compliance	MIL-STD-461C
Operating Temperature	-55 to +125 ^o C
Operating life	15 years (intended for LEO and GEO missions)

2. CIRCUIT BLOCK AND DESIGN ASPECTS

The indigenous High reliability (Hi-Rel) hybrid micro circuit flyback dc-dc converter basic block diagram is shown in Fig. 1. This triple output converter is designed to meet launch vehicle and spacecraft bus voltages and it can be from 24V to 45V. It maintains constant output voltage irrespective of changes in the load current and input supply voltage by changing the duty cycle of the Power MOSFET switch. The magnetic current sense and HKB voltage feedback is given to 1845A current mode PWM controller and it changes the duty cycle < 50% (i.e., discontinuous mode of operation). The flyback transformer stores the energy during switch on time and it transfers the energy to secondary winding during off time. Because of this, the reflected voltage from secondary winding and voltage spikes due to leakage inductance appears across the power switch. So the power transformer is made with less leakage inductance by changing the bifilar winding sequence.

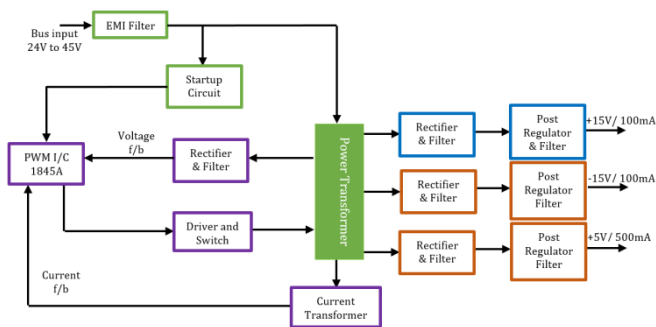


Fig. 1. Flyback topology for Space applications

This reduces the voltage spike and EMI related issues during EMI test. The input built-in common mode and single stage differential EMI filter maintains the fundamental current harmonics amplitude within 40dB μ A for MIL-STD-461C level. During variation in load current and input voltage, the post regulator maintains the constant output voltage with less power dissipation. The start-up bias regulator meets the initial power requirement of the PWM controller. Once HKB voltage is built-up the bias regulator will be turned off. The output capacitive filter is designed to meet stringent inertial systems voltage ripple and load transient requirements. The power stage low frequency pole and high frequency ESR zero is compensated by single-pole & single-zero lag compensation method. To improve noise immunity in the current feedback signal during lighter load condition, slope compensation is added.

3. DC-DC CONVERTER REALIZATION

Space grade dies are selected based on parameters such as radiation specification of 100K Rad (Si) SEE immunity up to LET threshold of 80 MeV/mg/cm², quiescent power, input voltage range, mode of operation, gate charge and frequency. In addition to technical compliance, de-rating analysis, worst case drift, tolerance analysis and FMECA as per MIL-STD-975, MIL-STD-1547 and reliability estimation as per MIL-HDBK-217F are carried out to meet necessary space qualification standards. Thermal and structural analysis of the mechanical model using the finite element method is carried out to establish a performance baseline, design margin and confidence in the mechanical configuration prior to finalization. Analysis with worst case operating temperatures (+125^oC) and vacuum conditions is carried out and junction temperatures of dies are maintained below 150^oC. Thick film hybrid assembly usually begins with an attachment of electrical components (semiconductor die, capacitors, diodes, etc.) by way of solder reflow or epoxy to a bare substrate Alumina (Al₂O₃). To realize a space worthy and reliable HMC, following design considerations are taken care of during the design stage. Current sensing is a major design parameter where factors like AC and peak currents, power loss, stability, bandwidth, transient response, and mechanical constraint determines the best technique to be implemented. With a dissipation of around 0.4W with 0.5 Ohm resistor ($I_{\text{primary RMS}}$ is 0.7A), resistive sensing will pose a thermal issue while packaging as a HMC. Additionally, when operating temperatures change from -55 to +125^oC, the power capability also reduces. Therefore, as thermal hotspots affect the case temperature, stress factors and reliability of converter and to maintain junction temperatures less than 150^oC, transformer sensing is implemented. The current transformer sensing used in HMC, where the primary winding will consist of a single turn with the secondary turns providing the current attenuation. With negligible power dissipation, thermal handling and performance is enhanced. The HMC version of DC-DC converter layout design and butterfly package is shown in Fig. 2. HMC DC-DC Manufactured in a facility fully qualified to ISRO Space Standards, these converters are fabricated utilizing ISRO qualified processes. They are encased in a hermetic 2.60" x 1.35" x 0.43" Kovar package and weight of 50grams. The package utilizes rugged glass to gold sealed feed-through pins for I/O interface. The output voltages can be pre-fixed to suit user requirements. They exhibit a high tolerance to environmental stresses such as temperature extremes, mechanical shock, vibration and radiation.



Fig. 2. Indigenous HMC DC-DC Converter with Built-in EMI filter

4. SIMULATION RESULT

A SPICE simulation of the current mode control flyback converter is carried out and the results are as shown in Fig. 3. In this simulation, input EMI filter and transformer leakage inductance & winding capacitance values are used from the practical measurement values. This simulation is carried out to find losses occurring in the MOSFET switch, transformer and output diodes and to analyse the feedback loop stability. The turn on response at the input of the post regulator is plotted and shows a monotonic output rise with minimal overshoot. Except post regulator, the major elements like MOSFET switch, transformer, output rectifiers and capacitors are modelled in this simulation.

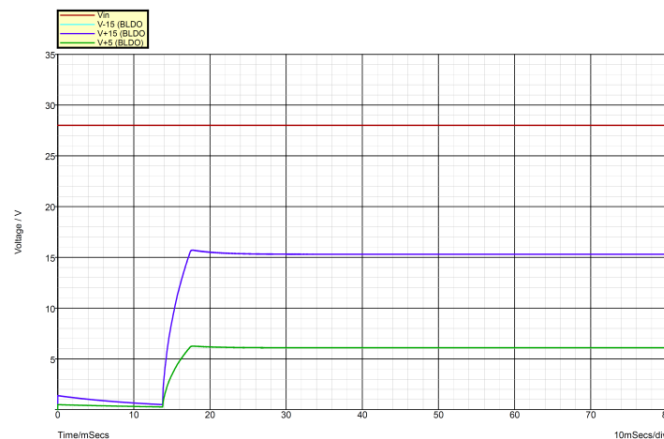


Fig. 3. Simulation result for Turn-ON response of the DC-DC

5. EXPERIMENTAL RESULTS

Flyback Converter performance is analysed in detail by observing various parameter like line regulation, load regulation, cross regulation, output voltage ripple, input current ripple, efficiency, step load response (transient and recovery), step line response (transient and recovery), start-up delay and overshoot.

5.1. Line, Load and Cross Regulation

The Nominal Input Bus voltage for the DC-DC characterization is taken as 28V for Launch Vehicle and 42V for Spacecraft applications. These high reliability applications demand line and load regulation requirement of within 0.5%. For the input voltage range of (24-45V), the achieved line regulation for +5V/500mA output is 0.04%, ±15V/100mA outputs are 0.02% and its plot is shown in Fig. 4.

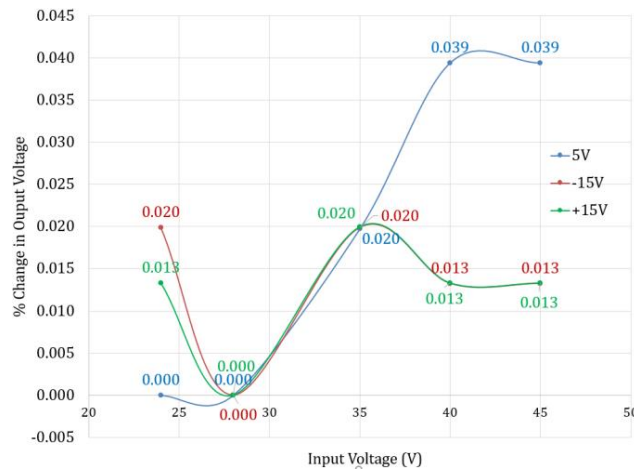


Fig. 4. Line Regulation (+5V/500mA, ±15V/100mA Outputs)

At 28V input voltage the no-load to 100% load regulation for +5V/500mA output is 0.12%, ±15V/100mA outputs are 0.04% and 0.08% which is as shown in Fig. 5. Similar values are obtained for remaining input voltages as well and all are within 0.2% at all outputs. Cross regulation of this Hi-Rel low power HMC dc-dc is almost zero and it is observed when 20% load in main output and 100% load in auxiliary outputs. At 42V input, cross regulations values for +5V/500mA output is 0.014%, ±15V/100mA outputs are 0.007% and its plot is as shown in Fig. 6. Similar values are obtained for remaining input voltages as well and all are within 0.02% at all outputs.

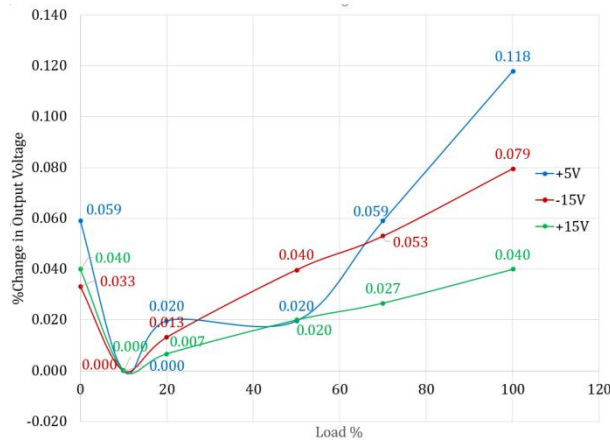


Fig. 5. Load regulation (+5V/500mA,±15V/100mA Outputs)

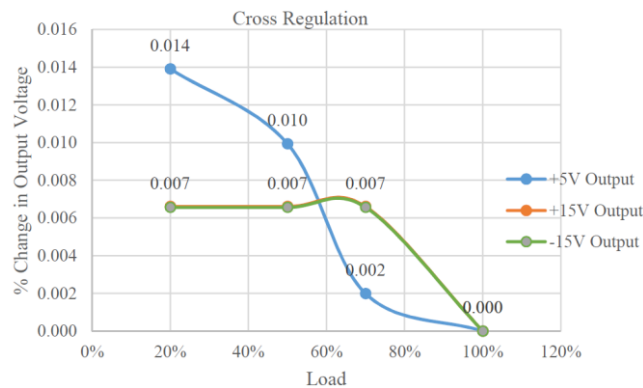


Fig. 6. Cross regulation (at +42V Input)

a. Output Power Vs Efficiency

The variation in efficiency with output power for the Hi-Rel triple output flyback converter at +42 V input is shown in Fig. 7. At 24V & 42V inputs the full load efficiency is 70%.

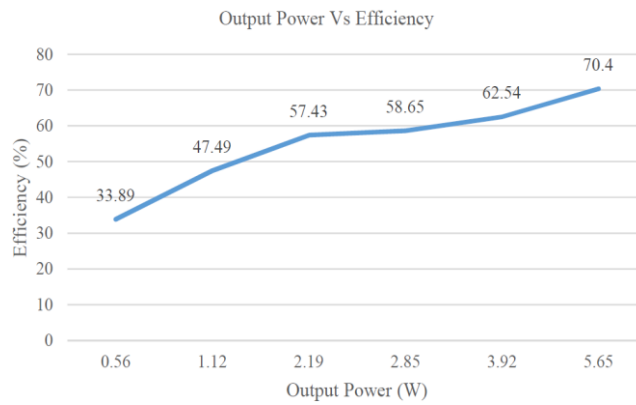


Fig. 7. Output Power Vs Efficiency (at +42V Input)

5.2. Efficiency Vs Switching Frequency

During design approach the switching frequency is varied by changing the oscillator frequency setting resistor (R_T). The efficiency variations are observed from 385 kHz to 630 kHz at all input range of voltages (24-45V). The maximum of 70.8% efficiency is obtained at 495 kHz, 28V input. Space grade version of triple output flyback converter efficiency for various switching frequency under nominal +42 V input and full load condition is shown in Fig. 8.

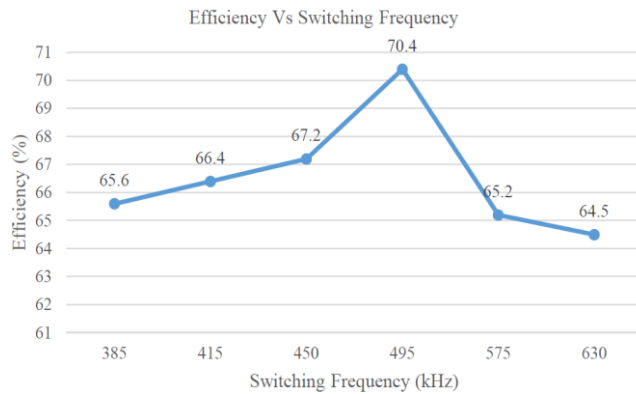


Fig. 8. Efficiency Vs Switching Frequency (at +42V Input)

5.3. Clock Signal and Gate Pulse

The clock and gate signal from Current mode PWM controller ($V_{in}=42V$, 100%load) of this HMC DC-DC converter is as shown in Fig. 9, 10.

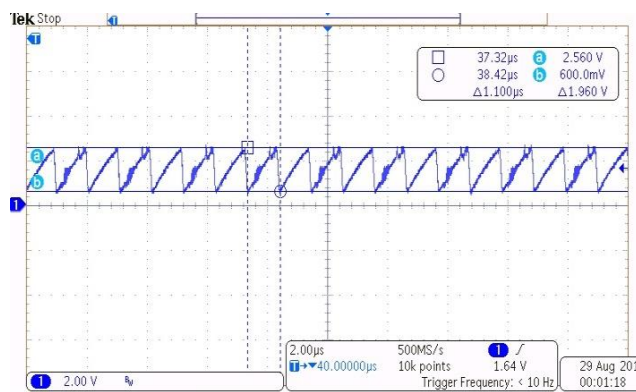


Fig. 9. Clock Signal

5.4. Stepload response

During 1553 bus communication the +5V output current changes from 500mA to 1050mA. To meet this step load with minimal voltage dip, the converter loop bandwidth and transformer inductance optimization is carried out. The step load response (100% to 210% load) is shown in Fig. 11. To meet the sensitive spacecraft electronics requirements, the output voltage ripple of the DC-DC converters needs to be less than 50mV. This HMC DC-DC converter output voltage ripple is 4mV at +5V/500mA output is shown in Fig. 12.

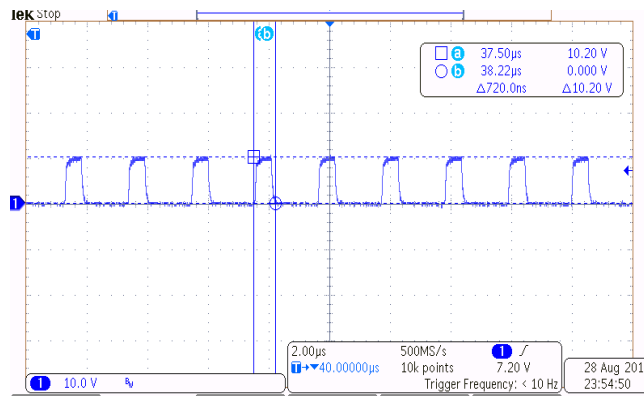


Fig. 10. Gate Pulse

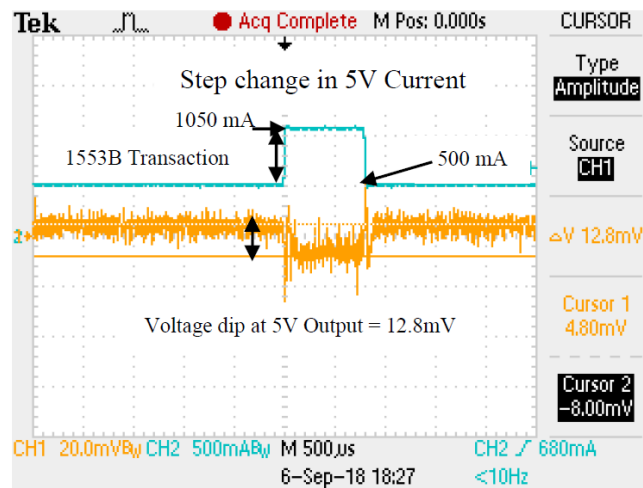


Fig. 11. Step load response at +5V Output

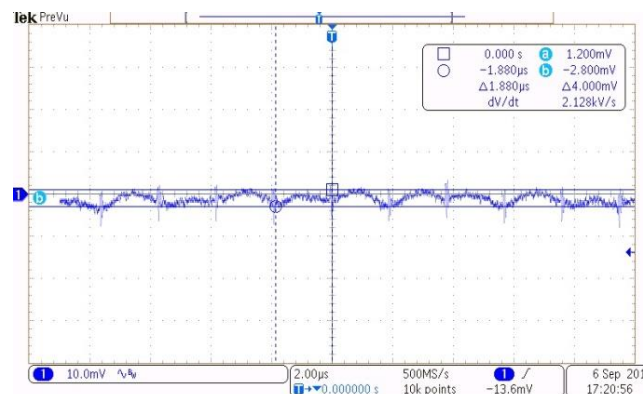


Fig. 12. +5V Output Voltage Ripple

5.5. MOSFET drain voltage & converter Turn ON response

To reduce the MOSFET drain to source voltage peak, leakage inductance optimization is carried out which is done by increasing the coupling factor of the transformer. At +42V input and 100% load the MOSFET drain to source voltage is 74V and transformer primary current peak is 1.46A. The MOSFET drain voltage, primary current, HKB current and +5V output current is shown in Fig. 13. This converter +5V Output Turn On response time is 28msec and turn off time is also less than 10msec. The Converter Turn On response of triple output HMC DC-DC converter is shown in Fig. 14.

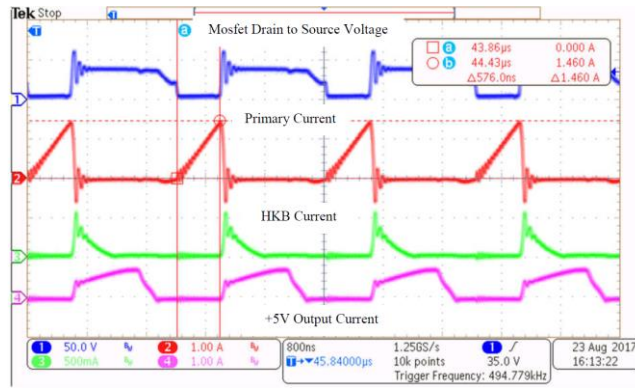


Fig. 13. MOSFET Drain Voltage and +5V Output Current (100% load)

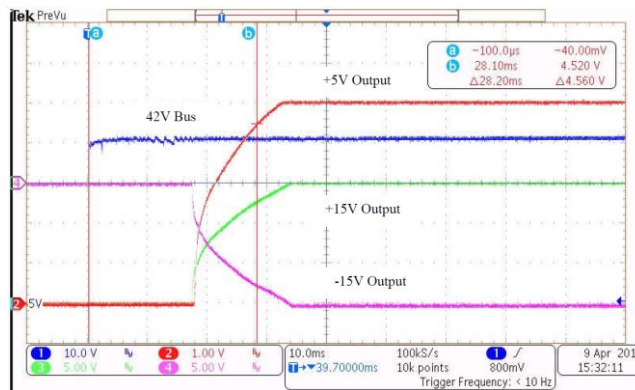


Fig. 14. Triple Output Converter Turn ON response (100% load)

5.6. PWM controller loop stability

The PWM controller loop stability is analysed by using vector stability analyser. The loop stability is measured across the injection resistor, which is added in the control loop path. The Phase margin at gain crossover frequency (5kHz) is 62.5° and gain margin at phase crossover frequency (75kHz) is 36.7dB. The converters power stage introduces a pole at 75 Hz and a zero at 95 kHz. To compensate this single pole – single zero lag compensator is used and its zero is fixed at 1.5 kHz and pole at 47.5 kHz. The HMC DC-DC converter PWM controller loop gain and phase at +42V input and 100% load is shown in Fig. 15.

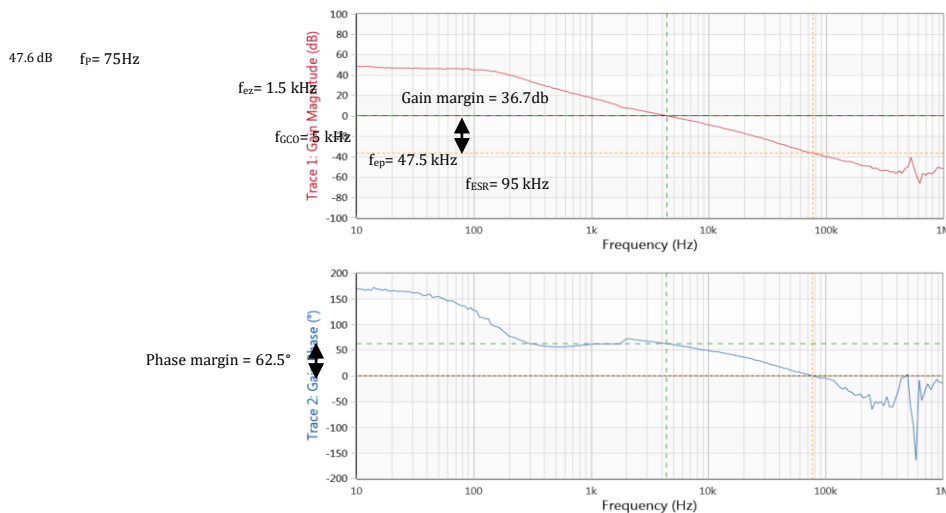


Fig. 15. PWM controller loop gain and phase (100% load)

5.7. EMI Test Results (MIL-STD 461 CE03 & CE01)

EMI testing of the converter is carried out at full power and +28V nominal input voltage and the levels are found to be well within the acceptance limits. Three major peaks are observed at 385 kHz (power supply frequency), 495kHz (converter switching frequency) and 1MHz (2nd order harmonics) in CE03 Plot. The plot of CE03 and CE01 test results are shown in Fig. 16, 17.

6. SUMMARY & CONCLUSION

Design aspects and specifications of dc-dc converter, dc-dc challenges for space use, HMC design, and achieved converter performance are discussed in this paper. Improvement of performance from the existing space grade converters in terms of efficiency, cross regulation (< 0.5%), output voltage ripple (< 20 mVpp) and EMI is achieved by proper selection of topology, circuit design components, layout design and comprehensive magnetics design.

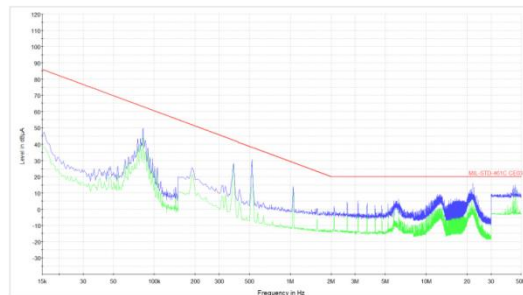


Fig. 16. Plot of CE03 test result

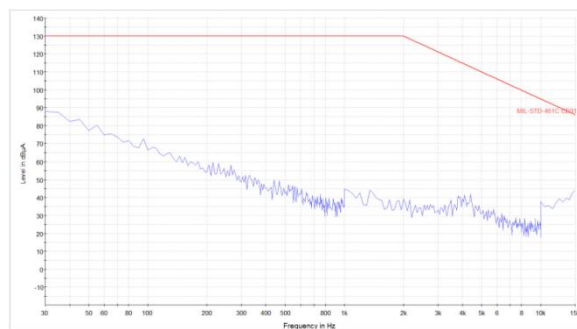


Fig. 17. Plot of CE01 test result

HMC 2.60" x 1.35" x 0.43" is realized with 35% reduction in size and 65% reduction in mass from PCB version. The size achieved is comparable with existing Hi-Rel dc-dc converters in the market, along with improved performance.

The Flight (Space & MIL) model of a high frequency miniaturized HMC flyback converter with triple output (+5V/500mA, ±15V/100mA) converter is realized and standalone testing including MIL-STD-461C EMI tests are completed. In qualification model, the endurance tests (i.e., active life tests for 2000Hrs @ +125°C), thermal vacuum tests, high temperature storage test (2000Hrs @ +125°C), environmental tests (thermal shock and thermal cycling test) and mechanical tests (mechanical shock and vibration tests) are done to qualify these high reliability HMC dc-dc converters and its performances are good. As the next phase of development, an HMC version of 40W triple output DC-DC converter is planned to realize with a smaller size and higher power density.

7. REFERENCES

- [1] Abraham I. Pressman, Keith billings, Taylor Morey, "Switching Power Supply Design," Third edition & Mc Graw Hill Publication, 2009.
- [2] Marian K. Kazimierczuk, "Pulse-width Modulated DC-DC Power Converters", John Wiley & Sons, 2008.
- [3] "Electromagnetic Emission and Susceptibility Requirements for the Control of Electromagnetic Interference", MIL-STD-461C, April 1980.
- [4] "Department of Defence Interface standard, Requirements for the Control of Electromagnetic Interference Characteristics of Subsystems and Equipment", MIL-STD-461E, August 1999.
- [5] Marty Brown, "Practical Switching Power Supply Design", Academic Press, INC, 2012.
- [6] Bernard Keogh, Isaac Cohen, "Flyback transformer design considerations for efficiency and EMI" Texas Instruments, 2017
- [7] Michele Sclocchi "Input Filter Design for Switching Power Supplies", National Semiconductor Corporation, 2010.
- [8] Ray Ridley, "Flyback Snubber Design", Power Magazine, 2005.
- [9] Richard Lee Ozenbaugh, "EMI Filter Design", Marcel Dekker, Inc., 2001.
- [10] L. Umanand, S.R. Bhat, "Design of Magnetic Components for Switched Mode Power Converter", Wiley Eastern Limited, 1992.
- [11] Joe Marrero, "Improving cross regulation of multiple output flyback converters", National Semiconductor, 2011.
- [12] Microchip, "Isolated flyback converter reference design", 2014.
- [13] Fairchild Semiconductor, "Design Guidelines for Off-line flyback converter using Fairchild Power Switch (FPS)", rev1.0.3 (1 200).
- [14] N. Coruh, S. Urgun, T. Erfidan, "Design and Implementation of flyback converters", 2010, pp. 1189-1193.
- [15] Picard, J. "Under the Hood of Flyback SMPS Designs", Texas Instruments Power Supply Design Seminar SEM1900, 2010.
- [16] Sullivan, C.R., Abdallah, T., and Fujiwara, T. "Optimization of a Flyback Transformer Winding Considering Two-Dimensional Field Effects, Cost and Loss" APEC 2001 Sixteenth Annual IEEE Applied Power Electronics Conference and Exposition (2001) 116-122.

A Novel Universal Reversible Logic on QCA

Snigdha Singh*¹, Abhinay Choudhary², Manoj Kumar Jain³

¹Research Scholar, Electronics Engineering Department, Institute of Engineering and Technology, 226021, India²Research Scholar, Electronics Engineering Department, Institute of Engineering and Technology, 226021, India

³Electronics Engineering Department, Institute of Engineering and Technology, 226021, India

snigdhas.03@gmail.com¹, svashuc@gmail.com², mkjain71@gmail.com³,

Corresponding author*: Phone: +918004663145

Abstract

Background/Objectives: The Modern VLSI industry is facing a great issue of shrinking size and scale reduction in the chip area which is at the cost of power and energy loss. These losses occur in the form of heat which may lead to the semiconductor chip diminished reliability or even destroy it. Reversible Logic approach is an effective counterfeit in this direction. **Methods/Statistical analysis:** For the sake of simulation QCADesigner 2.0.3 is opted as a tool. **Findings:** This paper deals with the Novel Proposed SA Reversible Logic as universal logic which holds a strong grip on all conservative gate designing. **Improvements/Applications:** As it is a universal logic can be used for designing of combinational as well as sequential circuits.

Keywords: Reversible Logic, garbage output, constant input, universal logic.

1. Introduction

The previous decade was fully dedicated to the remarkable achievements in the computers, antecedently computers were so cumbersome that they hold a very high areal occupancy but the downscaling motivated the mounting of plenty of components on a single board. The assimilation held due to the paradigmatic approach given by Moore¹ in 1965 stating that number of component on chip double every 18 months. This integration in the chip is at the cost of energy dissipation in form of heat dissipation leading to reduction in chip reliability or total destruction. Rolf Launders's^{2,3} stated that the energy dissipation observed can be estimated as $kT \ln 2 (2.8 * 10^{-21} J)$. The energy dissipation can be resolved if the logic is reversible in nature in spite of conservative logic stated by C.H. Bennett⁴. On considering a conventional Exclusive OR gate truth table (Table 1), we can observe that if the output is 0 then we can estimate output vector to be either (0, 0) or (1, 1) i.e. is an enigmatic condition. This can be removed if we insert additional output lines in such a way number input and output become equal. For converting the conventional logic to a reversible one the additional output lines are being added which is represented numerically as $\log_2 \mu$, here μ stands for the maximum times the output is being overlapped. From Table 1, $\mu=2$ which means additional output required for conversion of irreversible to reversible is $\log_2 2=1$. From the table 2 we can observe that the input and output vectors are non-overlapping in nature or we can say that if the output is known then we can recover the input from it. The block diagram of conventional Ex-OR gate is shown in figure 1 and Reversible Ex-OR in figure 2.

Reversible Logic⁵ can be defined as a bijective digital logic having the equal number of input-output terminals such that the unique mapping exists in between them. The mandatory condition for the Logic to be reversible is unique input-output pattern, zero fan-out, acyclic graph etc.

The remaining paper is arranged as section II encompasses of the key terms related to reversible circuit designing, section III builds the historical background of Quantum dot cellular Automata. The proposed Circuit and

simulation results are present in section IV and V. Section VI finally ends the paper with the conclusions made and future scope.

2. Key Terms

Constant inputs/Ancilla inputs: While realizing a reversible circuit a set of inputs are preset and reset termed as constant input for that circuit.

Quantum Cost: Quantum cost ⁶ is being termed as number of primitive gates i.e. NOT, CNOT, V and V+ in the equivalent quantum diagram. The following axioms are being followed:

$$\begin{aligned}V * V &= \text{NOT} \\V+ * V+ &= \text{NOT} \\V * V+ &= V+ * V = 1\end{aligned}$$

Alternatively, the layout in QCA also yields quantum cost by the formulation $\text{area} * \text{latency}^2$. In the critical path number of clock zones being employed is known as its latency.

Garbage output: The number of additional outputs being inserted in such a way that input and output become equal is termed as garbage output.

Delay: Delay can be defined as the maximal number of clock zones used in between input and output terminal.

Flexibility: The flexibility can be termed as the adaptability of the logic to perform different logical operations.

3. Background of QCA

Quantum Dot cellular automata ⁷ serves as the paradigm in the communication and information processing. In contrast to CMOS technology it has lower power as well energy dissipation. The fundamental unit in Quantum dot cellular Automata is QCA cell (Figure 3) consisting of the four vacant sites and two free electrons residing in between them. According to the electron position in the cell the polarization of the QCA cell ⁸ is being defined as polarization $P=1$ and $P=-1$ shown in figure 4.

QCA required clocking scheme for both combinational as well as sequential circuit designing. Four clock zones exist in QCA named as switch, hold, release and relax shown in figure 5.

4. Proposed Work

In case of conservative logic NAND, NOR act as universal logic but suffers from the information loss on bit manipulation so here a 4*4 Reversible universal Logic SA shown in figure 6 is being proposed which can implement all conservative logic gates.

The proposed SA Logic consists of input (A, B, C, D) and output (P, Q, R, S) so from the truth table in figure 7 it can be depicted as Reversible Logic. SA logic can be used to design all the conservative logic gates like AND, OR, NOT, Ex-OR, Ex-NOR, NOR, NAND etc. by setting the constant inputs. All the basic logic gates can be designed using it. Shown in Table 3 Therefore, it can be termed as universal logic. The Schematic on QCA is shown in figure 8.

5. Result and Simulation

The proposed universal logic has been verified on QCADesigner 2.0.3 ⁹ and choosing the bi-stable approximation option from the simulation window shown in figure 9. On taking in consideration the above parameters the waveforms of the SA universal logic is shown in figure 10.

6. Conclusion and Future Scope

This paper consists of the Universal SA Reversible logic implementation on QCA. The proposed logic is capable of implementing all the conservative logic gates. This a universal logic that's the reason it can be used as a basic building block in combinational as well as sequential circuit designing.

7. Acknowledgment

I would like to acknowledge the Electronics Department of Institute of Engineering and Technology for the constant support in the research work.

Figures

Figure 1. Conventional Ex-OR Gate Block Diagram

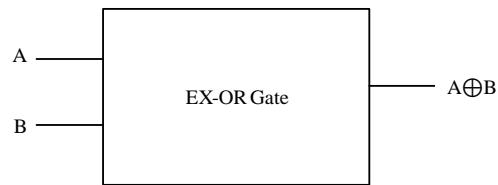


Figure 2. Reversible Ex-OR Gate Block Diagram

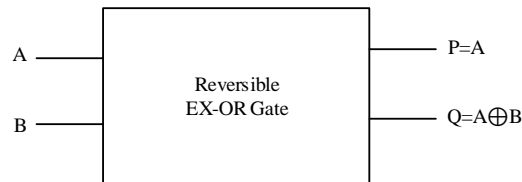


Figure 3. QCA Cell

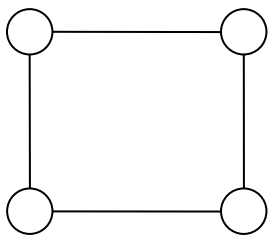


Figure 4. Two possible polarization in QCA (a) $P=+1$ (b) $P=-1$



Figure 5. Clocking zones in QCA

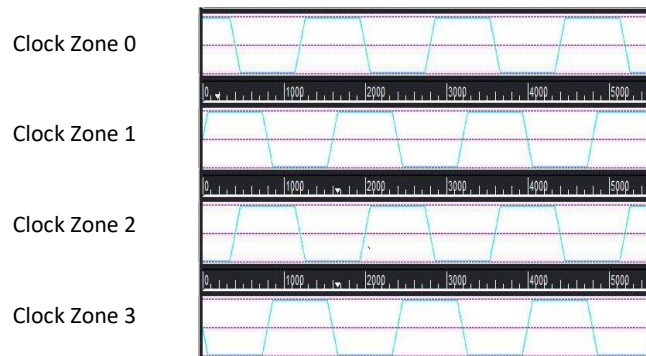


Figure 6. SA Universal Reversible Logic

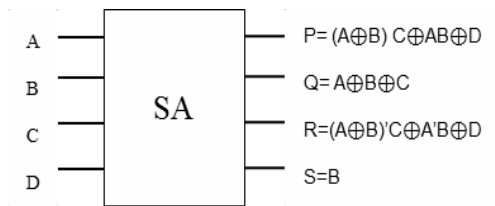
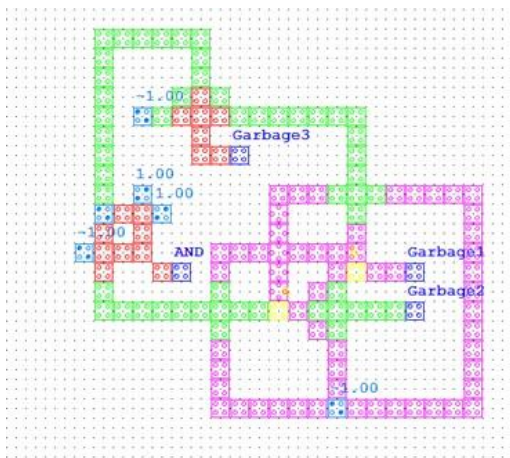


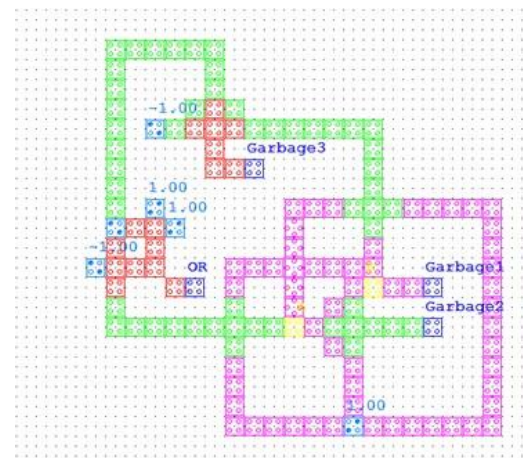
Figure 7. SA Logic Truth Table

Input				Output			
A	B	C	D	$P=(A\oplus B)C\oplus AB\oplus D$	$Q=A\oplus B\oplus C$	$R=(A\oplus B)'C\oplus A'B\oplus D$	$S=B$
0	0	0	0	0	0	0	0
0	0	0	1	1	0	1	0
0	0	1	0	0	1	1	0
0	0	1	1	1	1	0	0
0	1	0	0	0	1	1	1
0	1	0	1	1	1	0	1
0	1	1	0	1	0	1	1
0	1	1	1	0	0	0	1
1	0	0	0	0	1	0	0
1	0	0	1	1	1	1	0
1	0	1	0	1	0	0	0
1	0	1	1	0	0	1	0
1	1	0	0	1	0	0	1
1	1	0	1	0	0	1	1
1	1	1	0	1	1	1	1
1	1	1	1	0	1	0	1

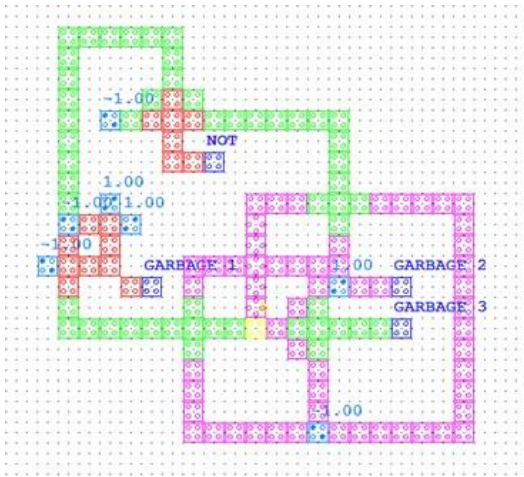
Figure8. SA logic as Universal Logic (a) AND (b) OR (c) NOT (d) EX-OR (e) EX-NOR (f) NOR (g) NAND



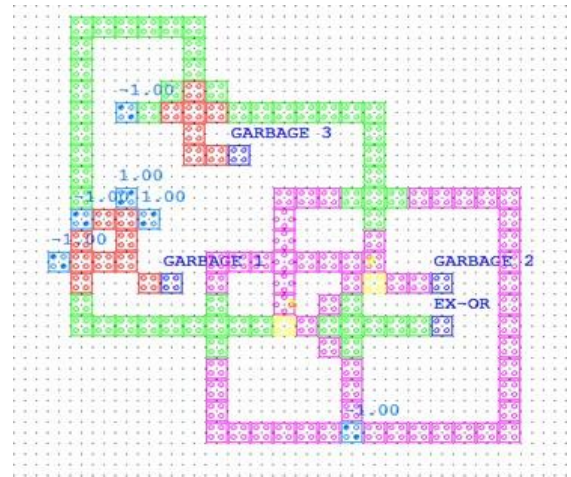
(a)



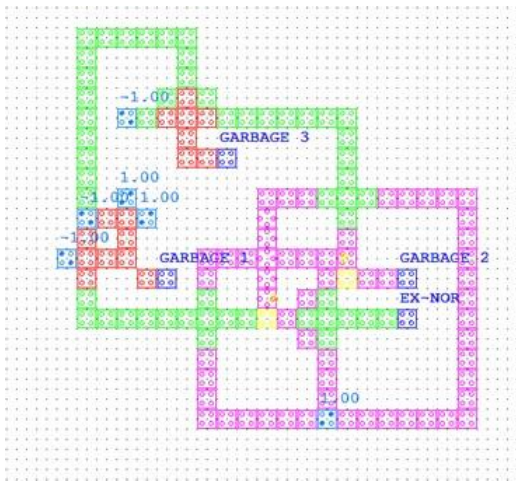
(b)



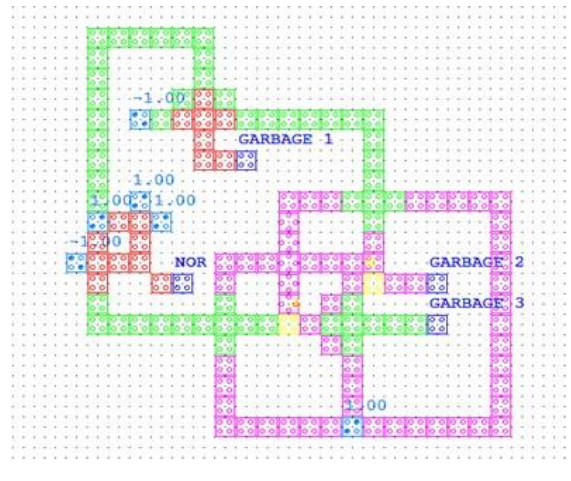
(c)



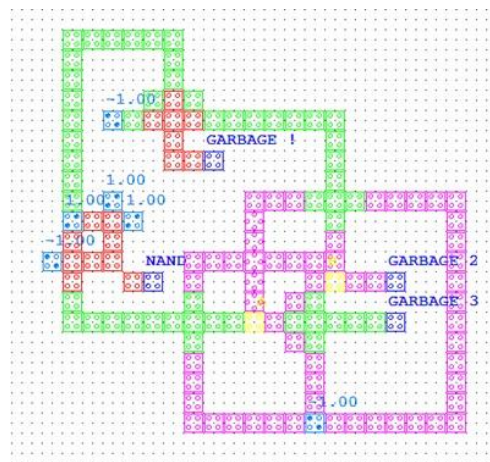
(d)



(e)



(f)



(g)

Figure 9. Bi-stable Approximations of QCA

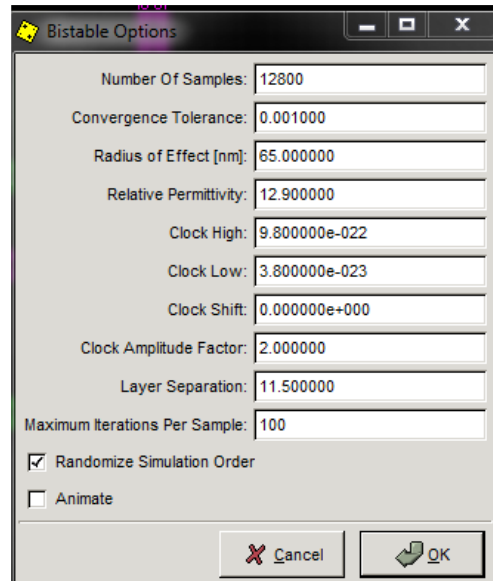
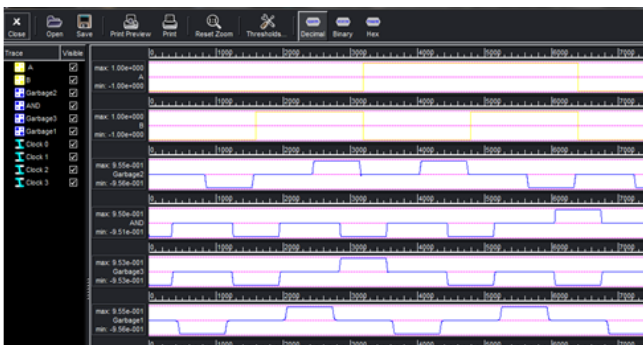


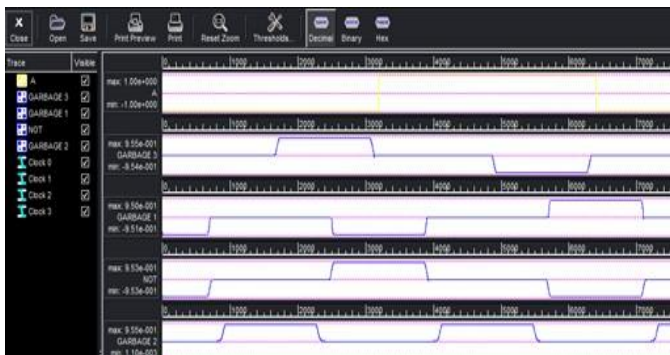
Figure 10. Waveform of SA logic as universal Logic (a) AND (b) OR (c) NOT (d) EX-OR (e) EX-NOR (f) NOR (g) NAND



(a)



(b)



(c)



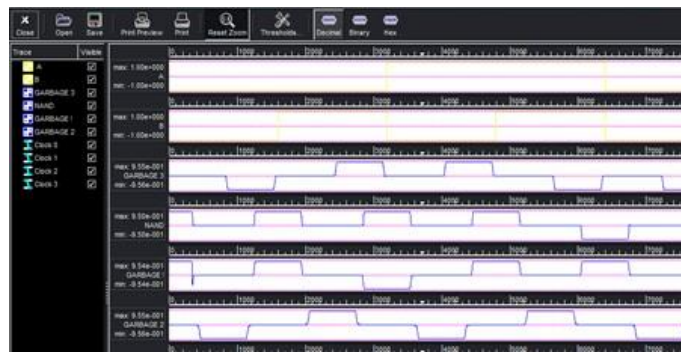
(d)



(e)



(f)



(g)

Tables

Table 1: Exclusive-OR Gate Truth Table

Input		Output
A	B	F
0	0	0
0	1	1
1	0	1
1	1	0

Table 2: Reversible Exclusive-OR Truth table

Input		Output	
A	B	P=A	Q=A⊕B
0	0	0	0
0	1	0	1
1	0	1	1
1	1	1	0

Table 3: Universality of SA Reversible

Gate Formed	Constant input used
AND	C=0, D=0
OR	C=1, D=0
NOT	B=1, C=0, D=0
EX-OR	C=0, D=0
EX-NOR	C=1, D=0
NOR	C=1, D=1
NAND	C=0, D=1

Logic

8. References

- [1] Gordon E. Moore, "Cramming more components onto integrated circuits," *Electronics*, volume 38, number 8, April 19, 1965.
- [2] R. Landauer, "Irreversibility and Heat Generation in the Computing Process," in *IBM Journal of Research and Development*, vol. 5, no. 3, pp. 183-191, July 1961
- [3] W. Keyes & R. Landauer, "Minimum Energy Dissipation in Logic," *IBM Journal of Research and Development*. 14. 152-157. 1970.
- [4] C. H. Bennett, "Logical Reversibility of Computation," *IBM Journal of Research and Development*, vol. 17, no. 6, pp. 525-532, Nov. 1973.
- [5] Snigdha Singh, Abhinay Choudhary, Manoj Kumar Jain, "A Brief Overview of Reversible Logic gate and Reversible Circuits," *International journal of Electronics Engineering*, volume 11, Issue 2 pp. 86-104 June - Dec 2019.
- [6] Robert Wille, Rolf Drechsler, "Towards a Design Flow for Reversible Logic," Springer book.
- [7] Craig S Lent, P Douglas Tougaw, Wolfgang Porod and Gary H Bernstein, "Quantum cellular automata," *Nanotechnology* 4, 49-57, 1993.
- [8] T. Cole and J. C. Luth, "Rules for a cellular automaton to model quantum-dot cellular automata," *Proceedings of the 2001 1st IEEE Conference on Nanotechnology. IEEE-NANO 2001 (Cat. No. 01EX516)*, Maui, HI, USA, 2001, pp. 391-396.
- [9] K. Walus, T. J. Dysart, G. A. Jullien and R. A. Budiman, "QCADesigner: A rapid design and simulation tool for quantum-dot cellular automata", *IEEE transactions on Nanotechnology*, vol. 3, no. 1, pp. 26-31, 2004.

AHP and GIS-based site suitability analysis for desirable innocuous facilities in an Urban Area

Ruchin Agarwal*¹, Amitabh Kumar Srivastava², Anjani Kumar Nigam³

¹Assistant Professor, Civil Engineering Department, Kamla Nehru Institute of Technology, Sultanpur, 228118, India

²Professor, Civil Engineering Department, Bundelkhand Institute of Engineering & Technology, Jhansi, 284128, India

³ Professor, Civil Engineering Department, Bundelkhand Institute of Engineering & Technology, Jhansi, 284128,

Indiaruchin_eng@yahoo.com¹, aks107@rediffmail.com², anjani.k.nigam@gmail.com³,

Corresponding author*: Phone: +0-876-526-8876

Abstract

Background/Objectives: An unabated influx of population into the urban areas results in the increase in pressure on the urban infrastructure. This is both due to the residential and commercial requirements of the increasing populace.

Methods/Statistical analysis: Change in the existing land-use thus becomes inevitable to satisfy the demands of the urban expansion. Hence, planners and decision-makers are faced with the challenge of how to define and control the land-use for sustainable urban development. Constant clash of interest of various groups of people makes the decision even more difficult. In this situation, AHP and GIS technology comes in handy to the planners and decision-makers for providing a suitable solution.

Findings: The present study deals with the problem of site selection for various desirable innocuous facilities (Residential area and Commercial area). These facilities are necessary to reduce the burden of requirements of the increasing populace. GIS and AHP methods have been used here to shortlist and rank the various site to be used for residential and commercial purposes. Residential site (RS5) and Commercial site (CS6) were found to be top-ranked among all other sites.

Improvements/Applications: GIS and AHP based integrated model can be applied to a variety of problems. This model proves to be very promising in situations where conflict of interests is of prime concern to the decision-maker due to the involvement of engineering, social, geographical, economic and political dimensions.

Keywords:AHP, GIS, Residential Area, Commercial Area, Urban Planning.

1. Introduction

Urban planning refers to planning with both spatial and aspatial components. Urban planning proposes different land-uses for various parcels of land.

Identification of a suitable land-use for a parcel of land is a source of major concern for urban planners and decision-makers¹. This will, in turn, depend upon a number of factors both spatial and aspatial. The combined effect of these factors will influence our choice of the decision on land-use.

Urban areas, in general, comprise of two major categories of land-uses:

1. Desirable Innocuous Facilities
2. Desirable Obnoxious Facilities.

Desirable Innocuous Facilities (for example residential areas, commercial areas, recreational areas, etc.) are supposed to form the heartland of the urban area. They are required to be placed in the near vicinity of the urban area to be directly used by the public at large.

On the other hand, Desirable Obnoxious Facilities (for example landfill sites, sewage treatment plant, etc.) though necessary are supposed to be placed as far as economically possible from the heartland of the urban area. They are required to be placed far from the vicinity of the public settlement.

GIS is a robust tool. It facilitates spatial analysis for the identification of suitable sites². Multi-criteria analysis can then be used to evaluate and rank the alternatives provided by the GIS analysis, thus helping the planners in the complex decision-making process³.

This paper deals with the site suitability evaluation of two desirable innocuous facilities namely residential areas and commercial areas.

A. Residential Area

An area that is utilized directly to satisfy the residential requirements of the population of an urban entity is termed as 'Residential Area'. A residential area does not just provide for dwellings but also for basic infrastructure to sustain a healthy living environment. These may include road network, sanitation facilities, vicinity to shopping complexes, parks, and other recreation activities center, etc.

Therefore, identifying a land parcel to be developed as a residential area is a complex decision-making task. It involves a number of parameters which may encourage or discourage the planners and decision-makers to consider a particular choice at hand.

B. Commercial Area

Those parts of the urban entity that are entrusted upon to provide for the economic activities are termed as 'Commercial Areas'. These areas are contributing components of the economy of the urban area, of which they are part. Commercial areas witness an influx of population during the morning and an outflux of the population during the evening from the nearby residential areas. This population is involved in economic activities on a daily basis. Therefore, commercial areas should have an excellent mode of transportation to facilitate this daily movement of people. Apart from this, the commercial area should have sanitation facilities, parks, and other activity centers, etc.

Therefore, identifying a land parcel to be developed as a commercial area is also a complex decision-making task. It involves a number of parameters which may encourage or discourage the planners and decision-makers to consider a particular choice at hand.

2. Materials and Methods

2.1. Methodology

2.1.1. Spatial Analysis

Spatial analysis (i.e. gathering, storing and analyzing) both spatial and aspatial data is done by software named Geographic Information System (GIS)^{4,5}. This analysis with reference to some complex problem help in arriving at a solution, which otherwise would have been difficult to deal with⁶⁻⁸. These capabilities add up to the robustness of GIS^{9,10}. Thereby making it helpful for planners and decision-makers to use it in a variety of applications. Site suitability analysis for various land uses is one such application¹¹. Thus making GIS a natural choice to be used in the site selection of the desirable innocuous facilities. This analysis provides a number of alternatives to the planners and decision-makers that can be taken into consideration.

2.1.2. Multi-Criteria Analysis

Multi-Criteria Analysis can then be used to rank the alternatives obtained from the Spatial Analysis for helping the planners and decision-makers in taking a well-informed and efficient decision. Analytical Hierarchy Process (AHP)

is one such tool to carry out Multi-Criteria Analysis ^{12,13}. In AHP, first of all, the hierarchy for the problem is established. The goals (objectives) are at the top, criteria are at levels, sub-criteria are at sub-levels and decision alternatives are at the bottom. Pairwise comparison of elements is then carried out at each hierarchy level. Eigenvectors are then computed and aggregated for them. The composite final vector of weight coefficients for alternatives is then obtained. The entries of final weight coefficients vector reflect the relative importance (value) of each alternative with respect to the goals stated at the top of the hierarchy. The alternative with the highest weight coefficient value is then taken as the best alternative.

2.2. Case Study

2.2.1. Study Area

The subject of focus in the present study is a rural to the semi-urban area in Sultanpur district of U.P. The study area has geographical extent of 260 19' 42.918" N to 260 25' 20.42" N latitude and 810 58' 30.897" E to 820 5' 4.079" E longitude and an area of 112.81 km². River Gomti flows across the study area, which mainly comprises of quaternary alluvium as soil. The study area (Fig. 1) is in a state of urbanization at a fast pace. Kurwar town being at the center of this transition (from rural to urban) is attracting the attention of planners. Thus, making this area a very suitable candidate to be considered for the present study.

2.2.2. Spatial Data

Following is the list of spatial data generated for carrying out the study:-

1. Land Use Map
2. Soil Map
3. Slope Map
4. Transportation Map
5. Drainage Map
6. Flood Map
7. Geological Map

2.2.3. GIS Analysis

A. Residential Area

Firstly, the site suitability for the residential area was carried out. A GIS model was developed for carrying out the spatial analysis on the basis of due deliberations amongst a group of 14 experts (team of academicians, people of municipal authorities, and researchers) and in lieu with the guidelines laid down in various literature available. Following parameters were considered to achieve this objective and the model was tuned accordingly.

1. Distance from Landfill: A residential area should be constructed at least 1500 m away from a landfill site.
2. Distance from Sewage Treatment Plant: A residential area should be constructed at least 1000 m away from an STP site.
3. Distance from Pond: A residential area should be constructed at least 100 m away from any lake or pond to avoid water body contamination.
4. Distance from Road: A residential area should be constructed at least 100 m away from the right of way of any state or national highway.

5. Distance from River: A residential area should be constructed at least 200 m away from a navigable river or stream.
6. Distance from Settlement: A residential area site should be at least 100 m away from any other residential area.

Also, a check for flood inundation should also be carried out. The residential area should not be affected by flood inundation.

Based on the criteria laid down as above a GIS model was developed, which was then used to carry out the spatial analysis for finding out the suitable site location for residential area site. Application of GIS model (Fig, 2) to the spatial data (created in due course of the study) resulted in ten candidate sites for prospective Residential Land-use. Fig 3 shows the map with various residential area candidate sites as per the respective locational criterion. The geographical location detail of these residential area sites is given in Table 1 along with geographic coordinates. These sites are designated as RS1 to RS10 for ease of notation as given in Table 1. Also, the detailed values of various spatial parameters for candidate sites are given in Table 2.

B. Commercial Area

Secondly, the site suitability for the commercial area was carried out. A GIS model was developed for carrying out the spatial analysis on the basis of due deliberations amongst a group of 14 experts (team of academicians, people of municipal authorities, and researchers) and in lieu with the guidelines laid down in various literature available. Following parameters were considered to achieve this objective and the model was tuned accordingly.

1. Distance from Landfill: A commercial area should be constructed at least 1500 m away from a landfill site.
2. Distance from Sewage Treatment Plant: A commercial area should be constructed at least 1000 m away from an STP site.
3. Distance from Pond: A commercial area should be constructed at least 100 m away from any lake or pond to avoid water body contamination.
4. Distance from Road: A commercial area should be constructed at least 100 m away from the right of way of any state or national highway.
5. Distance from River: A commercial area should be constructed at least 200 m away from a navigable river or stream.
6. Distance from Settlement: A commercial area site should be at least 500 m away from any other residential area.

Also, a check for flood inundation should also be carried out. The commercial area should not be affected by flood inundation.

Based on the criteria laid down as above a GIS model was developed, which was then used to carry out the spatial analysis for finding out the suitable site location for commercial area site.

Application of GIS model (Fig, 4) to the spatial data (created in due course of the study) resulted in ten candidate sites for prospective **Commercial Land-use**. Fig 5 shows the map with various commercial area candidate sites as per the respective locational criterion. The geographical location detail of these commercial area sites is given in Table 3 along with geographic coordinates. These sites are designated as CS1 to CS10 for ease of notation as given in Table 3. Also, the detailed values of various spatial parameters for candidate sites are given in Table 4.

2.2.4. AHP Analysis

AHP analysis was carried out on

1. The six criteria stated above in Table 2 to determine the most suitable residential area site from amongst the candidate sites.
2. The seven criteria stated above in Table 4 to determine the most suitable commercial area site from amongst the candidate sites. Based on the expert opinion collected from a group of 14 people consisting of academicians, researchers and people from municipal authorities, pair-wise comparison of each criterion were carried out. Thereafter, the weight of each criterion was calculated using the AHP analysis. These weights were then used to calculate the percentage suitability, which in turn provided the rank of each candidate site for residential area as shown in Table 5 and for the commercial area as shown in Table 6 below.

3. Results and Discussion

3.1. Residential Area Site Suitability

The candidate sites were then arranged according to their ranks for the creation of Map of residential area site suitability ranking as shown in Fig. 6 below. Residential area site RS5 is the most preferred one as per the GIS-AHP model with percentage suitability of 13.82%. Suitable values of this site (RS5) for criterion C1 and C3 made it the most preferred. Whereas on the other hand residential area site RS2 with percentage suitability of 6.35% is the least preferred one. Values of this site for criterion C1 and C6 have made this site the least preferred.

3.2. Commercial Area Site Suitability

The candidate sites were then arranged according to their ranks for the creation of Map of commercial area site suitability ranking as shown in Fig. 7 below. Commercial area site CS6 is the most preferred one as per the GIS-AHP model with percentage suitability of 12.748%. Suitable values of this site (CS6) for criterion C1, C5, C6, and C7 made it the most preferred. Whereas on the other hand commercial area site CS2 with percentage suitability of 8.03% is the least preferred one. Values of this site for criterion C3, C5 and C6 have made this site the least preferred.

4. Conclusion

Site selection for desirable innocuous facilities (i.e. residential area and commercial area) is a very challenging task involving socio-economical, environmental and technical dimension. Political influences and interests of locals also add to the complication. This study has hereby shown that a step-wise solution can be provided to the mentioned problem by breaking it into two parts. First being solved by GIS on the basis of very well defined spatial criteria. Second, being prioritizing the already finalized site choices so as to address conflicts and ambiguity in a rational manner. Therefore, this study justifies the proposition that the integration of GIS and AHP methods can be very fruitful in solving problems having multi-dimensional scope and conflict of interests of stakeholders.

Figures

Fig. 1: Study Area

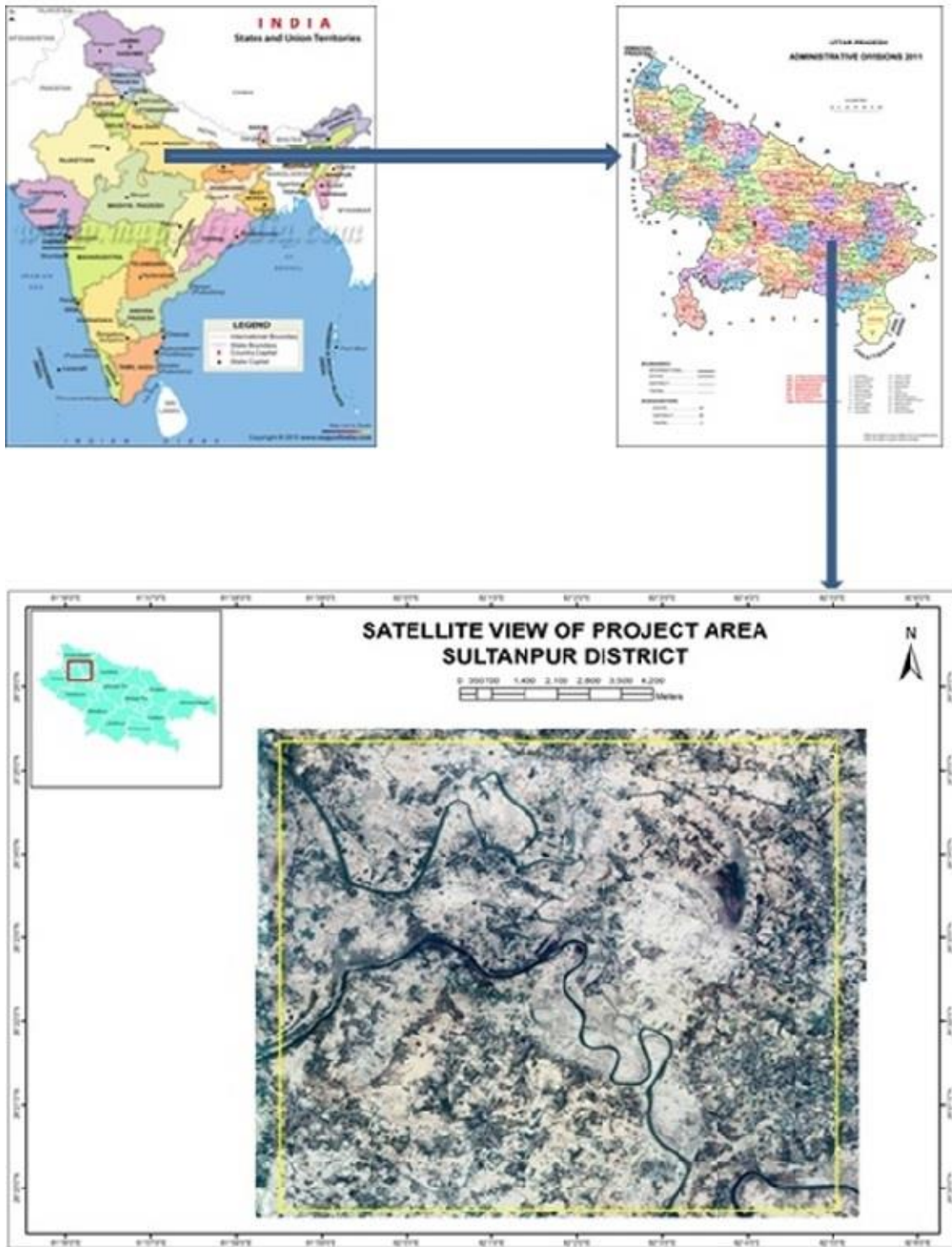


Fig. 2: GIS Model for Residential Area Site Selection

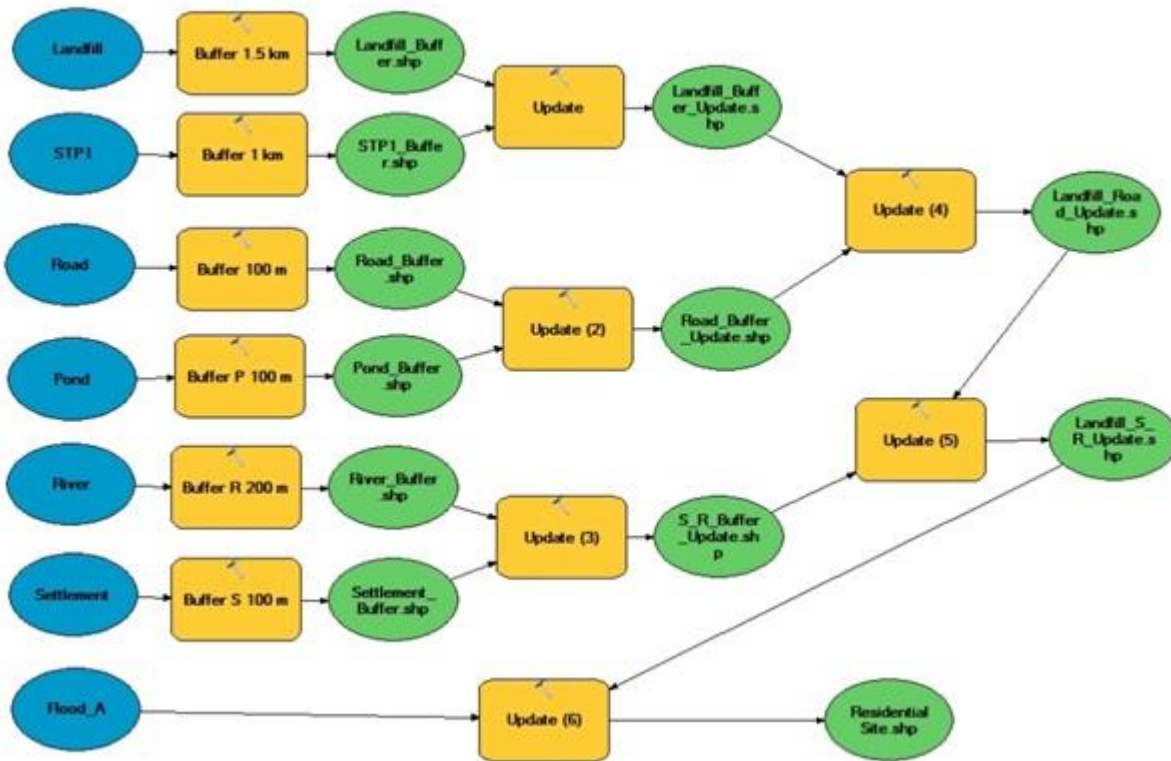


Fig 3. Map showing proposed location for Residential Area Site

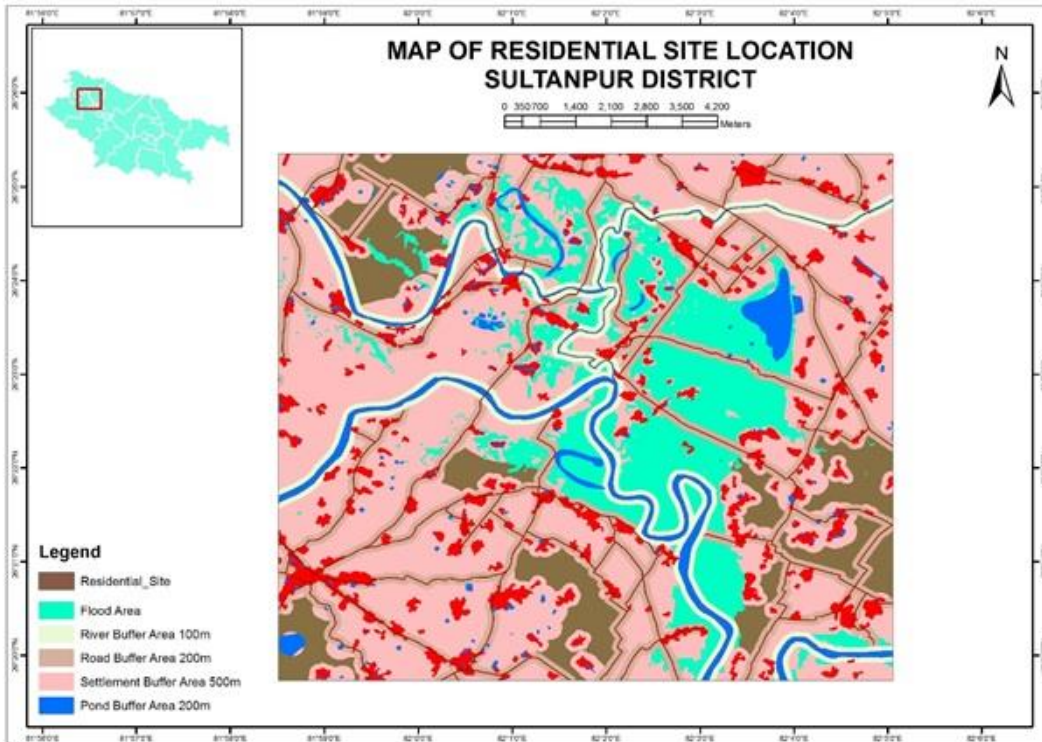


Fig. 4: GIS Model for Commercial Area Site Selection

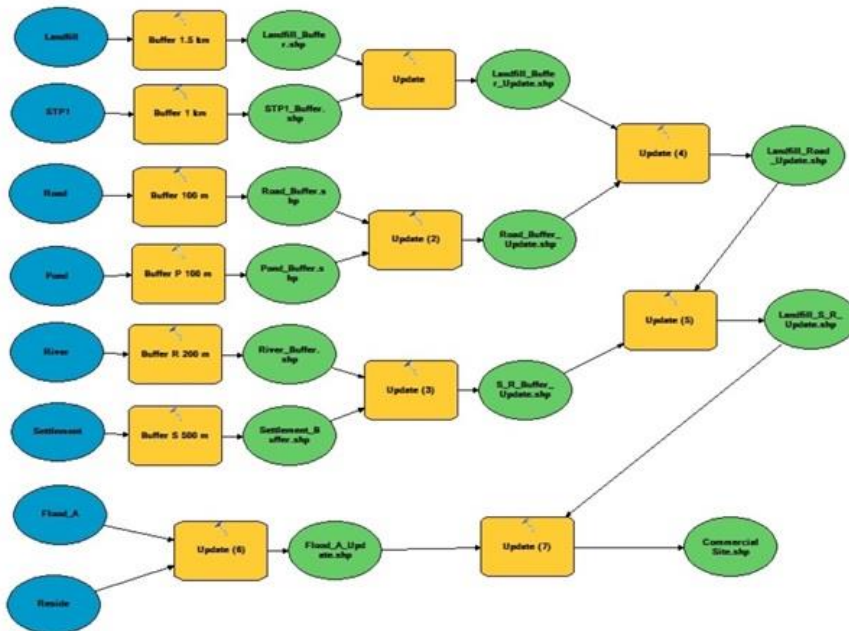


Fig. 5 Map showing proposed location for Commercial Area Site

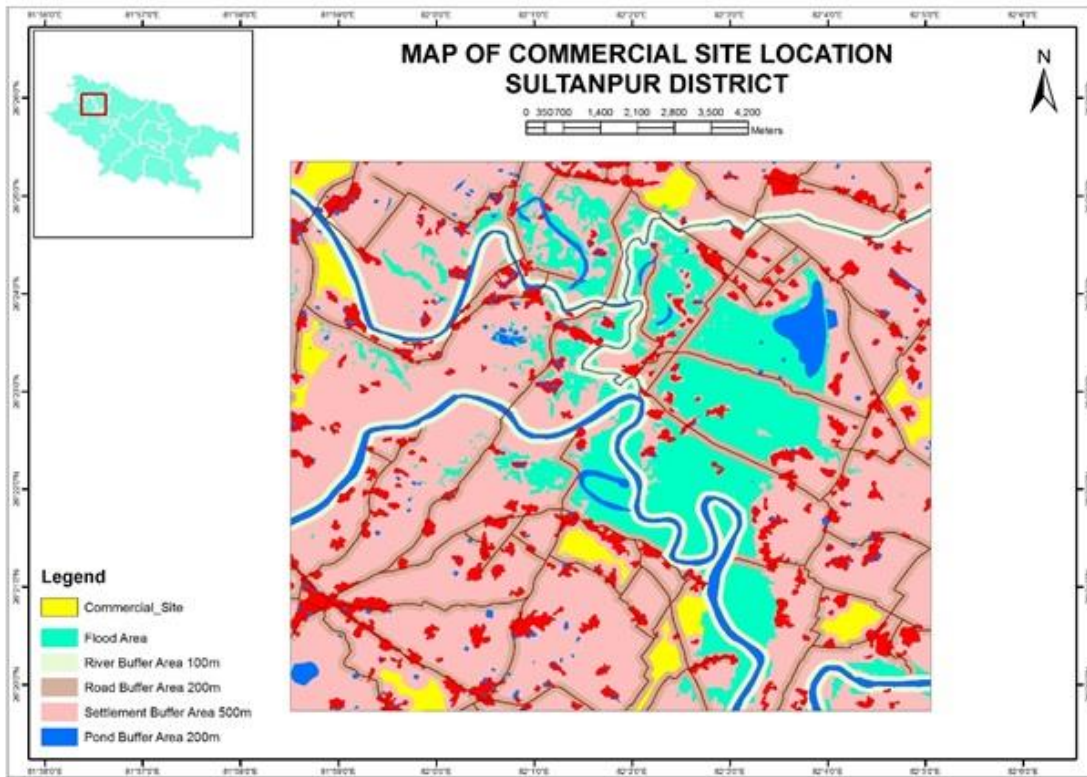


Fig. 6: Final Map showing rank-wise Residential Area Sites

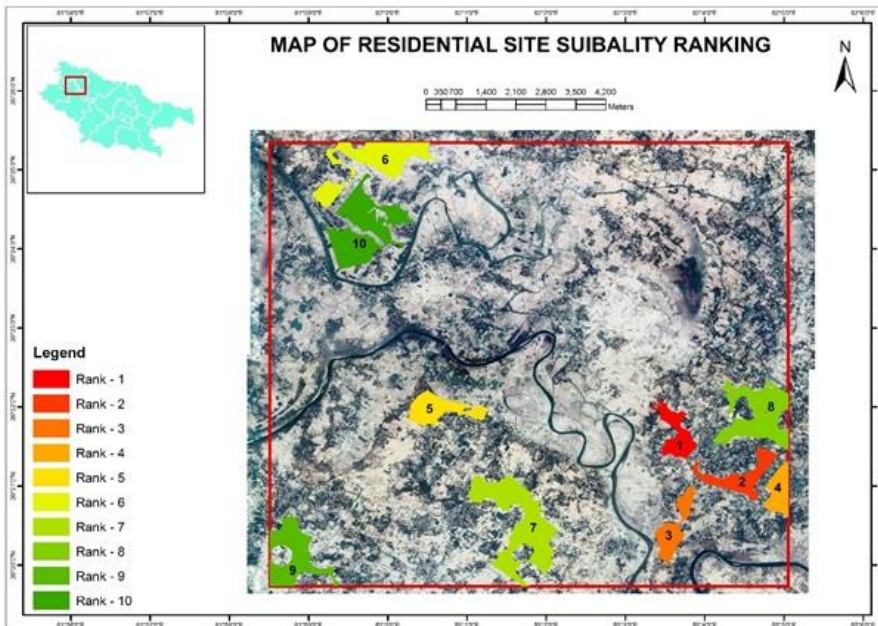
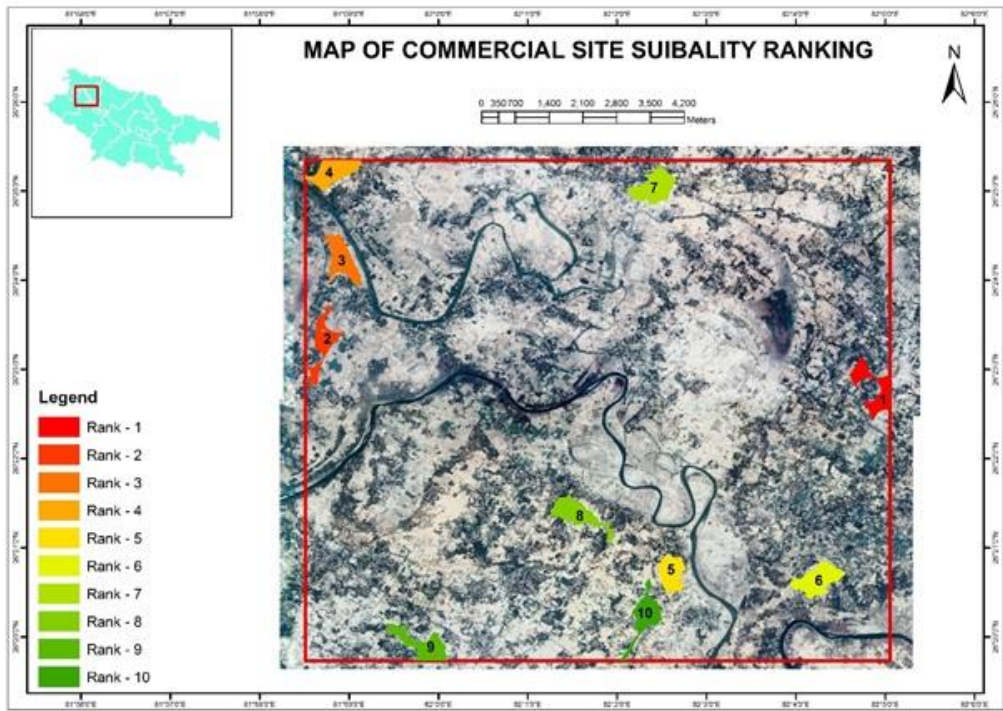


Fig. 7: Final map showing rank-wise Commercial Area Sites



Tables

Table1: Locational Coordinates of eight candidate site for residential area

Residential Area Site	Coordinates	
Residential Area Project Site 1 (RS1)	longitude	81° 59' 48.351" E
	latitude	26° 25' 5.559" N
Residential Area Project Site 2 (RS2)	longitude	81° 59' 41.593" E
	latitude	26° 24' 15.538" N
Residential Area Project Site 3 (RS3)	longitude	82° 4' 40.044" E
	latitude	26° 21' 54.384" N
Residential Area Project Site 4 (RS4)	longitude	82° 0' 39.143" E
	latitude	26° 21' 58.170" N
Residential Area Project Site 5 (RS5)	longitude	82° 3' 38.122" E
	latitude	26° 21' 40.115" N
Residential Area Project Site 6 (RS6)	longitude	82° 4' 27.711" E
	latitude	26° 21' 7.799" N
Residential Area Project Site 7 (RS7)	longitude	82° 4' 56.205" E
	latitude	26° 20' 56.117" N
Residential Area Project Site 8 (RS8)	longitude	82° 1' 38.563" E
	latitude	26° 20' 31.011" N
Residential Area Project Site 9 (RS9)	longitude	82° 3' 36.983" E
	latitude	26° 20' 28.398" N
Residential Area Project Site 10 (RS10)	longitude	81° 58' 48.332" E
	latitude	26° 20' 7.683" N

Table2: Values of various location criterions for different residential area sites

	Candidate Residential Area Sites									
	RS1	RS2	RS3	RS4	RS5	RS6	RS7	RS8	RS9	RS10
Level (C1)	90.79	88.03	89.17	91.24	98.70	99.54	97.79	99.84	94.61	101.47
Area (C2)	1.24	1.65	1.34	0.67	0.52	0.64	0.43	1.84	0.56	1.02
Distance Nearest Settlement (m) (C3)	980.31	723.71	183.26	233.60	140.99	206.32	692.23	210.25	270.72	1197.93
Distance Nearest Pond (m) (C4)	840.45	819.19	705.72	1356.45	521.56	226.12	978.98	302.52	1425.12	567.62
Distance Nearest River (m) (C5)	1461.64	862.21	2863.11	1198.52	976.79	2440.59	1649.10	2047.22	701.76	2877.42
Distance Nearest Road (m) (C6)	177.56	798.90	1061.38	503.64	609.96	480.81	403.60	877.51	394.84	437.49

Table 3: Geographic coordinates of six candidate site for commercial area

Commercial Area Site	Coordinates	
Commercial Area Project Site 1 (CS1)	longitude	81° 59' 48.351" E
	latitude	26° 25' 5.559" N
Commercial Area Project Site 2 (CS2)	longitude	81° 59' 41.593" E
	latitude	26° 24' 15.538" N
Commercial Area Project Site 3 (CS3)	longitude	82° 4' 40.044" E
	latitude	26° 21' 54.384" N
Commercial Area Project Site 4 (CS4)	longitude	82° 0' 39.143" E
	latitude	26° 21' 58.170" N
Commercial Area Project Site 5 (CS5)	longitude	82° 3' 38.122" E
	latitude	26° 21' 40.115" N
Commercial Area Project Site 6 (CS6)	longitude	82° 4' 27.711" E
	latitude	26° 21' 7.799" N
Commercial Area Project Site 7 (CS7)	longitude	82° 4' 56.205" E
	latitude	26° 20' 56.117" N
Commercial Area Project Site 8 (CS8)	longitude	82° 1' 38.563" E
	latitude	26° 20' 31.011" N
Commercial Area Project Site 9 (CS9)	longitude	82° 3' 36.983" E
	latitude	26° 20' 28.398" N
Commercial Area Project Site 10 (CS10)	longitude	81° 58' 48.332" E
	latitude	26° 20' 7.683" N

Table 4: Values of various spatial criteria for different commercial area sites

	Candidate Commercial Area Sites									
	CS1	CS2	CS3	CS4	CS5	CS6	CS7	CS8	CS9	CS10
Level (C1)	99.83	95.33	98.24	89.36	96.94	89.45	89.13	88.80	89.39	96.22
Area (C2)	0.37	0.33	0.39	0.29	0.37	0.35	0.32	0.36	0.39	0.35
Distance Nearest Settlement 1 (m) (C3)	385.11	535.65	308.53	442.18	330.86	561.03	255.61	844.88	321.91	422.55
Distance Nearest Settlement 2 (m) (C4)	470.77	465.16	318.26	462.03	404.28	184.14	697.72	377.54	396.77	374.19
Distance Nearest Pond (m) (C5)	252.42	1043.82	1093.69	748.79	923.61	437.66	530.86	723.98	556.79	399.48
Distance Nearest River (m) (C6)	5479.11	1195.59	885.21	384.93	1046.99	3680.59	1225.96	299.86	580.30	507.04
Distance Nearest Road (m) (C7)	508.79	408.05	416.10	324.72	577.78	586.27	247.36	303.37	521.69	318.43

Table 5: Percentage Suitability of Different candidate residential area sites

Sites	Percentage Suitability	Rankings
RS1	10.19	6
RS2	6.35	10
RS3	8.41	8
RS4	10.58	5
RS5	13.82	1
RS6	12.25	2
RS7	10.90	4
RS8	8.45	7
RS9	11.98	3
RS10	7.09	9

Table 6: Percentage suitability of different candidate commercial area sites

Sites	Percentage Suitability	Rankings
CS1	8.65	9
CS2	8.03	10
CS3	9.60	6
CS4	9.69	5
CS5	8.73	8
CS6	12.74	1
CS7	12.51	2
CS8	10.46	3
CS9	9.46	7
CS10	10.14	4

References:

1. Kumar M, Shaikh VR. Site Suitability Analysis for Urban Development Using GIS Based Multicriteria Evaluation Technique. *J Indian Soc Remote Sens.* 2012;41(2):417-424. doi:10.1007/s12524-012-0221-8
2. Zhao YW, Qin Y, Chen B, et al. GIS-based optimization for the locations of sewage treatment plants and sewage outfalls - A case study of Nansha District in Guangzhou City, China. *Commun Nonlinear Sci Numer Simul.* 2009;14(4):1746-1757. doi:10.1016/j.cnsns.2007.12.016
3. Anagnostopoulos KP, Gratiou M, Vavatsikos AP. Using the fuzzy Analytic Hierarchy Process for selecting wastewater facilities at prefecture level. *Eur Water.* 2007;19(20):15-24. http://www.ewra.net/ew/pdf/EW_2007_19-20_02.pdf.
4. Martínez-Graña AM, Goy JL, Zazo C. Water and wind erosion risk in natural parks -A case study in “Las Batuecas-Sierra de Francia” and “Quilamas” protected parks (Central System, Spain). *Int J Environ Res.* 2014;8(1):61-68.
5. Hijazi I, Lv Z, Li X, Zhong C, Koenig R, Schmitt G. Assessing Essential Qualities of Urban Space with Emotional and Visual Data Based on GIS Technique. *ISPRS Int J Geo-Information.* 2016;5(11):218. doi:10.3390/ijgi5110218
6. He C, Tian J, Shi P, Hu D. Simulation of the spatial stress due to urban expansion on the wetlands in Beijing, China using a GIS-based assessment model. *Landsc Urban Plan.* 2011;101(3):269-277. doi:10.1016/j.landurbplan.2011.02.032
7. Li X. Emergence of bottom-up models as a tool for landscape simulation and planning. *Landsc Urban Plan.* 2011;100(4):393-395. doi:10.1016/j.landurbplan.2010.11.016
8. Xie Z, Liu J, Ma Z, Duan X, Cui Y. Effect of surrounding land-use change on the wetland landscape pattern of a natural protected area in Tianjin, China. *Int J Sustain Dev World Ecol.* 2012;19(1):16-24. doi:10.1080/13504509.2011.583697
9. Burrough PA. Development of intelligent geographical information systems. *Int J Geogr Inf Syst.* 1992;6(1):1-11. doi:10.1080/02693799208901891
10. Burrough PA, McDonnell RA. Principles of Geographical Information Systems. *Econ Geogr.* 1998;75(4):333. doi:10.2307/144481
11. Collins MG, Steiner FR, Rushman MJ. Land-use suitability analysis in the United States: Historical development and promising technological achievements. *Environ Manage.* 2001;28(5):611-621. doi:10.1007/s002670010247
12. Saaty TL. What is the Analytic Hierarchy Process? In: *Mathematical Models for Decision Support.* ; 1988. doi:10.1007/978-3-642-83555-1_5
13. Saaty TL. Decision making with the analytic hierarchy process. *Int J Serv Sci.* 2008. doi:10.1504/IJSSCI.2008.017590

Real-Time Bridge Structural Health Monitoring using Internet of Things (IoT)

Rohit Samkaria¹, Varnita Verma^{*2}

¹National Wind Tunnel Facility, IIT Kanpur, Kanpur, Uttar Pradesh, Pin Code: 208016, India

^{2*} Department of Electrical and Electronics Engineering, University of Petroleum and Energy Studies, Dehradun, Uttarakhand, Pin code: 248007, India

rohit.samkaria93@gmail.com¹, varnitaverma2@gmail.com^{2*}

Corresponding author*: varnitaverma2@gmail.com

Abstract

Background/Objectives: In this paper, we have proposed the real-time structural health monitoring system with the help of the IoT (Internet of Things) technology for monitoring of various bridge parameters.

Methods/Statistical analysis: For data acquisition, the multiple sensor nodes designed placed alongside the bridge creating a wireless sensor network. The data from these sensor nodes send to the base station through XBee in the form of data packets. The data packets from each node is identified from its start and stop bit. The sensor data collected at the base station uploaded to the cloud through NodeMCU.

Findings: One of the most reasons for catastrophic failure of the bridges in India is due to the poor maintenance and this phenomenon accounts for more than 60% of bridges collapse. The utmost reasons are Bridge Scouring, Vibrations, Structural Integrity, and Natural Disasters. The current practice of Bridge Health monitoring is represented by collecting the various parameters and placing these parameters over the cloud so that they could be accessed anywhere throughout the globe where internet is available. The reliability of structural health monitoring system is confirmed data acquiring rate of the system, their field measured the result and early warning of disasters.

Improvements/Applications: This bridge health monitoring system is very easily accessible, feasible and durable through new automated remote monitoring technology.

Keywords: Structural Health Monitoring, IoT, XBee, NodeMCU, Sensor Nodes.

1. Introduction

In this particular research interested in to monitor the structural health, identify the damage and put the data of these parameters put over the cloud so that engineers who are specialized in the bridge health monitoring could detect these parameters at the earliest possible stage and avoid an unpredictable outcome, which leads to misfortune. Many of the bridges failures cause a fatality in the form of the human lives, damage of property and economic losses. Visual or localized experiment method such as acoustic or ultrasonic methods, magnetic field methods are in current trends for the most effective method utilized for the monitoring of bridge parameters [1]. The ability to monitor these parameters of the structure is becoming more important from the economic and life safety point of view [2]. For vibration measurement, the system presented is based on vibration collected from a network of acceleration sensor [3, 4]. Another analysis includes the changes in the model frequencies, changes in the measured mode shapes and changes in the measured flexibility coefficient. The main focused on applying a statistical process control (SPC) techniques known as "X-bar control chart" to vibration-based damage diagnosis [5, 6]. Bayesian profolistic methodology for structural health monitoring which uses a sequence of identified model parameter data sets up to compute the probability that continuously updated model stiffness parameter are less than a specified fraction of the corresponding initial model stiffness parameter [7]. Another factor, which contributes to bridging failure, are bridge overloaded and lateral impact forces from the trucks, barges/ships and trains [8, 9]. Scour is also one of the major contributors to bridge failure and Scour failure leads to occur suddenly and without warning or sign of distress to structure. There are many situations where the implementation of the Internet of Things (IoT) for

monitoring regular domestic condition that utilizes cloud computing [10]. Research to improve the tailing dam safety, a tailing dam monitoring and pre-alarm system (TDMPAS) based on Internet of Things (IoT) and Cloud Computing (CC) has accomplished with real-time monitoring of saturated line [11]. This paper includes the monitoring of various parameters of the bridges through cloud computing and reliability of the cloud-based monitoring system is compared with the available bridge monitoring system which provides early warning. A practical prototype has developed for this system, various parameters put over the cloud, and which are accessible through the internet.

2. System Description

The proposed system for implementing Cloud-Based Monitoring System for Bridges is shown in Figure 1 where various data-collecting sensors are placed over a bridge. The main parameters for Bridge health are its Scour level, Bridge Vibrations, Stress and Strain, Wind Pressure and Resistivity of Bridges.

[Figure 1]

The controller unit collects the data from various sensors placed over the bridge. The controller unit is capable of processing both the analog and digital data. The digital data is processed by the digital pins and analog data is converted to digital by Analog to digital conversion. The resolution of ADC is depended upon the number of bits of ADC. The ADC used in the model having 10 bits resolution. Figure 2 showing the block diagram of the model. The data is processed and fed to the controller. The controller unit performs all the operation over the data and sends this data to the Base station node through the RF modem which is capable to transmit data in the vicinity of the bridge. There are different nodes placed within the bridge each having a unique Identification Number (UIN). These data from all the different nodes is collected at the base node. The number of the critical point decides the total number of the nodes within the bridges should be placed to monitor bridge health failure rates are more.

[Figure 2]

3. Sensors

The Real-Time data acquisition designed sensor node is required to be equipped with the different sensors in order to acquire the relevant and sufficient data for bridge health monitoring. The different sensors embedded in sensor nodes are as follows:

3.1. Anemometer

Anemometer is used to detect the speed of wind and wind pressure. It is used with every node and detects the pressure of wind on the bridge. Whenever the pressure exceeds a certain specified limit at any point on the bridge, the node notifies the invigilator about it and suitable actions could be taken before any tragedy happen.

3.2. Strain gauge

Strain or tension on support wire and support pillar should be maintained minimum on bridges. The strain gauge is a sensor whose resistance varies with change in tension, force, weight, etc. The sensor is used at every node to measure tension on the support wire of bridge and support pillars.

3.3. Sonar(scour)

Scour monitoring is very necessary for the health of the bridge. Scour is depletion of the soil layer which is maintained to fix the pillars that support the bridge on river or lakes. It is very important to maintain the soil level that is why sonar is used to sense the soil level near the pillars. Sonar is a technique that is used to detect or sense the object on or underwater.

3.4. Platinum RTD (Resistance Temperature Detector)

This sensor measures the temperature of the object by correlating the resistance of the RTD element with temperature. It consists of a length of fine coiled wire wrapped around a ceramic or glass core. RTD's can process

temperature from -200 to 500°C. It is important to measure the temperature of asphalt pavements, structural steel, and concrete.

3.5. Vibration sensor

Vibration is a common phenomenon for a bridge but it can act as a very helpful phenomenon to monitor the health of the bridge. RKI-3107 is the vibration sensor which gives analog readings of the vibration and is connected with every node. So, whenever the vibration of the bridge increase certain defined value, the node notifies the invigilator of the bridge so, that suitable actions could be taken.

4. Hardware Implementation

The proposed system is validated using virtual simulation and at the same time sensors interconnected to Hardware. The figure below showing the Data Acquisition Board of Sensor node. In the sensor node, the various sensors correspond to the Structural Health Monitoring System are interconnected to the hardware with is Atmel Atmega328 microcontroller with Arduino IDE for coding as shown in figure 3. In this way, the multiple nodes are connected to the different points on the bridge to monitor various data.

[Figure 3]

These all nodes having Radio Frequency Modem especially XBee 2.4GHz operated module used to form a Wireless Sensor Network. The data from various sensors read through Analog to Digital Converter and Serial Peripheral Interface of the controller. This data framed in the form of packets and these data packets are sent to the base station through the RF Module.

Figure 4 showing the Circuit diagram of the base station where the primary unit is the RF Module that receives the data packets sent by the sensor node. The main consideration in the receiver unit is to differentiate the data packets of different sensor node and uploaded them to the cloud. For Cloud communication, NodeMCU controller is used.

[Figure 4]

5. Software Development

The Real-time Data Acquisition system is developed by using Atmel Microcontroller and NodeMCU controller for data uploading to the cloud. The frame chart for the system is developed using Embedded C language where various function developed to acquire data and to process data and to arrange the data in the form of packets and transmit to the base station. Figure 5 shows the flowchart of the software algorithm where each process is done step by step to acquire and process the data. The process data is transmitted to the base station where confirmation is sent back to the transmitter after receiving the desired data packets. If confirmation is not received within the desired duration then this data packet is again transmitted to the base station. Next data packet is only transmitted if the confirmation of previous packets is received. In the base station unit, the data is displayed on the Display and data at the same time it is uploaded to the cloud server. Before uploading the data to the cloud the network connectivity is checked by the ESP Module it connectivity will not available then the connection is terminated by the ESP Module and provide a warning on the display. If connectivity is available then it uploads the data packets to the cloud and from the cloud, this data is accessed by the user using Blynk App. The user authentication is required to access the data through the app and to do this a particular token which is generated by user app is need to be added in the frame chard of Embedded coding. [Figure 5]

6. Result and Discussion

The proposed system mainly focused on monitoring the bridge parameters, which are critical for collapsing of the bridges. This proposed research can simultaneously monitor the bride parameters and to upload these parameters

to the cloud. Blynk App is used to access the parameters and can provide the early indication of the parameters beyond their permitted value can be seen in figure 6. WSN Network ensures the data of all nodes placed alongside bridge should reach to the base station. The warning system code is designed according to the permitted values of different sensors.

[Figure 6]

7. Conclusion

This research helps us to have a check on bridge health monitoring on a real-time basis on the mobile app. The sensor technology used is advanced, robust, accurate and easy to implement. The proposed cloud-based testing system equipped with an advanced sensor used for the Anemometer, Thermistor, Strain gauge, accelerometer, Sonar, etc. The data collected with the help of sensors send to the server and that can be easily accessed by the mobile device. The data collection on a real-time basis and its integration with cloud help research to model the system for the estimation for predictive decay of bridge. The vast domain of structural healthcare to make structures robust enough to sustain natural calamities like earthquake, flood, toroid, etc. In order to make the early broadcast to the emergency conditions, these parameters can also play a major role. The ultimate aim of this research is to protect accident and safe life of people due to bridge structural damage and provide intuitive feedback to the observer regarding damage so that maintenance and measured steps can be taken on time.

FIGURES

Figure 1. Review Model of Proposed System

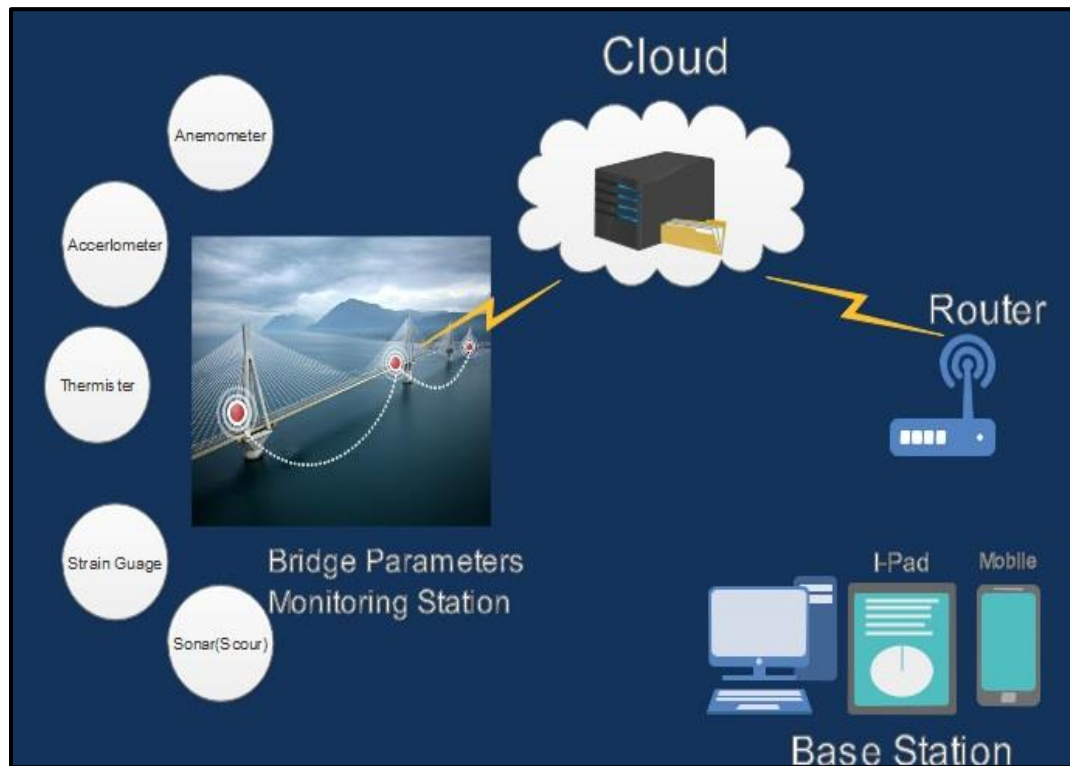


Figure 2. Block Diagram of the Cloud-Based Monitoring System for Bridge Structural Health Monitoring

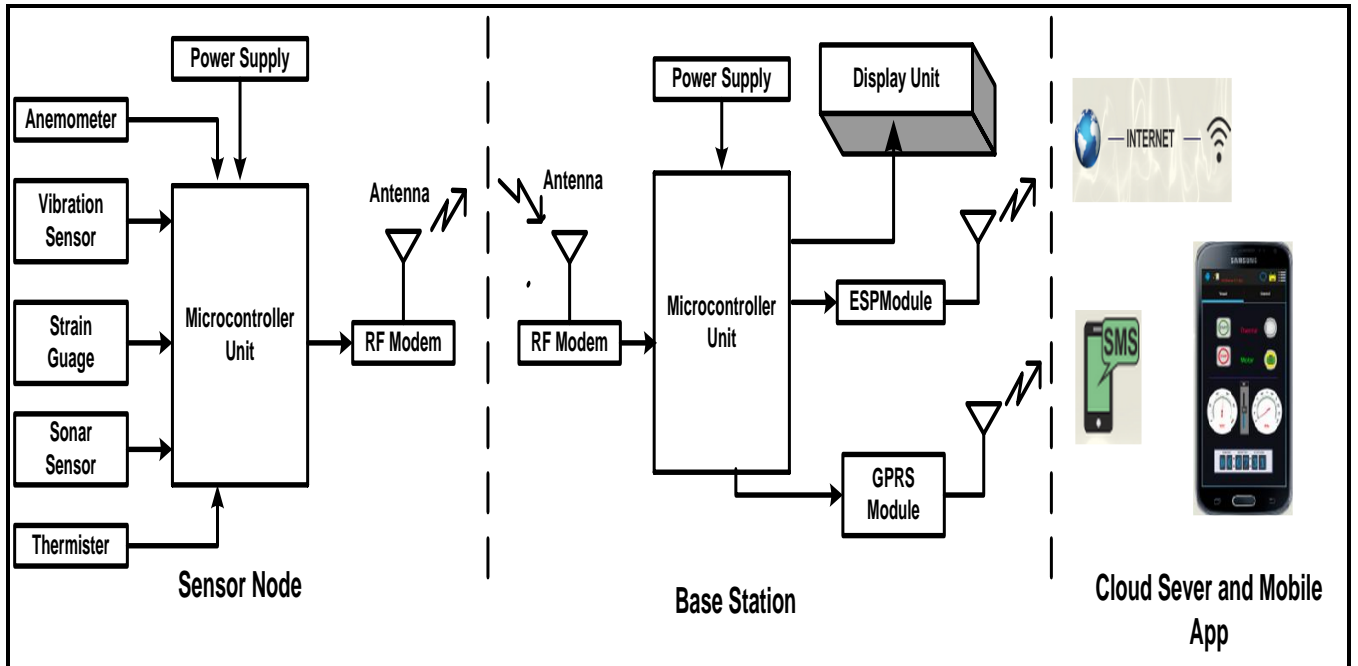


Figure 3. Circuit Diagram of Sensor Node

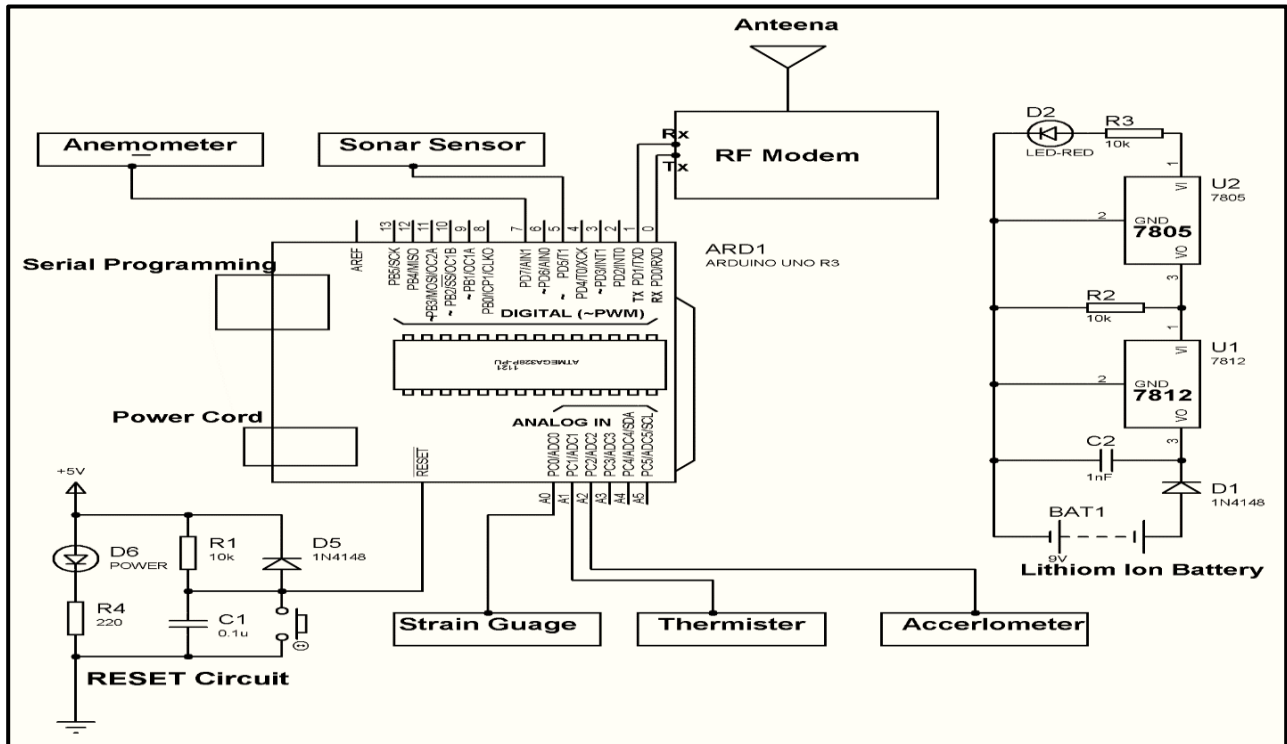


Figure 4. Circuit Diagram of Base Station

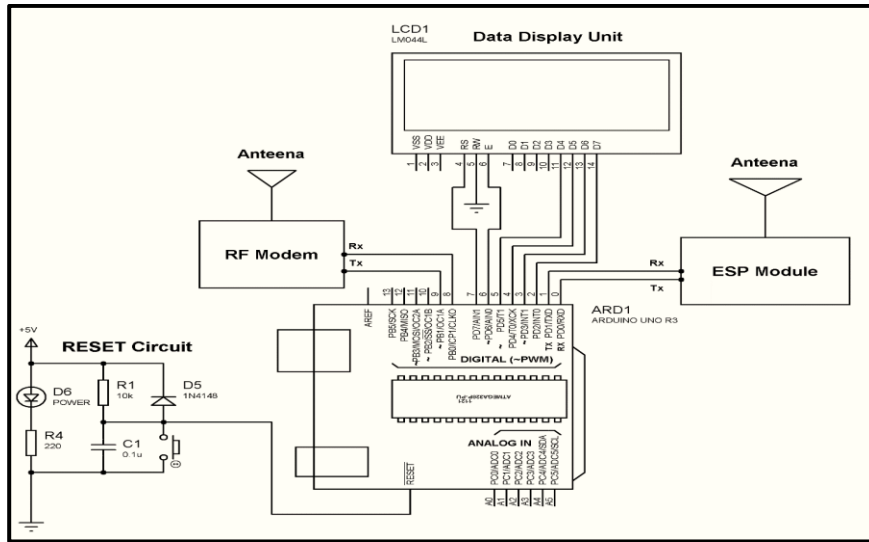


Figure6. The Developed Interface for Bridge Health Monitoring Using Blynk App.

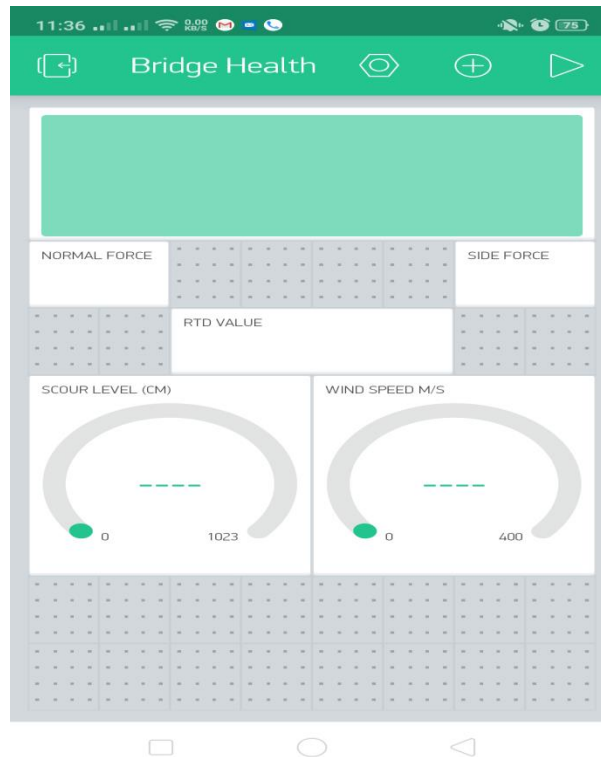
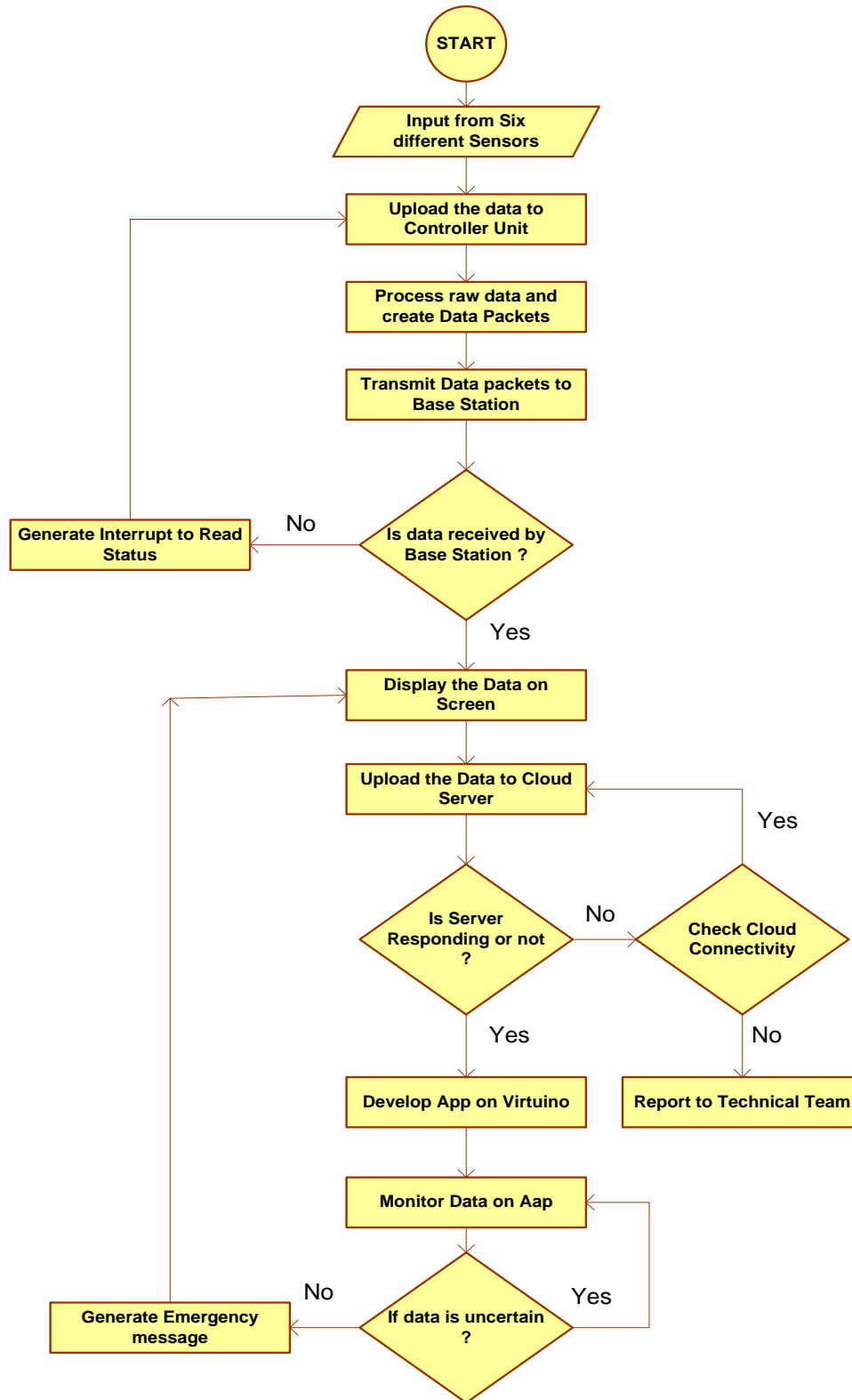


Figure 5. Flow Chart of Software Algorithm



8. References

- [1] Doebling, Scott W., Charles R. Farrar, and Michael B. Prime. "A summary review of vibration-based damage identification methods." *Shock and vibration digest* 30.2 (1998): 91-105.
- [2] Doebling, Scott W., et al. *Damage identification and health monitoring of structural and mechanical systems from changes in their vibration characteristics: a literature review*. No. LA--13070-MS. Los Alamos National Lab., NM (United States), 1996.
- [3] Varnita Verma, R Mishra, *Applications of Wireless Sensor Nodes in Structural Health Monitoring: A Review*, *HCTL Open International Journal of Technology Innovations and Research (IJTIR)* <http://ijtir.hctl.org> Volume 18, Issue 2, February 2016 e-ISSN: 2321-1814, ISBN (Print): 978-1-944170-16-5,
- [4] Sumitoro, Sunaryo, et al. "Long span bridge health monitoring system in Japan." *6th Annual International Symposium on NDE for Health Monitoring and Diagnostics*. International Society for Optics and Photonics, 2001 Sohn, Hoon, Jerry A. Czarnecki, and Charles R. Farrar. "Structural health monitoring using statistical process control." *Journal of Structural Engineering* 126.11 (2000): 1356-1363.
- [5] Vanik, Michael W., J. L. Beck, and SK2000 Au. "Bayesian probabilistic approach to structural health monitoring." *Journal of Engineering Mechanics* 126.7 (2000): 738-745.
- [6] Farrar, Charles R., and Keith Worden. "An introduction to structural health monitoring." *Philosophical Transactions of the Royal Society of London A: Mathematical, Physical and Engineering Sciences* 365.1851 (2007): 303-315.
- [7] Wardhana, Kumalasari, and Fabian C. Hadipriono. "Analysis of recent bridge failures in the United States." *Journal of Performance of Constructed Facilities* 17.3 (2003): 144-150.
- [8] Kelly, Sean Dieter Tebje, Nagender Kumar Suryadevara, and Subhas Chandra Mukhopadhyay. "Towards the implementation of IoT for environmental condition monitoring in homes." *IEEE Sensors Journal* 13.10 (2013): 3846-3853.
- [9] Sun, Enji, Xingkai Zhang, and Zhongxue Li. "The internet of things (IOT) and cloud computing (CC) based tailings dam monitoring and pre-alarm system in mines." *Safety science* 50.4 (2012): 811-815.
- [10] Singh, Rajesh, et al. "Application of icloud and wireless sensor network in environmental parameter analysis." *International Journal of Sensors Wireless Communications and Control* 7.3 (2017): 170-177.
- [11] Singh, Rajesh, et al. "Algorithm to read various sensors to detect the hazardous parameters in industry." *International Journal of Engineering & Technology* 7.2.6 (2018): 19-23.

A Review on Inter-Satellite links Free Space Optical Communication

Gayatri Tiwari¹, Ram Chandra Singh Chauhan²

¹Department of Electronics Engineering Institute of Engineering & Technology Lucknow, India ²Department of Electronics Engineering Institute of Engineering & Technology Lucknow, India
gayatri.10nov@gmail.com¹, rcschauhan@ietlucknow.ac.in²

Abstract –The Free space optical (FSO) communication possesses an advantage over two existing technologies optical fiber communication and wireless communication. Free space optical communication links have promising eminence over microwave communication links with high speed, low weight, and increased security so that they can be boarded conveniently on the satellite. Hence significant use of FSO is inter-satellite optical wireless communication (IsOWC) links, which will be deployed in the future in space. The need for constricting, lightweight, low-power electronics-aggravated by the thriving demand for large data flow rate and bandwidth is urging the use of optical technologies in defense and space. The advancement of the optical components and systems has made it very predominant along with its acceptability in space and defense. Yet a couple of significant components to be dealt with are tracking problems with misalignment of transmitter and receiver apertures and the progressions because of barometrical conditions. Efficiency of the free space optical communication system is seriously rotted due the angle of arrival (AoA) variance and including error pointing. The optical transmitter can be perfectly coordinated with the receiver by utilizing the pointing, acquisition, and tracking (PAT). However, this method is to be carried out under the airborne platform with required restrictions namely size, weight, and power. An overview of promising inter-satellite applications with the challenges have been discussed which sway the performance of the system and make the communication link unattainable.

Keywords: Angle-of-arrival variance (AoA), free-space optical communication, pointing, acquisition, and tracking (PAT).

1. INTRODUCTION

Ongoing years have seen enormous development in the field of information and communication techniques. The majority of this becomes conceivable with progression and utilization of Light wave technology in the field of communication. With fast, information transmission over larger distance has turned out to be conceivable [1]. This offered ascend to the optical wireless communication (OWC) being connected economically. Because of numerous points of interest over custom radio frequency signal (RF), OWC has been as of now connected in number of uses. LASER has been utilized seriously because of their coherent properties and in this way the equivalent is utilized to transmit information in space to convey between satellites orbiting in same or different orbits. This innovation has been named as inter-satellite optical wireless communications (Is-OWC) [2]. With properties like rapid and high limit, Is-OWC system empowers progressively successful, productive and steady activity of satellite system in years to come [3]. In this way by utilization of Is-OWC, a transformative space system can be shaped from satellites which can fill in as both backbone as well as user access nodes. [4-5].

The first inter-satellite links utilized microwaves radio frequency (RF ISL) worked under Ka- band frequency groups which prone to be helpful for mobile satellite system. It is helpful in mobile satellite system (MSS) for example, Iridium Next and Artemis, however with the quick improvement of satellite interchanges which requires a massive bit rate [6], further to proceed towards the optical ISLs is important as it is referred to by their focal points, for example, high information rate, an enormous transfer speed, long communication distance, minute transmission power with improved reliability and being cost effective, small antenna diameter and, more reliability and information security. Likewise, it is simple for multiplexing, De-multiplexing, exchanging, and directing adaptability of the system applications. The primary optical ISL between satellites utilizing laser light was set up between the European Space Agency's (ESA) and the French agency possessing Artemis satellite and the SPOT-4 a Earth perception satellite was the primary optical ISL utilizing laser light under the guidance of an experiment called Semiconductor Laser Inter satellite link experiment [8], [7]. For optical ISLs, three specialized parameters are important to set up an association between satellites; initial one is the frequency bands where it is in the scope of Tera Hertz (THz) to accomplishing huge information rate (Table I). The fundamental thought of transmission of the signal exposed to the free space experiences loss since zero absorption occurs in the signal. Reason to this loss is the non-alignment of the atmosphere.

And second one is a technique named as multiple access which is used for allocating the capacity of satellite transponder for the interference escaping among the approaching signal via satellites for the concerned earth stations [9], station limit is $C=B \log_2(1+S/N)$, where 'B' refers to the transfer speed, and S/N symbolizes ratio of signal to noise ratio. Thus the multiple wavelengths are utilized for the increment in the system limit at the time of

Table I. OPTICAL FREQUENCY AND TRANSMITTED POWER

Types of Laser	Wavelength(μm)	Transmitted Power
Solid state Laser Diode		
ALGaAs	0.8-0.9	About 100mW
InPAaGa	1.3-1.5	About 100mW

Nd:YAG	0.532	100mW
Gas Laser		
CO ₂	10.6	Several tens of watts

demand approaching towards the final extent of single optical channel [10].

The method of modulation is used which is supposed to be critical for the optimum modulation format [11] regarding a most extreme theoretical limit. This idea gives additionally phenomenal security which increases the immunity against jamming and interception [10]. The concerning point of this particular paper is to review about the inter satellite optical wireless communications, which transfers the data and collects the information among the satellites, and detailed examination with clarification of the need to choose optical transmission. A review on different difficulties looked by FSO communications system for inter-satellite links has been deliberated. Section I present the brief introduction on IS-OWC system. While Sections II discuss some related work and explain the different types of challenges for inter-satellite links confronted by FSO communication system. Section III discusses the advantages of IS-OWC over RF communication system. Last section is a conclusion and gives future perspective for the optical inter-satellite links.

1.1. Is-OWC SYSTEM

Communication between two satellites is represented in the fig. 1. Whereas, fig 2 describes the coverage of the Earth’s surface area by the inter satellite laser links.

By free space optics, signal is transmitted between two satellites in Is-OWC [38]. Block diagram of the Inter-satellite Wireless Optical Communication (Is-OWC) represented by the Figure 3.



Fig. 1 Inter-satellite Optical communications [13]



Fig. 2 Inter-satellite laser links around the Earth [13]

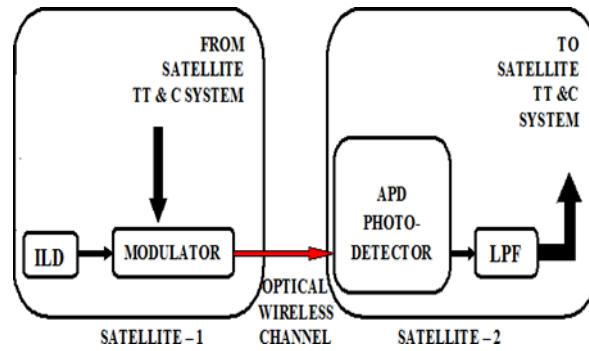


Fig.3 basic system block diagram for simplex communication in Is-OWC. [13]

1. Transmitter

LASER is a source which produces light and it is carried by transmitting satellites, as well as used for tracking, satellite telemetry, for communication system and an optical modulator [15]. The information which is regularly transmitted by a satellite is same as the zone of the satellite and following of attitude, picture getting the data for which transmission is done by a satellite are, for instance, the satellite territory and atmosphere following for isolated distinguishing satellite and communicating data got ready for handset system passing on satellite. The most liberal portion in the structure is light source as correspondence is done by transmitting light. Two sorts of optical light sources are used in optical correspondence, i.e., Light-emitting diode (LED) and injected laser diode (ILD). Development of these devices is done by semiconductor materials with the relationship of positive and negative charges semiconductor yielding photons or light imperativeness. Radiation of light from ILD monochromatic, sound and has over the top vivacity making it fitting for covering colossal division for transmitting in free space [16-17].

2. PropagationMedium

Considering the condition of Is-OWC framework, optical remote channel is viewed as the transmission medium. OWC channel is vacuum and free from losses like climatic losses in opposition to free space optics which is acquainted with a few losses attributable to climate and air debilitation [18]. Taking the perfect case, transmitting distance is the particular origin for signal attenuation. At the transmitter and the beneficiary side, utilization of optical antenna or optical lenses is formed. Broad divergence of light beam acceptance is allowed by the optical antenna.

3. Receiver

The signal on the recipient side of the Is-OWC incorporates a photodiode and a low pass channel. The detected received signal is accepted by photodiode that changes it into an electrical signal [19]. Photodiode involves positive and negative charged semiconductor connection, connected in reverse bias simply like in an optical light source [20-21]. Photons strike the junction then only an electrical signal is produced. Since having peculiar features as large amplification of weak light signals in free space optical transmission, APD is used [22].

2. RELATEDWORK AND CHALLENGES IN INTER-SATELLITE LINKS FREE SPACE OPTICAL COMMUNICATION

Atmospheric impacts which affects the result of communication between ground to satellite and satellite to ground. Free space optical innovation utilizes environmental window to breach having characteristics arbitrary as similar to time and space. For inter-satellite FSO links, different constraining elements incorporate availability of link, surround noise and pointing. The respective paper encompasses various difficulties experienced by data designers with respect to laser uplink/downlink just as inter-satellite FSO links. Free space optical links are not exposed to the climatic changes or the disturbances because of the clouds since the satellite orbits are placed distant from the atmosphere. For such situation, real test was performed using the acquisition and tracking of the respective two satellites moving at a considerable relative speed. Since large distances have to be covered by the inter-satellite, hence the strategy of the transmission should be of high power efficiency with relatively good sensitivity on the recipient part.

Thus the homodyne or heterodyne being the techniques of the coherent phase are placed convenient over direct detection methods at the inter-satellites free space optical links. At the resultant of view the above techniques present remarkable sensitivity at the receiver end delivered at high capacity links [23], [24]. Considering in today's time the most elevated transmission in between LEO to LEO at a high speed of 5.6 Gbps is the homodyne BPSK transmission. The European Data Relay Satellite System (EDRS) was created by the renowned European space agency which effectively exhibited interface among Alphasat in GEO and Sentinel-1 in LEO at 1.8 Gbps in 2014 [25]. A detailed examination of the elements of the inter-satellite FSO links were expected for 1000 km separation at a speed of 2.5 Gbps. On the contrary knowing the fact that there was no exposure of the free space optical links to the climates and air restrictions. The Doppler shift, background radiations, acquisitions, Point ahead angle, tracking and satellite platform stability were responsible to be the difficulties for any constraints to the FSO for every case. These difficulties are talked about as pursues.

1. Point ahead angle

The comparative movement between the transmitter and receiver terminals requires the arrival signal to offset from the beacon location with the goal to adequately hit the recipient upon an appropriate location known as spatial temporal location. The pointing of the offset is called PAA. The time taken to travel for the long distances of cross link is dependent on the comparative speed of the two satellites. The degree of the PAA is of hundreds of micro radians considering space optical links where as it is normally many miniaturized scale radians for satellite to satellite and ground to satellite. Fig.4 delivers the idea of PAA sharing the optical beam sent by LEO and time 'T' and arrival beam from GEO at 'T+4T'. So for exact pointing accuracy, the adjustment of the receiving and transmitting terminals is done utilizing link maintenance control and tracking algorithm [26, 27]. For most part, an impact observed named point ahead angular anisoplanatism is experienced for the condition PAA greater than isoplanatic edge from

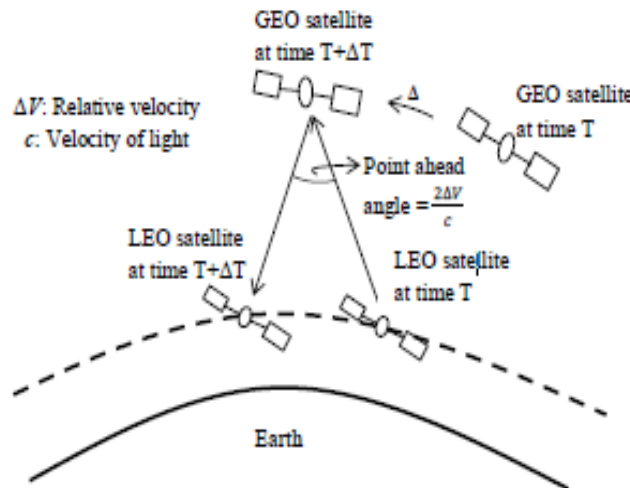


Fig. 4 Concept of PAA in space communications[26]

tracking direction. Generally it is brought about by the mismatch of the laser beam from the beacon path.

2. Doppler Shift

The variation in the recurrence of the received signal because of the relative movement among transmitter and receiver prompts Doppler impact. Occurring in inter orbit satellite links where the satellite in lower orbits travel quicker than at higher orbits. Range of movement to be rapid via information hand off framework is $\pm 7.5\text{GHz}$ for the transmission LEO and GEO respectively.

The two LEOs can possess higher move engendering in inverse ways. The frequency move generated by Doppler around 140 kHz move in a 2GHz clock time frame utilized for flagging. It requires a wide range of recurrence tuning for optical input filters or local oscillator (LO) lasers if there should be coherent optical link. This Doppler shift must be thought about for dependable FSO between satellite connections.

The Doppler shift achieves a greatest worth when the radial part of the relative speed achieves its most extreme. Carelessness of Doppler impact brings about loss of information and recurrence simultaneity issues at the beneficiary end. Incorporation of an optical phase lock loop (OPLL) procedure with the LO laser is needed for diminishing Doppler shift [28]. The agreeable recurrence tuning among the transmitters and LO at the collector is actualized to oppose the impact of Doppler shift. As far as a beat signal (distinction of transmitter and LO recurrence) is accessed, the recurrence procurement procedure starts with the adjustment of LO with an open recurrence control loop close to transmitter.

Recurrence tracking mode starts to lock on to the heterodyne recurrence control loop or homodyne loop, when the beat signal is retrieved. The utilization of the optical injection locking (OIL) method is other method; there is a downside that the locking recurrence range is constrained to commonly 1 GHz or less [29]. Both OPLL method and OIL procedure i.e., utilization of an optical phase injection lock loop (OIPLL) strategy, that is used to lock the recurrence and phase under Doppler shift circumstances. A pilot-bearer coherent LEO to ground downlink utilizing OIPLL Doppler recurrence move is shown in [30]. The impact of Doppler move in homodyne inter-satellite communication link is investigated in [31]. Ideal transfer speed of the optical filter is resolved for the whole length of recurrence movements to improve the framework execution. The recurrence move prompted by Doppler impact is portrayed for LEO satellite constellation with optical inter-satellite links in [32]. For coherent homodyne recipient with optical phase lock loop the Doppler shift recurrence compensator is researched in [33].

3. Satellite vibration and tracking

The LOS signal is received by acquiring and tracking of the signals, such signals are created by the satellite or by the on-board laser communication sub-assembly. The above process of tracking such signals is a tough task for the FSO links. The different unsettling influences created externally due to the satellite are there because of the various aspects such as thrusters, momentum wheels, gimbal packages and solar panels etc. There also exists various sources of noise caused by on-board laser communication system which comprises of Relative Intensity noise, background noise, dark current, shot noise, thermal noise and signal shot noise. Satellite vibration and tracking issues and the discussion for restitution contemplated in [34].

4. Background noise sources

The inter-satellite link observes some noises whose origin relies upon the detection method whether the system being pre-amplified or not optically. To detect the noise sources directly at the receiver's end it is often observed that the noise formation is coming from bulk dark current this is the detector as well as the receiver amplifier. Which results in pre-amplifier noise and thermal noise and lastly the noise due to the signal i.e., shot noise. The local oscillator shot noise leads the system sources of the noise to detect coherently. Whereas, the stellar and celestial radiant fluxes results in the background sources of noise. The light dispersing from optics structure comprised with the light falling on the detector adds to the background noises.

5. Acquisition, tracking and pointing (ATP)

In free space optical communication system pointing and acquisition of optical beam is a demanding concern in ground to satellite, inter satellite and satellite to ground links.

Vuong V. mai et al [43] studied about the high-elevation airborne stages are connected to each other with the help of optical communications in free space. As a result it developed as a promising answer for setting up remote systems for rustic and remote zones. The exhibition of FSOC framework is seriously corrupted due to the vacillation of angle of arrival (AoA) and pointing delusion. The arrangement of optical transmitter and recipient is accomplished by utilizing the pointing, acquisition, and tracking (PAT); however the above structure should be compatible to work inside the space conquering of various challenges on dimensions, weight and power. Because the platform of airborne is on the speedy shift, hence the PAT works quickly which is very alluring. As for the outage probability and for the most favorable beam dimension at the transmitter and receiver, the closed-form expression is allotted for this suggestion. For the précised derivation of the theory the Monte Carlo simulations is used for the confirmation. The airborne FSOC system with fixed beam dimension above outspread radius of AOA variation and pointing delusion having the adjustable beam control strategy conquer the system.

Yagiz Kaymak et al [44] have given an extensive overview on optical communications in free space use ATP structure. Provided mobile communications adopt ATP structure is a demanding fundamental. As for obtain Line of sight, the proper adjustment of FSO transmitted receiver is needed and this is possible by using ATP structure. The classification of overviewed ATP structure is done as per their working assumptions, valued cases, exercised technology. The preferences and inconveniences of reviewed ATP components are recorded and talked about. Additionally talk about current difficulties and future research headings.

Pointing and acquisition of optical beam turn into a primitive concern for the ground to satellite, inter satellite and satellite to ground FSO communication links. It happens because of the platform jitter disturbances, and narrow beam divergence of the optical beam [35]. Carrying wide range of FOV, coarse detection is executed under the mode of acquisition. At the receiver end there exist a detector which identifies based on the sensitivity of the position of the beacon signal. The receiver also continues to search for the required signal in its FOV side by side. While presentation of the free space optical link is constrained because of fluctuating pointing framework brought about by given stochastic systems: (i) following commotion made by the electro-optic tracker and (ii) vibrations made by inner satellite mechanical systems. The impact of satellite vibration and stage jitter is portrayed in [36]. The incorrect arrangement by any one may bring about connection disappointment or seriously debase the presentation of the framework.

The acquisition procedure is first tread for formation of free space optical link and it include the transmission scanning with its limited beacon signal over an ambiguity range. In large background radiations the beam location by the receiver helped with beacon signal which is having adequate peak power and small pulse rate. [37]. The once the guide signal is identified, the accepting terminal utilizes beam controlling components to point a relentless guide signal towards the starting terminal frequently balanced by fixed PAA. Fig. 5 demonstrates the essential idea of ATP for a space FSO correspondence framework.

The telescopic assists in collecting the uplink signal from the ground level which is further directed towards dichroic beam splitter-1. The splitter-1 will direct the coming signals to splitter-2 which later on guides the incoming signal to the ATP subsystem co-coordinating with signal's wavelength. Lastly the beam splitter-3 converges the images from the initial situation on the focal pixel array (FPA). The area of this point on the exhibit speaks to the course from the received reference point signal in respect to the telescope's pivot (the focal point of the exhibit).

Which opt for the telescopic approach for the FOV. By the above approach the spatial securing procedure is carried out and on the other hand capturing the ground zero situation of the station on to the FPA. Finally the signal is escorted from the satellite towards the receiver located at the base station thus shaping an interface for the LOS. Hence the reference point signal is obtained, governs the rational signal to taper down the FOV till the time the duo frameworks gets bolted among themselves. Hence to start discovering the signal at the receiver satellite signal range request in the space, the signal range should

be as per the requirement as well as the energy quotient (of the signal)

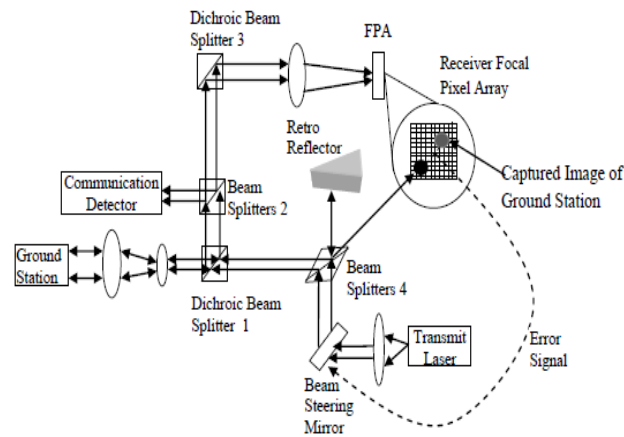


Fig. 5 The ATP system between Ground station and on-board satellite [45]

Obtained) should also be genuine to initiate the recurring circuit on its own. Regularly, the change from securing to following stage takes not exactly one second. At times, beaconless pointing utilizing divine reference source just [38], [39] is utilized to give an ideal pointing reference. This engineering furnishes a disentangled activity with extensive power sparing as it disposes of the need of additional reference point signal.

3. ADVANTAGES OF Is-OWC

In the previous years, the inter-satellite optical wireless communication has turned out to be well known because of the succeeding advantages:

1. *High Data Rates:* With the assistance of light as carrier frequency it is acceptable to be amplified using quick inter-satellite links [40]. Which flares up the information rates to Gbps to be used in the communication of the satellites optically.
2. *Unlicensed Spectrum:* The optical inter-satellite communication neither requires the necessity of license of spectrum nor for the co-ordination of the frequency as used in radio and microwave systems. Interference is certainly not a main task from or to system and furthermore, point-to-point laser signal is immensely difficult to intrude on, making it secure and safe.
3. *Smaller Wavelength:* The wavelength of light is significantly less with respect to microwaves. Signal wavelength of optical inter-satellite communication over RF/Microwave communication system is carrying huge variation. In this manner, RF/Microwave with respect to light wave describes the tapering nature of the thickness of the beam for respective magnitude of the signal. [41].
4. *Huge Bandwidth:* The transmitting data in any communication system is associated with the modulated carrier bandwidth. Data transmission of around 2000 THz is utilized as per the methods described for the high frequency optical carrier.
5. *Reducing Antenna Size:* The size necessity of the transmitter and receiver antenna is huge and furthermore massive if RF/Microwave system is to be dynamic. While the antenna size gets diminished to centimeters just as its carrier frequency is enormous, in optical inter-satellite communication system. Thus the satellite heaviness is reduced and power need is also decreased in optical inter-satellite communication system [42].
6. *Small width beam dimensions:* A small width beam is perceived for optical emission and its example a laser beam which is having diffraction restrained disparity in 0.01 to 0.1 μ rad. This shows transmitting force is engaged with a thin range giving an optical inter-satellite link giving sufficient isolation from its probable interferers.

The different focal points incorporate insusceptibility to the radio frequency interferences, faster communication, power efficiency, high accuracy or more all wireless optical communication doesn't contaminate the environment with electromagnetic radiations. All the subtleties determined are dynamic in an optical inter-satellite communication system since it can diminish the payloads and along these lines diminishing the cost.

4. CONCLUSION

As technology has advanced, methods for communication have additionally changed. Is-OWC is a phenomenal technology which has been generally utilized and investigated for terrestrial communication and broadcast purpose. As after contemplating the related work of this field it is presumed that to accomplish more work on the different quality components like increase in bandwidth, transfer capacity, to upgrade the number of clients that can take an interest in the communication all the while. Thus further upgrades should be possible so as to evacuate these challenges discussed above by utilizing trendy mechanisms. Different advanced modulation formats can be utilized too for improving existing limit of the Is-OWC systems.

5. REFERENCES

- [1] Someda SG. Electromagnetic Waves. Great Britain: Chapman & Hall, 1998.
- [2] Karafolas N et al. (2000). Optical satellite networks, *Journal of Lightwave Technology*, 18 (12), 1792-1806.
- [3] Franck L et al. (2002). Routing in networks of inter-satellite links, *IEEE Transactions on Aerospace and Electronic System*, 38 (3), 902-917.
- [4] Sharma, A., Chaudhary, S., Thakur, D., Dhasratan, Vigneswaran "A Cost-Effective High-Speed Radio over Fibre System for Millimeter Wave Applications", *Journal of Optical Communications*, Published Online: 2017-12-15 | DOI: <https://doi.org/10.1515/joc-2017-0166>.

- [5] K. K. Upadhyay, S. Srivastava, N. Shukla, and S. Chaudhary, "High-Speed 120 Gbps AMI-WDM-PDM Free Space Optical Transmission System," *Journal of Optical Communications*.
- [6] Heine, Frank, et al. Optical intersatellite communication operational Military communications conference, 2010-milcom 2010. IEEE, 2010.
- [7] Khalighi, Mohammad Ali, and Mustafa Uysal. "Survey on free space optical communication: A communication theory perspective
- [8] Purvinskas, R. A. J. (2003). Interplatform links. University of South Australia.
- [9] Wood, Lloyd, Will Ivancic, and Klaus-Peter Dörpelkus. "Using lightemitting diodes for inter-satellite links." *Aerospace Conference*, 2010 IEEE.
- [10] Chan, Vincent WS. "Optical satellitenetworks." *Journal of Lightwave Technology* 21.11 (2003): 2811.
- [11] Djordjevic, Ivan, William Ryan, and Bane Vasic. *Coding for optical channels*. Springer Science & Business Media, 2010.
- [12] Bjarklev, Anders, Dipak Chowdhury, Arun Majumdar, Masat aka Nakasawa, Carlo G. Somena, and Hans-Georg Weber. *Optical and Fiber Communications Reports*.
- [13] Shekhar S and Gupta A., "Inter-Satellite Optical Wireless Communication Link (IsOWC)", LAP Lambert Academic Publishing, 2014.
- [14] Chan V.W.S, "Free space optical communication", *Journal of Lightwave Technology*, 24 (12), 4750-4762.
- [15] Moli-Sanchez L et al., "Performance analysis of quantum cryptography protocols in optical earth-satellite and inter-satellite links", *IEEE Journal on Selected Areas in Communications*, 27 (9), 1582-1590.
- [16] Dang A, "Simultaneous Acquisition and Track Scheme with Multiple Terminals Based on Subspace Method for Optical Satellite Networks", *IEEE Transactions on Aerospace and Electronic Systems*, 46 (1), 263-277.
- [17] Ghosna F.J. et al., "Pulse Position Modulation Coding Schemes for Optical Inter-satellite Links", *Journal of IET*, 46 (4), 290-291.
- [18] Donner A et al., "Satellite networks for aeronautical communication: traffic modeling and link load analysis", *IET Communications*, 4 (13), 1594-1606
- [19] Chatzidiamentis ND, "Adaptive Subcarrier PSK Intensity Modulation in Free Space Optical System", *IEEE Transactions on Communications*, 59 (5), 1368-1377.
- [20] Xie W et al., "Received Signal Strength Reduction Analysis Based on the Wavelet Model in Inter-satellite Laser Communication", *IEEE Journal of Lightwave Technology*, 29 (15), 2327-2332.
- [21] Yang Y et al., "Research Bit Error Rate in the Presence of Local Wave front Aberration in Inter-satellite Laser Communication", *IEEE Journal of Lightwave Technology*, 29 (19), 2893-2898.
- [22] Arruego I et al., "In-orbit measurement of SET and DD effects on optical wireless links for intra-satellite data transmission", *IEEE Transactions on Nuclear Science*, 58 (6), 3067-3075.
- [23] B. Smutny, R. Lange, H. Kämpfner, D. Dallmann, G. Mühlhnikel, M. Reinhardt, K. Saucke, U. Sterr, B. Wandernoth, and R. Czichy, "In-orbit verification of optical inter-satellite communication links based on homodyne BPSK," *Proc. SPIE, Free-Space Laser Communication Technologies XX*, vol. 6877, 2008.
- [24] B. Smutny, H. Kaempfner, G. Muehlnikel, U. Sterr, B. Wandernoth, and F. Heine et al., "5.6 Gbps optical intersatellite communication link," *Proc. SPIE, Free Space Laser Comm. Tech. XXI*, vol. 7199, 2009.
- [25] "Laser link offers high speed delivery," *ESA Press Release*, 2014.
- [26] X. Ma, T. Herbst, T. Scheidl, D. Wang, and S. Kropatschek et al., "Quantum teleportation over 143 kilometres using active feed-forward," *J. Nature*, vol. 489, pp. 269-273, 2012.
- [27] Z. Zhou, H. H. Refai, P. G. LoPresti, and M. Atiqzaman, "Control algorithm development for mobile FSO node alignment," *IEEE/AIAA 28th Digital Avionics Systems Conference*, pp. 6.A.3-1 – 6.A.3.12, 2009.
- [28] M. Guelman, A. Kogan, A. Kazarian, A. Livne, M. Orenstein, and H. Michalik, "Acquisition and pointing control for inter-satellite laser communications," *IEEE Trans. on Aerospace and Elec. Sys.*, vol. 40, no. 4, pp. 1239-1248, 2004.
- [29] J. M. Kahn, "1 Gbit/s PSK homodyne transmission system using phase-locked semiconductor lasers," *IEEE Photon. Electron. Lett.*, vol. 1, no. 10, pp. 340-342, 1989.
- [30] O. Lidoyne, P. Gallion, C. Chabran, and G. Debarge, "Locking range, phase noise and power spectrum of an injection-locked semiconductor laser," *Proc. Inst. Elec. Eng.*, vol. 137, no. 3, pp. 147-154, 1990.
- [31] Y. Shoji, M. J. Fice, Y. Takayama, and A. J. Seeds, "A pilot-carrier coherent LEO-to-ground downlink system using an optical injection phase lockloop (OIPLL) technique," *J. Lightwave Tech.*, vol. 30, no. 16, pp. 2696-2706, 2012.
- [32] F. Zhao, S. Yu, J. Ma, and L. Tan, "Effect of Doppler shift on differential phase-shift keying receivers using interferometric demodulation and balanced detection in intersatellite laser communication links," *Opt. Eng.*, vol. 49, no. 10, 2010.
- [33] Q. Yang, L. Tan, and J. Ma, "Doppler characterization of laser inter-satellite links for optical LEO satellite constellations," *Opt. Comm.*, vol. 282, pp. 3547-3552, 2009.
- [34] T. Ando, E. Haraguchi, K. Tajima, and S. Yamakawa, "Coherent homodyne receiver with a compensator of Doppler shifts for inter orbit optical communication," *Proc. SPIE, Free-Space Laser Communication Technologies XXIII*, vol. 7923, 2011.
- [35] S. Arnon, "Power versus stabilization for laser satellite communication," *Appl. Opt.*, vol. 38, pp. 3229-3233, 1999.
- [36] T. Ho, *Pointing, acquisition, and tracking systems for free-space optical communication links*. PhD thesis, University of Maryland, 2007.
- [37] G. A. Koepf, R. Peters, and R. P. Marshalek, "Analysis of burst error occurrence on optical intersatellite link (ISL) design," *Proc. SPIE Opt. Technol. for Commun. Sat. Applica.*, vol. 616, pp. 129-136, 1986
- [38] T. N. T. Nguyen, "Laser beacon tracking for free-space optical communication on small-satellite platforms in low-Earth orbit," *Master's thesis*, Massachusetts Institute of Technology, 2015.
- [39] B. G. Boone, J. R. Bruzzi, B. Kluga, and W. P. Millard et al., "Optical communications development for spacecraft applications," *Johns Hopkins Apl. Tech. Digest*, vol. 25, no. 4, pp. 306-315, 2004.
- [40] C. Hindman and L. Toberton, "Beaconless satellite laser acquisition-modeling and feasibility," in *Military Comm. Conf. (MILCOM)*, pp. 41-47, 2004.
- [41] Chen H et al., "Approach for earth observation satellite real-time and playback data transmission scheduling", *Journal of Systems Engineering and Electronics*, 26 (5), 982-992.
- [42] Uysal M., "Optical Wireless Communications", Switzerland: Springer International Publishing, 2016.
- [43] Sanctis MD et al., "Satellite Communications Supporting Internet of Remote Things", *IEEE Internet of Things Journal*, 3 (1), 113-123.
- [44] Vuong V. mai et al., "Beam Size Optimization and Adaptation for High-Altitude Airborne Free-Space Optical Communication Systems", DOI:10.1109/JPHOT.2019.2901952 1943-0655 C _ 2019 IEEE.
- [45] Yagiz Kaymak et al., "A Survey on Acquisition, Tracking, and Pointing Mechanisms for Mobile Free-Space Optical Communications", DOI:10.1109/COMST.2018.28043231553-877X *IEEE Communications Surveys & Tutorials (Volume: 20 , Issue: 2 , Secondquarter 2018)*
- [46] H. Hemmati, *Deep Space Optical Communication*. John Wiley & Sons, New York, 2006.

Droid Analyzer: Efficient Framework for Android Malware Detection

Parvesh Mamgain¹Jasraj Meena²

¹Research Scholar Department of Information Technology Delhi Technological University
New Delhi, India²Assistant Professor Department of Information Technology Delhi
Technological University
New Delhi, India

mamgainparvesh@gmail.com¹jasrajengg@gmail.com²

Abstract — Android is a popular mobile platform with millions of applications. Its popularity has attracted the attention of malware developers. This has led to an increase in risk associated with Android devices. The growth of mobile malware is so huge that traditional techniques for malware detection are inefficient. Therefore, effective and robust malware detection techniques are required. Many researchers have proposed static and dynamic approaches for effective detection of android malware. In this research, we have proposed a fine-grained hybrid model for efficient android malware detection using multi-modal learning. We have extracted features from a set of 4000 applications by using static and dynamic analysis. We have used multi-modal learning to better classify the samples. We have compared our implementation with other techniques. Our analysis suggests that multi-modal learning yields good results.

Keywords — Static Analysis, Dynamic Analysis, Android, Malware Detection, Multi-Modal Learning

1. INTRODUCTION

Android is a popular mobile platform with millions of applications [1]. Android has a large market share and most of the users are using android devices. User devices hold sensitive information that can be exploited if fallen into the hands of a hacker. Sensitive information includes IMEI, contact list, saved passwords, etc. Malwares and other techniques are used by hackers to gain unauthorized access to user device. A malware is a malicious program used for malicious purposes like gaining unauthorized access, stealing information, etc. There are different types of malwares like viruses, spyware, Trojan horses, rootkits, backdoors, etc. [2]–[6]. Hackers use variety of techniques to distribute these malwares into user devices like repacked apps, malicious website, third-party app store, etc. Malware has grown exponentially from 2014 to 2019 as shown in fig. 1 [7]. There are many reasons for huge malware growth in android like Larger Attack Surface, Open Source and loose security in Google play store. These shortcomings have led to an increase in the growth of Android malware. According to Quick Heal annual threat report 2019, there is a huge increase in Android samples detection count from 2016 to 2019 [8]. Reports suggest the rise in profit-driven malware like ransomware, adware, potentially unwanted programs (PUP), premium SMS, etc. The report also suggests that malware infection rate is not uniform across the world rather it varies on the basis of geographical areas like mobile malware infections in Iran, Bangladesh, China, India, and Nepal are 35.12%, 28.3%, 27.38%, 21.91%, and 20.78% respectively. This data also suggests that there exist some countries that may become a victim of malware attack due to poor security infrastructure. Many researches have been studied for analyzing and detecting malware based on static and dynamic analysis using machine learning techniques. They work by extracting features from the applications and then building the model based on the feature vector.

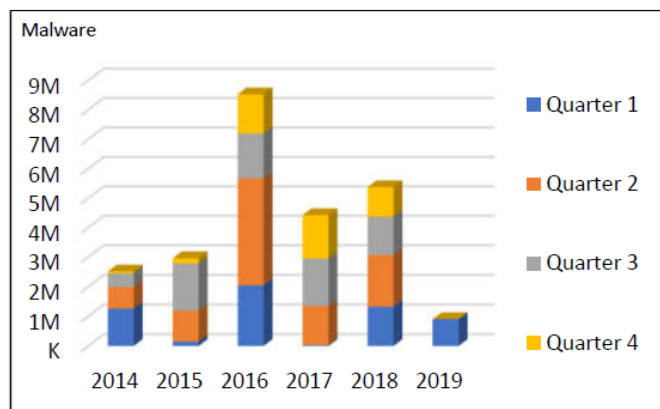


Fig. 1: Mobile Malicious Installation packages detected by Kaspersky Lab [2]

In this paper, we have proposed an efficient technique for effective android malware detection using a multi-modal deep neural network. We have compared our technique with other approaches [9], [10]. We have also extended these approaches for dynamic and hybrid analysis. We have performed the analysis by extracting features from a large dataset of 4000 applications using static and dynamic analysis. We have reduced the features by using Information Gain Attribute selection algorithm. The analysis has been carried out on a large dataset of 4000 applications with 2000 benign and 2000 malware applications. The benign apps are collected from AndroZoo Repository [11] and Malware apps are collected from VirusShare repository [12]. Our result shows that multi-modal neural network is an effective alternative and can be used for android malware detection. Our analysis also suggests that machine learning models yield a better result when features are provided in the form of different modalities separately rather than combining all the features into one long feature vector. The remaining part of this paper is arranged as follows. Section II briefly discusses related work. Section III discusses the implemented architecture for malware detection. Section IV discusses the results of our analysis and Lastly, Section V presents the conclusion.

2. RELATED WORK

Traditional malware detection methods are signature-based. A unique signature is generated for each malware found by extracting segments from code. Its drawbacks are ineffective to detect a zero-day error, Distribution of newly generated malware is a costly process and obfuscation attacks can bypass it. This leads to the development of heuristic-based detection approaches. Machine learning-based detection methods provide reliable and robust malware detection by extracting static and dynamic features. Static analysis-based approaches are widely popular [9], [10], [13]–[15]. Arp et al. proposed a static framework that uses permissions, activities, services, system events, etc. as features for classifying malware [10]. The research was based on support vector machine for model creation. Yuan et al. proposed a static framework using rotation forest model to better classify the dataset [9]. However, static approaches are inefficient to determine the obfuscated code. To detect obfuscated code, dynamic analysis approaches are used [16]–[19]. Feng et al. implemented a dynamic framework based on ensemble learning techniques [17]. They have used system calls, network logs, API Calls, etc. as features to better classify malware. Many types of research are carried out by using a combination of both techniques. It was found that the hybrid approach gives the best result [20]–[22]. Yuan et al. implemented a hybrid approach using both static and dynamic features and was able to

achieve good accuracy [21]. Deep learning is a relatively new field that is becoming popular now a days. Many researchers have used DNN for malware detection and achieved good results[23]–[25].

In comparison, our work is motivated by some of the above techniques and approaches, but with a focus on multi-modal learning using a deep neural network. We have used features extracted from a large dataset of 4000 applications using static and dynamic analysis, collected from AndroZoo [11] and VirusShare repository [7]. We have extracted a huge set of features from the application set. Considering the existence of noisy and redundant features, we have used a feature selection algorithm to reduce the size of the feature set. We have used information gain algorithm to reduce the size of the features. Our results show that recent advances in neural network approaches can be used as a better classifier when compared with traditional approaches.

3. PROPOSED FRAMEWORK

This section gives a brief overview of the proposed framework in depth. We have defined the general framework and then discussed the proposed framework in detail. Malware detection techniques that uses machine learning for effective malware detection follows this framework with modifications [26]. The steps are defined in the fig. 2. The research methodology can be broadly classified into four major steps which are as follows – Dataset Creation, Feature Extraction, Feature Selection and Model Creation.

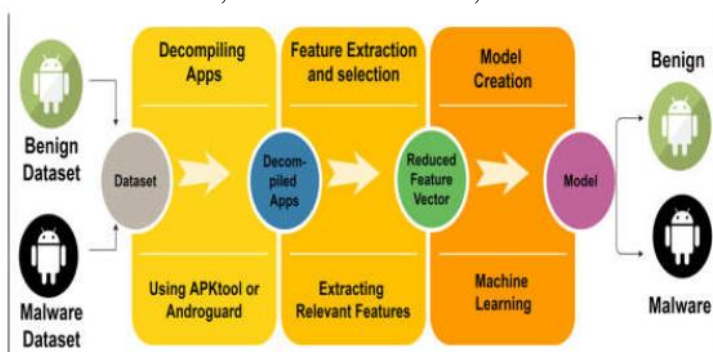


Fig 2: General Framework

In the initial phase, dataset is constructed by downloading apps from malware and benign repositories. For collecting malware applications, we can download apps from malicious websites or malware repositories like VirusShare [7]. We have used VirusShare repository for malware samples. For benign samples, we can download apps from play store or third party Appstore. We have used AndroZoo Repository for benign samples [6]. The Dataset is given in table 1.

TABLE 1: DATA SOURCE

DataSource	QUANTITY
AndroZoo (Benign)	2000
VirusShare(Malware)	2000

The next phase is feature extraction as shown in fig.2 In this phase, we extract features from a large set of application using static and dynamic analysis techniques. Here, we have

to use a feature representation technique. We have used binary representation for generating a feature vector. The feature vector is defined in equation 1.

$$X = \langle X_1, X_2, X_3, \dots, X_n \mid X_i = \text{feature} \rangle \quad (1)$$

Here, a feature is denoted by X_i where it can denote a component like intent, permission, API call, app component etc. These features are extracted by using static and dynamic analysis technique. We have used binary representation in our research. In binary representation, 1 denotes feature is present and 0 represent feature is not present as shown in equation (2).

$$f(x) = \begin{cases} 1 & \text{feature present} \\ 0 & \text{Otherwise} \end{cases} \quad (2)$$

As discussed, features can be extracted using static and dynamic analysis technique. In static analysis, we analyze the source code of the APK while in dynamic analysis, we execute the APK and extract features by monitoring its behavior. A feature vector is generated for each application denoting the behavior of the application. We have stored feature vector of each APK into a common CSV file. For extracting static features, there are many tools available like ApkTool [27] and Androguard [28]. We have used the Androguard framework for reverse engineering Android applications [28]. We have extracted API Calls, Permissions, System events (Components, Intents, Broadcast Receivers, and Services) and Opcodes from a large set of 4000 applications. For extracting dynamic features, we have used DroidBox framework for behavior analysis of android applications [29]. We have extracted Data leaks, File Accesses, Enforced permissions, and crypto calls from a large set of 4000 applications. In our research, we have extracted a total of 118333 features from the dataset each categorized into eight broad categories. The features are summarized in the table 2.

TABLE 2: FEATURE SET SUMMARY

CATEGORIES	NO. OF FEATURES EXTRACTED
S ₁ - API Calls	30105
S ₂ - Crypto Calls	51
S ₃ - Data Leaks	3
S ₄ - Enforced Permissions	1000
S ₅ - System Events	63112
S ₆ - Files	22392
S ₇ - Opcode	226
S ₈ - Permissions	1444

When the feature extraction phase is complete, we are usually presented with a large set of features. This results in a large number of computations and requires a lot of resources. Hence, feature selection techniques like Information Gain are used to minimize the dimensionality of the vector. Feature selection technique ranks the features on the basis of their contribution to malware detection. Best features are selected and rest features are removed thus reducing the size of the feature vector. We have used Information Gain as Attribute Selection algorithm to reduce the feature vector dimensionality. We have reduced the size of the feature vector by considering top features

based on their score. We have filtered the top features that have InfoGain score of greater than 0.1 except the data leaks feature as a number of features in it is already low. Let A be the set of all attributes and E set of all training examples. $V(x,a)$ be the value of specific example x for attribute a . H defines Entropy. $Values(a)$ represents a set of all values of a where $a \in A$. Information gain is defined by the following relation as shown in equation 3.

$$IG(E, a) = H(E) - \sum_{v \in values(a)} \left(\frac{|\{x \in E | V(x,a)=v\}|}{|E|} \cdot H(\{x \in E | V(x,a) = v\}) \right) \quad (3)$$

The final phase is model creation. In this phase, models are built using machine learning algorithms. Initially, the dataset consisting of malware and benign apps are split into two parts with 80% samples for training and 20% for testing. There are many factors that are used for determining the quality of the model like accuracy, F1, Recall, precision etc. These metrics help to justify the performance of the algorithm being used for model creation. We have used TensorFlow and keras (python-based framework) for implementing a deep neural network. We have implemented multi-model neural networks by varying no. of neurons present in hidden layer and no. of hidden layers in the network. Our results show the promising result with good detection accuracy. We have compared our approach with other techniques. Multi-Modal learning is an approach to learning a good model by using the joint representation of different modalities. Modality refers to the way in which something can be experienced. A problem can be labeled as a multimodal problem when it includes multiple such modalities. For example, consider a case of an image. An image is usually associated with a description (A long text describing the image), tags and pixel intensities. These all constitute the different modalities for the problem. Multi-Modal learning helps to learn such models that can solve these problems efficiently and effectively. Multi-Modal learning models are also capable of learning missing modalities given the observed ones. In a multi-modal learning approach, multiple models are built based on different modalities. All the models are then merged by using a merging layer and then final modal is used to predict the result. The process is shown in figure 3 as shown below.

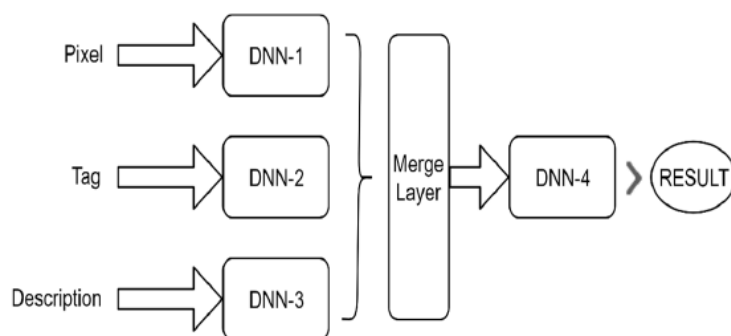


Fig 3: Multi-Modal Deep Neural Network (DNN)

In this research, we have implemented a hybrid modal based on multi-modal learning which is shown in fig.4. Our approach is categorized into four broad steps – dataset creation, feature extraction, feature selection, and model creation. These steps in detail are summarized below –

1. In the first step, the dataset is downloaded from repositories. Malware apps are collected from VirusShare repository [7] and benign apps are collected from AndroZoo repository [6]. We have collected a total of 4000 applications.
2. In the second step, the features are extracted from the collected dataset. We have used two approaches for feature extraction – static analysis and Dynamic analysis. We have

used Andro Guard for collecting static features and Droid box for collecting dynamic features. We have collected a total of 118333 features. All the data is persisted in a CSV file.

- In the next step, we have used Info Gain feature selection algorithm to reduce the feature vector dimensionality. Not only it helped in reducing the feature vector size but also helped in improving the computational time and accuracy of the classifiers.
- In the final step, we have implemented our proposed approach as shown in the fig. 4.1. We have categorized the features into eight broad categories. We have built a classifier for each feature category using a deep neural network. We then have used a Merge layer to merge all the models. Finally, we have built a DNN to predict the final result.

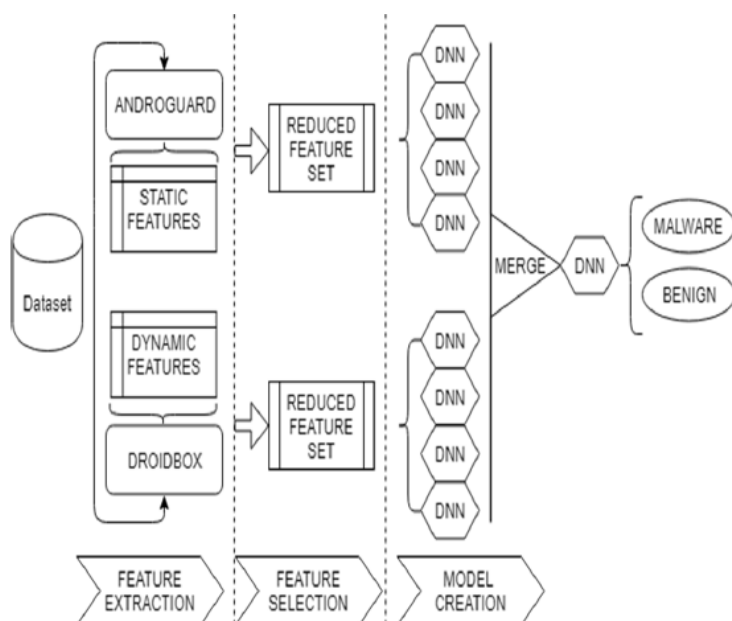
A multi-modal neural network contains a number of models that together provides an end result. It consists of an initial DNN and final DNN. The initial DNN has one input layer and 2 hidden layers each having n number of neurons. Each neuron having ReLU as the activation function. The count of neurons is varied in the network in order to tune it for better predictions. The final DNN has one merging layer, two hidden layers, and one final output layer. Each layer defined in this network has used ReLU function to be used as an activation function except the final output layer. The final output layer has used Sigmoid as the activation function.

Fig. 4: Proposed Architecture

4. EXPERIMENTAL RESULTS

This section briefly reported the performance of our implemented approach and compared it with other approaches. Our main motive is to demonstrate that multi-modal learning is an efficient and effective technique for detecting android malwares. We are able to achieve the best result that is 97.25% accuracy using this technique. We have used precision, F1, Recall, and accuracy as performance metrics. It is found that these measurements are very effective to assess the quality of classification in case of Android Malware detection. The metrics are defined in the equation 4-7.

$$Precision = \frac{TP}{TP + FP}$$



$$Recall = \frac{TP}{TP + FN}$$

$$Accuracy = \frac{TP + TN}{TP + FP + TN + FN}$$

$$FScore = 2 * \frac{Precision * Recall}{Precision + Recall}$$

We have divided the large dataset of 4000 applications with 80% samples for training and rest 20% samples for testing. TrainingsetisusedtobuiltthemodelandtheTestingsetisused to evaluate the model. We have split the dataset with 80% samples for training and 20% samples for testing. We have analyzedafewapproachesbasedonhowtheyhaveconstructed the feature vector. In comparison, we have focused on and comparedifferentmodelsbasedonasetoffeaturesusedinthe approach. All the feature set is broadly categorized into eight categories. In our approach, we have followed a notation to represent multi-modal architecture. The multi-modal network consistsofinitialandfinalDNN.TheinitialDNNhasoneinput layerand2hiddenlayerseachhavingnnumberofneurons.The final DNN has one merging layer, two hidden layers and an output layer with predefined neurons. Syntax to describe the multi-modal architecture is defined in equation8.

Representation: [[X1, X2, X3 ...] [X1, X2,X3...]] (8)

Here the first part represents the configuration of initial deep neuralnetworkandthesecondpartrepresentstheconfiguration of a final deep neural network. The Xi represents the count of neurons present in the hidden layer. The shape of the 1-Darray represents the total count of hidden layers. We have summarized our analysis in table 3. Based on the above analysis, we found that the best result is achieved when we use two hidden layers in both initial and final DNN with each hiddenlayerhaving20neurons.Thebestresultachievedis97.25% accuracy. We have compared our approach with two other approaches. Approach-1 is similar to DREBIN [10] and Approach-2 is similar to DroidDet [9]. Both these techniques are based on static analysis only. We have extended both the techniques for dynamic and hybrid analysis. We haveprovided a comparative analysis which is given in the below table4.

TABLE 3: MULTI-MODAL NEURAL NETWORK ANALYSIS

MULTI-MODAL NETWORK CONFIGURATION	ACCURACY	PRECISION	RECALL	F-SCORE
[[5,5,5] [5,5,5]]	96.12%	99.23%	93.25%	96.14%
[[5,5] [5,5]]	96.5%	98.98%	94.21%	96.54%
[[5][5]]	96.87%	99.24%	94.69%	96.91%
[[10,10,10] [10,10,10]]	96.87%	98.75%	95.81%	96.93%
[[10,10] [10,10]]	97%	99.24%	94.93%	97.04%
[[10][10]]	96.87%	99.24%	94.69%	96.91%
[[20,20,20] [20,20,20]]	96.75%	98.74%	94.93%	96.80%
[[20,20] [20,20]]	97.25%	99.24%	95.42%	97.29%
[[20][20]]	96.75%	98.74%	94.93%	96.80%
[[30,30,30] [30,30,30]]	96.62%	98.98%	94.45%	96.67%
[[30,30] [30,30]]	97.12%	99.24%	95.18%	97.17%
[[30][30]]	96.87%	98.99%	94.93%	96.92%

TABLE 4: COMPARATIVE ANALYSIS

APPROACH	MODEL	FEATURE SET	ACCURACY	PRECISION	RECALL	F-SCORE
APPROACH-1	SVM	STATIC	87.12%	88%	87%	87%
APPROACH-2	ROTATION FOREST MODEL	STATIC	87.37%	88%	87%	87%
EXTENDED APPROACH-1	SVM	DYNAMIC	72%	68.74%	53.25%	65.53%
		HYBRID	89.35%	85.88%	88.45%	89.44%
EXTENDED APPROACH-2	ROTATION FOREST MODEL	DYNAMIC	71.62%	66.40%	49.47%	62.60%
		HYBRID	91.5%	87.79%	88.59%	90.76%
OUR APPROACH	DEEP NEURAL NETWORK	STATIC	95.87%	98.64%	92.8%	95.67%
		DYNAMIC	72%	91.22%	50.48%	65%
		HYBRID	96.12%	94.61%	98.05%	96.30%
OUR APPROACH	MULTI-MODAL NEURAL NETWORK	HYBRID	97.25%	99.24%	95.42%	97.29%

5. CONCLUSION

In this paper, we have given a general overview of malware and its propagation techniques. We have also discussed different techniques for detecting malware with their strength and limitations. Keeping those limitations in mind, we have implemented a hybrid android malware detection technique using multi-modal learning to detect malwares in android devices. This model helped to overcome the problems of both static and dynamic analysis when used individually. We have also compared our approach with two other approaches and found that multi-modal learning yields a better result. We have also extended the approaches with dynamic and hybrid analysis.

We have also implemented a deep neural network and compared it with our approach. The result indicates that multi-modal learning is an effective technique and yields a better result when compared with other techniques. Our analysis also suggests that the model yields a better result when features are provided to it individually rather than combining all features into one long feature vector. In this research, we have used both static and dynamic features extracted from a large dataset of 4000 applications. The applications were collected from VirusShare and AndroZoo repository. We have achieved a good result with 97.25% accuracy.

6. REFERENCES

- [1] Statista, "Mobile OS Market Share," *www.Statista.Com*, 2018. [Online]. Available: <https://www.statista.com/statistics/266136/global-market-share-held-by-smartphone-operating-systems/>.
- [2] "First Kotlin-Developed Malicious App Signs Users Up for Premium SMS Services-TrendLabs Security Intelligence Blog." [Online]. Available: <http://blog.trendmicro.com/trendlabs-security-intelligence/first-kotlin-developed-malicious-app-signs-users-premium-sms-services/>.
- [3] Wikipedia, "WannaCry ransomware attack," *Wikipedia Foundation*, 2017. [Online]. Available: https://en.wikipedia.org/wiki/WannaCry_ransomware_attack.
- [4] "Android.Samsapo - Mobile Worm." [Online]. Available: https://www.symantec.com/security_response/writeup.jsp?docid=2014-050111-1908-99.
- [5] "Android/Trojan.AsiaHitGroup - Malwarebytes Labs_Malwarebytes Labs." [Online]. Available: <https://blog.malwarebytes.com/cybercrime/2017/11/new-trojan-malware-discovered-google-play/>.

- [6] “Mobile Spyware- Go Keyboard app.” [Online]. Available: <https://www.bleepingcomputer.com/news/security/popular-android-keyboard-app-caught-collecting-user-data-running-external-code/>.
- [7] K. Labs, “Kaspersky_Securelist Threat Report,” 2019. [Online]. Available: <https://securelist.com/threat-category/mobile-threats/>.
- [8] Q. Heal, “Quick Heal Annual Threat Report,” 2019.
- [9] H. J. Zhu, Z. H. You, Z. X. Zhu, W. L. Shi, X. Chen, and L. Cheng, “DroidDet: Effective and robust detection of android malware using static analysis along with rotation forest model,” *Neurocomputing*, vol. 272, pp. 638–646, 2018.
- [10] D. Arp, M. Spreitzenbarth, M. Hübner, H. Gascon, and K. Rieck, “Drebin: Effective and Explainable Detection of Android Malware in Your Pocket,” *Proc. 2014 Netw. Distrib. Syst. Secur. Symp.*, 2014.
- [11] K. Allix, T. F. Bissyandé, J. Klein, and Y. Le Traon, “AndroZoo: Collecting Millions of Android Apps for the Research Community,” pp. 468–471, 2016.
- [12] “VirusShare,” 2019. [Online]. Available: <https://virusshare.com/>.
- [13] J. Li, L. Sun, Q. Yan, Z. Li, W. Srisa-an, and H. Ye, “Significant Permission Identification for Machine Learning Based Android Malware Detection,” vol. 3203, no. c, 2018.
- [14] A. Firdaus, N. B. Anuar, A. Karim, M. Faizal, and A. Razak, “Discovering optimal features using static analysis and genetic search based method for Android malware detection *,” vol. 19, no. 6, pp. 712–736, 2018.
- [15] E. Billah, M. Debbabi, A. Derhab, and D. Mouheb, “MalDozer: Automatic framework for android malware detection using deep learning,” *Digit. Investig.*, vol. 24, pp. S48–S59, 2018.
- [16] S. Wang, Z. Chen, Q. Yan, B. Yang, L. Peng, and Z. Jia, “A mobile malware detection method using behavior features in network traffic,” *J. Netw. Comput. Appl.*, 2019.
- [17] P. Feng, J. Ma, C. Sun, and Y. Ma, “A Novel Dynamic Android Malware Detection System With Ensemble Learning,” *IEEE Access*, vol. 6, pp. 30996–31011, 2018.
- [18] W. You, B. Liang, W. Shi, P. Wang, and X. Zhang, “TaintMan: an ART-Compatible Dynamic Taint Analysis Framework on Unmodified and Non-Rooted Android Devices,” *IEEE Trans. Dependable Secur. Comput.*, vol. 5971, no. c, 2017.
- [19] L. Wei, W. Luo, J. Weng, Y. Zhong, X. Zhang, and Z. Yan, “Machine Learning-based Malicious Application Detection of Android,” *IEEE Access*, vol. PP, no. 99, p. 1, 2017.
- [20] S. Arshad *et al.*, “SAMADroid: A Novel 3-Level Hybrid Malware Detection Model for Android Operating System,” *IEEE Access*, vol. 6, pp. 4321–4339, 2018.
- [21] Z. Yuan, Y. Lu, and Y. Xue, “Droiddetector: android malware characterization and detection using deep learning,” *Tsinghua Sci. Technol.*, vol. 21, no. 1, pp. 114–123, 2016.
- [22] M. Sun, X. Li, J. C. S. Lui, R. T. B. Ma, and Z. Liang, “Monet: A User-Oriented Behavior-Based Malware Variants Detection System for Android,” *IEEE Trans. Inf. Forensics Secur.*, vol. 12, no. 5, pp. 1103–1112, 2017.
- [23] X. Su, D. Zhang, W. Li, and K. Zhao, “A Deep Learning Approach to Android Malware Feature Learning and Detection,” *2016 IEEE Trust.*, pp. 244–251, 2016.
- [24] D. Li, Z. Wang, and Y. Xue, “Fine-grained Android Malware Detection based on Deep Learning,” *2018 IEEE Conf. Commun. Netw. Secur.*, vol. 1, no. L, pp. 1–2, 2018.
- [25] M. A. Akcayol, “Permission Based Android Malware Detection With Multilayer Perceptron,” pp. 0–3, 2018.

- [26] R. Katarya and P. Mamgain, "A Survey on Android Malware Detection Techniques," *Int. J. Comput. Eng. Appl.*, vol. XII, 2018.
- [27] C. Tumbleson and R. Wiśniewski, "Apktool - A tool for reverse engineering 3rd party, closed, binary Android apps." [Online]. Available: <https://ibotpeaches.github.io/Apktool/>.
- [28] "Androguard - Reverse engineering Tool." [Online]. Available: <https://github.com/androguard/androguard>.
- [29] "GitHub - pjlanzt_droidbox_ Dynamic analysis of Android apps." [Online]. Available: <https://github.com/pjlanzt/droidbox>.

Chemical and Physical Analysis; Effect of the Ground Water at the Town of Achhnera, Agra

Sapna Tomar¹, O.P.Singh²

¹Department of Chemistry, RBSETC, Bichpuri, Agra, 283105

²Department of Physics, IET, Lucknow

Email: Sapnatomar_rbs@rediffmail.com, opsingh@ietlucknow.ac.in

Correspond Author: Phone: 91+9410668732, 91+8954696726

ABSTRACT

Ground water samples were taken in polythene bottles from achhnera namely site I station bazaar, site II Railway loco colony, site III- Rathiya mohalla, site IV- Jatwan mohalla, site V- Shekhan mohalla and site VI- Bajahera mohalla for studying. Experimental set up were performed for analysis of sample for total dissolved solids, Electrical conductivity and major ions eg., Ca⁺⁺, Mg⁺⁺, Nitrite, F⁻, Na⁺, K⁺. In this paper highlights the analytical results for main ions causal towards total dissolved solids. The experimental material is compared with the drinking water quality standard laid by Indian Council of Medical Research (I.C.M.R.), We found that water samples are no suitable for human due to high concentration of one parameter to the other. Most of the samples have total dissolved solids values a large amount than the most permissible level stipulated by ICMR. The high values of these parameters might have health implications and so they need notice.

Key Notes: Sample of Water, Conductivity, pH meter and Spectrometer

1. INTRODUCTION

According to W.H.O., about 80% of all the diseases of human beings are caused by water. Since these diseases are directly connected with human health, it's needed to bring alertness among the present and future generation about the consequences of water pollution. Pollution can be defined as "The addition of something to water which changes its natural quality". Contamination can also be defined as "Effluence is a alteration of the physical, chemical and biological properties of water, restricting or preventing its use in the a variety of applications where it usually plays a part.

With fast growing inhabitants and better living standard, the force on water supply is increase¹⁻². Rapid industrialization and urbanization contain led to discharge of industrial effluent which revolve pollutes the ecosystem. The removal of effluent has become a serious techno-economic difficulty particularly due to increasing cost of disposal and growing consciousness of pollution hazard. Ground water is an significant source of drinking water for much of the world's population and its quality of purity has no direct effect on human health. Ground water is normally a very good source of drinking water because of the cleansing properties of the soil. It is also used for irrigation and spraying and where surface water is limited for industrial purpose. Water is a universal solvent³ and it dissolves minerals from the rocks in which it is stored and thus physical and chemical quality of ground water depend on geology of particular area. The quality of ground water is the resultant of all the processes and reaction that act on the water from the moment, it condense in the atmosphere to the time it is discharged by a well⁴. The socio-economic increase of a region is severely constrained by non availability of safe drinking water⁵. Ground water meets domestic needs of extra than 80% rural and 50% urban population also fulfilling irrigation need of around 50% irrigation agriculture. Around two fifth of India's agriculture output is contributed from area irrigated by ground water. Contribution from ground water to India's Gross domestic product has been estimated to be 9% a reported⁶.

The most important objectives of the hydro chemical studies to identify the distribution of solute in ground water, and the appropriateness of the ground water for household and agriculture purpose. Bacterial contagion and total dissolved are two most important criteria for judging the quality of water for drinking purpose. U.P. State is characterized by high disappearance and extreme variation in temperature and Irregular rainfall⁷. In persistence of the work earlier complete related to ground water analysis and the results of ground water analysis presented in this paper Achhnera, Distt. Agra, ground water mainly contains no suspended particles and practically no bacteria. The suitability of ground water for domestic uses has been based on substance composition of dissolved solids⁸. The I.C.M.R(1975) has recommended highest desirable limit of 500mg/l and maximum permissible limit of 1500mg/l for total dissolved solids⁹.

2. MATERIALS AND METHODS

Sample were collected in polythene bottles from six different sites namely site I station bazaar, site II Railway loco colony , site III- Rathiya mohalla, site IV- Jatwan mohalla, site V- Shekhan mohalla and site VI- Bajahera mohalla from the depth of 35' and 75'ft. ulmost be concerned werein use during sampling

to remain away from any type of pollution Temperature and pH were measured at the time of collection itself. Physical attributes like Total suspended solids was evaluated by microprocessor. The conductivity was measured by conductivity meter. Major ions like Calcium, magnesium, and chloride were analyzed using the standard titrimetric method. Sulphate ion evaluation was completed by Spectrophotometrically. $\text{Na}^{++}, \text{K}^{++}$ ions analysis were complete using Systronic Flame Photometers.

3. RESULTS AND DISCUSSION

The consequences of the analysis are reported in table 1 and graph. In the present studies, the pH values in all the samples ranges from 7.60-7.78, which be well in the highest permissible level (6.5-9.2). The lesser value of pH may source tuberculation and decay while the higher value may create incrustation, residue deposit, and difficulties in chlorination for disinfection of water¹⁰.

EC of the ground water in all sites was under the permissible limit stipulated by ICMR. Conductivity is measurement of the dissolved solids in ms/cm. Conductivity varied from 650.00 – 663.00 ms/cm. Chloride ions was found from the range 350 to 390 mg/lit Chloride ions concentrations in a large amount of the samples were found higher than the attractive limit (i.e. 200ppm) but under the permissible limit (i.e. 1000ppm) for drinking water at all site. High chloride concentration indicated organic pollution.

Sodium was found from the range 346 to 385 mg/lit. Sulphate in most of the sample found from the range 162.00 to 185.00 mg/lit. It was found within the permissible limit (400 mg/lit, ISI. 1991).

Calcium is to crucial for healthy growth of bones and play important roles in biological system. Calcium varied from 88.80-97.18. Calcium was found in the entire sample higher than the highest desirable limit (75ppm) but under the permissible limit of ICMR i.e. 200ppm. Magnesium is a useful metal but toxic at higher concentration. Mg^{+} ranged from (60.28-70.58) mg/lit (highest desirable limit for magnesium by ICMR is 105 ppm).

4. CONCLUSION

It can be concluded from the results that the ground water in Achhnera town possess high desirable value of total dissolved solids, chloride sodium and magnesium ion conc. etc. Although not any of these factors pretense any serious health hazards thus far these humiliate quality of drinking water and therefore necessary to be treated.

5. ACKNOWLEDGEMENT

The authors gratitude ground water resources Lucknow for their help and logistic support. The authors also gratitude people of Achhnera town to provided whole hearted support during sampling procedure.

Table 1: Analytical and Physico-Chemical Parameter of Ground water

S.No	Location	Temp.	pH	Electric al Conductivity	Turbidity	Chloride Ions	Bicarbonate Ions	Ca ⁺⁺	Mg ⁺⁺	SO ₄ ⁻⁻	Nitrate	Flo rid e	Na ⁺	K ⁺	Total Solid
1	Station Bazar	18.80 (±0.10)	7.75 (±0.30)	655.00 (±1.12)	6.50 (±1.52)	360.00 (±0.27)	588.00 (±1.26)	92.80 (±0.65)	64.00 (±0.35)	165.00 (±0.54)	14.40 (±0.10)	Ab .	380 (±0.66)	7.80 (±0.16)	658 (±1.28)
2	Railway Loco Colony	19.30 (±0.01)	7.60 (±0.11)	650.00 (±0.64)	5.50 (±1.27)	350.00 (±0.44)	582.00 (±0.36)	88.80(±0.39)	60.28 (±0.32)	162.00 (±0.62)	1.65 (±0.06)	Ab .	344 (±0.13)	7.10 (±0.04)	653 (±1.52)
3	Rathiya Mohalla	19.00 (±0.03)	7.78 (±0.45)	668.00 (±0.45)	14.80 (±0.99)	390.00 (±0.76)	640.00 (±0.62)	97.18 (±0.29)	70.58 (±0.13)	185.00 (±0.12)	4.84 (±0.12)	Ab .	384 (±0.08)	10.46 (±0.24)	708 (±1.20)
4	Jatwan Mohalla	19.50 (±0.03)	7.64 (±0.60)	659.00 (±0.35)	8.34 (±0.67)	362.00 (±0.02)	590.00 (±0.34)	91.90 (±0.11)	66.00 (±0.11)	168.00 (±0.32)	2.24 (±0.06)	Ab .	355 (±0.04)	8.00 (±0.54)	680 (±0.90)
5	Shekhan Mohalla	19.88 (±0.02)	7.76 (±0.22)	662.00 (±0.26)	9.95 (±0.32)	365.00 (±0.12)	617.00 (±0.32)	95.50 (±0.17)	70.50 (±0.03)	174.00 (±0.94)	4.38 (±0.08)	Ab .	360 (±0.04)	9.56 (±0.06)	700 (±0.48)
6	Bajahera Mohalla	20.30 (±0.21)	7.62 (±0.09)	661.00 (±0.12)	9.90 (±1.11)	364.00 (±0.34)	615.00 (±1.52)	93.49 (±0.23)	69.38 (±0.09)	172.00 (±0.74)	3.23 (±0.06)	Ab .	356 (±0.12)	9.20 (±0.96)	685 (±1.20)

5. ACKNOWLEDGEMENT

The authors gratitude ground water resources Lucknow for their help and logistic support. The authors also gratitude people of Achhnera town to provided whole hearted support during sampling procedure.

REFERENCES

1. Batheja, K., Sinha, A.K. and Garg, J.; J. Environ. Sci. Engi.,2007, 49(3), 203
2. Kumar, R., Singh, R.D. and Sharma, K.D.; Water Resource of India, Curr. Sci. 2005,9(5), 794
3. Narsimhan, T.N.; Water Science and Society, Curr. Sci., 2005,89(5), 783 .
4. Gupta, S., Kumar, A., Ojha, C.K. and Seth, G.; Chemical Analysis of Ground Water of Sanganer Area jaipur in Rajastha, E. Sci. Engi., 2004,74 .
5. Kumar, A., Seth, G. and Samota, M. K.; Geochemical Studies of Fluoride in Ground Water of Rajasthan, Ind. J. Chem.,2005,2(6), 191 .
6. Burjia, J.S. and Romani, S.; Ground Water Development Present Scenario and Future Needs, Ind. Pub. Adm. XLIX ,2003,(3) 301 .
7. Ajmal, M., Khan, M.A. and Nomani, A.A.; Quality of Ganga River in U.P. and Bihar, IAWPL Tech. Annual IX, 1982,165 .
8. Duffy, C.J. and Brandes, D.; Dimension Reduction and Source Identification for Multi Species Ground Water Contamination, Conta. Hydro., 2001,48, 151.
9. Goel, P.K. and Sharma, K.P.; Environmental Guidelines and Standard in India, Ind. J.Environ.Sci., 1996,9(3), 182 .
10. Prasad, B.G.; Evaluation of Water Quality in Jadepalli Mandal of Gunter Disst. A.P., Environ.Pollution Techno. ,2003,2(3), 273 .

RF Performance Evaluation of Nanoscale FDSOI MOS transistors

Narendra Yadava *¹, R. K. Chauhan²

¹Research Scholar, Department of Electronics and Communication Engineering Madan Mohan Malaviya University of Technology Gorakhpur, Uttar Pradesh, 273016, India ²Department of Electronics and Communication Engineering Madan Mohan Malaviya University of Technology Gorakhpur, Uttar Pradesh, 273016, India

narendrayadava5@gmail.com¹, rkchauhan27@gmail.com²

Corresponding author*: Phone: +91-983-953-9800

Abstract

The paper puts forward the high frequency performance analysis of the single gate and double gate FDSOI MOSFET. The simplified small signal equivalent model for both the devices are developed in order to analyze the High frequency response of the device more accurately, and to extract other important high frequency (RF) parameters. The small signal equivalent model is utilized to obtain the Y parameter of the device and from which the minimum noise Figure and S parameter of the device are derived and provides its applicability in the design of RFICs. The derived S parameters are used to evaluate its high frequency losses. It is observed that in the SG FDSOI MOSFET the Insertion loss is 2.47 dB, the Transmission loss is 2.48 dB and the Reflection loss is 1.02 dB lower than that of DG FDSOI MOSFET while the Return loss is 0.05 dB higher as compared to that of DG FDSOI MOSFET. The analysis is carried out using Silvaco 2D ATLAS tool.

Keywords: FDSOI MOSFET, RFICs, Leakage current, Power dissipation, RF frequency.

1. Introduction

The demand for low power and RFIC applications are increasing day by day. This increasing demand leads to the need of high-density on chip integration in annexation with optimum performance ¹. To achieve these properties, the CMOS technology is clamped into the tenth of the nanometre range ². However, it becomes very arduous to preserve the performance of these devices in the nanoscale dimension due to its increased short channel effects (SCEs) ³⁻⁶.

To overcome the afore stated hindrances, since last two decade researchers are making great effort and even various device designs already has been proposed ⁷⁻¹³. SOI technology out of several MOS technology is preferred due to its several advantageous features like it highly suppress the leakage currents by using a buried oxide (BOX) insulating layer underneath the channel region and also its fabrication is easy and cost efficient ¹⁴⁻¹⁷.

Considering the FDSOI MOSFETs, In the Radio frequency operating range several losses take place so it is very essential to analyse these losses in order to characterize the device more accurately ²¹.

For RF applications several researches has already been carried out related to FDSOI MOS device design ¹⁹⁻²². *Lázaro & Iñiguez* compares the RF and noise performance of double gate (DG) and single gate (SG) SOI and observed that f_T of the DG SOI is greater in comparison to the SG SOI and hence DG SOI has larger BW in comparison to the SG SOI for RF applications ²³. *Mohan Kumar et al.* stated the impact of engineering in channel doping and gate electrode material on the analog and RF performance of FD SOI MOSFET and obtained that the gate engineered device has improved f_T and f_{MAX} while channel engineered device has reduced f_T with respect to single metal double-gate (DG) MOSFET ²⁴. Later, *Sarkar et al.* put forward the impact of gate engineering on analog and radio frequency (RF) performance of the DG MOSFET, and concluded that the use of triple metal gate electrode results in deviated peak horizontal electric field towards the source junction which results in improved carrier transference efficiency and

hence provides higher 1-dB compression point when compared to the single metal DG and double metal DG MOSFET making it suitable for high linearity ultra wide band (UWB) LNA design ²⁵. Pradhan *et al.* discusses the impact of stacking high-k gate insulating materials over a silicon dioxide material on analog and radio frequency (RF) performance of the nanoscale double gate FDSOI MOSFET and concluded that gate stacking using Silicon Nitride (Si₃N₄) as high-k dielectric material exhibit improved DIBL, reduced subthreshold slope (SS), better f_T and gain in comparison to the other dielectric materials making it suitable for large BW analog and RF applications ²⁶.

The analog and RF analysis of the above reported literatures only deals with either BW, short channel effects or power dissipation and their associated leakages. The losses in devices operating at the RF range has not been discussed by any of the earlier researchers. In this paper an analysis on the high frequency performance of the single gate and double gate FDSOI MOSFET is carried out in combined with their associated high frequency losses. The key Figure of merits (FOMs) used in the analysis are intrinsic capacitances (C_{gs} and C_{gd}), cut-off or unity current gain frequency (f_T) and frequency transconductance gain product (FTGP). The results obtained for RF analysis of the designed devices has been compared and contrasted with reported results. Also the simplified small signal equivalent models for DG FDSOI MOSFET has been proposed for the first time to extract its essential RF parameters.

2. Device Descriptions

The structure of both the devices is shown in Figure 1 and Figure 2 respectively. The Silicon dioxide (SiO₂) is used as an insulating material for gate as well as for the buried oxide (BOX) regions in the both devices. The drain and the source diffusion regions are n-type regions doped with Gaussian doping profile whereas the channel region is uniformly doped p-type region. The physical device models used in the simulation (Atlas simulator) are the Shockley-Read-Hall recombination model (SRH), the common mobility model (CONMOB) and Boltzmann statistic (BOLTZMAN) as a carrier transport statistic. The parameters used in the design of SG FDSOI and DG FDSOI MOS devices is described in TABLE 1.

[Figure 1]

[Figure 2]

[Table 1]

3. Small Signal Analysis

The small signal analysis is essential to examine the high frequency response of the MOS devices more precisely and also to easily extract other important high frequency parameter ²⁷. In small signal analysis, the Source and Substrate (Body) terminal are shorted together in order to realize the effective configuration as a two-port network. This method is the simplest method used for extracting the parasitic components of the MOS devices which are utilized in accurate RF measurement. For common two port-network, a particular current and voltage values are assigned to each of these ports. For two port analysis of the MOS devices, Source and Gate terminal are considered as input port while Source and Drain terminal are considered as output port. For a two-port network if V_2 , I_2 and V_1 , I_1 are considered as a voltage and current at the output and input port respectively, then it's short-circuit admittance parameter can be formulated as:

$$Y_{11} = I_1 / V_1 | V_2=0 \quad (1)$$

$$Y_{12} = I_1 / V_2 | V_1=0 \quad (2)$$

$$Y_{21} = I_2 / V_1 | V_2=0 \quad (3)$$

$$Y_{22} = I_2 / V_2 | V_1=0 \quad (4)$$

The admittance of this network is given by:

$$Y = \begin{pmatrix} Y_{11} & Y_{12} \\ Y_{21} & Y_{22} \end{pmatrix} \quad (5)$$

These Y parameters can be utilized to obtain the effective S parameters which is further used for high frequency analysis of the designed MOS devices. The Y parameters are used in the analysis because it is also known as “Transadmittance parameter” i.e., voltage controlled current source (VCCS) and it is a known fact that the MOSFET is inherently the VCCS.

The small signal equivalent model of the SG FDSOI MOSFET²⁸ is shown in Figure 3 in which C_{gs} is gate to source capacitance, C_{gd} is gate to drain capacitance, C_{sb} is source to body capacitance, C_{db} is drain to body capacitance, C_{gb} is gate to body capacitance, R_g is the gate resistance and R_s is the source resistance, R_d is the drain resistance and R_{sub} is the substrate resistance.

[Figure 3]

[Figure 4]

Figure 4 represents the small signal equivalent circuit of the double gate FDSOI MOSFET in which C_{gs} is gate to source capacitance which is a combination of C_{g1s} and C_{g2s} , C_{gd} is gate to drain capacitance which is a combination of C_{g1d} and C_{g2d} , C_{g1g2} is the capacitance between Gate1 and Gate2 terminals, R_{g1} and R_{g2} are the resistances across the Gate1 and Gate2 terminals respectively and R_s is the source resistance, R_d is the drain resistance and R_{sub} is the substrate resistance.

The gate to drain and gate to source capacitances are due to overlapping of gate electrode on the drain as well as source diffusion regions which depends upon the height of the gate electrode and responsible for fringe capacitances at the source as well as drain edges. Both the transition frequency f_T and the maximum oscillation frequency f_{max} are inversely proportional to all these capacitances and hence increase in capacitances results in decrease in f_T and f_{max} . Therefore, for better RF performance, the value of these capacitances should as small as possible. For distributed contact resistance model, the source and drain resistance is given by:

$$R_{Source} = R_{Drain} = R_C + \frac{L_{S/D}}{q\mu_0WNt_{si}} \quad (6)$$

Where, R_C is the contact resistance, $L_{S/D}$ is length of the source or drain electrode (for symmetric MOSFET), q is the charge on electron, W is the channel width N is the doping concentration of source or drain diffusion region, t_{si} is the silicon film thickness and μ_0 is the electron mobility under no bias condition.

3. Results and Discussion

The transfer characteristics of the single gate FDSOI MOSFET and double gate FDSOI MOSFET is obtained and shown here as Figure5. For all the figures shown here, the line with square mark represents the behaviour of single gate FDSOI MOSFET and the line with circular mark represents the behaviour of double gate FDSOI MOSFET. From Figure one can observe that with the increase in gate to source voltage, the drain current increase is larger in double gate FDSOI MOSFET as compared to single gate FDSOI MOSFET. The value of leakage current in double gate FDSOI MOSFET is found to be 0.15 A/ μm while it is equal to 0.09 A/ μm in the single gate FDSOI MOSFET. The I_{on}/I_{off} is 1.5×10^6 in double gate FDSOI MOSFET and 10^3 in the single gate FDSOI MOSFET. One can observe that the I_{on}/I_{off} and the leakage current for the double gate FDSOI MOSFET is larger which implies that it has high switching speed with high power dissipation. The intrinsic capacitances (C_{gd} and C_{gs}) are obtained by using small signal AC analysis after performing the DC analysis. In this work the, the intrinsic capacitances (C_{gd} and C_{gs}) are obtained by performing AC analysis at 1 MHz frequency with DC sweep voltage of 0V to 1.5V. Figure 6 shows the variation of C_{gd} and C_{gs} for varying gate to source voltage. It is observed that for double gate FDSOI MOSFET the value of both intrinsic capacitances (C_{gs} and C_{gd}) are smaller as compared to the single gate FDSOI MOSFET. Smaller value of intrinsic capacitances implies that it has high transconductance value and hence it is more suitable for high frequency applications.

[Figure 5]

[Figure 6]

The f_T can be evaluated by using Eq. (7). From the Figure 7 it is observed that in the double gate FDSOI MOSFET, the value f_T is larger in comparison to the single gate FDSOI MOSFET which reflects the higher gate controllability with higher transconductance and lower intrinsic capacitances (gate capacitances) as explained above.

Another key parameter for evaluating the analog and RF performance of the MOS devices is known as frequency transconductance gain product ($FTGP$) which is formulated in Eq. (8). $FTGP$ shows the trade-off between switching speed and intrinsic voltage gain. For high speed operation we have to compromise with the voltage gain. When voltage gain increases, the lower limit of the drain current increases and the upper limit remain same which shows that its Ion/Ioff ratio decreases and hence its switching speed decreases.

$$f_T \approx \frac{g_m}{2\pi(C_{gs}+C_{gd})} \quad (7)$$

$$FTGP = f_T \times \left(\frac{g_m}{I_D}\right) \times \left(\frac{g_m}{g_d}\right) = FTP \times A_V \quad (8)$$

[Figure 7]

[Figure 8]

Figure 8 to Figure 11 represents the variation of Y parameter (short circuit admittance parameter) with respect to the frequency up to 1THz. From Figure 8 and Figure 9 it is clearly observed that the *Real* (Y_{11}), *Real* (Y_{22}), *Real* (Y_{12}) and *Real* (Y_{21}) values for both the devices are frequency independent which implies that it is less sensitive to the high frequency signals.

[Figure 9]

[Figure 10]

[Figure 11]

Figure 10 and Figure 11 shows the variation of *Img* (Y_{11}), *Img* (Y_{22}), *Img* (Y_{12}) and *Img* (Y_{21}) values with respect to frequency for both the devices and from the Figure it is evident that the electrical characteristics exhibit by the both the devices are almost independent of the frequency upto several 100 GHz and beyond this it changes abruptly. The plots for Y parameters reveals that both the devices are exhibit almost similar performance in terms of frequency sensitivity.

[Figure 12]

Figure 12 represents the variation of minimum noise Figure with respect to frequency and it is observed that upto 100GHz of frequency range it is almost negligible and beyond this it increases abruptly. For single gate FDSOI MOSFET this increase is larger as compared to the double gate FDSOI MOSFET.

[Figure 13]

[Figure 14]

[Figure 15]

[Figure 16]

Figure 13 to Figure 16 represents variation of the S-parameters with respect to frequency. All the S-parameters are derived from the Y-parameters of the device (Eq. (9) to Eq. (12))¹⁹. From the plot it is observed that the all the parameters are frequency independent upto 10GHz of frequency range and beyond this the change is gradual in nature.

$$S_{11} = \frac{(1-Y_{11})(1+Y_{22})+Y_{12}Y_{21}}{(1+Y_{11})(1+Y_{22})-Y_{12}Y_{21}} \quad (9)$$

$$S_{12} = \frac{-2Y_{12}}{(1+Y_{11})(1+Y_{22})-Y_{12}Y_{21}} \quad (10)$$

$$S_{21} = \frac{-2Y_{21}}{(1+Y_{11})(1+Y_{22})-Y_{12}Y_{21}} \quad (11)$$

$$S_{22} = \frac{(1+Y_{11})(1-Y_{22})+Y_{12}Y_{21}}{(1+Y_{11})(1+Y_{22})-Y_{12}Y_{21}} \quad (12)$$

In the high frequency operating range several losses take place so it is very essential to analyse these losses in order to characterize the device more accurately. Some of the important losses associated with the devices in the microwave frequency range are as follows (Eq. (13) to Eq. (16))¹⁹:

Insertion loss:

$$10\log \frac{P_i}{P_o} = 20\log \frac{1}{|S_{21}|} = 20\log \frac{1}{|S_{12}|} \quad (13)$$

Transmission loss:

$$10\log \frac{P_i - P_r}{P_o} = 10\log \frac{1 - |S_{11}|^2}{|S_{12}|^2} \quad (14)$$

Reflection loss:

$$10\log \frac{P_i}{P_i - P_r} = 10\log \frac{1}{1 - |S_{11}|^2} \quad (15)$$

Return loss:

$$10\log \frac{P_i}{P_r} = 20\log \frac{1}{|S_{11}|} \quad (16)$$

Figure 17 to Figure 20 represents the losses associated with the devices at RF frequency range. From Figure 17 and Figure 19 it is found that the both Insertion losses and the reflection losses in the single gate FDSOI MOSFET is smaller in comparison to the double gate FDSOI MOSFET while from the Figure 18 and Figure 20 is found that the Transmission loss and the return losses in the single gate FDSOI MOSFET is larger as compared to the of double gate FDSOI MOSFET.

[Figure 17]

[Figure 18]

[Figure 19]

[Figure 20]

It is obtained that the leakage current in single gate FDSOI MOSFET is lower in comparison to the double gate FDSOI MOSFET which implies that the static power dissipation in the former device is lower. The transconductance and Ion/Ioff ratio of the double gate FDSOI MOSFET is greater than that of single gate FDSOI MOSFET and implies that double gate FDSOI MOSFET is suitable for fast switching and large BW applications.

In Table 2, the RF performances of the designed devices are compared with the various MOS devices reported in the literature and it is found that as the channel length decreases, (0.25 μm in Ref. [31], 40 nm in Ref. [26] and 20 nm in this work) the value of g_m increases due to which f_T of the device also increases and follows the $1/L$ (L =channel length) trend, but in contrary to this it is found that the value of $FTGP$ highly decreases which implies that the gain of the device decreases while switching speed increases.

[Table 2]

4. Conclusion

An analysis on the RF performance of the single and double gate FDSOI MOSFET is carried out. Also the small signal equivalent circuits are developed in order to analyse the RF response of the device more accurately, and to extract other important RF parameters.

The key FOMs used in the analysis are intrinsic C_{gs} & C_{gd} , f_T and $FTGP$. It is observed that the value of g_m for DGFDSOI is 38% larger than that of SGFDSOI, 97% larger than GSDGFDSOI (Ref. [26]) and 89% larger than SGFDSOI (Ref. [31]). The f_T for DGFDSOI is 37% larger than that of SGFDSOI, 99% larger than GSDGFDSOI (Ref. [26]) and 100% larger than SGFDSOI (Ref. [31]). The leakage current in single gate FDSOI MOSFET is 39% smaller in comparison to the double gate FDSOI MOSFET which implies that the static power dissipation in the former device is lower. The Ion/Ioff ratio of the double gate FDSOI MOSFET is 10^3 times greater than that of single gate FDSOI MOSFET and implies that its switching speed is higher. The derived S parameters are used to evaluate its high frequency losses. It is observed that in the SG FDSOI MOSFET the Insertion loss is 2.47 dB, the Transmission loss is 2.48 dB and the Reflection loss is 1.02 dB lower than that of DG FDSOI MOSFET while the Return loss is 0.05 dB higher as compared to that of DG FDSOI MOSFET.

References

1. J. Carballo, W. J. Chan, P. A. Gargini, A. B. Kahng and S. Nath, "ITRS 2.0: Toward a re-framing of the Semiconductor Technology Roadmap," 2014 *IEEE 32nd International Conference on Computer Design (ICCD)*, Seoul, 2014, pp. 139-146.
2. The International Technology Roadmap for Semiconductors, 2015. [Online]. Available from: <http://public.itrs.net/reports.html>
3. C. W. Pearce and D. S. Yaney, "Short-channel effects in MOSFET's," in *IEEE Electron Device Letters*, 1985July; 6(7), 326-328,
4. R. -. Yan, A. Ourmazd and K. F. Lee, "Scaling the Si MOSFET: from bulk to SOI to bulk," in *IEEE Transactions on Electron Devices*, 1992July; 39(7), 1704-1710.
5. J. -. Colinge, "Hot-electron effects in Silicon-on-insulator n-channel MOSFET's," in *IEEE Transactions on Electron Devices*, 1987Oct.; 34(10), 2173-2177.
6. B. Agrawal, V. K. De, J. M. Pimbley and J. D. Meindl, "Short channel models and scaling limits of SOI and bulk MOSFETs," in *IEEE Journal of Solid-State Circuits*, 1994Feb.; 29(2), 122-125.
7. C. H. Wann, K. Noda, T. Tanaka, M. Yoshida and Chenming Hu, "A comparative study of advanced MOSFET concepts," in *IEEE Transactions on Electron Devices*, 1996Oct.; 43(10), 1742-1753.
8. K. Suzuki, "Short channel epi-MOSFET model," in *IEEE Transactions on Electron Devices*, 2000Dec.; 47(12), 2372-2378,.
9. Kow-Ming, C. and W. Han-Pang (2004). "A simple 2D analytical threshold voltage model for fully depleted short-channel silicon-on-insulator MOSFETs." *Semiconductor Science and Technology*, 2004;19(12), 1397-1405.
10. P. Agarwal, G. Saraswat and M. J. Kumar, "Compact Surface Potential Model for FD SOI MOSFET Considering Substrate Depletion Region," in *IEEE Transactions on Electron Devices*, 2008March; 55(3), 789-795.

11. T. Yamada, Y. Nakajima, T. Hanajiri and T. Sugano, "Suppression of Drain-Induced Barrier Lowering in Silicon-on-Insulator MOSFETs Through Source/Drain Engineering for Low-Operating-Power System-on-Chip Applications," in *IEEE Transactions on Electron Devices*, 2013Jan.; 60(1), 260-267.
12. Vimal Kumar Mishra and R. K. Chauhan, "Area efficient layout design of CMOS circuit for high-density ICs", *International Journal of Electronics (U.K.)*, 2018; 105(1), 73-87.
13. Narendra Yadava, Vimal K. Mishra, R. K. Chauhan, "Analysis of N+N⁻ Epi-Source Asymmetric Double Gate FD-SOI MOSFET". *Intelligent Engineering Informatics*, Singapore, **Springer Singapore**, 2018.
14. A. Cathelin, "Fully Depleted Silicon on Insulator Devices CMOS: The 28-nm Node Is the Perfect Technology for Analog, RF, mmW, and Mixed-Signal System-on-Chip Integration," in *IEEE Solid-State Circuits Magazine*, Fall 2017; 9(4), 18-26.
15. N. Planes, S. Kohler, A. Cathelin, C. Charbuillet, P. Scheer and F. Arnaud, "28FDSOI technology for low-voltage, analog and RF applications," *2016 13th IEEE International Conference on Solid-State and Integrated Circuit Technology (ICSICT)*, Hangzhou, 2016; 10-13.
16. K. Suzuki and S. Pidin, "Short-channel single-gate SOI MOSFET model," in *IEEE Transactions on Electron Devices*, 2003May; 50(5), 1297-1305.
17. Jong-Tae Park and J. -. Colinge, "Multiple-gate SOI MOSFETs: device design guidelines," in *IEEE Transactions on Electron Devices*, 2002Dec.; 49(12), 2222-2229.
18. W. Neudeck, "An overview of Double-Gate MOSFETs," *Proceedings of the 15th Biennial University/Government/ Industry Microelectronics Symposium (Cat. No.03CH37488)*, Boise, ID, USA, 2003; 214-217.
19. J. J. Liou and F. Schwierz, "RF MOSFET: recent advances and future trends," *2003 IEEE Conference on Electron Devices and Solid-State Circuits (IEEE Cat. No.03TH8668)*, Hong Kong, China, 2003; 185-192.
20. A. Gupta, M. Shrivastava, M. S. Baghini, D. K. Sharma, H. Gossner and V. R. Rao, "Part I: High-Voltage MOS Device Design for Improved Static and RF Performance," in *IEEE Transactions on Electron Devices*, 2010Oct. 5; 62(10), 3168-3175.
21. J. Jeon and M. Kang, "Circuit Level Layout Optimization of MOS Transistor for RF and Noise Performance Improvements," in *IEEE Transactions on Electron Devices*, 2016Dec.; 63(12), 4674-4677.
22. A. J. Scholten *et al.*, "The New CMC Standard Compact MOS Model PSP: Advantages for RF Applications," in *IEEE Journal of Solid-State Circuits*, 2009May; 44(5), 1415-1424.
23. A. Lázaro, B. Iñiguez, "RF and noise performance of double gate and single gate SOI", *Solid-State Electronics*, 2006; 50(5), 26-842.
24. N. Mohankumar, B. Syamal and C. K. Sarkar, "Influence of Channel and Gate Engineering on the Analog and RF Performance of DG MOSFETs," in *IEEE Transactions on Electron Devices*, 2010April; 57(4), 820-826.
25. Angsuman Sarkar, Alope Kumar Das, Swapnadip De, Chandan Kumar Sarkar, "Effect of gate engineering in double-gate MOSFETs for analog/RF applications", *Microelectronics Journal*, 2012; 43(11), 873-882.
26. K.P. Pradhan, S.K. Mohapatra, P.K. Sahu, D.K. Behera, "Impact of high-k gate dielectric on analog and RF performance of nanoscale DG-MOSFET", *Microelectronics Journal*, 2014; 45(2), 144-151.
27. Tiya Dey Malakar, Partha Bhattacharyya & Subir Kumar Sarkar, "Analytical Surface Potential Modelling-Based Small Signal Analysis and RF Performance Characterization of DMG SOI MOSFET for Better RFIC Application", *IETE Technical Review*, 2018; 35(3), 282-291.
28. Guechol, K., et al. "Small-Signal and Noise Model of Fully Depleted Silicon-on-Insulator Metal-Oxide-Semiconductor Devices for Low-Noise Amplifier." *Japanese Journal of Applied Physics* 2006; 45(9R), 6872.
29. Behzad Razavi. "RF Microelectronics". *Prentice-Hall, Inc.*, Upper Saddle River, NJ, USA. 1998.
30. Sze, "Physics of Semiconductor Devices", *John Wiley & Sons* pp. 529 1981.
31. V. Kilchytska *et al.*, "Influence of device engineering on the analog and RF performances of SOI MOSFETs," in *IEEE Transactions on Electron Devices*, 2003March; 50(3), 577-588.
32. ATLAS user's manual, SILVACO Int, Santa Clara, CA (2014).

Tables

Table 1: Parameters used in the design of SG FDSOI and DG FDSOI MOS devices

Symbol	Parameter	Value
L	Channel length	20nm
t_{ox}	Gate oxide thickness	1nm
t_{box}	Buried oxide thickness (BOX)	3nm
t_{si}	Silicon substrate thickness	10nm
W	Width	50nm
N^+	Drain/Source doping concentration	$1e20cm^{-3}$
N_a	Channel doping concentration	$1e15cm^{-3}$

Table 2: RF Performance Comparison of the various MOS devices reported in the literature with the devices designed in this work

References	Device	V_G (V)	V_D (V)	C_{gs} (fF)	C_{gd} (fF)	g_m (S)	f_T (THz)
Ref. [31]	SGFDSOI	1	1.5	32	14.5	0.0115	0.038
Ref. [26]	GSDGFDSOI	1	0.5	0.77	0.30	0.0032	0.515
This Work	SGFDSOI	1	0.8	0.23	0.17	0.064	25.88
	DGFDSOI	1	0.8	0.21	0.18	0.102	41.15

Where, SGFDSOI=single gate FDSOI MOSFET, DGFDSOI=double gate FDSOI MOSFET and GSDGFDSOI=gate stack double gate FDSOI

MOSFET (with Si_3N_4 as high-k dielectric material)

Figures

Figure 1. Structure of designed SG FDSOI MOSFET

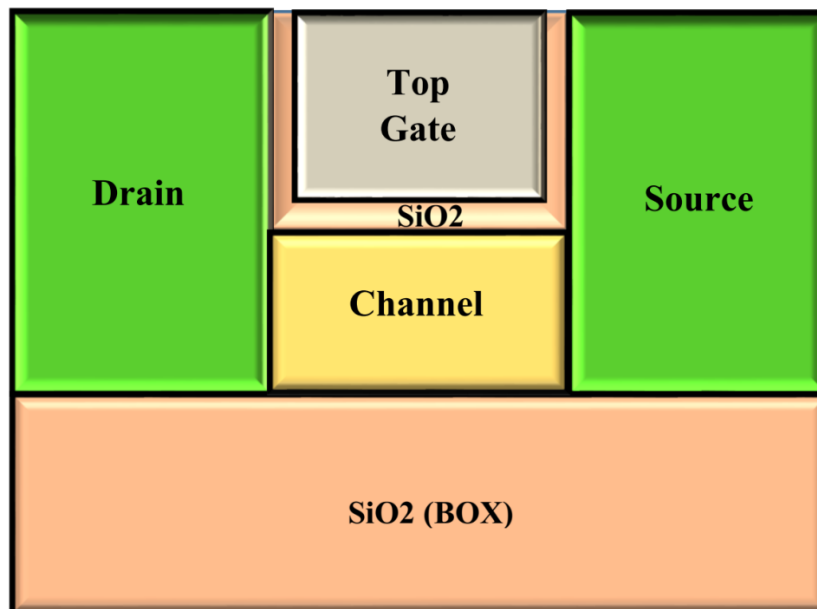


Figure 2. Structure of designed DG FDSOI MOSFET

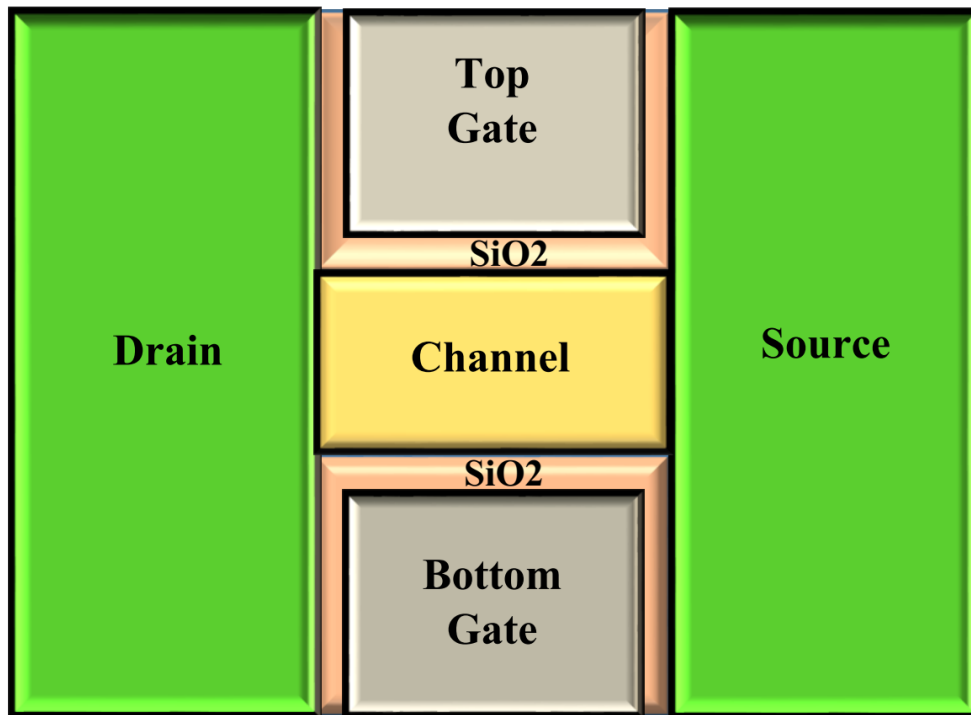


Figure 3. Small signal equivalent circuit of single gate FDSOI MOSFET

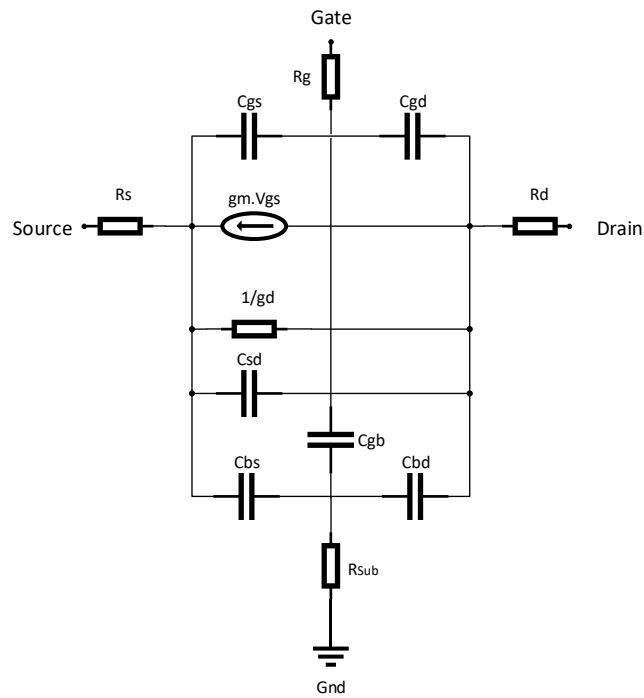


Figure 4. Small signal equivalent circuit of double gate FDSOI MOSFET

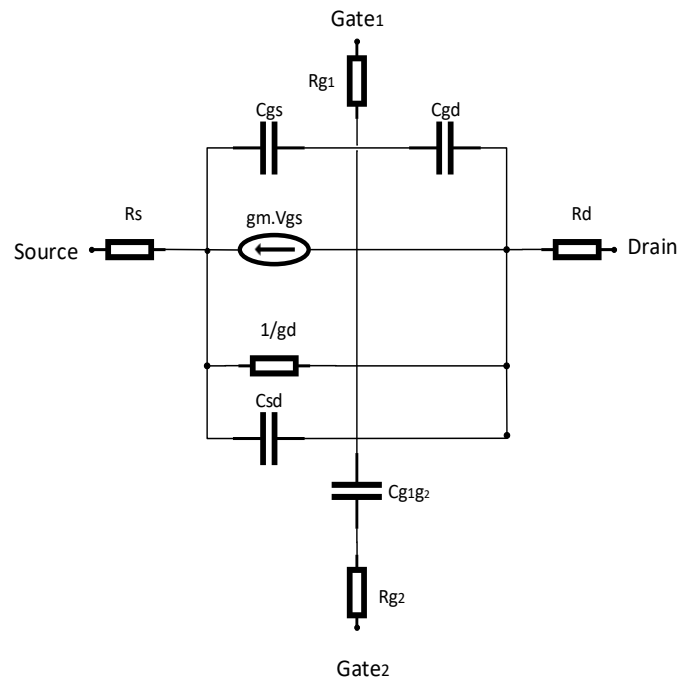


Figure 5. Drain current (I_D) versus gate to source voltage (V_{GS})

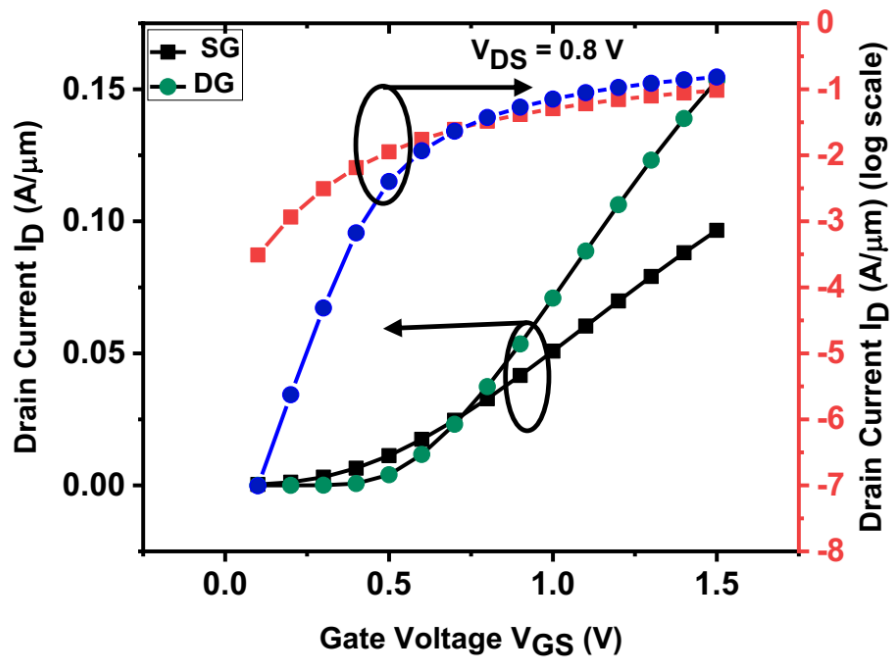


Figure 6. Intrinsic gate capacitances (C_{gs} and gate C_{gd}) versus gate to source voltage V_{GS}

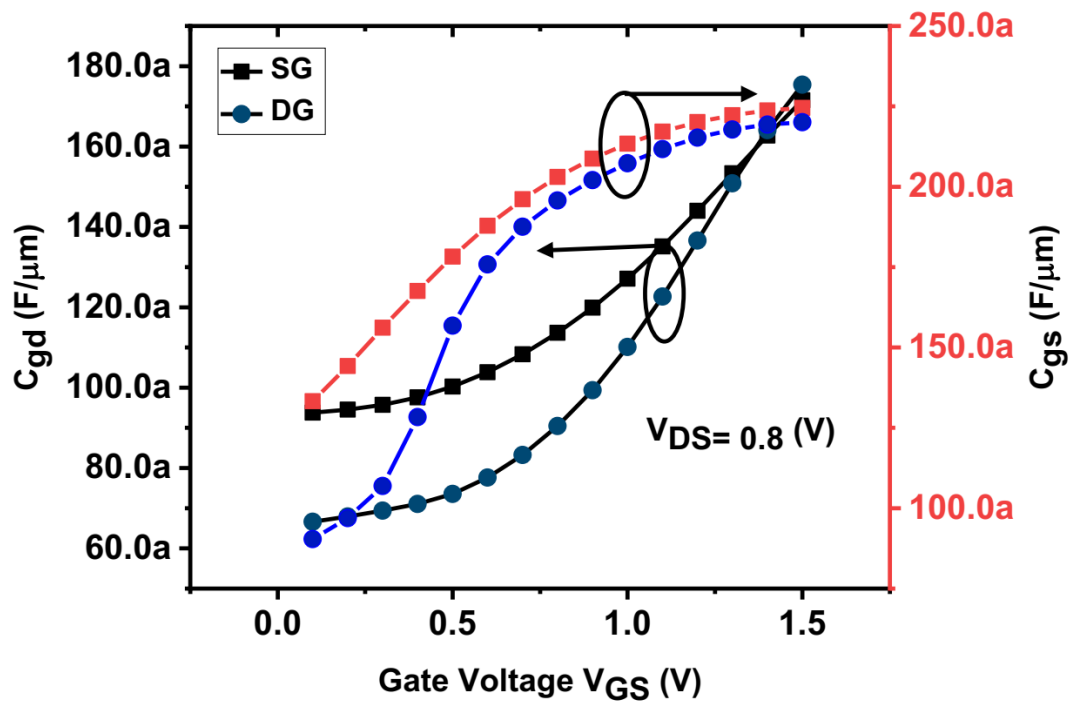


Figure 7. Cut off frequency (f_T) and frequency transconductance gain product (FTGP) versus gate to source voltage V_{GS}

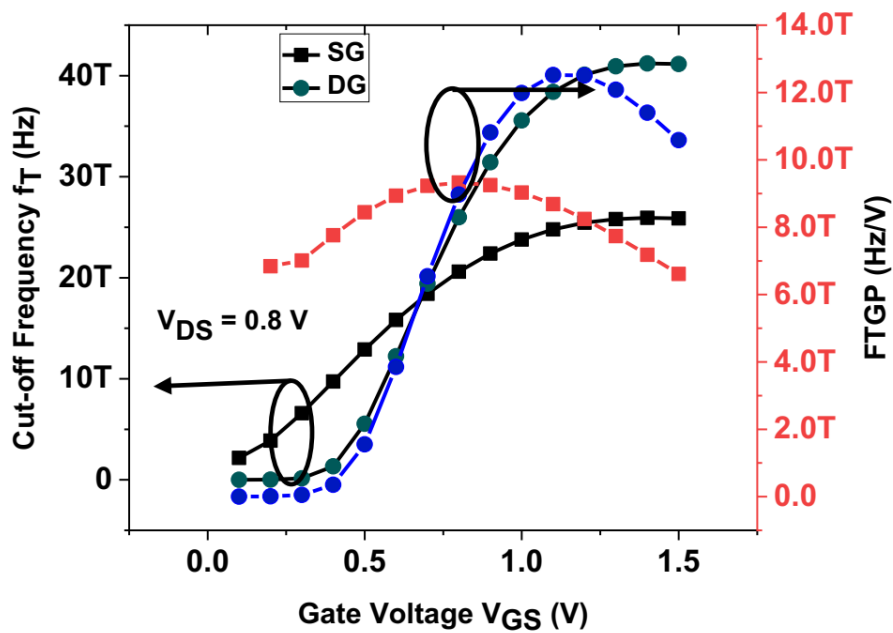


Figure 8. Real (Y_{11}) and Real (Y_{22}) versus frequency

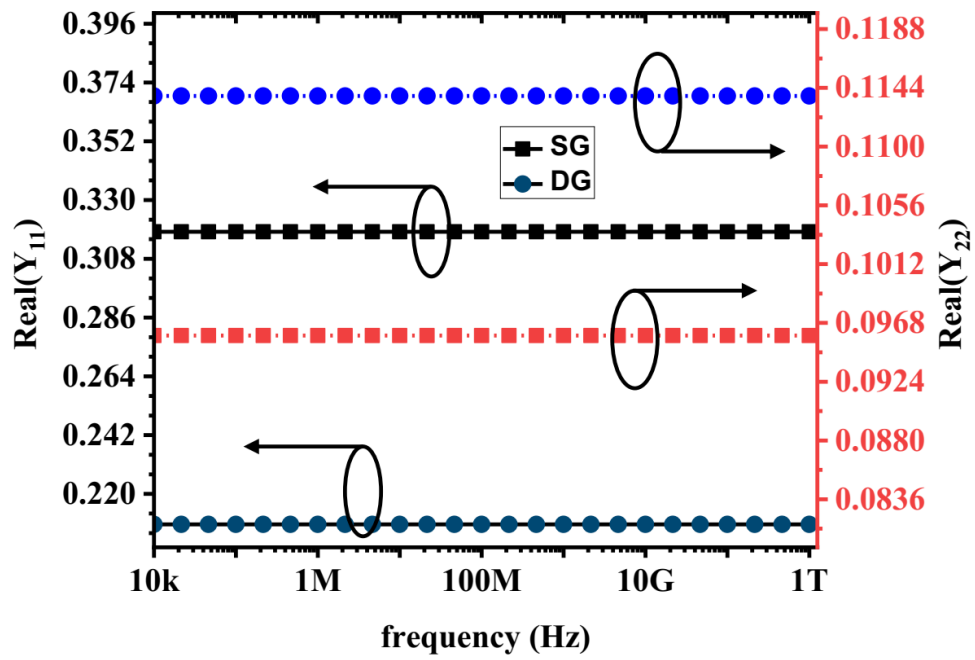


Figure 9. Real (Y_{12}) and Real (Y_{21}) versus frequency

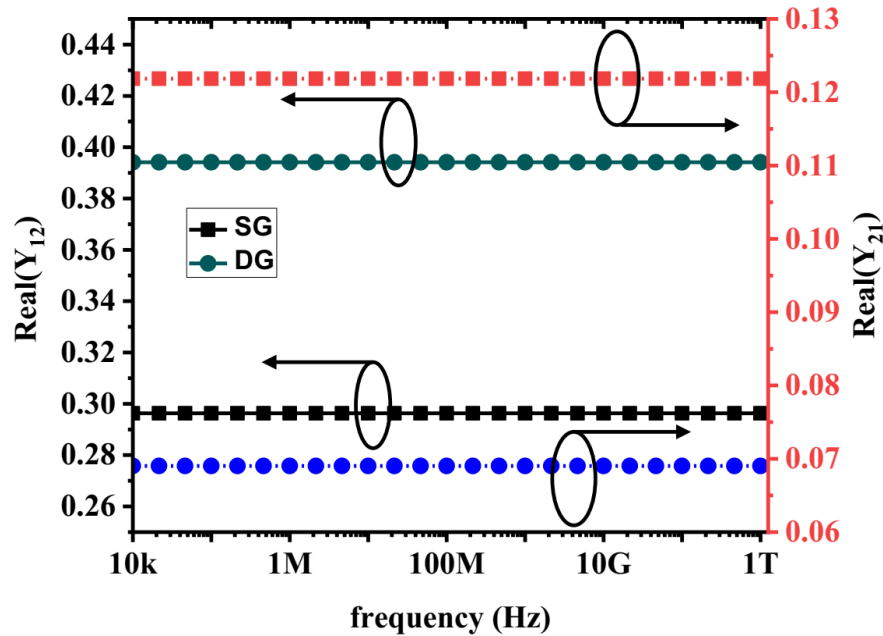


Figure 10. $Img(Y_{11})$ and $Img(Y_{22})$ versus frequency

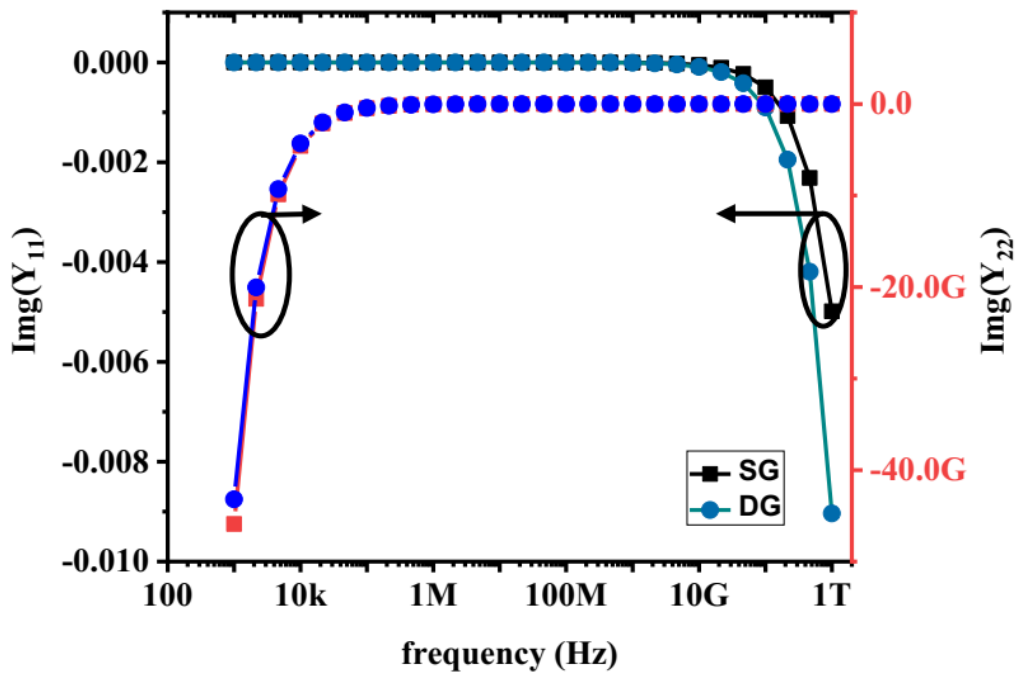


Figure 11. $Img(Y_{12})$ and $Img(Y_{21})$ versus frequency

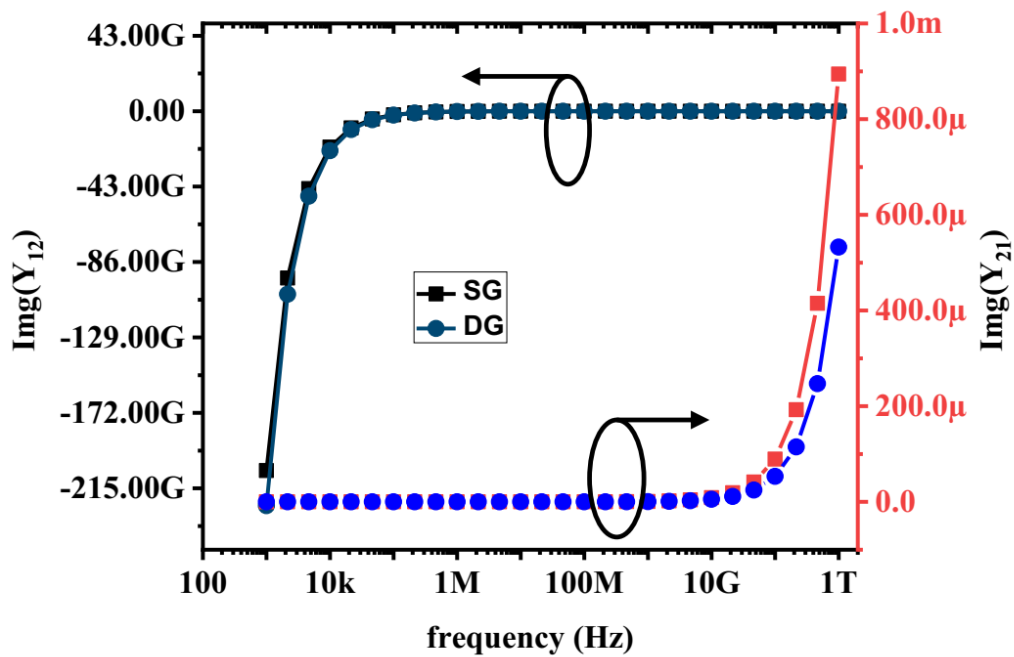


Figure 12. Minimum noise figure versus frequency

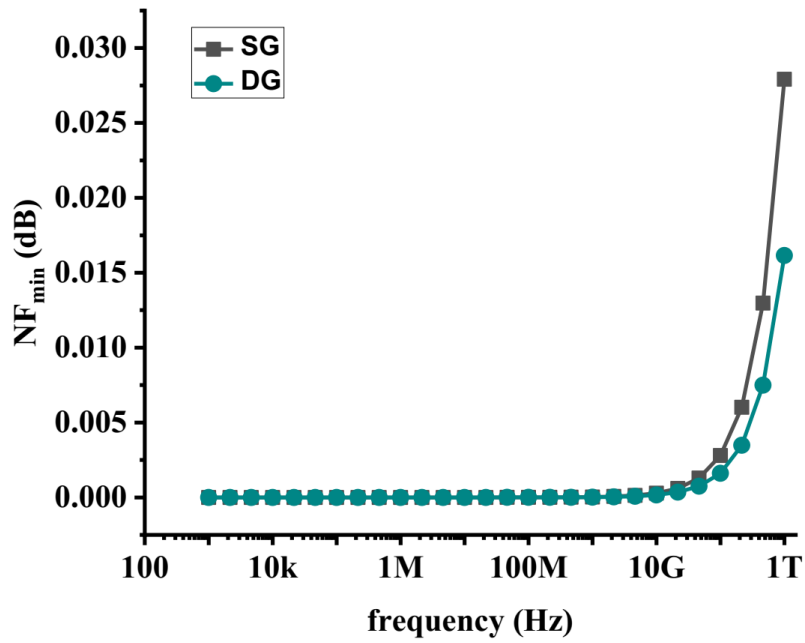


Figure 13. Real (S_{11}) and Real (S_{22}) versus frequency

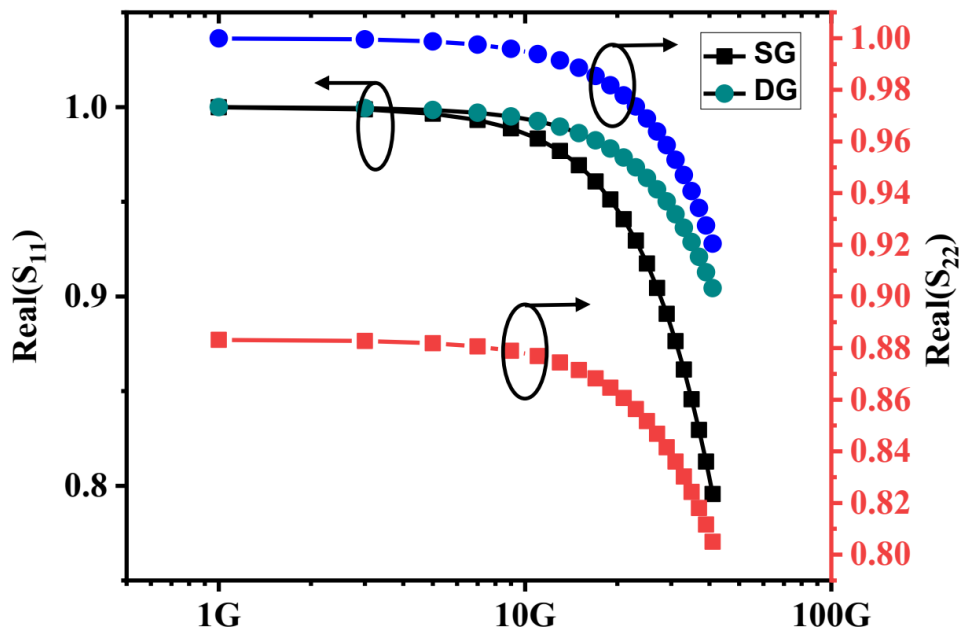


Figure 14. Real (S_{12}) and Real (S_{21}) versus frequency

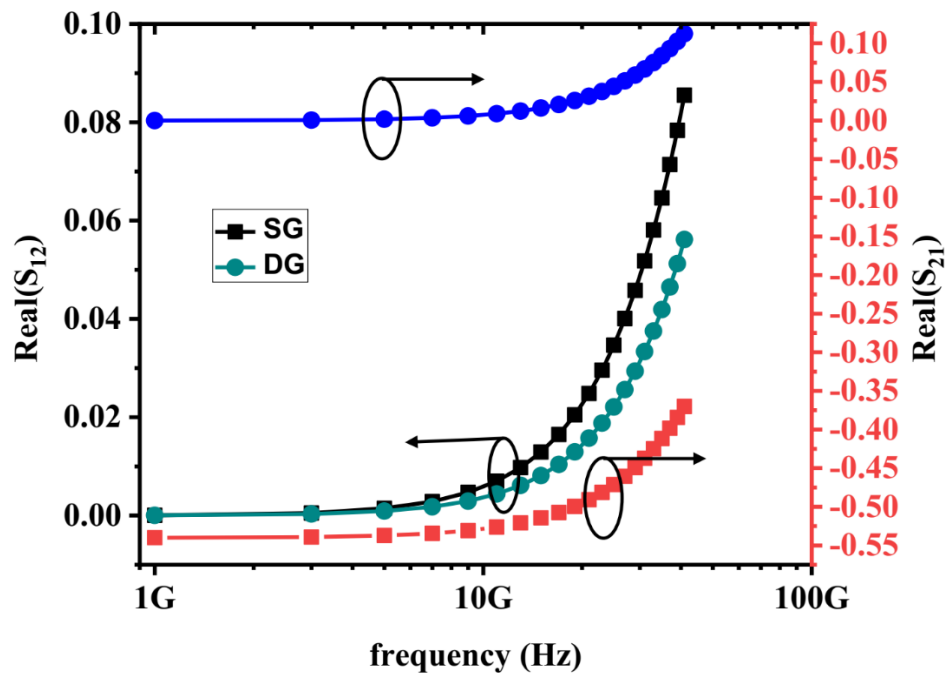


Figure 15. $\text{Im}g(S_{11})$ and $\text{Im}g(S_{22})$ versus frequency

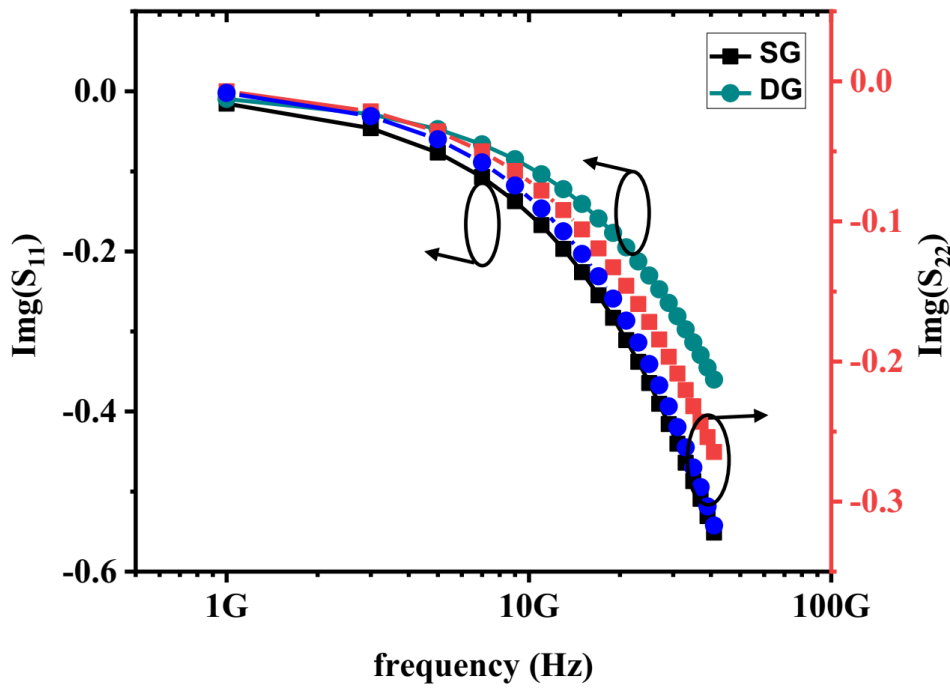


Figure 16. $\text{Img}(S_{12})$ and $\text{Img}(S_{21})$ versus frequency

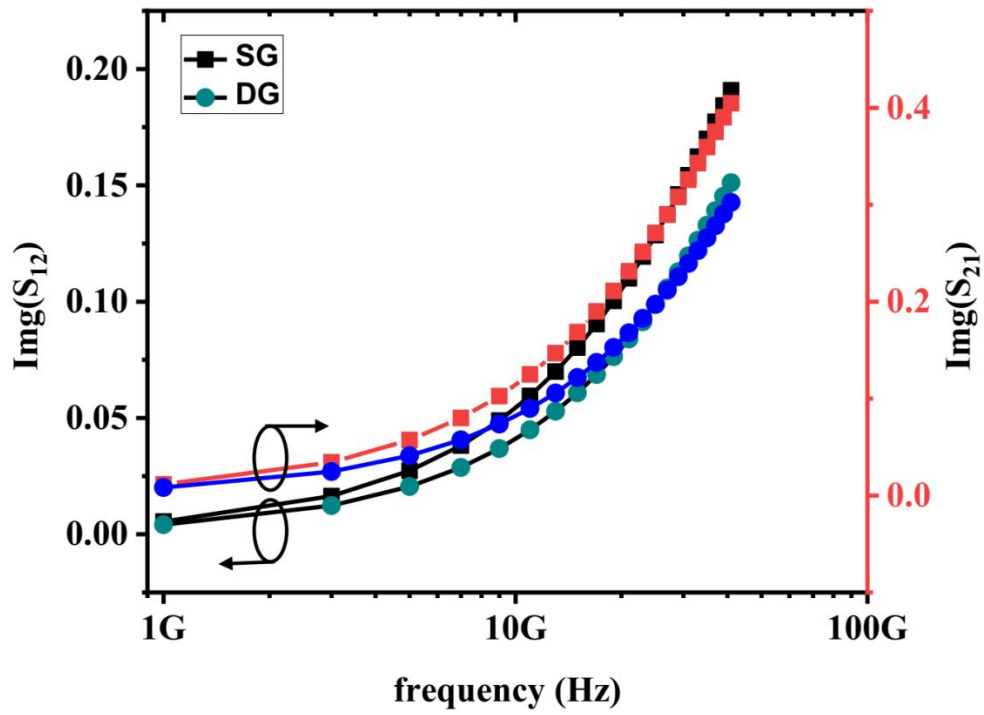


Figure 17. Insertion Loss versus frequency

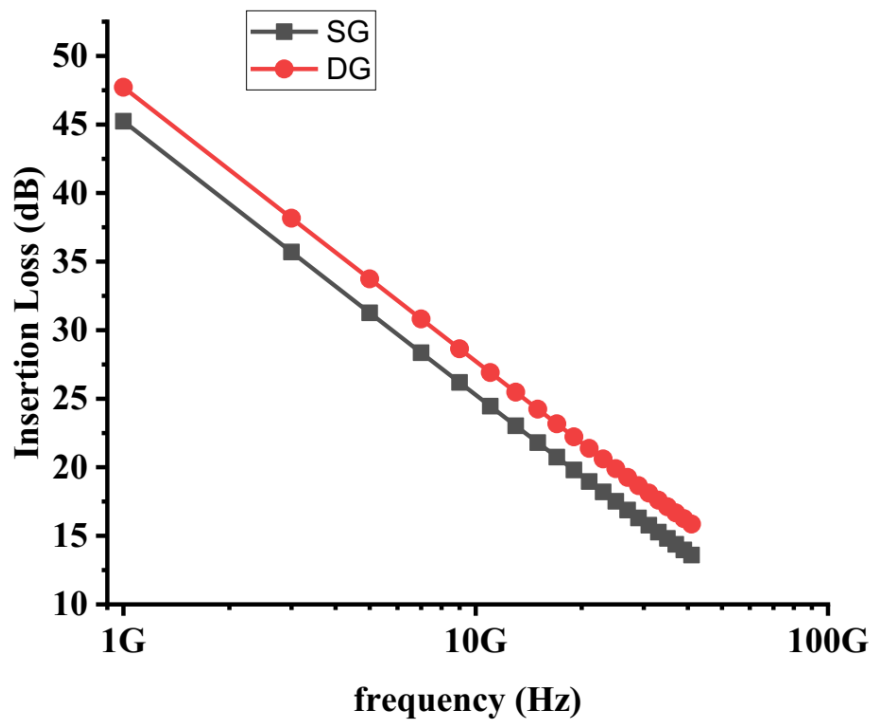


Figure 18. Transmission Loss versus frequency

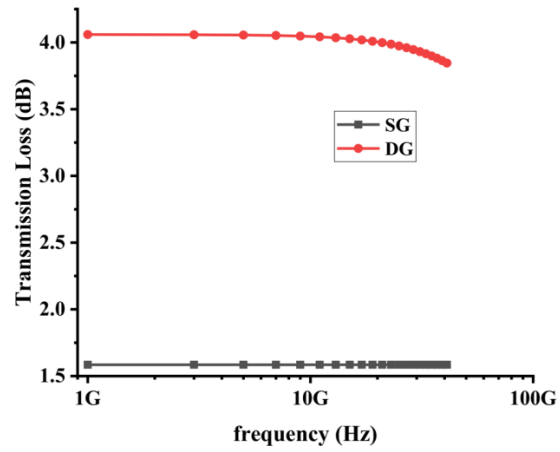


Figure 19. Reflection Loss versus frequency

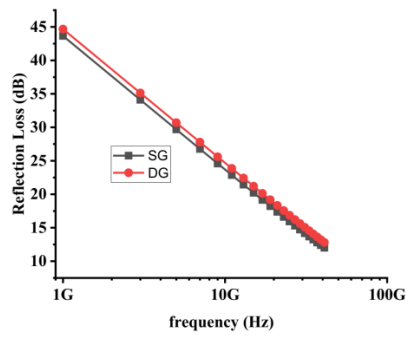
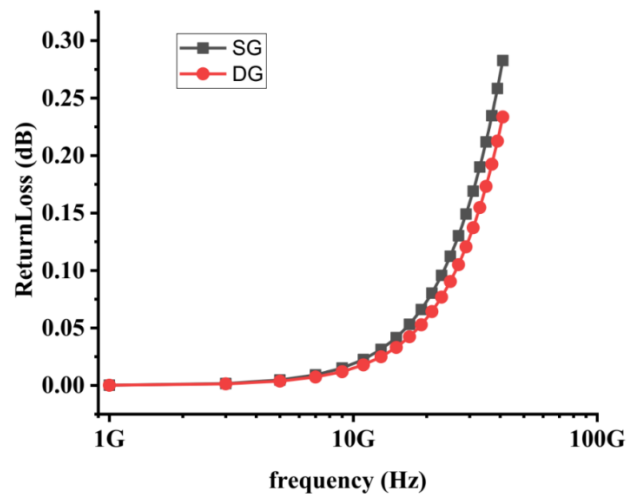


Figure 20. Return Loss versus frequency



International Conference on Defence and Space Technologies, ICDST 2019, Aug 23-25, 2019, IET Lucknow, India



International Conference on Defence and Space Technologies, ICDST 2019, Aug 23-25, 2019, IET Lucknow, India





International Conference on Defence and Space Technologies, ICDST 2019, Aug 23-25, 2019, IET Lucknow, India



International Conference on Defence and Space Technologies, ICDST 2019, Aug 23-25, 2019, IET Lucknow, India



International Conference on Defence and Space Technologies, ICDST 2019, Aug 23-25, 2019, IET Lucknow, India



International Conference on Defence and Space Technologies, ICDST 2019, Aug 23-25, 2019, IET Lucknow, India



International Conference on Defence and Space Technologies, ICDST 2019, Aug 23-25, 2019, IET Lucknow, India



International Conference on Defence and Space Technologies, ICDST 2019, Aug 23-25, 2019, IET Lucknow, India



International Conference on Defence and Space Technologies, ICDST 2019, Aug 23-25, 2019, IET Lucknow, India



International Conference on Defence and Space Technologies, ICDST 2019, Aug 23-25, 2019, IET Lucknow, India



International Conference on Defence and Space Technologies, ICDST 2019, Aug 23-25, 2019, IET Lucknow, India



International Conference on Defence and Space Technologies, ICDST 2019, Aug 23-25, 2019, IET Lucknow, India



International Conference on Defence and Space Technologies, ICDST 2019, Aug 23-25, 2019, IET Lucknow, India



International Conference on Defence and Space Technologies, ICDST 2019, Aug 23-25, 2019, IET Lucknow, India



International Conference on Defence and Space Technologies, ICDST 2019, Aug 23-25, 2019, IET Lucknow, India



International Conference on Defence and Space Technologies, ICDST 2019, Aug 23-25, 2019, IET Lucknow, India



International Conference on Defence and Space Technologies, ICDST 2019, Aug 23-25, 2019, IET Lucknow, India



International Conference on Defence and Space Technologies, ICDST 2019, Aug 23-25, 2019, IET Lucknow, India



International Conference on Defence and Space Technologies, ICDST 2019, Aug 23-25, 2019, IET Lucknow, India



International Conference on Defence and Space Technologies, ICDST 2019, Aug 23-25, 2019, IET Lucknow, India



International Conference on Defence and Space Technologies, ICDST 2019, Aug 23-25, 2019, IET Lucknow, India



International Conference on Defence and Space Technologies, ICDST 2019, Aug 23-25, 2019, IET Lucknow, India



International Conference on Defence and Space Technologies, ICDST 2019, Aug 23-25, 2019, IET Lucknow, India



International Conference on Defence and Space Technologies, ICDST 2019, Aug 23-25, 2019, IET Lucknow, India



International Conference on Defence and Space Technologies, ICDST 2019, Aug 23-25, 2019, IET Lucknow, India



International Conference on Defence and Space Technologies, ICDST 2019, Aug 23-25, 2019, IET Lucknow, India



International Conference on Defence and Space Technologies, ICDST 2019, Aug 23-25, 2019, IET Lucknow, India



International Conference on Defence and Space Technologies, ICDST 2019, Aug 23-25, 2019, IET Lucknow, India



International Conference on Defence and Space Technologies, ICDST 2019, Aug 23-25, 2019, IET Lucknow, India



International Conference on Defence and Space Technologies, ICDST 2019, Aug 23-25, 2019, IET Lucknow, India



International Conference on Defence and Space Technologies, ICDST 2019, Aug 23-25, 2019, IET Lucknow, India



International Conference on Defence and Space Technologies, ICDST 2019, Aug 23-25, 2019, IET Lucknow, India



International Conference on Defence and Space Technologies, ICDST 2019, Aug 23-25, 2019, IET Lucknow, India



International Conference on Defence and Space Technologies, ICDST 2019, Aug 23-25, 2019, IET Lucknow, India



International Conference on Defence and Space Technologies, ICDST 2019, Aug 23-25, 2019, IET Lucknow, India



International Conference on Defence and Space Technologies, ICDST 2019, Aug 23-25, 2019, IET Lucknow, India



Theme of Conference:

This conference is about to motivate engineering students, research scholars and faculty members to contribute the nation by producing technologies for defence of country and space technologies with their applications for human kind.

Call for Papers:

The authors are invited to submit their research / review papers and case studies/project-model / poster presentation in the myriad of conference themes listed below but not limited to:

Defence Technologies: Aeronautics, Air-Borne Systems, Armament Testing, Armaments, Artificial Intelligence & Robotics, Avionics, Ballistics, Bio-Energy, Bio-engineering, Camouflaging and Isotopes, Chemical & Biological Warfare, Cipher Systems, Combat Vehicles, Computational System, Cryptology, Electronic Warfare, Electronics & Communication Systems, Electronics & Optical Systems, Engineering Systems & Weapon Platforms, Explosives, Food Research, Gas Turbine, Health & Hygiene, High Altitude Agro-animal Research, High Energy Materials, High Energy Weapons, Laser Technology, Metallurgy, Microwave Devices, Missile & Strategic Systems, Missile & Strategic Systems, Naval Materials, Nuclear Medicine, Parachutes & Aerial Systems, Physiology, Psychological Research, Radars, Snow and Avalanche, Solid- State/ Semiconductor Materials, Sonar Systems, Terrain Research, Textiles, Polymers & Composites, Underwater Weapons, Wheeled Vehicles, High Energy Materials, Advanced Systems, Airworthiness & Certification, Information System and Documentation, Systems Integration, Systems Analysis, Missile Systems, Propellant, Life Sciences, Cryptology, Millimeter Wave and Semiconductor, Composite Materials, Sensors & MEMS, Propulsion Technology, Strategic Systems, Photonic Technologies, Plasmonics and Quantum Photonics, Systems Design.

Space Technologies: Aerospace, Aerospace Structures, Propulsion, Control, Guidance & simulation, Aerospace Materials, Composites & mechanical Systems, Transducers & Sensors, Structures & Fabrication, Avionics, Safety Engineering, Gravity Gradiometer, Precision Relative Navigation and Attitude Reference System, Ultrasonic Motor, Smart PCBs - Stress Strain Sensitive Films, Accelerometer, Vision Aided Inertial Navigation System - Image Processing Launch vehicle tracking system Launch pad Testing of liquid propulsion system, SATCOM Technology, SATCOM Applications, Mechanical Engineering Systems, Electronics Support Services, Antenna, System Reliability, Mission Development Area, Communication and Power, Integration and Checkout, Mechanical Systems, Controls and Digital, Reliability and Components, Systems Production, VLSI Design, CMOS Process Technology, Development and Educational Communication, Navigation Programme, Earth Observations, Mission Development and Remote Sensing-Sensor Technology, Remote Sensing Image Processing and Software Development, Satellite Data Reception & Ground Station, Earth, Ocean Sciences Applications, Aerial Remote Sensing, Earth and Climate Sciences, Disaster Management, Space Sciences, Investigation on Near

Earth Environment, Atmospheric Dynamics and Coupling, Sun and Solar System, Astronomy and Astrophysics, Space Instrumentation, Remote Sensing Data Analysis from Planetary Exploration Missions, Laboratory Study of Astro-materials, Study of Terrestrial Analogues of Moon and Mars, Payloads for Upcoming Planetary Missions, Meteorology, Weather and Climate, Radiation, Aerosols and Trace Gases, Microwave Atmospheric Studies, Signal and Data Processing, Radar and Lidar Instrumentation for Atmospheric Probing, Meteorology Facility for Launch-Vehicle.

Electronics and ICT: Soft Computing, Cloud Computing & Nano-Computing, Web Technology & Web Designing, Data Base Management System, Algorithms, Data Mining, Grid Computing & Internet Technology, Information & Data Security and Digital Security, Emerging Telecommunication Technology & Next Generation Network, Coding and Information Theory, Wireless, UWB, Ultrasonic Communications, Satellite Communications; Radio-over-Fiber, Free Space and Fiber-Optic Communications; Software Defined Radio, Cognitive Radio, Embedded System, Robotics, Industrial Instrumentation, Data Communication & Grid networking, Bio-Computation Technique, Biomedical Sensor & Instrumentation, Biomedical Applications, Nano-fabrications, Computer Integrated Manufacturing & its Subsystem, Future Technologies in Optical Communications, Security & Privacy in Optical Networks, Optical Networks and Components, Fiber Optic Sensors and Instrumentation, Energy Conversion, Management, Energy Efficiency and Energy Storage, Energy Policy, Planning & Economics, Green Technology & its Applications, Nano Technology & Photonics, **Nano-fabrication & Computing, Materials for Electronics**, Knowledge Management, Computer-Aided Diagnosis 3D-Computer Vision system & Application, Decision Making, Intelligent Systems and ICT Applications, Image, Speech and **Biomedical Signal Processing**, Biometrics & Authentication, Image Based Human-Computer Interaction, Biomedical Applications in Molecular, Structural, and Function Imaging, AI, Fuzzy Logic & Neural Systems, **Electrical** Power Electronics Converters and Drives, FACTS and HVDC technologies, Power System Economics & Restructured Power Systems, Distributed & Co-Generation, Energy Conservation, Optimal Control, Robust Control & Networked Control Systems, Nonlinear Systems and Control, Analysis and Design of Electrical Machines, Traction & Electric Vehicle Drives, Industrial Drives, Control of Electric Drives, Micro-electromechanical System, process & technology and application areas, Mechatronics, Microwave Devices / Components Design & Techniques, RF, Microwave & Millimeter wave systems and applications, Nano-scale Integration of Planar, Free-Space, and Mixed Subsystems, Reconfigurable system, Analog / Digital / Mixed-Signal Circuits, RF circuit design, MMIC & CMOS Circuits Remote Sensing and Geo-informatics.

Poster Presentation and Model Demonstration: Robotics, Bio Robotics, Artificial Intelligence, Neural Networks, Artificial Environment, mosquito modelling, Aerodynamics, Studies of Natural Systems, Logical Imagination and Proposals, Non-Conventional

Energy Resources, Clouds Spark and Lightening, Satellite Communication, Solar Energy and Stations for Satellites, Satellite Sensor Network, Image Processing, Soil Testing Based on Light Reflections, Applications of Satellite Technologies, Analysis of Historical Studies and Proposals, Applications for Defence System, Bio-Medical and Health in Space and Satellite, Mathematical Modelling and Research, Wireless Optical Communication, Space war, Nuclear Radiations and Defence, Missile Technologies and Defence System, Medical and Health after Nuclear Explosion, Air and Water purifier, Self Protections to be Used at Time of War, Earthquake and Tsunami, Sea Waves and Energy, Solar System and its Role in Universal System.

Tutorials on Important Topics

Tutorials/Lectures covering the recent important topics in the areas of defence and space technologies will be delivered by experts in the Defence, Space, Electronics and ICT fields. Certificates of attendance will be issued.

Registration Fees

Rs 3000/- for participant, Rs. 5000/- for Author,
The fees can be submitted online.

No fee for students as participants if registered on conference website.

Instruction for Authors

Prospective authors are invited to submit original and unpublished papers in the conference; full text manuscript in IEEE template is to be submitted & length of paper is limited to maximum of six pages. Authors are required to submit the papers through Easy Chair conference management system.

<https://easychair.org/my/conference?conf=icdst2019>

or e-mail the papers to icdst@ietlucknow.ac.in Papers must be only in .doc file format. Finally the selected papers for presentation in conference, may be published in selected SCI/Scopus indexed / UGC approved journals as per quality of papers after peer review and minor revisions as suggested by peer reviewers in the format of journals.

GMap location of IET Lucknow:

IET Lucknow, Sector F, Jankipuram, Lucknow, Uttar Pradesh 226021
<https://maps.google.com/?cid=12781453035130993833>

How To Reach IET Lucknow: From Amausi Airport Lucknow, one can book taxi directly to institute (35 Km away) locally known as Engineering College (Jankipuram) and from Charbagh Lucknow railway station to Engineering College (12 Km away).

From Amausi Airport or Charbagh railway station one may come to Munshi Pulia (7 Km away from IET) through Lucknow Metro train and then through taxi to Engineering College from Munsia-Pulia.

Important Dates: Abstract Registration: till 15 July 2019 Paper submission: till 31 July 2019

Review and Revision: till 15 Aug 2019

Conference date: 23-25 August 2019.

CONTACT: Dr. RCS Chauhan, Associate Professor, ECE, IET Lucknow,

email: icdst@ietlucknow.ac.in mob.ph.no. +91 9336050184

Student Coordinators

Mr. Abhinay Chaudhary
Mr. Aditya Verma

Ms. Snigdha Singh
Ms. Jyotsna Sharma

Chief Patron

Prof. Vinay Kumar Pathak, Hon. Vice Chancellor, AKTU, Lucknow

Patron

Prof. H.K.Paliwal, Director, IET Lucknow

General Chair

Prof. Yatindra Nath Singh, EE, IIT Kanpur

Conference Chair

Prof. V.K.Singh, ECE, IET Lucknow

Prof. S.R.P. Sinha, ECE, IET Lucknow

Advisory Committee

Dr. Ashish Dutta, ME, IIT Kanpur

Dr. Vineet Kansal, Pro VC, AKTU

Dr. Jaideep Srivastava, Prof, CSE, University of Minnesota, USA

Dr. K. V. Srivastava, IIT Kanpur

Dr. R. Govindarajan, IISC Bangalore

Dr. Nischal Verma, IIT Kanpur

Dr. Ruchir Gupta, IIT BHU

Dr. Barjeev Tyagi, IIT Roorkee

Dr. Satish Kumar Singh, IIIT Alld.

Dr. Rajeev Tripathi MNNIT Alld.

Dr. V. K. Srivastava, MNNIT Alld.

Dr. Vijaya Bhadauria, MNNIT Alld.

Dr. Rajeevan Chandel, NIT Hamirpur

Dr. Rachna Asthana, AITH Kanpur

Dr. Manoj K. Shukla, HBTU Kanpur

Dr. R.K. Chauhan, MMMUT Gorakhpur

Dr. D.K. Srivastava, BIET Jhansi

Dr. Neelam Srivastava, REC Kannauj

Dr. Manish Gaur, CAS, AKTU

Dr. G. Nagarajan, PEC Ponduchery

Dr. N.K.Singh, PhD, IIT BHU

Coordinator

Prof. Subodh Wairya, HoD, ECE, IET Lucknow.

Prof. O.P. Singh, TEQIP Coordinator, IET Lucknow

Convener

Dr. R.C.S. Chauhan, Asso. Prof., ECE, IET Lucknow.

Organizing Secretaries

Dr. Arun Kumar Tiwari, HoD, ME

Dr. Satyendra Singh, HoD, EE

Dr. Pradeep Bajpayee, Registrar

Manager

Conference Executive Committee

Prof. S.P. Tripathi, CSE

Prof. Bharti Dwivedi, EE

Prof. Kailash Narain, CE

Prof. Girish Chandra, CSE

Dr. Ram Pravesh Ram, CHE

Prof. Shailendra Sinha, ME

Prof. Sanjay Srivastava, ASD

Prof. A.K.Shukla, CE

Program Committee

Dr. Arun Kumar Singh, REC Kannauj

Dr. Arunima Verma

Dr.R.K.Singh

Mr. Amit Kumar

Ms. Richa Parihar

Mr. Pradeep Verma

Ms.Pooja Gupta

Ms. Gaytri Tiwari

Dr. S. N. Singh IIT Kanpur

Dr. K.S. Venkatesh, IIT Kanpur

Dr. KTV Reddy, IETE

Dr. T. Srinivas, IISC Bangalore

Dr. R. K. Pandey, IIT BHU

Dr. R. K. Singh, IIT BHU

Dr. K.V. Arya, IIIT Gwalior

Dr. Shekhar Verma, IIIT Alld.

Dr. A K. Singh, MNNIT Alld.

Dr. R.K.Nagaria, MNNIT Alld.

Dr. J.P. Saini, NSUT, Delhi

Dr. N.B. Singh, HBTU Kanpur

Dr. K. Raj, HBTU Kanpur

Dr. K.G. Upadhyaya, MMMUT

Dr. R.P. Payasi KNIT

Dr. Neelendra Badal, KNIT

Dr. S.P. Shukla, REC Banda

Dr. Rajeev Kumar, CoE, AKTU

Dr. Dilip Sharma, IEEE, UP

Dr. S.L. Shukla, PSIT Kanpur

About Lucknow City: Lucknow, the city of Nawabs, is state capital of Uttar Pradesh, highest populated state of India. The city also known as work place of Ex. Prime Minister of India, Shri Atal Bihari Vajpayee as MP from Lucknow city. In his tenure India could become atomic power.

About IET Lucknow: Institute of Engineering and Technology, Lucknow is well known engineering institution in North India. It was established in 1984 under UP state government. Through Uttar Pradesh State Entrance Examination (UPSEE) it gets the students for admission in UG/PG programs with top ranks. It offers UG programs in Electronics & Communication Engineering, Electrical Engineering, Mechanical Engineering, Computer Science & Engineering, Civil Engineering, Chemical Engineering, Information Technology and Electronics & Instrumentation Engineering. It offers PG programs as MCA, MBA and M.Tech in Bio-Technology, Micro-Electronics, Electric Drive and Control, Mechanical Engineering, Environment Engineering and Structural Engineering. It also offers PhD programs related with all departments offering UG/PG programs.

About Department of ECE: The Electronics & Communication Engineering department at IET Lucknow is producing quality engineers. The self financed UG program in Electronics & Instrumentation Engineering and PG program (M.Tech) in Micro-electronics are also running. In support of AKTU and TEQIP some teaching cum research fellows are doing their PhD degree under able supervision of senior faculty members involved in the research work of their areas.

Conference Objective and Scope: The conference objective is to increase the involvement of UG, PG, PhD students and faculty members of engineering institutions in research and projects development in field of defence and space research to make India a world leader in Defense and Space Technologies.

Institute of Engineering & Technology,
Lucknow, U.P.-226021

